N72-30336

NASA TECHNICAL TRANSLATION

NASA TT F-707

NASA TT F-707

CASE FILE COPY

PROPAGATION OF VISIBLE AND INFRARED WAVES IN THE ATMOSPHERE

by V. Ye. Zuyev

"Sovetskoye Radio" Press
Moscow, 1970

NATIONAL AERONAUTICS AND SPACE ADMINISTRATION • WASHINGTON, D. C. • JULY 1972

NASA TT F-707

PROPAGATION OF VISIBLE AND INFRARED WAVES IN THE ATMOSPHERE

By V. Ye. Zuyev

Translation of "Rasprostraneniye Vidimykh i Infrakrasnykh Voln v Atmosfere."
"Sovetskoye Radio" Press, Moscow, 1970

NATIONAL AERONAUTICS AND SPACE ADMINISTRATION

For sale by the National Technical Information Service, Springfield, Virginia 22151
$6.00

TABLE OF CONTENTS

Foreword vi

PART ONE. ABSORPTION OF VISIBLE AND INFRARED WAVES IN THE EARTH'S ATMOSPHERE. 1

Chapter 1. The Earth's Atmosphere as an Absorbing Medium . . . 1

1. Composition of the Atmosphere. Variations of Pressure and Temperature. 1
2. Distribution of Water Vapor in the Atmosphere. 5
3. Distribution of Ozone in the Atmosphere. 20
4. Distribution of CO_2, O_2, CH_4, N_2O, and CO in the Atmosphere. 21

Chapter 2. Origin and General Characteristics of the Absorption Spectra of Atmospheric Gases 24

1. Energy and Spectra of the Molecules. 24
2. Rotational Energy and Rotational Spectra of Molecules. . 26
3. Vibrational Energy and Vibrational-Rotational Spectra of Molecules. 35
4. Electron Energy and Electron Spectra of Molecules. . . . 43
5. Spectral-Line Shape. 43
6. Spectral-Line Strength 50
7. General Characteristics of the Absorption Spectra of Atmospheric Gases 52

Chapter 3. Absorption of Visible and Infrared Waves in a Homogeneous Atmosphere. 68

1. Basic Definitions. 68
2. Absorption by a Single Line 71
3. Absorption by Groups of Overlapping Lines. 76
4. Limits of Applicability of the Bouguer-Beer Law. 85
5. Fine Structure of Vibrational-Rotational and Purely Rotational Spectra of Water Vapor 89
6. Absorption Functions in Narrow Segments of the Vibrational-Rotational and Purely Rotational Spectra of Water Vapor 109
7. Fine Structure of the Absorption Spectrum of Carbon Dioxide 120
8. Absorption Functions in Various Segments of the CO_2 Spectrum. 124
9. Fine Structure and Absorption Functions in the Ozone Spectrum. 126
10. Fine Structure and Absorption Functions of the Oxygen Spectrum. 128
11. Fine Structure and Absorption Functions of the Spectra of Small Atmospheric Impurities 129
12. Absorption of Overlapping Lines and Bands. 132

13. Absorption of Radiation from Selective Sources. 134
14. Absorption of Laser Radiation in the Atmosphere 136

Chapter 4. Absorption of Visible and Infrared Waves in the Inhomogeneous Atmosphere. 153

1. Spectral Transmission (Absorption). The Transmission (Absorption) Function 153
2. Direct Calculation of Spectral Transmission and Transmission Functions 154
3. Approximate Calculation of the Absorption Function H. . 157
4. Approximate Method of Allowing for Temperature in Calculation of the Function H 161
5. Approximate Determination of the Spectral Transmission of the Inhomogeneous Atmosphere 163
6. Calculation of Absorption Function with Allowance for the Curvature of the Earth. 164
7. Experimental Investigations of the Absorption Functions H 167
8. Absorption of Laser Radiation in the Inhomogeneous Atmosphere. 168

PART TWO. SCATTERING OF VISIBLE AND INFRARED WAVES IN THE EARTH'S ATMOSPHERE. 175

Chapter 5. The Earth's Atmosphere as a Scattering Medium . . . 175

1. Clouds and Fogs 176
2. Hazes 183
3. Precipitation 193

Chapter 6. Single-Particle Scattering of Visible and Infrared Waves 195

1. The Polarized-Light Representation. 195
2. Scattering by a Plane Monochromatic Wave. 197
3. Scattering, Absorption, and Attenuation Coefficients. . 199
4. The Scalar Approximation in the Light-Scattering Problem 202
5. Scattering of an Inhomogeneous Field. 206
6. Laws Governing the Scattering of Visible and Infrared Waves by a Single Spherical Particle. 211
7. Scattering of Light by Nonspherical Particles 226

Chapter 7. Scattering of Visible and Infrared Waves in the Atmosphere. 228

1. Molecular Scattering of Visible and Infrared Waves. . . 229
2. Scattering of Waves by a System of Particles. 230
3. Investigations of the Scattering Matrix 233
4. Energy Characteristics of Scattering of Visible and Infrared Waves by Clouds and Fogs 234
5. Energy Characteristics of the Scattering of Visible and Infrared Waves by Haze. 251
6. Energy Characteristics of Scattering of Visible and Infrared Waves by Precipitation 266

7. Scattering Indicatrices of Polydisperse Aerosols 267
8. Scattering of Laser Radiation in the Atmosphere. 270
9. Influence of Measurement Apparatus on the Results of Experimental Investigations of the Scattering of Visible and Infrared Waves in the Atmosphere. 272

PART THREE. PROPAGATION OF SPATIALLY LIMITED BEAMS OF LIGHT IN THE ATMOSPHERE. 279

Chapter 8. Characteristics of Radiation from Various Types of Lasers 279

Introduction. 279
1. Ionic-Crystal Lasers 279
2. Glass Lasers 282
3. Gas Lasers 283
4. Semiconductor Lasers 285
5. Variation of Laser Emission Parameters Due to Various Causes. 286

Chapter 9. Propagation of Spatially Limited Beams of Optical Radiation in Atmospheric Aerolols 289

1. Brightness of Forward-Scattered Radiation. 289
2. Attenuation of Direct Radiation in Scattering Media. Limits of Applicability of Bouguer's Law. 303
3. Brightness of Backward-Scattered Radiation 306
4. Polarization Characteristics of Scattered Radiation. . . 309
5. Propagation of a Pulse of Directional Radiation in a Scattering and Absorbing Medium 311

Chapter 10. Nonlinear Effects Attending the Propagation of Strong Optical Radiation in the Atmosphere. 320

1. Probability of Multiphoton Processes 320
2. Calculation of Transition Probability by Successive Approximations. 324
3. Estimates of the Probability of Multiphoton Photoionization and Photodissociation. 326
4. The Spectroscopic Saturation Effect. 332
5. Absorption of Light with Consideration of the Saturation Effect. 335
6. Self-Focusing of the Laser Beam. 337
7. Effect of Strong Radiation Field on Atmospheric-Aerosol Particles 339

Chapter 11. Propagation of Limited Beams of Light in a Turbulent Atmosphere 349

1. General Remarks. 349
2. Theoretical Investigations of Parameter Fluctuations of Limited Beams Propagating in the Atmosphere 352
3. Experimental Studies of Parameter Fluctuations of Spatially Limited Beams Propagating in a Turbulent Atmosphere. 357

Appendix 1 369

Appendix 2 372

References 377

Index 416

PROPAGATION OF VISIBLE AND INFRARED WAVES IN THE ATMOSPHERE

V.Ye. Zuyev

ABSTRACT: The present monograph sets forth the basic results of theoretical and experimental investigations of various aspects of the problem of propagation of visible and infrared waves in the atmosphere. The generalization is based on the research of the author and his colleagues and on other studies carried out both in the USSR and abroad. Problems of the absorption and scattering of both monochromatic and nonmonochromatic radiation under various meteorological conditions, over various distances, and in various directions of propagation are examined in the first two parts of the book. The third part is devoted to a description of the propagation behavior of spatially limited beams of radiation from thermal sources and lasers in the atmosphere: the structure of the beam in various scattering media, the influence of atmospheric turbulence on beam parameters, and nonlinear effects that accompany the propagation of high-energy radiation in the atmosphere. The book is designed for a broad range of readers working in the fields of atmospheric optics and spectroscopy, meteorology, geophysics, geodesy and astrophysics, and opticoelectronic and laser engineering, as well as for senior students in the corresponding specialties.

/2

FOREWORD

/3

Recent years have witnessed a substantial increase in interest on the part of engineers and scientists in study of the propagation behavior of optical-wavelength electromagnetic waves in the earth's atmosphere. This interest is due primarily to the possibilities of using lasers in communications systems, data transmission, long-range distance measurement, optical radars, and other devices designed to work through the atmosphere. In addition, a broad range of meteorological, geophysical, and astrophysical problems requires increasingly accurate quantitative data on the propagation characteristics of visible and infrared radiation in the atmosphere. Foremost among these problems are: interpretation of satellite observational data on radiation and the associated solution of the inverse problems of satellite meteorology; calculation of radiant heat transfer in the atmosphere

and determination of the earth's planetary heat balance; determination of the radiation term in weather-forecasting equations; acquisition of astrophysical observational data that are free of the influence of the earth's atmosphere, etc.

Solution of these problems requires quantitative knowledge of a large number of variables that characterize the propagation of optical radiation in the atmosphere as both the characteristics of the radiation and the conditions of its propagation vary through wide ranges. These radiation characteristics include the width of the spectral interval or the degree of monochromaticity; power and its time variation (continuous and pulsed radiation); coherence; directivity and geometrical dimensions (ranging from the infinite wave to spatially limited beams, which are characterized by their initial diameter and divergence angle); the spatial homogeneity of the field. Propagation conditions depend on the instantaneous and mean temperature values, the total and partial pressures of the gaseous components of the atmosphere, /4
and the chemical composition, concentration, and size and shape spectra of atmospheric-aerosol particles, i.e., on the quantities that influence the parameters of radiation propagating in the atmosphere.

The author's first monograph [1] and the recently published ones of K.Ya. Kondrat'yev [2] and R. Goody [3] examined certain aspects of the interaction of optical radiation with the atmosphere. In [1], data on the absorption, scattering, and attenuation of thermal radiation in the visible and infrared bands in the atmosphere under various meteorological conditions were generalized. Reference [2] systematically sets forth problems in the calculation of heat transfer in the earth's atmosphere. The monograph of R. Goody [3] is devoted for the most part to the theory of absorption of thermal radiation by atmospheric gases.

The present monograph sets forth the results of theoretical and experimental research on various aspects of the problem of propagation of visible and infrared waves in the atmosphere that have been carried out both in the USSR and abroad.

The book consists of three parts. The first part examines problems of the absorption of visible and infrared radiation from thermal sources and lasers by atmospheric gases under various propagation conditions. The possible variations of these conditions and the mean vertical temperature, pressure, humidity, and absorbing-gas concentration profiles in the atmosphere are described in Chapter 1. Chapter 2 deals with the origin of the absorption spectra of atmospheric gases (water vapor, carbon dioxide, ozone, methane, nitrogen oxides, carbon monoxide, and oxygen). Chapters 3 and 4 analyze the results of theoretical and experimental studies of the absorption of optical radiation propagating in horizontal and slant directions under various conditions in the atmosphere.

Part Two of the Monograph sets forth the problems of aerosol and molecular scattering of visible and infrared radiation from thermal sources and lasers under various conditions in the atmosphere. These conditions are characterized in Chapter 5. The laws of scattering of optical radiation by a single particle are considered in Chapter 6. The results of theoretical and experimental study of the scattering of visible and infrared waves /5 under various conditions in the earth's atmosphere are set forth in Chapter 7.

Part Three of the book systematically discusses various aspects of the problem of propagation of spatially limited beams of laser and thermal-source radiation in the atmosphere. The basic parameters of the radiation from various types of lasers are considered in Chapter 8. Chapter 9 analyzes the results of studies of the structure of the luminous field in the cross section of a beam propagating through various scattering media. Nonlinear effects accompanying the propagation of high-energy luminous radiation in the atmosphere are handled in Chapter 10. In the last chapter, Chapter 11, the fluctuations of the parameters of spatially limited beams of radiation due to turbulent motions in the atmosphere are examined.

The author considers it a pleasant duty to thank the following colleagues of the Infrared Radiation Laboratory of the Siberian Physicotechnical Institute at Tomsk University: B.A. Antipov, P.A. Bokhan, A.G. Borovoy, Ye.A. Vedernikova, O.K. Voytsekhovskaya, V.N. Genin, L.I. Gerasimova, I.I. Ippolitov, M.V. Kabanov, G.M. Krekov, P.N. Kokhanenko, M.Ya. Krylova, V.P. Lopasov, E.V. Lugin, Yu.S. Makushkin, A.A. Nalivayko, L.I. Nesmelova, B.A. Savel'yev, I.V. Samokhvalov, V.A. Sapozhnikova, V.K. Sonchik, V.V. Fomin, S.S. Khmelevtsov, and N.A. Chernyavskaya for their wide-ranging assistance in the work on the manuscript of the book. The author is particularly grateful to Stanislav Dmitriyevich Tvorogov, who collaborated in writing Chapters, 4, 6, and 10 and §2 of Chapter 7. The author thanks G.P. Puchkov and S.I. Sokolov, who were most helpful in the technical design of the manuscript.

The author is deeply indebted to Profs. K.Ya. Kondrat'yev and A.A. Semenov for their valuable critical comments and recommendations made during the review of the manuscript.

Part One /7

ABSORPTION OF VISIBLE AND INFRARED WAVES IN THE EARTH'S ATMOSPHERE

Chapter 1

THE EARTH'S ATMOSPHERE AS AN ABSORBING MEDIUM

The earth's atmosphere is an absorbing medium of extraordinary temporal and spatial variability. The absorption of visible and infrared waves in the atmosphere depends strongly on the pressure, temperature, and concentration of the absorbing gases. Each of these quantities varies with altitude, in time, and as a function of geographical region within rather broad limits. Without knowing the patterns of the variations of these elements, no problem that requires quantitative data on the absorption of visible and infrared waves in the atmosphere can be solved.

The present chapter examines the laws of variation of the pressure, temperature, and absorbing-gas concentrations in the atmosphere. It is primarily concerned with the distribution of water vapor in the atmosphere, since this gas is the principal absorbing component. Moreover, this component is more variable than the others.

The variations of all of the elements of interest to us will be considered in greatest detail in the lowermost 30-km layer of the atmosphere, where the basic mass of all gases that absorb radiation in the visible and infrared is concentrated.

§1. COMPOSITION OF THE ATMOSPHERE. VARIATIONS OF PRESSURE AND TEMPERATURE

Pressure is the only one of the atmospheric variables influencing the absorption of visible and infrared radiation whose variability in time can practically always be disregarded at all heights in the lowermost 30-km layer of the atmosphere. The vertical pressure profiles may also be considered practically the same for various regions of the globe. /8

The atmosphere consists chiefly of nitrogen, oxygen, and argon, whose percentage contents are given in Table 1.1. The table also gives data on other components of the atmosphere with the exception of water vapor.

TABLE 1.1. COMPOSITION OF DRY AIR [3]

Atmospheric component	Mean volumetric concentration in troposphere, %	Remarks
N_2	78.084	Dissociates in the upper ionosphere; mixed at lower levels
O_2	20.946	Dissociates above 95 km; mixed at lower levels
Ar	$9.34 \cdot 10^{-1}$	Mixed up to 110 km; diffusion separation at higher levels
CO_2	$3.3 \cdot 10^{-2}$	Variations insignificant; mixed to 100 km; dissociates at higher levels
Ne	$1.818 \cdot 10^{-3}$	Mixed up to 100 km; diffusion separation at higher levels
He	$5.24 \cdot 10^{-4}$	Mixed up to 110 km; diffusion separation at higher levels
CH_4	$1.6 \cdot 10^{-4}$	Mixed in troposphere, oxidizes in stratosphere, dissociates in mesosphere
Kr	$1.14 \cdot 10^{-4}$	Mixed to 110 km; diffusion separation at higher levels
H_2	$5 \cdot 10^{-5}$	Mixed in troposphere and stratosphere; dissociates at higher levels
N_2O	$3.5 \cdot 10^{-5}$	Insignificant variations at ground surface; gradually dissociates in stratosphere and mesosphere
CO	$7 \cdot 10^{-6}$	A product of oxidation; content variable
O_3	10^{-6}	Subject to strong variations; of photochemical origin
NO_2 NO	From 0 to $2 \cdot 10^{-6}$	Industrial origin in troposphere; of photochemical nature in mesosphere and ionosphere

The atmosphere also contains traces of many other gases, but these have no substantial influence on the absorption of visible and infrared waves. Gases that absorb visible and infrared radiation but are not listed in Table 1.1 may be encountered in certain local regions. /9

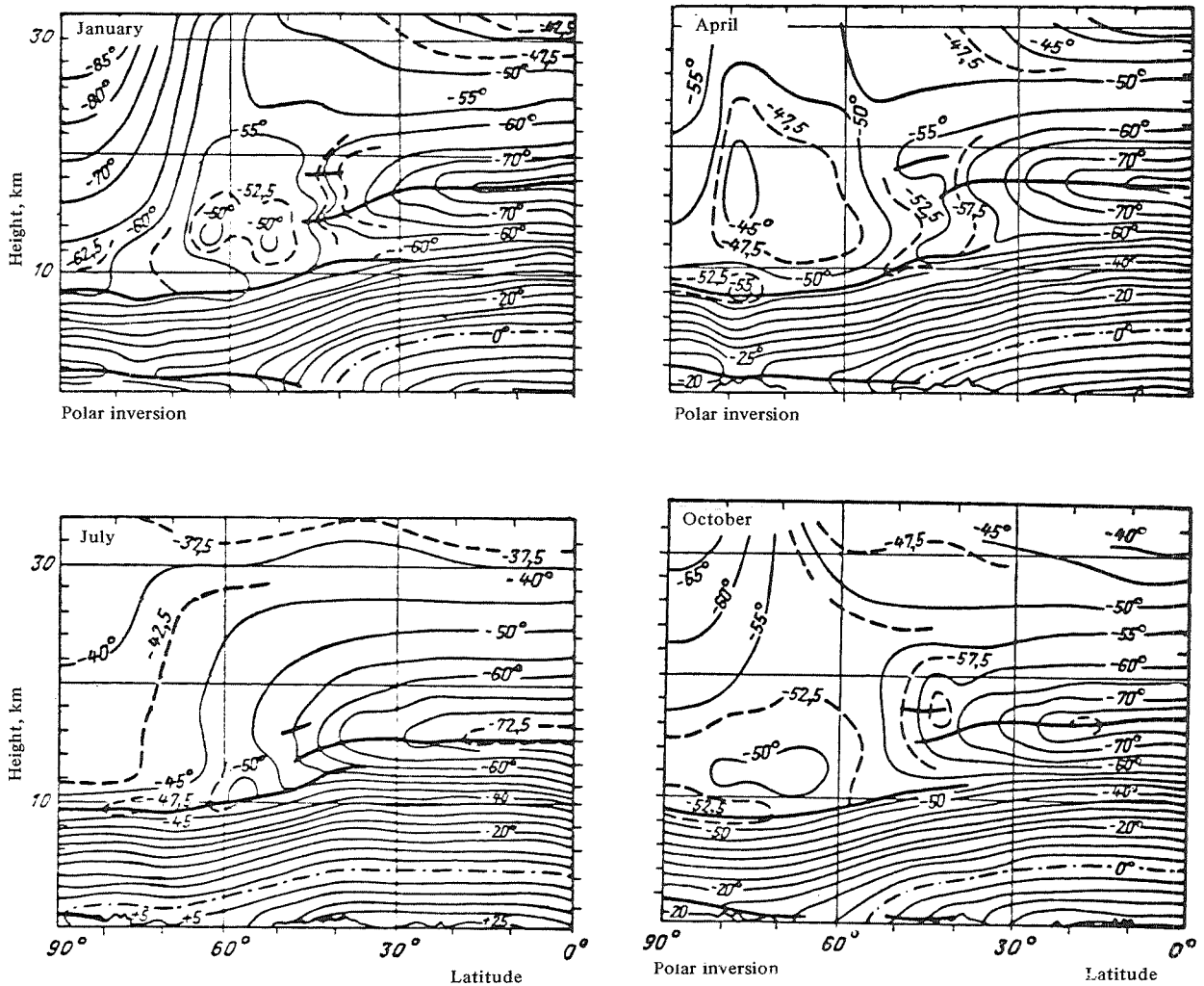

Figure 1.1. Annual Variation of Mean Atmospheric Isotherms Along the 80° W. Meridian at Heights from 0 to 30 km.

Note: Commas represent decimal points.

Averaged on the global scale, the pressure at sea level is 1013 mbar. This quantity varies between 980 and 1040 mbar [4]. Thus, the deviations from the mean pressure value lie in the approximate range $\pm 3\%$.

The decrease in pressure with height (vertical profile) is described rather well by the exponential law that follows from solution of the barometric equation.

Numerical values of the pressures at various heights in the lower 30-km layer are given in Appendix 1 in accordance with standard models of the atmosphere. This Appendix also gives data on pressure values at heights up to 100 km.

The mean vertical temperature profile indicates the presence of a number of layers in the atmosphere. The lowermost layer, in which the mean temperature decreases with increasing height, is usually known as the troposphere. Its vertical thickness depends on latitude and the time of year. It is 16-18 km in tropical regions and 7-10 km in polar regions. The next layer of the atmosphere, the stratosphere, extends upward to approximately 50 km. This layer is characterized first by a slow rise in temperature (up to about 20 km), and then a rapid rise. The boundary layer between the troposphere and the stratosphere, in which the vertical temperature gradient changes sign, is known as the tropopause.

The temperature reaches its maximum value at the upper boundary of the stratosphere. Then follows the stratopause, in which the vertical temperature gradient again changes sign. The atmospheric layer known as the mesosphere lies above 50 km and extends to 80-90 km. Here the temperature diminishes with altitude and reaches a mean value of approximately 200°K. Next is the mesopause, with another change in the sign of the temperature gradient, and the thermosphere, in which the temperature rises steadily.

Among all of these atmospheric layers, the troposphere has the least stable vertical temperature trend, especially in a layer 2-3 km thick at the bottom. Inversions in the vertical temperature profile are often observed in this layer.

Figure 1.1 [3] shows mean vertical profiles of the temperature field in the bottom 30-km layer of the atmosphere for the 80th meridian of western longitude in the northern hemisphere. The isotherms on the figure are given in °C. The heavy lines indicate the boundaries of the layers in which the temperature inversions are observed and levels with sharp changes in the vertical temperature gradient. /12

Appendix 1 gives the mean vertical temperature profiles used in the standard models of the atmosphere for various heights from 0 to 30 km. It also presents data on the mean temperature for heights from 25 to 100 km.

§2. DISTRIBUTION OF WATER VAPOR IN THE ATMOSPHERE

The following concepts are usually introduced to characterize air humidity: 1) the absolute humidity a, measured in grams per cubic meter; 2) the water vapor pressure e or its partial pressure, expressed in millimeters of mercury or in millibars; 3) the relative humidity r, the ratio of the partial pressure of the water vapor in the air to the saturation vapor pressure E at the given temperature, measured in percent; 4) the specific humidity q, the mass of water vapor per unit mass of moist air; 5) the mixing ratio δ, the mass of water vapor per unit mass of dry air; 6) the precipitated water layer ω characterizes the thickness of the layer of water that would be obtained if all of the water vapor in a given thickness of atmosphere were condensed; 7) the humidity deficit d, the difference between the maximum and actual water vapor partial pressures at a given temperature and pressure; 8) the dew point τ, the temperature of air cooled to saturation of the vapor present in it.

TABLE 1.2. VALUES OF SATURATION VAPOR PRESSURE E ABOVE FLAT SURFACE OF PURE WATER, ABSOLUTE HUMIDITY a, SPECIFIC HUMIDITY q, AND MIXING RATIO δ AT PRESSURE P = 1000 mbar AND VARIOUS TEMPERATURES

t, °C	E, mbar	a, g/m³	q, g/kg	δ, g/kg
—20	1,254	1,073	0,780	0,781
—10	2,863	2,357	1,782	1,786
0	6,108	4,845	3,808	3,822
10	12,270	9,39	7,67	7,73
20	23,37	17,27	14,67	14,89
30	42,43	30,33	26,82	27,56
40	73,78	65,30	47,20	49,54
50	123,40	82,76	80,51	87,56

Note: Commas represent decimal points.

The humidity characteristics are connected with one another by the following relationships [4, 5]:

$$a = 217\frac{e}{T}\,[\text{mb}] = 289.4\frac{e}{T}\;\;[\text{mmHg}]; \tag{1.1}$$

$$q = \frac{\delta}{1+\delta} = 0.622\,\frac{e}{P-0.378e};$$

$$\delta = \frac{q}{1-q} = 0.622\,\frac{e}{P-e}; \tag{1.2}$$

$$r = \frac{e}{E} \cdot 100\%; \quad d = E - e;$$
$$e = E_0 \cdot 10^{b\tau/c+\tau}, \qquad (1.3)$$

where T is the absolute temperature, P is the air pressure measured in the same units as e, E_0 = 4.58 mm Hg = 6.11 mbar, τ is measured in °C, and b and c are equal to 7.5 and 237.3 for water and 9.5 and 265.5 for ice.

Since $e \ll P$, $q \ll 1$, and $\delta \ll 1$ in the atmosphere, we obtain from (1.2)

$$q \cong \delta \cong 622 \frac{e}{P}.$$

The precipitated water layer ω' per kilometer is simply related to the absolute humidity expressed in grams per cubic meter as follows:

$$\omega' = 10e. \qquad (1.4)$$

The precipitated water layer concept is widely used in study of absorption of radiation by water vapor.

Table 1.2 presents values of E, a, q, and δ for P = 1000 mbar (ground layer of atmosphere) and various temperatures.

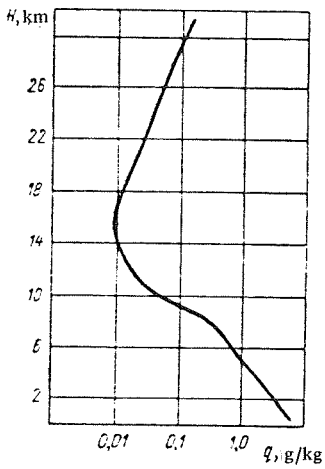

Figure 1.2. Mean Vertical Profile of Specific Humidity According to Gutnik [6].

The water-vapor concentration is extremely variable in time and space. It can be stated that any given measurement of the vertical humidity profile is nonrepeatable. Nevertheless, the pattern of the mean statistical horizontal and vertical profiles has now been studied rather thoroughly in the troposphere. /14

The mean altitude distribution of water-vapor concentration in the troposphere is described by the simple exponential relation [5]

$$e(z) = e(0)\, e^{-\alpha z}, \qquad (1.5)$$

where e(z) and e(0) are the water vapor partial pressures at height z and at the surface of the earth, respectively; α is

an empirical constant.

The water vapor concentration in the ground layer of the atmosphere may vary with time and space in the range from zero to 7%.

Great difficulty is encountered in measuring humidity in the stratosphere. As a result, more or less significant results have been acquired only in recent years. A summary of these results is given by Gutnik [6], who plotted a mean vertical specific humidity profile (Fig. 1.2), in the surveys of S.M. Malkevich, Yu.B. Samsonov, and L.I. Koprova [7] and Houghton [8], and in V.S. Komarov's paper [13].

TABLE 1.3. VALUES OF SPECIFIC HUMIDITY q_0 AND q_1 AND PARAMETERS α_0 AND α_1 IN FORMULAS (1.6) ACCORDING TO [7]

q_0, g/kg	α_0, km^{-1}	q_1, g/kg	α_1, km^{-1}	z_1, km
12,2	0,52	0,012	0,08	12
11,5	0,49	0,006	0,23	14
1,6	0,43	0,05	0	8
5,1	0,42	0,01	0,27	15
17,5	0,56	0,04	0	10
3,6	0,51	0,002	0,18	14
5,7	0,48	0,002	0,24	16
2,6	0,55	0,002	0,31	16

Note: Commas represent decimal points.

An analysis of the available data led the authors of [7] to the conclusion that there are two types of vertical water-vapor distribution in the stratosphere. The first type is characterized by a sharp drop in water-vapor concentration to very small specific-humidity values of the order of 10^{-3}-10^{-2} g/kg in the lower layers of the stratosphere (below 16 km). Concentration increases above this layer, reaching a value 1-2 orders higher at the maximum (for which data are available) altitude of 31 km than at the 16-km level. The second type of water-vapor altitude distribution is typified by constancy of specific humidity beginning at a certain height in the stratosphere. In either case, the dependence of specific humidity on height can be written

/15

$$q(z) = \begin{cases} q_0 e^{-\alpha_0 z}, & 0 \leqslant z \leqslant z_1, \\ q_1 e^{\alpha_1 (z - z_1)}, & z_1 \leqslant z \leqslant z_{\max}. \end{cases} \qquad (1.6)$$

We see from (1.6) that the parameter α_1 must be set equal to zero in describing the second type of humidity altitude distribution.

Table 1.3 presents values of the parameters that appear in (1.6), as obtained from analysis of measured results from various authors.

These two types of stratospheric specific-humidity distribution have come to be known in the foreign literature [10] as the "moist" and "dry" stratosphere models. Both assume the same distribution of water vapor with height up to the level of the tropopause. Thus, the difference between them is immaterial in calculations of infrared absorption in atmospheric thicknesses that include its lower layers. They may be significant in calculations of radiation absorption in the upper atmosphere.

The dispute between the partisans of the dry and moist stratosphere models continues to this day, since reports of measurements that favor one hypothesis in some cases and the other in others continue to appear. /16

In our opinion, this dispute cannot be resolved solely on the basis of analysis of isolated measurements. Statistical reduction of systematic measurements of the vertical water vapor concentration distribution is necessary. This approach has been implemented in [9, 11-13], the fundamental results of which will be set forth below.

1. Mean vertical specific humidity profile. Winter and summer mean vertical specific humidity profiles for middle latitudes are obtained from data on the mean values of temperature and relative humidity on the principal isobaric surfaces, as obtained by 95 aerological stations in the Soviet Union using the A-22 radiosonde. The mean values of these meteorological elements were computed from 280-370 time-separated pairs of observations in the 400-100-mbar layer and from 20-100 observations at the 50, 30, 20, and 10-mbar levels. Data obtained during the IQSY were used in the latter case. Corrections related to the systematic error of the measurements owing to the response lag of the radiosonde transducer were introduced into the mean specific-humidity values.

Figure 1.3 presents mean vertical specific humidity profiles for January and July and also shows Gutnik's profile. As we see from the figure, there is a very sharp decrease of specific humidity with altitude in the upper troposphere in all cases. The trend of the profiles in Fig. 1.3 is qualitatively similar to that of the Gutnik profile. However, the absolute specific-humidity values differ quite sharply at different heights. The mean January and mean July specific-humidity profiles for middle latitudes of the USSR lie to the right of the Gutkin profile. On the other hand, the profiles of specific regions may lie either

TABLE 1.4. MEAN SPECIFIC HUMIDITIES IN JANUARY AND JULY FOR THE RIGA, TASHKENT, AND IRKUTSK STATIONS ACCORDING TO [9], IN g/kg

Isobaric surface, mbar	Riga Sta.		Tashkent Sta.		Irkutsk Sta.	
	January	July	January	July	January	July
Surface	2,30	8,70	2,78	7,80	1,62	9,40
900	2,00	6,50	2,30	5,50	1,10	8,40
850	1,75	5,50	2,10	4,70	0,90	6,90
700	0,88	3,20	1,42	3,60	0,60	4,50
600	0,53	2,00	0,86	2,50	0,35	3,00
500	0,33	1,15	0,53	1,60	0,25	1,90
400	0,10	0,28	0,16	0,60	0,07	0,68
300	0,03	0,11	0,04	0,17	0,031	0,20
200	0,020	0,07	0,03	0,06	0,024	0,048
150	0,029	0,08	0,04	0,024	0,041	0,061
100	0,036	0,09	0,05	0,011	0,068	0,088
50	0,048	0,16	0,06	0,037	0,130	0,14
30	0,053	0,31	0,12	0,12	0,245	0,30
20	0,070	0,59	0,20	0,25	0,36	0,49
10	0,180	1,50	0,65	1,20	0,85	1,50

Note: Commas represent decimal points.

to the right or to the left of the Gutnik profile.

Table 1.4 presents monthly average values of specific humidity at the surface of the earth and on various isobaric surfaces for January and July in the Baltic region, central Asia, and eastern Siberia, as determined from single observations at the Riga, Tashkent, and Irkutsk stations.

Statistical reduction was applied to data from radio soundings of the atmosphere made four times daily at these stations for the surface of the earth and the isobaric surfaces from 900 to 100 mbar in January and July of each year from 1961 through 1966. Data obtained during the IQSY (1964-1965) were used for the levels from 50 to 10 mbar. There were from 560 to 740 observations at levels from the ground surface to 100 mbar at each station in January and July, and 30 to 150 observations in January and 50-180 in July at levels from 50 to 10 mbar. /17

The lowest mean specific humidity values are printed in boldface in each column of Table 1.4. We note that Table 1.4 was not corrected for the systematic measurement error due to radiosonde lag.

Table 1.5 presents mean vertical specific-humidity gradients as calculated from the data of Table 1.4. /19

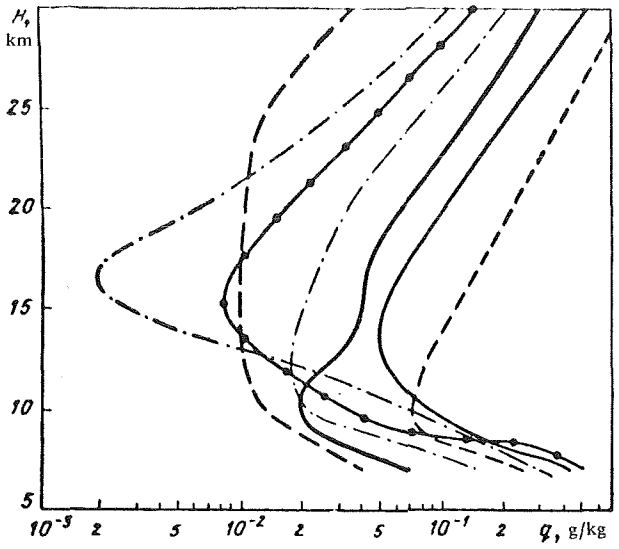

Figure 1.3. Mean Vertical Profile of Specific Humidity for the Middle Latitudes of the USSR (-----) and for the Barentsburg (-•-•-) and Ashkhabad (- -) Stations; -●- is Gutnik's Profile. The heavy lines are the January profiles and the light lines the July profiles.

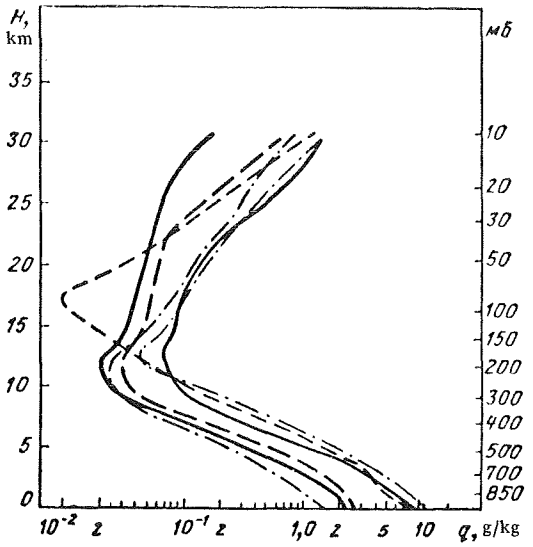

Figure 1.4. Monthly Average Vertical Specific Humidity Profiles for the Riga (-), Tashkent (- - -), and Irkutsk (-•-) Stations According to V.S. Komarov [9]. The heavy lines are the January profiles and the light lines the July profiles.

Figure 1.4 shows vertical profiles of the mean specific humidity for the three stations considered. The specific features of the behavior of the individual profiles are clearly evident from Table 1.4 and Fig. 1.4.

The fastest decrease in specific humidity with height occurs, as is seen from Table 1.4, below the 600-mbar level in the lower troposphere (height interval 0-4 km).

For all three stations, the lowest monthly average specific humidity value is observed near the tropopause, about 0.5-1 km above the minimum-temperature level.

Analysis of the individual observations for each of the stations indicates the presence of wide scatter of the vertical specific-humidity profiles. They can all be grouped into three classes. The first type includes profiles with a substantial increase in specific humidity with height above the tropopause level together with a rather substantial moisture content in the middle stratosphere (of the order of 0.1-0.5 g/kg). The second type is characterized by a constant specific humidity at various heights in the stratosphere and a low moisture content throughout the /20

TABLE 1.5. MEAN VERTICAL SPECIFIC HUMIDITY GRADIENTS FOR THE RIGA, TASHKENT, AND IRKUTSK STATIONS, IN g/kg/100 m

Layer, mbar	Riga Sta.		Tashkent Sta.		Irkutsk Sta.	
	January	July	January	July	January	July
0—900	0,03	0,22	0,05	0,23	0,05	0,10
900—850	0,05	0,20	0,04	0,16	0,04	0,30
850—700	0,07	0,15	0,05	0,07	0,02	0,25
700—600	0,04	0,12	0,06	0,11	0,03	0,15
600—500	0,02	0,09	0,03	0,09	0,01	0,11
500—400	0,02	0,04	0,02	0,05	0,01	0,06
400—300	0,004	0,009	0,006	0,021	0,002	0,024
300—200	0,0003	0,0013	0,0003	0,0036	0,0002	0,005
200—150	—0,0005	—0,0005	0,0005	0,0018	—0,0008	—0,0006
150—100	—0,0002	—0,0003	—0,0003	0,0004	—0,0009	—0,0009
100—50	—0,0003	—0,0018	—0,0002	—0,0006	—0,0013	—0,0010
50—30	—0,0002	—0,0050	—0,0020	—0,0028	—0,0038	—0,0053
30—20	—0,0008	—0,0140	—0,0040	—0,0065	—0,0058	—0,0095
20—10	—0,0027	—0,0180	—0,0110	—0,0190	—0,0120	—0,0202

Note: Commas represent decimal points.

stratospheric layer (of the order of 0.01-0.02 g/kg). Finally, profiles with a slow decrease in specific humidity with height in the stratosphere and a low middle-stratosphere moisture content (of the order of 0.01-0.02 g/kg) belong to the third type. Figure 1.5 presents examples of these three types of profiles.

Thus, the stratosphere may be both "moist" and "dry" in each specific observation. However, the mean statistical vertical profile of specific humidity indicates a rather substantial increase in this quantity with height in the stratosphere for all stations both in January and in July. To explain this fact, it will be necessary to answer the question: where does the large amount of moisture in the upper layers of the stratosphere originate? /21

2. Transport of water vapor from the troposphere into the stratosphere. One of the answers to the problem posed here may be found in V.S. Komarov's investigation [13] of vertical transport of water vapor from the troposphere to the stratosphere. This study was made on the basis of statistical analysis of data from radiosonde observations at 12 stations in the Soviet Union, which covered the entire area of the country more or less uniformly. Only radiosonde ascents in which humidity and wind speed and direction data were obtained for all isobaric surfaces were considered. Appropriate data for 9 standard levels were used in the analysis: 400, 300, 200, 150, 100, 50, 30, 20, and 10 mbar during the IQSY (1964-1965). The result of the study was acquisition of data on the repeatability of the directions of vertical

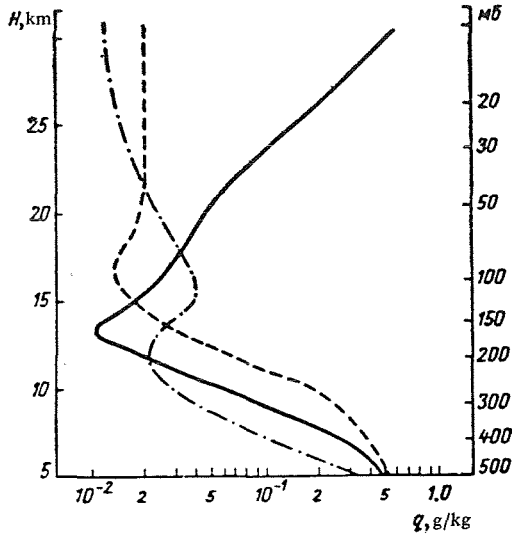

Figure 1.5. Examples of Different Types of Vertical Specific Humidity Profiles Obtained at Irkutsk on 28 July 1964 (-), at Tashkent on 7 July 1963 (- - -), and at Riga on 5 January 1966 (-•-).

motions characterizing the frequency with which the tropopause is pierced by ascending currents of air.

Analysis of the results indicates that the repeatability of vertical air motions in the tropopause region was 52-67% in January for 9 stations out of 12 and 52-64% in July for 10 out of 12. Descending air movements with repeatabilities from 52 to 60% predominate in the tropopause region for three stations in winter and two stations in summer.

Table 1.6 presents the average repeatabilities of upward and downward vertical air motions for the middle latitudes of the USSR in January and July for various layers of the atmosphere on clear and cloudy days. The table was compiled for $n \geq 30$ cases.

As we see from Table 1.6, the repeatability of the ascending and descending currents depends quite perceptibly on the cloudiness of the atmosphere. In cloudy weather, the repeatability of ascending air movements predominates both in winter and in summer throughout the troposphere and to the 100-mbar level in the stratosphere. For cloudy summer weather, the ascending air currents predominate over the descending currents both in the troposphere and in the stratosphere all the way up to the maximum radio-sounding altitude. These currents moisten the stratosphere. Thus, the stratosphere should be drier on clear days and more humid on cloudy days. This conclusion is consistent with the mean vertical specific humidity profiles of the stratosphere as obtained on clear and cloudy days. /23

3. **Variability of humidity field at various heights in the atmosphere.** In both the troposphere and the stratosphere, the humidity field varies strongly as a function of time and the physicogeographic region. Therefore, together with knowledge of the statistically averaged vertical humidity profiles, it is important to have data on the corresponding confidence intervals. The necessary calculations were performed for four stations situated in different climatic regions of the USSR. They were based on long-term radiosonde data for levels below 100 mbar and IQSY data for levels from 50 to 10 mbar.

TABLE 1.6. AVERAGE REPEATABILITIES OF ASCENDING AND DESCENDING VERTICAL AIR MOTIONS IN VARIOUS LAYERS OF THE ATMOSPHERE FOR THE MIDDLE LATITUDES OF THE USSR [13]

Layer, mbar	January						July							
	Clear		Ci, Cs, Ce clouds		Average		Clear		Ci, Cs, Ce clouds		Cb clouds		Average	
	asc.	desc.	asc.	desc.	asc.	desc.	asc.	desc.	asc.	desc.	asc.	desc.	asc.	desc.
400—300	49	51	63	37	56	44	51	49	57	43	56	44	55	45
300—200	51	49	58	42	56	44	44	56	52	48	54	46	52	48
200—150	43	57	58	42	58	48	48	52	52	48	53	47	52	48
150—100	40	60	51	49	51	49	46	54	62	38	56	44	53	47
100—50	32	68	50	50	40	60	57	43	60	40	56	44	55	45
50—30	31	69	37	63	40	60	60	40	60	40	50	50	54	46
30—20	32	68	—	—	44	56	51	49	58	42	42	58	55	45

Figures 1.6-1.13 present monthly average vertical specific humidity profiles for January and July and their confidence intervals. The latter characterize the number of cases in which profiles that fit within the given intervals were obtained.

Specific humidity can change within very short time intervals. These changes are governed by fluctuations in water-vapor content, which may cause corresponding fluctuations of a light ray propagating through the atmosphere [14]. At the present time, the problem of humidity fluctuations is only in the initial stage of investigation.

4. Total water vapor contents in various layers of the atmosphere. The total content of water vapor in both vertical and horizontal layers of the atmosphere is easy to obtain from data on the vertical specific-humidity profiles (Tables 1.7 and 1.8).

Knowledge of the precipitated-water layer between two points in the atmosphere is very important for solution of problems involving calculation of the absorption of visible and infrared radiation in the atmosphere. In this context, we take note of the method proposed in [15] for finding this quantity between any two points in the atmosphere with consideration of the earth's curvature and refraction when the vertical distribution of gas

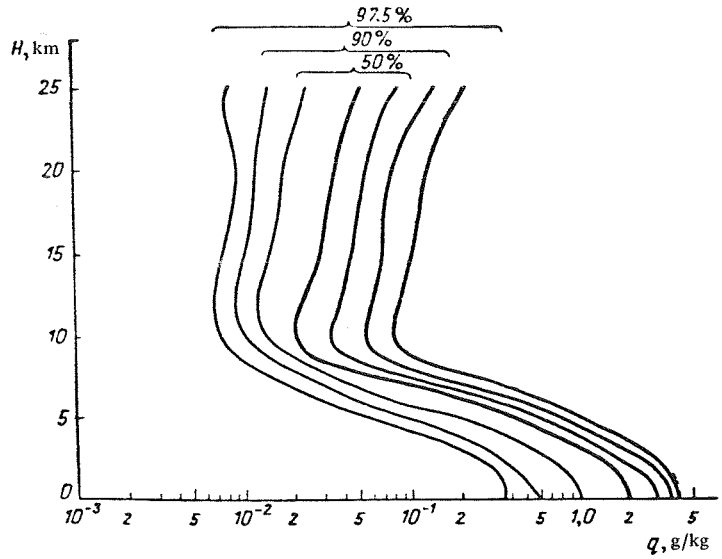

Figure 1.6. Mean Vertical Specific Humidity Profile in January for Boyeykovo Station and Confidence Intervals of its Variation (50, 90, and 97.5%).

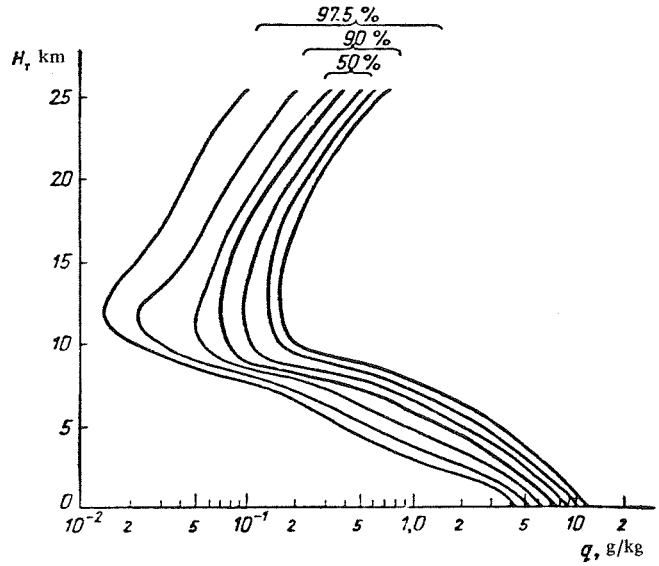

Figure 1.7. Mean Vertical Specific Humidity Profile in July for Boyeykovo Station and Confidence Intervals of its Variation (50, 90, and 97.5%).

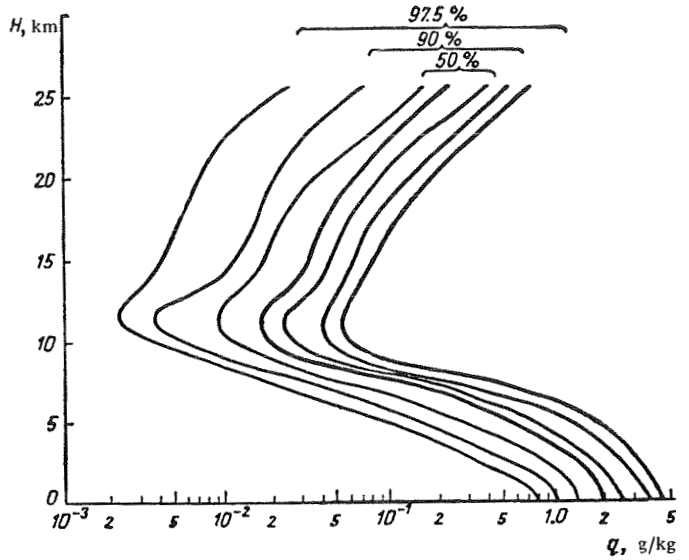

Figure 1.8. Mean Vertical Specific Humidity Profile in January for Alma-Ata Station and Confidence Intervals of its Variation (50, 90, and 97.5%).

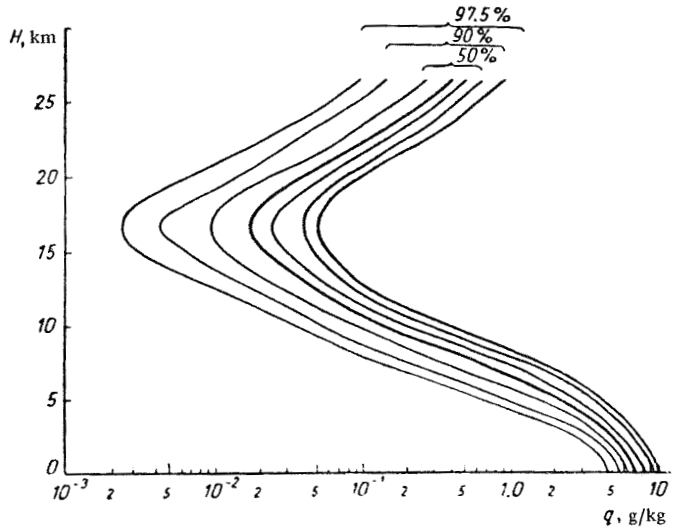

Figure 1.9. Mean Vertical Specific Humidity Profile in July for Alma-Ata Station and Confidence Intervals of its Variation (50, 90, and 97.5%).

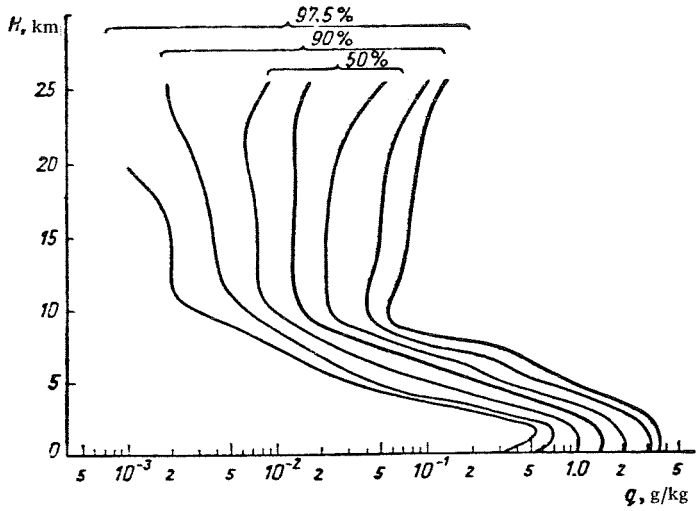

Figure 1.10. Mean Vertical Specific Humidity Profile in January for Murmansk Station and Confidence Intervals of its Variation (50, 90, and 97.5%).

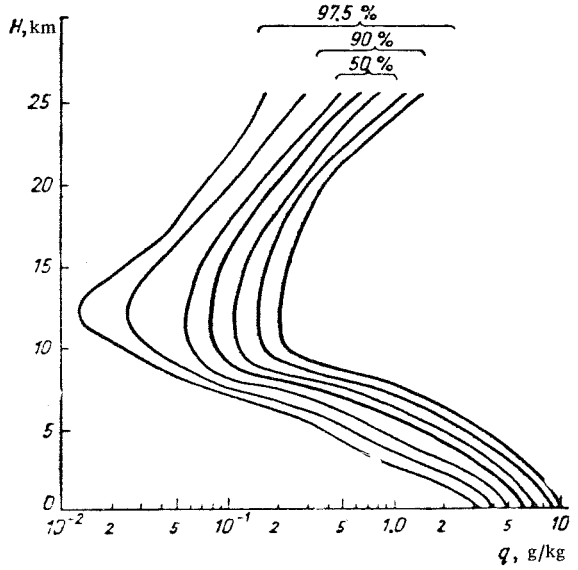

Figure 1.11. Mean Vertical Specific Humidity Profile in July for Murmansk Station and Confidence Intervals of its Variation (50, 90, and 97.5%).

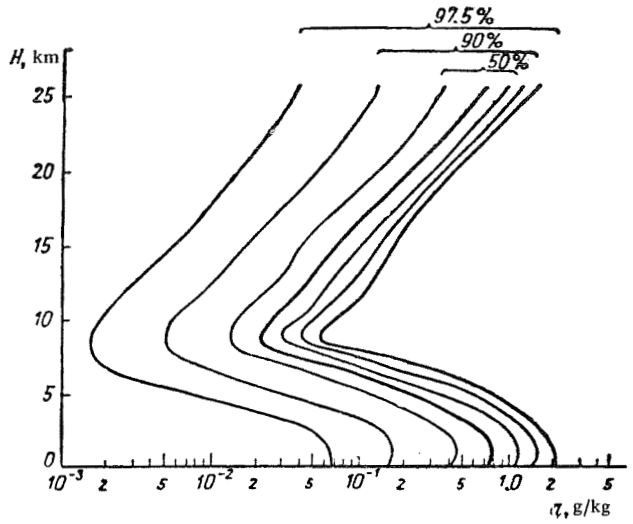

Figure 1.12. Mean Vertical Specific Humidity Profile in January for Nagayevo Station and Confidence Intervals of its Variation (50, 90, and 97.5%).

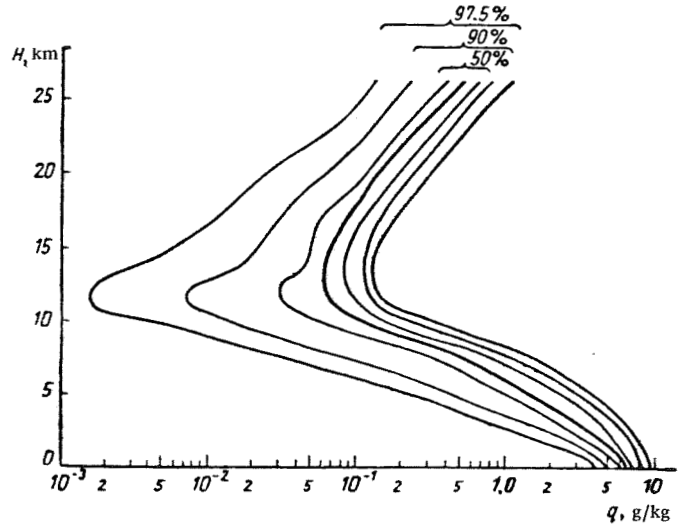

Figure 1.13. Mean Vertical Specific Humidity Profile in July for Nagayevo Station and Confidence Intervals of its Variation (50, 90, and 97.5%).

TABLE 1.7. MONTHLY AVERAGE VALUES OF PRECIPITATED WATER IN $cm \cdot km^{-1}$ IN LAYERS AT VARIOUS HEIGHTS FOR THREE STATIONS IN JANUARY AND JULY [13]

Layer, mbar	Riga Sta.		Tashkent Sta.		Irkutsk Sta.	
	January	July	January	July	January	July
Ground — 850	0,2070	0,7240	0,2490	0,6380	0,1290	0,8340
850—700	0,1340	0,4440	0,1790	0,4230	0,0770	0,5800
700—500	0,0620	0,2230	0,1000	0,1300	0,0430	0,3270
500—400	0,0110	0,0370	0,0180	0,0560	0,0560	0,0660
400—300	0,0030	0,0102	0,0051	0,0200	0,0024	0,0250
300—200	0,0013	0,0046	0,0018	0,0060	0,0017	0,0063
200—150	0,0007	0,0020	0,0009	0,0010	0,0010	0,0014
150—100	0,0006	0,0014	0,0008	0,0003	0,0013	0,0013
100—50	0,0001	0,0012	0,0001	0,0003	0,0019	0,0013
50—30	0,0004	0,0016	0,0006	0,0005	0,0017	0,0015
30—20	0,0001	0,0015	0,0005	0,0006	0,0011	0,0014
20—10	0,0003	0,0027	0,0011	0,0010	0,0016	0,0026

Note: Commas represent decimal points.

TABLE 1.8. MONTHLY AVERAGE VALUES OF PRECIPITATED WATER IN VARIOUS LAYERS OF THE ATMOSPHERE IN THE VERTICAL DIRECTION [13] FOR THREE STATIONS

Layer, mbar	Riga Sta.				Tashkent Sta.				Irkutsk Sta.			
	January		July		January		July		January		July	
	cm	%	cm	%	cm	%	cm	%	cm	%	cm	%
Ground-10*	0,673		2,334		0,903		2,026		0,442		3,022	
Ground-200*	0,666	99,0	2,300	98,5	0,893	98,8	2,014	99,5	0,414	93,5	2,962	98,0
Ground-500*	0,635	94,0	2,197	94,0	0,842	94,3	1,851	91,4	0,394	89,3	2,772	91,8
200 — 10	0,008	1,0	0,034	0,034	0,010	1,2	0,012	0,5	0,028	6,5	0,061	2,0

*These values were computed with respect to the precipitated water in the layer from the ground to 10 mbar.

Note: Commas represent decimal points.

concentration is regarded as known. The mass of absorbing gas is determined in [15] by the formula

$$\omega = \omega_{z_1} f(z_1) - \omega_{z_2} f(z_2), \qquad (1.7)$$

where ω_{z_1} and ω_{z_2} are the masses of absorbing gas in the vertical columns of atmosphere from heights z_1 and z_2 to ∞. An approximate expression proposed by G.V. Rozenberg [16] is used as the function f(z): /28

$$f(z) = (\cos z + ke^{-m\cos z})^{-1}, \qquad (1.8)$$

where m and k are constant coefficients.

5. Comparison of available data on the specific humidity in the stratosphere. Analysis of existing data on stratospheric specific humidity indicates that the quantitative values of this quantity obtained by various authors are widely scattered. Thus, both the yearly average profile of Gutnik [6] and the monthly average profiles constructed by V.S. Komarov [12] differ quite substantially from the profiles obtained by many other investigators in isolated measurements, including some made in recent years. Thus, Houghton's survey [8] analyzed many concrete measurements of humidity in the stratosphere, on the basis of which the author concluded that the mixing ratio is constant in the range $1\text{-}4 \cdot 10^{-3}$ g/kg, in- /30 dicating a dry stratosphere. In Gutnik's model, the lowest specific humidity at tropopause level is $9 \cdot 10^{-3}$ g/kg; in the January and July average profiles of V.S. Komarov, it is still larger. Above tropopause level, the specific humidity increases quite rapidly with height according to both Gutnik and V.S. Komarov. We note that a recent measurement of humidity in the mesosphere at heights of 70-80 km indicates a considerable content of moisture at these heights [17]. The authors of [17] obtained a value of 1.7 g/kg for the specific humidity. The moist-stratosphere model is also favored by the existence of nacreous and noctilucent clouds.

Nevertheless, it is not possible at this time to give a definite answer to the question as to why data obtained by different authors on the specific humidity differ so significantly. It appears to us that to answer this question, it will first be necessary to make highly reliable determinations of the measurement errors incurred with the various instruments and procedures. First of all, it will be necessary to solve the problem of the errors in humidity determinations made by the most widely used radiosonde method. This is because this is still the only method that yields data in quantities sufficient for statistically sound analysis.

3. DISTRIBUTION OF OZONE IN THE ATMOSPHERE

Because of the considerable influence of ozone on radiative processes in the atmosphere, it has been investigated in numerous papers, reviews and bibliographies of which can be found in the monographs and collections [18-21, 557, 560, 562, 865].

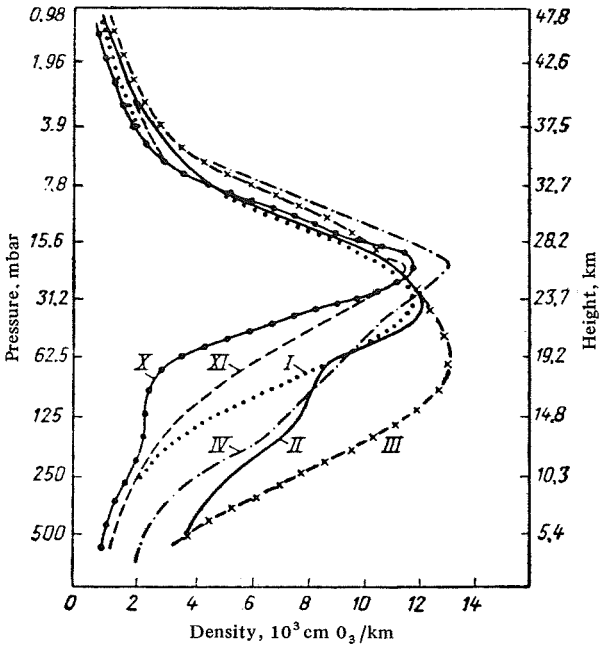

Figure 1.14. Monthly Average Vertical Ozone Profiles Obtained by Dütsch [22] for Arosa Station in 1956-57. The Roman numerals indicate the months.

An idea of the vertical ozone-concentration profile can be obtained from Fig. 1.14, from which it is evident that the monthly average ozone concentration may vary through a factor of about 6 at the heights of the maxima. Above and below the maximum, the range of variation of the monthly average concentrations is narrower the farther the height in question from the maximum of the layer. This relationship obtains for various geographical regions, although the absolute concentration values undergo marked variations with both time of day and time of year, /32 and also as functions of latitude and longitude.

The fluctuations of the monthly average total atmospheric ozone content can be judged from Table 1.9.

Table 1.9 shows that the monthly average values of the total ozone content vary in the range of 0.172-0.536 cm, i.e., through a factor of 3, from place to place and from month to month. The annual average values of the total O_3 content fluctuate on a small scale (from 0.394 cm to 0.204 cm, or through a factor of about 2).

Despite the very many measurements of atmospheric ozone concentration that have been made, no mean statistical vertical O_3 profile has as yet been constructed. Various sources cite averaged data from specific series of measurements (see, for example, Table 1.10).

In accurate calculations of visible and infrared absorption /33 in the atmosphere, it is necessary to take account not only of the variations of total ozone content, but also its height

TABLE 1.9. MONTHLY AVERAGE VALUES OF TOTAL OZONE CONTENT (IN cm) ACCORDING TO CERTAIN IGY STATIONS FOR 1958 [21]

No.	Station	Coordinates		I	II	III	IV	V	VI	VII	VIII	IX	X	XI	XII	Over year
		Latitude	Longitude													
1	Alert	82°30′ N	62°20′ E	0,259	0,480	0,536	0,470	0,429	0,355	0,331	0,292	0,299	0,320	0,366	0,370	0,376
2	Resolute	74°43′	94°59′W	0,376	0,502	0,499	0,491	0,419	0,373	0,344	0,306	0,323	0,339	0,427	0,321	0,394
3	Lerwick	60°08′	01°11′W	0,335	0,397	0,408	0,385	0,415	0,358	0,346	0,321	0,289	0,290	0,258	0,266	0,339
4	Oxford	51°46′	01°16′W	0,342	0,353	0,396	0,392	0,398	0,381	0,360	0,337	0,300	0,292	0,284	0,317	0,346
5	Arosa	46°47′	09°41′ E	0,347	0,340	0,394	0,401	0,358	0,352	0,338	0,314	0,292	0,292	0,288	0,308	0,335
6	El'brus	43°17′	42°25′ E	0,299	0,320	0,362	0,402	0,345	0,304	0,256	0,228	0,222	0,250	0,241	0,274	0,295
7	Washington	38°51′	77°02′W	0,330	0,373	0,359	0,367	0,364	0,333	0,313	0,315	0,289	0,295	0,285	0,315	0,328
8	Terishima	30°29′	140°18′ E	0,279	0,292	0,337	0,339	0,329	0,329	0,321	0,300	0,285	0,269	0,246	0,256	0,298
9	Tamanrasset	22°48′	05°31′ E	0,172	0,196	0,227	0,258	0,214	0,185	0,173	0,212	0,212	0,213	0,199	0,192	0,204
10	Mauna Loa	19°29′	155°36′ W	0,256	0,251	0,270	0,290	0,289	0,284	0,271	0,271	0,268	0,264	0,257	0,253	0,269
11	Kodaikanal	10°14′	77°28′W	0,227	0,224	0,233	0,247	0,240	0,249	0,246	0,244	0,241	0,239	0,237	0,217	0,237
12	Leopoldville	4°30′ S	15°00′W	0,257	0,253	0,252	0,245	0,239	0,244	0,245	0,249	0,254	0,245	0,251	0,244	0,248
13	Brisbane	27°28′	153°02′W	0,285	0,276	0,282	0,289	0,292	0,303	0,314	0,318	0,348	0,329	0,320	0,337	0,308
14	Wellington	41°17′	174°46′W	0,294	0,271	0,261	0,269	0,281	0,319	0,340	0,339	0,370	0,364	0,331	0,289	0,311
15	Argentinian Island	65°15′	64°16′W	0,295	0,259	0,234	0,251	0,289	0,301	0,278	0,298	0,324	0,300	0,350	0,309	0,291
16	Little America	78°12′	162°15′W	0,314	0,310	0,334	0,266	0,380	0,480	0,368	0,536	0,334	0,373	0,420	0,316	0,360

Note: Commas represent decimal points.

TABLE 1.10. OZONE CONCENTRATION C IN VARIOUS LAYERS OF THE ATMOSPHERE ACCORDING TO [23], $C = C_i \cdot 10^{-3}$

H, km	0—5	5—10	10—13	13—16	16—18	18—20	20—21	21—23
C_1, cm/km	1.9	4.1	5.8	7.6	11.1	15.6	16.8	17.5
C_2, cm/km	1.6	2.8	3.9	6.1	10,3	14.1	14.3	15,2

H, km	23—24	26—28	28—40.5	40.5—45.5	45.5—50.5	50.5—55.5
C_1, cm/km	10.8	6.5	1.6	0.3	0.1	0.1
C_2, cm/km	11.3	5.4	1.4	0,3	0.09	0.04

distribution. This is especially necessary in cases in which the calculation is being performed for spectral intervals in which the absorption of radiation is governed chiefly by O_3. Here it is most important to note the 9.0-10.3-μ range of wavelengths, which is occupied by the strongest ozone absorption band — a band which is, moreover, situated at the center of the long-wave atmospheric transparency window.

4. DISTRIBUTION OF CO_2, O_2, CH_4, N_2O, AND CO IN THE ATMOSPHERE

All of these gases have in common an approximately constant specific concentration at all heights, at least for the lower 30-

km layer of the atmosphere. The absolute oxygen concentration is practically independent of both time and locality up to approximately 90 km of altitude.

Many studies have been devoted to the CO_2 concentration. Measurements have now been made over all of the most characteristic areas of the globe: oceans, continents, in the Arctic and Antarctic, in rural localities and industrial cities, in the mountains and in the open atmosphere. A rather complete summary of the available data listing the measurement stations and the average minimum and maximum values obtained for the CO_2 concentration in the atmosphere will be found in [24-38]; it permits analysis of the problem and certain inferences. This analysis indicates that of the average CO_2 concentrations measured, in parts per million by volume of air, at 64 stations around the world, 60 lie in the range from 280 to 340. The values in the other four cases were as follows: 253 (England, at an altitude of 4-10 km), 256 (near Cape Horn, 56° S.), 354 (Pacific Ocean), and 650 (London). Interestingly, the average concentration near London is approximately 300. /34

The maximum deviation of the absolute concentration from its average value reached 46% in only one case (London: maximum concentration 900, minimum 425). It should also be noted that the London CO_2 concentrations were measured as far back as 1936 [24] and may require adjustment. As reported in [41], minimum and maximum CO_2 concentration values of 0.015 and 0.078% by volume, respectively, were obtained in [39, 40]. Using these data, we arrive at 0.015 and 0.09% by volume for the absolute minimum and maximum of atmospheric CO_2 concentration.

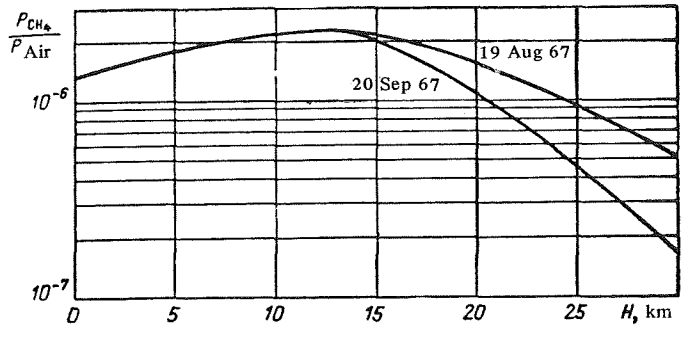

Figure 1.15. Vertical Profile of Ratio of Methane Pressure to Air Pressure According to Two Measurements Using an Automatic Balloon Spectrometer [866].

It follows from this analysis of available data on the atmospheric CO_2 concentration that the difference between the absolute minimum and maximum of concentration reaches large values. However, in calculating the absorption of infrared radiation by carbon dioxide in the earth's atmosphere, its concentration may be assumed constant at 0.03% by volume, since large deviations from this value are very seldom observed.

Data on the concentration of minor atmospheric impurities such as methane (CH_4), nitrous oxide (N_2O), and carbon monoxide (CO) have been acquired in a very limited number of studies. Seeley and Houghton [42] found values of $1.05 \cdot 10^{-6}$, $0.12 \cdot 10^{-6}$, and $0.12 \cdot 10^{-6}$ g/g for the mixing ratios of CH_4, CO, and N_2O, respectively. At these mixing-ratio values, the total contents of these gases in the entire vertical thickness of the atmosphere are 0.84, 0.10, and 0.10 atm·cm.

As is noted in [42], these data agree closely with the measured results of Migeotte's group [43]. Bouman and Shaw [44] obtained two concentrations of these gases in volumetric parts per million in the ground layer of air: 1.7 ± 0.03 (CH_4); 1.3 (CO); 0.28 ± 0.04 (N_2O). Here it is noted that the CO content varies widely. The same conclusion is drawn in Shaw's paper [45], in which the CO content of the entire atmospheric thickness was found to vary in the range from 0.04 to 0.13 atm·cm. The CH_4 content for the entire thickness of the atmosphere was determined most accurately in [46]. It was found to be 1.11 ± 16 atm·cm. /35

K.P. Vasilevskiy, V.A. Kazbanov, and V.A. Boldyrev [866] used an automatic high-resolution balloon spectrometer to investigate the transmission spectra of the atmosphere in two narrow bands around wavelengths of 3.31 and 3.39 μ at heights from 0 to 30 km. Reduction of the measured results yielded data on the vertical methane-content profiles of the atmosphere (Fig. 1.15).

The mixing ratios given for N_2O in [47, 48, 49] were $0.27 \cdot 10^{-6}$, $0.27 \cdot 10^{-6}$, and $0.05 \cdot 10^{-6}$ g/g, respectively. The differences are explained by the difficulties of interpreting the spectroscopic data [42].

Thus, the available data indicate that the CH_4, CO, and N_2O concentrations in parts per million range from 1.05 to 1.7, 0.04 to 1.3, and 0.12 to 0.5, respectively. Improvement of these ranges, like determination of the statistical average CH_4, N_2O, and CO concentrations in the atmosphere, requires the corresponding systematic measurements, which have not yet been made anywhere.

Chapter 2 /36

ORIGIN AND GENERAL CHARACTERISTICS OF THE ABSORPTION SPECTRA OF ATMOSPHERIC GASES

1. ENERGY AND SPECTRA OF THE MOLECULES

In first approximation, the energy of an isolated molecule can be presented in the form

$$E = E_{trans} + E_{el} + E_{vib} + E_{ro} \qquad (2.1)$$

where E_{trans} is the energy of translational motion, which depends on velocity and may assume any value, E_{el} is the energy of the electrons, and E_{vib} and E_{ro} are the vibrational and rotational energies. E_{el}, E_{vib}, and E_{ro} can assume only discrete values. Thus, they can vary only stepwise with either absorption or emission of a quantum of light at a definite frequency.

Formula (2.1) is valid only when the interaction of the various types of molecular motion can be disregarded. In the general case, the energy of a molecule is written

$$E = E_{trans} + E_{el} + E_{vib} + E_{ro} + E_{el.vib} + E_{el.ro} + E_{vib.ro}, \qquad (2.2)$$

where the last three terms are required to account for the interactions between the various types of molecular motion.

The electronic, vibrational, and rotational energies of a molecule differ in order of magnitude. Thus, the energy of the electron transitions is of the order of several electron-volts, the vibrational energy is reckoned in the tenths and hundredths of an electron-volt, and the rotational energies are in the thousandths and ten-thousandths of an electron-volt. In accordance with the energies, the electron spectra of the molecules occupy /37
the ultraviolet and visible regions of the spectrum, the vibrational spectra are in the near infrared, and the rotational spectra in the far infrared and microwave bands.

Since the molecule has both electronic and vibrational and rotational energies, and these energies change, generally speaking, simultaneously on emission or absorption, the electronic and

vibrational spectra are not manifested in pure form. Thus, depending on wavelength range, we deal either with an electronic-vibrational-rotational molecular spectrum, or with a vibrational-rotational spectrum, or with a purely rotational spectrum. For brevity, these spectra are often referred to as the electronic, vibrational, and rotational spectra, respectively.

Each electron state has a corresponding grid of vibrational energy levels characterized by a certain value of the vibrational quantum number v (Fig. 2.1). In turn, each vibrational level has a corresponding series of rotational levels, which are characterized by a certain value of the rotational quantum number j.

Referring to Fig. 2.1, it is easy to see why the electronic and vibrational transitions in the molecule cannot be observed in pure form. In fact, we deal in a set of molecules with statistically distributed values of the electronic, vibrational, and rotational energies. In each electron transition of the molecule, its vibrational and rotational energies change simultaneously. The entire aggregate of electron transitions gives rise to the electronic-vibrational-rotational spectrum, whose line strengths are determined by the energy-level distribution of the molecules and by the probabilities of the corresponding transitions.

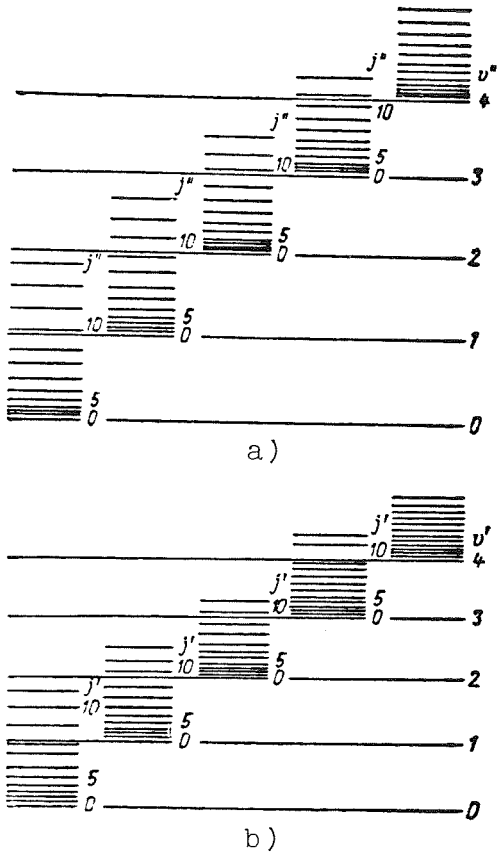

Figure 2.1. Diagram of Vibrational and Rotational Levels of Two Electronic States (a and b) of a Molecule (the single and double primes on the v and j indicate that the corresponding levels belong to the upper and lower electronic states of the molecule).

The electronic-vibrational-rotational spectrum is a set of bands. An electron band consisting of a set of vibrational-rotational bands corresponds to each set of transitions of the molecule between two electron states.

The number of different vibrational transitions accompanying a change in electron energy and the number of different rotational transitions associated with a change in the vibrational energy of the molecule may be very

large. This circumstance is responsible for the extremely complex structure of the molecular spectra. The nature of this structure /38
depends on the selection rules for transitions between energy levels with definite values of the set of quantum numbers. The selection rules will be discussed in greater detail below.

The highest vibrational levels of a lower electron state of the molecule may overlap the lower levels of the next higher elec- /39
tron state. Similarly, the rotational levels of neighboring vibrational states may also overlap (as is seen clearly from Fig. 2.1). This overlapping of the levels results in overlapping of the corresponding electronic and vibrational bands, to the further complication of the pattern of the molecular band spectrum.

In discussing the structure of various types of molecular spectra, it will be helpful to attend separately to the rotational, vibrational, and electronic molecular energies and their interaction.

2. ROTATIONAL ENERGY AND ROTATIONAL SPECTRA OF MOLECULES

In approximation, a rotating molecule can be regarded as a solid body (rigid top). The rotational behavior of molecules and

TABLE 2.1. CLASSIFICATION OF MOLECULES BY ROTATIONAL PROPERTIES

No.	Moments of inertia	Types of molecules	Atmospheric gases representing the corresponding types of molecules
1	$\mathcal{J}_a=0\ \mathcal{J}_b=\mathcal{J}_c\neq\neq 0$	Linear molecules	CO_2, N_2O, NO, CO, O_2, N_2
2	$\mathcal{J}_a\neq 0\ \mathcal{J}_b=\mathcal{J}_c\neq\neq 0$	Molecules of symmetrical-top type	None among atmospheric gases of planetary distribution
3	$\mathcal{J}_a=\mathcal{J}_b=\mathcal{J}_c$	Molecules of spherical-top type	CH_4
4	$\mathcal{J}_a\neq\mathcal{J}_b\neq\mathcal{J}_c$	Molecules of asymmetrical-top type	H_2O, O_3, HDO

their rotational spectra depend on the relation between the three principal moments of inertia $\mathcal{J}_a, \mathcal{J}_b$ and $\mathcal{J}_c$ about the three principal axes of inertia of the molecule. All molecules can be classified into four groups on the basis of their rotational properties (Table 2.1).

1. Linear molecules. The rotational energy of a linear mole- /40
cule equals [51]:

$$E = \frac{\vec{M}_p^2}{2\mathcal{J}}, \tag{2.3}$$

where $\vec{M}_p^2$ is the square of the angular momentum and $\mathcal{J}$ is the moment of inertia about the axis of rotation that passes through the molecule's center of gravity perpendicular to the molecule's axis.

The quantization of $\vec{M}_p^2$ is determined by the formula

$$\vec{M}_p^2 = \hbar^2 j(j+1), \tag{2.4}$$

where $\hbar = (h/2\pi)$, h is Planck's constant, and j is the rotational quantum number, which assumes integral values:

$$j = 0, 1, 2, 3, \ldots \tag{2.5}$$

From (2.4) and (2.3), we obtain an expression for the quantized molecular energy of rotation:

$$E_J = \frac{\hbar^2}{2\mathcal{J}} j(j+1) = Bj(j+1), \tag{2.6}$$

where

$$B = \frac{\hbar^2}{2\mathcal{J}} = \frac{2{,}80 \cdot 10^{-39}}{\mathcal{J}}\,[\mathrm{cm}^{-1}] = \frac{0{,}83 \cdot 10^{-28}}{\mathcal{J}}\,[\mathrm{sec}^{-1}] = \frac{0{,}83 \cdot 10^{-34}}{\mathcal{J}}\,[\mathrm{MHz}] \tag{2.7}$$

is known as the rotational constant.

TABLE 2.2. VALUES OF ROTATIONAL ENERGY E_j FOR VARIOUS VALUES OF THE ROTATIONAL QUANTUM NUMBER j

j	0	1	2	3	4	5	6	7	8	9	10
E_j	0	$2B$	$6B$	$12B$	$20B$	$30B$	$42B$	$56B$	$72B$	$90B$	$110B$

Table 2.2 presents values of E_j for various j.

The distance between adjacent energy levels /41

$$E_{j+1}-E_j=2B(j+1) \tag{2.8}$$

is proportional to j.

It is seen from (2.8) and (2.7) that the absolute values of the distances between rotational energy levels are inversely proportional to the moment of inertia of the molecule. The heavier and larger the molecule, the farther into the long-wave region should its rotational spectrum fall.

Simultaneously with quantization of the squared angular momentum $\vec{M}_p^2$, the projection of $\vec{M}_p^2$ onto a specified direction z is also quantized:

$$M_{pz}=\hbar m_j, \tag{2.9}$$

where m_j is the magnetic quantum number, which assumes 2j + 1 values:

$$m_j=j, j-1, \ldots, -j. \tag{2.10}$$

The energy of any free molecule is determined by its angular momentum and is independent of the projection of this momentum and, consequently, also of the quantum number m_j. However, the set of values of the quantum numbers j and m_j fully defines the rotational motion of a linear molecule, which has two degrees of freedom in rotational motion.

As we have noted, m_j assumes 2j + 1 values for a given j. Thus, a linear molecule has 2j + 1 degenerate states for a given j. The statistical weight of a rotational level with a given j equals g_j = 2j + 1 (j = 0, 1, 2, ...).

At thermal equilibrium, the number of molecules with a given j is determined by

$$n_j=(2j+1)\,n_0 e^{-\frac{\varepsilon_j}{kT}}=(2j+1)\,n_0 e^{-\frac{Bj(j+1)}{kT}}, \tag{2.11}$$

where n_0 denotes the number of molecules in the state with j = 0.

Only molecules with nonzero constant dipole moments can have purely rotational spectra. Linear molecules may have constant dipole moments when the centers of gravity of the positive and negative charges do not coincide.

The selection rules permit purely rotational transitions when

$$\Delta j = \pm 1. \tag{2.12}$$

We see from (2.12) and (2.8) that the frequencies of the possible successive rotational transitions differ by an amount 2B. Thus, the purely rotational spectrum of a linear molecule is obtained in the rigid-top approximation as a spectrum consisting of equidistant lines. /42

The rigid-top approximation assumes constancy of the distances between the nuclei in the molecule as it rotates. In actuality, these distances increase owing to centrifugal stretching, by an amount that increases with increasing rotational energy and, consequently, with increasing rotational quantum number j. The rotational constant B [see (2.7)] decreases with increasing distance between nuclei. This results in a shorter distance between the lines in the spectrum on the frequency scale.

For the case of moderate centrifugal stretching in the molecule, the quantum-mechanical theory of perturbations permits derivation of the following approximate formula for the rotational energy of the molecule:

$$E_j = Bj(j+1) - D[j(j+1)]^2. \tag{2.13}$$

The constant D does not exceed 10^{-4}B. It must be taken into account only at large j.

2. Molecules of the spherical-top type. Molecules of the spherical-top type ($\mathcal{J}_a = \mathcal{J}_b = \mathcal{J}_c \neq 0$) are the simplest nonlinear molecules. The rotational-energy levels of these molecules are determined by the same formula as the energy levels of linear molecules [see (2.6)]. However, there is a substantial difference in the properties of the rotational levels of these two molecule types. Spherical tops have three degrees of rotational freedom, so that three quantum numbers must be known for complete description of their rotational levels. In addition to the quantum numbers j and m_j, which characterize the rotational motion, the quantum number k is introduced to determine the projection of the angular momentum onto a longitudinal axis rigidly bound to the molecule.

The projection of the angular momentum onto the axis bound to the molecule is quantized in the same way as the projection of this momentum onto the fixed axis. Hence, like the quantum number m_j, the quantum number k assumes 2j + 1 values for a given j.

Hence the total degree of degeneracy of the rotational levels of a spherical-top molecule with respect to m_j and k is found to equal /43

$$g_j = (2j+1)^2. \tag{2.14}$$

There are (2j + 1) possible orientations of the molecule with respect to a fixed axis not bound to it for each value of j, and (2j + 1) orientations relative to an axis moving together with the molecule.

The rotational-state distribution of the molecules now takes the form

$$n_j = (2j+1)^2 n_0 e^{-\frac{E_j}{kT}} = (2j+1)^2 n_0 e^{-\frac{Bj(j+1)}{kT}}. \tag{2.15}$$

It follows from comparison of (2.15) and (2.11) that the number of molecules of the spherical-top type at high rotational levels (higher than j) will be larger than the number of linear molecules at the same B and T.

The influence of centrifugal stretching is taken into account in the same way for the rotation of spherical-top molecules as in the case of linear molecules, and is determined by the same formula (2.13).

3. Molecules of the symmetrical-top type. There are no molecules of this type among the atmospheric gases that are distributed on the planetary scale. Nevertheless, this problem must be examined.

Let us denote by a, b, and c the axes about which the principal molecular moments of inertia are related as

$$\mathcal{J}_a \leqslant \mathcal{J}_b \leqslant \mathcal{J}_c. \tag{2.16}$$

A symmetrical top may be prolate or oblate. For a prolate top

$$\mathcal{J}_a < \mathcal{J}_b = \mathcal{J}_c. \tag{2.17}$$

For an oblate top

$$\mathcal{J}_a = \mathcal{J}_b < \mathcal{J}_c.$$

Each of the moments of inertia has its corresponding rotational constant (A, B, or C):

$$A = \frac{h^2}{8\pi^2 \mathcal{J}_a}; \quad B = \frac{h^2}{8\pi^2 \mathcal{J}_b}; \; C = \frac{h^2}{8\pi^2 \mathcal{J}_c}. \tag{2.18}$$

The expression for the rotational energy of a rigid prolate top takes the form /44

$$E_{jk} = Bj(j+1) + (A-B)k^2; \quad (A > B),$$
$$j = 0, 1, 2, \ldots; \quad k = 0; \pm 1; \pm 2; \ldots; \pm j. \tag{2.19}$$

In the case of an oblate top

$$E_{jk} = Bj(j+1) + (C-B)k^2; \quad (C < B);$$
$$j = 0, 1, 2, \ldots; \quad k = 0; \pm 1; \pm 2; \ldots; \pm j. \tag{2.20}$$

The first term in (2.19) and (2.20) is identical in form with the expression for the rotational energy of a linear molecule or a spherical-top molecule [see (2.7)]. The second term depends on the absolute value of the quantum number k, which determines the projection of the angular momentum onto the symmetry axis of the molecule. While each level with a given j has a degree of degeneracy 2j + 1 of the relative quantum number k in the case of a spherical top, each level splits into j + 1 levels corresponding to the values |k| = 0, 1, 2, ..., j for symmetrical-top molecules. Thus, there is no need to indicate the sign of k.

The levels of molecules with given j and k have a degree of degeneracy 2(2j + 1), except for the level with k = 0. In the latter case, the degree of degeneracy is (2j + 1).

The selection rules for purely rotational transitions in symmetrical-top molecules permit transitions that satisfy the conditions

$$\Delta j = \pm 1; \quad \Delta k = 0. \tag{2.21}$$

From (2.18), (2.19), and (2.20), we obtain for the energy of a transition of the molecule between levels with quantum numbers j'k and j"k

$$\Delta E = E_{j'k} - E_{j''k} = B[j'(j'+1) - j''(j''+1)]. \qquad (2.22)$$

From (2.22), we have for the transition energy between neighboring levels ($\Delta j = 1$)

$$\Delta E = E_{j+1,\,k} - E_{jk} = 2B(j+1). \qquad (2.23)$$

Thus, as in the case of linear molecules, the purely rotational spectrum of molecules of the symmetrical-top type consists of equally spaced lines, and only those molecules of the symmetrical-top type that have nonzero constant dipole moments can have rotational absorption and emission spectra. /45

The influence of centrifugal stretching of the molecules is taken into account by the following formula for the rotational energy of a symmetrical-top molecule:

$$E_{jk} = E_{jk}^{(0)} - D_j j^2 (j+1)^2 - D_{jk} j(j+1) k^2 - D_k k^4, \qquad (2.24)$$

where $E_{jk}^{(0)}$ is the rotational energy of the rigid symmetrical top and is determined by (2.19) and (2.20); D_j, D_{jk}, and D_k are constants that are small compared with B, A, and C.

From (2.21) and (2.24), we now obtain for the possible rotational transitions in the molecules

$$\Delta E = E_{j+1,k} - E_{jk} = 2B(j+1) - 4D_j (j+1)^3 - 2D_{jk}(j+1)k^2. \qquad (2.25)$$

It is evident from this last formula that the rotational spectrum of a real molecule consists of converging lines, with j + 1 levels due to the values k = 0, 1, ..., j corresponding to each j.

4. Molecules of the asymmetrical-top type. For molecules of the asymmetrical-top type

$$\mathcal{J}_a < \mathcal{J}_b < \mathcal{J}_c; \quad A > B > C. \qquad (2.26)$$

In contrast to the cases considered above, the asymmetrical-top case cannot be described by simple analytical expressions. It is necessary to solve quadratic equations to determine the energy of rotation with j = 2 and j = 3. Equations of the third, fourth, and higher degrees are solved to determine the energies of levels with j > 3. These calculations have now been carried out up to j = 40 [52].

A qualitative picture of the rotational-energy levels of an asymmetrical-top molecule can be obtained by treating this molecule as a case intermediate between the cases of extremely prolate and extremely oblate tops.

It is easily seen that the less $\mathcal{J}_b$ differs from $\mathcal{J}_a$ or $\mathcal{J}_c$, the more closely will the asymmetrical top resemble the corresponding symmetrical top. The parameter

$$\varkappa = \frac{2B - A - C}{A - C} \tag{2.27}$$

is introduced to characterize the asymmetry of a top. For a prolate top we have $\kappa = -1$, while $\kappa = 1$ for an oblate top. When $B = +(A + C)/2$ (the most asymmetrical top), $\kappa = 0$. For a water molecule, for example, $\kappa = -0.430$. /46

TABLE 2.3. ENERGIES OF ROTATIONAL LEVELS OF THE WATER MOLECULE (cm^{-1}) [51]

$j=0$	$j=1$	$j=2$	$j=3$	$j=4$
0,0	1_{-1} 23.78	2_{-2} 70.09	3_{-3} 136.76	4_{-4} 222.07
	1_0 37.09	2_{-1} 79.43	3_{-2} 142.23	4_{-3} 224.81
	1_1 42.31	2_0 95.15	3_{-1} 173.31	4_{-2} 275.50
		2_1 134.98	3_0 206.35	4_{-1} 300.44
		2_2 136.24	3_1 212.24	4_0 315.83
			3_2 286.18	4_1 384.03
			3_3 286.93	4_2 385.44
				4_3 490.64
				4_4 490.79

For a molecule of the asymmetrical-top type, a level with a given j splits into 2j + 1 levels, which are identified with the aid of an index τ that assumes the values

$$\tau = -j,\ -j+1,\ \ldots,\ j-1,\ j. \tag{2.28}$$

The levels are arrayed in order of increasing energy from j_{-j} to j_{+j} (see, for example, Table 2.3).

Centrifugal stretching of asymmetrical-top molecules causes only an energy-level shift, which may be rather large for light molecules and large values of j. Allowance for the influence of centrifugal stretching of the molecules on the rotational levels is a rather difficult task. Solutions are presented in [53] for various particular cases.

Asymmetrical-top molecules have highly complex spectra. The selection rules permit transitions with rotational quantum number changes

$$\Delta j = 0, \pm 1. \tag{2.29}$$

Here, Q, R, and P branches correspond to transitions with $\Delta j = 0$, +1, and -1. /47

In addition to the selection rules (2.29), asymmetrical-top molecules are subject to restrictions on transitions that involve the symmetry properties of the inertia ellipsoid. The wave function may remain unchanged or reverse sign as the inertia ellipsoid rotates about the axis of rotation. In the former case, we speak of an even function (denoted by e), and in the latter of an odd function (denoted by o). Rotation of the ellipsoid through 180° about any two axes is equivalent to rotation through the same angle about the third axis. Thus, it is sufficient to consider the rotations of the ellipsoid about two axes. The following types of molecular symmetry are then possible: ee, eo, oe, and oo or ++, +-, -+, and --.

Depending on which of the principal axes lies in the direction of the molecule's dipole moment, we distinguish three types of selection rules: A, B, and C. The dipole moment is directed along the a axis in the first case, the b axis in the second, and the c axis in the third.

The dipole moment of the water molecule is directed along the b axis. In this case, the selection rules are of type B:

$$++ \leftrightarrow -- \quad \text{and} \quad +- \leftrightarrow -+. \tag{2.30}$$

For types A and C, we have, respectively,

$$++ \leftrightarrow -+ \quad \text{and} \quad +- \leftrightarrow -- \tag{2.31}$$

and

$$++\leftrightarrow+-\quad\text{and}\quad-+\leftrightarrow--. \tag{2.32}$$

If the dipole moment does not coincide in direction with any of the principal axes of rotation, we have all three types of selection rules.

As in the cases examined earlier, only those asymmetrical-top molecules with nonzero constant dipole moments can have purely rotational spectra. The atmospheric gases with such molecules include the basic absorbing components of the atmosphere: water vapor and ozone. The pure rotational spectra of H_2O and O_3 are highly complex and have large numbers of strong absorption lines distributed over a broad range of wavelengths.

3. VIBRATIONAL ENERGY AND VIBRATIONAL-ROTATIONAL SPECTRA OF MOLECULES /48

1. Vibrational energy of molecules. A molecule consisting of N atoms has 3N degrees of freedom, of which three pertain to translational motion of the center of gravity of the molecule as a whole and three or two to the rotational motion. Linear molecules have two rotational degrees of freedom and nonlinear molecules three degrees of freedom. Thus, a nonlinear molecule has 3N - 6 degrees of freedom of vibrational motion and, in the general case, 3N - 6 different vibration frequencies. The linear molecule has 3N - 5 vibrational degrees of freedom and 3N - 5 different vibration frequencies. In symmetrical molecules, certain frequencies coincide as a result of degeneracy.

The harmonic-oscillator model is the simplest model of molecular vibrational motion. Quantum mechanics gives the following familiar expression for the vibrational energy in this model:

$$E_v = h\nu\left(v+\frac{1}{2}\right), \tag{2.33}$$

where

$$\nu = \frac{1}{2\pi}\sqrt{\frac{k}{M}} \tag{2.34}$$

is the classical vibration frequency, v is the vibrational quantum number, which assumes integral values v = 0, 1, 2, 3, ..., k is the quasielastic force constant, and M is the mass of the oscillator.

As we see from (2.33), the energy levels of the harmonic oscillator are equidistant. Here the energy difference between neighboring levels is

$$E_{v+1} - E_v = h\nu. \qquad (2.35)$$

For a harmonic oscillator, the frequency of a quantum jump between neighboring vibrational levels coincides with the classical vibration frequency.

If the vibrations of a molecule are regarded as the aggregate of the vibrations of harmonic oscillators with frequencies ν_1, ν_2, ν_3, ..., then according to quantum mechanics the vibrational energy of the molecule takes the form /49

$$E_v = \left(v_1 + \frac{1}{2}\right) h\nu_1 + \left(v_2 + \frac{1}{2}\right) h\nu_2 + \left(v_3 + \frac{1}{2}\right) h\nu_3 + \ldots, \qquad (2.36)$$

where v_1, v_2, v_3, ... are the vibrational quantum numbers.

The vibrational states of the molecules are denoted by sets of values of these numbers. For example, the (001) state corresponds to the values $v_1 = 0$, $v_2 = 0$, $v_3 = 1$. The frequencies ν_1, ν_2, ν_3, etc. are commonly known as the fundamental vibration frequencies.

The selection rules permit transitions between harmonic-oscillator energy levels that satisfy the condition

$$\Delta v = \pm 1. \qquad (2.37)$$

Here, if the molecule is represented as an aggregate of harmonic oscillators, the quantum number of only one of the vibrations must change.

Thus, the selection rules permit transitions only between neighboring energy levels with the same frequency ν [see (2.35)].

The harmonic-oscillator model gives an oversimplified description of the true vibrations. Consideration of the anharmonicity of the molecular vibrations results in the appearance of terms of the second and higher orders in the energy expression (2.36). Thus, in the case of a diatomic molecule, we may derive the following approximate expression for E_V:

$$E_v = \left(v + \frac{1}{2}\right) h\nu - \left(v + \frac{1}{2}\right)^2 xh\nu, \qquad (2.38)$$

where x is the anharmonicity constant.

For an N-atomic molecule, the expression for the vibrational energy with consideration of anharmonicity takes the form [54]

$$E(v_1, v_2, \ldots) = \sum_i h\nu_i \left(v_i + \frac{1}{2}\right) + \sum_i \sum_k x_{ik} \left(v_i + \frac{1}{2}\right)\left(v_k + \frac{1}{2}\right) + \ldots, \qquad (2.39)$$

where x_{ik} are the anharmonicity constants and the coupling constants between individual vibrations.

The anharmonicity of the vibrations causes a decrease in the distance between neighboring vibrational-energy levels of the molecule with increasing vibrational quantum number. A series of frequencies that diminish in the order $v = 0 \leftrightarrow v = 1$; $v = 1 \leftrightarrow v = 2$, etc. appears instead of the single vibrational frequency. /50

The distance between levels decreases progressively with increasing vibrational quantum numbers v_1, v_2, and v_3 (Fig. 2.2).

When the anharmonicity of the vibrations is taken into account, the selection rules change significantly. Transitions that satisfy the condition

$$\Delta v = 2, 3, 4, \text{ etc.}, \qquad (2.40)$$

are now allowed. Also allowed are transitions in which two quantum numbers change simultaneously.

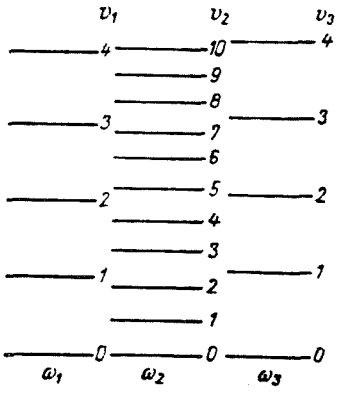

Figure 2.2. Vibrational Energy Levels of the H_2O Molecule.

Transitions characterized by a change of Δv by 2, 3, etc. give rise to corresponding harmonics of the fundamental vibration frequencies. On a simultaneous change of two or more vibrational quantum numbers, the so-called combination vibrational frequencies (sum and difference frequencies) make their appearance. Thus, in a real molecule, the number of vibrational frequencies is much larger than the number of its fundamental frequencies.

Vibrational anharmonicity may cause strong interaction between vibrations in the presence of accidental resonance. Thus, the CO_2 molecule has the almost coincident energy levels $\nu_1 = 1337\ cm^{-1}$ ($v_1 = 1$, $v_2 = 0$, $v_3 = 0$) and $2\nu_2$ ($v_1 = 0$, $v_2 = 2$, $v_3 = 0$). This accidental coincidence of energy levels belonging to the same symmetry class, which is known as Fermi resonance, causes interference between vibrational energy levels, which is manifested in shifts of the levels in opposite directions.

2. Vibrational-rotational molecular spectra. The energies of the vibrational and rotational quanta of the molecules are of the orders of 100-1000 cm^{-1} and 1-10 cm^{-1}, respectively. Thus, while the rotational spectra can be observed in pure form, the purely vibrational spectra can be observed only in extremely rare special cases. A change in the vibrational state of a molecule due to emission or absorption of energy is almost always accompanied by a change in rotational state. The smallness of the rotational-quantum energies as compared with those of the vibrational quanta explains the fact that rotation does not disturb the vibrational structure of the molecular spectrum. Since a series of rotational levels corresponds to each vibrational level, each vibrational transition in an aggregate of molecules becomes a series of lines or bands in the spectrum. Each of the lines corresponds to the same change in vibrational energy and a fully defined change in rotational energy. /51

Thus, the spectrum of the purely vibrational transitions of the molecule should be regarded as a skeleton about whose elements the vibrational-rotational bands are grouped. If we disregard the interaction of the molecular vibrations and rotations, its vibrational-rotational spectrum is easily presented as an additive superposition of the vibrational and rotational transitions allowed by the corresponding selection rules.

Let us first examine the nature of the vibrational structure of the spectra, which is the base of the vibrational-rotational bands. This structure is simplest in the case of diatomic molecules. The condition for the appearance of vibrational bands in the spectrum is a nonzero change in the molecule's dipole moment in the corresponding quantum jump. Diatomic molecules consisting of identical atoms and, consequently, having a zero dipole moment that does not change on vibrations cannot have vibrational-rotational spectra. The frequencies of these vibrations are said to be optically inactive.

The vibrational-transition spectrum of a diatomic molecule consisting of unlike atoms is easily obtained from (2.38), from which we have for the vibrational frequencies ν_k

$$\nu_k = \nu(1-x)(v''-v') - \nu x(v''^2 - v'^2), \qquad (2.41)$$

where v" and v' are the vibrational quantum numbers of the upper and lower states of the molecule.

It is evident from the last formula that the vibrational spectrum of a diatomic molecule consists of an aggregate of band series. Each band corresponds to an aggregate of transitions of the molecule from a given vibrational level to a neighboring one. We recall that the selection rules for an anharmonic oscillator, /52

for which (2.38) was derived, allow transitions with arbitrary vibrational quantum number changes. For example, for the series beginning with the zeroth vibrational level (v' = 0), we obtain from (2.41)

$$\nu_k(0, v'') = \nu(1-x)v'' - \nu x v''^2, \tag{2.42}$$

whence follows the next set of vibrational-transition frequencies and, consequently, of vibrational-rotational bands:

$$\nu_1 = \nu(1-2x); \quad \nu_2 = 2\nu(1-3x); \; \nu_3 = 3\nu(1-4x); \; \ldots \tag{2.43}$$

As we see from (2.43), the distance between neighboring lines decreases with increasing v" and increasing frequency. The lines of the series converge toward a certain limit corresponding to dissociation of the molecule. All other series are similar in structure.

This picture of the vibrational-rotational bands (in the form of an aggregate of band series) is also encountered in the case of monatomic molecules. However, owing to the complex vibrational-level scheme and the possibility of simultaneous excitation of a large number of vibrations (fundamental frequencies, harmonics, combination frequencies), these structures of individual vibrations overlap and the spectrum becomes highly complex.

Let us now examine the fine structure of the spectrum of individual vibrational-rotational bands. It will be convenient to begin with diatomic molecules. The vibrational-rotational energies for two levels characterized by the vibrational and rotational quantum numbers v", j", and v', j' can be written

$$E'' = E_{v''} + B_{v''} j''(j''+1), \tag{2.44}$$

$$E' = E_{v'} + B_{v'} j'(j'+1), \tag{2.45}$$

where $E_{V''}$ and $E_{V'}$ are determined by formulas of the type of (2.38) and the rotational energy is written for simplicity in the form Bj(j + 1).

In (2.44) and (2.45), account is taken of the interaction of /53
the molecule's vibrations and rotation with the aid of the rotational constant, which is a function of the vibrational quantum number v:

$$B_v = B_e - \alpha\left(v + \frac{1}{2}\right), \tag{2.46}$$

where B_e is the rotational constant of the nonvibrating molecule and α is a constant whose ratio to B_e is no more than a few hundredths.

As we see from (2.46), B_v diminishes linearly with increasing v. This is because the distance between atoms increases in the vibrating molecule, so that the moment of inertia also increases and the constant B_v decreases [see (2.7)]. We obtain from (2.44) and (2.45)

$$E'' - E' = E_{v''} - E_{v'} + B_{v''} j''(j''+1) - B_{v'} j'(j'+1). \tag{2.47}$$

The quantity $E_{v''} - E_{v'} = \nu_{00}$ determines the frequency of the purely vibrational transition, or the frequency of the so-called zeroth line, which would be obtained if $j'' = j' = 0$. The transition corresponding to the zeroth line is forbidden by the selection rules. The position of this line is determined by calculation.

Since the first difference in (2.47) may be much larger than the second, the position of the vibrational-rotational band in the spectrum is determined by the zeroth line.

For the transitions defined by (2.47), in contrast to the case of the purely rotational spectra, it is necessary to consider not only the values of $\Delta j = j'' - j' > 0$, but also the values of $\Delta j < 0$, and, in some cases, also $\Delta j = 0$. Then

if $\Delta j = j'' - j' = +1$, the transitions form an R branch,
if $\Delta j = j'' - j' = 0$, the transitions form a Q branch, (2.48)
if $\Delta j = j'' - j' = -1$, the transitions form a P branch.

Transitions with $\Delta j = +1$ correspond to frequencies greater than ν_{00}, and transitions with $\Delta j = -1$ correspond to frequencies smaller than ν_{00} (Fig. 2.3). For this reason, the R and P branches are also called positive and negative, respectively.

Transitions with $\Delta j = 0$ (Q branch) in diatomic molecules are allowed when the electronic angular momentum is nonzero (for example, in the NO molecule). For the Q branch, we obtain from (2.47) for the transition frequency ν_j /54

$$\nu_j = \nu_{00} + (B_{v''} - B_{v'})\, j\,(j+1). \qquad (2.49)$$

Since the difference $B_{v''}$ - $B_{v'}$ is very small, the lines of the Q branch are spaced very close together.

It is a convention to classify infrared absorption bands as parallel (denoted by the symbol ||) and perpendicular (denoted by ⊥). The bands that appear when the direction of the transition dipole moment coincides with the direction of the selected symmetry axis of the molecule are called parallel. Perpendicular bands are defined analogously.

We now turn to the fine-structure characteristics of the vibrational-rotational bands of molecules with differing rotational properties (linear and spherical, symmetrical, and asymmetrical tops).

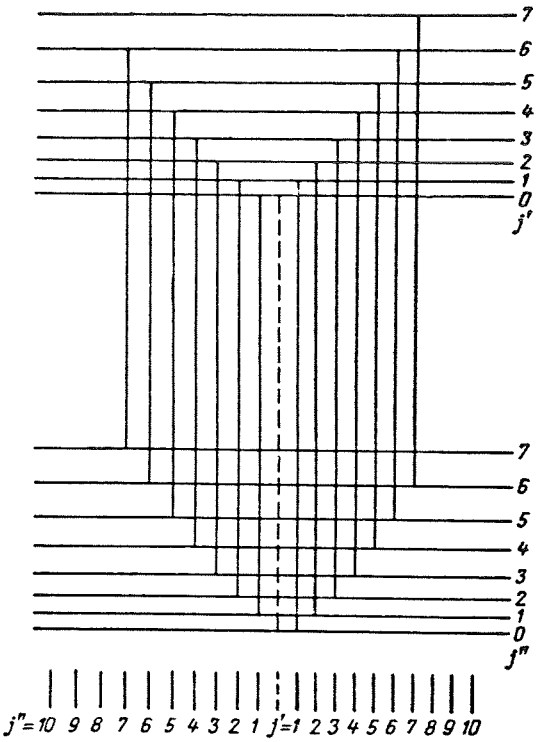

Figure 2.3. Scheme of Energy Transitions in Vibrational-Rotational Band.

/55

1. Linear polyatomic molecules. In the case of a linear polyatomic molecule, the positions of the rotational lines are determined by a formula similar to (2.47), except that now the rotational constants depend on all vibrational quantum numbers of the molecule:

$$B_{v_1, v_2, \ldots, v_k} = B_e - \sum_i \alpha_i \left(v_i + \frac{1}{2} g_i\right), \qquad (2.50)$$

where g_i is the degeneracy multiplicity of the i-th vibration.

In this case, the selection rules allow transitions in all three branches (R, Q, and P) for perpendicular bands. In the case of parallel bands, there is no Q branch, and the bands themselves are similar in structure to the bands of a diatomic molecule without an electronic angular momentum. Both parallel and perpendicular bands are encountered among the fundamental vibrational-rotational bands of linear molecules. For bands corresponding to vibrations in the direction of the valence bonds between atoms, the dipole moment is directed along the axis of the molecule (parallel bands). Deformational vibrations are responsible for the

appearance of perpendicular bands. In the case of CO_2, for example, the fundamental (001) bands with frequency ν_3 = 2349.3 cm^{-1} and the (010) bands with frequency ν_2 = 667.3 cm^{-1} are parallel and perpendicular, respectively. Both parallel and perpendicular bands are also encountered among the harmonics and combination frequencies. We note that the nature of a band (parallel or perpendicular) can be determined from the external appearance of the band spectrum. In the case of a parallel band, a minimum due to the absence of the Q branch is observed around the zeroth line. For a perpendicular band, there is a maximum due to the Q branch in the region of the zeroth line.

2. Molecules of the spherical-top type. In the case of spherical-top molecules, the positions of the rotational lines in a vibrational-rotational band are determined by the same formula as for linear molecules. The absorption bands consist of R, Q, and P branches. The interaction of the vibrational and rotational motions of the molecule cause splitting of triply degenerate vibrations.

3. Molecules of the symmetrical-top type. Molecules of the /56
symmetrical-top type, like linear molecules, have both parallel and perpendicular bands, for which there are different selection rules. The nature of the vibrational-rotational spectrum is found to be more complex than for linear and spherical-top molecules, especially if the dipole moment does not coincide in direction with the axis of the molecule. Since there are no symmetrical-top molecules among the atmospheric gases, we shall not dwell in greater detail on the fine-structure characteristics of the spectra of these molecules.

4. Molecules of the asymmetrical-top type. The purely rotational spectra and, accordingly, the vibrational-rotational spectra are most complex in molecules of this type. The dependence of the rotational constants A, B, and C on the vibrational quantum numbers is similar in character to (2.50). In the particular case of a triatomic molecule

$$\begin{aligned} A &= A_e - \alpha_{A_1}\left(v_1+\tfrac{1}{2}\right) - \alpha_{A_2}\left(v_2+\tfrac{1}{2}\right) - \alpha_{A_3}\left(v_3+\tfrac{1}{2}\right), \\ B &= B_e - \alpha_{B_1}\left(v_1+\tfrac{1}{2}\right) - \alpha_{B_2}\left(v_2+\tfrac{1}{2}\right) - \alpha_{B_3}\left(v_3+\tfrac{1}{2}\right), \\ C &= C_e - \alpha_{C_1}\left(v_1+\tfrac{1}{2}\right) - \alpha_{C_2}\left(v_2+\tfrac{1}{2}\right) - \alpha_{C_3}\left(v_3+\tfrac{1}{2}\right). \end{aligned} \qquad (2.51)$$

The constants α can be expressed in terms of the anharmonicity constants.

The selection rules for transitions in these molecules depend on the axis along which the transition dipole moment is directed.

In the general case, three types of bands result: A, B, and C (dipole moment directed along the a, b, and c axes, respectively). In the case of a symmetrical triatomic molecule XY_2, the dipole moment is directed either along the symmetry axis of the molecule or along the axis perpendicular to it that lies in the plane of the molecule. Perpendicular and parallel bands may then appear. For the particular case of the water molecule, the molecular axis coincides with the axis of the average moment of inertia, the parallel bands are of type B, and the perpendicular bands are of type A. Most of the H_2O bands are perpendicular.

The nature of the vibrational-rotational structure of the bands in molecules of all types and the positions, shapes, and strengths of the individual lines depend strongly on the interaction of the vibrational and rotational motions of the molecules. /57
Exact solution of the problem of fine-structure line positions requires consideration of the vibrational anharmonicity, centrifugal stretching of the molecules, resonance excitation of energy levels, and the influence of Coriolis forces. Proper allowance for all of these effects is a highly complex and difficult task.

4. ELECTRON ENERGY AND ELECTRON SPECTRA OF MOLECULES

The classification of molecular electron-energy levels and the selection rules for electron transitions are rather complex. With this in mind, and recognizing that all of the atmospheric gases except for oxygen lack electron spectra in the visible and infrared regions of interest to us, we do not consider it worthwhile to examine in detail the problem of the electron energy and electron spectra of molecules. As for the absorption spectrum of oxygen in the visible region, it will be described later.

We note that, despite the high complexity of the problem of quantitative calculation of the electronic-vibrational-rotational spectrum, it is precisely the solution of this problem that must be regarded as the most promising approach to correct investigation of the vibrational-rotational spectra. This problem will be examined in greater detail in the next chapter.

5. SPECTRAL-LINE SHAPE

In discussing transitions between discrete energy levels of a molecule, we have assumed that the absorption or emission processes associated with these transitions are characterized by fully defined frequencies. The spectra resulting from these transitions were assumed to consist of individual monochromatic lines. In fact, and for a variety of reasons, we never deal with strictly monochromatic lines. The real lines have fully defined contours whose shapes depend on the conditions under which light is absorbed or emitted by the molecules.

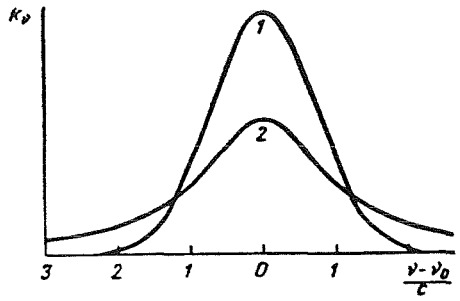

Figure 2.4. Contour Shapes of Lines Due to Doppler Broadening (1) and the Collision Effect, or the Effect of Radiative Damping (2) when the Strengths and Widths of the Lines are Equal.

Under the conditions of the earth's atmosphere, the contour shapes of spectral lines are determined chiefly by the following three effects: 1) radiative damping, 2) the Doppler effect, and 3) effects of collisions between molecules. /58

1. Natural spectral-line broadening. The transition of a molecule from one definite quantum-energy state to another takes place during a finite time interval. As a result, the vibrational process that accompanies this transition constitutes, as follows from the classical theory of radiation, an infinite set of frequencies in a definite spectral interval. The width of this interval depends on the time that the molecule spends in the excited state. If the molecules experience no external disturbances during absorption or emission of a given frequency, the resulting distribution of radiant intensity (absorption strength) over the frequencies will be the natural contour of the spectral line. Quantum mechanics gives us the following expression for this contour (Fig. 2.4, curve 2):

$$k(\nu)=\frac{1}{\pi}\frac{\gamma_N}{(\nu-\nu_0)^2+\gamma_N^2}, \tag{2.52}$$

where

$$\gamma_N=\frac{1}{2\pi\tau} \tag{2.53}$$

is the so-called natural line width and ν_0 is the center frequency of the line or the transition frequency for the hypothetical case corresponding to a time $\tau = \infty$ spent by the molecule in the excited state. /59

By the width of a line, we shall mean the spectral interval between the points ν_1, ν_2 on the contour that satisfy the condition

$$k(\nu_1)=k(\nu_2)=\frac{1}{2}k(\nu_0). \tag{2.54}$$

Expression (2.52) is often called the dispersion or Lorentz expression. We note that when the term dispersion contour is used, the reference is usually to the line contour obtained when the collision effect is considered.

For atmospheric gases, γ_N is very small. Actually, the most probable value of τ for the vibrational and rotational transitions of the atmospheric-gas molecules is of the order of 0.1 sec. At this value of τ, we have $\gamma_N = 3 \cdot 10^{-11}$ cm^{-1} [3]. This value is negligible compared to the line width due to both the Doppler and collision effects. In problems of the propagation of visible and infrared waves in the atmosphere, therefore, natural broadening of the spectral lines is not taken into account.

2. Doppler broadening of spectral lines. Assuming that thermodynamic equilibrium holds for the translational degrees of freedom of the molecule when the velocity distribution of the molecules is maxwellian, we obtain the following expression for the spectral-line contour (Fig. 2.4, curve 1), in which the broadening is due solely to the Doppler effect:

$$k(\nu) = \frac{S}{\sqrt{\pi}\alpha_D} \exp\left[-\left(\frac{\nu-\nu_0}{\alpha_D}\right)^2\right], \qquad (2.55)$$

where S is the strength of the line, which will be defined in the next section,

$$\alpha_D = \frac{\nu_0}{c}\sqrt{\frac{2kT\ln 2}{m}} \qquad (2.56)$$

is the Doppler half-width of the line, T is the absolute temperature, m is the mass of the molecule, c is the velocity of light, and k is Boltzmann's constant.

As we see from (2.56), α_D depends on ν_0, m, and T. The temperature varies on the average through no more than a factor of 1.5 in the lower atmosphere (troposphere and stratosphere). Thus, for a given spectral line (ν_0 = const, m = const), α_D can vary on a change in temperature within about ±15% of its average value, which corresponds to the average temperature. /60

Reference [3] cites two extreme values of α_D for atmospheric conditions and T = 300°K:

1) for the forbidden line of atomic oxygen at about 5577 Å

$$\alpha_D = 3{,}3 \cdot 10^{-2} \text{ cm}^{-1},$$

2) for the line of the rotational band of H_2O around 200 cm^{-1}

$$\alpha_D = 3{,}5 \cdot 10^{-4} \text{ cm}^{-1}.$$

3. Molecular-collision broadening of spectral lines. The interaction of a molecule that absorbs or emits light with neighboring molecules results in deformation of the energy levels and an associated broadening of the spectral lines. Clearly, this interaction must depend on pressure. Hence the effect in question is often referred to as the pressure-broadening or collision effect. If the absorption or emission processes take place in a pure gas, we sometimes speak of a self-broadening effect of the lines.

No exact solution of the problem of the influence of molecular collisions on spectral-line broadening has as yet been obtained with consideration of all properties of the collisions. All analyses deal only with binary molecular collisions, and the complex forces of the interacting molecules are described by interaction models: dipole-dipole, dipole-quadrupole, dipole-induced dipole.

Depending on the magnitude of the phase change in the molecule's absorption or emission due to collision with another molecule, a distinction is drawn between weak and strong collisions. The collisions considered in the kinetic theory are strong. The early theories of molecular-collision spectral-line broadening took only strong collisions into account. The prime example of these theories is that of Lorentz [55], which its author developed back in 1906. The results of this theory are widely used to this day. /61

According to the theory of strong collisions, the center of a spectral line is not shifted when the colliding molecules interact. In weak collisions, on the other hand, there is a shift in the line center. Both strong and weak collisions take place under real conditions. In application to atmospheric conditions (pressure $P < 1$ atm), the line contours obtained in the visible and infrared from strong-collision theory describe satisfactorily the central parts of spectral lines whose centers are not shifted with a change in pressure.

From the standpoint of quantum mechanics, energy transitions may take place in both colliding molecules as they interact. Collisions accompanied by energy transitions are conventionally known as nonadiabatic. Adiabatic collisions are those in which only the energy of the levels changes. In this classification of collisions, weak collisions can be regarded as adiabatic.

It follows from qualitative considerations that the theory of nonadiabatic collisions gives a better description of cases with high transition probabilities. On the other hand, adiabatic-collision theory is more suitable for description of transitions with low probabilities. For atmospheric conditions, the probabilities of molecular transitions are high in the infrared, so that nonadiabatic-collision theories are preferable here. The Anderson theory is an example of a theory of this class that is widely used in calculations.

In addition to the above classifications of theories advanced to account for pressure broadening of spectral lines, note should also be taken of one that views all theories as either impact or statistical. In the impact theories, it is assumed that the duration of collisions between molecules is negligibly short by comparison with the time between collisions. Statistical theories consider the distribution of the energy-level shift of the molecule at rest as a result of its interaction with all other molecules.

Since the Lorentz and Anderson theories have come into the widest practical use for description of spectral line-broadening effects due to collisions between molecules of atmospheric gases /62
in the visible and infrared, we shall present the results of only these theories.

The Lorentz theory gives the following well-known expression for the contour of a spectral absorption line:

$$k(\nu)=\frac{S}{\pi}\frac{\gamma_L}{(\nu-\nu_0)^2+\gamma_L^2}, \qquad (2.57)$$

which is frequently called the dispersion contour or Lorentz contour in the literature. In (2.57), S is the line strength, ν_0 is the position of the line center, and

$$\gamma_L=\frac{1}{4\pi\tau(v)} \qquad (2.58)$$

is the half-width of the line.

Here $\tau(\nu)$ is the lifetime of the absorbing or emitting molecule in the excited state and depends on its velocity v.

To find γ_L, it is necessary to take the dependence $\tau(v)$ into account. Usually, γ_L is found as the line width corresponding to the mean value of $\tau(v) = \bar{\tau}$. In this case, the kinetic theory of

gases yields the expression

$$\gamma_L = \frac{1}{2\pi\tau} = \sum_i n_i \sigma_i^2 \left[\frac{2kT}{\pi}\left(\frac{1}{m} + \frac{1}{m_i}\right)\right]^{1/2}, \qquad (2.59)$$

where n_i is the concentration of type i molecules, σ_i is the effective distance between the emitting or absorbing molecule and a type i molecule; m and m_i are the masses of these molecules. The effective distance is that at which there is an interaction of the molecules that causes broadening of the spectral line.

The concentration of molecules n_i in any gas mixture is proportional to pressure. Thus, it follows from (2.59) that the line width is proportional to pressure. Since pressure varies in a broad range under atmospheric conditions, the dependence of γ_L on P is very important. The dependence of γ_L on σ is also important, since σ depends not only on the pair of colliding-molecule types, but also on the energy levels of the molecules or on the rotational quantum number j. The temperature dependence of α_L [sic] is quite weak. It can be disregarded in solving many problems of the propagation of visible and infrared waves in the atmosphere. We shall /63 return more than once to the problem of γ_L as a function of various independent variables.

For the case of a two-component mixture, we obtain the following simpler expression for γ_L:

$$\gamma_L = \frac{1}{4}\left\{2\pi kT\left[N_a D_{aa}^2\left(\frac{2}{m_a}\right)^{1/2} + N_b D_{ab}^2\left(\frac{1}{m_a} + \frac{1}{m_b}\right)^{1/2}\right]\right\}^{1/2}, \qquad (2.60)$$

where the subscripts a and b pertain to absorbing and nonabsorbing molecules, N_a and N_b are the numbers of molecules a and b per unit volume, D_{aa} and D_{ab} are the total optical-collision diameters between molecules a $\leftrightarrow$ a and a $\leftrightarrow$ b, and m_a and m_b are the molecular masses.

The γ_L for a two-component mixture is often written in the still simpler form

$$\gamma_L = \gamma_L^0 \frac{P}{P_0}\sqrt{\frac{T_0}{T}}, \qquad (2.61)$$

where γ_L^0 is the half-width of the line under standard conditions (P_0 = 1 atm, T_0 = 273°K).

The theory of pressure broadening of spectral lines developed in 1949 by Anderson [56] is a quantum-mechanical nonadiabatic theory for molecular spectra. In this theory, it is assumed that transitions can take place in both colliding molecules. The impact-theory formula (2.59) is taken as the starting formula for γ_L, but the effective distances or optical-collision diameters are determined with consideration of the possible energy transitions in the colliding molecules. The following expression results for γ_L:

$$\gamma_L^{ij} = \sum_{j_2} \left[\frac{2kT}{\pi}\left(\frac{1}{m}+\frac{1}{m_0}\right)\right]^{1/2} n(j_2)\,\sigma^2(i, j, j_2), \qquad (2.62)$$

where $n(j_2)$ is the concentration of the perturbing molecules,

$$\sigma(i, j, j_2) = \sum_{j_2', i'} \sigma(i, i'; j_2, j_2'; j) + \sum_{j_2', j'} \sigma(i; j_2, j_2'; j, j'); \qquad (2.63)$$

i, i', j, j' are indices characterizing the states of the absorbing molecule, for which the transition i → j takes place without interaction with the perturbing molecule, and j_2 and j_2' are indices that characterize the state of the perturbing molecule. The molecular collision gives rise to transitions i → i' and j → j' in the absorbing molecule and $j_2 \rightarrow j_2'$ in the perturbing molecule. /64

Using the Anderson theory, Benedict and Kaplan [57, 58] made a detailed calculation of the half-widths of lines in the pure rotational spectrum of water vapor for collisions of its molecules with nitrogen and oxygen molecules. The results indicated that for H_2O-N_2 molecular collisions, γ_L varies from line to line in the range from 0.03 to 0.1 cm^{-1} at a pressure P = 1 atm. The data obtained in [57] and [58] will be examined in greater detail in the next chapter.

4. Combined action of Doppler and molecular-collision effects. Under real conditions, the Doppler and molecular-collision effects operate simultaneously. However, they differ substantially in importance at different altitudes, since the Doppler line-broadening effect does not depend on pressure. Broadening due to molecular collisions is maximal in the ground layer and diminishes with height in proportion to the pressure decrease. The Doppler line width is negligibly small in the ground layer as compared to the half-width due to the molecular-collision effect. The collision-governed width of each spectral line becomes equal to the Doppler

width at a certain height in the atmosphere. As height increases further, the Doppler width becomes larger and larger in comparison to the dispersion width.

If we set γ_L equal to 0.08 cm^{-1}, the most probable value for the atmospheric gases under standard conditions, then the heights at which $\gamma_L = \gamma_D$ are found to be 7 and 37 km for the extreme values $\gamma_D = 3.3 \cdot 10^{-2}$ cm^{-1} and $3.5 \cdot 10^{3}$ cm^{-1} (see paragraph 2 of the present section). For narrower dispersion lines, these heights will be correspondingly smaller, and vice versa. As these estimates show, it may be necessary to take account of both line-broadening effects in some cases beginning as low as the upper layers of the troposphere.

Joint analysis of the two spectral-line broadening effects results in the following expression for the absorption coefficient:

$$k(\nu) = \frac{k_0 y}{\pi} \int_{-\infty}^{\infty} \frac{e^{-t^2}}{y^2 + (x-t)^2} dt, \qquad (2.64)$$

where /65

$$k_0 = \frac{S}{\gamma_D}\left(\frac{\ln 2}{\pi}\right)^{1/2}; \quad y = \frac{\gamma_L}{\gamma_D}(\ln 2)^{1/2}; \quad x = \frac{\nu - \nu_0}{\gamma_D}(\ln 2)^{1/2}, \qquad (2.65)$$

S is the strength of the line and ν_0 is the center of the line.

5. Shape of far wings of lines. We see from Fig. 2.4 that the Doppler contour of the line drops off much more rapidly in the limbs than the dispersion contour. This means that when the Doppler and collision effects are in operation simultaneously, the far limbs of the line should be governed by dispersion. However, the question as to whether the dispersion contour correctly describes the far limbs of lines cannot be regarded as resolved. If we proceed from the qualitative considerations on which the hypotheses of the various pressure-broadening theories are based, we should expect the statistical and not the impact theories to give a better description of the shape of the far limbs of the lines. The presently available experimental data are totally inadequate for any definite conclusions in favor of either theory of the limbs of a line. The results at hand suggest that the shape of the far limbs may be different for different molecules.

6. SPECTRAL-LINE STRENGTH

The strength S of a spectral line is written in terms of the absorption coefficient $k(\nu)$:

$$S = \int_0^\infty k(\nu)\, d\nu. \tag{2.66}$$

For the strength of a specific transition of a molecule from a state with index j to a state characterized by index i, quantum mechanics gives the expression [3]:

$$S_{i,j} = \frac{n_j}{g_i n} \frac{8\pi^3 \nu_{i,j} |R_{i,j}|^2}{3hc} (1 - e^{-h\nu_{i,j}/kT}), \tag{2.67}$$

where n_j is the concentration of molecules in the lower state, n is the concentration of all molecules, g_i is a statistical weight, $n_{i,j}$ is the transition frequency, $|R_{i,j}|^2$ is the square of the dipole moment matrix element, T is the absolute temperature, and h, k, and c are Planck's constants, Boltzmann's constant, and the speed of light. /66

The dipole moment matrix element $\vec{M}$ is expressed in terms of the wave functions ψ_i and ψ_j of the states of the molecule:

$$R_{i,j} = \int \psi_i^* \vec{M} \psi_j \, dv. \tag{2.68}$$

The integration in (2.68) extends over the entire configuration space; dv is the element of this space. The wave functions are obtained by solving a Schrödinger equation.

The wave functions are subject to the orthogonality condition

$$\int \psi_i^* \psi_j \, dv = 0 \, (i \neq j). \tag{2.69}$$

With $\vec{M}$ = const, we obtain from (2.69) and (2.68)

$$\vec{M} \int \psi_i^* \psi_j \, dv = 0. \tag{2.70}$$

This last relation is the basis for our earlier statement to the effect that a transition of a molecule from one energy state to another with dipole emission takes place only when the dipole moment changes. We note that emission or absorption of light

takes place not only on dipole interaction of an electromagnetic field with matter. Spectral lines also appear when the magnetic dipole or electrical quadrupole of a molecule changes, with the accompanying corresponding energy transitions. However, these lines are of very low intensity. Transitions involving a change in the electrical dipole moment of a molecule produce line strengths 10^5 and 10^8 times higher in order of magnitude than are observed in cases when the magnetic dipole and electrical quadropole moments change.

The matrix elements $R_{i,j}$ are related to the familiar Einstein coefficients $A_{i,j}$, which characterize the probability of stimulated emission and absorption between levels of a molecule with indices i and j:

$$A_{i,j} = \frac{64\pi^4 \nu_{i,j}^3}{3hg_i c^3} |R_{i,j}|^2. \qquad (2.71)$$

We note that for electric-dipole emission, $A_{i,j}$ is of the order of 10^8, 10, and 1 sec^{-1} for electronic, vibrational, and rotational transitions, respectively. /67

The most difficult problem encountered in determining line strengths is that of finding the squares $|R_{i,j}|^2$ of the matrix elements.

7. GENERAL CHARACTERISTICS OF THE ABSORPTION SPECTRA OF ATMOSPHERIC GASES

We note first of all that we are interested in the absorption spectra of the atmospheric gases in the visible and infrared regions. We shall consider the spectra both of the basic absorbing gases (water vapor, carbon dioxide, ozone) and of the gases whose contributions to the integral absorption of visible and infrared radiation in the atmosphere is less significant, in some cases because of their relatively small absorption coefficients (oxygen) and in others because of their low concentrations (methane, carbon monoxide, nitrous oxide). The basic component of the atmosphere, nitrogen, has absorption bands only in the far ultraviolet. /68

The general pattern of the absorption spectrum of the earth's atmosphere is presented in Fig. 2.5, which has been borrowed from [3].

Let us now examine the absorption spectra of the atmosphere's basic constituents.

1. **Water vapor.** The water molecule forms an isosceles triangle with the oxygen atom at its vertex (Fig. 2.6). The angle θ

between the O-H bonds is 104°30'. The distance between the oxygen and hydrogen atoms is 0.958 Å.

The electron transitions in the H_2O molecule occur in the region of wavelengths shorter than 1860 Å (in the far ultraviolet).

The vibrational-rotational absorption spectrum of water vapor is exceedingly complex. This is primarily because the moments of inertia of the molecule about the three principal axes of the inertia ellipsoid differ sharply (they are equal to $\mathcal{J}_a = 1{,}004 \cdot 10^{-40}$; $\mathcal{J}_b = 1{,}929 \cdot 10^{-40}$; $\mathcal{J}_c = 3{,}014 \cdot 10^{-40}$ g·cm^{-2}).

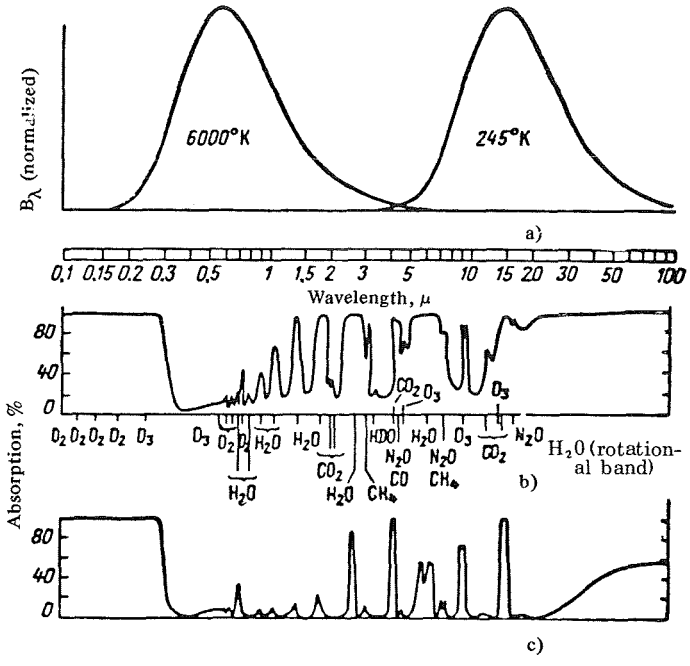

Figure 2.5. General Pattern of Absorption Spectrum of Atmospheric Gases. a) Black-body emission curves at 6000 and 245°K; b) absorption spectrum of solar radiation reaching the earth's surface; c) absorption spectrum of solar radiation reaching 11-km altitude. (Spectra b and c were obtained for middle latitudes at a solar zenith distance of 40° under most-probable conditions.)

In such cases, the rotational structure of the spectra of asymmetrical-top molecules is chaotic and complex. Figure 2.6 shows the axes a, b, and c about which the moments of inertia $\mathcal{J}_a$, $\mathcal{J}_b$, $\mathcal{J}_c$ of the water molecule are found. The absolute values of the moments of inertia are small, since the molecule contains two hydrogens. The distance between the rotational lines is therefore large.

The large values of the dipole moments of the molecule of H_2O and its isotopes give rise to a strong rotational spectrum. The dipole moments M of the molecule of H_2O and its isotopes are: M_b = /69
= 1.94D for H_2O, M_b = 1.87D for D_2O, M_a = 0.64D and M_b = 1.70D for HDO.

Lines of the following four water isotopes have been detected in the solar spectrum: H_2O^{16}, H_2O^{18}, H_2O^{17}, and HDO^{16}, which are present in the atmosphere in the proportions 99.73, 0.2039, 0.0373, and 0.0298. The rotational and vibrational constants of the first three isotopes differ insignificantly. The lines of the H_2O^{18} molecule are shifted from the corresponding H_2O^{16} lines by amounts from 1 to 11 cm^{-1}. This shift is twice as large for the H_2O^{17} molecule

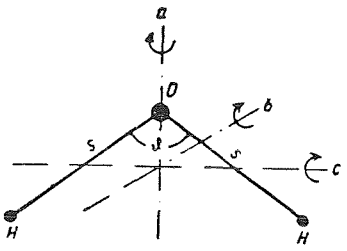

Figure 2.6. Diagram of Structure of H_2O Molecule.

[3]. The rotational constants for the molecules H_2O^{16} and HDO^{16} appear in Table 2.4.

The purely rotational absorption spectrum of water vapor occupies a very broad wavelength range extending from about 8 μ to several centimeters.

In addition to the three principal vibrational-rotational bands, which owe their origin to the fundamental vibrations at frequencies ν_1, ν_2, and ν_3 (Table 2.5), a considerable number of harmonics and combination frequencies are observed in the vibrational-rotational spectrum of H_2O in the visible and infrared regions (Tables 2.6 and 2.7).

Figure 2.7 presents a diagram of the fundamental vibrations /70

TABLE 2.4. ROTATIONAL CONSTANTS OF THE MOLECULES HHO^{16} AND HDO^{16} IN THE GROUND STATE (cm^{-1}) [3]

Axis	HHO^{16}	HDO^{16}
a	27.79	23.38
b	14.51	9.06
c	9.29	6.38

TABLE 2.5. FREQUENCIES OF THE PRINCIPAL BANDS OF THE MOLECULE H_2O [3]

Band	Transition	Center of band, cm^{-1}	
		HHO^{16}	HDO^{16}
ν_1	000—100	3657.05	2723.66
ν_2	000—010	1594.78	1403.3
ν_3	000—001	3755.92	3707.47

of the molecule, which give rise to the appearance of the frequencies ν_1, ν_2, and ν_3. The deformational vibration ν_2 has the lowest frequency. Transitions of the molecule involving the fundamental frequencies ν_1 and ν_3 create overlapping bands in a region in which the first harmonic of the ν_2 band falls. The overlapping /71 of the bands ν_1, ν_3, and $2\nu_2$ causes a complex interaction between the corresponding energy levels.

In addition to the fundamental bands, harmonics, and combination frequencies, bands of higher states in which the vibrational transition is not from the ground state are observed in the solar spectrum (Table 2.8).

The band strengths of the higher states depend very strongly on temperature, since temperature is a major factor in determining

TABLE 2.6. BANDS OF H_2O IN THE VISIBLE REGION OF THE SPECTRUM [3]

Transition	Center of band		Type	Strength, cm
	cm^{-1}	μ		
000—411	18 394	0.54	*A*	$2 \cdot 10^{-23}$
000—203	17 495	0.57	*A*	$1 \cdot 10^{-22}$
000—401	16 899	0.59	*A*	$3 \cdot 10^{-22}$
000—302	16 898	0.59	*B*	$3 \cdot 10^{-23}$
000—321	16 822	0.59	*A*	$2 \cdot 10^{-22}$
000—113	15 832	0.63	*A*	$2 \cdot 10^{-23}$
000—311	15 348	0.66	*A*	$2 \cdot 10^{-22}$
000—103	14 319	0.69	*A*	$1 \cdot 10^{-21}$
000—400	14 221	0.70	*B*	$1 \cdot 10^{-22}$
000—301	13 831	0.72	*A*	$3 \cdot 10^{-21}$
000—202	13 828	0.72	*B*	$2 \cdot 10^{-23}$
000—221	13 653	0.73	*A*	$6 \cdot 10^{-21}$
000—013	12 565	0.79	*A*	$1 \cdot 10^{-22}$
000—112	12 408	0.81	*B*	$6 \cdot 10^{-21}$
000—211	12 151	0.82	*A*	$6 \cdot 10^{-23}$
000—210	12 140	0.82	*B*	$1 \cdot 10^{-22}$
000—131	11 813	0.85	*A*	$2 \cdot 10^{-21}$

the populations of the corresponding vibrational levels of the H_2O molecule. However, the population of the fundamental vibrational state may be regarded as practically temperature-independent.

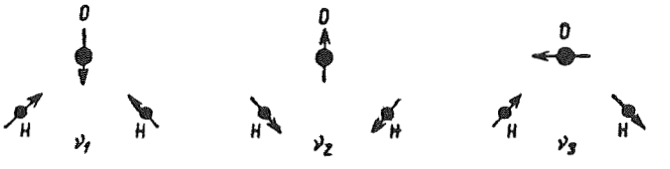

Figure 2.7. Diagram of Fundamental Vibrations of the H_2O Molecule.

/72

As we have noted, the vibrational-rotational spectra of the water isotopes HHO^{18} and HHO^{17} are similar to the spectrum of HHO^{16}, except that they are slightly shifted. The ratios of the line strengths of these isotopes and those of HHO^{16} correspond to their concentration ratios. The bands of HDO (Table 2.9) differ markedly from those of HHO^{16}

/73

Analysis of the vibrational-rotational spectrum of water vapor indicates that the fundamental ν_2 band, which corresponds to deformational vibration of the molecule, is the strongest and broadest absorption band. This band is centered around a wavelength of 6.25 μ. The literature refers to it frequently as the 6.3-μ band. In a vertical column of atmosphere, this band absorbs

TABLE 2.7. BANDS OF H_2O IN THE NEAR INFRARED REGION OF THE SPECTRUM [3]

Band	Transition	Center of band		Type	Strength, cm
		cm^{-1}	μ		
ρ	000—003	11 032	0.91	*A*	$2 \cdot 10^{-21}$
	000—102	10 869	0.92	*B*	$4 \cdot 10^{-22}$
σ	000—201	10 613	0.94	*A*	$1 \cdot 10^{-20}$
	000—300	10 600	0.94	*B*	$6 \cdot 10^{-22}$
τ	000—121	10 329	0.97	*A*	$2 \cdot 10^{-21}$
	000—220	10 284	0.97	*B*	$< 4 \cdot 10^{-23}$
	000—041	9 834	1.01	*A*	$6 \cdot 10^{-23}$
φ	000—012	9 000	1.11	*B*	$3 \cdot 10^{-22}$
	000—121	8 807	1.13	*A*	$8 \cdot 10^{-21}$
	000—210	8 762	1.14	*B*	$1 \cdot 10^{-23}$
	000—130	8 274	1.20	*B*	$7 \cdot 10^{-24}$
	000—031	8 374	1.19	*A*	$3 \cdot 10^{-23}$
ψ	000—002	7 445	1.34	*B*	$1 \cdot 10^{-21}$
	000—101	7 250	1.37	*A*	$1{,}5 \cdot 10^{-19}$
	000—200	7 201	1.38	*B*	$1{,}5 \cdot 10^{-20}$
	000—021	6 871	1.45	*A*	$1 \cdot 10^{-20}$
	000—120	6 775	1.47	*B*	$2 \cdot 10^{-22}$
Ω	000—011	5 331	1.87	*A*	$2{,}2 \cdot 10^{-19}$
	000—110	5 235	1.91	*B*	$7 \cdot 10^{-21}$
	000—030	4 667	2.14	*B*	$3 \cdot 10^{-22}$

TABLE 2.8. BANDS OF THE HIGHER STATES OF H_2O [3]

Transition	Frequency		Type	Strength (at 259°K), cm
	cm^{-1}	μ		
010—001	2161.14	4.62	*A*	$2 \cdot 10^{-22}$
010—100	2062.27	4.84	*B*	$8 \cdot 10^{-23}$
010—020	1556.82	6.42	*B*	$9 \cdot 10^{-22}$
010—010	0—500	∞ — 20	*B*	$4.6 \cdot 10^{-20}$

all of the solar radiation at the wavelengths from approximately 5.5 to 7.5 μ [59]. The center of the second-strongest band, ν_3, is situated at around 2.66 μ. The ν_1 and $2\nu_2$ bands are centered around 2.74 and 3.17 μ. Under typical conditions, the ν_1, ν_3, and $2\nu_2$ bands totally absorb solar radiation in a vertical column of atmosphere in the spectral region from approximately 2.6 to 3.3 μ. In a spectrum obtained with low resolution, the other vibrational-rotational water-vapor bands group to form absorption bands

TABLE 2.9. BANDS OF HDO^{16} [3]

Transition	Frequency		Strength, cm	
	cm^{-1}	μ	Of type A component	Of type B component
000—010	1403,3	7.12	$5 \cdot 10^{-23}$	$2{,}3 \cdot 10^{-22}$
000—100	2723,66	3.67	$5 \cdot 10^{-22}$	$< 5 \cdot 10^{-24}$
000—020	2782,16	3.59	$1.4 \cdot 10^{-23}$	$9 \cdot 10^{-24}$
000—001	3707,47	2.69	$3 \cdot 10^{-22}$	$1{,}4 \cdot 10^{-22}$
000—110	4100,05	2.43	$2 \cdot 10^{-23}$	$< 1 \cdot 10^{-24}$
000—030	4145,59	2.41	$2 \cdot 10^{-23}$	$< 1 \cdot 10^{-24}$
000—011	5089,59	1.96	$3 \cdot 10^{-23}$	$1{,}6 \cdot 10^{-23}$
000—200	5363,59	1.86	$3 \cdot 10^{-23}$	$< 2 \cdot 10^{-24}$
000—101	6415,64	1.55	$1 \cdot 10^{-24}$	$9 \cdot 10^{-24}$
000—021	6452,05	1.54	$2 \cdot 10^{-24}$	$< 5 \cdot 10^{-25}$
000—012	8611,22	1.16	$5 \cdot 10^{-24}$	$< 5 \cdot 10^{-25}$

centered around 1.87, 1.38, 1.1, 0.94, 0.81, and 0.72 μ . There are several weak bands in the visible region of the spectrum.

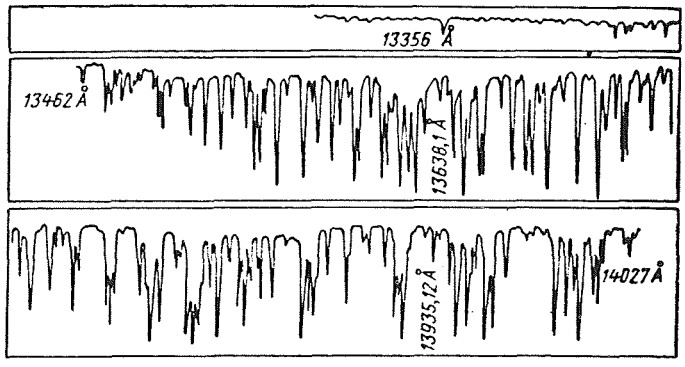

Figure 2.8. Absorption Spectrum of the Part of the Vibrational-Rotational Band of Water Vapor Around 1.38 μ [60].

The fine structure of the vibrational-rotational spectrum of water vapor is extremely complex and confused. Each band of this spectrum consists of hundreds and even thousands of individual lines whose identification is a very difficult problem. Use of spectral instruments of even the highest resolution does not always make it possible to resolve completely all of the lines in the /74
fine structure of the spectrum. By way of illustration, Fig. 2.8 shows a width of only 0.07 μ from the spectrum of the H_2O vibrational-rotational band in the region of the 1.38-μ band as recorded by a high-resolution instrument [60]. Theoretical calculation of the center positions, strengths, and half-widths of the individual lines requires correct allowance for the complex interaction of the vibrational and rotational levels of the molecule.

2. **Carbon dioxide.** The symmetrical linear CO_2 molecule, whose C-O bond length is 1.1632 Å in the fundamental vibrational

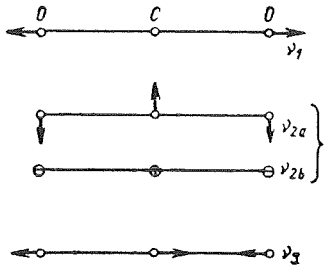

Figure 2.9. Diagram of Fundamental Vibrations of the CO_2 Molecule.

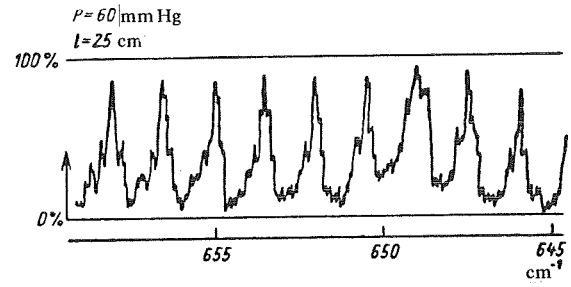

Figure 2.10. Section of Absorption Spectrum of CO_2 in 15.0-μ Band as Recorded with High Resolution in [61].

TABLE 2.10. FUNDAMENTAL BANDS ν_2 AND ν_3 OF THE CO_2 MOLECULE [3]

Isotopic variety	Percentage content	Center of band, cm^{-1}	
		ν_2	ν_3
$C^{12}O^{16}O^{16}$	98.420	667.40	2349.16
$C^{13}O^{16}O^{16}$	1.108	648.52	2283.48
$C^{12}O^{16}O^{18}$	0.408	662.39	2333

state, has three fundamental vibration frequencies: ν_1, ν_2, and ν_3, which are diagrammed in Fig. 2.9. The rotational constant of the molecule in the fundamental vibrational state is 0.3895 cm^{-1}. The deformational vibration ν_2 is doubly degenerate. In the latter case, it is necessary to consider, in addition to the selection rules discussed in §3 of this chapter, selection rules for the vibrational quantum numbers of the vibrational angular momentum:

$$\Delta l = 0, \pm 1. \tag{2.72}$$

Owing to the symmetry of the molecule, the dipole moment does not change in the fundamental ν_1 vibration, so that this vibration does not appear in the infrared spectrum. The frequency ν_1 is approximately twice the frequency ν_2.

The fundamental vibrational-rotational bands $\nu_2(00^\circ0\text{-}01^10)$ and $\nu_3(00^\circ0\text{-}00^\circ1)$ are perpendicular and parallel, respectively. Thus, the ν_3 band does not have a Q branch.

The statistical weights of the levels of the CO_2 molecule with even values of j are zero. As a result, there are only lines with odd j in the fine structure of the vibrational-rotational bands.

The CO_2 molecule has the isotopes $C^{12}O_2^{16}$, $C^{13}O_2^{16}$, $C^{12}O^{16}O^{17}$, and $C^{12}O^{16}O^{18}$, whose percentage contents with respect to the total

carbon dioxide content in the atmosphere are 98.420, 1,108, 0.0646 and 0.4078%, respectively. There are also two rare CO_2 isotopes. /75

Table 2.10 gives the center positions of the ν_2 and ν_3 bands of the three CO_2 isotopes most widely encountered in the atmosphere [3].

Together with 14 bands of higher states, the fundamental vibrational-rotational band ν_2, which is centered around 15 μ, occupies a rather broad interval of the spectrum, from about 12 to 20 μ. In the central region of this band (∿13.5-16.5 μ), a vertical column of atmosphere absorbs the solar radiation completely. This entire aggregate of bands is often referred to in the literature as the 15.0-μ band (Table 2.11). Figure 2.10 shows part of the spectrum of the 15-μ CO_2 band. We see from this figure that not all of the lines in this segment of the spectrum are resolved by the instrument. We note that the region of the 15-μ band is extremely rich in fine-structure lines. Thus, for example, Drayson [62] counted about 2000 lines in the course of calculating the CO_2 absorption coefficients in the region of this band (or, more precisely, set of bands). /76

TABLE 2.11. CO_2 BANDS IN THE 15-μ REGION [3]

Isotopic variety	Transition	Center of band		Molecular strength of band*, cm	E", cm^{-1}
		cm^{-1}	μ		
$C^{12}O^{16}O^{16}$	00^00-01^10	667,40	15,0	$7,89\cdot10^{-18}$	0,0
$C^{13}O^{16}O^{16}$	00^00-01^10	648,52	15,4	$7,9\cdot10^{-20}$	0,0
$C^{12}O^{18}O^{16}$	00^00-01^10	662,39	15,1	$3,7\cdot10^{-20}$	0,0
$C^{12}O^{16}O^{16}$	01^10-02^00	618,03	16,2	$1,75\cdot10^{-19}$	667,4
—	01^10-10^00	720,83	13,9	$2,3\cdot10^{-19}$	667,4
—	01^10-02^20	667,76	15,0	$6,2\cdot10^{-19}$	667,4
—	10^00-03^10	647,02	15,5	$4,2\cdot10^{-20}$	1285,43
—	10^00-11^10	791,48	12,6	$8,2\cdot10^{-22}$	1285,43
—	02^20-03^10	597,29	16,7	$5,83\cdot10^{-21}$	1335,16
—	02^20-11^10	741,75	13,5	$5,2\cdot10^{-21}$	1335,16
—	02^20-03^30	668,3	15,0	$3,2\cdot10^{-20}$	1335,16
—	02^00-03^10	544,26	18,4	$1,64\cdot10^{-22}$	1388,19
—	03^30-04^20	581,2	17,2	$1,56\cdot10^{-22}$	2003,28
—	03^30-12^20	756,75	13,2	$2,2\cdot10^{-22}$	2003,28
—	03^10-12^20	828,18	12,1	$1,8\cdot10^{-23}$	1932,45
—	03^10-12^00	740,5	13,5	$5,2\cdot10^{-22}$	1932,45
—	04^40-13^30	769,5	13,0	$1,5\cdot10^{-23}$	2674,76

*These data were obtained with respect to the total number of molecules of all isotopic varieties. Each strength value contains the Boltzmann fundamental-state multiplier.

Note: Commas represent decimal points.

TABLE 2.12. ABSORPTION BANDS OF CO_2 AT 5.2 AND 4.8 μ [3]

Band, μ	Isotopic variety	Transition	Center of band		E'', cm^{-1}	Molecular strength of band at 259°K, cm
			cm^{-1}	μ		
5.2	$C^{12}O_2^{16}$	000—03^{1}0	1932.45	5.17	0	$2.4 \cdot 10^{-21}$
4.8	$C^{13}O_2^{16}$	000—11^{1}0	2037.08	4.90	0	$4.0 \cdot 10^{-22}$
	$C^{12}O_2^{16}$	000—11^{1}0	2076.86	4.81	0	$3.2 \cdot 10^{-20}$
	$C^{12}O_2^{16}$	01^{1}0—12^{2}0	2093.35	4.77	667.40	$2.0 \cdot 10^{-21}$
	$C^{12}O_2^{16}$	01^{1}0—200	2129.79	4.69	667.40	$8.0 \cdot 10^{-22}$

TABLE 2.13. ABSORPTION BAND OF CO_2 AROUND 2.7 μ [3]

Isotopic variety	Transition	Center of band		E'', cm^{-1}	Molecular strength of band at 259°K, cm
		cm^{-1}	μ		
$C^{12}O_2^{16}$	000—02^{0}1	3613.03	2.76	0	$1.0 \cdot 10^{-18}$ (1.4×10^{-18})
—	000—101	3714.56	2.69	0	$1.3 \cdot 10^{-18}$ ($2 \cdot 10^{-18}$)
—	01^{1}0—03^{1}0	3580.81	2.79	667.40	—
—	01^{1}0—11^{1}1	3723.05	2.68	667.40	—
$C^{13}O_2^{16}$	000—02^{0}1	3527.70	2.83	0	$1.1 \cdot 10^{-20}$
—	000—101	3632.92	2.75	0	$1.4 \cdot 10^{-20}$
—	01^{1}0—03^{1}1	3498.72	2.85	667.40	—

The fundamental vibrational-rotational absorption band of $C^{12}O_2^{16}$ at ν_3 = 2349.16 cm^{-1} causes very strong absorption in the atmosphere in the 4.3-μ region. This band is overlapped by two others: the fundamental band of the molecule $C^{13}O_2^{16}$ at ν_3 = = 2283.48 cm^{-1} and the combination-frequency band $\nu_1 + \nu_3 - 2\nu_2$ /77 (02°0-10°1) centered around 2429.37 cm^{-1}. Together, these bands form a region of the absorption spectrum that is usually called the 4.3-μ CO_2 band in the literature. All of these bands are parallel and, consequently, do not have Q branches. The 4.3-μ band is so narrow and its strength so great that up to a height on the order of 20 km the solar radiation is completely absorbed in a vertical column of atmosphere in a region extending approximately from 4.2 to 4.4 μ.

In addition to these 15.0- and 4.3-μ bands, in which the absorption is due chiefly to the fundamental vibrational-rotational bands ν_2 and ν_3 of the $C^{12}O_2^{16}$ molecule, carbon dioxide has bands /78 centered around 10.4, 0.4, 5.2, 4.8, 2.7, 2.0, 1.6, and 1.4 μ and

TABLE 2.14. ABSORPTION BANDS OF CO_2 AROUND 2.0, 1.6, and 1.4 μ [3]

Band, μ	Isotopic variety	Transition	Center of band		E'', cm^{-1}	Molecular strength of band at 259°K, cm
			cm^{-1}	μ		
2.0	$C^{12}O_2^{16}$	00^00-04^01	5100	1.96	0	$1.6\cdot10^{-20}$
	$C^{12}O_2^{16}$	00^00-12^01	4978	2.00	0	$3.7\cdot10^{-20}$
	$C^{12}O_2^{16}$	00^00-20^01	4853	2.06	0	$1.0\cdot10^{-20}$
	$C^{12}O_2^{16}$	01^10-05^10	5132	1.94	667.40	—
	$C^{12}O_2^{16}$	01^10-13^11	4965	2.01	667.40	—
	$C^{12}O_2^{16}$	00^10-21^11	4808	2.07	667.40	—
	$C^{13}O_2^{16}$	00^00-04^01	5046	1.98	0	$1.8\cdot10^{-22}$
	$C^{13}O_2^{16}$	00^00-12^01	4887	2.04	0	$4.1\cdot10^{-22}$
	$C^{13}O_2^{16}$	00^00-20^01	4748	2.10	0	$1.1\cdot10^{-22}$
	$C^{12}O^{16}O^{18}$	00^00-04^01	5042	1.98	0	$7\cdot10^{-23}$
	$C^{12}O^{16}O^{18}$	00^00-12^01	4905	2.03	0	$1.5\cdot10^{-23}$
	$C^{12}O^{16}O^{18}$	00^00-20^01	4791	2.08	0	$4\cdot10^{-23}$
1.6	$C^{12}O_2^{16}$	00^00-06^01	6503	1.53	0	—
	$C^{12}O_2^{16}$	00^00-14^01	6350	1.57	0	—
	$C^{12}O_2^{16}$	00^00-22^01	6228	1.60	0	$2.9\cdot10^{-22}$
	$C^{12}O_2^{16}$	00^00-20^01	6076	1.64	0	—
1.4	$C^{12}O_2^{16}$	00^00-00^03	6973	1.43	0	$8.6\cdot10^{-22}$

a series of weaker bands in the region from 1.24 to 0.78 μ. None of these bands is particularly broad (their widths are on the order of 0.1 μ).

Two parallel bands in the 10-μ region have vibrational frequencies of 1063.8 cm^{-1} (02^00-001 transition) and 961.0 cm^{-1} (100-001 transition). The bands for which data are given in Tables 2.12, 2.13, and 2.14 are responsible for the absorption around 1.4, 1.6, 2.0, 2.7, 5.2, and 4.8 μ.

In Tables 2.12, 2.13, and 2.14, the strengths of the bands were determined with respect to one CO_2 molecule with allowance for all of its isotopic varieties. /79

3. Ozone. The dipole moment of the O_3 molecule (Fig. 2.11) is 0.58D. The electronic transitions in the molecule give rise to the Hartley and Huggins bands in the ultraviolet (wavelengths shorter than 3400 Å) and the Chappuis bands in the 4500-7400-Å region (visible region). The maximum value of the absorption coefficient in the Chappuis bands is $5\cdot10^{-21}$ cm^2, so that only 7% of the solar radiation is absorbed at an atmospheric mass of two.

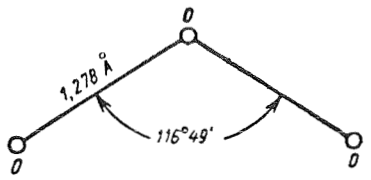

Figure 2.11. Structure of the Ozone Molecule.

TABLE 2.15. POSITIONS OF THE FUNDAMENTAL BANDS OF THE O_3 MOLECULE [3]

Band	O_3^{16}, cm^{-1}	$O^{16}O^{18}O^{16}$, cm^{-1}	$O^{16}O^{16}O^{18}$, cm^{-1}
ν_1	1110 (?)	1080	1095
ν_2	701.42	697	688
ν_3	1045.16	1008	1029
Percentage content	99.4	0.21	0.41

All three fundamental vibrational frequencies of the O_3 molecule are active in infrared absorption. They form vibrational-rotational bands centered at $\nu_1 = 1110\ cm^{-1}$ (9.1 μ), $\nu_2 = 710\ cm^{-1}$ (14.1 μ), and $\nu_3 = 1043\ cm^{-1}$ (9.6 μ). The ν_1 band is very weak and overlaps the ν_3 band. The overlap gives rise to strong interaction between the corresponding molecular energy levels.

Three isotopic modifications of the ozone molecule are detected in the atmosphere: O_2^{16}, $O^{16}O^{18}O^{16}$, and $O^{16}O^{16}O^{18}$ (Table 2.15).

The harmonics and combination vibrational frequencies of O_3 /80 produce vibrational-rotational bands in the 2.7, 3.27, 3.59, 4.75, and 5.75-μ regions, of which the strongest is the 4.75-μ band. All of these bands are on the order of 0.1 cm^{-1} in width.

Normally, only the absorption of the 9.6-μ O_3 band, which occurs in the center of the long-wave 8-13-μ atmospheric transparency "window," is taken into account in study of the absorption of solar radiation by the earth's atmosphere. In a vertical column of atmosphere, a central region of this band about 1.0 μ in width absorbs approximately half of the solar radiation. The other bands are either overlapped by stronger H_2O or CO_2 absorption bands or are of low strength. The 9.6-μ band is very rich in fine-structure lines that have not yet been resolved experimentally. Experiment has yielded the molecular constants for the excited vibrational state. These constants, together with those of the ground state, which have been determined from the purely rotational microwave spectrum of O_3, enable us to calculate the fine structure of the band.

The O_3 molecule has a strong purely rotational spectrum in the microwave region.

4. Oxygen. Oxygen occurs in the molecular and atomic states in the atmosphere. Atomic oxygen is formed as a result of dissociation of molecular oxygen under the action of solar ultraviolet radiation. This dissociation produces the atoms that go

TABLE 2.16. RED BANDS OF THE O_2^{16} MOLECULE [3]

Transition	Center of band, μ	Strength of band, * cm	Characterization of band strength in solar spectrum**
0.0	0.7621	$4.3 \cdot 10^{-22}$	s
0.1	0.6884	$2.0 \cdot 10^{-23}$	s
0.2	0.6288	$5.1 \cdot 10^{-25}$	ms
0.3	0.5796	$2.0 \cdot 10^{-26}$	ms
0.4	0.5384	$8.1 \cdot 10^{-28}$	—
1.1	0.7710	$2.7 \cdot 10^{-27}$	ls
1.2	0.6970	$2.3 \cdot 10^{-28}$	ls
1.3	0.6379		ms

*The band strengths are referred to the number of molecules in the initial state.
**s stands for a strong band, ms for a band of medium strength, and ls for a band of low strength.

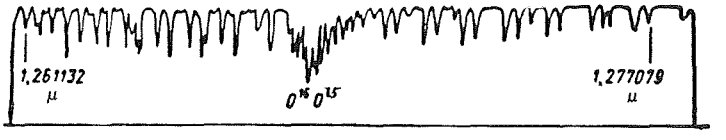

Figure 2.12. Solar Spectrum in the Region of the O_2^{16} Absorption Band at 1.2683 μ [63].

into production of ozone.

Atomic oxygen has no allowed electronic dipole-radiation transitions in the visible and infrared. A series of forbidden transitions produces a solitary line at 5571 Å and a multiplet in the 6300-6364-Å region. These lines are weak ones, and need be taken into account only in study of the luminescence of the upper atmospheric layers.

Molecular oxygen has strong electronic bands in the ultraviolet and relatively weak ones in the red and near infrared regions (Table 2.16).

The O_2^{16} molecule has two conspicuous bands in the near infrared, centered around 1.2683 μ (0-0 transition) (Fig. 2.12) and 1.0674 μ (0-1 transition). /81

Owing to the symmetry of the O_2^{16} molecule, only lines with alternating values of the rotational quantum number j appear in its band spectra.

The molecule of the isotopic oxygen modification $O^{16}O^{18}$ has bands in the red region around 0.7620 μ (0-0 transition), 0.6901 μ (0-1 transition), and 0.6317 μ (0-2 transition). These bands contain lines with all values of j owing to the diminished symmetry of the $O^{16}O^{18}$ molecule as compared with O_2^{16}.

In addition to these molecular electronic bands, oxygen also /82 has diffuse bands in the ultraviolet, visible and near infrared regions due to the molecular complexes $[O_2]_2$. The spectra of these complexes are studied in the papers of Dufay [64] and V.I. Dianov-Klokov [65]. The band strengths of the complexes are moderate. They are also overlapped by the stronger ozone and water-vapor bands. It appears that allowance for absorption in the $[O_2]_2$ bands may be necessary only in occasional special cases (for example, for nearly horizontal slant-path propagation).

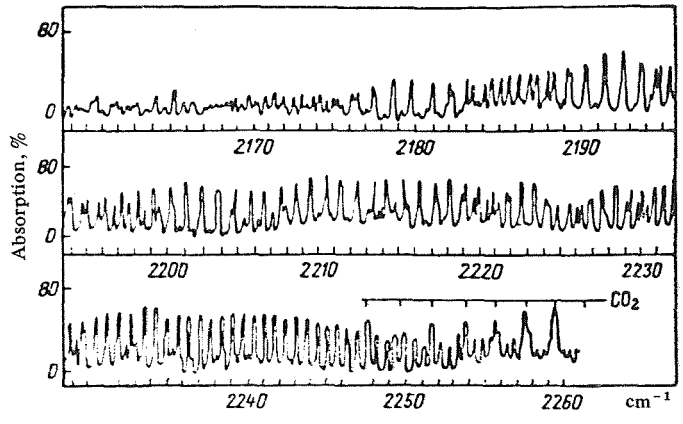

Figure 2.13. Spectrum of ν_3 Band of N_2O Molecule Recorded Using a Cuvette 15 cm Long at an N_2O Partial Pressure of 10 mm Hg [3]. Lines from the combination $\nu_3 + \nu_2 - \nu_2$ and several CO_2 absorption lines also fall into the region of the ν_3 band.

5. Nitrous oxide. The molecule of nitrous oxide N_2O is an asymmetrical linear molecule whose dipole moment and rotational constant are 0.166D and 0.4182 cm^{-1}, respectively, for the basic isotopic modification $N_2^{14}O^{16}$.

TABLE 2.17. N_2O BANDS IN THE SOLAR SPECTRUM [3]

Center of band		Transition	Type	Molecular strength of band under standard conditions, cm
cm^{-1}	μ			
4730.86	2.11	$00^00—20^01$	Parallel	—
4630.31	2.16	$00^00—12^01$	»	—
4417.51	2.27	$00^00—00^02$	»	—
4389.06	2.28	$01^10—01^12$	»	—
3481.2	2.87	$00^00—10^01$	»	$1.29 \cdot 10^{-18}$
3365.6	2.97	$00^00—02^01$	»	—
2798.6	3.57	$00^00—01^11$	Perpendicular	$9 \cdot 10^{-20}$
2577	3.88	$01^10—21^10$	Parallel	—
2563.5	3.90	$00^00—20^00$	»	$1.6 \cdot 10^{-18}$
2461.5	4.06	$00^00—12^00$	»	$4.3 \cdot 10^{-19}$
2223.5	4.50	$00^00—00^01$	»	$6.88 \cdot 10^{-17}$
2210	4.52	$01^10—01^11$	»	—
1285.0	7.78	$00^00—10^00$	»	$9.78 \cdot 10^{-18}$
1167.0	9.56	$00^00—02^00$	»	$4.08 \cdot 10^{-19}$
588.8	17.0	$00^00—01^10$	Perpendicular	$7.75 \cdot 10^{-19}$

The strong electronic bands of N_2O appear in the far ultraviolet.

All three fundamental vibration frequencies $\nu_1 = 1285.6$ cm^{-1} (7.8 μ), $\nu_2 = 288.8$ cm^{-1} (17.0 μ), and $\nu_3 = 2223.5$ cm^{-1} (4.6 μ) (Fig. 2.13) are active in the infrared spectra.

The N_2O molecule has many harmonic, combination-frequency, and higher-state bands. Thus, there are 23 bands in the frequency region above 8000 cm^{-1}, 18 between 4417 and 1880 cm^{-1}, 14 between 4062 and 7431 cm^{-1}, and 7 between 2209.53 and 2798.30 cm^{-1}, not counting higher-state bands [3]. Most of these bands are very weak. Nine bands, certain data on which are given in Table 2.17, appear in the solar spectrum. /83

The N_2O molecule has 12 stable isotopes, which are formed by combinations of N^{14}, N^{15}, O^{16}, O^{17}, and O^{18} atoms. The vibrational-rotational spectrum of the basic isotopic modification $N_2^{14}O^{16}$ and those of some of the isotopes have been studied in greater or lesser detail.

6. Methane. The molecule of methane CH_4 is tetrahedral. CH_4 has electronic bands in the far ultraviolet (wavelengths shorter than 1450 Å). The molecule's high degree of symmetry causes strong degeneration of the vibrational energy levels. Of the 9 /84

TABLE 2.18. BANDS OF METHANE IN THE SOLAR SPECTRUM [3]

Center of band		Transition	Molecular strength of band under standard conditions, cm
cm^{-1}	μ		
6005	1.67	0000—0020	$3.6 \cdot 10^{-20}$
5861	1.71	0000—1101	—
5775	1.73	0000—0111	—
4420	2.20	0000—0110	—
4313	2.32	0000—0011	—
4216	2.37	0000—1001	—
4123	2.43	0000—0102	—
3019	3.31	0000—0010	$1.26 \cdot 10^{-17}$
3823	3.55	0000—0101	—
2600	3.85	0000—0002	$1.04 \cdot 10^{-17}$
1306	7.66	0000—0001	$6.9 \cdot 10^{-18}$

fundamental frequencies, one is doubly degenerate and two are triply degenerate. Thus, the molecule is found to have only four fundamental vibrations with different frequencies. The ν_1 band is fully symmetrical, ν_2 is double degenerate, and ν_3 and ν_4 are triply degenerate. The only bands that appear in the infrared are $\nu_3 = 3020.3$ cm^{-1} (3.3 μ) and $\nu_4 = 1306.2$ cm^{-1} (7.7 μ). The vibrational frequencies of the optically inactive bands ν_1 and ν_2 are 2914.2 and 1526 cm^{-1}, respectively. The vibration frequencies of the first harmonic of the ν_2 band and the ν_1 and ν_3 bands are closely similar. Overlapping of these three bands results in strong interaction among the vibrational-rotational transitions. This interaction eliminates the degeneracy of the fundamental ν_3 and ν_4 bands and greatly complicates the fine structure of the spectrum.

In addition to the two fundamental vibrational-rotational bands, methane has many harmonics and combination frequencies (Table 2.18), of which 9 are found in the solar spectrum.

TABLE 2.19. CENTER POSITIONS OF CO BANDS [66]

Band	1—0	2—0	3—1	4—2	5—3	6—4	7—5	3—0	4—0
Calculation, cm^{-1}	2143, 2740	4260, 0646	4207, 1664	4154, 4056	4101, 7820	4049, 2958	3996, 9466	6350, 4404	8414, 4702
Observation, cm^{-1}	2143, 2740	4260, 0646	4207, 1680	4154, 4040	—	—	—	6350, 436	8414, 458

/85

Methane does not have a purely rotational spectrum.

7. Carbon monoxide. In virtue of its simplicity, the spectrum of carbon monoxide has been studied in rather great detail. This molecule has a dipole moment of 0.1D. The purely rotational spectrum lies in the far infrared and microwave regions.

The fundamental vibrational-rotational band of the $C^{12}O^{16}$ molecule occurs at around 2143.2 cm^{-1} (4.67 μ). The first harmonic of the band is centered around 4260 cm^{-1}.

Table 2.19 gives the center positions of the various CO bands as listed in [66].

The carbon monoxide molecule has two isotopic modifications: $C^{12}O^{16}$ and $C^{13}O^{16}$.

The fine structures of many vibrational-rotational CO bands have been quite thoroughly studied. The results of these researches will be examined in the next chapter.

Chapter 3 /86

ABSORPTION OF VISIBLE AND INFRARED WAVES IN A HOMOGENEOUS ATMOSPHERE

1. BASIC DEFINITIONS

1. Absorption coefficient. Optical thickness. Spectral Transmission (absorption). In our usage, the absorption coefficient $k(\nu)$ of a medium for radiation at frequency ν is the coefficient of proportionality in Bouguer's law, written in the differential form

$$dI(\nu) = -k(\nu) I(\nu) dl, \tag{3.1}$$

where $dI(\nu)$ is the attenuation of radiation of intensity $I(\nu)$ after passage through a thickness dl of the medium.

Integration of (3.1) with respect to the layer thickness l yields the well-known expression of Bouguer's law for a homogeneous medium:

$$I(\nu) = I_0(\nu) e^{-k(\nu)l}, \tag{3.2}$$

where $I_0(\nu)$ and $I(\nu)$ are the intensities of the radiation before and after passage through the thickness l of the medium.

The optical thickness τ of the layer l of the medium is the argument of the exponential in (3.2):

$$\tau = k(\nu) l. \tag{3.3}$$

The limits of applicability of (3.1) and (3.2) will be considered in §4.

The quantities

$$f(\nu) = \frac{I(\nu)}{I_0(\nu)}; \quad A(\nu) = \frac{I_0(\nu) - I(\nu)}{I_0(\nu)} \tag{3.4}$$

will be referred to as the spectral transmission and spectral absorption, respectively. /87

2. Absorption and transmission functions. Integral absorption. The absorption function A of radiation in a spectral interval $\Delta\nu = \nu_2 - \nu_1$ is the ratio of the radiation absorbed by the layer of medium to the radiation incident on this layer. The transmission function T is analogously defined.

In accordance with this definition, we may write

$$A = \frac{\int_{\nu_1}^{\nu_2} [I_0(\nu) - I(\nu)]\, d\nu}{\int_{\nu_1}^{\nu_2} I_0(\nu)\, d\nu}; \quad T = \frac{\int_{\nu_1}^{\nu_2} I(\nu)\, d\nu}{\int_{\nu_1}^{\nu_2} I_0(\nu)\, d\nu}. \tag{3.5}$$

For a homogeneous layer, we apply (3.4) to (3.5) to obtain

$$A = \frac{\int_{\nu_1}^{\nu_2} I_0(\nu) A(\nu)\, d\nu}{\int_{\nu_1}^{\nu_2} I_0(\nu)\, d\nu}, \quad T = \frac{\int_{\nu_1}^{\nu_2} I_0(\nu) f(\nu)\, d\nu}{\int_{\nu_1}^{\nu_2} I_0(\nu)\, d\nu}. \tag{3.6}$$

As we see from (3.6), the absorption and transmission functions in the spectral interval $[\nu_1, \nu_2]$ characterize the average values of spectral absorption and spectral transmission in this interval.

In the particular case with $I(\nu) = \text{const} \in [\nu_1, \nu_2]$

$$A = \frac{\int_{\nu_1}^{\nu_2} A(\nu)\, d\nu}{\nu_2 - \nu_1}, \quad T = \frac{\int_{\nu_1}^{\nu_2} f(\nu)\, d\nu}{\nu_2 - \nu_1}, \tag{3.7}$$

or, applying (3.4) and (3.2),

$$A = \frac{1}{\nu_2 - \nu_1} \int_{\nu_1}^{\nu_2} (1 - e^{-k(\nu)l})\, d\nu;$$
$$T = \frac{1}{\nu_2 - \nu_1} \int_{\nu_1}^{\nu_2} e^{-k(\nu)l}\, d\nu. \tag{3.7a}$$

In another particular case, in which $k(\nu) = \text{const} \in [\nu_1, \nu_2]$,

$$A = A(\nu); \quad T = f(\nu). \tag{3.8}$$

The functions A and T depend [see (3.5) and (3.6)] not only on the absorbing properties of the medium, which are expressed by $A(\nu)$ or $f(\nu)$, but also on the spectral radiant flux density of the source, $I_0(\nu)$. Hence to characterize those absorbing properties of a medium in a given spectral interval $[\nu_2, \nu_1]$ that do not depend on the function $I_0(\nu)$, the notion of the integral absorption B is introduced; it is the value of the integral /88

$$B = \int_{\nu_1}^{\nu_2} A(\nu)\, d\nu. \tag{3.9}$$

It is easily seen that the maximum integral absorption occurs at $A(\nu) = 1$ over the entire spectral range and equals $\Delta\nu = \nu_2 - \nu_1$. The integral absorption is expressed in frequency units and can be regarded as the width of a certain spectral interval in which the integral absorption equals a given value for $A(\nu) = 1$. In this sense, the integral absorption is often known as the equivalent width of the interval (line, band, etc.) in question.

Expressions (3.1)-(3.9) were derived for the case in which the frequency ν is taken as the spectral corrdinate. Formally identical formulas are obtained if the wavelength λ is used as the spectral coordinate.

Bearing in mind the relation between ν and λ:

$$\nu[\mathrm{cm}^{-1}] = 10^4/\lambda[\mu], \tag{3.10}$$

it can be shown that (3.5) and (3.6), written in terms of ν and λ with (3.10), give the same numerical values of A and T. However, Formulas (3.7) are not equivalent when expressed in terms of ν and λ, i.e.,

$$\begin{aligned} \frac{\int_{\nu_1}^{\nu_2} A(\nu)\, d\nu}{\nu_2 - \nu_1} &\neq \frac{\int_{\lambda_1}^{\lambda_2} A(\lambda)\, d\lambda}{\lambda_2 - \lambda_1}; \\ \frac{\int_{\nu_1}^{\nu_2} f(\nu)\, d\nu}{\nu_2 - \nu_1} &\neq \frac{\int_{\lambda_1}^{\lambda_2} f(\lambda)\, d\lambda}{\lambda_2 - \lambda_1}. \end{aligned} \tag{3.11}$$

The smaller the spectral interval $[\nu_1, \nu_2]$ or the equivalent $[\lambda_1, \lambda_2]$, the weaker does inequality (3.11) become. In the limit as /89

$\nu_2 - \nu_1 \to 0$ or $\lambda_2 - \lambda_1 \to 0$, $A(\nu) = A(\lambda)$ and $T(\nu) = f(\lambda)$.

We note that (3.10) is rigorously valid for a vacuum. When radiation propagates in a medium with a refractive index $n \neq 1$, it is necessary to take account of the dependence $\lambda = \lambda_0 n^{-1}$, where λ and λ_0 are the wavelength in the medium and in vacuum, respectively.

We stress that the expressions for the absorption and transmission functions, (3.7) and (3.7a), are often written in the literature without the stipulation that they are valid only for the case in which the frequency dependence of the incident radiant intensity can be disregarded within the spectral interval $\Delta\nu = \nu_2 - \nu_1$. In practice, these expressions can be used to calculate the absorption functions of radiation from thermal sources in narrow spectral regions (of the order of 0.1 μ wide).

2. ABSORPTION BY A SINGLE LINE

The absorption spectrum of any isolated molecule presents a set of individual spectral lines whose positions, strengths, and shapes are uniquely determined by the corresponding quantum changes in the electronic, vibrational, and rotational energies of the molecule. Thus, the spectral line is the basic element in the spectrum of a molecule. This is why the numerous papers whose results are generalized in the series of monographs and reviews [67-71] have been devoted to study of the absorption behavior of the individual spectral line. We have considered some aspects of single-line absorption in Chapter 2. Here we shall dwell only on a few problems that are prerequisites to exposition and understanding of the material that follows.

1. Line contour shape. As we have already noted, the shapes of absorption-line contours are determined under the conditions of the earth's atmosphere by the finiteness of the molecule's excited-state lifetime, the Doppler effect, and effects of collisions of molecules of the absorbing gas with one another and with molecules of nonabsorbing or extraneous gases. Formulas describing the line contour due to a particular effect or combination of effects were given above [see (2.55), (2.57), and (2.64)].

Strictly speaking, none of these formulas can pretend to exact description of the line contour under real atmospheric conditions. It is therefore very important to know the cases in which and the accuracy with which a given expression can be used to describe the true line contour. /90

The requirements as to the accuracy with which the real line contour shape is described depend strongly on the nature of the particular problem. For example, suppose that we have to determine the integral absorption function in a very broad spectral interval for a black or gray radiator. In this case, the accuracy

requirements for the shapes of individual lines are less stringent, since both the central part of the line and its limbs will contribute to the integral absorption. If, on the other hand, we must know the absorption function in a relatively narrow interval that contains only the central parts of certain lines or, conversely, includes only the limbs of widely spaced lines, the distribution of the energy absorbed by the line at the center and in the limbs now becomes very important. Finally, the accuracy of line-contour description is subject to the most rigid requirements when the absorption of monochromatic radiation in the atmosphere is to be determined.

In the overwhelming majority of studies of the absorption of visible and infrared waves in the atmosphere, use is made of the dispersion or Lorentz line contour. This is because the dispersion contour, though quite simple, gives an adequate description of the center of the line at heights averaging up to 30 km, where the basic mass of the gases that absorb in the visible and infrared regions is concentrated [1].

New problems in the solution of which the dispersion contour either does not give the required accuracy or cannot be used have arisen in recent years. These are for the most part problems related to the use of lasers in various systems designed to work through the atmosphere, inverse problems of satellite meteorology, and problems requiring more accurate calculation of radiant fluxes in the atmosphere. To solve these problems, it is necessary to have data on the contour of the central part of the line at the heights at which the Doppler effect can no longer be neglected as compared to the collision broadening of the lines. The dispersion /91
contour is definitely not valid for description of the true absorption in the far limbs of lines. Let us briefly consider the results of investigations of the Lorentz-Doppler contour and shape of the remote limbs of lines.

A theoretical study by S.G. Rautian and I.I. Sobel'man [72] examined various cases of line contours governed by the combination of the Doppler and Lorentz effects. These effects are regarded both as statistically independent and statistically dependent. It was shown in [72] that the real contour of a line should have less intense limbs than the Lorentz contours. In the limbs, line strength diminishes in proportion to the fourth power of frequency rather than the second, as would follow from the dispersion contour.

For statistically dependent line broadening due to the Doppler and Lorentz effects, the authors of [72] obtained asymmetrical line contours that were shifted from the center.

Drayson [62] calculated the integral absorption of a line for Lorentz and Lorentz-Doppler contours. Various values of the product $S\omega$, where S is the line strength and ω is the precipitated layer of absorbing gas, were used in the calculation. It was

found that for the average values of $S\omega$, the integral absorption of a line with a mixed contour at low pressures (great heights in the atmosphere) may exceed the integral absorption of the Lorentz-contour line by a factor of more than two. Thus, as the pressure changes from 100 to 0.5 mbar (heights from 16 to 55 km), the error due to disregard of the Doppler effect in calculation of the integral absorption of the line varies from 0.05 to 60%. This error is about 5% at a pressure of 10 mbar (heights 30 km). It was shown in Plass and Fivel's paper [73] that for the extreme cases of small and large $S\omega$, the Doppler effect can be disregarded up to 50 km in calculating the integral absorption of a line.

Thus, it follows from [62] that in calculating the integral absorption for individual lines and, consequently, groups of lines, the Doppler effect need not be taken into account up to 30 km to obtain accuracy no worse than 5%. We stress that this conclusion pertains to determination of integral line absorption and cannot be extended to calculation of the absorption of monochromatic radiation in the atmosphere. Methods of calculating the absorption coefficient for a spurious line contour are examined in [74-77]. /92

Winters, Silverman, and Benedict [78] published the results of experimental studies of absorption in the 4.3-μ CO_2 band. Analysis of the results indicated that beyond 5 cm^{-1} from the line center, the absorption coefficient $k(\nu)$ diminishes more rapidly than the dispersion contour indicates. The authors of [78] proposed the following empirical expression for $k(\nu)$, which describes the results of their experiment satisfactorily:

$$k(\nu)=\left(\frac{\gamma}{\pi}\right)[(\nu-\nu_i)^2+\gamma^2]\,e^{-a(|\nu-\nu_i|-\Delta\nu_0)^b};\ |\nu-\nu_i|>\Delta\nu_0, \qquad (3.12)$$

where γ is the half-width of the line, a and b are empirical constants that depend on the species of the broadening gas, and, according to Benedict's estimates, the quantity $\Delta\nu_0$ does not exceed 3 cm^{-1}.

Murcray et al. [79] measured the spectral absorption of solar radiation in the 4.3-μ band at heights from 10 to 30 km with 0.5 cm^{-1} resolution. When the calculation was applied, this resolution was found to be sufficient to permit line-to-line interpretation of the spectrum. When the calculated results were compared with experimental data, the agreement was found to be satisfactory if the Lorentz contour was used at high altitudes and the contour (3.12) proposed by Benedict for lower altitudes. The latter was used in calculating the high-frequency limb of a band.

Burch et al. [80, 81] made experimental studies of spectral absorption by water vapor and carbon dioxide in the wavelength

range from 0.6 to 5.5 μ. Analysis of the results led the authors to the conclusion that one of the existing expressions for the contour shape of the far limbs of a line is suitable for accurate description of the experimental data. The experiment indicated that the shapes of the far limbs are different for H_2O and CO_2 and depend, for a given absorbing gas, on the absorption band, the extraneous gas, and the temperature.

Thus, while the central part of a line is more or less satisfactorily described by the existing formulas for line contours, this is by no means the case for the remote limbs of the line. A new effort on the part of the theoreticians is needed here. Analysis of the available experimental data indicates that the formulas for the far limbs must take account of the absorbing and extraneous gases, the properties of the absorption band, and the temperature dependence. /93

2. **Integral absorption and absorption function of a single line.** An expression for the integral absorption of an isolated nonoverlapping line with a dispersion contour was obtained in the well-known paper of Ladenberg and Reiche [82]:

$$B=\int_{-\infty}^{+\infty} A(\nu)\,d\nu = 2\pi\gamma f(x); \qquad (3.13)$$
$$f(x)=xe^{-x}[J(x)+J_1(x)],$$

where

$$x=\frac{S\omega}{2\pi\gamma},$$

$J_0(x)$ and $J_1(x)$ are zeroth- and first-order Bessel functions of a purely imaginary argument and ω is the mass of the absorbing gas, which is sometimes known as the precipitated layer of the gas. Values of the function f(x) have been tabulated for various x by Elsasser [83] and for x from 0.01 to 10 in the monograph of K.Ya. Kondrat'yev [84].

From (3.13), we obtain for the extreme cases

$$B=S\omega \quad \text{for} \quad x\ll 1, \qquad (3.14)$$
$$B=2\sqrt{S\gamma\omega} \quad \text{for} \quad x\gg 1. \qquad (3.15)$$

Given a constant intensity of the incident radiation $I(\nu)$ = = const within the spectral interval $\nu_2 - \nu_1$ occupied by the line, the absorption function for a single line of dispersion shape takes the form

$$A = \frac{\int_{\nu_1}^{\nu_2} (1 - e^{-k(\nu)\omega})\, d\nu}{\nu_2 - \nu_1}, \qquad (3.7a)$$

where $k(\nu)$ is determined by (2.57).

A general expression for the function A was obtained in [85]: /94

$$A = 1 - e^{-x(1+\cos 2\delta)} - \frac{e^{-x}}{2b} \sum_{n=0}^{\infty} \delta_n (-1)^n J_n(x) B_n(\delta), \qquad (3.16)$$

$$B_n(\delta) = -4n \left[\sum_{k=0}^{n} \delta_k (-1)^{n-k} \frac{\sin 2k\delta}{2k} - \frac{\sin 2(n-1)\delta}{2(n-1)} \right], \qquad (3.17)$$

$x = S\omega/2\pi\gamma$, S and γ are the strength and half-width of the line, ω is the mass of the absorbing gas, δ = arc tan b, $2b\gamma$ is the width of the spectral interval in which the function a is defined, and $J_n(x)$ is an n-th order Bessel function of an imaginary argument.

The following asymptotic values for A can be obtained from (3.16):

1) $x \ll 1$, $A = 2x\delta/b$; (3.18)

2) $x \gg 1$, $A = 1 - e^{-z^2} + \sqrt{\pi z}\,[1 - \Phi(z)]$; (3.19)

3) $b \gg 1$, $A = A_1 + A_2$, $A_1 = \frac{\pi}{b} x e^{-x} [J_0(x) + J_1(x)]$, (3.20)

$$A_2 = 1 - e^{-z^2} - \sqrt{\pi z}\,\Phi(z); \qquad (3.21)$$

4) $b \gg 1$, $x \ll 1$, $A = \frac{S\omega}{2\gamma b}$. (3.22)

In (3.19) and (3.21), $\Phi(z)$ is the error probability integral and the argument $z = \frac{1}{b}\sqrt{2x}$.

Let us compare the above asymptotic formulas for the absorption functions with the corresponding formulas for the single-line integral absorption B [(3.14) and (3.15)].

As we see from comparison of (3.22) and (3.14), the expressions for A and B are identical but for a constant factor. This means that physical implications that proceed from analysis of one formula are applicable to the other. Thus, neither A nor B depends on pressure in this case.

Comparison of (3.19) and (3.15) for x >> 1 indicates that in this case the physical implications of the expression for the

integral line absorption cannot be used in examining the problem of the absorption function in a fixed spectral interval. For example, B is expressed in terms of the square root of the absorbing mass (the so-called square-root law for the single line), while A has a totally different expression and the square-root law cannot be used to describe the single-line absorption function at large x (large ω or low pressures). /95

We note in conclusion that neither the absorption function A nor the integral absorption B of a single line depends on pressure at $x \ll 1$ with sufficiently large B, when arc tan b can be replaced by $\pi/2$ [see (3.18), (3.22), and (3.14)]. For $x \gg 1$, the mass ω of the absorbing gas and the pressure P figure equally in the corresponding expressions for A and B [see (3.19) and (3.15), which contain the half-widths $\gamma = \gamma^0 P$].

3. ABSORPTION BY GROUPS OF OVERLAPPING LINES

The spectra of all atmospheric gases consist of groups of overlapping lines. Depending on the source of the radiation whose absorption in the atmosphere must be determined, the overlap of the lines must be considered either for specific wavelengths (for example, in the case of gas lasers) or in certain spectral intervals. In the former case, it is necessary to know the absorption coefficients with which the spectral absorption can be determined; in the latter case, the absorption functions are determined.

One of three approaches is used to find the absorption functions: 1) one based on consideration of the absorption at the particular frequency of each spectral line; 2) one based on the spectrum-model formulas; 3) experimental determination of the appropriate variables under natural or laboratory conditions. Let us consider each of these approaches.

1. Direct calculation of absorption functions. For the case in which the pressure is constant along the ray path and the intensity of the incident radiation is constant in the interval $[\nu_1, \nu_2]$, the absorption function for a group of overlapping lines (a band) occupying the spectral interval $[\nu_1, \nu_2]$ takes the form

$$A = \frac{1}{\nu_2 - \nu_1} \int_{\nu_1}^{\nu_2} (1 - e^{-k(\nu)\omega})\, d\nu, \tag{3.23}$$

where /96

$$k(\nu) = \sum_i S_i b_i(\nu); \tag{3.24}$$

$b_i(\nu)$ is the contour of the i-th line normalized to unity. In

this last formula, the summation extends over all lines contributing to absorption of radiation at frequency ν.

If we assume that all lines contributing to this absorption have dispersion contours, we obtain from (3.24)

$$k(\nu)=\sum_i S_i \frac{\gamma_i}{\pi} \frac{1}{(\nu-\nu_{0i})^2+\gamma_i^2}. \qquad (3.25)$$

Thus, direct calculation of the absorption functions requires knowledge of the center positions, strengths, and half-widths of all lines that may contribute to the absorption of radiation in the spectral interval of interest. Calculation and experimental determination of the atmospheric-gas line parameters is an extremely complex task. Only during the last few years has appreciable progress been made in this problem. There have been several publications in which direct calculations of absorption functions are presented for certain atmospheric-gas bands, and a number of papers have been devoted to experimental determination of the line parameters. We shall discuss these studies when we deal with concrete research results for certain atmospheric gases in the sections that follow. Here we should stress only that, despite considerable mathematical and computational difficulties, direct calculation of the absorption functions is unquestionably of high promise, since it yields the most universal data with no restrictions on the width of the spectral interval for which the absorption function must be known.

In conclusion, we take note of the approximate method of direct absorption-function calculation proposed in our work [86].

The formula obtained for the absorption function is general in nature and can be used to calculate the absorption of radiation in various narrow segments of the spectrum in which the absorption lines can be described by the dispersion contour with constant half-width. What is important is that this formula takes account of absorption in the given interval by lines whose centers are located outside this interval. /97

2. **Method of absorption-spectrum models.** The direct calculation of the absorption functions is quite laborious and cannot always be carried out owing to inadequacy of data on the parameters of individual lines in the absorption spectra of atmospheric gases. This has resulted in widespread use of the spectrum-model method to calculate absorption functions. In this method, the spectra of the atmospheric gases are modeled by a certain set of hypotheses as to the distribution and strengths of the lines. The dispersion line contour is assumed in all models, and the half-widths of all lines are assumed to be the same. Let us briefly examine the basic models that are in use for calculation of

atmospheric-gas absorption functions (this problem is set forth in greater detail in the monograph of R. Goody [3] and our paper [88]).

1. The absorption function in the Elsasser model. This model assumes equal line strengths S, equal half-widths γ, and uniform line spacing d within the segment of the spectrum under consideration. If this segment is wide enough so that the number of lines in it can be considered large, the following expression can be obtained for the absorption coefficient:

$$k(\nu)=\frac{S\,\mathrm{sh}\,\beta}{d}\,\frac{1}{\mathrm{ch}\,\beta-\cos t}, \quad t=\frac{2\pi\nu}{d}; \quad \beta=\frac{2\pi\gamma}{d}. \tag{3.26}$$

Substituting (3.26) into (3.23) and manipulating, we obtain

$$A=\mathrm{sh}\,\beta\int_0^{x'} e^{-\xi\,\mathrm{ch}\,\beta}J_0(\xi)\,d\xi, \tag{3.27}$$

$$x'=\frac{S\omega}{d\,\mathrm{sh}\,\beta}, \tag{3.28}$$

where $J_0(\xi)$ is a zeroth-order Bessel function of a purely imaginary argument.

Integration within the limits indicated means that A is calculated in the spectral interval occupied by one line. However, /98 when we remember that $k(\nu)$ is a periodic function with period d in this model, the value of A for any spectral interval containing n lines will also be determined by (3.27).

The following expression for the absorption function can be derived from (3.27) [88]:

$$A=\mathrm{sh}\,\beta x'e^{-x'\,\mathrm{ch}\,\beta}J_0(x')-\mathrm{th}\,\beta x'e^{-x'\,\mathrm{ch}\,\beta}J_1(x')+\frac{\mathrm{sh}^3\beta}{\mathrm{ch}\,\beta}\int_0^{x'}\xi e^{-\xi\,\mathrm{ch}\,\beta}J_0(\xi)\,d\xi. \tag{3.29}$$

For the atmosphere, $\beta \ll 1$ (the distance between lines is much greater than their half-widths). For this case, we obtain from (3.29)

$$A=\beta x e^{-x(1+\beta^2/2)}[J_0(x)+J_1(x)]+\beta^3\int_0^{x}\xi e^{-\xi(1+\beta^2/2)}J_0(\xi)\,d\xi, \tag{3.30}$$

$$x=\frac{\omega S}{2\pi\gamma}. \tag{3.31}$$

Let us examine the asymptotic expressions for A that follow from (3.30):

1) $x \ll 1$. Series expansion of (3.30) yields

$$A = \beta x = \frac{S}{d}\omega. \tag{3.32}$$

In this case, the absorption function does not depend on pressure. It should be noted that (3.32) can also be obtained directly from (3.29), and, consequently, that the inference drawn here is independent of β.

2) $x \gg 1$. Use of the asymptotic representations of the Bessel functions for large values of the argument leads in this case to the relation

$$A = \Phi\left(\sqrt{\frac{1}{2}\beta^2 x}\right) = \Phi\left(\frac{1}{2}\sqrt{\pi S \gamma \omega}\right) \tag{3.33}$$

It follows from this formula that the absorption function depends on the product ωP but not on ω and P taken separately. We stress that this conclusion pertains only to the case of $\beta \ll 1$.

3) $x \gg 1$ and $\beta^2 x \ll 1$ (practically nonoverlapping lines). /99
It follows directly from (3.33) that

$$A = \beta\sqrt{\frac{2x}{\pi}} = \frac{2}{d}\sqrt{\pi\gamma S\omega}. \tag{3.34}$$

4) $x \approx 1$. With this hypothesis, $\beta^2 x \ll 1$ and the expansion of the integral in (3.30) in powers of x gives

$$A = \beta x e^{-x}[J_0(x) + J_1(x)]. \tag{3.35}$$

We note that in [89] and [90], the expression of the square-root law (3.34) was obtained from the Elsasser model for the extreme case with $\omega \ll 1$ and $\beta \ll 1$. The error of this derivation was pointed out in our paper [88].

2. Absorption function in statistical model. The basic premise of the statistical model, which was first put forth by Goody [91], consists in the assumption of a random distribution, one subject to the laws of probability theory, of the line positions and strengths in the spectrum and equality of their half-widths. The

notion of the statistical model was further developed in the work of Plass [92], Godson [93], and Kaplan [94].

We note that the analytical expressions obtained in [91]-[94] actually give the value of the spectral absorption for a certain frequency and not the value of the absorption function. A correct mathematical analysis of the statistical model on the basis of a "mean measured absorption coefficient" was given by V.N. Sochnikov [95]. Below we present formulas for the function A in which the deficiency tolerated in [91-94] is eliminated.

In the case of the statistical model, the absorption function takes the following form for a rather broad interval $\nu_2 - \nu_1$ with equiprobable distribution of the lines:

$$A = 1 - \frac{1}{\nu_2 - \nu_1} \int_{\nu_1}^{\nu_2} d\nu \exp\left\{ -\frac{1}{\bar{d}} \int_{\nu_a}^{\nu_b} d\nu' \times \int_0^\infty Q(S)\left[1 - e^{-\frac{\omega S \gamma}{\pi} \frac{1}{(\nu-\nu')^2+\gamma^2}}\right] dS \right\}, \quad (3.36)$$

where Q(S) is the probability density function, normalized to unity, of the line-strength distribution, d is the average distance between lines, and $\nu_a - \nu_b = D$ is the interval the lines in which contribute to absorption in the segment $\nu_2 - \nu_1$ under consideration. /100

If we also assume that $|\nu_b - \nu_a| >> |\nu_2 - \nu_1|$

$$A = 1 - \exp\left\{ -\frac{1}{\bar{d}} \int_{-\infty}^{\infty} d\nu' \int_0^\infty Q(S)\left[1 - e^{-\frac{S\gamma\omega}{\pi} \frac{1}{\nu'^2+\gamma^2}}\right] dS \right\}. \quad (3.37)$$

Goody [91], examining the case in which

$$Q(S) = \frac{1}{\bar{S}} e^{-S/\bar{S}}, \quad (3.38)$$

where $\bar{S}$ is the average line intensity, obtained

$$A = 1 - \exp\left[-\frac{\bar{\beta}\bar{x}}{(1+2\bar{x})^{1/2}} \right], \quad (3.39)$$

where

$$\bar{x} = \frac{\bar{S}\omega}{2\pi\gamma}; \quad \beta = \frac{2\pi\gamma}{\bar{d}}. \quad (3.40)$$

Plass [92] and Godson [93] considered the case in which all lines have the same strength, i.e.,

$$Q(S)=\delta(S-\bar{S}_0), \tag{3.41}$$

and obtained

$$A=1-\exp\{\bar{\beta}\bar{x}_0 e^{-\bar{x}_0}[J_0(\bar{x}_0)+J_1(\bar{x}_0)]\}, \tag{3.42}$$

where

$$\bar{x}_0=\frac{\bar{S}_0\omega}{2\pi\gamma}. \tag{3.43}$$

Formula (3.39) has the following asymptotic expressions:

1) $\bar{x}\ll 1$,

$$A=\bar{\beta}\bar{x}=\frac{\bar{S}}{\bar{d}}\omega; \tag{3.44}$$

2) $\bar{x}\gg 1$,

$$A=1-\exp\left(-\sqrt{\frac{1}{2}\bar{\beta}^2\bar{x}}\right). \tag{3.45}$$

Formula (3.42) has analogous asymptotic representations, except that $\bar{x}$ must be replaced by $\bar{x}_0$ in (3.44) and by $4\bar{x}_0/\pi$ in (3.45). /101

As in the case of the Elsasser model, the absorption function does not depend on pressure at small $\bar{x}$ and depends on the product ωP at large $\bar{x}$.

Relations (3.38) and (3.41), which determine the line-strength distribution, are highly arbitrary. However, the calculations performed by V.N. Sochnikov [95] for a Boltzmann line-strength distribution showed that in this case the values of the function A practically coincide with those obtained from (3.39) and (3.42).

3. Absorption function in combined model. In this model, which was proposed by Kaplan [94] and Plass [92], it is assumed that all lines in the particular segment of the spectrum can be broken up into several groups within each of which they are equally spaced and have equal strengths and half-widths, i.e., are described by the Elsasser model. The groups themselves, on the other hand, are distributed randomly, like the lines in the statistical model.

In this case, the expression for A is written

$$A = 1 - \prod_{j=1}^{N} \operatorname{sh}\beta_j \int_{x_j}^{\infty} e^{-\xi \operatorname{ch}\beta_j} J_0(\xi)\, d\xi, \qquad (3.46)$$

where

$$\beta_j = \frac{2\pi\gamma}{d_j}; \quad x_j = \frac{S_j\omega}{d_j \operatorname{sh}\beta_j}; \qquad (3.47)$$

d_j is the distance between lines in the j-th group described by an Elsasser model with a line strength S_j and N is the number of groups.

The limit relations for $\beta_j << 1$ are obtained in much the same way as in the Elsasser model:

1) all $x_j << 1$,

$$A = \sum_{j=1}^{N} x_j\beta_j = \omega \sum_{j=1}^{N} S_j/d_j; \qquad (3.48)$$

2) all $x_j >> 1$,

$$A = 1 - \prod_{j=1}^{N} \left(1 - \Phi\sqrt{\tfrac{1}{2}\beta_j^2 x_j}\right); \qquad (3.49)$$

3) all x_j of the order of unity, /102

$$A = \prod_{j=1}^{N} \{1 - \beta_j x_j e^{-x_j}[J_0(x_j) + J_1(x_j)]\}. \qquad (3.50)$$

As in the preceding models, A is independent of pressure for small x_j, but the absorption function depends on the product ωP at large x_j.

4. Quasistatistical model. This model was proposed by Wyatt, Stull, and Plass [96] and is based on the same basic idea as the statistical model. The spectral interval $\Delta\nu$ in which the

absorption function must be determined is broken up into smaller intervals δ, within each of which the statistical model is employed. To a substantial degree, this method eliminates the basic shortcoming of the statistical model — the assumption that the line positions and strengths are randomly distributed within a particular interval. Actually, the smaller the spectral interval, the more valid should this hypothesis of the statistical model become.

Within each interval δ, the lines are divided into five strength groups, for each of which the spectral transmission at the center of the interval $f_i(\nu)$ is determined. Then a simple cross-multiplication of the values obtained for $f_i(\nu)$ gives the spectral transmission at the center of the interval δ, which is regarded as the mean spectral transmission of the interval. Knowing the mean spectral transmissions in the intervals δ, it is not difficult to find the transmission function in the broader interval Δ. This procedure permits quite correct allowance for the contributions made to absorption in the given spectral interval by lines centered outside the interval.

We note that the technique of breaking the spectral interval under study into small intervals with use of the statistical model was also applied in the work of V.N. Sochnikov [95, 97].

5. Certain general conclusions. Comparison of the basic formulas for the absorption function in these models indicates that the argument is in all cases

$$x = \frac{S\omega}{2\pi\gamma^0 P}, \qquad (3.51)$$

where S is the integral strength of the lines in the Elsasser model; $S = \bar{S}$ or $S = \bar{S}_0$ in the statistical model and $S = S_j$ in the combined model. /103

Depending on the magnitude of x, some simple asymptotic formula for the absorption function will be valid in each of the models. It is essential that the parameter x depends on the ratio ω/P and not on the pressure P or the mass of the absorbing gas ω taken separately.

In the case $x \ll 1$, the absorption function is independent of pressure in each of the spectrum models. It can be shown that the inequality $x \ll 1$ is equivalent to the condition $\omega k(\nu) \ll 1$ for all ν in the particular interval $\Delta\nu = \nu_2 - \nu_1$ [88]. The word "equivalent" is used here in the sense that both conditions lead to the same result.

For $x \gg 1$, the absorption function depends on $\sqrt{\omega P}$ in all models. It can be shown that the corresponding asymptotic formulas

derive from the general expression (3.23) for the absorption function for $(\nu - \nu_i)^2 >> \gamma^2$. The physical significance of this condition is that the magnitude of the integral in (3.23) is determined by integration over the segments occupied by the limbs of the lines.

Plass [98] considered the limits of applicability of the various absorption-function formulas in the case of the Elsasser, statistical, and combined models. Our numerical calculations showed that the transitional region between the asymptotic cases $x << 1$ and $x >> 1$ is relatively small. It can be assumed in approximation that the first type of dependence merges directly into the second type.

In all models, the absorption-function expressions contain such characteristics of the spectral lines falling in the interval of interest as the distance between them and their strengths and half-widths. At the present time, we have inadequate data, both theoretical and experimental, on these characteristics of the lines. Therefore the coefficients that appear in the formulas for the absorption functions and embody the parameters of the lines are usually regarded as fitting parameters in practical applications of the models and are determined from experimental data. Methods of determining these parameters for the statistical-model case were elaborated in detail by Godson [99, 100].

Another factor that limits the possibilities of the spectrum- /104
model method is the assumption of constant line width, i.e., neglect of the existing dependence of line half-width on rotational quantum number.

In spite of these shortcomings, calculations of absorption functions that make use of the model representations give accuracy that is satisfactory for practical purposes.

In addition to the simplicity of the calculations themselves the model method has another important advantage in that the calculations can be used for quantitative estimation of atmospheric infrared absorption for situations whose experimental realization is either impossible or would be so expensive and time-consuming that the cost of the experiments would be all out of proportion to the results (for example, study of propagation at high altitudes along either horizontal or slant paths, etc.). Another important feature of the model method is that it can be used to obtain formulas for the absorption function A in terms of elementary functions, so that the dependence of this function on its arguments can be analyzed in general form.

It must also be noted that because of the limited resolution of spectral instruments, it is not the spectral absorption $A(\nu)$ or transmission $f(\nu)$ that is measured in experimental studies, but the absorption (transmission) function in one or another spectral

interval, which depends on the parameters of the spectrometer.

Finally, the model-theory formulas may prove most helpful when direct-method absorption-function calculations are used. They can substantially reduce the volume of computational work after the center positions, strengths, and half-widths of the lines in the respective segments of the spectrum have been calculated by the direct method.

3. Experimental determination of absorption function. Numerous studies, the basic results of which will be examined below, have been devoted to experimental determination of the absorption functions of various atmospheric gases under laboratory and natural conditions. Here, however, we shall discuss the advantages and /105
disadvantages of experimental absorption-function determinations as compared with the mathematical methods considered above.

In experimental determination of the absorption functions, there is no need to take special account of line overlapping, since this is done automatically. The methods of absorption-function measurement are relatively simple, although this can by no means be said of the equipment used.

In addition to the complexity of the apparatus, the experimental method of finding absorption functions also has certain other shortcomings. Of these, the most important one is associated with the limiting resolution of spectral instruments, which distorts the true picture of the spectrum and gives rise to errors in the determination of absorption functions in relatively narrow spectral intervals (with widths smaller than that of the whole absorption band). In many cases, experimental determination of absorption functions is a very difficult task (for example, measurements of absorption functions on horizontal paths at various heights or along slant paths, when the end points of the measurement path are in the atmosphere).

In concluding our section on methods of absorption-function determination, we should note that each of the methods considered has both advantages and disadvantages and an equal right to exist. Development of any of the methods considered may bring closer the acquisition of sufficiently accurate quantitative data on the absorption functions of atmospheric gases in various segments of the visible and infrared regions.

4. LIMITS OF APPLICABILITY OF THE BOUGUER-BEER LAW

The definitions of the absorption coefficient $k(\nu)$ [see (3.1)] and the absorption functions A [see (3.7a)] assumed validity of the Bouguer-Beer law. The same assumption is made in the derivation of analytical expressions for the absorption functions in all spectrum models. Finally, validity of the Bouguer-Beer law is also usually assumed in the processing of experimental data. This

calls for a review of the limits of applicability of this law. Here a distinction should be drawn between the actual and apparent deviations from the law. We shall consider both types of deviations. /106

The Bouguer-Beer law was derived on the basis of two fundamental assumptions, which were subsequently analyzed theoretically by A.A. Gershun [101] and Strong [102]. To characterize these assumptions, let us write the law in the form

$$I(\nu) = I_0(\nu)\, e^{-k(\nu)cl}. \qquad (3.52)$$

It is assumed in the derivation of (3.52) that the absorption coefficient $k(\nu)$ depends neither on the intensity $I_0(\nu)$ of the incident radiation nor on the concentration c. The first assumption was tested experimentally by S.I. Vavilov [103], who demonstrated its validity as $I_0(\nu)$ varies through almost 20 orders for electronic transitions with short atomic excited-state lifetimes τ. In studies of electronic transitions with large τ, S.I. Vavilov found that the absorption coefficient depended on $I_0(\nu)$.

To the best of our knowledge, the dependence of the coefficient $k(\nu)$ on $I_0(\nu)$ has not been verified for vibrational-rotational transitions in the spectra of the atmospheric gases. However, certain conclusions can be drawn in this matter on the basis of the fact that the integral absorption figures calculated for solar radiation in the earth's atmosphere for specific lines and line groups without consideration of the dependence of $k(\nu)$ on $I_0(\nu)$ have agreed closely with experimental data, as in Houghton's work [104]. Similar results have been obtained in a number of other studies for broad spectral intervals that included whole absorption bands. This indicates that the dependence of $k(\nu)$ on $I_0(\nu)$ is immaterial for the lines and bands studied at values of $I_0(\nu)$ that are characteristic for the solar spectrum. No further definite conclusions are possible without further research. It appears that a dependence of $k(\nu)$ on $I_0(\nu)$ should be expected when powerful lasers are used as radiation sources. The dependence of $k(\nu)$ on $I_0(\nu)$ should then manifest differently for different lines.

The fact that $k(\nu)$ is independent of concentration C means that each molecule absorbs radiation independently of other molecules. Numerous experimental studies have shown that this assumption is valid for small concentrations of the absorbing substance. Increasing the absorbing-gas concentration and adding an extraneous gas enhances the intermolecular-interaction effects, which change the values of the absorption coefficients and result in true deviations from the Bouguer-Beer law. This effect was first observed experimentally by Angström [105] in the infrared, during a study of the integral absorption by carbon dioxide. Schaefer [106] investigated the spectral absorption in the 2.7- and 4.3-μ CO_2 bands /107

and also found $k(\nu)$ to depend on partial pressure. Eva von Bahr [107] studied the absorption of infrared radiation by mixtures of various absorbing and extraneous gases and came to the conclusion that the observed deviations from the Bouguer-Beer law are due to intermolecular collisions. Intermolecular interactions cause a broadening of the spectral absorption lines that depends on the partial pressures of the absorbing and extraneous gases and on the temperature. In turn, spectral line broadening causes a change in $k(\nu)$.

The Bouguer-Beer law can be regarded as valid when applied to absorption of infrared radiation in the atmosphere, where the total pressure varies little with time at a given height and the partial pressures of the absorbing gases are low by comparison with the total pressure — this in most cases in which high accuracy of the solution is not required. Here it must be remembered that the absorption coefficient $k(\nu)$ will be different for different heights of horizontal-path propagation at a given frequency ν, since the total and partial pressures of the absorbing components depend on height. When it is necessary to determine certain absorption characteristics of infrared radiation during horizontal-path propagation with high accuracy, it must be borne in mind that at a 1% by volume concentration of the atmosphere's principal absorbing component (water vapor), the contribution to line broadening due to collisions between water molecules will be approximately 5% of the contribution from collisions between water and air molecules.

Let us now consider the apparent deviation from the Bouguer-Beer law due to limited instrument resolution in experimental research on absorption. /108 We know that the beam of light leaving any spectrometer contains a range of frequencies determined by the instrument's resolution. The highest resolution that has been attained in diffraction-grating spectrometers in the near infrared is 0.025 cm^{-1} [108]-[110]. On the other hand, the half-widths of individual lines in vibrational-rotational absorption bands (see §5) in the lower layers of the atmosphere varies from a few hundredths to a few thousandths of a reciprocal centimeter. /109 This means that the spectral width of the instrument's slit is of the same order of magnitude as the absorption-line width, even when high-resolution instruments are used. Several lines or even groups of lines fall on the exit slits of standard spectrometers. The spectral transmission $T(\nu)$ registered by the instrument will not be equal to its true value $f(\nu)$. Actually, $T(\nu)$ will characterize the transmission function after distortion by the spectrometer's instrumental function for an interval $\Delta\nu$ equal to the spectral width of the instrument's exit slit (Figs. 3.1 and 3.2).

The distorting effect of the spectrometer on the true picture of the spectrum and the resulting deviation from the Bouguer-Beer law are larger the lower the resolution of the instrument and the stronger the dependence of the absorption coefficient on frequency. Only when $k(\nu)$ = const in the spectral interval under consideration will the measured spectral transmission equal the true value.

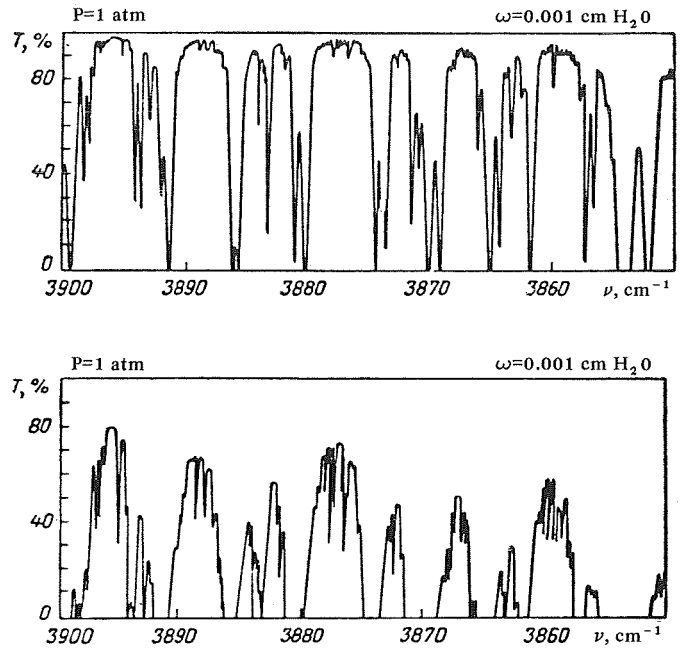

Figure 3.1. Fully Resolved Absorption Spectrum of Water Vapor in the Segment 3850-3900 cm^{-1} (2.56-2.6 μ) at Pressure P = 1.0 atm and Precipitated Water Layer w = 0.001 cm (Upper Curve) and w = 0.01 cm (Lower Curve) [189].

The measured spectral absorption A'(ν) is related to the true absorption A(ν) and the instrumental function S by

$$A'(\nu)=\int_{-\infty}^{\infty} S(\nu-\nu')\,A(\nu')\,d\nu'.$$

If the instrumental function is assigned as a gaussian distribution, then A'(ν) assumes the form /110

$$A'(\nu)=\frac{\sqrt{\ln 2}}{a^2\sqrt{\pi}}\int_{-\infty}^{\infty}\exp\left\{-\frac{\ln 2}{a^2}(\nu-\nu')^2\right\}A(\nu')\,d\nu',$$

where a is the half-width of the instrumental function. Applying the Fourier transformation, we may write

$$A(\nu)=\frac{1}{2\pi}\int_{-\infty}^{\infty}\frac{A'(\omega)}{S(\omega)}\exp(-i\omega\nu)\,d\omega,$$

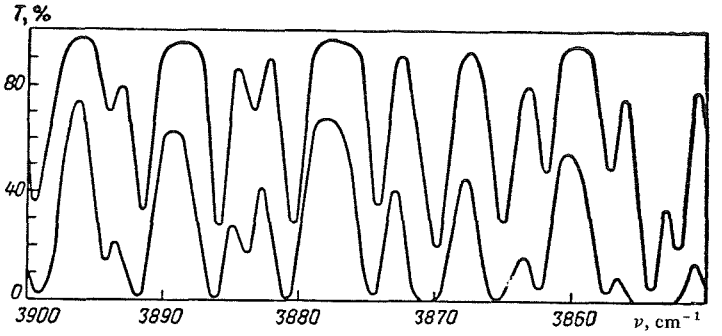

Figure 3.2. Water Vapor Absorption Spectrum Obtained by Multiplying T(ν) (Fig. 3.1) by an Instrumental Function with Width 2a = 2.0 cm^{-1} [189].

where A'(ω) and S(ω) are the transforms of A(ν) and S(ν).

Kostkowski and Bass [784] performed extensive calculations of A(ν) for cases in which the absorption lines are of the dispersion shape and the instrumental function is described by a gaussian distribution.

A detailed theoretical investigation of the influence of the spectrometer on the results of spectral and integral transmission measurements appeared in a paper by Nielsen, Thornton, and Dalle [111], where it was shown for the first time that the integral absorption of a band as a whole does not depend on instrument slit width. This was subsequently confirmed experimentally by Howard [112] and in our own studies [113, 114]. V.P. Kozlov and Ye.O. Fedorova [115] derived a formula that can be used to estimate the maximum error in determination of the integral transmission with a spectrometer on a segment $\Delta\nu$ from its known instrumental function.

The influence of the spectrometer on the results of absorption-spectrum measurements, which is governed by the instrumental function, the spectral slit width, and the scanning speed, and selection of optimum measurement conditions have been investigated in numerous studies (see, for example, the reviews [116, 117, 785] and the papers [118-123]).

5. FINE STRUCTURE OF VIBRATIONAL-ROTATIONAL AND PURELY ROTATIONAL SPECTRA OF WATER VAPOR

Let us consider the state of theoretical and experimental research on the center positions, strengths, and half-widths of the lines in the vibrational-rotational and purely rotational spectra of water vapor.

1. Line center positions. 1. Theoretical investigations. The /111
positions ν_{0i} of absorption-line centers can be calculated on the basis of the quantum theory of absorption. To find ν_{0i}, it is necessary to know the molecular energy levels the combination of transitions between which in accordance with the known selection rules enables us to acquire the unknowns. The vibrational-rotational levels of the molecule can be obtained in approximation on the basis of simple addition of the vibrational and rotational energies determined separately.

The detailed analysis of the molecular vibrational energy problem carried out by Dennison [124], Bonner [125], Escart [126], and others showed that solution of the quantum-mechanical problem of the anharmonic oscillator requires knowledge of the anharmonicity constants. Finding these constants requires use of the corresponding experimental data. Using this approach, G.A. Khachkuruzov [127] calculated the energies for the first 100 vibrational levels of the water molecule.

The problem of determining the rotational energy of asymmetrical-top molecules, of which the water molecule is a representative, was solved by Wang [128] and Ray [129]. Ray introduced the concept of the asymmetry parameter and showed that the problem can be reduced to finding a certain quantity that depends only on this parameter. The Ray method was developed and advanced to the stage of numerical calculations by King, Hainer, and Cross, who published tables for calculation of the rotational energy up to $j = 12$ [130]. In [131], they pointed out a procedure for calculating the rotational energy for $j > 12$, following which Erlandsson calculated the rotational energies up to $j = 40$ [52].

Thus, an approximate mathematical apparatus for calculation of the vibrational-rotational energy of the H_2O molecule has been developed. The accuracy with which the ν_{0i} are determined is quite adequate for solution of many problems that require knowledge of the transmission functions for spectral segments that are not too narrow. When the problem requires data on the spectral transmission $T(\nu)$, as in the use of the laser as a radiation source, the approximation is not valid, especially for lines due to transitions with large j. Accurate determination of the vibrational-rotational energy levels of the molecule and, consequently, of the ν_{0i} values, requires that the interaction between vibration and rotation be taken into account. The first attempt to do so /112
was made by Wilson and Howard [132] by the perturbation method. They showed that allowance for the interaction gives rise in the rotational-energy operator to new terms, whose coefficients were referred to as "centrifugal-distortion constants." Wilson [133] succeeded in finding an analytical relation between these constants and the parameters of the molecules. M.A.Yel'yashevich's paper [134] was devoted to the same problem of determining the

vibrational-rotational energies; the author obtained general formulas for the centrifugal-distortion constants.

Schaffer and Nielsen [135] found the values of the vibrational-rotational energy and the centrifugal-distortion constants of molecules of the type XY_2 and derived an equation for determination of most of the anharmonicity constants. Solution of the Schrödinger differential equation for the asymmetrical top was also the subject of Majumdar's papers [136, 137], which included numerical calculations of the vibrational-rotational energy for $j = 10$. Comparison of the calculations with the data of Benedict [138] showed that they differ by no more than 3.49 cm^{-1} at energy values from 1114.6 cm^{-1} ($j_\tau = 10_{-10}$) to 2698.6 cm^{-1} ($j_\tau = 10_{10}$), indicating good agreement between theory and experiment.

However, this accuracy is totally inadequate when the line positions are calculated for solution of problems involving quantitative estimation of the absorption of laser light in the atmosphere, or for problems in which the absorption functions must be found in narrow spectral intervals. Thus, until recently, the theoretical results had not delivered the required accuracy in determination of line-center positions. The author's laboratory therefore initiated the corresponding studies, the results of which are published in detail in [139-147, 343, 779].

To find the system of vibrational-rotational levels, it is necessary to solve the complete Schrödinger equation for vibrational-rotational motion of the nuclei in the molecule:

$$H\psi = E\psi, \tag{3.53}$$

where H and ψ are the vibrational-rotational Hamiltonian and the wave function of the molecule and E are the eigenvalues of the energy operator.

For a molecule of the type XY_2, the vibrational-rotational Hamiltonian is written /113

$$H = H_v + \frac{1}{2}\sum_{\alpha\beta}\mu_{\alpha\beta}P_\alpha P_\beta - \frac{1}{2}g_z P_z, \tag{3.54}$$

where H_v is the Hamiltonian of the anharmonic vibrations of the system of nuclei written either exactly [132, 135, 148, 149] or approximately [145]; P_α is the operator of the projection of the total angular momentum onto the α axis of a coordinate system rigidly bound to the molecule ($\alpha = x, y, z$), $\mu_{\alpha\beta}$ is a certain known

[132] function of the normal coordinates q_k (k = 1, 2, 3), $g_z = \mu_{zz}P_z + P_z\mu_{zz}$; $P_z = \sum_{ik} G^z_{ik} q_i P_k$ is the projection of the vibrational angular momentum onto the z axis, and the G^z_{ik} are the Coriolis constants.

Since it is impossible to solve the Schrödinger equation with a Hamiltonian of the form (3.54) in closed form, various approximate methods are used. The usual approach is as follows. By means of a unitary transformation [134] or a sequence of contact transformations [150-153], the matrix of the operator H is reduced to diagonal form in the vibrational quantum numbers. Then the rotational-energy operator is separated from the diagonal elements and the problem of the eigenvalues of a nonrigid asymmetrical top is solved.

We shall also follow the same general procedure, except that we shall diagonalize the matrix of the operator H with the aid of perturbation theory. In (3.54), we take as our zeroth approximation $H^0 = H_v$; then the perturbation operator is

$$\hat{w} = \frac{1}{2}\sum_{\alpha\beta}\mu_{\alpha\beta}P_\alpha P_\beta - \frac{1}{2}g_z P_z, \qquad (3.55)$$

and the matrix elements $\langle v|x|v'\rangle$ are noncommutative operators with respect to the rotational variables. If the standard working formulas of ordinary perturbation theory are used, difficulties resulting from the indeterminacy of the order of the matrix elements arise as early as the third approximation. However, it is possible to determine uniquely the order in which the matrix elements follow one another in the course of writing the perturbation-theory formulas.

Let us consider the range of applicability of perturbation theory in this case. /114

As we know, the condition for applicability of perturbation theory is written [154]

$$\left|\frac{\langle v|\hat{w}|v'\rangle}{E_v - E_{v'}}\right| \ll 1. \qquad (3.56)$$

We note that, as pointed out by Yel'yashevich [134], the ratio of the last term to the next-to-last term is approximately equal to λ in the expansion of the vibrational-energy operator. For light molecules such as the water molecule, $\lambda \approx 10^{-1}$.

Performing simple estimates, we can then write

$$\left|\frac{\langle v|w|v'\rangle}{E_v - E_{v'}}\right| \approx \lambda^3 j^2, \tag{3.57}$$

where j is the rotational quantum number, the E_v are the eigenvalues, and the $\langle v|$ are the eigenfunctions of the operator $H^0 = H_v$.

Thus, the applicability condition for perturbation theory is satisfied in this case for rotational levels with quantum numbers $j < 31$. It must be noted that these estimates may not hold true for those vibrational levels whose energies are approximately equal (random degeneracy), so that this method must be used with caution in such cases.

Equation (3.57) enables us to estimate the orders of the contributions from the various approximations to the rotational-energy operator $H_R^{[v]}$ with respect to the zeroth approximation. The Hamiltonian of the effective rigid asymmetrical top is taken as the zeroth approximation:

$$(H_R^{[v]})^{(0)} = \frac{1}{2}\sum_\alpha a_{\alpha\alpha} P_\alpha^2, \tag{3.58}$$

where $a_{\alpha\alpha} = \langle v_1 v_2 v_3 | \mu^0_{\alpha\alpha} | v_1 v_2 v_3\rangle_0$ are the effective rotational constants.

Owing to the special properties of the perturbation operator, the corrections are found to be different for each approximation. For the n-th approximation, there are n + 1 terms for n even and n terms for n odd. The orders of these terms are, generally speaking, different for each j. For example, terms in the eighth power of the projections of the angular momentum from the fourth approximation become larger with increasing j (for $j \geq 10$) than terms in the sixth power of the angular-momentum projections from the third approximation, i.e., the contributions from the individual terms are redistributed. /115

Redistribution of the contributions is also observed within each approximation. For example, the largest contribution to the nonrigid-top Hamiltonian in the second approximation for $j < 10$ should be expected from terms with P_α^2, while terms with P_α^4 make the largest contribution for $j \approx 30$.

A detailed analysis of the problem has made it possible to estimate the absolute error incurred in calculating the matrix elements of the operator $H_R^{[v]}$ for any $1 \leq j \leq 30$ and the maximum

error in determining the energy of the rotational levels. Thus, if the error for j = 10 is not to exceed 0.1 cm^{-1}, it is necessary to consider all terms containing P^2, P^3, P^4, P^5, P^6, and P^8 up to the fourth approximation. At the same time, it is unnecessary to consider terms with P^7. After transformation using the commutation relationships, the nonrigid-top Hamiltonian $H_R^{[v]}$ can be written as follows in the fourth approximation:

$$H_R^{[v]} = \sum_{\alpha} b_{\alpha\alpha} P_\alpha^2 + \sum_{\alpha\beta\gamma\delta} \tau_{\alpha\beta\gamma\delta} P_\alpha P_\beta P_\gamma P_\delta + \sum_{\alpha\beta\gamma\delta\varepsilon\eta} [\alpha\beta\gamma\delta\varepsilon\eta] P_\alpha P_\beta P_\gamma P_\delta P_\varepsilon P_\eta + \\ + \sum_{\alpha\beta\gamma\delta\varepsilon\eta\nu\xi} [\alpha\beta\gamma\delta\varepsilon\eta\nu\xi] P_\alpha P_\beta P_\gamma P_\delta P_\varepsilon P_\eta P_\nu P_\xi. \quad (3.59)$$

Simple but cumbersome calculations result in analytical expressions for the effective rotational constants $b_{\alpha\alpha}$ and the centrifugal-distortion constants $\tau_{\alpha\beta\gamma\delta}$, $[\alpha\beta\gamma\delta\varepsilon\eta]$ and $[\alpha\beta\gamma\delta\varepsilon\eta\nu\xi]$. For example,

$$[\alpha\beta\gamma\delta\varepsilon\eta\nu\xi] = \sum_k \mu_{\alpha\beta}^k \mu_{\nu\xi}^k \frac{\tau_{\gamma\delta\varepsilon\eta}^k}{2\hbar\omega_k^3} + \sum_{ik} \mu_{\alpha\beta}^k \mu_{\gamma\delta}^i \mu_{\varepsilon\eta}^k \mu_{\nu\xi}^i \frac{1}{\omega_i^2 - \omega_k^2} \left(v_k + \frac{1}{2}\right). \quad (3.60)$$

Here ω_i is the fundamental frequency, $\tau_{\gamma\delta\varepsilon\eta}^k$ is the linear coefficient of the expansion of the centrifugal-distortion constants of second order in the vibrational quantum numbers, and $\mu_{\alpha\beta}^k = \left(\frac{\partial \mu_{\alpha\beta}}{\partial q_k}\right)_{q=0}$. We now write the complete Schrödinger vibrational-rotational equation as follows: /116

$$[H_v + H_R^{[v]} + H_{Rv} - H_R^{[v]}]\psi = E\psi, \quad (3.61)$$

where H_{Rv} is introduced to denote the second and third terms in (3.54).

Perturbation theory is used in solving Eq. (3.61). The operator $H_v + H_R^{[v]}$ is taken as the zeroth approximation. It then follows from the method for obtaining the operator $H_R^{[v]}$ that the total vibrational-rotational energy

$$E = E_v + E_R^{[v]} \quad (3.62)$$

accurate to the discarded terms in $H_R^{[v]}$.

In the second approximation of perturbation theory, the normalized complete vibrational-rotational functions are represented in the form

$$\psi_{vj\tau} = (1 + C^{(2)}_{vj\tau,\ vj\tau})\,\psi_v\psi^{[v]}_{j\tau} + \sum_{v'j'\tau'}{}' (C^{(1)}_{vj\tau,\ v'j'\tau'} + C^{(2)}_{vj\tau,\ v'j'\tau'})\,\psi_v\psi^{[v']}_{j'\tau'}, \qquad (3.63)$$

where

$$C^{(1)}_{vj\tau,\ v'j'\tau'} = \langle v'j'\tau' | RH_{Rv} | vj\tau\rangle; \qquad (3.64)$$

$R = 1/(E_V - H_V)$ is the operator of the resolvent in the vibrational problem:

$$\begin{aligned} C^{(2)}_{vj\tau,\ v'j'\tau'} = {} & [\langle v'j'\tau' | R_{Rv} | v'j'\tau'\rangle - \langle vj\tau | H_{Rv} | vj\tau\rangle]\,\langle v'j'\tau' | R^2 H_{Rv} | vj\tau\rangle \\ & + \tfrac{1}{4} b_{zz}(vv')\,\langle j\tau' | P_z^2 | j\tau\rangle + \tfrac{1}{4}\sum_{\alpha\beta} [b_{\alpha\beta z}(vv')\,\langle j\tau' | P_\alpha P_\beta P_z | j\tau\rangle + \\ & + b_{z\alpha\beta}(vv')\,\langle j\tau' | P_z P_\alpha P_\beta | j\tau\rangle] + \tfrac{1}{4}\sum_{\alpha\beta\gamma\delta} t_{\alpha\beta\gamma\delta}(vv')\,\langle j\tau' | P_\alpha P_\beta P_\gamma P_\delta | j\tau\rangle; \end{aligned} \qquad (3.65)$$

$$C^{(2)}_{vj\tau,\ vj\tau} = \frac{1}{2}\sum_\alpha b_{\alpha\alpha}(vv)\,\langle j\tau | P_\alpha^2 | j\tau\rangle + \frac{1}{4}\sum_{\alpha\beta\gamma\delta} t_{\alpha\beta\gamma\delta}(vv)\,\langle j\tau | P_\alpha P_\beta P_\gamma P_\delta | j\tau\rangle. \qquad (3.66)$$

The constants $b_{\alpha\alpha}(vv)$ are analogous to the corrections to the effective rotational constants, while the constants $t_{\alpha\beta\gamma\delta}$ are analogous to the corrections applied to the centrifugal-distortion constants: /117

$$\begin{aligned} b_{zz}(vv) &= \frac{1}{2}\langle v | g_z R^2 g_z | v\rangle; \\ b_{\alpha\alpha}(vv) &= \pm i\hbar\,\langle v | g_z R^2 \mu_{xy} | v\rangle, \quad \alpha = x,\ y; \quad t_{\alpha\beta\gamma\delta}(vv) = \langle v | \mu_{\alpha\beta} R^2 \mu_{\gamma\delta} | v\rangle. \end{aligned} \qquad (3.67)$$

As for the constants $b_{\alpha\beta z}(vv')$, $b_{z\alpha\beta}$, b_{zz}, and $t_{\alpha\beta\gamma\delta}$, they take the form

$$A(vv') = (-1)^n \langle v' | R_a R_b | v\rangle, \qquad (3.68)$$

a and b are the operators g_z and $\mu_{\alpha\beta}$ in various combinations and n is the number of operators g_z among a and b.

Estimates of the contributions of various terms in the second, third, and fourth approximations to the nonrigid-top Hamiltonian for j = 1(1)30 have been calculated on the basis of the above expression. The data obtained permit determination of the highest order of the approximation for the operator $H_R^{[v]}$ that must be used to find the position of the center of the corresponding line with the required accuracy for a certain j. The rest of the solution procedure reduces to the following. All of the coefficients appearing in the expression for $H_R^{[v]}$ are determined and the operator matrix is constructed and numerically diagonalized. Then the eigenvalues of the operator $H_R^{[v]}$ are found and (3.67) is used to determine the values of the total vibrational-rotational energy, from which the centers of the corresponding lines are easily found by applying the selection rules.

2. Experimental studies. Many studies have been devoted to the fine structure of the purely rotational and vibrational-rotational spectra of water vapor. The first investigations of the vibrational-rotational bands were carried out by Sleator [155] and Sleator and Phelps [156], although the resolution attained did not permit analysis of the rotational spectrum. Plyler and Sleator [157] and later Plyler [158] therefore investigated the fundamental bands with improved resolution. Using the data of [157 and 158] and the results of their own measurements in the photographic region of the spectrum, Mecke et al. [159-161] submitted the first analysis of the rotational structure of the individual bands and determined the moments of inertia and geometrical parameters of the water molecule. /118

Nielsen [162] investigated the water-vapor spectrum with high resolution in the region of the fundamental vibrational frequencies and the combination bands $(\nu_1 + \nu_3)$ and $(\nu_2 + \nu_3)$. Nelson and Benedict [163] investigated the region of the spectrum from 1.34 to 1.97 μ with resolution somewhat higher than in [162]. In [164], Benedict and Plyler made another investigation of the 2.7-μ band at high resolution. The authors of [164] submitted a new identification of the lines in the ν_1 band, expanded the structural analysis of the ν_3 band, and presented values for the rotational terms (100) and (001) of the states up to j = 13. Additional data from analysis of the fine structure of the water-vapor spectrum are given in the papers of Benedict [165]. Plyler, Gailar, and Wiggins [60] made a high-resolution study of the water-vapor vibrational-rotational spectrum and determined with high accuracy some of the wavelengths needed for spectrometer calibration.

The spectrum of water vapor in the 4.5-5.7 and 6.6-13-μ regions was investigated in detail by Benedict, Claassen, and Shaw [166]. The results included a more detailed analysis of the rotational structure of the ν_2 band, determination of the ground-state rotational terms to j = 18, calculation of the terms of the (010) and (020) states, and values of a number of rotational constants of the H_2O molecule. The spectral region from 5.26 to 7.14 μ was investigated in detail at high resolution by Dalby and Nielsen [167]. High-resolution flame studies of the segment of the water-vapor spectrum around 1.9 μ [168] yielded data on high levels of the vibrational state and on absorption bands between high vibrational levels: (021) → (010) and (031) → (020).

The purely rotational water-vapor absorption spectrum was investigated at high resolution by Barnes and Benedict [169], who improved upon Mecke's data. The most detailed investigation in the 18-135-μ region was carried out by Randall, Dennison, Ginsberg, and Weber [170] and by Dennison [171], who registered more than 200 absorption bands. N.G. Yaroslavskiy and A.Ye. Stanevich [172] greatly expanded the region of the rotational absorption spectrum that has been investigated at high resolution. Their measurements were made in the 20-2500-μ interval. New data on the purely rotational water-vapor spectrum in the 55-1000-μ wavelength band were obtained by N.I. Furashov [173]. /119

Let us briefly discuss the work done on the fine structure of the water-vapor absorption spectrum under natural conditions. In most cases, the sun was used as the radiation source. In measurements made under natural conditions, the spectra of atmospheric gases other than water vapor are registered along with the water-vapor absorption spectrum. It is therefore not always possible to make a complete identification of the lines owing to the resulting overlap of the spectra. Nevertheless, most lines have been identified.

The first atlas of the solar absorption spectrum of the earth's atmosphere was published by Minnaert, Mulders, and Houtgast in 1940 [174]. This atlas covered the spectral region from 3612 to 8771 Å, which is readily accessible to photographic registration of the spectrum. In 1947, Babcock and Moore [175] published their data on the solar spectrum in the wavelength range from 6600 to 13 495 Å. Mohler et al. made measurements and compiled an atlas of the solar spectrum in the range from 0.8 to 2.6 μ [176]. In [177] and [178], Mohler and Benedict identified the lines listed in this atlas. A group of Ohio University investigators published an atlas of the solar spectrum for the regions from 3.0 to 5.2 μ [179] and 7 to 13 μ [180]. A total of more than 1600 lines, of which more than 70% are water-vapor lines, has been observed in the 1-13-μ region.

Working at the Jungfrau alpine station in Switzerland (elevation 3580 m), Migeotte, Neven, and Swenson recorded the solar

spectrum from 2.8 to 23.7 μ [181]. In this atlas, the authors of [181], working with Benedict, identified more than 3600 individual lines [182]. Using an improved apparatus, Delbouille and Roland [183] prepared a new atlas of the solar spectrum at the same Jungfrau station. About 10,500 lines were detected in the relatively narrow region from 0.75 to 1.2 μ.

Farmer and Key [184] recorded the solar spectrum at an elevation of 5200 m in the Bolivian Andes in the wavelength range from 7 to 400 μ. The spectrum was obtained with a resolution of 0.3 cm^{-1} from 7 to 30 μ, and new telluric absorption lines of H_2O were registered. In the 40-400-μ region, the solar radiation is absorbed practically completely in the column of atmosphere above 5.2 μ [sic], except for a relatively narrow atmospheric transparency window around 345 μ detected by the authors of [184]. /120

An absorption spectrum of the ground layer of atmosphere for a distance of 16.3 km, recorded with high resolution in the range from 5400 to 8250 Å, was published by Curcio [185] in 1963. Owing to the relatively high resolution and the great thickness of atmosphere, a substantial number of weak absorption lines were detected in [185] in the visible region of the spectrum.

In 1966, Moore, Minnaert, and Houtgast [186] published tables of the absorption spectrum of the earth's atmosphere containing about 24,000 lines in the region from 2935 to 8770 Å.

Oppenheim and Goldman [187] compiled an atlas of the water-vapor absorption spectrum in the regions of the 1.9- and 2.7-μ bands at 1200°K. Lines due to transitions between high-energy vibrational-rotational levels of the H_2O molecule were recorded in this atlas.

Let us review the basic experimental research that has been done on the water-vapor absorption spectrum under laboratory and natural conditions. The positions of many lines of both the vibrational-rotational and the purely rotational spectra of H_2O have now been determined. However, it must be noted that many close lines stayed unresolved in many cases even when the spectra were recorded with the highest possible resolution. Groups of lines are often taken for individual lines. This applies especially to segments of the spectrum in which both strong and weak lines are closely spaced simultaneously. The accuracy with which the line centers are determined in the ultraviolet, visible, and near infrared regions varies from a few hundredths to 0.1-0.2 Å.

2. Line strengths. 1. Theoretical investigations. No fundamental difficulties are encountered in calculating the line strengths of the spectra of rigid asymmetrical-top molecules. We now have quite detailed data [188, 878] that yield an approximate picture of the line strengths in the purely rotational spectrum of water vapor. The true picture of the spectrum can be obtained by

solving the problem of rotation of a nonrigid top.

In exact calculations of the line strengths in the vibrational-rotational spectrum of water vapor, it is necessary to take account of the nonrigidity of the molecule and the interaction of all forms of its motion. Usually, the line strengths in the vibrational-rotational bands of H_2O are found in the following procedure [879, 880]. It is assumed that the strength of the line /121

$$S = S_{ro}S_{vib}, \qquad (3.69)$$

where S_{ro} is the strength of the corresponding line from the purely rotational spectrum, whose value is assumed to be known; S_{vib} is a cofactor that takes account of the vibration-rotation interaction. S_{vib} is determined from experiment. It is assumed that S_{vib} is the same for all lines in a given vibrational-rotational band. With this hypothesis, integration of (3.69) over the band yields the experimentally determined integral strength of the band on the left and, on the right, the product of S_{vib} by the sum of the strengths of the lines due to the corresponding purely rotational transitions.

On the basis of this scheme, the strengths of lines in the vibrational-rotational absorption bands ν_1, $2\nu_2$, and ν_3 in the 2.7-μ region (2857-4444 cm^{-1}) were calculated in [879, 880].

In a series of calculations performed by Benedict and Calfee [881], data were obtained on the line strengths of the absorption bands in the 1.9- and 6.3-μ regions. In these calculations, some account was taken of the interaction between the vibrational and rotational motions of the H_2O molecule. The tables published by the authors of [881] contain information on the center positions, strengths, and half-widths of the lines in the $\nu_2\nu_3$, $\nu_1\nu_2$, and $3\nu_2$ bands around 1.9 μ and the ν_2 band around 6.3 μ. The tabulation was carried out for lines with $j \leq 20$. This reference also includes data on all three parameters of the fine structure of the four "hot" bands (021-010; 100-010, 020-010, 001-010), the bands of the isotopes H_2O^{17} and H_2O^{18}, and the ν_2 bands of HDO. It contains 4110 absorption lines of the 1.9-μ (4212-6254.3-cm^{-1}) band and 5054 lines in the 6.3-μ (640-2885-cm^{-1}) region.

The tables include lines whose strengths exceed 0.0001 $cm^{-1}/g \cdot cm^{-2}$. The central region of the ν_2 band (1400-1850 cm^{-1}), which included lines with strengths greater than 0.001 $cm^{-1}/g \cdot cm^{-2}$, is an exception. The line parameters of the purely rotational H_2O spectrum were calculated for 640-1000 cm^{-1}. This was done to make the data as complete as possible over the entire range of wavelengths investigated.

We note that the highest line-strength values found in the 1.9- and 6.3-μ bands were 1042.7 (line at 5413.90 cm^{-1}) and 10976.2 $cm^{-1}/g \cdot cm^{-2}$ (the 1684.84-cm^{-1} line), respectively. /122

The hypothesis that S_{vib} is constant for all lines of the band, on which this scheme is based, is, strictly speaking, inaccurate. It does not consider the specifics of the interaction between the vibrational and rotational motions of the molecule for the individual lines. This circumstance may lead to substantial errors in calculating the strengths of lines due to transitions between high-energy levels of the molecule.

An attempt was made in our laboratory to devise a new scheme for calculation of line strengths in the vibrational-rotational spectrum of water vapor with consistent allowance for the vibration-rotation interaction in the molecule [139-141, 147, 190, 220, 779, 907]. We describe the results obtained.

The expression for the strength of the line is written in the form [191]

$$S_{vR}^{v'R'} = \frac{8\pi^3 N}{hcz} \Delta\omega [2-(-1)^{|\tau|}] e^{-\frac{hc}{kT}\omega_{\tau R}} \times [1-e^{-\frac{hc}{kT}\Delta\omega}] |\langle v'R'|M_z|vR\rangle|^2. \quad (3.70)$$

Here $\Delta\omega = \omega_{v'R'} - \omega_{vR}$, $\omega_{v'R'}$, and ω_{vR} are the levels of the upper and lower states, M_z is the component of the electric-dipole-moment vector in a fixed coordinate system, N is the number of particles of the absorbing gas per unit volume, z is the partition function, τ is the rotational quantum number, h is Planck's constant, c is the velocity of light, k is Boltzmann's constant, T is the temperature, and |vR> is the complete vibrational-rotational wave function. The component M_z can be written

$$M_z = \Phi(zx)\mu_x + \Phi(zy)\mu_y, \quad (3.71)$$

where μ_x and μ_y are the projections of the dipole-moment vector onto coordinate axes rigidly bound to the molecule and Φ(zx) and Φ(zy) are direction cosines.

It follows from the symmetry of the H_2O molecule [134] that only the second term contributes to M_z for parallel bands when the /123 vibration-rotation interaction is disregarded. The quantities μ_x and μ_y are series-expanded in normal coordinates.

The function (3.63) can be used to obtain for the quantity $\langle vR|M_z|v'R'\rangle$ in (3.70)

$$\langle vR|M_z|v'R'\rangle = \langle vR|M_z|v'R'\rangle_0 + C^{(1)}_{v'R',\,vR}[\langle vR|M_z|vR\rangle_0 - \langle v'R'|M_z|v'R'\rangle_0] + \sum_{v''R''}[C^{(1)}_{vR,\,v''R''}\langle v''R''|M_z|v'R'\rangle_0 + \langle vR|M_z|v''R''\rangle_0 C^{(1)}_{v'R',\,v''R''}]. \quad (3.72)$$

Here we have discarded terms containing the coefficients $C^{(2)}$, since their contributions to the matrix element are of higher orders of smallness. The second term in (3.72) is identically equal to zero, since $\langle R|\Phi|R\rangle \equiv 0$ owing to the symmetry of the molecule. The matrix elements on the right in (3.72) are calculated with the functions of the zeroth approximation $\psi^0_{vR} = \psi_v\psi^{[v]}_R$. Here the rotational wave function $\psi^{[v]}_R$ is presented in the form of an expansion in the wave functions of the rigid symmetrical top:

$$\psi^{[v]}_R = \sum_{k=-j}^{j} g^{[v]}_{k\tau}|jkm\rangle. \quad (3.73)$$

In the third term of (3.72), we are obliged to extend the summation over the rotational structure of intermediate vibrational states. Let us examine this term of (3.72) more closely. Applying (3.64) and (3.61), we can present it in the form

$$\frac{1}{2}\sum_{R''v''}\sum_{g}\Big\{\sum_{\alpha\beta}\Big[\frac{\langle v'|\bar{\mu}_g|v''\rangle\langle v''|\mu_{\alpha\beta}|v'\rangle}{E_v - E_{v''}} \times \langle R'|\Phi(z_g)|R''\rangle\langle R''|P_\alpha P_\beta|R\rangle + \frac{\langle v'|\mu_{\alpha\beta}|v''\rangle\langle v''|\mu_g|v\rangle}{E_{v'} - E_{v''}} \times \langle R'|P_\alpha P_\beta|R''\rangle\langle R''|\Phi|(zg)|R\rangle\Big] - \frac{\langle v'|\mu_g|v''\rangle\langle v''|g_z|v\rangle}{E_v - E_{v''}} \times \langle R'|\Phi(zg)|R''\rangle\langle R''|P_z|R\rangle - \frac{\langle v'|g_z|v''\rangle\langle v''|\mu_g|v\rangle}{E_{v'} - E_{v''}}\langle R'|P_z|R''\rangle\langle R''|\Phi(zg)|R\rangle\Big\}. \quad (3.74)$$

With (3.73), the rotational partition functions take the form /124

$$\sum_{\substack{k''\tau'' \\ kk'}} g^{[v]}_{k\tau}(g^{[v'']}_{k\tau''})^2 g^{[v']}_{k'\tau'}\langle jkm|P_\alpha P_\beta|jk''m\rangle \times \langle jk''m|\Phi|j'k'm'\rangle, \quad (3.75)$$

$$\sum_{\substack{\tau''k \\ k'}} g^{[v]}_{k\tau}(g^{[v'']}_{k\tau''})^2 g^{[v']}_{k'\tau'}\langle jkm|P_z|jkm\rangle \times \langle jkm|\Phi|j'k'm'\rangle. \quad (3.76)$$

The summation over k" in (3.75) is elementary, since the $\langle jkm|P_\alpha P_\beta|jk"m\rangle$ are nonzero only for k" = k, k ± 2. Further, since the matrix $g_{k\tau}^{[v]}$ is normalized [130], we have $\sum_{\tau"} (g_{k\tau"}^{[v"]})^2 = 1$.

The matrix elements of the direction cosines are expressed in terms of products of Clebsch-Gordan coefficients; we should note that this approximation does not violate the selection rules for the rotational quantum numbers j and τ.

Let us turn to calculation of the sums over intermediate vibrational quantum states. The matrix elements that figure in these sums are computed with the aid of the functions of the three-dimensional anharmonic oscillator. The normal-coordinate functions μ, $\mu_{\alpha\beta}$, g_z, and v are presented in the form of series in the normal coordinates, e.g.,

$$v = \sum_i \omega_i^2 q_i^2 + \sum_{ik} a_{iik} q_i^2 q_k + \sum_{ikl} a_{iikl} q_i^2 q_k q_l + \ldots \qquad (3.77)$$

In the expansion (3.77), the ratio of a succeeding term to the preceding term equals λ. According to Yel'yashevich's estimates [134], $\lambda \sim 10^{-1}$. Further, the fact that the orders of the coefficients in the expansions of v, g_z, μ, and $\mu_{\alpha\beta}$ increase in the same fashion enables us to assume validity of this estimate for all of these quantities. This is confirmed by direct calculations according to [190, 193, 194]. To estimate the order of the contribution to the matrix element from the dipole moment using (3.74), it is necessary to calculate the order of

$$\mu_{\alpha\beta}^0 P_\alpha P_\beta \frac{1}{E_v - E_{v"}} = \varepsilon j^2.$$

Direct calculations in accordance with Yel'yashevich's estimates [134] yield $\varepsilon \sim \lambda^2$ for small j. We note that the quantity $g_z P_z/(E_v - E_{v'})$ is also of the order of λ^2. /125

In computing the contribution from (3.74), we shall limit ourselves to terms of order no higher than λ^3. The contribution from (3.74) can be estimated with the formulas for the matrix elements μ and the operator g_z on the basis of the functions of the anharmonic three-dimensional oscillator [142, 144]. Owing to the cumbersomeness of the final results, we present, by way of illustration, only the contribution of (3.74) for the 000-010 vibrational transition:

$$\langle 000j\tau \mid M_z \mid 010j'\tau'\rangle = \langle 000j\tau \mid M_z \mid 010j'\tau'\rangle_0 \times$$
$$\times\left[1+\alpha+\beta\frac{S'}{S}+\gamma\frac{S(k)}{S}\right];\quad \beta=\frac{\mu_0\mu_{xx}^{(2)}\hbar}{\sqrt{2}\,\mu_2\omega_2};$$
$$\alpha=\frac{\hbar\mu_0}{2\mu_2\omega_2}(\mu_{xx}^2+\mu_{zz}^2)+\frac{\mu_3\mu_{zz}^{(0)}\zeta_{23}^z\hbar}{2\omega_3\mu_2}\frac{\omega_2+\omega_3}{\omega_3-\omega_2};$$
$$\gamma=-\frac{\mu_0\mu_{zz}^{(2)}\hbar}{\mu_2\omega_2}-\frac{\mu_3\mu_{zz}^{(0)}\zeta_{23}^z\hbar}{\omega_3\mu_2}\frac{\omega_3^2+\omega_2^2}{\omega_3^2-\omega_2^2}; \qquad (3.78)$$
$$S=\sum_{kk'}g_{k\tau}^{[v]}(j)\,g_{k'\tau'}^{[v']}(j')\,[(1j-1k\mid j'k')+(1j1k\mid j'k')];$$
$$S(k)=\sum_{kk'}kg_{k\tau}^{[v]}(j)\,g_{k'\tau'}^{[v']}(j')\,[(1j-1k\mid j'k')-(1j1k\mid j'k')];$$
$$S'=\sum_{kk'}g_{k\tau}^{[v]}(j)\,g_{k'\tau'}^{[v']}(j')[\sqrt{(j-k)(j+1+k)}\,(1j0k+1\mid j'k')+$$
$$+\sqrt{(j+k)(j-k+1)}\,(1j0k-1\mid j'k')].$$

This approximation takes account of the anharmonicity of the vibrations, the nonrigidity of the molecule, and the Coriolis interaction.

We note that, in contrast to the zeroth approximation, the vibrational-rotational interaction leads in the matrix elements of the dipole moment to the appearance of its components on the x and y axes. The component is directed along the x axis for parallel bands and along the y axis for perpendicular bands. Here the selection rules in the rotational spectrum, which are governed by the symmetry of the molecule, are not violated.

2. Experimental investigations. Experimental determination of line strengths is a highly complex task. The basic difficulty stems from the need to take line overlapping into account. As of this writing, the strengths of a very limited number of lines in the water-vapor absorption spectrum have been determined.

Benedict, Claassen, and Shaw [166] found the strengths of certain rotational lines and lines from the vibrational-rotational ν_2 band under laboratory conditions at relatively high temperatures and H_2O concentrations. The intensities of a series of lines in the vibrational-rotational spectrum of H_2O were determined by K.P. Vasilevskiy in the region of the bands centered around 2.7 μ [195-197]. Sanderson and Ginsburg [198] measured the strengths of three lines of the pure rotational spectrum of water vapor at around 92, 170, and 188 cm^{-1}. Saidy [199] determined the strengths of three rotational and two vibrational-rotational H_2O lines. A brief abstract of Bolle's paper [200] reports on determination of the strengths of a series of weak H_2O lines in the 8-20-μ region from atmospheric emission spectra by comparison of the results of measurements with calculation of the monochromatic absorption. This comparison indicated a disagreement of about 30% between the results for the weakest lines, with the calculated figures smaller than the experimental ones. The disagreement was apparently due to failure to consider the vibrational- /126

rotational interaction in the molecule in the line-strength calculations.

Goldman and Oppenheim [187, 201] measured the strength of one line in the 6.3-μ band. They used the results to determine the integral strength of the band in much the same way as was done in [202] and [203] for the 2.7-μ band.

Burch and Gryvnak's paper [81] reports the results of measurement of water vapor and CO_2 absorption in the region from 0.6 to 5.5 μ, from which, among other things, information can be extracted on the strengths and half-widths of several hundred of the most important H_2O lines. However, the paper gives no data on the parameters of the lines.

The strength and half-widths of a series of lines in the limbs and central region of the ν_2 band were determined in [885-887]. The strengths of several lines in the visible region of the spectrum around 0.69 μ were measured in [888].

3. Half-widths of lines. 1. Theoretical investigations. Applying Anderson's theory [56], Benedict and Kaplan [57] calculated the half-widths γ of lines in the rotational spectrum of water vapor to $j = 13$ and those of several lines from the ν_2 band of the vibrational-rotational spectrum with collisions between the water molecules and nitrogen molecules. The authors of [57] also investigated the temperature dependence of line half-width in the range /127 from 220 to 2400°K and the vibration-rotation interaction effect.

The basic results of the calculations can be stated as follows. At 300°K, the half-widths of the lines vary from 0.11115 $cm^{-1} \cdot atm^{-1}$ for the 1_1-1_{-1} lines to 0.032 $cm^{-1} \cdot atm^{-1}$ for the 14_{-13}-13_{-13} lines. Analysis of the results brought out a decrease in line half-width with increasing j and a decrease in γ as the orbital rotational quantum number τ increases at fixed j.

For the range of temperatures characteristic for the stratosphere, the following formula was obtained for description of γ as a function of T: $\gamma(T)/\gamma(300) = (T/300)^n$.

Here, n varies from line to line, averaging 0.62 at T = 260°K. Strong variations of the γ-T dependence from line to line are noted for temperatures in the region from 300 to 2400°K.

In [58], Benedict and Kaplan used the method developed here to present calculated results for the half-widths of purely rotational water-vapor lines with H_2O-H_2O and H_2O-O_2 molecular collisions. It was found that the line half-widths range from 0.5663 to 0.6607 $cm^{-1} \cdot atm^{-1}$ at 300°K.

For the molecular collisions H_2O-H_2O and H_2O-N_2, the calculated ratios of the line half-widths vary in the range from 1.90 to 6.85 from line to line. For the broadest and strongest lines,

which correspond to small j, this ratio lies in the range from 4.5 to 6.0. The average value of this ratio for the entire rotational band was found to be 5.49.

In the papers of Benedict and Kaplan, and in those of Gates, Calfee, Hansen, and Benedict [879, 880, 189, 881], line half-widths in the vibrational-rotational water-vapor spectrum were calculated without consistent allowance for the interaction between the vibrational and rotational motions of the molecule.

An attempt was made in [139-141] to take this interaction into account. The reasoning was essentially as follows. If the complete vibrational-rotational eigenfunction is expressed by

$$\psi_{vj\tau} = \psi_v \psi_{j\tau}^{[v]}, \tag{3.79}$$

where ψ_n is the vibrational wave function obtained with consideration of anharmonicity and $\psi_{j\tau}^{[v]}$ is the wave eigenfunction of the nonrigid top, the system of contributions of the familiar Anderson theory can be used to obtain the line half-widths [56]. /128

Using the Dirac nomenclature for the wave functions, we have for the half-width of a spectral line

$$\gamma(vj\tau m \to v'j'\tau'm') = \frac{Nv}{2c} \sum_{j_2} B_{j_2}\sigma_{j_2}; \tag{3.80}$$

$$\sigma_{j_2} = \int_0^\infty 2n\rho S_{j_2}(\rho)\,d\rho; \tag{3.81}$$

$$S_{j_2}(\rho) = \frac{1}{2}\sum_{M_2} \frac{\langle vj\tau m;\ j_2M_2 | P^2 | vj\tau m;\ j_2M_2\rangle}{(2j+1)(2j_2+1)} + \frac{1}{2}\sum_{M_2} \frac{\langle v'j'\tau'm';\ j_2M_2 | P^2 | v'j'\tau'm';\ j_2M_2\rangle}{(2j'+1)(2j_2+1)}; \tag{3.82}$$

$$P = \frac{1}{\hbar}\int_{-\infty}^{+\infty} e^{\frac{-H_0 t}{i\hbar}} C(t) e^{\frac{H_0 t}{i\hbar}}\,dt, \tag{3.83}$$

where N is the particle concentration per unit volume, v is the average particle velocity, ρ is the impact parameter, the vjm are the quantum numbers denoting the level from which the transition occurs, v'j'm' are the quantum numbers of the final level, j_2M_2 are the quantum numbers of the perturbation states of the molecule, Bj_2 is the population of state j_2, which is defined by a Boltzmann distribution, C(t) is the potential energy of interaction between the absorbing and perturbing molecules, and H_0 is the Hamiltonian of an isolated absorbing molecule.

Proceeding from [204], we obtain for the dipole-quadrupole interaction of two systems of charges

$$C(t)=\sum_{\alpha\beta}\left[\frac{5}{2}\frac{D_{\alpha\beta}R_\alpha R_\beta(\vec{M}\vec{R})}{R^7}-\frac{D_{\alpha\beta}R_\alpha M_\beta}{R^5}\right], \tag{3.84}$$

where α and β assume the values x, y, and z, the D are the tensor components of the perturbing-molecule quadrupole moment, M_β and R_α are the components of the dipole moment and the distance R between the interacting molecules on the axis of a fixed reckoning system centered on the H_2O molecule.

Using matrices for conversion from the components of the dipole-moment vector and the quadrupole-moment tensor in the fixed system to a system bound to the molecule, it is easy to obtain an expression for C(t) from (3.84): /129

$$C(t)=\sum_{\substack{m_1k_1\\m_2k_2}} C^{j_1j_2}_{m_1k_1m_2k_2}D^{j_1}_{m_1k_1}D^{j_2}_{m_2k_2}, \tag{3.85}$$

where $m_1 = 1, 0, -1$; $m_2 = 2, 1, 0, -1$; $k_1 = 1, -1$; $k_2 = 0$; $j_1 = 1$; $j_2 = 2$; the D^j_{mk} are generalized spherical functions.

Substituting (3.83) into (3.84) and applying (3.85), we obtain after certain manipulations

$$\begin{aligned}S_{j_2}(\rho)=\frac{1}{2}\sum|a^{12}_{m_1k_1m_2k_2}|^2\langle j_2M_2|D^2_{m_2k_2}|j_2'M_2'\rangle\times\\ \times\langle j_2'M_2'|D^2_{m_2'k_2'}|j_2M_2\rangle\langle j\tau m|D^1_{m_1k_1}|j''\tau''m''\rangle\times\\ \times\langle j''\tau''m''|D^1_{m_1'k_1'}|j\tau m\rangle\frac{1}{(2j+1)(2j_2+1)}+\\ +\text{ a similar term for the final state,}\end{aligned} \tag{3.86}$$

where

$$a^{12}_{m_1k_1m_2k_2}=\left\langle v\left|\frac{1}{\hbar}\int_{-\infty}^{\infty}e^{-i\omega_{\alpha\beta}t}C^{12}_{m_1k_1m_2k_2}(t)\right|v\right\rangle, \tag{3.87}$$

$$\omega_{\alpha\beta}=\frac{E_{v''j''\tau''}-E_{vj\tau}+E_{j_2}-E_{j'_2}}{\hbar}. \tag{3.88}$$

In (3.87), the summation is extended over all indices except v, j, m, and j_2 for the original state and v', j', m', and j_2 for the final state.

Using the representation (3.73), the relation between the rotor wave functions and the D functions, and the expression for the integral of the product of the three D functions in terms of Clebsch-Gordan coefficients [205] and summing in (3.86) over m, m", M_2, and M_2', we obtain

$$S_{j_2}(\rho) = \sum |a^{12}_{m_1 k_1 m_2 k_2}|^2 \frac{(g_k^{[vj\tau]})^2 (g_{k''}^{[v''j''\tau'']})^2}{15} \times$$
$$\times (jj_1 k - k_1 | j'' k'')^2 (2j_2 00 | j_2' k_2') +$$
$$+ \text{ a similar term for the final state,} \qquad (3.89)$$

where (abcd|ef) are the Clebsch-Gordan coefficients.

The summation over m_1, m_2, and k_1 in (3.89) can be carried out using Appendix C of [71]. We finally obtain /130

$$\sum_{m_1 k_1 m_2} |a^{12}_{m_1 k_1 m_2 k_2}|^2 = \frac{D^2 \mu^2_{vv''}}{\hbar^2 v^2 \rho^6} f(x) \qquad (3.90)$$

where

$$f(x) = \frac{1}{288}\{x^6 [18k_3^2 + 12k_2^2 + 78k_1^2 + 84k_0^2]| + x^4 [-32k_2^2 - 96k_1^2]\};$$
$$x = \frac{\rho}{v}\omega_{\alpha\beta};$$
$$\mu^2_{vv''} = |\langle v_i' | \mu_{x'} + i\mu_{y'} | v'' \rangle|^2,$$

$k_n(x)$ are Hankel functions, for which the representation (8, 432, 5) of [207] is used, μ_x and μ_y are the dipole-moment components of the H_2O molecule in a fixed coordinate frame. After substitution of (3.89) with regard to (3.90), the integral of (3.81) diverges for small ρ. This is a consequence of the fact that the distance between the charge systems is assumed to be larger than the dimensions of the systems themselves in the derivation of (3.84).

Following [71], we assume

$$S(\rho) = 1 \quad \text{for} \quad 0 \leqslant \rho \leqslant \rho_0.$$

With this, we obtain from (3.82)

$$\sigma_{j_2} = \pi\rho_0^2 + 2\pi \int_{\rho_0}^{\infty} S_{j_2}(\rho)\, d\rho. \qquad (3.91)$$

Omitting certain intermediate operations, we obtain the following formulas for the half-width of a spectral line from (3.80), (3.89), (3.90), and (3.91):

$$\gamma(vj\tau m \to v'j'\tau'm') =$$
$$= \frac{Nv}{2c} \sum_{j_2} B_{j_2}\rho_{j_2}^2 (vj\tau m \to v'j'\tau'm') \times$$
$$\times \rho_{j_2}^2 (vj\tau m \to v'j'\tau'm') =$$
$$= \rho_0 \left\{ 1 + \frac{1}{45\hbar^2 v^2 \rho_0^6} \sum D^2 \mu_{vv''}^2 (g_k^{[vj\tau]})^2 \times \right.$$
$$\times (g_{k''}^{[\tau''j''\tau'']})^2 (j \mid k - k_1 \mid j''k'')^2 (j_2 j_2 00 \mid j_2' 0)^2 f(x_0) +$$
$$+ \text{ a similar term for the final state,}$$

/131

$$f(x_0) = \frac{1}{32} x_0^6 [3k_2(x_0) k_4(x_0) + 2k_1(x_0) k_3(x_0) +$$
$$+ 13k_0(x_0) k_2(x_0) - 3k_3^2(x_0) - 2k_2^2(x_0) + k_1^2(x_0) - 14k_0^2(x_0) -$$
$$- \frac{x_0^4}{3} \int_{x_0}^{\infty} \frac{1}{x} [k_2^2(x) + 3k_1^2(x)]\, dx,$$

where

$$x_0 = \left| \frac{\rho_0}{v} \omega_{\alpha\beta} \right| > 0,$$

since its sign is everywhere without influence on the results, as was seen in the course of the calculations.

In these last expressions, D is the quadrupole moment of the perturbing molecule, $\mu_{vv''}^2$ is the square of the dipole-moment matrix elements of the v → v" transition, elements for which analytical expressions can be obtained [142].

2. Experimental investigations. Experimental studies of line half-widths are usually conducted simultaneously with determination of the line strength and present a rather complex task. This is because very limited data have thus far been obtained on the half-widths of H_2O absorption lines.

Becker and Autler [208] determined the half-width of H_2O lines in the microwave region of the H_2O rotational spectrum (ν_0 = = 0.744 cm^{-1}). The authors of [208] found that collisions between molecules broaden the line by an amount 4.7 times larger than collisions between water and air molecules.

The half-widths of a series of lines in the region of the 2.7-μ band were measured by K.P. Vasilevskiy [195-197]. A detailed investigation of the broadening effects of various gases

was made for the line centered at $\nu_0 = 4025.38$ cm^{-1}. The acquired experimental data are described accurately by the formula

$$\gamma = \gamma^0 (P_a + \sigma_{a,b} P_b), \qquad (3.92)$$

where γ^0 is the half-width of the lines at an effective pressure $P = P_a + \sigma_{a,b} P_b = 1$ atm and a temperature $T = 293°K$; P_a and P_b are the partial pressures of the absorbing and extraneous gases, and $\sigma_{a,b}$ is the relative effectiveness of optical collisions between molecules a and molecules b.

For collisions between molecules of H_2O and CO_2, air, N_2, and Ar, the values of $\sigma_{a,b}$ were found equal to 0.239, 0.170, 0.165, and 0.123, respectively, indicating a strong dependence of γ on the nature of the broadening gas. The line broadening due to collisions between water molecules was found to be six times that resulting from collisions between water and air molecules. /132

The half-width of the line centered at $\nu_0 = 914.03$ cm^{-1} was measured by Saidy [199]. Sanderson and Ginsburg [198] determined the half-widths of three lines and found them to be approximately 1.5 times larger than indicated by calculations based on the Anderson theory. The half-width of the 1_1-1_{-1} line ($\nu_0 = 18.6$ cm^{-1}) was determined in [786] for collisions of water molecules with one another and with air, oxygen, and nitrogen molecules. Its values were found equal to 0.5 ± 0.2; 0.05 ± 0.01; 0.03 ± 0.02; and 0.06 ± 0.02 cm^{-1}·atm^{-1}, respectively. The half-widths of the 4_0-5_{-4} ($\nu_0 = 10.86$ cm^{-1}); 2_2-3_{-2} ($\nu_0 = 6.1$ cm^{-1}) and 3_1-4_{-3} ($\nu_0 = 12.67$ cm^{-1}) lines for collisions between water and air molecules were measured in [787-789]; the half-width values of these lines were found equal to 0.101; 0.107 ± 0.005; and 0.105 ± 0.004 cm^{-1} in the ground layer of the atmosphere.

6. ABSORPTION FUNCTIONS IN NARROW SEGMENTS OF THE VIBRATIONAL-ROTATIONAL AND PURELY ROTATIONAL SPECTRA OF WATER VAPOR

1. Direct calculation of absorption functions. Cowling [209] calculated the absorption functions for segments 25 cm^{-1} wide in the region of the purely rotational water-vapor spectrum from 100 to 350 cm^{-1}. The data on the line positions and strengths were borrowed from [170]. The line half-widths were assumed constant at values from 0.05 to 0.4 cm^{-1}. Using theoretical data on the line parameters of the purely rotational H_2O spectrum, Benedict [210] calculated absorption functions for various frequency intervals. It was found that for broad enough intervals, the values obtained for these functions differed little from those calculated by the spectrum-model method.

Calfee [189] calculated the absorption functions in segments of the vibrational-rotational spectrum of water vapor in the infrared. The calculation was based on experimental data on the line-center positions. The strengths and half-widths of the lines were determined by the method described in the preceding section. /133 No systematic allowance was made for the vibrational and rotational motions of the H_2O molecules.

The relation obtained for spectral absorption as a function of wavelength was multiplied by the spectrometer instrumental function to permit, on the one hand, comparison of the calculated results with experiment and, on the other, investigation of the influence of the spectrometer's parameters on the nature of the spectrum recorded with it.

A.G. Pokrovskiy [882] derived algorithms and calculated the spectral absorption and absorption functions in a narrow segment of the spectrum (3795-3836 cm^{-1}) and for a single line (ν_0 = = 1677.95 cm^{-1}). An important advantage of the algorithms used in this study is that they take account of both the Doppler and the dispersion line contours. The data on absorption at various heights that were obtained for the single line indicate clearly the need to consider Doppler broadening in the central region of the line beginning at heights as low as 10 km.

K.Ya. Kondrat'yev and Yu.M. Timofeyev [211] calculated absorption functions for eight narrow segments of the spectrum, ranging in width from 5.3 to 8.5 cm^{-1}, in the 20-50-μ region for pressures of 1000, 500, 100, and 10 mbar and temperatures of 300, 260, and 220°K. Analysis of the temperature curves of the absorption functions indicated that they are governed chiefly by the effect of temperature on the strength of the lines, which is unique for each specific segment of the spectrum. Thus, the quantity m in the temperature correction to the transmission function

$$f(T) = (T/T_0)^m$$

varies from 0.86 to 4.0 for the segments studied.

Yu.M. Timofeyev [883] used a direct calculation of the absorption functions A to estimate the errors incurred in computing A by the approximate method. It was shown in [883] that these methods are subject to the largest errors when the mixing ratio of the absorbing gas increases with increasing height.

K.Ya. Kondrat'yev and Yu.M. Timofeyev [884] analyzed the possibilities of direct calculation of transmission functions in narrow segments of the atmospheric-gas absorption spectra for various stratifications of the atmosphere. They pointed out the promise of this method for overlapping bands and solution of inverse problems.

A calculation of the absorption functions for specific segments of the vibrational-rotational water-vapor spectrum in the visible and infrared regions was carried out in our paper [780] on the basis of theoretical data on the center positions, strengths, and half-widths of the lines. /134

2. Calculations of absorption functions using the spectrum-model method. Plass and Stull [212] calculated infrared absorption functions for water vapor and CO_2 in relatively narrow segments of the spectrum 10-20 cm^{-1} wide, using the statistical, combined, and Elsasser models. The experimental data of Howard, Burch, and Williams [213] were used to determine the fitting parameters.

A new series of absorption-function calculations was made in the work of Wyatt, Stull, and Plass for narrow segments of the spectrum in the fundamental vibrational-rotational bands of water vapor [214] and CO_2 [215], using a quasistatistical model proposed by the authors (see §3). The water-vapor absorption functions were calculated in the range of wavelengths from 1 to 10 μ for spectral intervals 2.5 cm^{-1} wide in the 997.5-3400-cm^{-1} region and 20, 50, and 100 cm^{-1} wide in the 1000-10,000-cm^{-1} region. In the last three cases, the data were obtained at intervals of 10, 25, and 50 cm^{-1}, respectively. The absorption functions for the 2.5-cm^{-1} intervals were calculated using the results of [166]. The rest of the data were obtained on the basis of calculated relative line strengths in the vibrational-rotational spectrum of water vapor as given in [214] and reduced to an absolute scale by application of the experimental results from [216].

The absorption functions for these spectral intervals were calculated for 15 values of the precipitated layer of water vapor ω from 0.001 to 50 cm, for seven values of the pressure P: 1.0, 0.5, 0.2, 0.1, 0.05, 0.02, and 0.01 atm, and three values of the temperature T: 200, 250, and 300°K.

Some of the data obtained were published in [217] together with the calculation procedure; this reference also gives a table of transmission-function values for segments 100 cm^{-1} wide at T = 300°K and P = 1 atm for 15 values of ω.

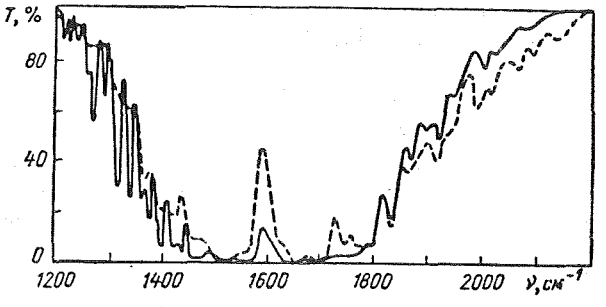

Figure 3.3. Absorption Functions in Narrow Segments of the Spectrum in the 6.3-μ H_2O Band According to the Experimental Data of [216] and Calculation [214]. Solid curve represents experiment, P = 805 mm Hg, w = 0.0707 cm; dashed line represents calculation for P = 760 mm Hg, w = = 0.1 cm.

Figure 3.3 compares the calculated [214] and experimental [216] results for the strongest and widest vibrational-rotational band of water vapor at 6.3 μ. The satisfactory agreement shown in the figure between the two sets of data indicates the possibility of quite accurate calculation of absorption functions in narrow spectral segments by means of band models if their fitting parameters are correctly determined from the experimental data [216, 218]. /135

In an attempt to obtain values of the absorption functions for spectral intervals 0.1 μ wide that would be convenient for practical use, we made the corresponding calculation [219] on the basis of fitting parameters obtained in [212], except for the 3.2, 1.87, 1.38, and 1.1-μ absorption bands, for which we used the statistical-model formula with the fitting parameters obtained in [213]:

$$T=\exp\left[\frac{-\frac{\omega}{\omega_0}k\gamma}{\bar{d}\left(\gamma^2+\frac{\omega}{\omega_0}\frac{k\gamma}{\pi}\right)^{1/2}}\right]=\exp\left[\frac{-\frac{\omega}{\omega_0}\alpha}{\left(1+\frac{\omega}{\omega_0}\delta\right)^{1/2}}\right], \qquad (3.93)$$

where $\alpha = k/\bar{d} = 1.97$ and $\delta = k/\pi\gamma = 6.67$ are the fitting parameters determined from the experimental data and ω_0 is the precipitated layer of water vapor corresponding to T = 0.5. The calculation was made for the following total-pressure values: 1.0, 0.9, 0.7, 0.5, 0.3, 0.1, 0.05, and 0.01 atm, which correspond to heights of 1, 3, 5, 10, 16, 21, and 31 km in the atmosphere. The values of the precipitated water layer were adjusted for each height so as to cover distances from 0.1 to 100 km at the humidities encountered in the real atmosphere. /136

All calculated data were transferred to diagrams from which the transmission-function value can be found directly for a given interval of width 0.1 μ for any values of the pressure P and precipitated layer ω encountered in horizontal layers of the atmosphere on distances from 0.1 to 100 km and at heights from 0 to 30 km [790].

3. Experimental determination of absorption functions. Quite a few papers have been devoted to experimental determination of absorption functions. The groups of Howard [112, 213], Burch [216, 221], and B.M. Golubitskiy [791-793] performed the most extensive studies.

Howard's group investigated the spectral absorption of the fundamental vibrational-rotational bands of H_2O in the infrared at 6.3, 3.2, 2.7, 1.87, 1.38, 1.1, and 0.94 μ and the 3.7 [μ] band of HDO. Reduction of the experimental data yielded the following empirical relationships for the integral absorption of the bands:

$$\int_{\nu_1}^{\nu_2} A(\nu)\,d\nu = c\omega^{1/2}(P+P_a)^k, \tag{3.94}$$

$$\int_{\nu_1}^{\nu_2} A(\nu)\,d\nu = C + D\lg\omega + K\lg(P+P_a), \tag{3.95}$$

where ω and P_a are the precipitated layer in cm and the water vapor partial pressure in mm Hg; $P = P_{N_2} + P_a$ is the total pressure, and c, k, C, D, and K are empirical constants.

Formulas (3.94) and (3.95) describe the integral absorption of the band at small and large values of ω, respectively, as given in [112] for each band. The integral absorption of the band is determined for intermediate values of ω by extrapolating the data obtained from (3.94) and (3.95).

The results obtained by Howard's group were very quickly put to use in various calculations. Larmor and Passman [222] used them as a basis for compiling a series of tables for the transmission of radiation by the atmosphere at sea level and at various heights in spectral intervals taken every 0.1 μ. Langer [223] determined the transmission in the atmosphere's most important transparency windows. Roach [224] calculated the absorption of solar radiation in a cloudless atmosphere. These data were used extensively in our own work to calculate the integral absorption function and absorption functions in spectral intervals occupied by specific bands [225]. /137

Burch's group used spectroscopic apparatus of resolution higher than in [213], so that it was possible to obtain more reliable information on absorption in narrow segments of the spectrum and to investigate absorption-band broadening effects on changes in the total and partial pressures of the absorbing and nonabsorbing gases. The absorbing gases studied were H_2O, CO_2, N_2O, CO, and CH_4. The problem consisted in determining $B = C_{a,a}/C_{a,b}$, which characterizes the ratio of the abilities of the gas to broaden lines due to collisions among its molecules (self-broadening) and collisions with molecules of an extraneous gas, for which the authors used N_2.

The experimental results showed that B varies over the spectrum (Table 3.1). This becomes understandable when we remember that the optical-collision diameters vary from line to line. For example, B changes from 0.9 to 0.13, i.e., increases by a factor of one and a half, from 2250 to 2175 cm^{-1} for the 2224-cm^{-1} N_2O band.

Formulas that give a close approximation of the experimental data for the integral absorption of the bands were arrived at on

TABLE 3.1. VALUES OF THE SELF-BROADENING COEFFICIENTS B OF ABSORPTION LINES AND BANDS FOR H_2O, N_2O, CO_2, CO, AND CH_4 ACCORDING TO VARIOUS AUTHORS

Gas	Bands, cm^{-1}	Authors	B
Water vapor H_2O	5332, 3756, 1595	Burch etal [226]	5±1.5
	500 cm^{-1} region	region Palmer [227]	11−6T *
	Line 4025,4	Vasilevskiy and Neporent [195]	6
	4 lines in the 500-600 cm^{-1} region	Izatt [228]	3.6−5.5
N_2O	2224, 1285, 1167	Burch et al [226]	1.12±0.07
	1285	Goody and Wormell [229]	1.27±0.04
	1167	Goody and Wormell	1.35±0.07
	2224	Cross and Daniels [230]	1.29
CO_2	3716, 3609, 2350 961, 875—495	[226]	1.30±0.08
	3716, 3609, 2350, 961, 875—495	Edwards [231]	$2+0.5P_a$ **
CO	2143	[226]	1.02±0.06
	4260	[226]	1.08±0.06
CH_4	3020	[226]	1.30±0.08
	1306	[226]	1.38±0.08

*T is the spectral transmission T(ν).
**P_a is the CO_2 partial pressure in the atmosphere.

the basis of reduction of measured data in [216]:

$$\int_{\nu_1}^{\nu_2} A(\nu)\,d\nu = c\,[\omega P_e^a]^b, \tag{3.96}$$

$$\int_{\nu_1}^{\nu_2} A(\nu)\,d\nu = C + D \lg [\omega P_e^a], \tag{3.97}$$

where a, b, c, C, and D are empirical constants, $P_e = P + (B - 1)P_a$ is the effective pressure, including the total pressure P, the partial pressure P_a, and the self-broadening coefficient B of the lines.

TABLE 3.2. RANGES OF VALUES OF PRECIPITATED WATER-VAPOR LAYER IN MEASUREMENTS OF INTEGRAL ABSORPTION IN VARIOUS H_2O BANDS IN [213, 216]

Bands μ	Precipitated layer ω, cm	
	Howard [213]	Burch [216]
0.94	0.01—3.85	
1.1	0.01—3.85	
1.38	0.01—3.85	
1.87	0.01—3.85	0.003—0.11
2.7	0.002—2.4	0.003—0.11
3.2	0.002—2.4	0.003—0.11
6.3	0.02—1.2	0.002—0.07

A valuable result of this series of studies consists in the fact that it was not limited to water vapor and CO_2, but also included minor impurities. Thus, it is now possible to make quantitative estimates of the role of trace impurities in infrared absorption under natural atmospheric conditions. /138

Table 3.2 presents the ranges of variation of the precipitated water layer in centimeters for various absorption bands as realized in the experiments of the Howard and Burch groups. /139

A new series of measurements of water-vapor absorption spectra in the 0.6-5.5-μ region made by Burch et al. [81] makes it possible to determine absorption functions in very narrow segments of the spectrum in the visible and infrared regions. In this series, the measurements were made at various temperatures extending up to 1800°K.

B.M. Golubitskiy et al. [791-793] made experimental studies of the water vapor absorption functions for spectral segments ranging from 3 to 20 cm^{-1} in width in the wavelength band from 1 to 14 μ. The measurements were made at various water-vapor temperatures and various values of the precipitated-water layer equivalent to its thickness in the ground layer of the real atmosphere, which reaches 12 cm. Reduction of the measured results yielded an empirical relation that satisfactorily describes the dependence of the transmission function on the precipitated water layer ω and the pressure P:

$$T_\lambda = \exp\{-\beta_\lambda \omega^{m_\lambda} P^{n_\lambda}\}, \qquad (3.98)$$

where β_λ, m_λ, and n_λ are empirical parameters determined for spectral intervals of various widths.

The authors of [785-787] affirm that (3.98) describes the measured absorption-function data with rather high accuracy (the relative error does not exceed 6-8% for values of $\omega \leq 12$ cm and $P \leq 1$ atm). Their comparison showed satisfactory agreement of the available experimental data on the absorption functions with the calculated data according to (3.98).

A paper by M.S. Kiseleva [794] proposed empirical formulas that give an approximate description of the absorption function in a given spectral interval when its value lies in the range $0.05 \leq A \leq 0.9$.

Stauffer and Walsh [232] measured the transmission of a mixture of water vapor and nitrogen in the 14-20-μ range. They obtained a set of curves plotted for various values of the total and partial pressures. The precipitated water layer was varied from 0.0037 to 1.163 cm, the nitrogen pressure from 0.00286 to 0.805 atm, and the water-vapor pressure from $0.264 \cdot 10^{-3}$ to $11.5 \cdot 10^{-3}$ atm. The results of the measurements were in good agreement with Benedict's calculations [210].

Palmer [233] measured transmission functions in the region of the purely rotational H_2O spectrum for various values of the H_2O and nitrogen partial pressures, nitrogen being the extraneous gas. Transmission functions for intervals 10 cm^{-1} wide were found in the 500-320-cm^{-1} region, for 5-cm^{-1} intervals in the 340-200-cm^{-1} region, and for seven overlapping intervals 50 cm^{-1} wide in the region from 200 to 500 cm^{-1}. The data obtained agree well with Benedict's calculations [210] for wide intervals. As the spectral interval is narrowed, the experimental data deviate further from the calculations.

Burch and Reisman [234] measured the absorption by water vapor and its mixtures with nitrogen in the region of the long-wave transparency window around 340 μ.

4. Integral strengths of absorption bands. Knowledge of the integral strengths of absorption bands is highly important for investigation of the fine structure of the spectra and determination of the absorption functions of both whole bands and specific parts of bands. This explains the rather numerous papers devoted to measurements of the integral strengths of bands of various atmospheric gases, including water vapor. New measurements of the strengths of a series of bands have been made in recent years in /141
spectra recorded at high temperatures.

Goldstein [235] measured the integral strengths of the 1.38, 1.87, 2.7, and 6.3-μ bands at temperatures of 200, 400, 600, and 727°C. The emission spectra of water vapor were investigated at

various temperatures in a series of papers by Ferriso and Ludwig et al. [236-239]. The 6.3-μ band was recorded at temperatures of 540, 1030, 1535, 1850, and 2200°K. The fine structure of the spectrum was practically washed out at temperatures above 1800°K, so that integral-strength measurements were easier. Spectral emission in the 10-22-μ region was recorded at temperatures of 590, 850, 1040, 1640, 1830, and 2200°K. Transmission spectra of H_2O were measured in a broad range of wavelengths from 1 to 25 μ at 2750°K. The authors of [236-239] found the integral strengths of various bands from emission-spectrum measurements.

Goldman and Oppenheim [240] determined the integral strengths of the 1.87 and 2.7-μ bands on the basis of H_2O emission spectra at 1200°K.

Reference [241] presents the results of measurements of water-vapor absorption as the temperature varies from 300 to 1100°K, which were used to obtain the integral strengths of the vibrational-rotational bands around 1.38, 1.87, and 6.3 μ and that of the shortwave end of the rotational band to a wavelength of 20 μ.

The integral-strength values obtained by various authors for the H_2O bands are assembled in Table 3.3.

5. Absorption by far limbs of strong lines. The role of the far limbs of strong lines in the absorption of radiation in the atmospheric transparency windows is a major one. The continuous absorption due to the far limbs of strong lines may be the dominant factor in determination of absorption functions in the transparency windows. It is therefore most important to have accurate enough data on the absorption coefficients and functions of the so-called continuum. To this we should add that it is precisely through the spectral intervals of the transparency windows that most radiant transfer takes place in the atmosphere.

The idea that the continuous absorption in remote limbs of strong lines might be important in the attenuation of radiation in the windows was advanced by Elsasser back in 1938. Arbitrarily setting the coefficient of continuous absorption equal to 0.1 per unit of air mass in the 8-13-μ region, Möller [244] estimated the /142
value of this absorption for meteorological purposes. The existence of continuous absorption in the 8-13-μ window is confirmed in the measurements of Gebbie et al. [245] and Taylor and Yates [246] in the ground layer and those of Adel [247] and Anthony [248] using the sun as the radiation source. V.G. Kastrov represented the absorption coefficient in the 8-13-μ interval as the sum of the continuous-absorption coefficients according to Adel and the weak-line absorption coefficients according to Weber and Randall [249].

Roach and Goody made a quantitative experimental study of the continuous absorption in the 8-13-μ window in 1958 [250]. /143

TABLE 3.3. INTEGRAL STRENGTHS OF H_2O ABSORPTION BANDS ACCORDING TO VARIOUS AUTHORS

Bands, μ	Integral strength, $cm^{-2} \cdot atm^{-1}$	Measurement temperature K	Authors
6,3	300±20%	273	[236]
	350±15%	2750	[239]
	220±22 *		[201]
	247±10%	273	[235]
2,7	230±15%	2750	[239]
	206±21 **	1000	[235]
	177±18 ***	1000	[235]
	182±36 **	530—2200	[242]
	165±33 ***	530—2200	[242]
	198±20 **	1200	[240]
	180±18 ***	1200	[240]
	192±28	300	[202]
	172±7	300	[203]
1,87	22,3±2,2 **	873	[235]
	23,7±1,7 **	1000—2200	[243]
	18,0±2,7 **	1200	[240]

*Reduced to standard conditions.
**Reduced to 300°K.
***Reduced to 300°K and corrected by the authors of [203].

Measurements made at London and Ascot (a rural locality) of the attenuation of solar infrared radiation in selected narrow segments of the spectrum with a resolution of about 7 cm^{-1} made it possible to separate the selective absorption of weak lines falling in the particular segment from the total attenuation. The measurements were made on clear days. Values about 50 times larger than those due to aerosol attenuation in such weather according to Volz [251] were obtained at Ascot for the continuous-attenuation coefficients. The attenuation at London was several times the attenuation at Ascot, a fact attributed to the heavy pollution of the London atmosphere. A major deficiency of Roach and Goody's work consisted in their failure to make measurements of attenuation in the visible region, data from which could have been used to separate aerosol attenuation.

Another study in quantitative investigation of continuous absorption in the same 8-13-μ window was performed in 1963 by Bignell, Saidy, and Sheppard [252], who eliminated the methodological deficiencies of the first study, which included, in addition to the lack of measurements in the visible region, a low spectrometer resolution. The studies were made by two methods for 19 frequencies in the 1202-479-cm^{-1} (8.32-20.9-μ) range: 1) using

TABLE 3.4 VALUES OF THE COEFFICIENT k_a OF CONTINUOUS ABSORPTION BY FAR LIMBS OF STRONG WATER-VAPOR LINES FOR VARIOUS WAVELENGTHS ACCORDING TO [252] (PRESSURE P = 1 atm, ABSOLUTE HUMIDITY 12 mbar)

λ, μ	8.32	8.66	8.86	9.13	10.14	10.40	11.10
k_a, $g^{-1} \cdot cm^2$	0.074	0.0601	0.0595	0.0625	0.0666	0.0685	0.0925
λ, μ	11.44	11.82	12.02	12.20	12.66	13.96	
k_a, $g^{-1} \cdot cm^2$	0.105	0.114	0.119	0.119	0.158	0.6±0.2	
λ, μ	16.38	17.02	17.88	18.83	20.12	20.88	
k_a, $g^{-1} \cdot cm^2$	0.8±0.1	1.4±0.1	1.7±0.1	2.0±0.1	3.0±0.1	4.1±0.1	

TABLE 3.5. VALUES OF COEFFICIENT k_a OF CONTINUOUS ABSORPTION BY FAR LIMBS OF STRONG WATER VAPOR LINES IN VARIOUS NARROW SEGMENTS OF THE SPECTRUM ACCORDING TO [253]

λ, μ	3.58	3.70	8.15	8.30	8.53	8.76	8.86
k_a, cm^{-1}	0.07	0.062	0.15	0.12	0.10	0.10	0.095
λ, μ	9.10	10.18	10.40	10.62	10.92	11.11	
k_a, cm^{-1}	0.090	0.085	0.085	0.090	0.11	0.12	
λ, μ	11.51	11.98	12.18	12.72	12.95	13.95	
k_a, cm^{-1}	0.15	0.15	0.16	0.21	0.22	0.225	

the sun as the source (1202-790-cm^{-1} range); 2) on horizontal paths of 200 and 400 meters using a Nernst lamp (range from 716 to 479 cm^{-1}). The results of the measurements indicated that the continuous absorption coefficient varies from 0.06 to 4.1 $g^{-1} \cdot cm^{-2}$ in the wavelength band studied. More detailed data appear in Table 3.4.

A special laboratory study of CO_2 absorption showed that its effects on the measured results can be disregarded outside of the spectral range from 790 to 560 cm^{-1} (12.7-18 μ).

Table 3.5 lists values of the continuous-absorption coefficient obtained from measurements of the solar spectrum at the alpine station of the Atmospheric Physics Department of Leningrad University on Mt. El'brus [253].

Data on the continuous-absorption coefficients have also been obtained in [874-875] for the 8-25-μ wavelength range and in [876] for the 8-14-μ range.

In conclusion, we stress the need for continuing quantitative /144
experimental research on this phenomenon. Such investigations are important primarily because theoretical solution of this problem is difficult without analytical expressions that describe quantitatively and with sufficient accuracy the remote limbs of spectral absorption lines.

7. FINE STRUCTURE OF THE ABSORPTION SPECTRUM OF CARBON DIOXIDE /145

A considerable number of experimental and theoretical studies have been devoted to the fine structure of the vibrational-rotational spectrum of CO_2. The bands around 15 and 4.3 μ were subjected to most detailed analysis in the early papers. The bands around 15 μ are important in the absorption of long-wave radiation in the atmosphere. The 4.3-μ bands are so strong that their absorption can be detected even in the thermosphere. Investigators have attempted to use this circumstance to reconstruct vertical temperature profiles up to high altitudes with the aid of appropriate outgoing-radiation measurements [254].

The possibility of using the CO_2 absorption bands in the 4.3- and 15.0-μ regions and at other frequencies to solve inverse problems of satellite meteorology has given rise in recent years to a substantial number of publications in which the fine structures of all of the fundamental bands were investigated. Below we set forth briefly the results of research done by various authors on specific absorption bands.

1. **Bands around 15.0 μ.** The detailed structure of the band spectrum was first investigated theoretically in this region by Kaplan [255] and Yamamoto and Sasamory [256]. These authors obtained data on the line positions and strengths. The calculation was made for the basic isotope without consistent allowance for the interaction between the molecule's vibrational and rotational motions and the Coriolis interaction. The relative strengths of the lines in the bands of this region were computed by Wyatt, Plass, and Stull [212, 215].

The most accurate experimental data on the center positions of lines in the region of the 15.0-μ bands were obtained by Gordon and McCubbin [257]. The authors of this paper succeeded in attaining very high spectral resolution at the practical limit of echelette interferometry. This enabled them to determine the line-center positions accurate to within a few thousandths of a cm^{-1}. Comparison of the experimental data obtained with theory indicated that they agree to within 0.01 cm^{-1} for most lines, with the maximum disagreement not exceeding 0.027 cm^{-1}.

The half-widths γ of the lines in these bands were determined /146 experimentally by Kaplan and Eggers [258] and Madden [61]. In the former study, only strong lines were considered, and the value obtained for γ was 0.064 cm^{-1}. However, Kaplan subsequently reviewed the results of this work and found a value of 0.075 cm^{-1} for γ under standard conditions. Madden [61] found the line half-width to depend on the rotational quantum number, which is different for each of the bands in the region under investigation.

The half widths and strengths of a series of lines in the P and R branches of the 10^00-00^01 band were determined in [795-797] using a CO_2-nitrogen laser as the radiation source. In this case, the emission- and absorption-line centers coincide and the expressions for the Doppler and Lorentz line contours are simplified and can be used for quite accurate determination of the parameters of the corresponding lines.

TABLE 3.6. DATA ON CO_2 BANDS AROUND 4.3 μ INVESTIGATED IN [79]

Isotope	State	Allowed values of j	Center of band cm^{-1}	Greatest value of j
$C^{12}O_2^{10}$	0 0^0 0	Even	2349.5	70
$C^{13}O_2^{16}$	0 $1^{\pm1}$ 0	Even and odd	2339.2	54
$C^{13}O_2^{16}$	0 0^0 0	Even	2283.7	70
$C^{13}O_2^{16}$	0 $1^{\pm1}$ 0	Even and odd	2273.4	54
$C^{12}O^{18}O^{16}$	0 0^0 0	Even and odd	2331.8	48
$C^{13}O^{18}O^{16}$	0 0^0 0	Even and odd	2266.0	48

2. Bands in the 4.3-μ region. The center positions and strengths of lines in these bands have been studied on several occasions by various authors. The most important results were obtained in the work of Nielsen and Yao [259], Benedict, Herman, and Silverman [260], Winters, Silverman, and Benedict [78], Wyatt, Plass, and Stull [212, 215], Courtoy [261], Gray and Selvidge [262], Kyle, D. Murcray, F. Murcray, and Williams [79], and Migeotte, Neven, Swenson, and Benedict [182]. Reference [259] gives an analysis of the ν_3 bands for the isotopes $C^{12}O_2^{16}$ and $C^{13}O_2^{16}$, [260] investigated the R branches of the bands, and [261] obtained the most detailed trace of the spectrum in the 4.3-μ region.

The strengths of the lines were computed in [212, 215] in the eight isotopic modifications of CO_2. The relative line strengths for transitions from the molecular states 00^00 and 01^10 are obtained in [262]. The positions and strengths of about 300 lines were calculated in [79]. The calculation indicated that the 80

strongest lines make a 97.1% contribution to the integral strengths of the bands. Table 3.6 presents data on the bands studied in [79].

The line half-widths γ in the region of the 4.3-μ band have not been thoroughly studied. In calculations of the absorption coefficients and functions, γ is usually assumed to be uniform at 0.066 cm^{-1} under standard conditions.

3. Bands in 2.7- and 2.05-μ regions. The positions of the line centers and their strengths have been studied in greater detail in the regions of the 2.7- and 2.05-μ bands than in any other bands, thanks to the work of Calfee and Benedict [263]. /147

The authors of [263] calculated the center positions and strengths of 2826 lines in the region of the 2.05-μ band and 4790 lines in the region of the 2.7-μ band. In this paper, all molecular parameters used in the calculations for each band are tabulated in detail. The line positions are calculated with account of the interaction between the vibrational and rotational motions of the molecule due to centrifugal distortion and Coriolis forces. The line strengths were calculated without consistent consideration of the vibrational-rotational interaction in the molecule. The scheme described in §5 was used to calculate the line strengths, along with data on the band intensities obtained in the studies of Burch's group.

The table of line-center frequencies and line strengths given in [263] covers all rotational levels of the molecule with rotational quantum numbers $j \leq 100$. This means that it covers practically all lines that can appear in measurements in the earth's atmosphere. In a review of [263], Williams [264] states that he is among those prepared to offer a reward for the discovery of lines not tabulated in [263].

The relative strengths of the lines in these bands were calculated in [212, 215].

A whole series of papers by various authors has been devoted to experimental study of the fine structure of the spectrum and specific elements of it in the regions of the 2.7- and 2.05-μ absorption bands. A bibliography of these papers can be found in the well-known monographs of Hertzberg [798] and Goody [3] and in the paper of Gordon and McCubbin [265]. /148

The most detailed experimental study of line positions in the 2.7-μ region was carried out in [265]. Its authors measured the center positions in 10 bands of the isotope $C^{12}O_2^{16}$, one band of the isotope $C^{13}O_2^{16}$, and two bands of the isotope $C^{16}O^{16}O^{18}$. All measurements were accurate to ± 0.005 cm^{-1}.

K.P. Vasilevskiy et al. [266] measured the half-widths of several dozen lines in the $4\nu_2 + \nu_3$ (2.5-μ) absorption band. The

measurements were made both with pure CO_2 and with $CO_2 + N_2$ mixtures. The strengths and half-widths of almost all lines in the P and R branches of the band were determined. In pure CO_2, the line half-widths γ vary in the range from 0.126 to 0.06 $cm^{-1} \cdot atm^{-1}$ as the rotational quantum number varies from 4 to 50-56. In the gas mixture, γ varies from 0.122 to 0.09 $cm^{-1} \cdot atm^{-1}$.

4. Weak absorption bands. In addition to the strongest CO_2 bands discussed above, there are numerous very weak bands whose fine structure can be brought out either theoretically or in experiments under laboratory conditions with large absorbing masses of carbon dioxide. These bands lie in the spectral regions around 10.4, 9.4, 5.2, 4.8, 1.6, and 1.4 μ and in the intervals between them and between the strong absorption bands, or in the atmospheric transparency windows, including the visible region of the spectrum.

The fine structure of the weak CO_2 bands has not been studied adequately because their role in atmospheric processes is a minor one and their investigation is a rather difficult task. A bibliography of the work done will be found in the monographs [1, 3] and the paper [267].

To recapitulate, analysis of the results of theoretical and experimental study of the fine structure of the CO_2 absorption spectrum suggests the following conclusions. The most comprehensive data on the line-center positions have been determined in experimental studies. Here, the center positions have been found for most lines in all of the fundamental bands with errors of 0.005-0.1 cm^{-1}. Line-center positions have also been calculated /149
for the overwhelming majority of lines. These calculations have not taken systematic account of the vibrational-rotational interaction in the molecule for the individual lines. The errors incurred by this omission are yet to be evaluated.

The largest volume of data on the line strengths has been obtained by calculation. There are very few lines whose strengths have been determined experimentally. Like their positions, the strengths of lines have been calculated without systematic correction for the vibrational-rotational level interaction of the molecule.

There are very few data, either calculated or experimental, on the half-widths of lines in any of the CO_2 vibrational-rotational bands. In all calculations, the line half-widths have been assumed constant within the particular band, although this is not, strictly speaking, the case.

The imprecision in determination of all three line parameters has its strongest effects on the magnitude of the absorption coefficient in the regions of the line centers.

8. ABSORPTION FUNCTIONS IN VARIOUS SEGMENTS OF THE CO_2 SPECTRUM

As in the case of water vapor, the absorption functions in various segments of the CO_2 spectrum are determined by three methods, whose results will be examined below.

1. Direct calculation of absorption functions. Drayson [62] made a detailed calculation of the absorption functions in the interval from 12 to 18 μ. A total of about 2000 lines were used in the calculation, in which their half-widths were assumed constant at 0.064 cm^{-1} at a pressure of 1 atm and a temperature of 298°K. The existing dependence of line half-width on rotational quantum number was not taken into account. The strength, center-position, and half-width data on the lines were used to determine the absorption coefficient, which was used, in turn, to compute the absorption functions.

In the absorption-coefficient calculations, the term γ^2 in the line-contour expression

$$k(\nu) = \frac{S}{\pi} \frac{\gamma}{(\nu - \nu_0)^2 + \gamma^2}$$

was discarded for frequencies that satisfy the condition $(\nu - \nu_0) > 7.0$ cm^{-1}. The error introduced by this operation did not exceed 10^{-4} of $k(\nu)$ at any pressure. /150

The absorption band was broken into short intervals at least 0.001 cm^{-1} wide in the regions of the line centers and 0.1 cm^{-1} wide in the limbs of the lines. The absorption functions were obtained for segments 0.1 cm^{-1} wide and then averaged for intervals 5 cm^{-1} wide.

The calculated results were compared with the experimental data of Burch's group and Yamomoto's calculations. Satisfactory agreement was obtained in the comparison for pressures of 0.2 and 1.0 atm. For low pressures, substantial disagreements were obtained for the central part of the band; in Drayson's opinion [62], they may have been due to errors in determination of the integral band strength (it was taken equal to 194 cm^{-1} in [62]) or to disregard of the dependence of line half-width on rotational quantum number. We note, however, that Grayson's data disagree with those of Yamomoto so strongly at very low pressures that these factors could hardly be the explanation. Thus, for example, this disagreement is more than two orders of magnitude in the absorption function for the spectral segment centered around 15.1 μ for a pressure P = 1 mbar [268]. It is as yet difficult to conjecture as to the true causes of such a strong disagreement.

2. Calculation of absorption functions from spectrum-model formulas. The absorption functions in narrow segments of the CO_2

vibrational-rotational bands were calculated in the studies of Plass, Stull, and Wyatt [212, 215, and 270]. In the first reference, data were obtained on the absorption functions in segments 10-20 cm^{-1} wide in the regions of the 15, 4.3, 2.7, and 2.0-μ bands. In [215], the quasistatistical model was used to compute the absorption functions in segments 2.5 cm^{-1} wide in the 500-1000 cm^{-1} (1-20 μ) interval for three temperatures T: 200, 250, and 300°K, for the same seven pressure values as in the calculations with water vapor: 1.0, 0.5, 0.2, 0.1, 0.05, 0.02, and 0.01 atm and 15 values of the mass of CO_2 from 0.2 to 10,000 atm·cm. We note that the one-kilometer layer of atmosphere at the earth's surface is characterized by a CO_2 mass of about 30 atm·cm. The absorption functions were also obtained in [215] for the above values of the calculation parameters in 20, 50, and 100-cm^{-1} intervals whose centers were spaced at 10, 25, and 50 cm^{-1}, respectively. Some of the data obtained in [215] were published in [269]. Comparison of the calculated data of [215] with the experimental data of [216] showed that they agree closely. /151

To obtain results suitable for practical use using the numerical values of the fitting parameters obtained in [212], we calculated the CO_2 absorption functions for spectral intervals 0.1 μ wide. The absorption functions were calculated in spectral segments 0.1 μ in width in the 15, 4.3, 2.7, and 2.0-μ bands for pressures of 1.0, 0.9, 0.7, 0.5, 0.3, 0.1, 0.05, and 0.01 atm and CO_2 masses corresponding to horizontal-path propagation distances from 0.1 to 100 km at each height. The results obtained were presented in detailed graphs in the monograph [1] and in the article [790].

Reference [271] reports calculations of absorption functions in the region of the 9.4- and 10.4-μ CO_2 bands. The value used for the line half-widths was $\gamma = 0.07$ cm^{-1}; values of 0.016 and 0.030 $cm^{-2} \cdot atm^{-1}$ were taken for the integral band strength at 300°K. Comparison of the calculated results with experimental data for the temperature range from 296 to 555°K indicated satisfactory agreement between the two groups of data.

Gray and McClatchey [272] calculated the absorption functions of mixtures of CO_2, N_2O, and CO in the spectral region from 4.2 to 4.8 μ. The calculated results were presented for various heights in a homogeneous atmosphere. Originally, 99 vibrational levels were included in the calculation. However, it was then found that the result remains practically unchanged if only 27 are used.

3. Experimental determination of absorption functions. The most detailed data on the absorption functions in the regions of the fundamental CO_2 vibrational-rotational bands were obtained by the groups of Howard [213, 220], Burch [216, 273], and B.I. Golubitskiy [792-868].

The first groups of studies resulted in a series of traces of the absorption spectra of CO_2-N_2 mixtures in the regions of the absorption bands around 1.4, 1.6, 2.0, 2.7, 4.3, 4.8, 5.2, and 15.0 μ at various partial pressures of the components. The measurements were made with wide variation of the CO_2 absorbing mass. In the second group of studies, the absorbing masses were considerably smaller than in [213, 220] for recording of the spectra of the 2.7, 4.3, and 15.0 μ bands, but the weak 9.4- and 10.4-μ bands were studied with very large masses: from 48 to 11,200 atm·cm. It will be recalled that the mass of CO_2 in a one-kilometer horizontal layer of ground air is 30 atm·cm. /152

As in the investigations of water vapor, the data from measurements of the CO_2 absorption spectra made it possible in both groups of studies to find empirical formulas for the integral absorption of the entire bands. These relations were the same as in the case of water vapor [see (3.94), (3.95), and (3.96), (3.97)]. The empirical constants were found separately for each band.

The experimental studies of the absorption functions in segments of the CO_2 spectrum from 5 to 15 cm^{-1} in width that were carried out by B.M. Golubitskiy's group [792, 867, 868] made it possible to find an empirical formula for the absorption function at various absorbing CO_2 masses and air pressures.

Burch and Gryvnak [81] made a detailed study of CO_2 absorption in the spectral region from 0.6 to 5.5 μ as the pressure was varied in a very broad range (from a few thousandths of a mm Hg to 15 atm). The authors of [81] identified 30 new absorption bands. Integral strengths were determined for the most important bands.

Experimental data an the integral absorption of various CO_2 bands at elevated temperatures were obtained in the studies of Edwards [231, 274, 275].

The most accurate determination of the integral strength of the 15-μ CO_2 band was made in [276]; it was found to equal 200 ± 10 $cm^{-2}\cdot atm^{-1}$. A comparison with the data of other investigators was made in [276]. Values ranging from 170 ± 18 to 218 ± 5 $cm^{-2}\cdot atm^{-1}$ were obtained for this quantity in five other studies. However, there are two additional papers in which the integral strength of the band was reported at 330 ± 90 and 146 ± 18 $cm^{-2}\cdot atm^{-1}$.

9. FINE STRUCTURE AND ABSORPTION FUNCTIONS IN THE OZONE SPECTRUM

Fine structure has been studied theoretically and experimentally in the vibrational-rotational and purely rotational spectra of ozone in a number of papers, bibliographies of which will be found in [1, 3, 277].

The most detailed analysis of the fine structure of the overlapping 9.1- and 9.6-μ O_3 bands is due to Clough and Kneizis [277, 278]. /153

The authors computed the center positions and strengths of more than 1200 and 1800 absorption lines in the 995-1070-cm^{-1} and 1065-1155-cm^{-1} spectral regions, respectively. The Coriolis interaction between the lines of the ν_1 and ν_3 bands was taken into account. The results were used to find the spectral-absorption contour of O_3 and then to compare it with the corresponding experimental curves of White, Alpert, Debell, and Chapman [279], which were recorded with a resolution of 0.08-0.06 cm^{-1}. The value obtained by Walshaw [280] for the integral strength of the ν_3 line, 455 $cm^{-2} \cdot atm^{-1}$ under standard conditions, was used in calculating the line strengths.

Nexsen [281] measured the structure of the ν_2 ozone band around 14 μ and was the first to attempt an analysis of this band.

Reference [282] reported an experimental structural study of the $\nu_1 + \nu_3$ combination band centered around 4.7 μ under natural and laboratory conditions. Using the results obtained in [282], Trajmar [283, 284] analyzed the fine structure of the band.

Gora [285] made an analysis of the fine structure of the purely rotational O_3 spectrum. New data for the high-resolution O_3 spectrum in the 80-92-cm^{-1} region were obtained in [286].

A.P. Gal'tsev and V.M. Osipov [889] calculated the strengths and center positions of lines in the 4.7-μ band, as well as absorption functions in segments 10 cm^{-1} wide in the spectra of the 9.6- and 4.7-μ bands.

The most complete experimental data on the absorption functions of the 9.6-μ O_3 band were obtained by Walshaw [287]. His measurements were made under laboratory conditions with precipitated O_3 layers from 0 to 1.5 cm and pressures from 0.5 to 760 mm Hg. In [890], the precipitated O_3 layer reached 4.7 cm and the eight pressure values ranged from 10 to 400 mbar and more.

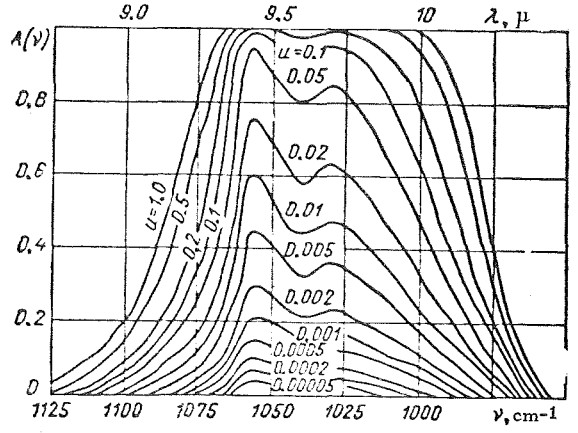

Figure 3.4. Spectral Absorption Curves in 9.65-μ Ozone Band for Various Values of the Precipitated Layer u, as Plotted in [289].

A rather complex empirical formula was proposed for the absorption function of the entire band on the basis of reduction of the measurement results in [287]; a simpler formula was taken in [280] for the absorption functions in three spectral intervals into which the band was broken: 990-1110 cm^{-1} (center of band), 960-990 and 1080-1110 cm^{-1} (ends of band). /154

Quantitative data on absorption in the 4.7-μ ozone band were also obtained in [287]. Using Walshaw's data on the infrared absorption in the 9.6- and 4.7-μ bands, Altschuller [288] constructed diagrams that can be used to estimate the absorption in these bands under atmospheric conditions. Also using Walshaw's data, Elsasser [289] constructed extremely useful curves that characterize the spectral transmission in this band with low resolution for various values of the precipitated ozone layer (Fig. 3.4).

10. FINE STRUCTURE AND ABSORPTION FUNCTIONS OF THE OXYGEN SPECTRUM

Line positions in the fine structure of the red band system in the atmospheric-oxygen absorption spectrum were investigated by Babcock and Herzberg [799]. The distribution of line strengths in the 0.76-μ band (0-0 transition) and the half-widths of the lines were measured by T.G. Adiks and V.I. Dianov-Klyukov [800], who also determined the oscillator strength of the band. The average values of the line half-widths for $O_2 \leftrightarrow O_2$ molecular collisions and collisions between oxygen and air molecules were found to be 0.085 and 0.077 $cm^{-1} \cdot atm^{-1}$, respectively. No substantial dependence of line half-width on rotational quantum number was detected in [800]. /155

Using the data obtained for the band oscillator strength, the average line strength, data on the line positions [799], and the distribution of their strengths in the band [801], the authors of [800] calculated the absorption functions of the band in the ground layer of atmosphere.

The absorption function of the 0.76-μ band was also calculated by Wark and Mercer [802] on the basis of their own data on the integral absorption of the band. Note is taken in [800] of the fact that the authors of [802] were obliged to adjust the value of the integral band strength in order to obtain agreement between calculation and experiment. In view of the possibility of using the 0.76-μ oxygen absorption band to determine the heights of cloud tops from artificial earth satellites, a great deal of attention has recently been devoted to its study [802-804].

The dependence of the equivalent widths S of the telluric O_2 lines in the 0.69-μ band on atmospheric temperature was investigated in [891]. The results indicated that the values of S change differently with rising temperature depending on the rotational levels at which they begin.

11. FINE STRUCTURE AND ABSORPTION FUNCTIONS OF THE SPECTRA OF SMALL ATMOSPHERIC IMPURITIES

1. Methane. More than a score of papers, a bibliography of which up to 1964 appears in [237], have been devoted to study of the vibrational-rotational absorption spectrum of methane. The ν_3 band was investigated by Allen and Plyler [290]. A high-resolution spectrum of the ν_2 band was obtained in [292]. The appearance of the forbidden ν_2 band in the spectrum is due to the vibrational-rotational interaction. Reference [292] gives, in addition to an analysis of the line positions, calculations of their relative strengths on the basis of the formulas obtained earlier in [291].

Data on the absorption functions of the CH_4 bands at 3.33, 6.45, and 7.65 μ, the N_2O bands at 3.9, 4.05, 4.5, 7.78, 8.55, 14.5, and 17.0 μ, and the CO bands at 2.32 and 4.76 μ were obtained by Burch's group [216, 293, 294]. The measurements were made both with the pure gases and in mixtures with nitrogen and other extraneous gases. The N_2O, CH_4, and CO concentrations were varied in ranges that more than cover their values under natural conditions. /156

TABLE 3.7. VALUES OF THE RELATIVE BROADENING COEFFICIENTS F^b AND RELATIVE OPTICAL-COLLISION DIAMETERS $d_{a,a}/d_{a,b}$ FOR VARIOUS GASES ACCORDING TO [216]

Absorbing gas	Band, cm^{-1}	P_a, mm Hg	P_b, mm Hg	Broadening gas	F^b	$\frac{d_{a,a}}{d_{a,b}}$
N_2O	2224	10	15—990	O_2 CH_4	0.83 1.08	0.93 0.94
	1285	100	80—900	O_2 CO_2 CO	0.72 1.17 0.97	0.87 1.14 0.99
CO	2143	100	100—2900	CH_4	1.12	0.96
CO_2	2350	50	30—650	O_2	0.81	0.92
CH_4	3020	50	50—2450	CO_2	1.25	1.15

The research done has yielded not only data on the integral absorption, but also information on the coefficients B, which characterize the relative effectiveness of collisions of molecules of the absorbing gas with one another and with molecules of the extraneous gas N_2 (see Table 3.1). Further, values of the relative optical-collision diameters $d_{a,a}/d_{a,b}$ (the subscripts a and b

nertain respectively to the absorbing and extraneous gases) and values of the relative broadening coefficients $F^b = P_{N_2}/P_b$, where P_b is the gas pressure required to produce the same line-broadening effect as that due to N_2, were also obtained in [216] (Table 3.7).

The data obtained by Burch's group on the integral absorption of the bands of these gases enable us to determine the absorption functions of these bands and make quantitative estimates of the role of each band in the attenuation of infrared radiation /157 from sources with a continuous spectrum at various temperatures.

B.M. Golubitskiy's group [793-869] made experimental studies of the absorption functions in narrow segments of the methane spectrum. Reduction of the measured results yielded the parameters that appear in the empirical formula for the absorption functions.

Edwards and Menard [274] derived relations for the integral absorption in the 7.6 and 3.3-μ CH_4 bands on the basis of model representations. The parameters of the relationships were determined for temperatures of 300, 555, and 833°K.

2. Nitrous oxide. The line-center positions in the fine structure of the vibrational-rotational and purely rotational N_2O spectra have now been studied in considerable detail. The corresponding bibliography is available in Goody's monograph [3] and in Howard and Garing's review [296].

The strengths and half-widths of the N_2O absorption lines have not been adequately studied. Using the harmonic-oscillator approximation, Gray [297] calculated relative strengths for the lines of the 4.6-μ band for the temperature range from 200 to 300°K. A band integral strength of 1850 $cm^{-2} \cdot atm^{-1}$ at 300°K was used to determine the absolute values of the line strengths. Having data on the line strengths and assuming their half-widths to be uniform at 0.05 cm^{-1} under standard conditions, the author of [297] employed a statistical model to compute absorption functions for narrow spectral segments of the band.

Abels and Ford [298] measured the strengths and half-widths of more than 70 lines in the 5.3-μ N_2O band. The authors of [298] found the line half-widths to depend on rotational quantum number.

Oppenheim and Goldman [299] used an approximate method based on the formulas for the absorption function in the Elsasser model and experimental data on the low-resolution absorption function to obtain the line half-widths. They found a half-width $\gamma^0 = 0.08$ $cm^{-1} \cdot atm^{-1}$ at a temperature of 300°K for part of the 4.5-μ band when nitrogen is used as the broadening gas.

Rank et al. [300] found the strengths of specific lines in the region of the 3.9-μ N_2O band.

Various molecular and force constants of the molecule were found in [301, 302]. /158

The integral strengths of the N_2O bands were investigated by Burch's group [216], Abels and Shaw [303], and Yamada and Person [304]. Absorption functions were measured in narrow segments of the fundamental N_2O bands by B.M. Golubitskiy's group [869-870]. Absorption functions of overlapping N_2O and CO absorption bands in the 2200-cm^{-1} region were measured in [305].

3. Carbon monoxide. The vibrational-rotational and purely rotational spectra of CO have been studied in some detail in virtue of their relative simplicity. Bibliographies can be found in Goody's monograph [3] and in the paper by Rank, Pierre, and Wiggins [66]. The last article cites detailed data on the molecular and force constants of the molecule.

The strengths and half-widths of lines in the vibrational-rotational bands of CO have been studied experimentally in the paper of Benedict et al. [307]. Shaw and France [308] found the half-widths and strengths of individual lines in the fundamental 4.6-μ band. Dowling and Hall [309] measured line half-widths in the purely rotational CO spectrum in the range from 100 to 3 cm^{-1}. A strong dependence of the line half-width γ on the rotational quantum number j was discerned in [307] and [308] (as j varied from 1 to 25, γ decreased from 0.1 to 0.05 cm^{-1} under standard conditions).

An analysis of the fine structure of the spectrum was carried out in [310] for the "hot" CO bands, which consist of lines with large rotational quantum numbers.

The integral absorption of the CO bands was measured by Burch's group [216] and Gryvnak and Shaw [311] at various partial pressures of the CO and the extraneous gases. Reference [312] reports an experimental study of the integral absorption in the fundamental 4.6-μ CO vibrational-rotational band at temperatures of 300, 273, and 198°K in a broad range of pressures and absorbing gases. The integral absorption of the fundamental band (interval from 1900 to 2450 cm^{-1}) was measured in [313] at temperatures of 300, 600, 900, 1200, and 1500°K with the pressure varied from 0.25 to 3 atm for path lengths of 1, 5, 10, and 20 cm in the cuvette with the gas. The integral absorption of the fundamental band and its first harmonic (region of 4050-4450 cm^{-1}) were also computed in [313] for various temperatures and pressures.

The absorption functions were measured in [793] in narrow segments of the CO spectrum. /159

TABLE 3.8. ABSORPTION BANDS OF ATMOSPHERIC GASES FOR WHICH EMPIRICAL COEFFICIENTS IN (3.98) WERE OBTAINED FOR CALCULATION OF ABSORPTION FUNCTION IN [791-793, 867-870]

Gas	Band, μ										
H_2O	0,94	1,1	1,38	1,87	2,7	6,3	8—14	14—40*	Continuum 1—14		
CO_2	1,4*	1,6*	2,0	2,7	4,3	4,8	5,2	9,6	10,4	15,0	
N_2O	2,12	2,3	2,94	3,04	3,57	3,86	4,0	4,5	7,8	8,6	15*
CH_4	2,3	3,3									
CO	7,6	4,7									
O_3	9,6*	4,75*									
O_2	1,26*										
N_2	4,3*										

*Empirical coefficients obtained by reducing data of other investigators.

Note: Commas represent decimal points.

Shaw and Houghton [314] calculated the integral absorption of the 4.6-μ band from data obtained in [307] on the strengths, half-widths, and shapes of the lines. Edwards calculated the integral absorption of the same band [306].

In concluding our discussion of the absorption functions of atmospheric gases, we summarize the basic data (Table 3.8) obtained by B.M. Golubitskiy's group [791-793, 867-870]. It is a distinctive feature of this series of studies that its results are convenient for practical use and make possible quick determination of the absorption functions in relatively narrow segments of the spectrum for various pressures and absorbing masses of the gases. The fact that broad ranges of absorbing gaseous masses were covered in the measurements is a special merit of these studies. We note that the absorption of N_2 in the 4.3-μ region is due to complexes [871, 872]. On the basis of calculated absorption functions for narrow segments of the spectrum in the bands listed in Table 3.8, V.L. Filippov and S.O. Mirumyants [873] constructed nomograms for calculation of the atmosphere's spectral transparency in the 2.8-5.6-μ region.

12. ABSORPTION OF OVERLAPPING LINES AND BANDS /160

In the real atmosphere, it is often necessary to deal with absorption in overlapping lines and bands of the same gas or of different gases. It is therefore necessary to take account of line overlapping in the determination of absorption coefficients and functions. As concerns the absorption coefficients, this problem is quite simply solved theoretically when all parameters of the lines contributing to the absorption at a given frequency

ν are known. In this case, the resultant absorption coefficient is calculated as the sum of the absorption coefficients of all lines.

Since the data presently available for the intensities and half-widths of atmospheric-gas absorption lines are quite inadequate, it is impossible in most cases to determine the monochromatic-radiation absorption coefficients theoretically. Experimental determination of these quantities is now possible only through the use of lasers as radiation sources.

The transmission function of a segment $\Delta\nu = \nu_2 - \nu_1$ of a composite band consisting of overlapping bands of n gases takes the form

$$T = \frac{1}{\Delta\nu}\int_{\nu_1}^{\nu_2} T(\nu)\,d\nu = \frac{1}{\Delta\nu}\int_{\nu_1}^{\nu_2}\prod_{i=n} T_i(\nu)\,d\nu, \qquad (3.99)$$

where $T(\nu)$ is the spectral transmission of the gas mixture for radiation at frequency ν and $T_i(\nu)$ is the same quantity for the i-th gas.

The following expression can be derived from (3.99) for the absorption function in the segment $\Delta\nu$ for the most commonly encountered case, in which bands of two atmospheric gases overlap:

$$A = \frac{1}{\Delta\nu}\int_{\nu_1}^{\nu_2} A(\nu)\,d\nu = \frac{1}{\Delta\nu}\int_{\nu_1}^{\nu_2} A_1(\nu)\,d\nu + \frac{1}{\Delta\nu}\int_{\nu_1}^{\nu_2} A_2(\nu)\,d\nu - \frac{1}{\Delta\nu}\int_{\nu_1}^{\nu_2} A_1(\nu)\,A_2(\nu)\,d\nu, \qquad (3.100)$$

where $A_1(\nu)$, $A_2(\nu)$, and $A(\nu)$ are the spectral absorptions of radiation at frequency ν for the first and second gases and their mixture, respectively.

Thus, the absorption function of the composite band is smaller than the sum of the absorption functions of the individual gases by an amount $A' = \frac{1}{\Delta\nu}\int_{\nu_1}^{\nu_2} A_1(\nu)\,A_2(\nu)\,d\nu$ stemming from the overlapping of bands of two gases. /161

Data for determining the spectral absorption of atmospheric gases, which is required to calculate A', have begun to appear only during the past few years. The early studies devoted to determination of the absorption function for overlapping bands were experimental.

Before turning to the results of the individual studies, let us write an approximate expression for the transmission of a mixture of two gases, which follows from (3.99):

$$T = T_1 \cdot T_2, \qquad (3.101)$$

where T_1 and T_2 are the absorption functions for the first and second gases in the interval $\Delta\nu$ for which T is found.

In his very first series of studies, Howard attempted to find the integral absorption functions of a mixture of water vapor and CO_2 in the region of the 2.7-μ band from available data on these functions for H_2O and CO_2 taken separately. Reduction of the corresponding measurements indicated that the transmission function of a segment $\Delta\nu$ of a complex band consisting of H_2O and CO_2 lines can be represented with accuracy sufficient for practical purposes in the form of the product of the absorption functions in the H_2O and CO_2 bands taken separately.

Hoover, Hathaway, and Williams [305, 315] made an experimental study of the spectral transmission in the bands of CO, N_2O, CH_4, and their mixtures. The limits of applicability of (3.101) for description of the absorption functions of the corresponding gas mixtures were found for the CO and N_2O bands in the region of 2200 cm^{-1} and for the CH_4 and N_2O bands around 1300 cm^{-1}. The experimental data obtained were compared with the calculations of Gray and McClatchey [316]. The absorption functions in narrow segments of the spectra of mixtures of the gases CO_2, N_2O, and CO in the region from 4.2 to 4.8 μ were also calculated in the latter paper. The calculations were made with the formulas of the Elsasser model [272].

Penner and Varanasi [317] calculated the absorption in overlapping bands of water vapor and CO_2 in the 2.7- and 15-μ regions at temperatures above 800°K. /162

Expressions for the equivalent width of two overlapping lines were obtained in the papers of Sakai [318, 319] and Plass [320]. The method proposed in [318] was extended by Sakai to the case of overlapping bands [321].

13. ABSORPTION OF RADIATION FROM SELECTIVE SOURCES

Accurate calculations of radiant heat transfer in the atmosphere require knowledge of the absorption functions for sources with both continuous and selective emission spectra. In accordance with the well-known law of Kirchhoff, all gases that absorb radiation in the visible and infrared regions of the spectrum have the corresponding electronic, vibrational-rotational, and purely rotational emission spectra. In radiant heat transfer calculations,

it is necessary to consider both the radiant fluxes from the sun and the earth that penetrate the corresponding atmospheric thicknesses and the radiant fluxes emitted by the atmosphere itself. The latter problem requires knowledge of the laws governing absorption of selective radiation in a selectively absorbing medium.

A second group of problems, for which it is necessary to know the absorption of nonselective sources in the atmosphere, is associated with the development of rocketry and jet aviation. The high exhaust-jet temperatures excite the highest-energy transitions in the molecules and emission of the so-called "hot" bands of the atmospheric gases. Study of the emission spectra of the jets at various distances from them requires knowledge of how the emission of these sources is absorbed.

Depending on the species of the emitting and absorbing gases and their temperatures, we encounter one or a combination of the following possible cases: 1) the centers of the emission and absorption lines coincide; 2) the centers of the emission and absorption lines are shifted with respect to one another, and 3) the emission and absorption lines do not coincide at all.

The first case occurs when both the emission and the absorption are due to the same gas, which is at the same temperature. /163
In the second case, the same gas emits and absorbs, but the conditions of emission differ from those of absorption. Finally, the third case may be encountered when one gas emits and another absorbs or when the gas concerned emits bands with practically no absorption manifestation under the conditions of the atmosphere. It usually involves the "hottest" absorption bands. The absorption function for the radiation from a selective source in the spectral interval $\Delta\nu = \nu_2 - \nu_1$ can be written [322]

$$A = \frac{\int_{\nu_1}^{\nu_2} \left[1-\exp\left(-\sum_i k_{e_i}\omega_e\right)\right]\left[1-\exp\left(-\sum_i k_{a_i}\omega_a\right)\right] d\nu}{\int_{\nu_1}^{\nu_2} \left[1-\exp\left(-\sum_i k_{e_i}\omega_e\right)\right] d\nu}, \qquad (3.102)$$

where k_{e_i} and k_{a_i} are the absorption coefficients of the i-th spectral line in the emitting and absorbing gases and ω_e and ω_a are the precipitated layers of the emitting and absorbing gases.

For direct calculation of exact quantitative data on the absorption coefficients and functions of selective-source radiation, it is necessary to know all fine-structure elements of both the emission and absorption spectra. Our knowledge of these elements is presently totally inadequate. Recourse is therefore taken either to spectrum models or to experiment to find the absorption

functions.

Plass [322, 323] obtained a series of expressions for the absorption functions of selective-source radiation for various cases of line overlapping both in the radiation source and in the absorbing medium (nonoverlapping lines, overlapping lines described by the Elsasser model, overlapping lines described by the statistical model). Cases in which the pressure, temperature, and concentration of the absorbing gas change along the path of the ray were also examined in [322].

A numerical calculation presented in [322] indicated that when the same line participates both in emission and in absorption, the absorption function of the flame is substantially larger /164 than that for a source with a continuous emission spectrum.

Selective-source absorption by carbon dioxide was calculated in the papers of M.V. Podkladenko et al. [324, 325].

Burch and Gryvnak [81] carried out experimental studies of the absorption of the emission from hot H_2O and CO_2 by the same gases at standard temperature. The absorption functions of CO_2 for a flame at a temperature of 2800°K and various pressures and path lengths in the cuvette were investigated experimentally in [326]. The cuvette temperature was 24°C. The authors of [326] reported relatively high transmission in the segments of the spectrum from 2.5 to 3.5 and from 4.0 to 5.5 μ. Thus, the transmission function was found equal to 0.2 in a layer of CO_2 equivalent in absorbing mass to the ground-to-50-km layer of the earth's atmosphere in the 4.0-5.5-μ segment.

14. ABSORPTION OF LASER RADIATION IN THE ATMOSPHERE

The high monochromaticity, directivity, and coherence of laser radiation and the possibility of generating ultrashort-period pulses and attaining "giant" powers give rise to a number of specific features of the propagation of this radiation in the atmosphere as compared to that of the radiation from other sources.

The line half-widths of gas-laser emission are considerably smaller than the line half-widths in the absorption spectra of the atmospheric gases. As a result, quantitative estimation of the absorption of laser light in the atmosphere requires highly accurate knowledge of the positions, strengths, and shapes of the lines in the spectra of the atmospheric gases. All quantitative data on the absorption spectra of atmospheric gases that existed before the appearance of lasers have been found unsuitable for evaluation of laser-light absorption in the atmosphere [1].

The interaction of a spatially confined beam of light with an aerosol results in a change in the intensity of the light in the direction of propagation owing to direct attenuation in accordance

with the Bouguer law and to single and multiple scattering. The contributions of the directly attenuated and scattered light vary /165
with depth of penetration into the scattering medium. The luminous field in the medium is found to depend not only on the latter's optical properties, but also on the geometrical parameters of the source.

Together with the coherence of the radiation, the small diameters of laser beams and their slow divergence result in a spot-like space-time structure of the beam propagating in a turbulent atmosphere.

The giant powers of laser radiation give rise to a series of nonlinear effects, which accompany the laser radiation in the atmosphere. Foremost among these effects, we should note: 1) the spectroscopic saturation effect (the absorption coefficient depends on the power of the radiation incident on the absorbing layer); 2) many-photon effects (excitation, ionization, and dissociation of atoms and molecules of the atmospheric gases that do not absorb radiation at the particular frequency at low radiated powers); 3) effects of the radiation on atmospheric-aerosol particles (light pressure, vaporization, explosion, etc.); 4) stimulated Raman scattering; 5) self-focusing of the beam.

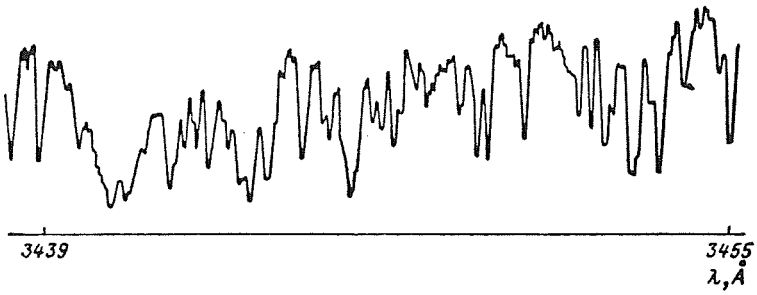

Figure 3.5. Record of Fine Structure of the Atmosphere's Absorption Spectrum Around $\lambda = 0.345\ \mu$ [174].

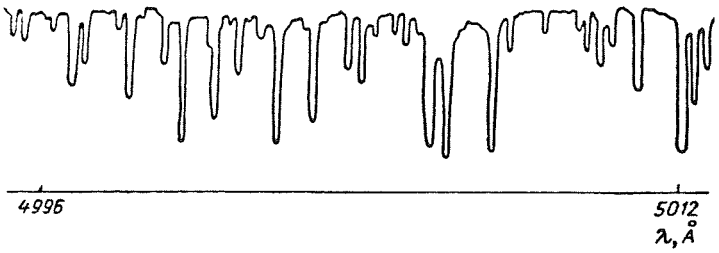

Figure 3.6. Record of Fine Structure of the Atmosphere's Absorption Spectrum Around $\lambda = 0.5\ \mu$ [174].

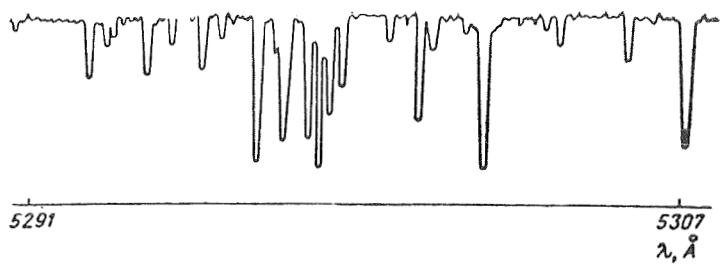

Figure 3.7. Record of Fine Structure of the Atmosphere's Absorption Spectrum Around λ = = 0.53 μ [174].

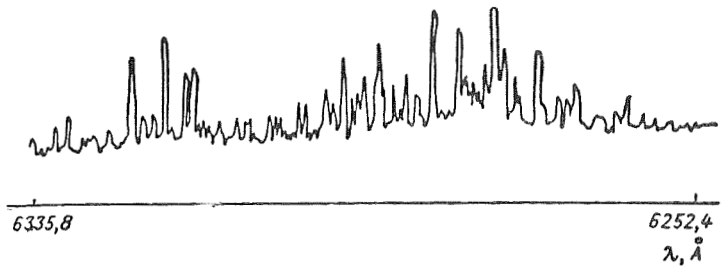

Figure 3.8. Record of Fine Strucutre of the Atmosphere's Absorption Spectrum Around λ = = 0.63 μ [185].

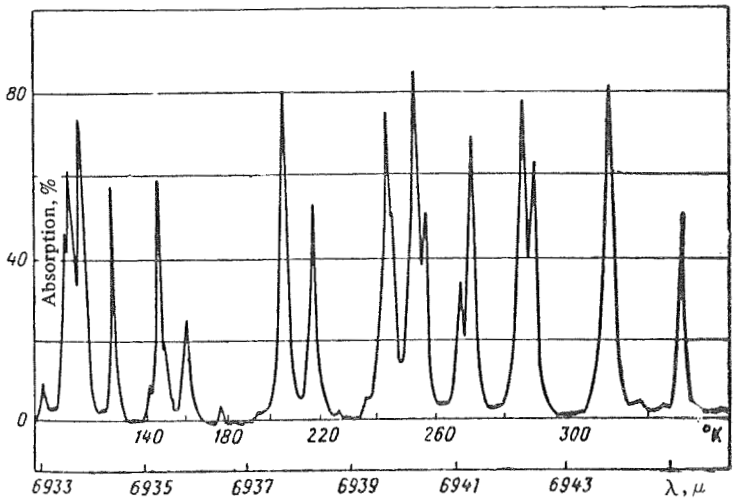

Figure 3.9. Record of Fine Structure of the Atmosphere's Absorption Spectrum Around λ = = 0.69 μ [295].

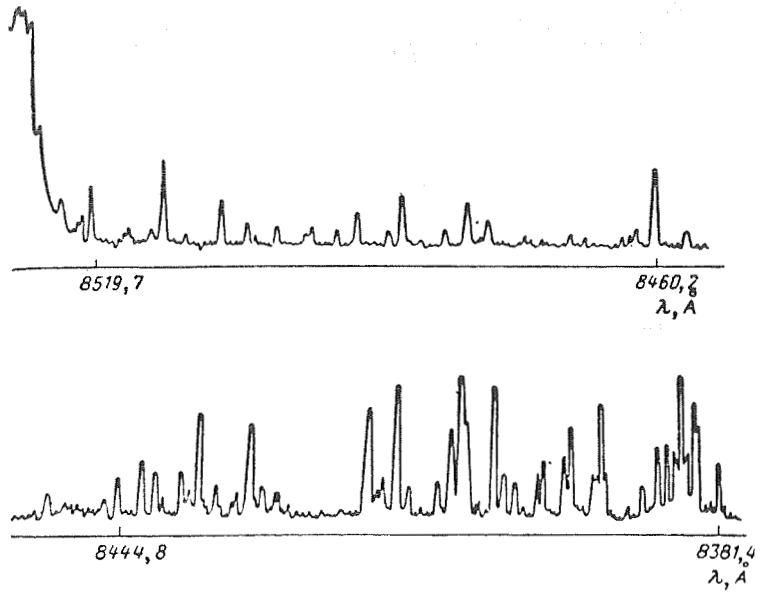

Figure 3.10. Record of Fine Structure of the Atmosphere's Absorption Spectrum Around λ = = 0.84 μ [185].

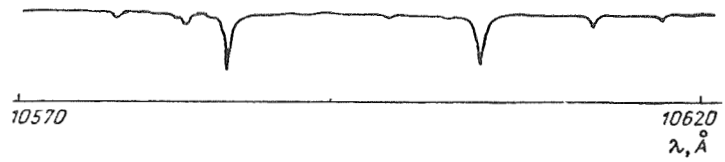

Figure 3.11. Record of Fine Structure of the Atmosphere's Absorption Spectrum Around λ = = 1.06 μ [183].

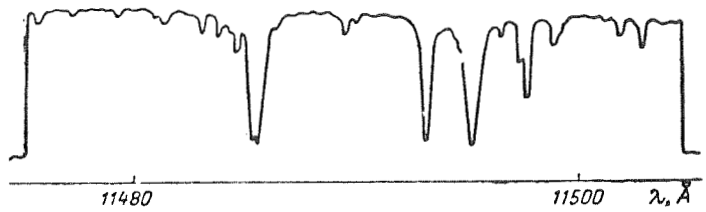

Figure 3.12. Record of Fine Structure of the Atmosphere's Absorption Spectrum Around λ = = 1.15 μ [183].

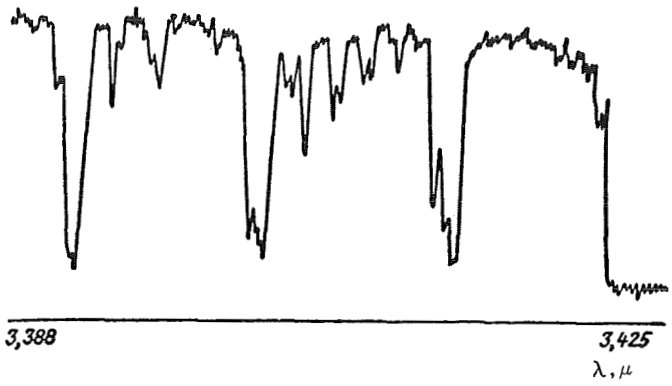

Figure 3.13. Record of Fine Structure of the Atmosphere's Absorption Spectrum Around λ = = 3.39 μ [181].

Figure 3.14. Record of Fine Structure of the Atmosphere's Absorption Spectrum Around λ = = 3.51 μ [181].

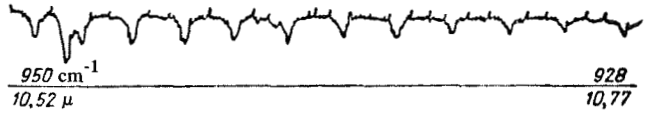

Figure 3.15. Record of Fine Structure of the Atmosphere's Absorption Spectrum Around λ = = 10.6 μ [181].

The bright promise offered by the use of lasers in various devices designed to work through the atmosphere (communications, data transmission, optical radar, distance measuring, etc.) requires intensive study of all aspects of the propagation of laser light in the atmosphere.

1. General fine-structure pattern of the absorption spectrum of the earth's atmosphere in the laser-radiation regions. A general picture of the fine structure of the atmosphere's absorption spectrum in the segments in which the most widely used lasers radiate can be assembled on the basis of existing literature data. Figures 3.5-3.15 present absorption spectra of the earth's atmosphere as recorded by various authors with high resolution in the segments in which the most commonly encountered lasers radiate: the first harmonic of the ruby laser (λ = 0.345 μ), the argon gas laser (λ = 0.5 μ), the first harmonic of the neodymium-glass laser (λ = 0.53 μ), the helium-neon gas laser (λ = 0.63 μ), the ruby laser (λ = 0.69 μ), the gallium arsenide semiconductor laser (λ = = 0.84 μ), the neodymium-glass laser (λ = 1.06 μ), the helium-neon gas laser (λ = 1.15 μ), the helium-neon gas laser (λ = 3.39 μ), the xenon-helium gas laser (λ = 3.51 μ), and the carbon dioxide-nitrogen gas laser (λ = 10.6 μ). /166

Figures 3.5-3.15 bring out clearly the extremely sharp selectivity of atmospheric absorption in all of the laser bands. It should be noted that all of the figures represent records of the absorption spectrum of the earth's atmosphere that were obtained at high but finite resolution, which smooths out the actually even sharper absorption selectivity. For example, far from all of the absorption lines on any given figure have been resolved as individual lines. It is easily seen that if the wavelength of the laser radiation changes for any reason, the absorption of this radiation in the atmosphere may also change substantially. This /170 can be illustrated by reference to the most widely used ruby laser. In Fig. 3.9, the spectral absorption of the entire thickness of the atmosphere, as recorded with high resolution using the sun as the radiation source, is plotted against the axis of ordinates. A wavelength scale in angstroms and a scale of the temperatures T at which the ruby laser generates the respective wavelengths appear on the axis of abscissas. It is easily seen from the figure that the absorption of ruby-laser radiation in the atmosphere may vary substantially depending on the temperature of the laser's generating medium. It should be noted that there are no strong absorption lines in the region in which the ruby laser radiates.

These figures also make it easy to understand why very weak lines may be significant factors in the absorption of laser light when the centers of these lines coincide with the centers of emission lines of the laser. Hence the neglect of absorption by weak lines that is justified in calculating absorption functions in broad segments of the spectrum is by no means applicable to calculations of laser-light absorption. Until recently, the absorption of water vapor, carbon dioxide, and ozone was usually taken into account in calculation of absorption functions in relatively narrow segments of the spectrum. The absorption in whole vibrational-rotational bands of small impurities such as methane, nitrous oxide, and carbon dioxide was disregarded. This neglect

TABLE 3.9. POSITIONS OF EMISSION LINES OF VARIOUS GAS LASERS AND NEARBY ABSORPTION LINES OF ATMOSPHERIC GASES [295]

Gases	Wavelength of laser radiation in air, Å	Nearest atmospheric-gas absorption lines, Å	Notes
He—Ne	6328,172	None	
O_2	8146,2	None in earth's atmosphere	1
He—Ne	10798	None	
He—Ne	10845	None	
He—Ne	11143	11143,32—H_2O	
He—Ne	11177	11175,59—H_2O	
		11177,45—?	
		11177,49—H_2O	
He—Ne	11390	Unidentified line	
He—Ne	11409	None	2
He—Ne	11522,76	11522,77—H_2O	
		11523,19—H_2O	
		11523,73—H_2O	
		11524,20—H_2O	
		11524,23—H_2O	
He—Ne	11601	11600,21—H_2O	
		11601,05—H_2O	
He—Ne	11614	11613,84—H_2O	
He—Ne	11767	11768,37—H_2O	
He—Ne	11985	11984,8 —?	
He—Ne	12066	12067,24—H_2O	
Ne	15231	15230,59—H_2O	
Ar	16180	None	
Kr	16900	16900,97—H_2O	
		16901,41—CH_4	
		16901,3 —H_2O	
Kr	16935,81	16935,1 —CH_4	
		16936,25—CH_4	
		16937,22—H_2O	
Ar	16940,59	16940,13—H_2O	
Kr	17843	17843,37—H_2O	3
Ar	17930	17934,71—H_2O	4
Kr	18185	18180 —H_2O	5
Kr	19211	— —H_2O	3
Xe	20262,28	20260,75—CO_2	
		20263,21—CO_2	
He	20603	20604,57—CO_2	
		20615,75—H_2O	
		20618,04—CO_2	
Ne	21019	21018,45—CO_2	6
Kr	21165	21165,76—$OC^{18}O$	4
Kr	21902,53	21899,5 —H_2O	4
Xe	23193,28	23192,89—H_2O	
		23194,44—CH_4	
Kr	25234	25234,39—H_2O	3
	25414	— —H_2O	3
Xe	26268,95	—H_2O	3
Xe	26510,96	—H_2O	3
Xe	26600,6	—H_2O	3
	31069,14	31053,8 —H_2O	2
		31081,5 —H_2O	
Ne	33333	33336,3 —CH_4	
Xe	33666,5	33658,6 —CH_4	
		33666,6 —CH_4, H_2O	
		33676,8 —CH_4	

Note: Commas represent decimal points.

TABLE 3.9 (Cont'd.)

Gases	Wavelength of laser radiation in air, Å	Nearest atmospheric-gas absorption lines Å	Notes
Ne	33913,17	33913,0 —CH_4	
Xe	34341	34344,1 —CH_4	
		34348,7 —CH_4	
		34352,1 —CH_4	
		34357,2 —CH_4	
Xe	35070,4	35069,5 —?	4
Xe	36209	36205,5 —CH_4	
Xe	36503	36501,0 —HDO, CH_4	6
Xe	36788,36	36790,1 —CH_4	6
Xe	36848,56	—	6
Ne	37734	37732,9 —CH_4, HDO	4
Xe	38686	38686,7 —N_2O	
Xe	38939,74	38937,5 —N_2O	
Xe	41516		4
Xe	41516		4
Xe	46096	46096,8 —N_2O, CO	
Ne	54072	54077,1 —CO, H_2O	7
Xe	55738	— —H_2O	
Cs	71821	71600,9 —H_2O	
		71801,4 —H_2O^{17}	
Xe	73147	73042,3 —H_2O, CH_4	
		73143,8 —CH_4	
		73181,3 —CH_4, H_2O	
Xe	90040	90057,6 —O_3	
Xe	97003,36	96979,1 —O_3	
Xe	122990		4
Xe	122630	122564 —CO_2	4
		122731 —H_2O	
Xe	129130	129134 —CO_2	6
Ne	182760	182505 —H_2O	5
Ne	182820	182989—H_2O	
Ne	183040	182989—H_2O	3
Ne	183970		4
Xe	185010	184771—H_2O	5
Ne	185910	185805—CO_2, H_2O	4
Ne	185970		
Ne	203510	203215—H_2O	5

Notes: 1) Absorption by atomic oxygen; 2) between two strong H_2O lines; 3) total absorption; 4) practically no absorption; 5) limb of H_2O line; 6) weak lines; 7) solar CO.

is all the more justifiable the wider the spectral segment for which the absorption function is determined, since the small-impurity absorption bands occupy rather narrow segments.

In calculating the absorption of laser light, it is not admissible to disregard the absorption of either bands or lines solely on the basis of their known strengths. It is first necessary to have highly accurate knowledge of the center positions of the absorption lines and the laser emission lines.

Table 3.9, which has been borrowed from Long's paper [295], presents data on the positions of the emission lines of 67 gas lasers and nearby atmospheric-gas absorption lines as observed by various investigators in high-resolution absorption spectra.

2. Requirements as to accuracy of determination of absorption-line centers. /173 Let us assume that we know the centers of laser-radiation lines with very high accuracy and that the half-widths of the emission lines are much smaller than those of the absorption lines. The latter assumption is quite sound for gas lasers.

Following [327], let us estimate the accuracy with which the line centers must be determined in the absorption spectra of atmospheric gases in order to evaluate quantitatively the absorption of laser light in the atmosphere. This accuracy depends: 1) on the total and partial pressures and the temperature, or on the height at which the laser radiation propagates; 2) on the distance between the laser emission line and the center of the absorption line.

As was indicated in Chapter 2, the central region of an atmospheric-gas absorption line is described satisfactorily in the lowermost 20-30-km layer of the atmosphere by the dispersion contour:

$$k(\nu)=\frac{S}{\pi}\frac{\gamma}{(\nu-\nu_0)^2+\gamma^2},$$

where $k(\nu)$ is the monochromatic absorption coefficient for the frequency ν, S, $\gamma = \gamma^0(P_a + \sigma_{ab}P_b)$, and ν_0 are the strength, half-width, and center position of the absorption line, γ^0 is the half-width of the line for standard conditions, P_a is the pressure of the nonabsorbing gas, P_b is the pressure of the absorbing gas, and σ_{ab} is the effectiveness of collisions between molecules of the /174 absorbing and nonabsorbing gases. In the bottom 30-km layer of atmosphere, the product $\sigma_{ab}P_b$ can be disregarded as small by comparison with P_a for all gases that absorb in the infrared. We may therefore assume that $\gamma = \gamma^0 P$, where P is the total pressure.

Further recognizing the weak dependence of γ^0 on temperature $\left(\gamma^0 \sim \frac{1}{\sqrt{T}}\right)$ and the rather small variations of the latter with height, we may assume γ^0 to be independent of height with accuracy sufficient for practical purposes.

With the assumptions adopted above, we calculated the values of $k(\nu)$ for $S = 1$, $\gamma^0 = 0.03$ and 0.1 $cm^{-1} \cdot atm^{-1}$, and $P = 1$ and 0.1 atm. The values of γ^0 used in the calculation corresponded to the minimum and maximum absorption-line half-widths of water vapor, the atmosphere's principal absorbing component. The pressures of 1.0 and 0.1 atm correspond to heights of 1 and 16 km above sea level.

The calculated results for $k(\nu)$ for these four cases appear in Table 3.10.

Table 3.11 presents the values of the coefficient $k(\nu)$ for the same four cases, but not for a unit line strength. For convenience in interpretation of the calculated results, the values of $k(\nu)$ at the line center ($\Delta\nu = 0$) were taken as 100 in all four cases.

As we see from the tables, the value of $k(\nu)$ diminishes by a factor of 10 at a distance $\Delta\nu = 0.3$ cm^{-1} from the line center for the broadest lines (which are, as a rule, also the strongest ones) in the ground layer of the atmosphere ($P = 1$ atm); the same decrease takes place over as little as $\Delta\nu = 0.1$ cm^{-1} for narrow lines. At a 16-km height, $k(\nu)$ decreases by one order of magnitude at distances of 0.03 cm^{-1} and 0.01 cm^{-1} for broad and narrow lines, respectively. But $k(\nu)$ decreases by a factor of 100 at $\Delta\nu = 0.1$ cm^{-1} and 0.03 cm^{-1} for broad and narrow lines at this height.

Thus, if monochromatic laser radiation falls into the center of a water-vapor absorption line, evaluation of $k(\nu)$

TABLE 3.10. VALUES OF $k(\nu)$ AT VARIOUS DISTANCES FROM THE CENTER OF A LINE OF STRENGTH $S = 1$ FOR VARIOUS LINE HALF-WIDTHS

$\Delta\nu$, cm^{-1}	$\gamma^0 =$ $P = 0{,}1\ cm^{-1} \cdot atm^{-1}$, $P = 1$ atm	$\gamma^0 =$ $P = 0{,}03\ cm^{-1} \cdot atm^{-1}$, $P = 1$ atm	$\gamma^0 =$ $P = 0{,}1\ cm^{-1} \cdot atm^{-1}$, $P = 0{,}1$ atm	$\Delta\nu$, cm^{-1}	$\gamma^0 =$ $P = 1\ cm^{-1} \cdot atm^{-1}$, $P = 1$ atm	$\gamma^0 =$ $P = 0{,}03\ cm^{-1} \cdot atm^{-1}$, $P = 1$ atm	$\gamma^0 =$ $P = 0{,}1\ cm^{-1} \cdot atm^{-1}$, $P = 0{,}1$ atm
0	3,18	10,6	31,8	0,1	1,59	0,9	0,3
0,005	3,17	10,3	25,4	0,2	0,6	0,2	0,1
0,01	3,15	9,5	15,9	0,3	0,3	0,1	0,04
0,02	3,06	7,3	6,4	0,4	0,2	0,06	0,02
0,03	2,92	5,3	3,2	0,5	0,1	0,04	0,01
0,04	2,74	3,8	1,9	1,0	0,03	0,01	
0,05	2,54	2,8	1,2	2,0	0,01		

Note: Commas represent decimal points.

TABLE 3.11. VALUES OF k(ν) AT VARIOUS DISTANCES FROM THE LINE CENTER FOR VARIOUS HALF-WIDTHS REDUCED TO A SINGLE SCALE AT $\Delta\nu = 0$

$\Delta\nu$, cm^{-1}	$\gamma = 0,1$ $cm^{-1} \cdot atm^{-1}$, $P = 1$ atm	$\gamma = 0,03$ $cm^{-1} \cdot atm^{-1}$, $P = 1$ atm	$\gamma = 0,1$ $cm^{-1} \cdot atm^{-1}$, $P = 0,1$ atm	$\gamma = 0,03$ $cm^{-1} \cdot atm^{-1}$ $P = 0,1$ atm
0	100	100	100	100
0,005	99,8	97,3	80,0	26,5
0,01	99,1	89,5	50,0	8,3
0,02	96,2	69,2	20,1	2,3
0,03	91,7	50,0	10,1	1,0
0,04	86,2	36,0	6,0	0,6
0,05	80,0	26,5	3,8	0,4
0,1	50,0	8,3	1,0	0,1
0,2	20,1	2,2	0,3	0,02
0,3	10,1	1,0	0,1	0,01
0,4	6,0	0,6	0,06	0,01
0,5	3,8	0,4	0,03	—
1,0	1,0	0,1	—	—
2,0	0,3	—	—	—

Note: Commas represent decimal points.

requires, together with exact knowledge of the laser radiating frequency, knowledge of the position of the absorption-line center with very high accuracy. In the ground layer of the atmosphere, this accuracy amounts to a few hundredths of a cm^{-1} and increases substantially with height. None of the atmospheric absorption spectra recorded until recently (atlases of spectra) guarantees this high accuracy in determination of the line-center positions. Accordingly, these atlases must be used with great caution even in rough quantitative estimation of k(ν) near line centers.

As the laser radiation frequency moves away from the center of an atmospheric-gas absorption line, the requirements as to the accuracy of determination of the position of this center relax. A quantitative measure of these requirements is afforded by the tables.

These conclusions are valid not only for the water-vapor absorption spectrum. They may also be applied to the absorption spectra of other atmospheric gases, since the half-widths of their lines are of the same order.

3. Results of studies of the absorption of laser radiation in the atmosphere. 1. Theoretical investigations. In view of the stringent accuracy requirements for determination of the line positions, as well as their strengths and half-widths, it is necessary in theoretical solution of the problem of calculating atmospheric-gas absorption spectra to take account of all factors that influence the characteristics of the spectra.

All of these characteristics are most strongly influenced by the interaction of the vibrational and rotational motions of the

molecules, which increases in importance the larger the rotational quantum number with which we deal in calculating the absorption lines. Incidentally, it is a general rule that lines with large /177
rotational quantum numbers fall in the practically important spectral intervals between absorption bands (in the atmosphere's transparency windows).

Of all of the atmospheric gases, water vapor, the principal absorbing component of the atmosphere, has the most complex vibrational-rotational spectrum. For this reason, the author's laboratory began with water vapor in its attempt at correct quantitative calculation of the positions, strengths, and half-widths of the lines and the absorption coefficients with consistent allowance for the interaction of the molecule's vibrational and rotational motions.

The method used to calculate the center positions of the lines and their strengths and half-widths was examined in detail in §5. The data obtained on all three parameters of the H_2O absorption lines were then used to find the monochromatic absorption coefficients in specific narrow segments of the water vapor vibrational-rotational spectrum in the regions in which the most common lasers radiate. The calculation was performed for several pairs of values of the temperature and pressure that are characteristic for specific heights in the atmosphere. A dispersion line contour was assumed. Thus, we used the expression

$$k(\nu)=\sum_i \frac{S_i(T)}{\pi}\frac{\gamma_i(T,\ P)}{(\nu-\nu_{0i})^2+\gamma_i^2(T,\ P)}$$

for the monochromatic absorption coefficient.

Analysis of tee spectral variation of the H_2O absorption coefficient in the spectral interval studied shows the extreme selectivity of $k(\nu)$ even in regions that have no strong absorption lines. Thus, the absorption coefficient varies through several orders as the wavelength changes by only a few reciprocal centimeters in the regions in which lasers with wavelengths of 0.84 μ (semiconductor gallium arsenide laser) and 1.06 μ (neodymium-glass laser) emit. The absence of corresponding experimental data on the monochromatic absorption coefficients unfortunately precludes an estimate of the accuracy of these calculations.

Water vapor is responsible for the absorption of the radiation from most lasers. In several cases, however, the laser radiation falls into segments of the spectra of other atmospheric /178
gases. For example, the absorption of radiation from $CO_2 + N_2$ (10.6-μ region) and He + Ne (wavelength 3.39 μ) lasers is due in the former case to carbon dioxide and water vapor simultaneously, but practically entirely to methane in the latter case.

No difficulty is encountered in calculating monochromatic absorption coefficients for CO_2-nitrogen lasers in the region of 10.6 μ. We obtained the components of this coefficient due to carbon dioxide and water vapor absorption. At the line centers of the P branch of the CO_2 band with rotational quantum numbers j from 14 to 28, the carbon dioxide component of the absorption coefficient in the ground layer of the atmosphere varies from 0.12 to 0.19 km^{-1}. The water-vapor component of the absorption coefficient is governed in the narrow spectral segment occupied by these lines by the continuous absorption by the limbs of far blue lines, and is practically independent of wavelength. Its value is 0.08 km^{-1} at a humidity of 10 g/m^3 in the ground layer of the atmosphere [192].

The data on the parameters of the individual lines are presently inadequate for theoretical calculation of monochromatic absorption coefficients in the region of the methane bands and in most parts of the spectra of other atmospheric gases.

We note in conclusion that, despite a certain amount of progress made in theoretical solution of the problem of the absorption coefficients for monochromatic radiation in the atmosphere, we are still very far from being in a position to predict the absorption of monochromatic or quasimonochromatic radiation in the atmosphere with sufficient accuracy, and would be even if we knew the spectral composition of this radiation in advance with high accuracy. As a result, the absorption characteristics of radiation from various lasers in the atmosphere can still be determined most reliably on the basis of the corresponding experimental studies.

2. Experimental investigations. A series of studies in experimental determination of the absorption of radiation from various types of lasers has been performed in the author's laboratory. The results have been published in [328-331, 782, 806, 908-910].

Direct experimental determination of the absorption coefficients of atmospheric gases in the radiating regions of lasers is practically impossible owing to the inadequate resolution of the best types of spectrometers. However, if the lasers themselves are used as radiation sources in the measurements, the absorption coefficients or functions for specific lasers can be obtained directly from experiment. In the case of gas lasers, such measurements may yield what are practically absorption coefficients. For other types of lasers, the experiment yields directly either the absorption function or an averaged absorption coefficient. /179

Experimental studies of the absorption of radiation from various lasers have taken two trends in the author's laboratory: 1) studies using a multiple-pass vacuum cell; 2) studies performed under natural conditions over an outdoor course. In the former

case, it is possible to investigate pure absorption, while in the latter it is necessary to separate the absorption from the total attenuation. However, large thicknesses cannot be produced in the cell measurements. Thus, the cell and outdoor measurements complement one another.

In the cell measurements, we obtained absorption coefficients for the radiation of helium-neon lasers at wavelengths of 1.15 and 3.39 μ. The absorption coefficient for 1.15 μ in the ground layer was found to be 0.3 mm^{-1}, where the mm^{-1} is a reciprocal millimeter of precipitated water. Since the absorption of this radiation is due to water vapor, the value of the absorption coefficient in reciprocal distance units or in dB/km would depend on humidity. The attenuation coefficient in the ground layer at a humidity of 12 g/m^3 equals 16 dB/km.

TABLE 3.12. TRANSMISSION T OF NONTURBID ATMOSPHERE FOR LASER RADIATION AT WAVELENGTH OF 1.15 μ FOR VARIOUS VALUES OF THE ABSOLUTE HUMIDITY a AND DISTANCES OF 0.1, 0.5, AND 1.0 km IN THE GROUND LAYER OF THE ATMOSPHERE

D, km	T			
	a = 1 mm/km	a = 5 mm/km	a = 10 mm/km	a = 15 mm/km
0.1	0,97	0.86	0.74	0.64
0.5	0,86	0.47	0.22	0.11
1.0	0,74	0.22	0.05	0.01

Table 3.12 lists values of the transmission coefficient in the ground layer of a nonturbid atmosphere for 1.15-μ laser light and various humidities.

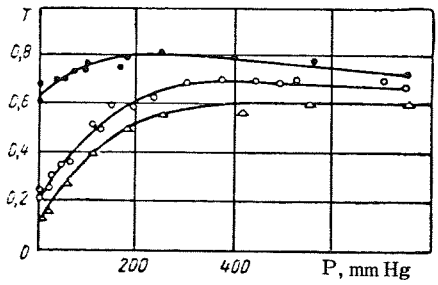

Figure 3.16. Transmission of Laser Light with Wavelength λ = 3.39 μ as a Function of Total Pressure at Various Methane Partial Pressures and a Geometrical Layer Thickness L = 64 m.

The absorption coefficient for laser radiation at 3.39 μ was found equal to 1.4 km^{-1} or 6 dB/km for the ground layer. The absorption of this radiation is due to methane. It must be stressed that in calculating the absorption of radiation from thermal sources, it is customary to neglect methane absorption owing to the very small concentration of this impurity (which is in the parts per million by volume). The strong absorption of laser light at 3.39 μ that was observed in the measurements indicates that in this case we may not even consider neglect of absorption by methane. The relatively strong absorption in this case is due to the fact that the centers of the methane absorption and laser emission lines practically coincide. /180

This is explained by the increase in atmospheric transparency that was observed in our measurements in the region of the laser radiation at 3.39 μ when the total pressure of the gas mixture was increased and the methane content remained constant (Fig. 3.16).

TABLE 3.13. RADIATION PARAMETERS OF LASERS USED IN OUTDOOR MEASUREMENTS

Laser type	Radiation wavelength μ	Radiated power	Radiating mode	Beam divergence
Helium-neon gas	0.63	10 mW	Continuous multimode	1'
Ruby solid	0.69	1 mW	Pulsed	1.5'
Gallium arsenide semiconductor	0.84	1 mW	Pulsed	20'
Neodymium-glass solid	1.06	0.1 mW	Pulsed	3'
Helium-neon gas	1.15	10 mW	Continuous multimode	1'
Helium-neon gas	3.39	20 mW	Continuous multimode	1'
Helium-xenon gas	3.51	20 mW	Continuous multimode	2'
Carbon dioxide-nitrogen gas	10.6	1 mW	Continuous multimode	2'

The outdoor-range measurements of the absorption of lasers with various wavelengths were made at much greater thicknesses than those in the cuvette. The distances over which the measurements were made varied from several hundred meters to 3.5 km (the longest path in the cuvette was 96 m).

The lasers whose parameters are listed in Table 3.13 were used as radiation sources in the outdoor measurements. /181

The absorption coefficient for 1.15-μ laser radiation was found to be the same in the outdoor measurements as it was in the cuvette. For the 3.39-μ laser, the absorption coefficient varied under natural conditions from one series of measurements to another, ranging from 1.4 to 5.0 km^{-1}. Thus, the lowest absorption-coefficient value agrees with that measured under laboratory conditions. Further study will be necessary to determine the cause of the absorption-coefficient variations. It is possible that

they were due to a corresponding change in the methane concentration at the locality of the measurements.

The measured attenuation was not resolved into components due to molecular absorption and aerosol scattering in the measurements /182
with the $CO_2 + N_2$ laser (wavelength 10.6 μ). The values obtained for the attenuation coefficients lie in the range from 0.12 to 4 dB/km. This range of variation of the attenuation coefficient is due to the varying weather conditions under which the measurements were made (haze with visibility $S_m \geq 2$ km, snow storms, light fog).

The absorption of the ruby-laser radiation varied as a result of changes in working-element temperature. The range of the absorption coefficient for a humidity of 10 g/m^3 was 1.1 to 4.7 dB/km.

The absorption of the laser radiation at 0.63, 0.84, 1.06, and 3.51 μ was completely masked in the outdoor investigations by the errors of measurement, which ranged up to 10-30%, depending on weather conditions and distance.

Edwards and Burch [332] measured the absorption of a helium-neon laser radiating at $\lambda = 3.30$ μ, using a small cell. The result of the measurements was a determination of the distance between the centers of the laser emission and methane absorption lines and the half-widths of the CH_4 line, which were found equal to 0.003 ± 0.002 cm^{-1} and 0.13 ± 0.04 cm^{-1}, respectively, under standard conditions, indicating that the centers of the emission and absorption lines practically coincide.

Chu and Hogg [333] measured the absorption of 3.39-μ gas-laser radiation at a distance of 2.9 km under natural conditions. They found a value of 5.5 ± 0.05 dB/km for the attenuation coefficient, in close agreement with the results of Edwards and Burch [332] and our own cell measurements, but not with the results of our outdoor measurements. We note in passing that in a new series of measurements, we again obtained absorption coefficients 1.5-3 times larger than those of [332, 333] and our cell measurements. The causes of these discrepancies are still unclear.

Long and Lewis [334] measured the absorption of a helium-neon gas laser radiating at 1.15 μ. The absorption coefficients obtained in [334] and in our own measurements agree satisfactorily.

McCubbin and Darone [335] used a CO_2-nitrogen laser to measure the absorption in several lines of the 10.4-μ CO_2 band in a /183
mixture of gases in which the absorbing and extraneous gases were placed under various pressures. They determined the strengths and half-widths of the lines from their measured results. Similar measurements are reported in [795-797].

Long and McCoy [336] measured the absorption of the radiation of a CO_2 laser in nitrogen in a long cuvette. The radiation was

generated on a line of the P branch with a rotational quantum number $j = 20$. For a CO_2 pressure of 0.25 mm Hg and a nitrogen pressure of 760 mm Hg, which correspond to conditions in the ground layer of the atmosphere, the authors of [336] found an absorption coefficient of 1.125 dB/km for the center of the emission line. We should note that radiation can be generated in various lines with a CO_2-N_2 mixture. In [337], for example, the positions of 17 lines that yield laser radiation were measured in the $(01^{1}1) \rightarrow (11^{1}0)$ band in the interval from 897.00 to 911.33 cm^{-1}. More than 100 generation lines of the CO_2 and N_2O molecules have been detected in the 9-11-μ interval [805]. Since the strengths of the lines in the CO_2 absorption spectrum vary with rotational quantum number, we should expect different absorption-coefficient values for lasers that radiate in different lines.

Thus, in speaking of the coefficient of laser-light absorption, it is necessary to have highly accurate knowledge of the positions of not only the atmospheric-gas absorption lines, but also of the laser emission lines. We stress once again that there is no point in speaking of absorption coefficients for laser radiation unless the half-widths of the emission lines are much smaller than those of the absorption lines. This condition may be regarded as satisfied for all practical purposes in the case of gas lasers. If, on the other hand, it is not satisfied, then Bouguer's law cannot be used to describe the absorption of the laser's radiation. It is then necessary to determine the absorption function for selective radiation sources.

Chapter 4

/184

ABSORPTION OF VISIBLE AND INFRARED WAVES IN THE INHOMOGENEOUS ATMOSPHERE

1. SPECTRAL TRANSMISSION (ABSORPTION). THE TRANSMISSION (ABSORPTION) FUNCTION

Written in differential form, the relation for the intensity change of radiation in an absorbing medium takes the form (see Chapter 3):

$$dI_\nu = -I_\nu k(\nu)\rho(l)\,dl, \tag{4.1}$$

where I_ν is the intensity of the radiation at frequency ν, $k(\nu)$ is the absorption coefficient, ρ is the density of the absorbing gas, and dl is an element of the ray path in the absorbing medium.

If the absorption coefficient is a function of points along the ray path, we speak of propagation in an inhomogeneous medium. The reason why the atmosphere is inhomogeneous in this sense is quite obvious: the half-widths and strengths of the lines, which determine $k(\nu)$, depend on pressure and temperature; the latter (see Chapter 1) vary strongly with height and depend on the geographical coordinates of the point in question. Thus the absorption coefficient is a function of points on the path of the ray in slant-path propagation in the atmosphere or in the case of horizontal propagation over distances for which the earth's curvature is significant.

Integrating (4.1), we obtain an expression for the spectral transmission

$$F(\nu) = \frac{I_\nu}{I_{0\nu}} = \exp\left(-\int_{(l)} \rho(l)\,k(\nu,\ l)\,dl\right), \tag{4.2}$$

where $I_{0\nu}$ is the intensity of the radiation at frequency ν at the /185 beginning of the path. The argument of the exponential is a curvilinear integral of the first kind, which can be evaluated with respect to points along the ray path. Strictly speaking, the integration should be carried out over the actual path of the ray with consideration of refraction. However, the refraction effect is usually left out of account in spectral-transmission determinations.

As in the case of the homogeneous atmosphere, the spectral absorption $A(\nu)$ is determined by the simple relation

$$A(\nu) = 1 - T(\nu), \tag{4.3}$$

By definition, the transmission function F and the absorption function H for an inhomogeneous path are written as follows in the spectral interval $\Delta\nu = \nu_2 - \nu_1$:

$$F = \frac{1}{\nu_2 - \nu_1} \int_{\nu_1}^{\nu_2} \exp\left[- \int_{(l)} \rho(l)\, k(\nu, l)\, dl \right] d\nu, \tag{4.4}$$

$$H = 1 - F. \tag{4.5}$$

It will be recalled that (4.4) and (4.5) are valid for the case in which the spectral density of the source radiation is constant in the interval $\Delta\nu$. The function F is the ratio of the radiant flux that has passed through a given layer of inhomogeneous atmosphere to the flux that was incident on the layer in the given spectral interval $\Delta\nu$. The function H is similarly defined.

2. DIRECT CALCULATION OF SPECTRAL TRANSMISSION AND TRANSMISSION FUNCTIONS

As we see from (4.2), direct calculation of $F(\nu)$ requires knowledge of the functions $\rho(l)$ and $k(\nu,l)$. The distribution of absorbing-gas concentration in the atmosphere has by now been more or less thoroughly studied (see Chapter 1). In any event, the function $\rho(l)$ can be assigned at least as the statistically averaged vertical concentration profile of the gas in question.

The absorption coefficient for radiation of frequency ν is the sum of the coefficients of the individual spectral lines $k(\nu, l) = \sum_i S_i(l) b_i(\nu, l)$, where S_i and B_i are the total strength and the contour of the line. The summation in this last relationship can be performed only numerically. The argument of the exponential in (4.2) is now equal to $\sum_i \int_{(l)} \rho(l)\, S_i(l)\, b_i(\nu, l)\, dl$, i.e., the terms of the /186

series depend on frequency otherwise than in the case of the homogeneous atmosphere and depend on the form of the meteorological-element distributions. This means that the sum in question must be recalculated in each concrete case. Moreover, the integrals in the last relationship cannot, as a rule, be expressed in terms of elementary functions.

If we assume validity of the dispersion spectral-line contour, we have

$$k(\nu, l) = \sum_i \frac{S_i[T(l)]}{\pi} \frac{\gamma_i[T(l), P(l)]}{(\nu - \nu_{0i})^2 + \gamma_i^2[T(l), P(l)]}, \qquad (4.6)$$

where T(1) and P(1) are the temperature and effective pressure at point 1.

Thus, the following data must be available for direct calculation of the spectral transmission (absorption) of the inhomogeneous atmosphere with (4.2) and (4.6): 1) the concentration distribution of the absorbing gases and the temperature and the distribution of effective pressure along the ray path; 2) the positions ν_{0i} of the lines contributing to absorption of radiation at frequency ν; 3) the strengths and half-widths of these lines at the corresponding temperature and effective-pressure values. It must be stressed that accurate calculation of $F(\nu)$ requires line-parameter data determined with extremely high accuracy (see §13 of Chapter 3). This applies in particular to calculation of the spectral transmission in the central regions of the lines.

Only recently have we had reason to hope for the acquisition of spectral-transmission data by direct calculation of this quantity. Using data on the parameters of the water-vapor lines obtained by the method described in §5 of Chapter 3, our laboratory has performed calculations of this nature for a limited number of wavelengths.

The problem of direct calculation of absorption functions for an inhomogeneous atmosphere is even more complex.

The need to consider an integral in the argument of the exponential must now be added to the difficulties encountered in absorption-function calculations owing to calculation of the integral over a certain frequency band, which were described in Chapter 3. It is easily seen that this greatly complicates the problem /187 since the integrations with respect to ν and l are not commutative. Except for certain rather uninteresting particular cases of the distribution of the meteorological elements and absorption spectra, only numerical calculation of (4.4) is possible. However, the large volume of computational work, the need to examine each particular case, and the abundance of parameters render this procedure extremely complex. A few papers in which the absorption functions have been obtained for slant paths in the atmosphere by direct calculation with allowance for the absorption of each line have now been published.

Kyle, D. Murcray, F. Murcray, and Williams [79] calculated absorption functions in the 4.3-μ band (interval from 2235 to 2415 cm^{-1}). The transmission spectrum was first calculated with very close spacing. The calculation was performed for 1800 points in the indicated spectral interval. The resulting dependence of

the spectral transmisson on wavelength was then multiplied by the instrumental function of the spectrometer used in the measurements [79]. The positions and strengths of the CO_2 lines were calculated without systematic allowance for the interaction between the vibrational and rotational motions of the molecule. The line half-widths were assumed to be uniform at 0.066 cm^{-1} under standard conditions for all lines. A CO_2 concentration of 0.033% by volume was assumed for all heights. Despite the approximate nature of the calculation, its results agreed satisfactorily with experiment. This fact indicates that, as we have already noted, the requirements as to the accuracy of line-parameter determination are not as stringent for calculation of absorption functions as they are for calculation of spectral absorption.

A similar calculation for the 15.0-μ CO_2 band was performed by Drayson [62], who included about 2000 lines in the 12-18-μ interval. As we noted in Chapter 3, the author of [62] used a mixed Lorentz-Doppler line contour for pressures below 100 mbar. The dispersion contour was used for pressures above 100 mbar. The atmosphere was divided into 34 layers such that the temperature changed by no more than a few degrees within each layer. The calculation was carried out for six zenith angles. The averaged data for spectral intervals 5 cm^{-1} wide were presented for various atmospheric thicknesses.

Calfee and Gates [338] calculated a fully resolved water-vapor absorption spectrum in the region from 3848 to 3860 cm^{-1}. /188
No other gases have absorption lines on this segment. As in [62], the calculation procedure assumes that the atmosphere can be broken up into layers. Ten layers were taken for heights above 13.7 km (the tropopause). After transformation by applying the spectrometer instrumental function, the data acquired were compared with corresponding measured results. By comparing the calculated and experimental data, the authors were able to determine the vertical humidity profiles for a rather large number of cases. The initial data on the half-widths and strengths of the absorption lines were obtained without systematic allowance for the interaction of the vibrational and rotational motions of the H_2O molecule. The line-center positions were taken from experiment.

Generally speaking, the absorption functions were determined in all of these studies [79, 62, 338] on the basis of spectral-transmission data obtained for a large number of wavelengths. The line-parameter information used in the calculations could not have given sufficiently accurate values for the true spectral transmission at the corresponding specific wavelengths. Nevertheless, the absorption-function values obtained by this method can describe the true absorption in finite spectral intervals quite satisfactorily. This reflects the fact that exact knowledge of the line positions is not necessary for absorption-function calculations. What is of first importance is that the line in question lie in the interval $\Delta\nu$ under consideration. Further, failure to consider

the vibrational-rotational interaction in the molecule affects most strongly the parameters of weak lines that cannot contribute substantially to the value of the absorption function.

3. APPROXIMATE CALCULATION OF THE ABSORPTION FUNCTION H

The basic idea behind approximate methods of calculating the function H consists essentially of reducing the problem to a problem of finding the absorption function for the case in which the absorbing-gas concentrations, pressure, and temperature are constant over the path of the ray. Usually, either the effective-absorbing-mass method or the Curtiss-Godson approximation is used here.

In the former method, the effective absorbing mass is so selected as to satisfy the relation /189

$$H = A(P_0, \omega^*), \tag{4.7}$$

where P_0 is the pressure at the surface of the earth and ω^* is the effective absorbing mass.

The expression usually used for ω^* is

$$\omega^* = \int_{l_1}^{l_2} \rho(l) \left[\frac{P(l)}{P_0}\right]^{(n)} dl. \tag{4.8}$$

The value of the parameter n is adjusted.

The formula

$$\omega^* = \int_{l_1}^{l_2} \rho(l) \frac{P(l)}{P_0} \left(\frac{T_0}{T(l)}\right)^{1/2} dl \tag{4.9}$$

is sometimes used for ω^*. In (4.8) and (4.9), $\rho(l)$ is the density of the absorbing gas, $P(l)$ and $T(l)$ are the pressure and temperature at point l, and P_0 and T_0 are the pressure and temperature at the surface of the earth.

According to the Curtiss-Godson approximation or the weighted-average-pressure method, the absorption function H is written

$$H = A(\bar{P}, \omega), \tag{4.10}$$

$$\bar{P} = \frac{\int_{l_1}^{l_2} \rho(l) P(l)\, dl}{\int_{l_1}^{l_2} \rho(l)\, dl}, \tag{4.11}$$

$$\omega = \int_{l_1}^{l_2} \rho(l)\, dl. \tag{4.12}$$

The weighted-average-pressure method was proposed independently by Curtiss in 1952 and Godson in 1953 [3]. Rather many calculations have since been made for the absorption function of atmospheric gases on slant paths in the atmosphere. The method gives fair results for segments of the water-vapor and carbon-dioxide absorption bands, not only in approximating weak and strong lines, for which formulas (4.10)-(4.12) were derived, but also for intermediate values of the parameter x [see formula (3.52)]. Use of the weighted-average-pressure method for all values of the parameter x was defended in our paper [339]. In the case of the 9.6-μ ozone absorption band, the Curtiss-Godson approximation does not give sufficient accuracy for intermediate values of x. /190

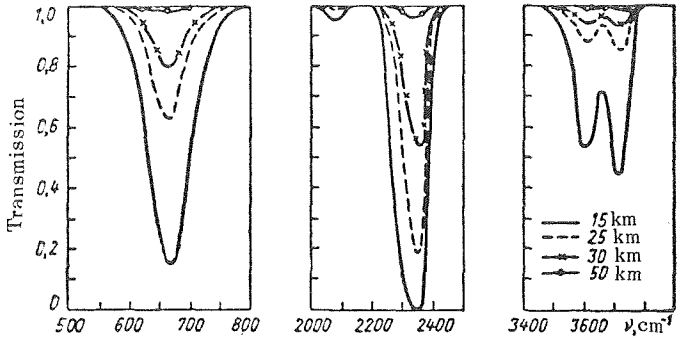

Figure 4.1. Transmission in 15.0-, 4.3-, and 2.7-μ CO_2 Bands for the Vertical Thicknesses of the Atmosphere Above 15, 25, 30, and 50 km According to Plass [342] (the calculation was performed with averaging over the spectrum in intervals 50 cm^{-1} wide).

Plass [340] obtained a series of formulas for calculation of the absorption functions H from known data on the homogeneous-atmosphere absorption function. Plass derived exact expressions for the function H in the weak- and strong-line approximations when the absorbing-gas concentration and temperature do not vary along the ray path. Analogous expressions were obtained for the case of pressure, concentration, and temperature variable along the ray path. In addition, a procedure for approximate calculation of the /191

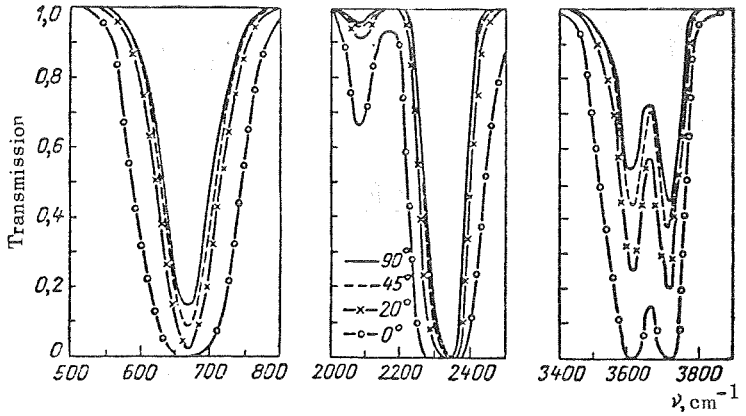

Figure 4.2. Transmission in 15.0-, 4.3-, and 2.7-μ CO_2 Bands for Atmospheric Thicknesses Penetrated by a Ray from a Height of 15 km at Angles θ = 0°, 20°, 45°, and 90° to the Local Horizon, According to Plass [342] (the calculation was made with averaging over the spectrum in intervals 50 cm^{-1} wide).

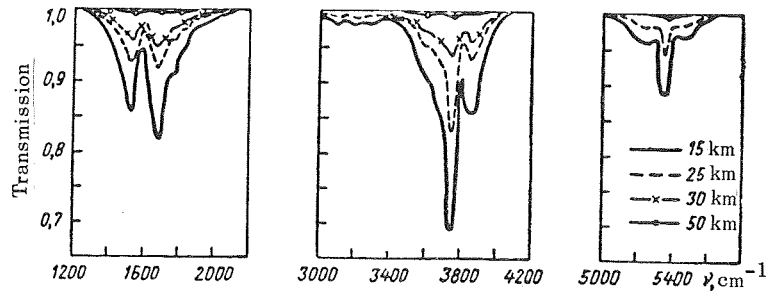

Figure 4.3. Transmission in 6.3-, 2.7-, and 1.87-μ H_2O Bands for the Vertical Thicknesses of Atmosphere Above 15, 25, 30, and 50 km, According to Plass [342] (calculation performed with averaging over the spectrum in intervals 50 cm^{-1} wide for the moist-stratosphere model).

function H was developed in [340]. The initial data on the homogeneous-atmosphere absorption functions, which are needed to determine the function H, can be presented in the form of theoretical or empirical relationships or tabulated.

In [341, 342], Plass used the formulas and tabular data on the homogeneous-atmosphere absorption functions that had been

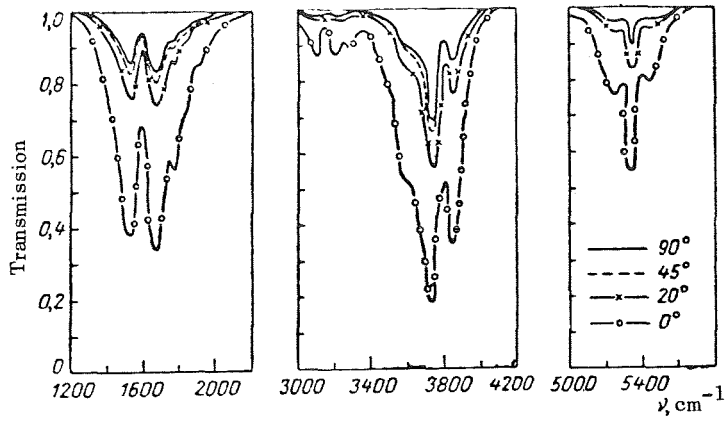

Figure 4.4. Transmission in 6.3-, 2.7-, and 1.87-μ Bands for Atmospheric Thicknesses Penetrated by a Ray from a Height of 15 km at angles θ = 0°, 20°, 45°, and 90° to the Local Horizon According to Plass [343] for the Moist-Stratosphere Model with Averaging over 50-cm^{-1}-wide Spectral Intervals.

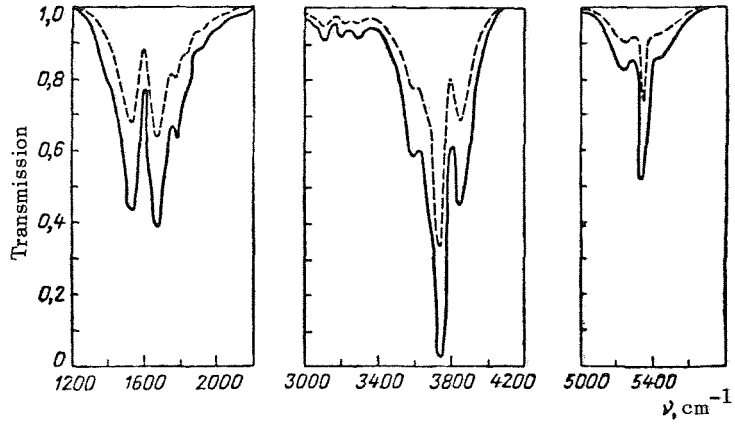

Figure 4.5. Transmission in 6.3-, 2.7-, and 1.87-μ H_2O Bands as Calculated by Plass [343] for Dry and Moist Stratosphere Models and the Thickness of Atmosphere Penetrated by a Ray in Horizontal Propagation from a Point at a Height of 30 km: ——) moist stratosphere; ---) dry stratosphere.

obtained in [340] to perform extensive calculations of the absorption functions H in narrow spectral segments of the fundamental water-vapor and carbon-dioxide vibrational-rotational bands with allowance for the altitude changes of pressure, absorbing-gas concentration, and temperature.

Some of the calculated results obtained by Plass for the functions H appear in Figs. 4.1-4.5.

Our laboratory calculated absorption functions H for segments of the water-vapor and carbon-dioxide spectra 0.1 μ wide for a defined atmospheric model that took account of the altitude variations of pressure, temperature, and H_2O and CO_2 concentrations. /193
The calculation covered all of the fundamental H_2O and CO_2 vibrational-rotational bands. The values of H were obtained at 1-km intervals for the bottom 30-km layer of atmosphere. The results were set forth in detail in the author's monograph [1]. Absorption functions were calculated for the whole 6.3-, 3.2-, 2.7-, 1.87-, 1.38-, 1.1-, and 0.94-μ water-vapor and 15.0-, 5.2-, 4.8-, 4.3-, 2.7-, 2.0-, 1.6-, and 1.4-μ carbon-dioxide vibrational-rotational bands for various directions in the bottom 8-km layer of atmosphere in our paper [59]. References to other papers may be found in [1] and [342].

4. APPROXIMATE METHOD OF ALLOWING FOR TEMPERATURE IN CALCULATION OF THE FUNCTION H

When the function H is calculated, its temperature dependence is often disregarded because the temperature varies with height in a relatively narrow range. Nevertheless, it is necessary in many cases to take the temperature dependence of H into account. Below we set forth an approximate method for consideration of this dependence, one that is suitable for application to the vibrational-rotational spectra of water vapor and carbon dioxide.

The temperature dependence of the function H is defined in terms of the temperature dependence of the absorption line half-widths and strengths. The latter dependence is expressed approximately by the following formulas:

$$\gamma_i(T) = \gamma_{0i}\frac{P(l)}{P_0}\left(\frac{T_0}{T(l)}\right)^{1/2} = \gamma_{0i}\frac{T_0^{1/2}}{P_0}\beta(l), \tag{4.13}$$

$$S_i(T) = S_i(T_0)\left[\frac{T_0}{T(l)}\right]^{3/2} \times \exp\left[-E_i(T(l)-T_0)(kT(l)T_0)^{-1}\right], \tag{4.14}$$

where γ_{0i} is the half-width of the i-th line under the standard conditions $P = P_0$; $T = T_0$; $S_i(T_0)$ is the strength of the i-th line at standard temperature, E_i is the energy of the lower level from which the transition responsible for the line begins, and $\beta(l) = \frac{P(l)}{[T(l)]^{1/2}}$.

We shall henceforth consider γ_{0i} to be temperature-independent.

For lines of the vibrational-rotational spectra, E_i can be represented approximately by /194

$$E_i = E_{iv} + E_{iR}, \tag{4.15}$$

where E_{iv} and E_{iR} are the vibrational and rotational energies of the lower state of the i-th line. Recognizing that $E_{iv} >> E_{iR}$ (see Chapter 2), we can put

$$E_i = E_{iv}. \tag{4.16}$$

Within a given vibrational-rotational band, E_{iv} is independent of the rotational quantum number. Further, we may take the energy of the ground vibrational state as E_{iv} for the fundamental vibrational-rotational bands of water vapor and carbon dioxide. Analysis of the fundamental vibrational-rotational bands of these gases indicates that each of them consists of lines belonging to different vibrational transitions. However, most of these overlapping transitions have the ground state as the lower state and, most importantly, their strengths are substantially higher than those of transitions from nonground states. In absorption-function calculations, therefore, the rotational lines of these transitions can be disregarded. We might replace E_v by the average $\bar{E}_v = \Sigma E_{vk}\tau_k$, where E_{vk} is the vibrational energy of the lower state of the k-th transition (that forming the given band) and τ_k is its relative strength ($\Sigma\tau_k = 1$). However, estimates show that $\bar{E}_v$ is close to the ground-state energy. We may therefore write

$$\left.\begin{aligned} S_i(T) &= S_i(T_0)\varphi, \\ \varphi &= (T_0/T)^{3/2}\exp\left(-C(T-T_0)(TT_0)^{-1}\right), \end{aligned}\right\} \tag{4.17}$$

where ϕ does not depend on i and C is a certain quantity corresponding to the lines of the H_2O and CO_2 spectra. We stress that this approximation (ϕ independent of i) is not possible for lines of the rotational spectrum, because it is based on the inequality $E_{iv} >> E_{iR}$. In the described approximation

$$k_\nu = \sum S_i(T_0)\, b_i(\nu, \beta), \tag{4.18}$$

$$A = A(\omega', \beta), \quad \omega' = \omega\varphi, \tag{4.19}$$

where

$$\beta = P\sqrt{\frac{T_1}{T_2}}$$

Consequently, the scheme developed in [1, 339] for calculating H emerges unchanged after substitution of β for P and ρφ for ρ'. The final result can now be written /195

$$\left.\begin{aligned} H &= A(m', \bar{\beta}), \\ m' &= \int \varphi(l)\rho(l)\,dl, \\ \bar{\beta} &= \frac{\int \beta(l)\varphi(l)\rho(l)\,dl}{m'}. \end{aligned}\right\} \qquad (4.20)$$

5. APPROXIMATE DETERMINATION OF THE SPECTRAL TRANSMISSION OF THE INHOMOGENEOUS ATMOSPHERE

Formula (4.2) can be used to calculate the spectral transparency along an inhomogeneous path in the general case. However, the difficulties noted above oblige us to seek certain approximate methods.

The weighted-average-pressure method can be extended to our case, with the final formula for F(ν) written in the form

$$F(\nu) = I_\nu / I_{0\nu} = \exp[-\omega k(\nu, \bar{P})], \qquad (4.21)$$

where ω and P are defined by (4.11) and (4.12).

If we consider the variations of temperature over the ray path, we have for the vibrational-rotational spectrum

$$F(\nu) = \exp(-m' k(\nu, \bar{\beta})) \qquad (4.22)$$

and can use (4.20) in calculating m' and $\bar{\beta}$.

It must be noted that formulas (4.21) and (4.22) are now obviously a rougher approximation than the analogous results for the absorption function.

It is shown without difficulty that these relations are asymptotically valid for spectral segments in which the absorption is governed by the limbs of lines. The results of (4.10)-(4.12) and (4.20) proceed directly from (4.21) and (4.22), although this does not, of course, mean that the converse holds true.

However, it is easy to cite cases that do not fit into the scheme developed, e.g.: 1) absorption at the center of a line; 2) absorption of frequency ν due to lines with different lower vibrational-energy levels.

There is as yet no numerical material that would enable us to establish the accuracy of the approximate expressions obtained in §§4 and 5. /196

6. CALCULATION OF ABSORPTION FUNCTION WITH ALLOWANCE FOR THE CURVATURE OF THE EARTH

In many cases, it is necessary to have the inhomogeneous-atmosphere absorption functions with consideration of the earth's curvature. Let us consider the corresponding exact formulas and an approximate method for solving this problem.

We first write out certain geometrical relationships that will be used later.

Let the geographical coordinates of the source and receiver of the radiation and their elevations above sea level be given. All quantities pertaining to the source will be subscripted 1 (point 1) and those pertaining to the receiver will be subscripted 2 (point 2).

We introduce a Cartesian coordinate system with its origin at the center of the earth, its z axis pointed at the North Pole, and its x axis directed through Greenwich, so that the x, y, and z axes form a right trihedral. We define the polar coordinates r, θ, and ϕ in this system in the usual manner. The Cartesian and polar coordinates are related as usual:

$$\begin{gathered} x = r\sin\theta\cos\varphi;\ y = r\sin\theta\sin\varphi;\ z = r\cos\theta; \\ r = \sqrt{x^2+y^2+z^2};\ \cos\theta = z/r;\ 0 \leqslant \theta \leqslant \pi; \\ \sin\varphi = (y/r)\sin\theta;\ \cos\varphi = (x/r)\sin\theta. \end{gathered} \tag{4.23}$$

The height of a point above the surface of the earth will be denoted by h. It is easily shown that

$$\begin{gathered} \text{if } \xi \text{ is the eastern longitude of a point, then } \phi = \xi, \\ \text{if } \xi \text{ is the western longitude of a point, then } \phi = 2\pi - \xi, \\ \text{if } \eta \text{ is the northern latitude of a point, then } \theta = \pi/2 - \eta, \\ \text{if } \eta \text{ is the southern latitude of a point, then } \theta = \pi/2 + \eta, \end{gathered} \tag{4.24}$$

$$r = R + h,$$

R is the radius of the earth.

It follows from (4.10)-(4.12) that in order to determine the function H, it is necessary to evaluate integrals of the type /197

$$B = \int F(l)\, dl, \tag{4.25}$$

where F(1) is a certain function of points on the ray path and the integration is extended over the ray path.

In calculating ω, the function F coincides with the concentration distribution of the absorbing gas, and in the calculation of $\bar{P}$

$$F = \rho(1)P(1).$$

In the general case, F depends on the geographic coordinates of the point and its height. It is now easy to construct the function F(r, θ,ϕ) from formulas (4.24). We shall assume that this procedure has been completed. Then r, θ, and ϕ will be functions of the path points 1. Applying the usual rule for operations with curvilinear integrals of the first kind, we can derive the following exact formulas for calculation of the function H:

$$B = \int_0^s F[r(l),\ \theta(l),\ \varphi(l)]\, dl, \tag{4.26}$$

$$s = \sqrt{r_1^2 + r_2^2 - 2r_1 r_2 \cos\delta}, \tag{4.27}$$

$$\cos\delta = \cos\theta_1 \cos\theta_2 + \sin\theta_1 \sin\theta_2 \cos(\varphi_2 - \varphi_1), \tag{4.28}$$

$$r(l) = \left(r_1^2 + l^2 + 2l\,\frac{r_1 r_2 \cos\delta - r_1^2}{s}\right)^{1/2}, \tag{4.29}$$

$$\cos\theta(l) = \frac{r_1 \cos\theta_1 + l\cos\gamma}{r(l)},\quad 0 \leqslant \theta \leqslant \pi, \tag{4.30}$$

$$\cos\varphi(l) = \frac{r_1 \sin\theta_1 \sin\varphi + l\cos\beta}{r(l)\sin\theta(l)}, \tag{4.31}$$

$$\sin\varphi(l) = \frac{r_1 \sin\theta_1 \sin\varphi_1 + l\cos\alpha}{r(l)\sin\theta(l)}, \tag{4.32}$$

$$\cos\alpha = \frac{r_2 \sin\theta_2 \cos\varphi_2 - r_1 \sin\theta_1 \cos\varphi_1}{s}, \tag{4.33}$$

$$\cos\beta = \frac{r_2 \sin\theta_2 \sin\varphi_2 - r_1 \sin\theta_1 \sin\varphi_1}{s}, \tag{4.34}$$

$$\cos\gamma = \frac{r_2 \cos\theta_2 - r_1 \cos\theta_1}{s}. \tag{4.35}$$

Calculations of the integrals B by the exact formulas (4.26)-(4.35) presuppose quite extensive information on the meteorological situation over various geographic regions. /198

Let us now examine an approximate method of evaluating the integrals with respect to the ray paths, one that may be found

adequate for most practical applications.

For the sake of definition, let us assume that the receiver of the radiation is higher than the source; needless to say, this will not affect the generality of the result, because the integrals under consideration are invariant under transposition of the limits of integration.

Let us denote by x_3, y_3, and z_3 the coordinates of a point (point 3) situated above the straight line passed through the locations of the receiver and the source and at the shortest possible distance from the coordinate origin. Then

$$\begin{aligned} x_3 &= x_2 + t^*(x_1 - x_2), \\ y_3 &= y_2 + t^*(y_1 - y_2), \\ z_3 &= z_2 + t^*(z_1 - z_2), \\ t^* &= \frac{x_2(x_2 - x_1) + y_2(y_2 - y_1) + z_2(z_2 - z_1)}{(x_2 - x_1)^2 + (y_2 - y_1)^2 + (z_2 - z_1)^2}. \end{aligned} \tag{4.36}$$

The formula for t* can also be written

$$t^* = \frac{r_2(r_2 - r_1 \cos\delta)}{r_1^2 + r_2^2 - 2r_1 r_2 \cos\delta}. \tag{4.37}$$

It follows from this last formula that $t^* > 0$.

There are two possible cases of location of points 1, 2, and 3, depending on t*:

$$\begin{aligned} &1)\ 0 \leq t^* \leq 1, \text{ point 3 between 1 and 2,} \\ &2)\ t^* > 1, \quad \text{point 1 between 2 and 3.} \end{aligned} \tag{4.38}$$

We now take advantage of two facts: 1) the vertical profile of the meteorological characteristics is much less variable than the horizontal profile; 2) that part of the atmosphere where the absorbing-component concentration is highest is most important for infrared absorption. Bearing these facts in mind, we can substitute the coordinates of the point on the path that is closest to the earth's surface for $\theta(1)$ and $\phi(1)$ in the exact formulas (4.26)-(4.35). These will be the coordinates of point 3 if the first variant of (4.38) is realized, and the coordinates of point 1 for the second variant of (4.38). Further, as follows from (4.10-(4.12) and the formulas describing the distribution of the pressure and the H_2O and CO_2 concentrations in the troposphere, the function F takes the form $\exp(-\alpha h)$, where α is a certain constant. Formula (4.26) is integrated from a point at a distance r' from the origin of the coordinate system introduced above to a point at a distance r" from

/199

this origin with an angle σ between these directions. The integral defined in this manner will be denoted by $B(\alpha, \sigma, h', h'')$, where h' and h'' are the heights of points r' and r'' above the earth's surface. Regarding r' and r'' as quite small compared to R, we can obtain for $B(\alpha, \sigma, h', h'')$

$$B(\alpha, \sigma, h', h'') = e^{-\alpha h'} \sqrt{\frac{\pi R}{2\alpha}} \frac{1}{\sin\psi} e^{\xi_0^2} [\Phi(\xi^*) - \Phi(\xi_0)]. \tag{4.39}$$

Here Φ is the probability integral defined by

$$\Phi(z) = \frac{2}{\sqrt{\pi}} \int_0^z e^{-z'^2} dz', \tag{4.40}$$

$$\xi^* = \xi + \xi_0, \quad \xi = l \sqrt{\frac{\alpha}{2R}} \sin\psi,$$

$$\xi_0 = \left(\frac{\alpha R}{2}\right)^{1/2} \operatorname{ctg}\psi, \tag{4.41}$$

$$\cos\psi = \frac{r'' \cos\sigma - r'}{l}, \quad \sin\psi = \sqrt{1 - \cos^2\psi}.$$

The angle σ is easily determined from the relations

$$\sigma = \sigma'' - \sigma', \quad \cos\sigma' = \frac{r_3}{R + h'}, \quad \cos\sigma'' = \frac{r_3}{R + h''}.$$

The geometrical sense of ψ is as follows: it is the angle between the direction of r' and the straight line joining points r' and r''. Particular cases of (4.39) will be found in the monograph [1].

As follows from the material of Chapter 1, the quantity α introduced there is, generally speaking, different for different heights if we consider the altitude distribution of the concentration of any absorbing gas in the troposphere and stratosphere. In this situation, the path of integration must be broken up into segments within which α has a fixed value.

7. EXPERIMENTAL INVESTIGATIONS OF THE ABSORPTION FUNCTIONS H /200

It is practically impossible to reproduce the inhomogeneous atmosphere under laboratory conditions with its continuous variations of pressure, temperature, and absorbing-gas concentrations. For this reason, the absorption functions H are measured under /201 natural conditions using the sun as the radiation source.

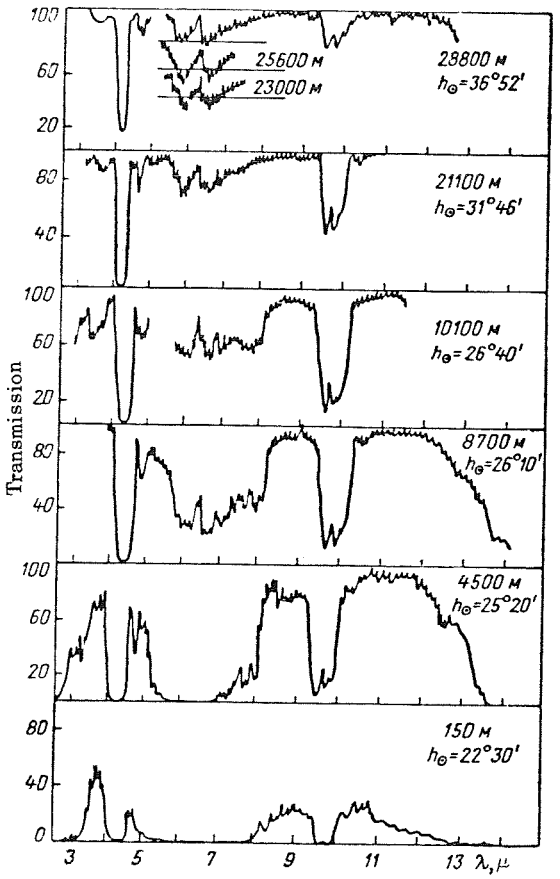

Figure 4.6. Transmission of Various Atmospheric Thicknesses from Various Levels According to K.Ya. Kondrat'yev et al. [344] in the 3-13-μ Region (the authors of [344] attribute the absorption above 20 km in the 6.3-μ band to moisture present in the spectrometer).

We now have a substantial number of measurements of H obtained from the ground and from various heights with various spectral resolutions in all of the fundamental vibrational-rotational absorption bands of the atmospheric gases (Figs. 4.6-4.12). The H_2O absorption bands at 6.3, 3.2, 2.7, 1.87, 1.38, and 1.1 μ and the 4.3- and 2.7-μ CO_2 and 9.6-μ O_3 absorption bands have been studied in greatest detail. Measurements have been made from various heights using equipment lifted on aircraft or balloons. The altitudes covered range up to 20 km in the former case and 30 km in the latter.

In studies made under natural conditions, it is not the pure absorption of solar radiation in the atmosphere that is measured, but instead its attenuation due to absorption plus aerosol and molecular scattering. To minimize /205 the influence of aerosol scattering, measurements are made only on the clearest cloudless days. As for molecular scattering, its influence can be taken into account when necessary, since the corresponding coefficients have been determined with sufficient accuracy in a broad range of wavelengths (see Chapter 6).

The most complete data on the functions H were obtained by the groups of K.Ya. Kondrat'yev [253, 344, 807], B.S. Neporent and Ye.O. Fedorova [348, 808, 809, 877], Murcray [79, 345-347], Gates [349, 350], Houghton [351-353] and Cummings [354]. Another series of results was obtained in [355-357].

8. ABSORPTION OF LASER RADIATION IN THE INHOMOGENEOUS ATMOSPHERE

The emission-line half-widths of many lasers are smaller than

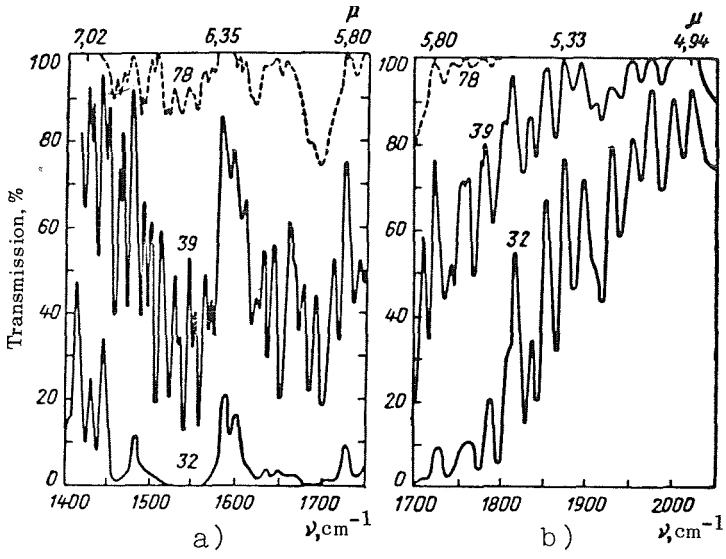

Figure 4.7. Transmission of Various Atmospheric Thicknesses from Various Levels in the Spectral Region from 1400 to 2050 cm^{-1} According to [345]. Curve 32: pressure P = = 453 mbar, height z = 6.3 km, sec θ = 2.75, air mass w = 1.23, precipitated CO_2 layer u = 295 atm·cm; curve 39: P = 270 mbar, z = = 9.9 km, sec θ = 2.42, w = 0.646, u = 155 atm·cm; curve 78: P = 23.8 mbar, z = 25.5 km, sec θ = 1.517, w = 0.0356, u = 8.54 atm·cm.

those of the absorption lines of atmospheric gases. Quantitative evaluation of the absorption of laser radiation therefore requires data on the spectral absorption for fixed frequencies in certain very narrow segments of the spectrum. Generally speaking, such data can be calculated when the center positions, strengths, and contour shapes of the lines contributing to absorption at the particular frequency are known with very high accuracy. Moreover, such calculations require data on the altitude distributions of pressure, temperature, and the absorbing-gas concentrations.

In principle, a quantitative estimate of the absorption of laser light can be obtained from measurements of the spectral absorption of solar radiation in the earth's atmosphere. The spectral resolution of the instruments must be exceptionally high to avoid distortions due to the instrumental functions of the spectrometers. In addition, the positions of the absorption and laser emission lines must be known accurate to within no more than 10^{-2}-10^{-4} cm^{-1}, depending on the distance between the centers of the absorption and emission lines (see §14 of Chapter 3). The

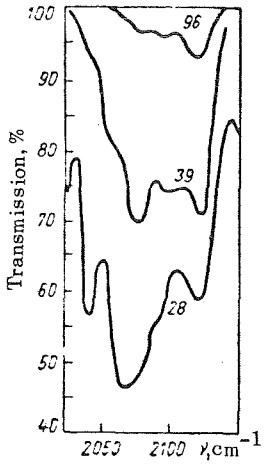

Figure 4.8. Transmission of Various Atmospheric Thicknesses from Various Levels in Spectral Region from 2000 to 2150 cm^{-1} According to [345]. Curve 28: pressure P = 557 mbar, height z = 4.8 km, sec θ = 2.97, air mass w = 1.63, precipitated CO_2 layer u = = 395 atm·cm; curve 39: P = = 279 mbar, z = 9.9 km, sec θ = 2.42, w = 0.646, u = 155 atm·cm; curve 96: P = 10.3 mbar, z = 30.9 km, sec θ = = 1.321, w = 0.0135, u = 324 atm·cm.

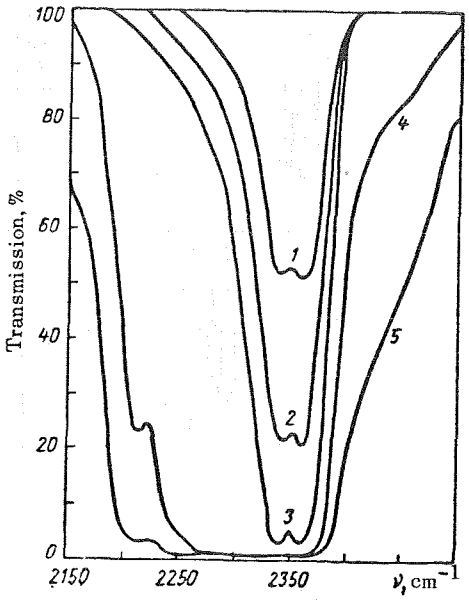

Figure 4.9. Transmission of Various Atmospheric Thicknesses from Various Levels in Spectral Region from 2150 to 2500 cm^{-1} According to [345]. Curve 1: pressure P = 10.3 mbar, height z = 30.9 km, sec θ = 1.273, air mass w = 0.0130, precipitated CO_2 layer u = = 3.12 atm·cm; curve 2: P = = 18.6 mbar, z - 27.1 km, sec θ =1.476, w - 0.0272, u - 6.53 atm·cm; curve 3: P - 41.5 mbar, z = 21.9 km, sec θ = 1.63, w = = 0.0668, u = 16.0 atm·cm; curve 4: P = 453 mbar, z = 6.3 km, sec θ = 2.75, w = 1.23, u = = 295 atm·cm; Curve 5: P = 764 mbar, z = 2.3 km, sec θ = 3.45, w = 2.60, u = 624 atm·cm.

absorption of laser radiation in an inhomogeneous atmosphere can also be measured using the laser as the radiation source.

In §5, we examined an approximate method that we proposed for calculation of the spectral absorption in an inhomogeneous atmosphere, one that reduces this problem to one of the spectral absorption of a homogeneous atmosphere. It is assumed that the solution of this last problem is known. /206

Plass [409] derived a number of useful formulas for estimating the absorption of laser light propagating on slant paths in

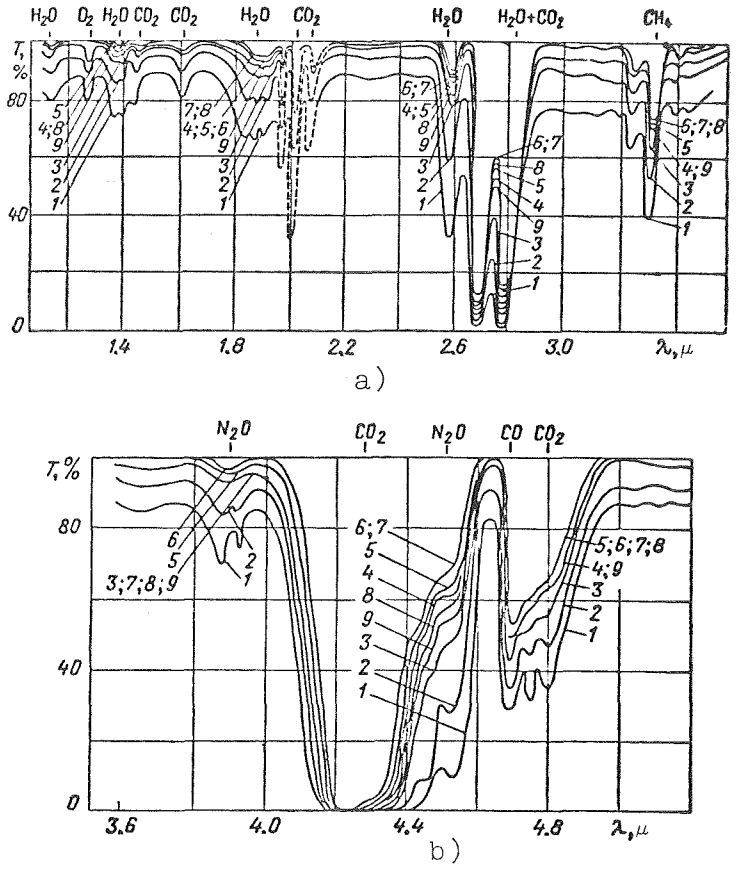

Figure 4.10. Transmission of Atmosphere at Various Heights in the Regions from 1 to 3.5 (a) and 3.5 to 5.5 (b) μ for Low Sun During the Summer According to [804]:

Curve No.	Height, km	Altitude of sun
1	12	1°57′
2	13	2°39′
3	14	3°24′
4	15	4°24′
5	15.6	4°54′
6	16	5°54′
7	14.6	7°06′
8	13.8	8°15′
9	12.8	91°8′

the atmosphere. For the case in which the volume concentration of the absorbing gas can be assumed constant at all heights and the temperature dependence of the line strengths and half-widths can be disregarded, Plass obtained the following expression for the spectral transmission of monochromatic radiation at frequency μ on a slant path:

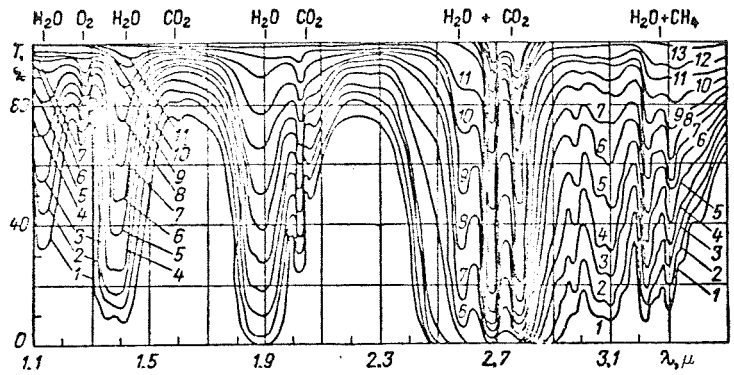

Figure 4.11. Transmission of Atmosphere at Various Heights in Region from 1 to 3.5-μ According to [804].

Curve No.	Height, km	Altitude of sun
1	0	20°10′
2	1,0	20°50′
3	2,3	21°20′
4	3,4	22°00′
5	4,4	22°40′
6	5,6	23°20′
7	6,8	24°00′
8	8,5	24°30′
9	9,8	25°10′
10	11,5	25°50′
11	12,5	26°30′
12	15,4	27°40′
13	17,6	28°20′
14	19,6	29°30′
15	22,1	30°40′
16	24,0	32°40′

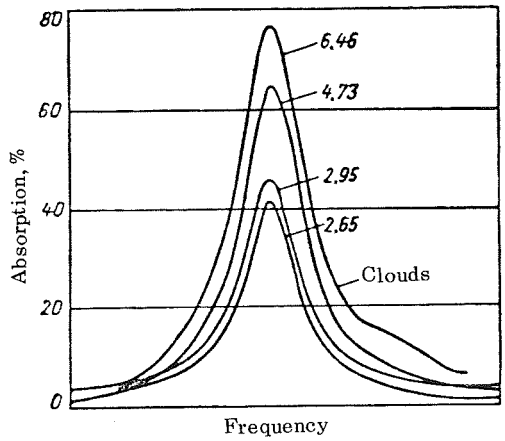

Figure 4.12. Transmission of the Entire Thickness of the Atmosphere in the Region of the Water-Vapor Absorption Line Centered Near 6943.8 Å for Various Air Masses According to Long's Measurements [295] of December 26, 1965.

$$F(\nu)=\prod_i[(1+\xi_{0i}^2)/(1+\xi_{1i}^2)]^{\vartheta}, \qquad (4.42)$$

where

$$\xi_{0i}=\gamma_{0i}(\nu-\nu_{0i})^{-1}, \qquad (4.43)$$

$$\xi_{1i}=\gamma_{1i}(\nu-\nu_{0i})^{-1}, \qquad (4.44)$$

$$\vartheta_i=\frac{S_i c P_{s_i}\sec\theta}{2\pi\gamma s_i g}. \qquad (4.45)$$

Here γ_{0i} and γ_{1i} are the half-widths of the i-th line at the beginning and end of the slant path, c is the volume concentration of the absorbing gas, P_{s_i}

and γ_{ji} are the effective pressure and half-width of the line under standard conditions, θ is the angle between the propagation direction and the vertical, g is the acceleration of gravity, and ν_{0i} and S_i are the center and strength of the i-th line.

Reference [409] also examined the case in which the temperature and concentration of the absorbing gas vary along the path of the ray. The product of the line strength by the gas concentration c is written in the form

$$Sc = S_s c_s \gamma_s^{-m} \gamma^m. \tag{4.46}$$

This yields the following expression for $F(\nu)$:

$$F(\nu) = \exp\left\{-2\vartheta_s \gamma_s^{-m} \int_{\gamma_0}^{\gamma_1} \gamma^{m+1} [(\nu-\nu_0)^2+\gamma^2]^{-1} d\gamma\right\}, \tag{4.47}$$

where

$$\vartheta_s = S_s c_s P_s \sec\theta / 2\pi\gamma_s g. \tag{4.48}$$

S_S, c_S, γ_S, and P_S are the values of S, c, γ, and P under standard conditions and m is a number that is, generally speaking, different for each line and dependent on height. For a water-vapor line in the troposphere, m is found to be approximately 4. In this case we obtain from (4.48) /207

$$F(\nu) = \exp\left(\vartheta_s \xi_s^{-4}\left\{\frac{1}{2}(\xi_1^4-\xi_0^4)-(\xi_1^2-\xi_0^2)+\ln[(1+\xi_1^2)(1+\xi_0^2)^{-1}]\right\}\right), \tag{4.49}$$

where

$$\xi_0 = \gamma_s(\nu-\nu_0)^{-1}. \tag{4.50}$$

Finally, Plass considered the case in which the center of an absorption line with a dispersion contour may be pressure-shifted. In this case, the absorption coefficient becomes

$$k(\nu) = \frac{S}{\pi}\frac{\gamma}{(\nu-\nu_0+A\gamma)^2+\gamma^2}, \tag{4.51}$$

where $A\gamma$ defines the shift of the line center and depends on pressure, since γ depends on pressure.

Using (4.51), we easily obtain a formula for $F(\nu)$:

$$F(\nu)=\{[(1+A\xi_0^2)+\xi^2]/[(1+A\xi_1^2)+\xi_1^2]\}^{\vartheta(1+A^2)^{-1}}\times \\ \times\exp[(1+A^2)^{-1}\cdot 2\vartheta A\{\mathrm{tg}^{-1}[(1+A^2)\xi_1+A]- \\ -\mathrm{tg}^{-1}[(1+A^2)\xi_0+A]\}], \tag{4.52}$$

where ν_0 is the position of the line center at zero pressure.

Formulas (4.51) and (4.52) are valid for atomic lines, whose shifts in the visible region have been observed experimentally. A value of 0.725 was found for A. No pressure-connected line-center shifts have as yet been observed in the vibrational-rotational absorption spectra of the atmospheric gases. Use of lasers for this purpose will no doubt help solve this important problem. If there is a shift, it will be necessary to take it into account in determining $F(\nu)$.

Long [295] made an experimental study of the atmospheric transmission with high resolution in the region of ruby-laser radiation, using the sun as a radiation source. Figure 3.9 presents the spec- /208
tral-absorption curve obtained at solar altitudes from 17.4° to 19.3°. The spectrum was recorded on the 6933-6946 Å segment, which includes the radiation from ruby lasers operating at various crystal temperatures. As the figure shows, the spectral absorption can vary from 0 to 80% on a change in radiation wavelength by less than 1 Å.

Figure 4.12 presents the results of Long's more detailed studies [295] of atmospheric transmission in the region of the water-vapor absorption line at 6943.8 Å, a region into which ruby-laser light falls when the crystal temperature is 305-310°K. The curve shows transmission curves obtained on December 26, 1965 for four air-mass values: 6.46, 4.73, 2.95, and 2.65. We see from the figure that the absorption in the central part of the line increases from approximately 40% to 80% on a change in air mass from 2.65 to 6.46. We note that this result characterizes the winter absorption of the atmosphere. The absorption increases strongly in all water-vapor lines when the corresponding measurements are made in summer.

Part Two /209

SCATTERING OF VISIBLE AND INFRARED WAVES IN THE EARTH'S ATMOSPHERE

Chapter 5

THE EARTH'S ATMOSPHERE AS A SCATTERING MEDIUM

Electromagnetic waves in the visible and infrared regions are attenuated during propagation in the earth's atmosphere as a result of absorption by the gaseous components and as a result of scattering: 1) on molecule-density fluctuations (molecular scattering), 2) on aerosol particles (aerosol scattering), and 3) on inhomogeneities due to turbulent motions in the atmosphere.

The coefficients of attenuation due to scattering of the radiation on micro- and macroturbulent inhomogeneities are negligibly small by comparison with the coefficients of molecular and aerosol scattering.

The attenuation of visible and infrared light by molecular scattering in the atmosphere has been studied quite thoroughly. We now have extensive tables of the coefficients of molecular or Rayleigh scattering in a broad range of wavelengths in the ultraviolet, visible, and infrared regions.

The coefficients of Rayleigh scattering are practically independent of time and place. The coefficients of aerosol scattering, on the other hand, depend strongly on the dimensions, chemical composition, and concentration of the aerosol particles, which are subject to wide variations in time and space. Thus, quantitative evaluation of the atmospheric attenuation of visible and infrared light due to aerosol scattering requires reliable data on all of the fundamental characteristics of the atmospheric aerosol.

Even though the dimensions, concentration, and chemical composition of the atmospheric-aerosol particles vary over extremely broad ranges, certain characteristic aerosol types can be distinguished (clouds, fogs, hazes, precipitation, dust). The present chapter is devoted to the spectra of the dimensions, chemical composition, and concentration of the particles of the most characteristic atmospheric aerosols. /210

1. Spectra of particle dimensions. The processes in which clouds and fogs form are related to a multitude of wide-ranging factors that determine the growth of droplets (the dependence of growth rate on the concentration, size distribution, and nature of the condensation nuclei, on the temperature and cooling rate of the air, and on the scale and intensity of turbulence). All of this has thus far precluded theoretical solution of the problem of the size-distribution functions of the particles.

The existing analytical expressions have been derived as approximating relationships in reduction of the corresponding experimental histograms. The overwhelming majority of experimental data obtained by various investigators both in the USSR [358-360 and others] and abroad [361, 362 and others] indicate that the size-distribution functions of cloud and fog particles are single-peak asymmetrical curves similar to that shown in Fig. 5.1.

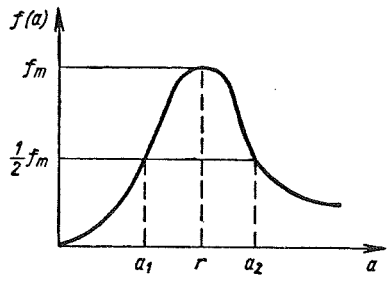

Figure 5.1. Typical Particle-Size Distribution Curve for Water Clouds and Fogs.

We present the most commonly encountered approximating expressions for the particle-size distribution functions of liquid-drop clouds and fogs.

In 1951, Best [363] used the following formula to reduce the experimental data of the foreign investigators Deem, Mazur, Frisch, and Hagemann [361]:

$$1-F=\exp\left[\left(\frac{d}{b}\right)^c\right], \qquad (5.1)$$

where F is the fraction of liquid water in the cloud per water droplet smaller than d in diameter and b and c are parameters.

It was found that the parameter c varies from 12 to 29 and b from 1.92 to 4.90. Investigating the size distribution of 300,000 droplets, Rittberger [362] found that the parameter b actually varies in a much broader range, from 0.4 to 12.5. We therefore concluded that the Best formula cannot be applied in cloud physics.

In 1952, A.Kh. Khrgian and I.P. Mazin [364] used the formula /211

$$f(a)=Aa^2e^{-ba} \qquad (5.2)$$

where A is a normalizing factor and b is a parameter, to reduce a

large amount of systematized data on cloud-drop sizes that had been collected by A.M. Borovikov [365].

In 1954, L.M. Levin [366] proposed the use of the logarithmically normal distribution that describes the size spectrum of grains of gold in placers in the case of multiple crushing [367] to describe the size distribution of cloud droplets:

$$f(a)=\frac{1}{\sqrt{\pi t}}\frac{1}{r}e^{-\frac{1}{4}-\frac{1}{t}(\ln\tau)^2}, \tag{5.3}$$

where $\tau = a/r$, r is the most probable radius, and t is a parameter.

In 1958, noting the complexity of the analytical expression for the logarithmically normal law and certain inconveniences encountered in its use in theoretical calculations, L.M. Levin [368] proposed a gamma distribution for description of the cloud-droplet spectrum; in our nomenclature, this distribution would be written

$$f(a)=\frac{1}{\Gamma(\mu+1)}\mu^{\mu+1}\frac{a^{\mu}}{r^{\mu+1}}e^{-\mu\frac{a}{r}}, \tag{5.4}$$

where $\Gamma(\mu + 1)$ is a gamma function, which equals $\mu!$ for integral μ, and r and μ are parameters.

We note that A.Kh. Khrgian and I.P. Mazin's formula is a particular case of the gamma distribution with $\mu = 2$. In turn, the gamma distribution is a particular case of the four-parameter distribution [369]: /212

$$f(a)=Aa^{\mu}e^{-\beta a^{\gamma}}. \tag{5.5}$$

These expressions for f(a) are those used most extensively; other formulas can be found in [358, 370, 371].

A.Kh. Khrgian and I.P. Mazin's formula was used by the authors to describe the drop sepctrum in reducing a large amount of statistical material (more than 660,000 droplets in stratiform clouds were measured). The important advantage of this formula over the others is its simplicity. A.Kh. Khrgian and I.P. Mazin show in [372] that in the case of stratus clouds that do not yield precipitation, their formula, Best's formula, and the expression for the logarithmically normal law approximate the experimental particle-spectrum curves with errors of the same order of magnitude.

Investigating the applicability of the various expressions for f(a) for approximation of experimental cloud and fog droplet-size data on the basis of a large amount of statistical material collected by the El'brus expedition, L.M. Levin showed in [358] that A.Kh. Khrgian and I.P. Mazin's formula gives a good result for the droplet-size range with radii a > 5 μ, while the logarithmically normal law and the gamma distribution describe the droplet-spectrum pattern satisfactorily for practically the entire range of dimensions investigated by the author in clouds and fogs. In a study of the microstructure of thick cumulus clouds, Huang Mei-Yuan [360] concluded that the gamma distribution is valid for the description of the particle-size spectra in these clouds as well.

2. **Quantitative data on microstructure parameters.** Methods of determining the microstructure parameters are considered in detail in the specialized monographs [359, 361, 370]. Depending on the investigator's objective, he may be interested in one or another combination of the following characteristics of the particle-size distribution curve [358, 361]:

1) the arithmetic mean radius a_1;
2) the root-mean-square radius a_2; /213
3) the root-mean-cube radius a_3;
4) the most probable or modal radius r;
5) the radius of the drops that make the largest contribution to the geometrical cross section, a_Q;
6) the radius of droplets making the largest contribution to the water content of the space, a_q;
7) the median radius a_{in};
8) the minimum and maximum radii r_{min} and r_{max};
9) the particle concentration N per cm^3.

The first seven characteristics have certain interrelationships for which analytical expressions have been derived for all of the distribution functions considered [358, 359, 364]. In order to use A.Kh. Khrgian and I.P. Mazin's formula, it is necessary to know only one of the characteristics. To use the gamma-distribution or the logarithmically normal law, it is necessary to know any two. Usually, the values of a_1 and r are determined in experiment.

The most important investigations of cloud microstructure, which were made for the most part by foreign authors prior to 1957, are summarized in B.J. Mason's monograph [361]. The results of Soviet and foreign research done up to 1960 are analyzed in the monograph by A.M. Borovikov et al. [359]. The analysis of data on the numerical values of the cloud and fog microstructure parameters that are cited in these monographs and in the monograph [358] and the papers [360, 371, 373-384] enable us to draw a number of definite conclusions as to the applicability of one or

another of the approximation formulas for description of the particle-size spectrum and the ranges of variation of the average values of specific parameters:

1. The simple and easy-to-handle single-parameter formula of A.Kh. Khrgian and I.P. Mazin is fully applicable to stratiform clouds. To determine the particle spectrum from this formula, it is sufficient to know only the arithmetic-mean radius of the cloud droplets. The experimental statistical material given in [359] serves as a basis for recommending $a_1 = 5$ μ for St, Sc, Ns, and Ac clouds. The results of other studies of these same cloud types gave average values of a_1 in the range from 5 to 10 μ. On the one hand, this disagreement may be explained by the failure of the early experiments to consider the capture coefficient for small droplets, which may shift a_1 by 1-2.5 μ [359], and, on the other, regional peculiarities may have asserted themselves with their characteristic values of a_1 and values of μ other than 2 [385]. /214

2. A.Kh. Khrgian and I.P. Mazin's formula is not suitable for approximation of narrow particle spectra. In this case, generally speaking, we may also make use of a single-parameter function, setting the parameter μ for the gamma distribution equal to the value most commonly encountered in such clouds. However, without fixing the value of the parameter μ, the gamma distribution can be used to describe with accuracy sufficient for practical purposes the spectra of the droplets in any clouds, at any stage in their development and in various parts of their volume. A larger value of μ will correspond to a narrower size spectrum. Thus, L.M. Levin [358] obtained values of μ ranging from 4 to 8 for high-mountain clouds and fogs, with $\mu = 8$ in more than 70% of cases. In a study of warm cumulus clouds. V.I. Kazas [378] found $\mu = 8$-10 in 72% of cases. Huang Mei-Yuan [360] obtained values of μ from 0.5 to 5.5 for thick cumulus clouds, depending on level above the cloud base. The investigations of G.T. Nikandrova [386] also indicate variation of the parameters μ and r of the gamma distribution as functions of height above the base of the cloud.

If, using the relation between the average a_1 and the most probable r particle radii, we determine the values of μ for the data given in [361] on the microstructures of various clouds, we find that it equals 2 for stratus, stratonimbus, and fair-weather cumulus clouds, 7 for stratocumulus clouds, 9 for altocumulus, and 0.33 for thick cumulus and cumulonimbus clouds. Thus, taking into account all of this information, we may conclude that the parameter μ varies in extremely broad limits from 0.33 to 10. To summarize all data on the most probable radius, its value varies from approximately 3 to 10 μ for all clouds. We note that we are speaking here of the variation of the average characteristics. For specific clouds and, in particular, for specific local regions and in various phases of the development of a given cloud, these variations are considerably broader owing to the inevitable /215

fluctuations of the microstructural characteristics of the clouds [358, 360].

3. As in the case of clouds, the overwhelming majority of results from study of fog microstructures indicate that their size spectra are approximated by the gamma distribution. The average most probable radius can vary in the approximate range from 2 to 10 μ. As concerns μ, there are not yet sufficient data for a confident estimate.

All of the information on cloud microstructure that we have considered is characterized by reference to single-peak distribution curves. We should note that double-peak distribution curves are sometimes observed (see, for example, [382, 387, 388]).

3. Water contents of clouds and fogs. To characterize fully the microstructure of a cloud or fog, it is necessary to know the particle concentration n per unit volume in addition to the size distribution function of the particles. This concentration can be determined from knowledge of the function f(a) and the water content q, meaning the amount of liquid water present in the droplets in a unit volume and usually expressed in grams per cubic meter. In view of the great importance of this characteristic and the relatively simple technique of determining it, it is measured in the USSR not only by individual researchers, but also by a network of aerological sounding stations. Methods of measuring water content are considered in detail in [359, 361, 370].

Table 5.1 presents a summary of data on the water contents of various clouds and fogs as obtained by various authors. It also lists average water-content characteristics for various clouds and fogs, which may differ substantially from the water-content values at different levels and at different stages in the development of a given cloud. The average water contents of clouds also depend on temperature. It is precisely this dependence that causes the scatter of the average water-content values given in Table 5.1 from data of [359]. On the other hand, the water contents of clouds of a given type may differ substantially at a given temperature when the clouds have formed and developed under different conditions [376].

As we see from Table 5.1, the average water-content values for clouds of the various forms, except for thick cumulus clouds, fluctuate in not too broad a range: 0.1-0.3 g/m^3. The maximum contents may reach 3-4 g/m^3 and even 43 g/m^3. However, such contents are extremely seldom encountered in St, Sc, Ac, Ns, and As clouds. We shall therefore consider the reproducibility of the water contents of various cloud forms at various temperatures, which is of great practical importance. /216

After processing about 5000 aircraft measurements, V.Ye. Minervin [391] plotted reproducibility curves for the average

TABLE 5.1. WATER CONTENTS OF VARIOUS CLOUDS AND FOGS ACCORDING TO VARIOUS INVESTIGATORS

Cloud	No. of measurements	Water content, g/m^3			Author	Area of measurements
		Minimum	Average	Maximum		
Sc, St, Ac	752	—	0,17 * (0,08—0,23)	1,15	A. M. Borovikov [359]	Riga
Sc, St, Ac	571	—	0,27 * (0,08—0,38)	1,79	Same	Minsk
Sc, St, Ac	493	—	0,23 * (0,11—0,28)	1,89	» »	Vnukovo
St, Sc, Ac	4897		0,21 * (0,09—0,33)	3,14	» »	All CAO stations
Ns, As	184		0,22 * (0,07—0,23)	1,56	» »	Riga
Ns, As	123		0,31 * (0,14—0,35)	1,11	» »	Minsk
Ns, As	156		0,23 * (0,09—0,28)	0,87	» »	Vnukovo
Ns As	1654		0,22 * (0,145—0,356)	1,56	» »	All CAO stations
Various forms	493		0,11 * (0,005—0,161)		L. T. Matveyev and V. S. Kozharin [359	Leningrad
Cu, Cb, Ac	} 2157			1,5	Pettit [359]	Canada
Sc, St, Ac				1,4	Same	»
Ac—As						
St, Sc	327 **			0,9	Lewis [359]	USA
Ac, Ac—As	246 **			0,5	Same	»
Cu, Cb	324 **			1,8	» »	»
Cu cong	102		1,7 ***	4,1 ***	V. A. Zaytsev [359]	USSR
Sc	74 flights	0,06	0,30	1,30	Klein Walker [361]	USA
Cu	> 1000		1,2 (0,47—1,91)		Huang Mei-Yuan [360]	USSR
Sc	Network data	0,08	0,17—0,32	0,6	V. Ye. Minervin [389]	»
Ns	Network data	0,03	0,18—0,35	0,6	V. Ye. Minervin [389]	USSR
As—Ns	} 2137		0,154	0,77	A. I. Voskresenskiy [376]	Arctic
St			0,10	0,58		»
Sc			0,12	0,67	I. M. Dolgin [375]	»
Cu	21	0,05	0,14	0,20	V. I. Kazas [378]	USSR
	22 flights		7—12	43	Schumacher [390]	Western Europe
Fog	21 flights	0,1		0,22	Radford [361]	
Fog				0,4	Kuroiwa and Kinoshita [361]	Japan
Winter fog		10^{-4}		10^{-2}	Okita [383]	»
Ocean fog			$4{,}2 \cdot 10^{-3}$		Wiener et al. [380]	
Fog			0,10—0,30	0,60	A. L. Dergach [313]	Arctic

*Data computed on the basis of the measured results given in [359] for the average water contents of clouds at various temperatures. Limits of variation of the averages are indicated in parentheses.

**Results of measurements in supercooled clouds.

***Data pertaining to densest zones of thick cumulus clouds.

Note: Commas represent decimal points.

water contents of air-mass and frontal clouds at various temperatures. Analysis of the curves indicates that the reproducibility maxima of the average water contents of these clouds range from 0.1 to 0.3 g/m^3 at temperatures from -25 to +15°C. Clouds with

average water contents of 1.0 g/m^3 have practically zero reproducibility. Analogous data were obtained by Pettit in Canada and Lewis in the USA [359].

Most papers reporting on the particle-size spectra of clouds and fogs give little attention to acquisition of data on the concentrations of large particles, despite the fact that they may make a very large contribution to cloud water content.

Some data on the concentrations of large particles in clouds were obtained in the work of A.M. Borovikov, I.P. Mazin, A.N. Nevzorov [392, 393], and Okita [394]. It was found that the concentration of large particles (particles with radii larger than 75, 85, 130, 200, 300, 400, 500, 650, and 800 μ were registered in the measurements) depends strongly on the form of the cloud and varies widely within a given cloud. The size distribution of the large particles is described in some cases by an exponential law and in others by a reciprocal power law. Often, not a single large particle is encountered over many kilometers.

4. Average values of microstructure parameters and water content of clouds and fogs. As we have noted, the average size spectra of the various cloud forms and those of fogs are approximated satisfactorily by a gamma distribution with the parameter μ between 1 and 10 and the parameters r between 3 and 10 μ. The values of the water content q vary approximately from 10^{-2} to 43 g/m^3. Naturally, these ranges of variation of the parameters μ, r, and q must be covered in calculating attenuation coefficients for real clouds and fogs of various forms and in various stages of development. In practical use of the data from such a calculation, however, it is very important to know the average or most probable /219 values of these parameters (Table 5.2).

TABLE 5.2. MOST PROBABLE VALUES OF THE GAMMA-DISTRIBUTION PARAMETERS r AND μ AND THE WATER CONTENTS OF VARIOUS LIQUID-DROP CLOUDS AND FOGS

Type of cloud	r, μ	μ	q, g/m^3
Thick cumulus Cu cong	6	3	1.2
Cumulus Cu	6	3	0.2
Cumulonimbus Cb	6	1	
Stratocumulus Sc	5	2	0.1
Stratus St	5	2	0.1
Stratonimbus Ns	5	2	0.2
Altostratus As	5	2	0.2
Altocumulus Ac	5	2	0.1
Fogs, radiative	5	6	0.1
Fogs, advective	5	3	0.1

5. Chemical composition of cloud and fog particles. It is usually assumed in calculations of the aerosol-attenuation coefficients of clouds and fogs that the particles consist solely of pure water. In the overwhelming majority of cases, this approximation may be regarded as quite sound, since the concentration of the impurities in cloud and fog droplets is very low. The work of O.P. Petrenchuk and V.M. Drozdova [395], which presents results of measurements of impurity concentrations in cloud droplets and precipitation in certain regions of the European USSR may be cited as a quantitative illustration. It was found that the total contents of the ions $SO_4^{\cdot\cdot}$, $Cl^{\cdot}$, $HCO_3^{\cdot}$, $NO_3^{\cdot}$, $NH_4^{\cdot}$, $Na^{\cdot}$, $K^{\cdot}$, $Mg^{\cdot\cdot}$, and $Ca^{\cdot\cdot}$ in cloud water taken in the Leningrad region and in the northern and southwestern (vicinity of Kiev) European USSR average 11.0, 13.0, and 15.1 mg/liter, respectively. In precipitations, these contents were 13.7, 14.6, and 37.1 mg/liter in the same regions. The authors of [395] found that cities have a strong influence on the impurity contents of cloud water and precipitation. Thus, the total impurity content in the cloud water was found to be 300 mg/liter in one of the flights over Dnepropetrovsk, about 120 mg/liter over Odessa, and approximately 10 mg/liter between these cities. Copper, iron, beryllium, vanadium, cobalt, chromium, molybdenum, manganese, aluminum, zinc, nickel, and silicon were found in concentrations above $2 \cdot 10^{-3}$ mg/liter in the polluted precipitation. /220

However, the impurity concentration does not exceed 1% even in the most heavily polluted clouds and precipitation. Recognizing that the complex refractive indices of aqueous solutions of the impurities detected are practically no different at these concentrations from the complex refractive index of pure water, we may assume that the impurities present in the cloud water and precipitation have no substantial influence on their attenuation coefficients.

2. HAZES

The term "haze" is usually understood as connoting the most frequently encountered state of turbidization of the atmosphere by particles of relatively small size, with $S_m > 1$ or 2 km. The particles may be solid or liquid, wettable or nonwettable. The solid particles may have various shapes, while the liquid particles are spherical. Particles with a solid nucleus and a water envelope are usually to be expected. The shapes of such two-layered particles depend on the size relation between the nuclei and the envelopes.

Existing methods of experimental investigation cannot yet give us a precise answer to the question as to the shape of these particles. Nor can the available data on the particle sizes pretend to high accuracy. The dimensions of aerosol particles depend strongly on processes of condensation, sublimation, and vaporization of moisture in the atmosphere. We shall present the

available experimental data on the microstructural characteristics of hazes, which must be applied with the reservations stated above.

1. Size spectra of haze particles. C. Junge [396, 894] classifies aerosol particles into three size groups: 1) "Aitken nuclei" (particle radii r = 10^{-7} to 10^{-5} cm); 2) large particles (r = 10^{-5}-10^{-4} cm); 3) giant particles (r > 10^{-4} cm). From the standpoint of attenuation of visible and infrared waves in the atmosphere, atmospheric aerosol particles can be classified as optically active and inactive. The former include particles with marked influence on attenuation. We shall call particles optically inactive if their attenuation of radiation can be disregarded. The largest particle size that can be regarded as optically inactive depends on the wavelength λ of the radiation. The larger the λ, the larger the corresponding critical particle size. Analysis of the attenuation coefficients indicates that particles with linear dimensions smaller than 0.1 μ may be considered optically inactive for any wavelength in the visible or infrared. /221

Two characteristic cases can be discerned on the basis of most of the available data regarding the nature of the haze-particle size spectrum: 1) a multipeak distribution for the dimensions of particles smaller than about 0.1 μ, observed in [397 and 398]; 2) a single-peak distribution that has been obtained by many authors for particle sizes a > 10^{-2} μ. As in the case of clouds, different authors proposed different analytical expressions for the particle-size distribution function. Thus, the experimental results from measurements of urban aerosols made by M.M. Fedorov [399], K.P. Makhon'ko [400], and Spurny and Pich [401] are approximated satisfactorily by a logarithmically normal distribution [see (5.3)]. As was noted in [400], this distribution law was detected experimentally for rock [402] and uranium [403] ore dust. The distributions of the giant chloride and sulfate condensation nuclei measured by Padzimek [404, 405] are described satisfactorily by A.Kh. Khrgian and I.P. Mazin's formula [see (5.2)].

Junge [406] showed that the part of the distribution curve characterizing large particles is satisfactorily approximated by an expression that has come to be known in the literature as the Junge distribution:

$$N = Ca^{-\beta}. \qquad (5.6)$$

Here a is the particle radius, C is a constant that depends on particle concentration and is determined experimentally, and β is a constant that assumes a value of 3 for continental aerosols at the ground surface.

The Junge formula has come into rather widespread use. The value of the exponent β characterizes the slope of the large-droplet branch of the distribution curve. Different investigators have obtained different values for β. Thus, in measurements above /222
various regions of the USSR, A.G. Laktionov [407, 408] obtained values of β equal to 3, 4, and 5, respectively, at heights of 100 m, 1 km, and 2-3 km for large particles (a > 4 μ). Okita [410] obtained values of β ranging from 1.7 to 3.2 for nonhygroscopic giant nuclei.

Junge [411, 412] obtained β = 2 in measurements at heights from 12 to 21 km in the stratosphere at various latitudes (40° S to 70° N) for particles ranging in size from 0.1 to 2 μ.

TABLE 5.3. AEROSOL PARTICLE DISTRIBUTION FUNCTIONS ACCORDING TO [413]

Particle diameter, μ	Tropospheric aerosols	Stratospheric aerosols
0.5-0.1	$n \approx a^{-5/2}$	$n \approx a^{-2}$
Above 0.5	$n \approx a^{-19/4}$	$n \approx a^{-4}$

Assuming dynamic equilibrium between the processes of formation, coagulation, and precipitation of aerosols, Friedlander [413] introduced certain reasonable assumptions to obtain the theoretical expressions given in Table 5.3 for the distribution functions.

Thus, the theoretical values of β obtained by Friedlander for the troposphere and stratosphere lie in the range from 2 to 4.75. G.M. Idlis [414] obtained a formula similar to (5.6) with β = 4 for the distribution function of cosmic-dust particles.

As a result of measurements made in the ground layer of the atmosphere during the summer of 1967 in the region of Ryl'sk (Kursk region), L.S. Ivlev [810] detected the existence of two basic types of particle-size distribution. Among the 100 particle-size distribution spectra processed in the range from 0.1 to 5 μ, approximately every third case presents a Junge-type distribution with the exponent β = 4 (first distribution type). In the second type, the counted concentration has a minimum in the range of particle sizes from 0.25 to 0.6 μ and a small maximum for particles with dimensions from 2 to 3 μ.

Fenn [811] detected deviations from the Junge particle-size /223
distribution. He found a maximum in the particle-size distribution around 0.4 μ and another at larger sizes, as well as minima in the 0.2-0.25-μ and 0.4-0.5-μ regions.

The results of sky-brightness observations made by Bullrich's group [812] indicate that the size spectrum of particles larger than 1 μ is subject to a Junge distribution with the parameter β = 4 and an upper limit a_2 = 10 μ.

Summarizing, we may apparently conclude that, according to the results of most investigators, the optically active part of the atmospheric-aerosol size-distribution curve can be approximated roughly by formula (5.6), in which β may vary from 2 to 5. It must, however, be stressed that specific realizations of the particle-size spectrum may differ substantially from the smoothed distribution (5.6), which, as is correctly noted by G.V. Rozenberg [895], reflects the properties of the real distributions only in their most general features. The real distributions are often curves with one or more maxima [811, 812, 896].

There are as yet very few data on the variations of the distribution maximum.

In measurements on urban dust, K.P. Makhon'ko [400] found that the dimensions of the most numerous particles vary from 0.06 to 0.34 μ. In an investigation of various aerosols over the USA, Goetz, Priening, and Kallai [415] found no particles smaller than 0.1 μ, although the spectrometer that they used was capable of measuring particles down to 0.08 μ. The most probable particle size varied from 0.2 to 0.5 μ in [415]. Junge [411] found 0.03 μ for this dimension. On the basis of these data, and bearing in mind what was said above concerning the role of small particles in attenuation, we may propose a value of 0.1 μ as the smallest particle size in the corresponding calculations using (5.6).

We note in conclusion that the Junge formula is only an approximating expression that describes more or less correctly the real distributions of the largest haze particles. It does not cover all possible concrete distributions. However, the available experimental data are still inadequate as a basis for the corresponding statistical analysis and establishment of the frequency with which a given particle-size distribution is encountered. /224

2. **Particle concentration.** Depending on the distribution function used, we are interested either in the total particle concentration including the fine-droplet fraction or in the particle concentration in a given size range. In either case, it is necessary to know how the quantity in question varies as a function of place, time, and height. It is well known that these variations are enormous: in the atmospheres above large industrial cities, the aerosol concentration ranges into the tens of thousands of particles per cm^3 and beyond, while the cleanest air samples taken in rural localities may contain tens of particles per cm^3, and in some cases fewer than 10 [416].

Studying the altitude distribution of particle concentration in the atmosphere, A.Kh. Khrgian [416] showed theoretically that the law of concentration decrease should be exponential. A similar result was obtained by A.G. Laktionov [417]. I.I. Gayvoronskiy [418] confirmed this experimentally for condensation nuclei up to a height of 4 km. Generalizing data from various investigators, Penndorf [419] concluded

an exponential decrease of the concentration of particles with sizes of 0.06-1 μ up to a height of 5 km. A theoretical and experimental justification of the exponential decrease of condensation - nucleus concentration in the size range from 10^{-2} to 1 μ up to a height of 4-6 km

$$N(z) = N(0)\,e^{-z/n} \qquad (5.7)$$

is given in the papers of Ye.S. Selezneva [420, 421, 900]. In (5.7), N(z) and N(0) are the concentrations at heights z and 0 and h is an empirical constant that differs for different stations. The numerical values obtained for N(0) and h in investigations of condensation nuclei above various regions of the USSR are also given in the papers by A.L. Dergach [422] and A.I. Voskresenskiy [376].

A detailed investigation of atmospheric-aerosol particle concentration was made by Junge et al. for heights from 6 to 27 km [411, 412, 423-426]. These studies have considerable merit in that particles of different sizes (0.01-0.1 μ, 0.1-1.0 μ and up) were investigated separately. The basic results of these studies /225 reduce to the following. The concentration of condensation nuclei is practically independent of height in the upper troposphere, while it decreases sharply with height in the lower troposphere and in the stratosphere. An aerosol layer with maximum concentration at heights from 15 to 23 km was detected for particles with sizes in the 0.8-1-μ range. It was found that the particle concentration in this layer varies through a factor no larger than 3 with time. Measurements made at various latitudes led the authors to conclude that this layer is of planetary nature. As in the case of the condensation nuclei a weak variation of large-particle concentration with altitude is observed in the upper layers of the troposphere; at heights of 10-15 and 23-27 km, on the other hand, the concentration rises and falls sharply.

Very few giant particles (a > 1 μ) are found in the stratosphere. This is consistent with the research data of Durbin [427-429], who reported that these particles make a substantial contribution to the concentration only near the earth's surface. Their concentration diminishes very rapidly with height. The largest measured value at a height of 0.8 km was 2.5 cm^{-3}. Values of 4000, 2800, and 1000 m^{-3} were obtained for the concentration of particles larger than 3 μ at heights of 13-16, 20, and 17-29 km, respectively, in [430].

Extensive data on the concentration of particles with dimensions r > 4 μ at heights from 0.1 to 3.0 km over various regions of the USSR were obtained in A.G. Laktionov's study [431]. It was found that the concentrations of these particles depend strongly on the underlying surface. Thus, at a height of 0.2 km

above various seas (Aral, Okhotsk, Barents), the particle concentrations were approximately the same at 1.5-5 particles per liter. At the same height above coastal land regions, the particle concentration varied strongly, taking values of 1.5 liter^{-1} above tundra, 30 liter^{-1} above wooded steppes, and 65 liter^{-1} above sandy areas. A sharp decrease in particle concentration is observed during the spring in steppe regions. Thus, the winter concentration of particles with $r > 4$ μ was 3 liter^{-1} at a height of 0.1 km, while the summer value was 60 liter^{-1}.

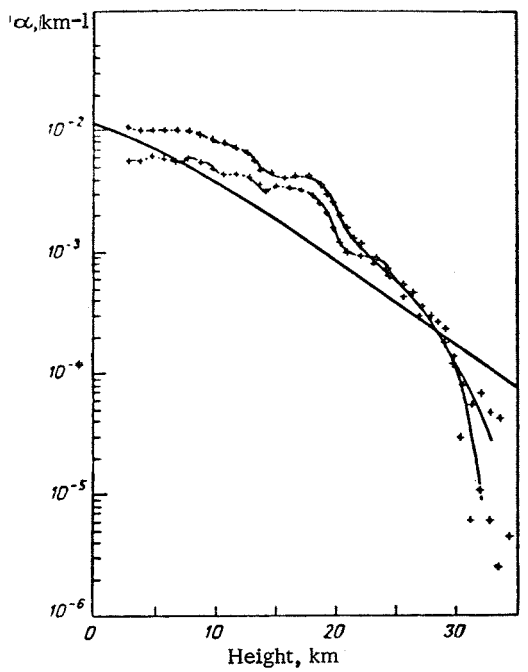

Figure 5.2. Examples of Vertical Aerosol-Attenuation Coefficient Profiles with Indistinct Structure Obtained by Elterman [444] on April 9, 1964 and December 10, 1964; The Solid Curve is the Height Curve of the Rayleigh-Scattering Coefficient.

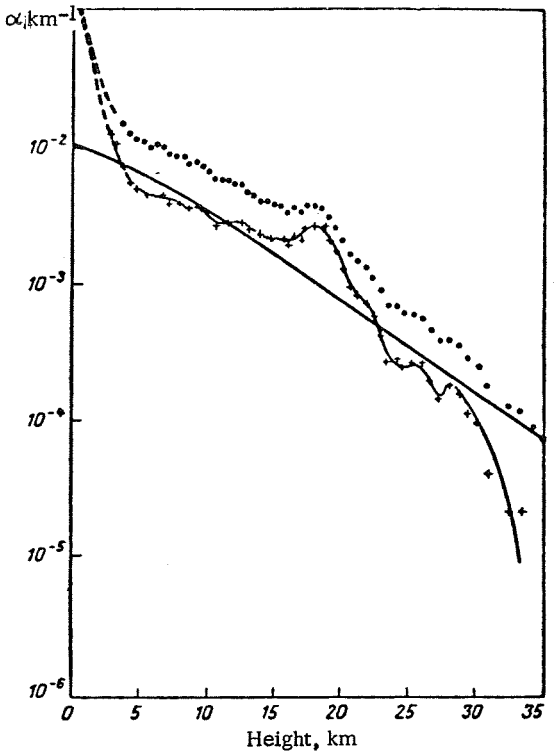

Figure 5.3. Example of Vertical Aerosol-Attenuation Coefficient Profile with Moderately Distinct Structure Obtained by Elterman [444] on May 8, 1964 (Curve drawn through crosses); The Solid Curve is the Altitude Curve of the Rayleigh-Scattering Coefficient and the Dots Characterize Attenuation-Coefficient Values.

No direct measurements of aerosol-particle concentration have as yet been made at heights above 30 km, although the presence of aerosols has been detected up to and above a height of 100 km from analysis of /226
the results of optical searchlight-probing experiments [432] and in rocket launchings. Thus, Rossler and Vassy [433] found that

aerosol scattering is stronger than Rayleigh scattering at heights up to 50 km. A maximum of the aerosol layer occurs at a height of 25 km, and a minimum at the tropopause level. A.Ye. Mikirov [434] obtained atta on the aerosol component of attenuation at heights from 48 to 102 km. The aerosol attenuation was above-Rayleigh at all heights, and another aerosol layer was detected at heights of 80 km and higher. It was shown in the investigations of G.P. Gushchin [435] and Yu.I. Rabinovich [436] that the aerosol attenuation of visible light in the layer of atmosphere above 6 km is 20-30% of the attenuation in the underlying layer. These results suggest the presence of substantial aerosol-particle concentrations in the upper layers of the atmosphere. At the same time, a value of about $2 \cdot 10^{-4}$ was obtained for the optical thickness of the atmosphere above 25 km in the study of Newkirk and Eddy [446], indicating negligible importance of aerosol attenuation at great heights. /227

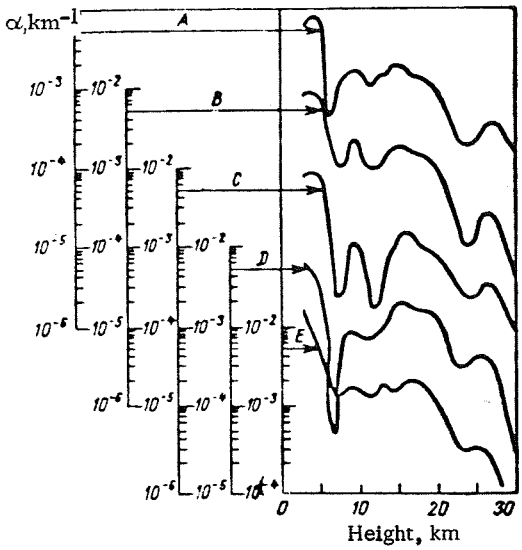

Figure 5.4. Examples of Vertical Aerosol Attenuation Coefficient Profiles with Strongly Pronounced Structure Obtained by Elterman [444] from 20 Hours 8 Minutes on April 12, 1964 to 2 Hours 19 Minutes on April 13, 1964.

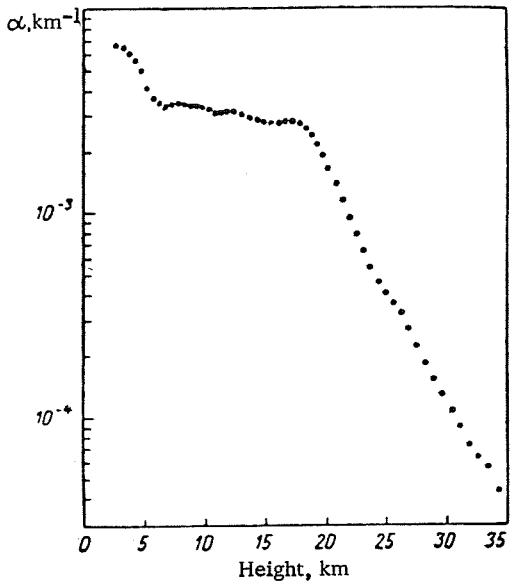

Figure 5.5. Average Vertical Profile of Aerosol Attenuation Coefficient Obtained by Elterman [444] by Averaging 105 Individual Profiles.

In recent years, substantial data on the altitude variation of atmospheric-aerosol particle concentration on cloudless days has been obtained by probing the atmosphere with searchlight and laser beams [437-444]. The most complete data were obtained by Elterman [441-444]. The atmosphere was sounded in the region of New Mexico up to heights /228

of 70 km throughout the year from December 1963 to December 1964 with a distance of 30.2 km between the source and the receiver. The measurements were made on a wavelength of 0.55 μ. Aerosols were found to be present at all heights. However, the aerosol density was very low above 35 km. Reference [444] presents 105 vertical aerosol attenuation coefficient profiles. All of the profiles were classified into three types: 1) with indistinct structure (Fig. 5.2); 2) with moderately distinct structure (Fig. 5.3); 3) with strongly pronounced structure (Fig. 5.4). Figure 5.5 presents the vertical aerosol attenuation coefficient profile obtained by averaging the 105 individual profiles.

Analysis of the individual aerosol attenuation coefficient profiles indicates the presence of aerosol layers with by no means /229
constant stratification. The aerosol layer discovered by Junge at heights from 15 to 23 km is not clearly in evidence in all soundings. In many cases, the aerosol attenuation coefficient varies little with height in the layer from approximately 5 to 18 km. This fact was also reflected in the trend of the averaged profile.

Comparison of the average values of the aerosol attenuation coefficient with the values of the molecular scattering coefficient produces the following picture. At heights from 0 to approximately 10 km and above 25 km, the molecular scattering coefficient is larger than the aerosol attenuation coefficient. The widest differences between these coefficients occur at heights in the approximate range 18 to 22 km and at 35 km. In the former case, the aerosol attenuation coefficient is approximately 2-2.5 times the molecular scattering coefficient, but this relation is reversed in the latter case.

In recent years, K.Ya. Kondrat'yev's group has conducted a /230
broad program of experimental research in atmospheric optics, using various types of equipment lifted on balloons to heights of 25-30 km. One of the basic parts of this program was devoted to study of the optical properties of the aerosols and their stratification. Measurements indicated the presence of aerosol layers at various heights. The vertical particle-concentration profile varies in a broad range (Fig. 5.6). Both the heights of the aerosol layers and the absolute concentrations of the particles at various heights were subject to variations [344, 445, 813].

The material examined above indicates a wide diversity of the data on the vertical atmospheric-aerosol concentration profiles. Despite the fact that considerable data have by now been obtained on the particle concentrations at various heights and in various geographic regions, this information is still not sufficient for solution of the question as to the average statistical particle-concentration profiles. However, many practical problems require knowledge of certain average values of this quantity to characterize aerosol models of the atmosphere.

Approximating Junge's experimental data on the concentration of particles with sizes from 0.08 to 1.0 μ at various heights, we have constructed the following aerosol model of the atmosphere [1]:

$$
\begin{aligned}
&N(z) = N(0)\,e^{-bz}, \quad z \leqslant 5 \text{ km},\\
&N(z) = 0.03, \quad 5 \text{ km} \leqslant z \leqslant 15 \text{ km},\\
&N(z) = 0.03\,e^{0.06z}, \quad 15 \text{ km} \leqslant z \leqslant 20 \text{ km},\\
&N(z) = 0.1\,e^{-0.09z}, \quad z \geqslant 20 \text{ km},
\end{aligned}
\qquad (5.8)
$$

where N(z) and N(0) are the particle concentrations at heights z and 0.

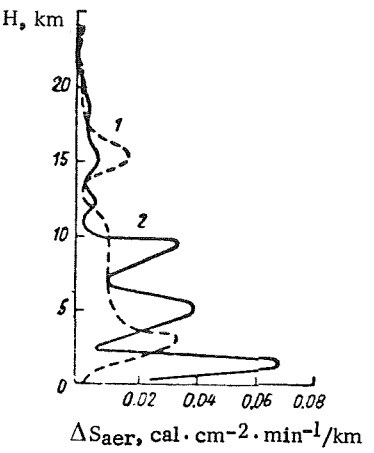

/231

Figure 5.6. Vertical Profile of Aerosol Attenuation of Direct Solar Radiation According to K.Ya. Kondrat'yev et al. [445]: 1) autumn; 2) summer.

Elterman [447, 448] generalized the available data on aerosol attenuation coefficients to construct an aerosol model of the atmosphere.

In this model, the particle size distribution function does not vary with height, and the particle concentration at the surface of the ground was assumed equal to 200 cm^{-3} at a meteorological visibility S_m = 25 km. Values of the concentration at other heights are given in Table 5.4.

Figure 5.7 shows the vertical profile of aerosol-particle concentration as constructed from the data of Table 5.3. We note that the Elterman model does not take account of the possible variations of the parameters of the particle-size distribution function. As is seen from the material considered above, these variations may be quite wide. Hence it follows that particle concentration can vary over a rather broad range even at a given meteorological visibility. /232

We note in conclusion that the atmospheric models considered here are highly approximate statistical-average pictures of the aerosol stratification in the real atmosphere. More or less substantial deviations of the real aerosol particle concentration profiles from those assumed in the models may be observed in any given concrete case.

Apart from the variations of the size and concentration spectra of the atmospheric aerosol, great importance attaches to the chemical composition of the particles, which determines the components of their complex refractive index. A change in these components may have a substantial influence on the corresponding optical

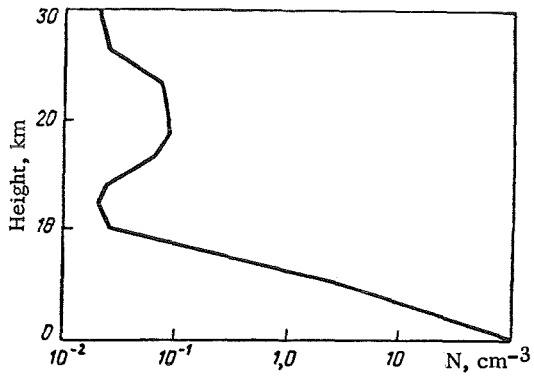

Figure 5.7. Vertical Profile of Aerosol-Particle Concentration in the Atmosphere as Assumed in the Elterman Model [447].

properties of the aerosol (scattering coefficients, scattering indicatrices, etc.). We should expect differences in these characteristics not only for oceanic and continental aerosols, but also for different genetic types of both. /233

There have been, conservatively, several tens of reports published recently on the particles of continental and oceanic aerosols (for example, [814-819]). Nevertheless, the data obtained are quite inadequate for any more or less definite conclusions as to the chemical composition of either oceanic or continental aerosol particles. It is usually assumed in calculations of the atmospheric-aerosol scattering coefficients that the particles consist of water. In this case, the refractive index is taken at 1.33. The calculations have been made for transparent particles in a number of cases, for which the refractive index assumes various discrete values from 1.2 to 1.5 [820].

TABLE 5.4. AEROSOL-PARTICLE CONCENTRATIONS AT VARIOUS HEIGHTS IN THE ELTERMAN MODEL

Height, km	0	1	2	3	4	5	6	7
concentration, cm^{-3}	200	87	38	16	7,2	3,1	1,1	0,4
Height, km	8	9	10	11	12	13	14	15
concentration, cm^{-3}	0,14	0,05	0,026	0,023	0,021	0,023	0,025	0,041
Height, km	16	17	18	19	20	21	22	23
concentration, cm^{-3}	0,067	0,073	0,080	0,090	0,086	0,082	0,080	0,076
Height, km	24	25	26	27	28	29	30	31—50
concentration, cm^{-3}	0,052	0,036	0,025	0,024	0,022	0,020	0,019	0

Note: Commas represent decimal points.

Future atmospheric-aerosol models will undoubtedly have to recognize the size, concentration, and chemical-composition ranges of the particles, as well as the variations of these characteristics under real conditions.

3. PRECIPITATION

All forms of precipitation are characterized by the presence of large particles, for which the values of the parameter $\rho = 2\pi a/\lambda$ (λ is the wavelength and a is the particle radius) are such that the attenuation coefficient may be assumed proportional to particle cross-sectional area (see Chapters 6 and 7). To find the aerosol attenuation coefficients in precipitation, therefore, it is more important to know their intensity or water content than their microstructural parameters. The latter have been studied more or less thoroughly for rain.

Studies of the microstructure of rainfalls [449-453] indicate that with rare exceptions, the size distributions of the droplets are characterized by single-peak, asymmetrical curves, as in the case of clouds and fogs.

TABLE 5.5. MAXIMUM AND MINIMUM VALUES OF THE CHARACTERISTICS OF RAINS [451-453]

Amount of rain	I, mm/h	ω, g/m^3	n, m^{-3}	a_{max}, mm	a_{max} [sic], mm	α, km^{-1}
Minimum	0,3	0,02	80	0,7	0,025	0,10
Maximum	57	1,98	19 750	3,2	0,3	3,34

The microstructure parameters vary with the rate of rainfall and the distance from the cloud shedding the rain. Kelkar [449] showed that with increasing distance downward from the base of the cloud, the relative number of small droplets increases steadily as a result of their evaporation as they fall. Mason and Andrews [450] observed substantial variations of the microstructure parameters for different types of rains. Ye.A. Polyakova [451-453] obtained the most complete set of rain-microstructure data (Table 5.5). /234

The data of Table 5.4 characterize the scatter of the microstructure parameters of the most frequently encountered rains. We note that in very rare cases, intensities I and water contents ω much larger than those indicated in Table 5.4 may be observed in rain. Thus, the record rainfall rate registered in the USSR, 3.74 mm/min (224 mm/hour) occurred at Sochi in 1913; in 1911, a heavy rainfall at Panama yielded 12.6 mm/min, which corresponded

to a water content of 38 g/m^3, and rates up to 21.5 mm/min (1290 mm/hour) have been recorded in the Hawaiian Islands [416].

The size-distribution function of raindrops was approximated in [451] by a gamma distribution with the parameter $\mu = 2$. Marshall and Palmer [454] used the same distribution with $\mu = 0$. L. M. Levin [368] considers μ to be variable between 0 and 2.

I.L. Zel'manovich [455] studied the microstructure of falling snow. Particle sizes were identified with the radii of the spots left on filter paper after the snowdrops had thawed. Using the formula $dn/dr = Ar^2e^{-\beta r}$ for the particle size distribution function, where r is the particle radius, the author of [455] found values of the parameters A and β on the basis of experimental data obtained on the attenuation coefficient and the number of snowflakes. The single-peak distribution curves constructed using the values obtained for A and β were found to agree well with the experimental data.

Chapter 6 /235

SINGLE-PARTICLE SCATTERING OF VISIBLE AND INFRARED WAVES

1. THE POLARIZED-LIGHT REPRESENTATION

Let us consider a plane monochromatic wave whose electric-field strength $\vec{E}$ has the complex form

$$\vec{E} = \vec{E}_0 e^{-i\omega t + i\vec{k}\vec{r}}. \tag{6.1}$$

Here ω is the frequency of the field, the direction of $\vec{k}$ coincides with the direction of wave propagation, $k = m_a\omega/c$, m_a is the refractive index of the medium, c is the velocity of light, and $\vec{E}_0$ is a constant vector perpendicular to $\vec{k}$. The magnetic-field strength $\vec{H}$ is related to $\vec{E}$ in the usual manner:

$$\vec{H} = m_a [\vec{n}, \vec{E}], \tag{6.2}$$

where $\vec{n} = \vec{k}/k$.

The electromagnetic-field energy flux calculated per unit area is determined by the Umov-Poynting vector:

$$\vec{P} = \frac{c}{4\pi} [\mathrm{Re}\,\vec{E}, \mathrm{Re}\,\vec{H}]. \tag{6.3}$$

Since radiation receivers respond to the energy characteristics of the fields, the time-averaged components of (6.3) are the quantities measured in optics. Time averaging results from the fact that the time required for experimental analysis of the field properties is much longer than the period of the light wave's oscillations.

Let us now consider the complete set of measurable quantities. The first is the total intensity of the wave, defined as the time-averaged value of P. Then it is also possible to measure the time-averaged intensity of the oscillations along a given straight line. These oscillations can be separated by placing a suitably oriented analyzer on the path of the wave. These characteristics constitute the entirety of the experimentally determinable information on a light beam. This information can be described /236

quantitatively as follows. It is necessary to substitute (6.1) and (6.2) into (6.3) and recognize that all terms in the multipliers $\exp(\pm i2\omega t)$ vanish on time averaging. Then we have for the total intensity I

$$I = \frac{c}{8\pi} m_a (\vec{E}_0, \vec{E}_0^*). \tag{6.4}$$

We now introduce a certain Cartesian coordinate system x, y, z, with respect to which the wave in question propagates in the negative direction of the third axis. Then the vector $\vec{E}_0$ lies in the plane formed by the unit vectors on the first two axes. The direction of the straight line along which the intensity of the vibrations must be measured can be assigned as an angle η with respect to the first axis. If $I(\eta)$ is the intensity of the corresponding vibrations, it is easy to obtain from (6.4)

$$I(\eta) = \frac{c}{16\pi} m_a (S_1 + S_2 \cos 2\eta + S_3 \sin 2\eta). \tag{6.5}$$

If a supplementary device that introduces a constant phase difference δ into mutually perpendicular components of the field (for example, a quarter-wave plate) is placed in the path of the light beam, we have

$$I(\eta) = \frac{c}{16\pi} m_a [S_1 + S_2 \cos 2\eta + (S_3 \cos\delta - S_4 \sin\delta) \sin\eta]. \tag{6.6}$$

In (6.5) and (6.6), S_j is the Stokes parameter, which is defined as follows:

$$\begin{aligned} S_1 &= E_{01}E_{01}^* + E_{02}^*E_{02}, \\ S_2 &= E_{02}E_{02}^* - E_{01}E_{01}^*, \\ S_3 &= E_{02}E_{01}^* + E_{02}^*E_{01}, \\ S_4 &= i(E_{02}E_{01}^* - E_{02}^*E_{01}). \end{aligned} \tag{6.7}$$

Here E_{0j} are the first and second components of the vector $\vec{E}_0$.

Comparing (6.4) and (6.7), we can write a formula for the total intensity: /237

$$I = \frac{c}{8\pi} m_a S_1. \tag{6.8}$$

It is easily shown that S_1 and S_4 are invariant under rotations about the third axis and that S_2 and S_3 are transformed in

accordance with the representation

$$S_2' = S_2 \cos 2\psi + S_3 \sin 2\psi, \quad S_3' = -S_2 \sin 2\psi + S_3 \cos 2\psi,$$

where S_2' and S_3' are the values of the Stokes parameters in the system rotated about the third axis with respect to the original system through an angle ψ.

It can be shown further that the end of the vector $\vec{E}$ of the wave (6.1) describes a certain ellipse. A wave of this type is therefore said to be elliptically polarized. The polarization ellipse can be described by the angle ϕ between the semimajor axis of the ellipse, the first unit vector of the selected coordinate system, and the ellipticity β, defined by $\tan \beta = a_2/a_1$, where a_1 and a_2 are the semiminor and semimajor axes of the ellipse, respectively, and β is positive in the case of right-hand rotation (about $\vec{k}_0$) and negative in the opposite case. The following relationships result from certain calculations:

$$\begin{aligned} S_2 &= S_1 \cos 2\beta \cos 2\varphi, \\ S_3 &= S_1 \cos 2\beta \sin 2\varphi, \\ S_4 &= S_1 \sin 2\beta. \end{aligned} \tag{6.9}$$

Formulas (6.6), (6.8), and (6.9) can be used to calculate the characteristics of the polarization ellipse from the results of the corresponding measurements.

2. SCATTERING BY A PLANE MONOCHROMATIC WAVE

Let us now identify the field considered in §1 with a wave incident upon a certain object. Let us place the coordinate origin at the center of the object and its first axis in coincidence with the semimajor axis of the wave's polarization ellipse. We shall denote the unit vectors of this system by $\vec{I}_1$, $\vec{I}_2$, and $\vec{I}_3$.

The material of the object in question has a complex refractive index $m_b \neq m_a$ and, consequently, presents a certain optical inhomogeneity. A scattered field must therefore exist outside of the object. Henceforth, all quantities characterizing the incident wave will be superscripted (0) and those of the scattered wave (a). /238

Let us consider a certain point $\vec{r}$, at which the scattered field is investigated. We shall denote by Q the plane that contains the selected point and the propagation direction of the incident wave (i.e., the third axis of the selected reference frame).

We introduce a system of g-coordinates with the unit-vector right trihedral $\vec{g}_1$, $\vec{g}_2$, $\vec{g}_3$, where $\vec{g}_3 = -\vec{l}_3$, $\vec{g}_1$ is perpendicular to the plane Q and $\vec{g}_2$ is parallel to it. In the g-system, the Stokes parameters $S_j^{(0)}$ of the scattered wave have the form (6.9) and ϕ is the azimuth angle of the point $\vec{r}$.

It is more convenient to analyze the scattered wave in a j system whose unit-vector right trihedral is defined as follows: $\vec{j}_3 = \vec{r}/r$, $r = |\vec{r}|$, $\vec{j}_1$ is perpendicular to Q and $\vec{j}_2$ is parallel to this plane. It follows from the linearity of the Maxwell equations and the radiation principle that the scattered wave in the wave zone can be represented in the form

$$E_1^{(a)} = \frac{e^{-i\omega t+ikr}}{ikr}(a_{11}(\theta, \varphi)E_1^{(0)} + a_{12}(\theta, \varphi)E_2^{(0)}),$$
$$E_2^{(a)} = \frac{e^{-i\omega t+ikr}}{ikr}(a_{21}(\theta, \varphi)E_1^{(0)} + a_{22}(\theta, \varphi)E_2^{(0)}). \qquad (6.10)$$

In (6.10), r, θ, and ϕ are the polar coordinates of the point $\vec{r}$, $E_i^{(0)}$ are the components of $\vec{E}_0^{(0)}$ in the g system, and $E_j^{(a)}$ are the components of the scattered field in the j system. The magnetic field strength $\vec{H}$ of the scattered wave is again calculated with (6.2). The functions $a_{ij}(\theta, \phi)$ are determined by the shape and dimensions of the particle and the properties of its material.

The wave (6.10) takes the form considered in §1, because its characteristics are constant at all points of a sphere of fixed radius; $E_2^{(a)} = 0$ in the wave zone and the factors $\exp(-i\omega t + i\vec{k}\vec{r})$ and $\exp(-i\omega t + ikr)$ are essentially identical. In the j system, therefore, we can introduce the Stokes parameters $S_j^{(a)}$ of the scattered light and again define relations (6.7). If the Stokes parameters are written in the form of a single-column matrix {S}, it is easily found that

$$\{S^{(a)}\} = \frac{1}{k^2r^2}\{M\}\{S^{(0)}\}. \qquad (6.11)$$

Relation (6.11) defines the scattering matrix {M}, which, as follows from the meaning of the Stokes parameters, contains essentially all of the information regarding the scattered light. Let us write out the scattering-matrix components in explicit form: /239

$$M_{ij} = \frac{1}{2}\sum_{\alpha,\beta=1}^{2}|a_{\alpha\beta}|^2 e_{\alpha\beta ij}, \quad i, j = 1, 2,$$

$$\varepsilon_{\alpha\beta ij} = \begin{pmatrix} 1 & 1 & 1 & 1 \\ -1 & 1 & -1 & 1 \\ -1 & -1 & 1 & 1 \\ 1 & -1 & -1 & 1 \end{pmatrix};$$

$$M_{13} = \mathrm{Re}\,(a_{12}a_{11}^* + a_{21}a_{22}^*), \quad M_{41} = -\mathrm{Im}\,(a_{12}a_{22}^* + a_{21}a_{11}^*),$$
$$M_{23} = \mathrm{Re}\,(a_{21}a_{22}^* - a_{12}a_{11}^*), \quad M_{43} = -\mathrm{Im}\,(a_{11}a_{22}^* + a_{12}a_{21}^*),$$
$$M_{31} = \mathrm{Re}\,(a_{12}a_{22}^* + a_{21}a_{11}^*), \quad M_{44} = \mathrm{Re}\,(a_{11}a_{22}^* - a_{12}a_{21}^*),$$
$$M_{32} = \mathrm{Re}\,(a_{12}a_{22}^* - a_{21}a_{11}^*), \quad M_{24} = \mathrm{Im}\,(a_{21}a_{22}^* - a_{12}a_{11}^*),$$
$$M_{33} = \mathrm{Re}\,(a_{11}a_{22}^* + a_{12}a_{21}^*), \quad M_{42} = -\mathrm{Im}\,(a_{12}a_{22}^* - a_{21}a_{11}^*),$$
$$M_{14} = \mathrm{Im}\,(a_{12}a_{11}^* + a_{21}a_{22}^*), \quad M_{34} = -\mathrm{Im}\,(a_{11}a_{22}^* - a_{12}a_{21}^*).$$

The explicit form of the coefficients a_{ij} is determined after solving the corresponding electrodynamic boundary-value problem, which reduces to solution of the Maxwell equations with the condition that the tangential field component at the interface between media with differing electromagnetic characteristics is continuous. This is a highly complex problem, and solutions for it have been found only in certain particular cases. In the case of spherical particles, $a_{12} = a_{21} = 0$, a_{11} and a_{22} depend only on θ and at $\theta = \pi$, i.e., when the propagation direction of the scattered wave coincides with the incidence direction, $a_{11} = a_{22}$. We note further that M_{11} is essentially the same as the scattering indicatrix.

3. SCATTERING, ABSORPTION, AND ATTENUATION COEFFICIENTS

It follows from (6.8) and (6.11) that the intensity $I^{(a)}$ of scattered light is determined as follows:

$$I^{(a)} = \frac{m_a c}{16\pi k^2 r^2}\,(S_1^{(0)}M_{11} + S_2^{(0)}M_{12} + S_3^{(0)}2M_{13} + S_4^{(0)}M_{14}). \qquad (6.12)$$

Then the direction of the Umov-Poynting vector, as indicated by formulas (6.2), (6.3), and (6.10), coincides with the direction of the unit vector $\vec{j}_3$. Hence the energy flux of the scattered field $P^{(a)}$ through a sphere of large enough radius equals $\int I^{(a)} r^2 \sin\theta\, d\theta\, d\phi$. The ratio of this last quantity to the intensity of the incident light determines the scattering coefficient σ_s. /240

Substituting (6.12) into the definition of the flux and using (6.8) to calculate the intensity of the incident light and relations (6.9), we find

$$\sigma_s = \frac{1}{2k^2}\int (M_{11} + M_{12}\cos 2\beta\cos 2\varphi + \\ + 2M_{13}\cos 2\beta\sin 2\varphi + 2M_{14}\sin 2\beta)\sin\theta\, d\theta\, d\varphi. \qquad (6.13)$$

Formula (6.13) readily yields formulas for σ_s in the cases of scattering of linearly polarized light ($\beta = 0$) and circularly polarized light ($\beta = \pm\pi/4$ depending on the polarization direction). If the particle is spherical, we can use the properties of the a_{ij} to obtain in this case

$$\sigma_s = \frac{\pi}{k^2}\int_0^{\pi} M_{11}\sin\theta\, d\theta \tag{6.14}$$

irrespective of the polarization state of the incident light.

The absorption coefficient σ_a is defined as the ratio of the flux of the total-field Umov-Poynting vector across a sphere of radius r to the intensity of the incident light, taken with its sign reversed. It is easily seen that the flux defined above is equal in absolute magnitude to the amount of field energy absorbed in the volume under consideration. The minus sign indicates an energy sink.

According to the field-superposition principle and formulas (6.3), the Umov-Poynting vector $\vec{P}$ can be written in the form $\vec{P} = \vec{P}^{(0)} + \vec{P}^{(a)} + \vec{P}'$, where

$$\vec{P}' = \frac{c}{8\pi}\operatorname{Re}\{[\vec{E}^{(a)}, \vec{H}^{(0)*}] + [\vec{E}^{(0)}, \vec{H}^{(a)*}]\}. \tag{6.15}$$

The vector $\vec{P}'$ in (6.15) is time-averaged.

By the definition of the absorption coefficient,

$$\sigma_a = -\frac{1}{I^{(0)}}\int (\vec{P}, \vec{j}_3)\, ds, \tag{6.16}$$

where, as usual, $ds = r^2\sin\theta d\theta d\phi$.

The sum of the scattering and absorption coefficients will be defined as the attenuation coefficient σ: /241

$$\sigma = \sigma_a + \sigma_s. \tag{6.17}$$

If we substitute the expression for $\vec{P}$ into (6.16) and recognize that the integral vanishes with the first term and yields the scattering coefficient with the second, we obtain from (6.17)

$$\sigma = -\frac{1}{I_0}\int (\vec{P}', \vec{j}_3)\, ds. \qquad (6.18)$$

After substituting (6.15) into (6.18), we can write the integrand in explicit form, using (6.1) and (6.10) for the electric-field components and (6.2) for the magnetic-field components. We then have integrals of the type $\int F(\theta, \phi)\exp[ikr(1 + \cos\theta)]\sin\theta d\theta$. Since $kr >> 1$ in the wave zone, these integrals can be evaluated by the stationary-phase method. The following expression for σ is obtained after certain calculations [456]:

$$\sigma = -\frac{1}{k^2}\mathrm{Re}\int_0^{2\pi}[(a_{11}+a_{22})+\cos^2\beta\cos 2\varphi\,(a_{22}-a_{11})+$$
$$+(a_{12}+a_{21})\cos 2\beta\sin 2\varphi+i\,(a_{21}-a_{12})\sin 2\beta]\,d\varphi. \qquad (6.19)$$

All functions a_{ij} in (6.19) have the argument $\theta = \pi$.

In essence, the results of (6.19) represent the well-known optical theorem, generalized to the case of elliptically polarized light and a scattering particle of arbitrary shape.

For spherical particles, we may write on the basis of the corresponding properties of the a_{ij} and (6.19) that

$$\sigma = -\frac{4\pi}{k^2}\mathrm{Re}\,a(\pi) \qquad (6.20)$$

irrespective of the polarization state of the incident wave. Here $a(\pi) = a_{11}(\pi) = a_{22}(\pi)$ represents the amplitude of the forward-scattered wave.

As we see from (6.19), calculation of the attenuation coefficient requires knowledge of the amplitude of a wave scattered at a small angle to the propagation direction of the incident wave. The reasons for this are quite simple if we remember that any experimental scheme for the determination of σ by its nature involves consideration of interference between the incident wave and a wave scattered at small angles. Since integrals of the type given above do not depend on the upper limit when evaluated by the stationary-phase method, it can be shown that the σ determined from (6.17) coincides with the screening coefficient η. The latter is defined precisely by the scheme of the experiment: $\eta = I_0^{-1}(\Pi_0 - \Pi)$, where Π and Π_0 are the amounts of energy recorded by the radiation receiver when the particle is in the radiant flux and outside it. From a purely computational standpoint, formula (6.19) is helpful in that it permits use of any approximate

/242

information on the amplitudes of the light scattered at small angles for determination of σ.

4. THE SCALAR APPROXIMATION IN THE LIGHT-SCATTERING PROBLEM

We shall call substitution of the solutions of the Maxwell vector equations by the solution of the Helmholtz scalar equation for a certain function ψ the scalar approximation. The Helmholtz equation takes the form

$$\Delta\psi + k^2 V(\vec{r})\psi = 0. \tag{6.21}$$

The advantage of the scalar approximation is that it is considerably easier to find the approximate solution of (6.21) in many cases than to find an asymptotic solution of the Maxwell equations. It is also found that such solutions cover the range of small scattering angles, and this makes it possible to seek certain approximate representations for the attenuation coefficient. We note also that replacement of the Maxwell equations by the Helmholtz equation has been discussed in [457-459] with the object of ascertaining the sense of the "scalar perturbation" that figures in the theory of optical diffraction.

Let us first discuss the scalar approximation for spherical particles. The solution of (6.21) is usually sought for the following boundary conditions at the surface of a sphere of radius a:

$$\psi_1 + \psi_2 = \psi_3, \quad P_0(\partial(a\psi_1 + a\psi_2)/\partial a) = P_1 \frac{\partial}{\partial a}(a\psi_3),$$

where ψ_1, ψ_2, and ψ_3 are functions that describe the incident, external, and internal waves (with ψ representing the plane wave) and P_1 and P_0 are certain constants. /243

The following proposition can be proven [460]: in the range of small scattering angles, the solution of the Maxwell equations for the potential of the field of a sphere can be represented as the sum of the half-solutions of (6.21) with $P = P_0 = 1$ and $P_0 = 1/P = m$, where m is the relative complex refractive index of the material of the sphere. The first solution corresponds to oscillations of the electrical type, and the second to magnetic oscillations. This proposition can be established by simple comparison of the corresponding solutions with $\theta \simeq \pi$.

Using the proposition formulated above and certain methods of quantum collision theory, we may, for example, obtain all results of Chapter II of van de Hulst's well-known monograph [461]. By way of example, we cite an expression for the coefficient of attenuation of light by a two-layered transparent sphere whose

dimensions are much greater than the wavelength:

$$\sigma = \pi r_2^2 (2 - x_1 - x_2), \quad x_1 = [2 - k(\rho_2, \beta)]\,[1 - a_1/a_2],$$

$$x_2 = 4 \int_0^{a_1/a_2} \cos\{\rho_2 \sqrt{1 - \xi_2} + \rho_2 [(n_1 - 1)/(n_2 - 1) - 1] \sqrt{(r_1/r_2)^2 - \xi^2}\}\, \xi\, d\xi.$$

The subscript 1 is used for quantities pertaining to the "nucleus" and the subscript 2 for the "envelope," $k = \sigma'/\pi a_2^2$, σ' is the attenuation coefficient for a sphere of radius a_2, $m = n_2$, $\rho_2 = 2\pi a_2 (n_1 - 1)/\lambda$, and λ is the wavelength of the scattered light.

We write out one more formula for the refractive index α of a medium containing N particles with radii $a >> \lambda$:

$$\alpha = 1 + Na^2 \frac{2\pi}{k} \left\{ e^{-\rho \operatorname{tg}\beta} \frac{\cos\beta}{\rho} \cos(\rho - \beta) + e^{-\rho \operatorname{tg}\beta} \frac{\cos^2\beta}{\rho^2} \sin(\rho - 2\beta) + \frac{\sin 2\beta \cos^2\beta}{\rho^2} \right\},$$

$$k = 2\pi/\lambda, \quad \rho = 2(n - 1)ka, \quad \operatorname{tg}\beta = \varkappa/(n - 1), \quad m = n + i\varkappa.$$

We now turn to analysis of the scattering of light at small angles by particles of arbitrary shape and dimensions considerably in excess of the wavelength of the scattered light. It is found that the field can be written in this case in terms of a certain scalar function. With certain assumptions, this quantity coincides with the result of Kirchhoff diffraction theory as applied to describe Fraunhofer diffraction. /244

Let us introduce the vector and scalar potentials $\vec{A}$ and ϕ of the electromagnetic field, the relations $\vec{H} = m_a \operatorname{curl} \vec{A}$, $\vec{E} = -(m_a/c)(i\omega\vec{A})$ and write the Lorentz condition in the form $\operatorname{div} \vec{A} + (m_a/c)(i\omega\phi) = 0$. The expediency of using this notation for $\vec{A}$ and ϕ for scattering problems will be pointed out below.

Using the above relations, the following equation can be obtained for $\vec{E}$ from the Maxwell equations:

$$\vec{E}(\vec{r}) = \vec{E}_0 e^{-i\vec{k}\vec{r}} + B(\vec{r}) \int U(\vec{r}')\, \vec{E}(\vec{r}')\, G(\vec{r}/\vec{r}')\, d\vec{r}'. \tag{6.22}$$

Here $B(\vec{r}) = (4\pi)^{-1}(k^2 + \text{grad div})$, $G(\vec{r}/\vec{r}') = e^{-ikR}/R$, $R = |\vec{r} - \vec{r}'|$, $U = m^2 - 1$ inside the particle and $U = 0$ outside it; $m = m_j/m_a$.

The scheme of the subsequent solution is as follows. The field $\vec{E}_j$ inside the particle is found from (6.22) and then, using the formulas

$$\left.\begin{aligned} \vec{E}_a &= \frac{e^{-ikr}}{r}(C_\theta i_\theta + C_\varphi i_\varphi), \\ C &= \frac{k^2}{4\pi}\int U(\vec{r}')\,\vec{E}_j(\vec{r}')\,e^{-ik\vec{r}\vec{r}'}\,d\vec{r}' \end{aligned}\right\} \qquad (6.23)$$

which follow from (6.22), the scattered field $\vec{E}_a$ in the wave zone is determined. Here i_θ and i_ϕ are the unit vectors of a spherical coordinate system with its origin at the center of the particle.

The derivation of (6.22) and (6.23) indicates that representation of the absolute term in (6.22) in the form of the incident wave and reduction of the region of integration to the volume of the particle are possible only if the above notation is used for the field potentials and the Lorentz condition.

Solution of (6.22) by successive approximations gives $\vec{E}_j = \sum_{n=0}^{\infty}\vec{D}_n$, where $\vec{D}_0 = \vec{E}_0 e^{-ik\vec{r}}$ and for $n \neq 0$ /245

$$\begin{aligned} \vec{D}_n(\vec{r}) = B(\vec{r})\int d\vec{r}_1 U(\vec{r}_1)\,G(\vec{r}/\vec{r}_1)\times \\ \times B(\vec{r}_1)\int d\vec{r}_2 U(\vec{r}_2)\,G(\vec{r}_1/\vec{r}_2)\,B(\vec{r}_2)\ldots B(\vec{r}_{n-2})\times \\ \times\int d\vec{r}_{n-1}U(\vec{r}_{n-1})\,G(\vec{r}_{n-2}/\vec{r}_{n-1})\times \\ \times B(\vec{r}_{n-1})\int d\vec{r}_n U(\vec{r}_n)\,G(\vec{r}_{n-1}/\vec{r}_n)\,\vec{E}_0 e^{-ik\vec{r}\vec{r}_n}. \end{aligned} \qquad (6.24)$$

Let us assume, in addition, that the complex refractive index of the particle substance varies little over a distance of the order of the wavelength. Then, evaluating the last integral in (6.24) by the stationary-phase method and applying the operator B, we can satisfy ourselves that in virtue of the assumption made, the second term, which is related to the operator grad div, can be disregarded. Since $B(\vec{r}_{n-1})\int d\vec{r}_n U(\vec{r}_n)G(\vec{r}_{n-1}/\vec{r}_n)\vec{E}_0 e^{-ik\vec{r}_n}$ differs from the vector $\vec{E}_0 e^{-ik\vec{r}_{n-1}}$ only by a scalar multiplier in this approximation, the procedure described above can be continued. This will be equivalent to setting the operator B equal to $k^2(4\pi)^{-1}$. Then the transformation (6.24) is, with our assumptions, analogous to the calculations in the corresponding section of Schiff's paper [462]. We therefore present only the final result for the vector $\vec{C}$:

$$\vec{C} = -\vec{E}_0 \frac{ik}{2\pi} \int e^{-i(q_1 x_1 + q_2 x_2)} dx_1 dx_2 \times$$
$$\times (1 - e^{-\frac{ik}{2} \int U(\vec{r}) dx_3}), \qquad (6.25)$$

where $\vec{q} = \vec{k} - \vec{k}_a$, and integration extends over the volume of the particle with the x_3 axis directed along $\vec{k}$.

If $|m| >> 1$, the second term in (6.25) can be dropped. Then the formula for the diffracted-field components that follows from (6.23) and (6.25) will constitute the well-known result of the Kirchhoff method for Fraunhofer diffraction.

It is clear that in essence, relations (6.23) and (6.25) expand the scope of the scalar approximation to include large particles of arbitrary shape. /246

If the argument of the exponential in the parentheses in (6.25) is small, then the relation $\vec{C} = (k^2/4\pi) \times \int U(\vec{r}) e^{-i(q_1 x_1 + q_2 x_2)} d\vec{r}$ follows immediately from (6.25). For the case of small scattering angles, this expression, together with (6.25), is the starting point for analysis of wave propagation in a turbulent atmosphere (see, for example, [463]) and analysis of Gans-Rayleigh scattering (to use the terminology in [461]).

Formulas (6.23), (6.21), and (6.19) yield the following expression for the attenuation coefficient σ of the light:

$$\sigma = 2\mathrm{Re} \int (1 - e^{-\frac{ik}{2} \int U(\vec{r}) dx_3}) dx_1 dx_2.$$

To illustrate this last relation, we present an expression for the attenuation coefficient of a nonabsorbing ellipsoid with near-unity relative refractive index:

$$\frac{\sigma}{S} = 2 - \frac{4}{\pi} \left(\frac{\cos b}{b^2} + \frac{\sin b}{b} \right) + \frac{4}{b^2} \sum_{n=0}^{\infty} (-1)^n (1 - P^2) \times$$
$$\times \frac{\partial^{2n}}{\partial z^{2n}} J_0(z) + \frac{4\sqrt{1-P^2}}{b} \sum_{n=0}^{\infty} (-1)^n (1 - P^2) \frac{\partial^{2n}}{\partial z^{2n}} J_1(z).$$

Here

$$z = b\sqrt{1-P^2};$$
$$P = 4S/(SV\sqrt{a});$$
$$b = 2k(m-1)/\sqrt{a};$$
$$a = a_1^{-2} \cos^2 \alpha_1 + a_2^{-2} \cos^2 \alpha_2 + a_3^{-2} \cos^2 \alpha_3,$$

S is the area of the projection of the ellipsoid onto the perpendicular plane, v is the volume of the ellipsoid, α_j is the angle between k and the j-th principal semiaxis of the ellipsoid with length a_j, and J_0 and J_1 are Bessel functions.

If $\vec{k}$ is parallel to one of the principal axes of the ellipsoid, then σ/S will be equal to the corresponding expression for a sphere with radius equal to the length of the semiaxis along which the wave incident upon the ellipsoid propagates.

It appears that this last formula plays the same role as the formula for the coefficient of attenuation by "soft" spheres, i.e., it describes with qualitative certainty the behavior of the coefficient of attenuation by ellipsoids of arbitrary dimensions. /247

5. SCATTERING OF AN INHOMOGENEOUS FIELD

We shall call a wave inhomogeneous if its form differs from that described in §1. It may be either a nonmonochromatic wave or a nonplane wave or one that has an inconstant vector $\vec{E}_0$. Any combination of these causes is also possible.

In the case under consideration, all measured quantities can be constructed from the components of the matrix $D(\vec{r}_1, \vec{r}_2, t_1, t_2)$, where $\vec{r}_1$ and $\vec{r}_2$ are certain arbitrary points of the field and t_1 and t_2 are arbitrary points in time. Formally, the matrix D can be described as follows. We represent the vectors $\vec{E}$ and $\vec{H}$ by single-column matrices whose elements are components of the vector in a certain coordinate system. We shall denote these matrices by E and H. Then

$$D(\vec{r}_1, \vec{r}_2, t_1, t_2) = \langle E(\vec{r}_1, t_1)\,\overline{H}(\vec{r}_2, t_2)\rangle, \tag{6.26}$$

where the bar over the H denotes transposition of the matrix and the symbol < > indices that each component of the tensor $E\overline{H}$ is time-averaged in accordance with the rule

$$\langle f_1 f_2\rangle = \lim_{T\to\infty}\frac{1}{2T}\int_{-T}^{T} f_1(\vec{r}_1, t_1+\xi)\, f_2(\vec{r}_2, t_2+\xi)\, d\xi,$$

here f_1 and f_2 are certain components of $\vec{E}$ and $\vec{H}$.

The analysis then deals with stationary fields for which D depends only on the difference $t_2 - t_1$ and which admit of the expansion

$$D(\vec{r}_1, \vec{r}_2, t_1, t_2) = \int \Gamma(\vec{r}_1, \vec{r}_2, \omega) e^{-i\omega(t_1-t_2)} d\omega, \qquad (6.27)$$

where the components of the matrix Γ are the Fourier components of the corresponding elements of matrix D.

The Stokes parameters at a certain point $\vec{r}$ are constructed from the components of D with $\vec{r} = \vec{r}_1 = \vec{r}_2$ and $\tau = t_1 - t_2 = 0$. According to (6.26) and (6.4), for example, the total intensity equals $\mathrm{Sp}D(\vec{r}, \vec{r}, t_1, t_1)$. Experimental schemes for determination of $D(\vec{r}_1, \vec{r}_2, t_1, t_2)$ are examined in [464]. For example, the components of $D(\vec{r}, \vec{r}, t_1 - t_2)$ are developed in analysis of interference in the scheme of Young's experiment, and the $D(\vec{r}_1, \vec{r}_2, 0)$ are required for analysis of diffraction at rather large apertures. In the scalar variant, D is usually known as the coherence function. /248

Let us now examine an arbitrary electromagnetic field scattered by a certain object [465]. We shall assume that the medium external with respect to the object is nonmagnetic and spatially homogeneous.

The basic idea of the calculations performed below is quite familiar. We denote by $\vec{F}(\vec{r}, t)$ and $\vec{F}_b(\vec{r}, t)$ the electric $\vec{E}(\vec{r}, t)$ or magnetic $\vec{H}(\vec{r}, t)$ vectors of the incident and total fields outside the object (t is time and $\vec{r}$ are the coordinates of a certain point). The relation $\vec{F}_b(\vec{r}, t) = \hat{T}\vec{F}(\vec{r}, t)$ determines the interaction operator $\hat{T}$, which is linear within the framework of linear electrodynamics. We must find the operator on the assumption that the solution of the problem of scattering of a plane monochromatic wave on the object in question is known. The operator $\hat{T}$ can be found by expanding the incident field in plane waves and using the linearity of $\hat{T}$.

It follows from the Maxwell equations and the relation between $\vec{E}$ and the electric-induction vector that

$$\Delta\vec{F} - \frac{1}{c^2}\frac{\partial^2\vec{F}}{\partial t^2} - \frac{1}{c}\int \vec{F}(\vec{r}, \tau)\frac{\partial^2 f}{\partial \tau^2} d\tau = 0, \qquad (6.28)$$

where $f(\tau)$ is the relaxation function (see, for example, [466]).

Using the apparatus of δ functions, it can be shown that real $\vec{F}$ that satisfy (6.28) are subject to the expansions

$$\vec{F}(\vec{r}, t) = 2\mathrm{Re}\int \frac{\omega\sqrt{\varepsilon(\omega)}}{2c}\vec{G}\left(\frac{\omega\sqrt{\varepsilon}}{c}\vec{k}_0\omega\right)e^{\frac{-i\omega\sqrt{\varepsilon}\vec{k}_0\vec{r}}{c}+i\omega t}d\vec{k}_0 d\omega,$$

$$\frac{\omega\sqrt{\varepsilon}}{2c}\vec{G}\left(\frac{\omega\sqrt{\varepsilon}}{c}\vec{k}_0, \omega\right) = \frac{1}{(2\pi)^4}\int \vec{F}(\vec{r}', t')e^{-i\omega t+i\vec{k}\vec{r}'}k^2\,dk\,d\vec{r}'\,dt'. \qquad (6.29)$$ /249

where $\omega \in [0, \infty]$; $d\vec{k}_0 = \sin\beta d\beta d\psi$; β and ψ are the coordinates of the unit vector $\vec{k}_0$ on the unit sphere, $\varepsilon(\omega) = 1 + \int f(\tau)\exp[-i\omega\tau]d\tau$ is the dielectric constant for frequency ω, and c is the velocity of light.

The condition div $\vec{F}$ = 0 yields the relation $\vec{G}\left(\frac{\omega\sqrt{\varepsilon}}{c}\vec{k}_0, \omega\right)\vec{k}_0 = 0$, and the Maxwell equations give $G_{\vec{H}} = \left(\frac{c}{\omega}\right)^2 [\vec{k}_0\vec{G}]$. These last relationships signify that (6.29) represents the expansion of the incident field in plane waves.

The expansion (6.29) assumes quadratic integrability of $\vec{F}(\vec{r}, t)$ over time. In optics, however, it is often necessary to deal with the contrary case, because the measured quantities are constructed from components of the tensor D.

Following [464], we can introduce the quadratically integrable function

$$\vec{F}^{(T)}(\vec{r}, t) = \begin{cases} \vec{F}(\vec{r}, t), & |t| \leqslant T, \\ 0, & |t| > T, \end{cases} \qquad (6.30)$$

whose tensor F_{pq} coincides with the corresponding tensor of the function $\vec{F}$. We shall assume that the described procedure has always been carried out.

After commutation of $\hat{T}$ with the sign of the integral in (6.29), it will in fact operate on a plane monochromatic wave. When such a wave is scattered, the field outside the object is composed of the incident and scattered fields, i.e., $\hat{T} = \hat{P} + \hat{T}_a$, where $\hat{P}$ is an operator that does not change the plane wave and $\hat{T}_a$ is the scattering operator. The latter is usually determined as follows (see [461] and §2). The incident field is written in a coordinate system with unit vectors $\vec{g}_1$, $\vec{g}_2$, $\vec{g}_3$, where $\vec{g}_1$ is perpendicular to the plane containing the vector $\vec{k}_0$ and the vector r, which connects the coordinate origin to the point at which the scattered field is observed, $\vec{g}_2$ is parallel to this plane, and $\vec{g}_3 = \vec{k}_0$. The components of the scattered field are then obtained in a system with /250 the unit vectors $\vec{m}_1$, $\vec{m}_2$, $\vec{m}_3$; here $\vec{m}_3 = \vec{r}_0 = \vec{r}/|r|$, the vector $\vec{m}_1$ is perpendicular and $\vec{m}_2$ is parallel to the above-described plane.

All vectors in (6.26)-(6.30) are defined in an arbitrary coordinate system with unit vectors $\vec{I}_1$, $\vec{I}_2$, $\vec{I}_3$ and its origin at the center of the scattering object. In this system, therefore, the scattering operator $\hat{T}_a = \hat{N}^{-1}\hat{T}_g\hat{M}$, where $\hat{T}_g$ is the scattering operator of the plane wave in the system $\vec{g}_1$, $\vec{g}_2$, $\vec{g}_3$, $\hat{M}$ is the transformation that translates the vector defined in $\vec{k}$ space from the system ($\vec{I}_1$, $\vec{I}_2$, $\vec{I}_3$) to the system ($\vec{g}_1$, $\vec{g}_2$, $\vec{g}_3$) and N is the transformation that translates this vector from the system ($\vec{I}_1$, $\vec{I}_2$, $\vec{I}_3$) to the system ($\vec{m}_1$, $\vec{m}_2$, $\vec{m}_3$). It can be shown that the energy of the field is invariant under these transformations, i.e., that the field obtained after the respective transformation is equivalent to the original field.

To make it possible to introduce the operator matrices in the usual manner, we present the vectors as single-column matrices whose elements are the components of the vector in the system ($\vec{I}_1$, $\vec{I}_2$, $\vec{I}_3$). It then follows from (6.29) and (6.30) and the expression for the scattering operator in ($\vec{I}_1$, $\vec{I}_2$, $\vec{I}_3$) that

$$F_b(\vec{r}, t) = F(\vec{r}, t) + \frac{2\mathrm{Re}}{(2\pi)^4}\int U^{(\vec{E},\vec{H})}(\omega, \vec{k}_0, \vec{r})\,F(\vec{r}', t')\times \\ \times e^{i\vec{k}\vec{r}-i\omega(t-t')}\,d\vec{k}\,d\omega\,d\vec{r}'\,dt' \equiv F + F_a, \qquad (6.31)$$

where F and F_b are the matrices corresponding to $\vec{F}$ and $\vec{F}_b$; $U = N^{-1}T_g^{(\vec{E},\vec{H})}$; $\hat{N}$ and $\hat{M}$ are the invariant matrices of the operators N and M whose explicit forms are written out below; $T_g^{(\vec{E},\vec{H})}$ is the matrix of the operator $\hat{T}_g$ in the system ($\vec{g}_1$, $\vec{g}_2$, $\vec{g}_3$). The latter matrix equals $T_g^{(\vec{E})}$ if $\vec{F}$ is understood as $\vec{E}$, and is $T_g^{(\vec{H})}$ when $\vec{F}$ denotes the vector $\vec{H}$. The matrices $T_g^{(\vec{E})}$ and $T_g^{(\vec{H})}$ are determined on solution of the Maxwell equations obtained after elimination of the time multiplier.

In deriving (6.31), it is necessary to recognize that the action of the scattering operator on the complex-conjugate terms in (6.29) leads to complex-conjugate expressions for the scattered fields. This can be demonstrated by using the integral equation given in §4 for the scattering amplitude. /251

Let us denote the matrices D for the total and incident fields by D_b and D_0.

Substituting (6.31) into the definition of D and dropping terms containing the factor exp[i(ω' + ω")t] in the integrand, we arrive at the expression

$$D_b = \frac{2}{(2\pi)^8} \operatorname{Re} \lim_{T\to\infty} \frac{1}{2T} \int U^{(\vec{E})}(\omega', \vec{k}_0', \vec{r}_1)\, E(\vec{r}', t') \times$$
$$\times \overline{H(\vec{r}'', t'')}\, U^{(\vec{H})+}(\omega'', \vec{k}_0'', \vec{r}_2)\, e^{i\vec{k}'\vec{r} - i\omega'(t'-t_1-\xi) - i\vec{k}''\vec{r}'' + i\omega''(t''-t_2-\xi)} \times$$
$$\times d\vec{k}'\, d\vec{k}''\, d\vec{r}'\, d\vec{r}''\, d\omega'\, d\omega''\, dt'\, dt''\, d\xi +$$
$$+ \frac{2}{(2\pi)^4} \operatorname{Re} \lim_{T\to\infty} \frac{1}{2T} \int_{-T}^{T} E(\vec{r}_1, t_1+\xi)\, \overline{H(\vec{r}'', t'')} \times$$
$$\times U^{(\vec{H})+}(\omega'', \vec{k}_0'', \vec{r}_2)\, e^{-i\vec{k}''\vec{r}'' + i\omega''(t''-t_2-\xi)}\, d\vec{k}''\, d\vec{r}''\, d\omega''\, d\xi +$$
$$+ \frac{2}{(2\pi)^4} \operatorname{Re} \lim_{T\to\infty} \frac{1}{2T} \int_{-T}^{T} U^{(\vec{E})}(\omega', \vec{k}_0', \vec{r}_1)\, E(\vec{r}', t')\, \overline{H(\vec{r}_2, t_2+\xi)} \times$$
$$\times e^{i\vec{k}'\vec{r}' - i\omega'(t'-t_1-\xi)}\, d\vec{k}'\, d\vec{r}'\, d\omega'\, dt'\, d\xi + D_0.$$

Here and below, the symbol "+" on the matrix $U^{(H)+}$ signifies a Hermitian conjugate matrix.

Substituting the variables $t' = \tau' + \xi$, $t'' = \tau'' + \xi$, $\xi = \eta$, using the spectral expansion of D_0, and integrating with respect to τ', τ'', ω', and ω'', we find

$$D_b = \frac{2}{(2\pi)^6} \operatorname{Re} \int U^{(\vec{E})}(\omega, \vec{k}_0', \vec{r}_1)\, \Gamma(\vec{r}', \vec{r}'', \omega) \times$$
$$\times U^{(\vec{H})+}(\omega, \vec{k}_0'', \vec{r}_2)\, e^{i\vec{k}'\vec{r}' - i\vec{k}''\vec{r}'' + i\omega(t_1-t_2)}\, d\vec{k}'\, d\vec{k}''\, d\vec{r}'\, d\vec{r}''\, d\omega +$$
$$+ \frac{2}{(2\pi)^3} \operatorname{Re} \int \Gamma(\vec{r}_1, \vec{r}'', \omega)\, U^{(\vec{H})+}(\omega, \vec{k}_0'', \vec{r}_2)\, e^{-i\vec{k}''\vec{r}'' + i\omega(t_1-t_2)} \times$$
$$\times d\vec{k}''\, d\vec{r}''\, d\omega + \frac{2}{(2\pi)^3} \operatorname{Re} \int U^{(\vec{E})}(\omega, \vec{k}_0', \vec{r}_1) \times$$
$$\times \Gamma(\vec{r}', \vec{r}_2, \omega)\, e^{i\vec{k}'\vec{r}' - i\omega(t_1-t_2)}\, d\vec{k}'\, d\vec{r}'\, d\omega + D_0. \qquad (6.32)$$

In the case of quadratically integrable functions /252

$$\Gamma_{pq}(\vec{r}', \vec{r}'', \omega) = E_p(\vec{r}', \omega)\, H_q^*(\vec{r}'', \omega).$$

Otherwise,

$$\Gamma_{pq}(\vec{r}', \vec{r}'', \omega) = \lim \frac{1}{2T} E_p^{(T)}(\vec{r}', \omega)\, H_q^{(T)*}(\vec{r}'', \omega).$$

Here E_p, $E_p^{(T)}$, H_q, $H_q^{(T)}$ are the Fourier components of the components E, $E^{(T)}$, and H, $H^{(T)}$, and the symbol * signifies the complex conjugate.

The explicit form of the components of the matrices of operators $\hat{M}$ and $\hat{N}$ can be obtained from the relations

$$\vec{g}_1 = (\sin\alpha)^{-1}[\vec{k}_0 \times \vec{r}_0],$$
$$\vec{g}_2 = (\sin\alpha)^{-1}[\vec{k}_0 \times [\vec{k}_0 \times \vec{r}_0]], \quad \vec{g}_3 = \vec{k}_0,$$
$$\vec{m}_1 = (\sin\alpha)^{-1}[\vec{k}_0 \times \vec{r}_0],$$
$$\vec{m}_2 = (\sin\alpha)^{-1}[[\vec{k}_0 \times \vec{r}_0] \times \vec{r}_0], \quad \vec{m}_3 = \vec{r}_0.$$

The expressions are given in greater detail in [465].

6. LAWS GOVERNING THE SCATTERING OF VISIBLE AND INFRARED WAVES BY A SINGLE SPHERICAL PARTICLE

1. Efficiency factors of attenuation, scattering, and absorption. The attenuation K, scattering K_s, and absorption K_a efficiency factors are notions introduced in examining the scattering of electromagnetic waves by a spherical particle:

$$K = \frac{\sigma}{\pi a^2}, \quad K_s = \frac{\sigma_s}{\pi a^2}, \quad K_a = \frac{\sigma_a}{\pi a^2}. \tag{6.33}$$

As will be seen from (6.33) and the definition given in §3 for the coefficients σ, σ_s and σ_a, the functions K, K_s, and K_a are numerically equal to the ratios of the energies attenuated, scattered, and absorbed by the particle to the energy incident upon its geometrical cross section πa^2.

1. Analytical expressions for the function K, K_s, and K_a. The Mie theory, which is set forth in systematic detail in the monographs of K.S. Shifrin [467] and H. van de Hulst [461], yields /253 general formulas for K, K_s, and K_a. The expressions for the functions K, K_s, and K_a are infinite series, with K, K_s, and K_a dependent on two arguments, which characterize the relative dimension ρ and relative refractive index m of the particle:

$$\rho = \frac{2\pi a}{\lambda}, \tag{6.34}$$

$$m = \frac{m_1}{m_2}, \tag{6.35}$$

where λ is the wavelength of the scattered radiation and m_1 and m_2 are the complex refractive indices of the particle and the medium.

As applied to the conditions for scattering of radiation in the atmosphere, the relative complex refractive index may be considered equal to the refractive index of the particle, i.e., we may set $m = m_1 = n - i\kappa$, where n is the ordinary refractive index and κ is the absorption index of the material of the particle.

In a number of asymptotic cases, the expressions for the functions K, K_s, and K_a are obtained in finite form. Some of the asymptotic formulas, which we shall subsequently need, are given below.

1. Small particles. Small particles are those for which $\rho << 1$. In this case, asymptotic formulas for K and K_s are obtained by using the expansions of the Bessel and Hankel functions that appear in the expressions for K and K_s in powers of ρ. Different formulas are obtained for different $|m|$. We shall be interested in the case in which $|m|$ is small, for which the following formulas were obtained in [467] and [468]:

$$K(\rho, m) = \sum_{n=1}^{5} P_n \rho^n, \quad P_1 = 4 \operatorname{Im}\left(\frac{1-m^2}{m^2+2}\right), \quad P_2 = 0,$$

$$P_3 = 2 \operatorname{Im}\left[\frac{-2(m^2-1)(m^2-2)}{(m^2+2)^2} + \frac{m^2-1}{15} - \frac{m^2-1}{3(2m^2+3)}\right],$$

$$P_4 = \frac{8}{3} \operatorname{Re}\left(\frac{m^2-1}{m^2+2}\right)^2,$$

$$P_5 = 2 \operatorname{Im}\left(\frac{3}{175}\frac{m^2-1}{m^2+2}\frac{m^6+20m^4-200m^2+200}{m^3-2} - \right.$$

$$\left. - \frac{1}{56}\frac{m^2-1}{3m^2+4} - \frac{(m^2-1)(2m^2-3)}{315}\right). \qquad (6.36)$$

For transparent particles, setting $\kappa = 0$ in (6.37), we obtain /254

$$K(\rho, m) = K_s(\rho, m) = \frac{8}{3}\rho^4\left(\frac{m^2-1}{m^2+2}\right)^2. \qquad (6.37)$$

As we see from (6.37), the single-particle scattering coefficient in this particular case is inversely proportional to the fourth power of wavelength, as in the case of molecular (Rayleigh) scattering, if we consider its real refractive index to be constant. In other cases, the relationship becomes highly complex and does not resemble that which follows from the familiar Rayleigh law.

Expressions for $K(\rho, m)$ and $K_s(\rho, m)$ for large m and $m = \infty$ are given in [461] and [467].

2. Large particles. Particles are large if their $\rho \gg 1$. Analysis of the problem with direct application of the Mie formulas is extremely difficult in this case, since, as was shown by Debye, all terms with n from 1 to ρ must be retained in the sums. In the case of raindrops, for example, it is necessary to retain several thousand terms. K.S. Shifrin [469] analyzed this case for a transparent particle by considering a scattered field consisting of geometrical-optical beams and beams of radiation diffracted on the contours of the drop. After calculations for the case of an absorbing particle that are similar to those given in [469], we can obtain for $K(\rho, m)$

$$K(\rho, m) = 2 - \frac{8\sqrt{n^2-\varkappa^2}}{(n+1)^2+\varkappa^2}\frac{n}{n-1}\times$$
$$\times\frac{e^{-2\rho\varkappa}}{\rho}\sin\left[2\rho(n-1)-2\operatorname{arctg}\frac{\sqrt{n^2+\varkappa^2}}{\sqrt{n^2+\varkappa^2}+1}\frac{\varkappa}{\sqrt{n^2+\varkappa^2}+n}\right]. \qquad (6.38)$$

For transparent particles, we have from (6.38)

$$K_s(\rho, m) = 2 - \frac{8n^2}{\rho(n+1)^2(n-1)}\sin[2\rho(n-1)]. \qquad (6.39)$$

It follows from (6.38) and (6.39) that in the case $\rho \to \infty$, the functions K and K_s tend to 2 irrespective of the value of m. This means that extremely large particles scatter twice as much radiation as is incident on their geometrical cross sections.

3. Particles with $|m - 1| \to 0$ ("soft" particles). This case was examined in detail in [461]. We note that particles of water and water aerosols can be regarded with accuracy sufficient for practical purposes as "soft." /255

A rather simple and convenient formula was derived in [461] for large "soft" particles ($\rho \gg 1$):

$$K(\rho, m) = 2 - 4e^{-\rho' \operatorname{tg}\beta}\frac{\cos\beta}{\rho'}\sin(\rho'-\beta) -$$
$$- 4e^{-\rho' \operatorname{tg}\beta}\left(\frac{\cos\beta}{\rho'}\right)^2\cos(\rho'-2\beta) + 4\left(\frac{\cos\beta}{\rho'}\right)^2\cos^2\beta, \qquad (6.40)$$

where

$$\rho' = 2\rho(n-1); \quad \operatorname{tg}\beta = \frac{\varkappa}{n-1}, \qquad (6.41)$$

and for a transparent particle

$$K_s(\rho, m) = 2 - \frac{4}{\rho'}\sin\rho' + \frac{4}{\rho'^2}(1-\cos\rho'). \qquad (6.42)$$

Expressions (6.40)-(6.42) reproduce quite accurately the trend of the K and K_s curves (including even small values of ρ) obtained on the basis of tabulation of the exact Mie formulas.

2. Results of tabulation of the functions K, K_s, and K_a. If none of the conditions considered above is satisfied, the functions K, K_s, and K_a can be obtained only by calculation on the basis of the exact Mie formulas. Here, in order to obtain sufficient accuracy in the calculation, it is necessary to retain on the order of ρ terms in the series. The calculations are highly cumbersome; for this reason, they had been carried out only for occasional values of the parameters m and ρ prior to the advent of high-speed electronic computers.

Quite numerous calculations have now been performed for various m and ρ as a result of the great interest in data on the functions K, K_s, and K_a on the part of specialists in various branches of science, especially chemists, geophysicists, and meteorologists. By far the largest number of calculations has been made for real refractive indices: $0.60 \leq m \leq 2.105$ and $m = \infty$.

We shall be most interested in the results of calculations of the functions K, K_s, and K_a for particles of atmospheric aerosols, and primarily for particles of water, whose absorption index is so small in the visible region of the spectrum that it can be disregarded compared to the refractive index. It is usually assumed that water has a real refractive index in the visible region /256 and a complex one in the infrared (see Chapter 7).

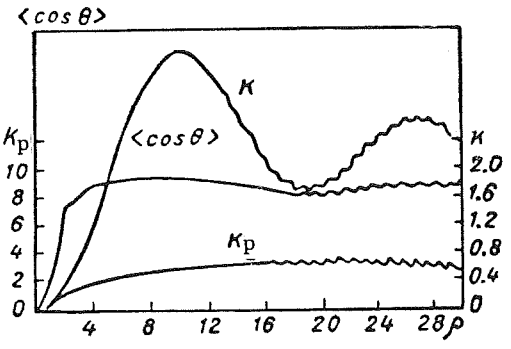

Figure 6.1. Function K, Scattering-Indicatrix Asymmetry Factor <cos θ>, and Light-Pressure Cross Section K_p for Dielectric Spheres with m = = 1.20 According to [477]. Calculation performed for ρ = 0.5 (0.1) 10 (0.05) 20 (0.025) 30.

The most complete data on the functions K, K_s, and K_a for atmospheric-aerosol particles were obtained in [470-483]. References to other studies can be found in these sources and in the monograph [1].

Figures 6.1-6.20 present the most characteristic results from calculations of the functions K, K_s, and K_a by various authors.

As we see from Figs. 6.1-6.3, the dependence of K on the parameter ρ is characterized for transparent dielectric spheres with m from 1.20 to 1.50 by the presence of a series of large-

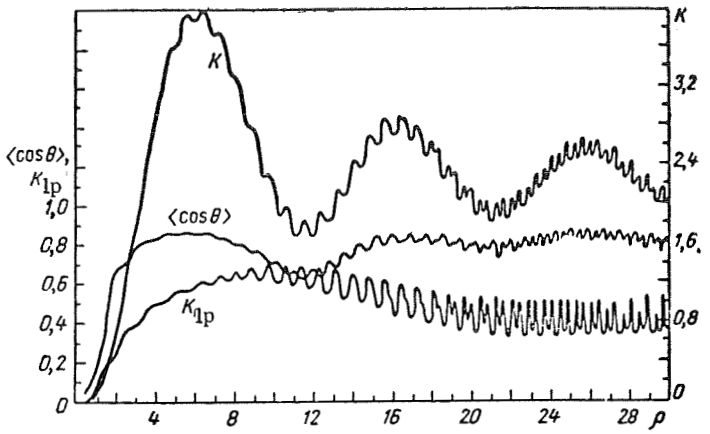

Figure 6.2. Function K, Asymmetry Factor <cos θ> of Scattering Indicatrix, and Light-Pressure Cross Section K_{1p} for Dielectric Spheres with m = 1.33 According to [477]. Calculations performed for ρ = 0.5 (0.1) 10 (0.05) 20 (0.025) 30.

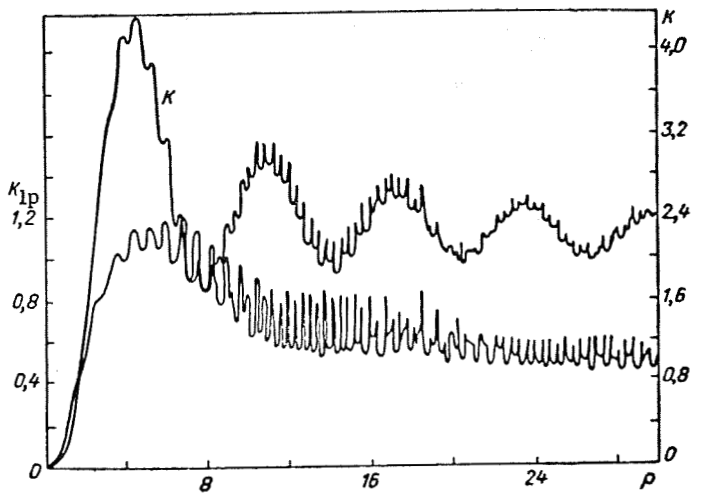

Figure 6.3. Function K and Light-Pressure Cross Section K_{1p} for Dielectric Spheres with m = 1.5 According to [477]. Calculations performed for ρ = 0.5 (0.1) 10 (0.05) 20 (0.025) 30.

scale and a large number of small-scale maxima. These peaks owe their origin to the interference nature of the phenomena of electromagnetic-wave scattering on particles.

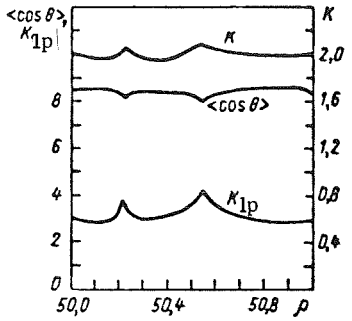

Figure 6.4. Function K, Scattering Indicatrix Asymmetry Factor <cos θ> and Light-Pressure Cross Section K_{1p} for Dielectric Spheres with m = = 1.33 for ρ = 50(0.01)51 According to [477].

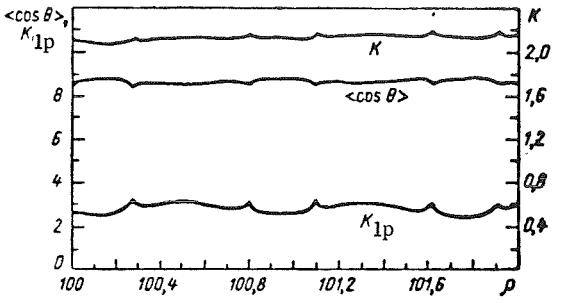

Figure 6.5. Function K, Scattering-Indicatrix Asymmetry Factor <cos θ> and Light-Pressure Cross Section K_{1p} for Dielectric Spheres with m = = 1.33 for ρ = 100(0.01)102 According to [477].

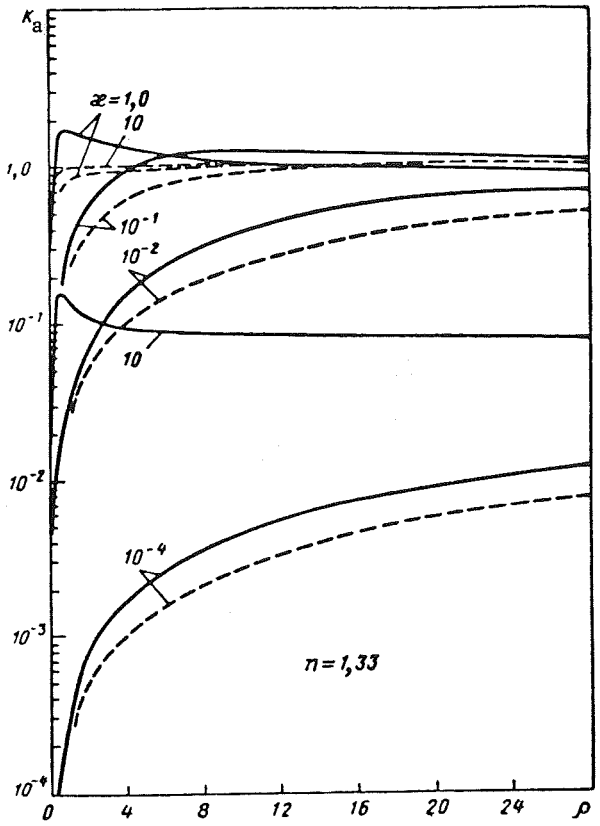

Figure 6.6. Functions K_a for Spheres with n = 1.33 and κ = 10^{-4}, 10^{-2}, 10^{-1}, 1, and 10 and Various ρ as Calculated by Plass [479] from the Exact Formulas of the Mie Theory (Solid Curves) and by the Approximate Formula (6.43).

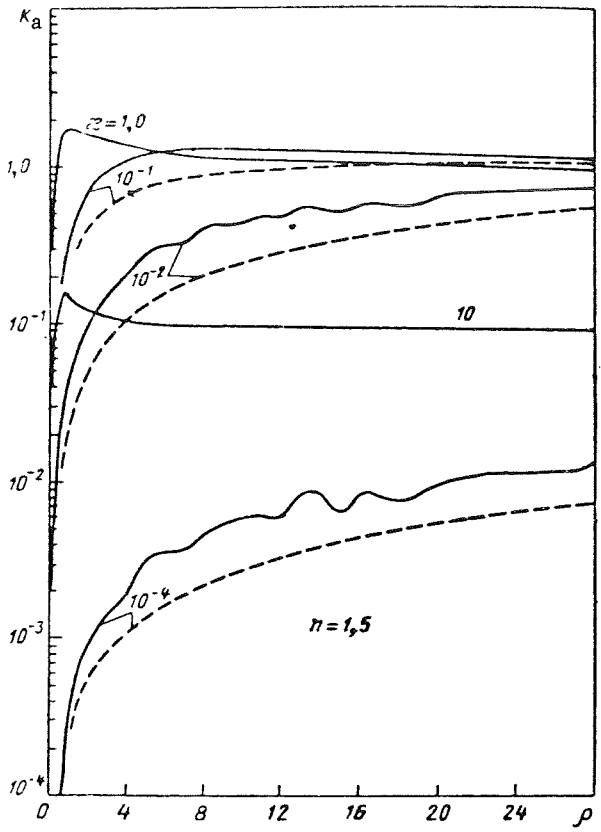

Figure 6.7. Functions K_a for Spheres with n = 1.5 and $\kappa = 10^{-4}$, 10^{-2}, 10^{-1}, 1, and 10 and Various ρ as Calculated by Plass [479] by the Exact Mie Formulas (Solid Curves) and by the Approximate Formula (6.43).

Irwine's calculations [477] of the factor with a step $\Delta\rho$ = = 0.01 show that the small-scale peaks are observed at values up to ρ = 50 and ρ = 100 (Figs. 6.4 and 6.5).

Plass [479] calculated the functions K, K_s, and K_a for spheres with refractive indices n = 1.01, 1.33, 1.5, and 2 and absorption indices $\kappa = 10^{-4}$, 10^{-2}, 10^{-1}, and 10 for values of ρ from 0 to 30 (see, for example, Figs. 6.6-6.11). /258

Along with the exact values of the functions K_a, Figs. 6.6 and 6.7 show approximate values obtained from the van de Hulst formula [467]:

$$K_a = 2Q(4\rho\varkappa), \tag{6.43}$$

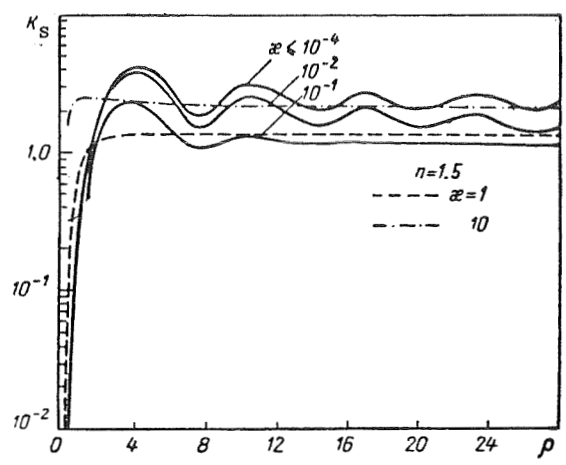

Figure 6.8. Function K_s as a Function of ρ According to [479] for Spheres with n = 1.33 and $\kappa \leq 10^{-4}$, 10^{-2}, 10^{-1}, 1, and 10.

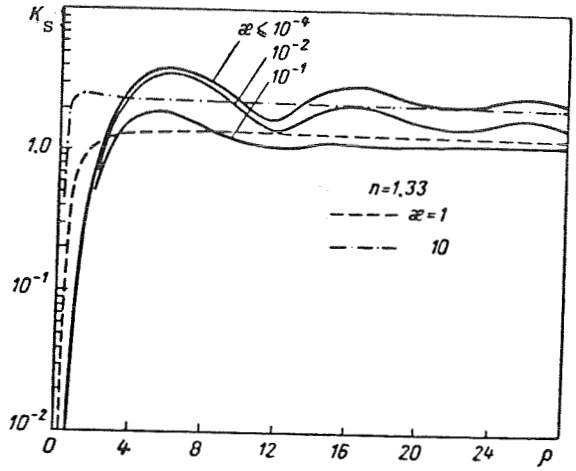

Figure 6.9. Function K_s as a Function of ρ According to [479] for Spheres with n = 1.5 and $\kappa \leq 10^{-4}$, 10^{-2}, 10^{-1}, 1, and 10.

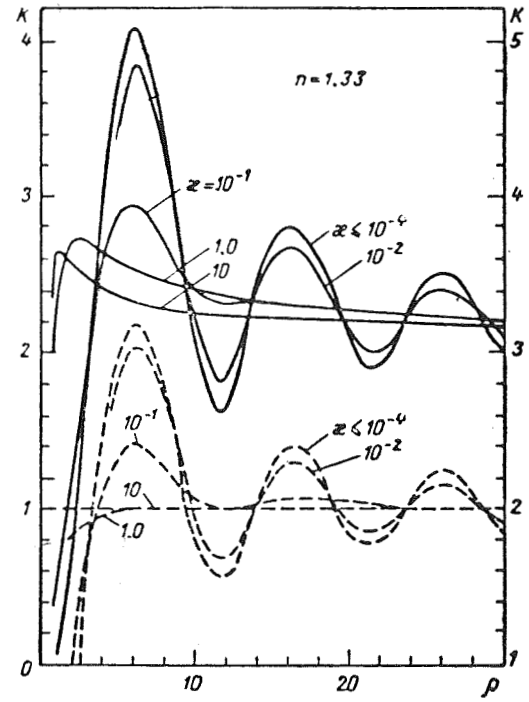

Figure 6.10. Function K as a Function of ρ According to [479] for Spheres with n = 1.33 and $\kappa \leq 10^{-4}$, 10^{-2}, 10^{-1}, 1, and 10 as Calculated by the Exact Mie Formulas (Solid Curve, Left Ordinate Axis) and the Approximate Formula (6.40).

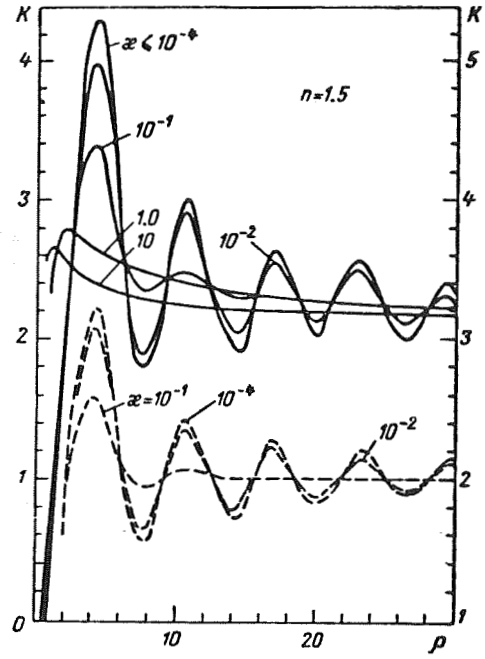

Figure 6.11. Function K as a Function of ρ According to [479] for Spheres with n = 1.5 and $\kappa \leq 10^{-4}$, 10^{-2}, 10^{-1}, 1, and 10 as Calculated by the Exact Formulas (Solid Curves, Left Ordinate Axis) and the Approximate Formula (6.40).

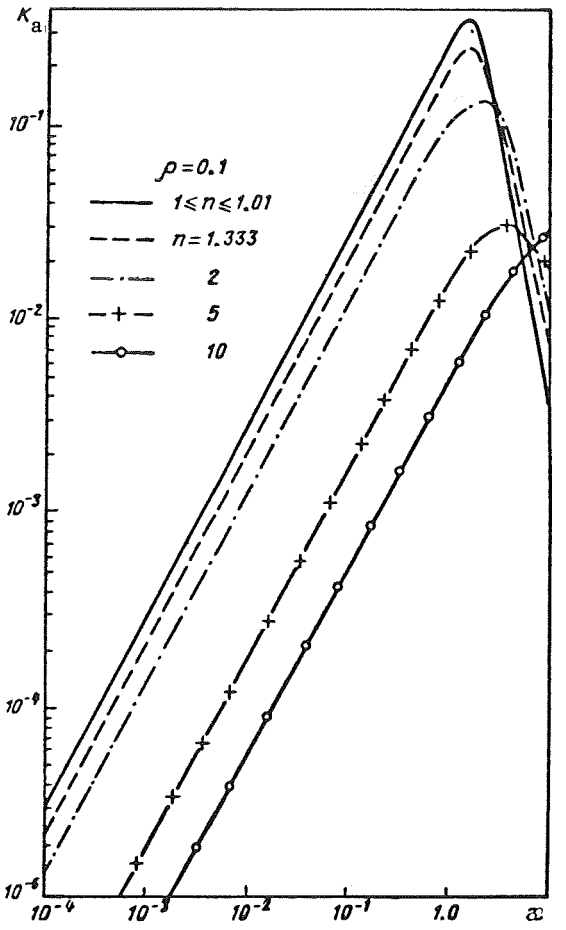

Figure 6.12. Function K_a as a Function of κ for Spheres with ρ = 0.1 and Various Values of n According to [480].

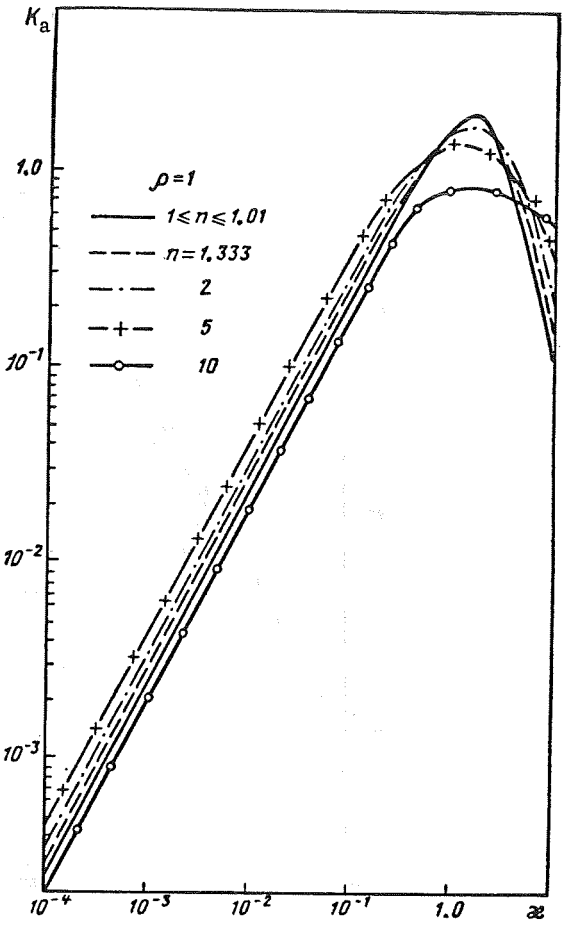

Figure 6.13. Function K_a as a Function of κ for Spheres with ρ = 1.0 and Various Values of n According to [480].

where

$$Q(\omega)=\frac{1}{2}+\omega^{-1}e^{-\omega}+\omega^{-2}(e^{-\omega}-1). \qquad (6.44)$$

Like Figs. 6.6 and 6.7, Figs. 6.10 and 6.11 also give exact and approximate values of the function K. The latter were calculated by the approximate van de Hulst formula (6.40). /262

The influence of κ on the values of the functions K_a and K_s at various n is illustrated by Figs. 6.12-6.17.

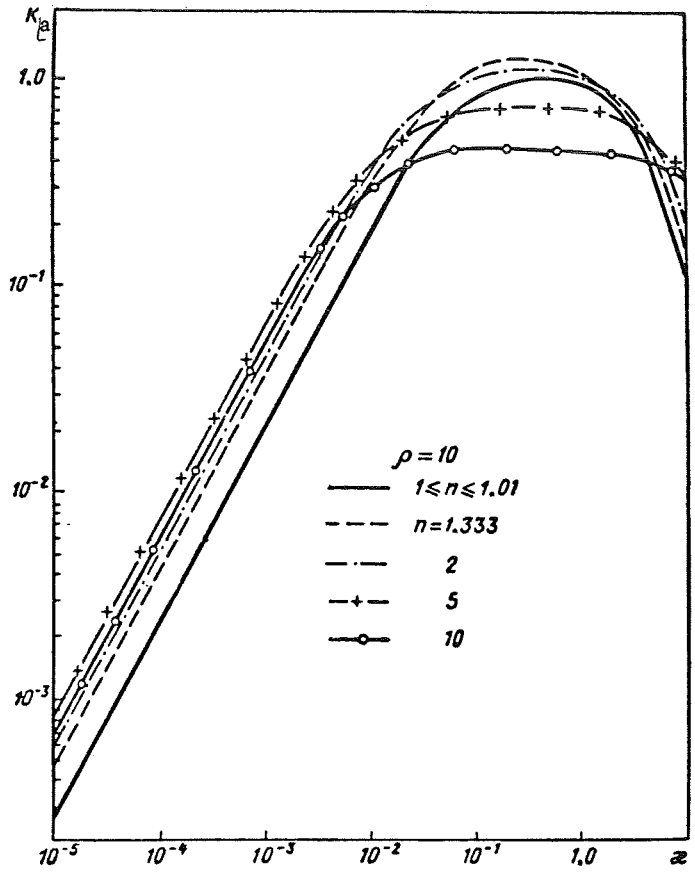

Figure 6.14. Function K_a as a Function of κ for Spheres with $\rho = 10$ and Various Values of n According to [480].

Figures 6.18-6.20 show the functions K, K_a, and K_s for water spheres with values of ρ from 0 to 30 and three wavelengths: λ = = 4, 6, and 10 μ, according to [474].

It is interesting to know the values of the functions K, K_a, and K_s when the particles of the atmospheric aerosol (for example, in the case of haze) can be regarded as two-layered or multi- /263
layered spheres. The corresponding calculations were performed in [484-487]. K, K_a, and K_s were calculated in [486] for two-layered spheres with soot nuclei and water envelopes. The calculated data were presented in the form of graphs of the functions K for values of ρ from 0.1 to 250 and various values of the ratio of the particle and nucleus radii. Analysis of the results showed

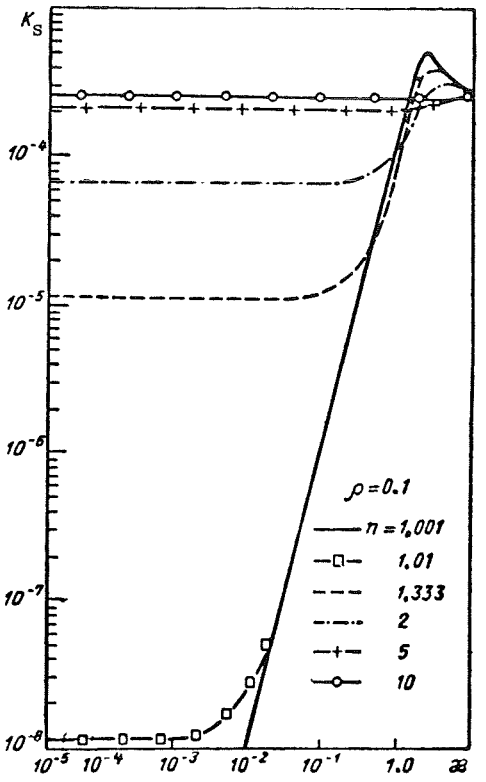

Figure 6.15. Function K_s as a Function of κ for Spheres with ρ = 0.1 and Various Values of n According to [480].

that if the nuclear radius is smaller than 0.1 of the radius of the entire sphere, the particle can be regarded as single-layered. Reference [487] considers a homogeneous spherical nucleus surrounded by concentric envelopes with different refractive-index values. It was shown that these concentric spheres can be replaced by a homogeneous envelope with the average refractive-index value. /269

The above results from calculations of the functions K, K_a, and K_s were obtained for standard temperature. Generally speaking, exact calculation of the attenuation of visible and infrared waves on atmospheric-aerosol particles requires knowledge of these functions for various temperatures. However, the corresponding calculations have not yet been performed because the literature offers no data on the temperature dependence of the complex refractive indices of atmospheric aerosols. There is only one paper by Plass [488] in which the functions K_s and K_a are calculated for spherical aluminum oxide particles in the temperature

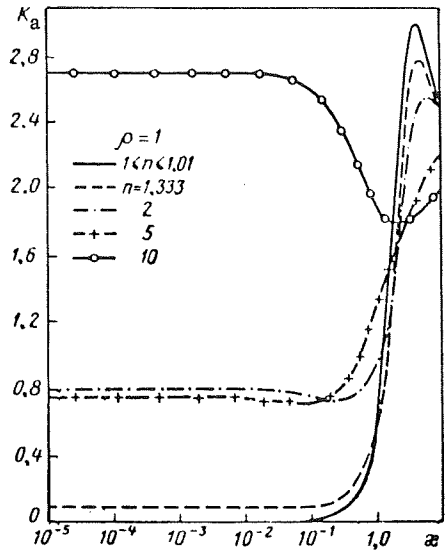

Figure 6.16. Function K_s as a Function of κ for Spheres with ρ = 1.0 and Various Values of n According to [480].

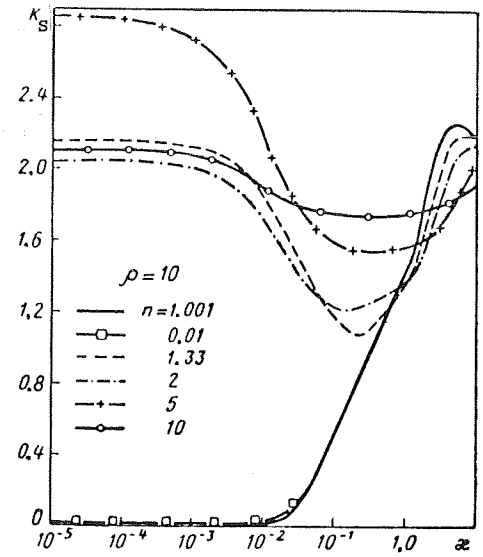

Figure 6.17. Function K_s as a Function of κ for Spheres with ρ = 10.0 and Various Values of n According to [480].

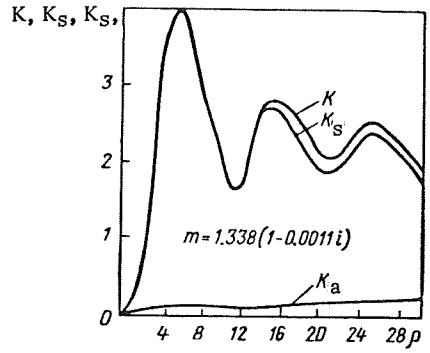

Figure 6.18. Functions K, K_s, and K_a for Water Spheres with ρ from 0 to 30 and Wavelength λ = 4 μ According to Herman [474].

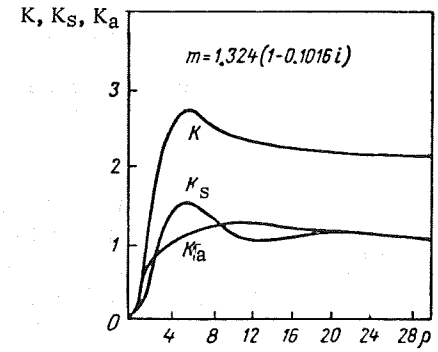

Figure 6.19. Functions K, K_s, and K_a for Water Spheres with Values of ρ From 0 to 30 and Wavelength λ = 6 μ According to Herman [474].

range from 1200 to 2020°C. Particle radius and wavelength were varied from 0.1 to 10 μ and from 0.5 to 6.0 μ, respectively. It was found that at a wavelength λ = 2 μ, K_a varies through a factor of 40 as the temperature varies from 1200 to 2020°C. In the same /270

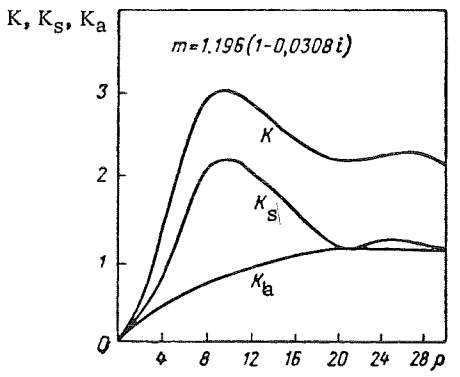

Figure 6.20. Functions K, K_s, and K_a for Water Spheres with Values of ρ from 0 to 30 and Wavelength λ = 10 μ According to Herman [474].

temperature range, K_a increases by factors of 7 and 2 for wavelengths of 0.5 and 6.0 μ. Under the same conditions, the function K_s varies only from 5 to 15% for various wavelengths.

Approximating expressions for the function K. A number of authors have found approximating expressions for the dependence of the function K on m for various m. L.M. Levin [358] derived the corresponding formula for K(ρ) for arbitrary ρ and m = 1.33 (water spheres in the visible region).

Deirmenjian [489] analyzed an approximating expression for functions K(ρ, m) that is valid for arbitrary ρ and complex m satisfying the condition |m| < 2. In [489], K was represented in the form

$$K = (1 + D) K_1, \tag{6.45}$$

where K_1 is the function defined by (6.40) and (6.42) and (1 + D) is an approximation factor.

The function D(ρ, m) has the expression /271

$$\begin{aligned}
D_1 &= \frac{n-1}{2n}\frac{5(n-1)}{4{,}08}[d(\beta)+1]-\frac{5(n-1)-\rho'}{5(n-1)\,d(\beta)}, \\
&\rho' \leqslant 5(n-1) \leqslant \frac{4.08}{1+3\operatorname{tg}\beta}; \\
D_2 &= \frac{n-1}{2n}[d(\beta)+1]\frac{\rho'}{4.08}, \quad 5(n-1) \leqslant \rho' \leqslant \frac{4.08}{1+3\operatorname{tg}\beta}; \\
D_3 &= \frac{n-1}{2n}\frac{d(\beta)+1}{1+3\operatorname{tg}\beta}, \quad \frac{4.08}{1+3\operatorname{tg}\beta} \leqslant \rho' \leqslant \frac{4.08}{1+\operatorname{tg}\beta}; \\
D_4 &= \frac{n-1}{2n}\frac{d(\beta)+1}{d(\beta)}\frac{40.8}{\rho'}, \quad \rho' > \frac{4.08}{1+\operatorname{tg}\beta}; \\
d(\beta) &= (1+\operatorname{tg}\beta)(1+3\operatorname{tg}\beta).
\end{aligned} \tag{6.46}$$

The values of ρ' and β are determined by formulas (6.42).

It is shown in [489] that the functions K(ρ, m) obtained with (6.45) and (6.46) approximate the calculated data of Johnson and

Terrell [470], which were obtained with the exact Mie formulas, with an error no greater than 4%. We note that $K(\rho, m)$ was calculated up to $\rho = 17.5$ in [470]. Our comparison of the results of calculations by formulas (6.45) and (6.46) and by the asymptotic formula (6.38) showed that this accuracy of approximation is maintained for $\rho > 17.5$.

2. Scattering indicatrices. The notion of the scattering coefficient of a particle in a given direction can be introduced to characterize the properties of a particle that scatters radiation at various angles from the direction of the incident wave. On the other hand, the concept of the scattering indicatrix $f(\theta)$ or the angular scattering function is used most frequently in practice to characterize the spatial pattern of radiation scattering by a particle; it is given by the ratio of the radiant intensity scattered by the particle in a given direction to the energy flux scattered in all directions:

$$f(\theta) = \frac{I(\theta)}{\int\limits_{4\pi} I(\theta)\, d\omega}, \qquad (6.47)$$

where $I(\theta)$ is the intensity of the light scattered by the particle in the direction of the angle θ and $d\omega$ is an elementary solid angle.

Rather many papers, a bibliography of which can be found in the monographs [461, 467, and 1], have been devoted to calculations of the scattering indicatrices of spherical particles of various sizes and for various wavelengths in the visible and infrared spectra. /272

Particle scattering indicatrices have now been calculated for various realistic refractive-index values. Calculations have been made only recently for particles with a complex refractive index in a broad range of variation of both the refractive index and the absorption index. The most complete and sufficiently accurate data have been obtained by K.S. Shifrin and I.L. Zel'manovich [481, 482].

Angular scattering functions have been tabulated in [481] for angle values 0° (0.1°) 5° (1°) 90°, and in the region of the primary rainbow at 135-140° with a 0.2° step. Reference [482] gives values of all scattering-matrix components and the components of the field of the scattered wave for the water droplet in the visible and infrared regions. The tables of [482] can be used to find all characteristics of the scattered field, including the scattering indicatrix, degree of polarization, and degree of polarization ellipticity. The tables of [482] contain the data indicated above for 12 bands of the spectrum in the wavelength

range from 0.4 to 12 μ. The wavelengths are so selected as to cover, with a certain approximation, the components of the complex refractive index of water throughout the entire range.

All scattered-field characteristics were calculated for 51 values of the parameter ρ = 0.5 (0.5) 6 (1) 20 (2) 50 (5) 100 and 43 values of the scattering angle θ = 0, 0.5, 0.1, 0.2, 0.5, 1, 2, 5, 10 (10) 130, 135 (0.5) 140 (10) 170, 175, 178, 179, 179.5, 179.8, 179.9, 179.95, and 180°. Thus, highly detailed data have been obtained for small forward and backward scattering angles.

We note that the values of Δλ given by the authors of [482] require substantial correction according to the new data obtained in our study (see Chapter 7) and listed in Appendix 2 on the components n and κ of the complex refractive index of water.

Penndorf [490] analyzed the behavior of the function $i_1 + i_2$ that appears in the expressions for the attenuation coefficient and scattering indicatrix of a particle for angles θ = 0, 90, and 180° at m = 1.33. As a result, he detected strong oscillations of this function with ρ. The frequency and amplitude of these oscillations increase with increasing angle θ. Thus, if the oscillation amplitude at θ = 0 is taken as 0.1, it increases to 5 and 500 for angles of 90 and 180°, respectively. We note that observation of these oscillations became possible as a result of calculations with a very small step Δρ = 0.1. /273

Let us examine the analytical representations of the spherical-particle scattering indicatrix. Clark [491] represented the scattering indicatrix in terms of Legendre polynomials $P_n(\cos\theta)$:

$$f(\theta) = 1 + \sum_{n=1}^{\infty} a_n(\rho) P_n(\cos\theta) \qquad (6.48)$$

and calculated the coefficients $a_n(\rho)$ for values of ρ from 1 to 30 and m = 1.33.

K.S. Shifrin obtained the following approximate formula in [467] for the scattering indicatrix of large particles:

$$f(\theta) = \frac{1}{2}\left[\frac{\tau(\theta)}{2} + \rho^2(1+\cos\theta)^2 \frac{J_1^2(\rho\sin\theta)}{(\rho\sin\theta)^2}\right], \qquad (6.49)$$

where τ(θ) is the part of the indicatrix due to geometrical-optical beams, which was calculated in [467] with a step Δθ = 5° for spheres with m = 1.33, and J_1 is a Bessel function.

In conclusion, let us describe the qualitative variation of the spherical-particle indicatrix as a function of particle size and the components of the complex refractive index. Small particles with $m \sim 1$ and $\rho \to 0$ have a symmetrical Rayleigh indicatrix; small particles with $m = \infty$ reflect much more radiation backward than forward. We note that different authors have taken values of m in the range 1.33-1.5 [423, 492, 820] for atmospheric aerosols in the visible region of the spectrum.

As ρ increases from 0 to ∞, the scattering indicatrix of atmospheric-aerosol particles changes shape continuously, becoming increasingly asymmetrical and elongated in the forward direction (the Mie effect). The following numerical example is given in [492] to illustrate this circumstance. For particles with $m = 1.5$ and radii $a = 0.5$, 1.5, 5.0, and 12.5 μ, the ratio of the radiant fluxes with wavelength 0.5 μ ($\rho = 6.28$, 18.84, 62.8, and 157) that are scattered forward and backward equals 17, 74, 823, and 16,000. This ratio is often called the asymmetry coefficient of the indicatrix.

This pattern of scattering-indicatrix variation with atmospheric-aerosol particle size is strongly influenced by the complexity of the particle refractive index and Penndorf's oscillations of the intensity of the radiation scattered at various angles, which depend on θ, ρ, and m. /274

7. SCATTERING OF LIGHT BY NONSPHERICAL PARTICLES

Although many investigators have noted that the shapes of most atmospheric aerosols can be represented by spheres, this problem still merits special attention, because particles of dust, ice crystals, and particles of crystalline clouds actually have arbitrary shapes. It is important to know how the optical properties of the particles are influenced by their shape. Results in this problem have been obtained in considerable volume and are collected in the monograph of H. van de Hulst [461] (ellipsoids, circular cylinders, circular disks, and particles of other shapes with various ρ and m and various orientations relative to the incident radiation). K.S. Shifrin [467] investigated the optical characteristics of rod- and disk-shaped particles, which were approximated by ellipsoids.

Analysis of the available results indicates that the optical characteristics of variously shaped particles depend strongly on the ratio of the maximum and minimum particle dimensions, their orientation relative to the incident radiation, the degree of the latter's polarization, and the value of the complex refractive index. For example, for a strongly elongated transparent rod all of whose linear dimensions are much smaller than the wavelength, the ratio of the scattering coefficients for orientation against the field and with the field is 6.25 for $m = 2$ and 1.64 for $m = 1.64$ [461]. Naturally, the ratios will be different for a

similar absorbing rod. A change in the dimensions of the rod results in corresponding changes in this ratio.

The optical characteristics of variously shaped particles may differ strongly from those of a spherical particle of the same volume. It is therefore always necessary to exercise caution in applying the results of the Mie theory to nonspherical particles. At the same time, if the particle shape does not differ very greatly from spherical (for example, ellipsoids with semiaxis ratios smaller than 1.5-2, cubes, cylinders with near-unity ratios of height to diameter, etc.), then such characteristics of the /275
particle as its scattering indicatrix and attenuation, scattering, and absorption coefficients differ little from the corresponding characteristics of the spherical particle of equal volume.

We take note of one practically important way to use the results of the Mie theory for nonspherical particles. If some optical characteristic of the particle is averaged over all possible particle spatial orientations, its volume can then be expressed analytically in terms of the volume of a spherical particle with the same optical characteristic. K.S. Shifrin [467] obtained such a relation for the scattering indicatrix of ellipsoidal particles:

$$v^* = \sqrt{\varphi(t)}\, v,$$

where v* and v are the respective volumes of the sphere and ellipsoid whose scattering indicatrices coincide, t = a/b is the semiaxis ratio of the ellipsoid, and $\phi(t)$ is a function that has been tabulated in [464] and assumes values from 1 to 0.23 as t varies from 1 to 10. For example, $\phi(t) = 0.93$ and 0.71 at t = 2 and 3.

Relationships of this kind can be derived for various scattering characteristics and for particles of other shapes.

Chapter 7 /276

SCATTERING OF VISIBLE AND INFRARED WAVES IN THE ATMOSPHERE

The scattering of visible and infrared waves in the earth's atmosphere is due primarily to density fluctuations of the air and to aerosol particles. In the former case, we deal with molecular or Rayleigh scattering, and in the latter with aerosol scattering. In addition, at least two more types of scattering may occur in the atmosphere: scattering on small-scale and large-scale inhomogeneities due to turbulent motions of the air and Raman scattering. However, neither of these types of scattering makes a substantial contribution to the attenuation of visible and infrared radiation in the atmosphere as compared with the first two. In this chapter, which is devoted chiefly to description of the energy losses sustained by electromagnetic waves in the atmosphere, we shall therefore not concern ourselves with the phenomena of scattering of turbulent inhomogeneities or Raman scattering.

Molecular scattering has been quite thoroughly studied. Extensive tables of scattering coefficients in the visible and infrared have now been compiled; they enable us to determine quantitatively and quite accurately the energy losses of waves propagating in any direction in the atmosphere. In describing molecular scattering, we shall therefore confine ourselves for the most part to certain tabulated data on the scattering coefficients and optical thicknesses of the Rayleigh atmosphere.

In speaking of aerosol scattering, we generally have in mind not only the scattering, but also the absorption of wave energy by the particles. It would therefore be more correct to speak of aerosol attenuation, which is governed both by the scattering phenomenon and by the phenomenon of absorption of radiant flux by aerosol particles.

Despite the diversity of size spectra and the broad ranges /277
of variation of the concentration and chemical composition of atmospheric-aerosol particles, certain characteristic types of aerosols that differ substantially in their ability to scatter electromagnetic waves in the optical band can be distinguished. Foremost among these types are clouds, fogs, and hazes. It is therefore no accident that much of the chapter's material is devoted to discussion of the scattering of visible and infrared waves by these aerosols. Further, although precipitation cannot be classed as an aerosol, the attenuation of radiation on passage through it is also covered in this chapter, since the nature of wave scattering on particles of precipitation is the same as that on particles

of hazes, clouds, and fogs.

1. MOLECULAR SCATTERING OF VISIBLE AND INFRARED WAVES

The Cabannes-Rayleigh theory of molecular scattering of light yields the following expression for the scattering coefficient in gases:

$$\sigma_{RGH}(\lambda)=\frac{8\pi^3(n^2-1)^2}{3N\lambda^4}\frac{6+3\delta}{6-7\delta}, \qquad (7.1)$$

where N is the number of molecules per unit volume, n is the refractive index of the medium, λ is the wavelength of the radiation, and δ is the depolarization factor of the scattered radiation, which equals 0.035 according to recent measurements [447]. /278

TABLE 7.1. COEFFICIENTS OF MOLECULAR SCATTERING σ_{RGH} AT TEMPERATURE t = 15°C AND PRESSURE P = 1013 mbar. OPTICAL THICKNESSES τ_{RGH} OF A VERTICAL LAYER OF THE ENTIRE ATMOSPHERE. SOURCE: [493] and [494]

Wavelength λ,μ	σ_{RGH}, km^{-1}	τ_{RGH}	Wavelength λ,μ	σ_{RGH}, km^{-1}	τ_{RGH}
0,30	$1,446\cdot10^{-1}$	1,2237	0,65	5,893	0,0499
0,32	1,098	0,9290	0,70	4,364	0,0369
0,34	$8,494\cdot10^{-2}$	0,7188	0,80	2,545	0,0215
0,36	6,680	0,5653	0,90	1,583	0,0134
0,38	5,327	0,4508	1,06	$8,458\cdot10^{-4}$	0,0072
0,40	4,303	0,3641	1,26	$4,076\cdot10^{-4}$	0,0034
0,45	2,644	0,2238	1,67	$1,327\cdot10^{-4}$	0,0011
0,50	1,716	0,1452	2,17	$4,586\cdot10^{-5}$	0,0004
0,55	1,162	0,0984	3,50	$6,830\cdot10^{-6}$	0,0001
0,60	$8,157\cdot10^{-3}$	0,0690	4,00	4,002	0,0000

Note: Commas represent decimal points.

Penndorf [493] calculated the molecular scattering coefficients for various wavelengths in the range from 0.2 to 20 μ by formula (7.1). The data obtained in [493] can be used to calculate the molecular-scattering optical thicknesses τ_{RGH} for various geometrical thicknesses of the atmosphere.

Tables 7.1 and 7.2 present data on the coefficients σ_{RGH} and τ_{RGH} for various wavelengths and geometrical atmospheric thicknesses. We note that the Rayleigh-scattering coefficient

TABLE 7.2. COEFFICIENTS σ_{RGH} FOR VARIOUS HEIGHTS z AND THE OPTICAL THICKNESSES τ_{RGH} OF LAYERS OF ATMOSPHERE (z-∞) FOR WAVELENGTHS λ = 0.30, 0.55, and 1.06 μ, ACCORDING TO [447]

Hgt. z, km	$\lambda = 0.30\mu$		$\lambda = 0.55\mu$		$\lambda = 1.06\mu$	
	σ_{RGH}, km^{-1}	$\tau_{RGH} \times (z-\infty)$	σ_{RGH}, km^{-1}	$\tau_{RGH} \times (z-\infty)$	σ_{RGH}, km^{-1}	$\tau_{RGH} \times (z-\infty)$
0	$1.446 \cdot 10^{-1}$	1.2237	$1.162 \cdot 10^{-2}$	0.0984	$8.458 \cdot 10^{-4}$	0.0072
5	$8.693 \cdot 10^{-2}$	0.6538	$6.988 \cdot 10^{-3}$	0.0526	5.085	0.0038
10	4.881	0.3212	3.924	0.0258	2.855	0.0019
15	2.999	0.1471	1.848	0.0118	1.345	0.0009
20	1.049	0.0672	$8.436 \cdot 10^{-4}$	0.0054	$6.138 \cdot 10^{-5}$	0.0004
30	$2.173 \cdot 10^{-3}$	0.0146	1.747	0.0012	1.271	0.0001
40	$4.716 \cdot 10^{-4}$	0.0035	$3.791 \cdot 10^{-5}$	0.0003	$2.758 \cdot 10^{-6}$	0.0000
50	1.212	0.0010	$9.743 \cdot 10^{-6}$	0.0001	$7.089 \cdot 10^{-7}$	0.0000

calculated by (7.1) has the dimensions of reciprocal length.

2. SCATTERING OF WAVES BY A SYSTEM OF PARTICLES

The exact electrodynamic formulation of the problem of wave scattering by a system of particles, methods of its solution, and certain results that have already been obtained have been discussed quite broadly in the literature (see, for example, [494]-[503]). The methodological crux of the solution of this problem consists in the following. It is assumed that the solution of the single-particle light-scattering problem is known and that all unknown physical quantities can be obtained after appropriate statistical averaging over the particle positions.

A certain field composed of the field of the wave incident upon the particle system and the fields scattered by the individual particles exists in the particle-filled medium. The scattered fields are written on the basis of the familiar solution, with each particle subject to the action of its own so-called effective field. We may therefore write

$$\left.\begin{aligned} \psi(\vec{r}) &= \psi_0(\vec{r}) + \sum_{j=1}^{N} T(\vec{r}, \vec{r}_j)\,\tilde{\psi}(\vec{r}_j), \\ \tilde{\psi}(\vec{r}_j) &= \psi_0(\vec{r}) + \sum_{j' \neq j} T(\vec{r}_j, \vec{r}_{j'})\,\tilde{\psi}(\vec{r}_{j'}), \end{aligned}\right\} \qquad (7.2)$$

where ψ is a certain component of the field, $\vec{r}_j$ are the coordinates of the j-th particle, ψ_0 is the corresponding component of the incident wave, $\vec{r}$ is the radius vector of an arbitrary point, T is the scattering operator, and $\tilde{\psi}$ is the effective field. The

first equation in (7.2) gives the magnitude of the field in the medium, while the second represents essentially a system of equations for determining the values of the effective fields acting on individual particles. The sum in (7.2) defines a fixed scattering-particle configuration.

The next step consists in averaging Eqs. (7.2) over all configurations. Formally, this is done by multiplying both sides of the equations by the configuration distribution function and integrating with respect to the corresponding variables. Here the configuration distribution function depends strongly in the general case on the nature of particle interaction. In general form, the corresponding calculations can be carried through to completion if the particles are assumed to be noninteracting (ideal-gas-type model) or if we confine ourselves to the first terms of the expansion in Virial coefficients. It is also necessary to assume that the distances between particles are substantially greater than the length of the light wave in order to be able to use the asymptotic form of the scattering operator in the wave zone. We note further that the effective field is usually assumed equal to the average field at the position of the particle, since the two fields differ by an amount of the order of 1/N, where N is the number of particles. This assumption makes it possible to analyze only one equation for the average field.

The question as to the intensity of the light is handled in the identical manner. In the scalar variant, this quantity can be defined as $|\psi|^2$. After multiplying both sides of Eqs. (7.2) by the corresponding complex-conjugate terms, the resulting expressions are again averaged over the configurations for a given distribution function. /280

If we consider noninteracting particles, the usual transfer equation is obtained for the radiant intensity in the medium; if particle interaction is taken into account in the usual manner, certain corrections to this equation result.

The relationship for the attenuation coefficient $\alpha(\lambda)$ calculated per unit of ray-path length makes its appearance automatically in such an analysis:

$$\alpha(\lambda) = N \int_0^\infty \sigma(a, \lambda) f(a)\, da, \qquad (7.3)$$

where N is the number of particles per unit volume, $\sigma(a, \lambda)$ is the attenuation coefficient for radiation with wavelength λ and a particle of radius a (here and below, the scattering particles are assumed spherical), and f(a) is the particle size distribution function, whose sense is defined by the relation $N_a da = Nf(a)da$,

where N_a is the number of particles having radii in the range from a to a + da.

The origins of formula (7.3) are easily traced with the aid of the optical theorem (see §2 of Chapter 6). The attenuation coefficient of a certain volume can be determined by the scheme described in §3 of Chapter 6 for finding the screening coefficient. This gives us the relation $\alpha = 4\pi/k^2 \operatorname{Im} A$, where A is the amplitude of the field scattered forward by all particles. In virtue of the superposition principle, $A = \sum A_j$, where A_j is the amplitude of the wave scattered forward by the j-th particle. The combination of the last two relations together with (6.20) indicates that $\alpha = \sum \sigma_j$, where σ_j is the attenuation coefficient of the j-th particle. On introduction of the distribution function f(a), this last sum can be written in the form of (7.3).

Relation (7.3) and the equality $\sigma(\lambda, a) = \sigma_s(\lambda, a) + \sigma_a(\lambda, a)$, where σ_s and σ_a are the scattering and absorption coefficients for radiation with wavelength λ and a particle of radius a, automatically yield expressions for the polydisperse scattering $\alpha_s(\lambda)$ and absorption $\alpha_a(\lambda)$ coefficients: /281

$$\alpha_s(\lambda) = N \int_0^\infty \sigma_s(\lambda, a) f(a)\, da, \tag{7.4}$$

$$\alpha_a(\lambda) = N \int_0^\infty \sigma_a(\lambda, a) f(a)\, da. \tag{7.5}$$

The equation for the change in the intensity I of radiation propagating on a certain path can be written in the usual manner with the coefficient $\alpha(\lambda)$:

$$dI(\lambda) = -I(\lambda)\alpha(\lambda)\, dl. \tag{7.6}$$

Integration of (7.6) yields the familiar relation for the aerosol component of atmospheric transparency:

$$T(\lambda) = I/I_0,$$

where I_0 is the intensity of the radiation at the start of the path:

$$T(\lambda) = \exp\left(-\int_{(l)} \alpha(\lambda, l)\, dl\right). \qquad (7.7)$$

The integration in (7.7) is performed by points on the path, and $\alpha(\lambda)$ generally varies along the ray path. This variation results from the corresponding changes in the size spectrum and concentration of the particles.

Relation (7.7) describes the intensity variation of information-carrying direct radiation. We note that it is impossible to register only the direct radiation experimentally, since this would require receivers with zero angular aperture. Generally speaking, the angular aperture of the receiving system can be made as small as we please, but not zero. As a result, receiving systems always register, along with the direct radiation attenuated in accordance with (7.7), light that has been singly and multiply scattered by aerosol particles and is to be regarded as one of the background noises. This fact causes the measured values (scattering coefficient, $T(\lambda)$, and others) to depend on the conditions of the experiment.

3. INVESTIGATIONS OF THE SCATTERING MATRIX

/282

As we have noted in §2 of Chapter 6, the scattering matrix M contains complete information on the light field scattered by the particles. Knowledge of the components of this matrix permits quantitative solution of any problem involving scattering of waves by particles.

Despite the obvious importance of the problem of investigating the matrix M for atmospheric aerosols, the amount of data obtained thus far on the components of this matrix is inadequate. On the one hand, this situation is explained by the complexity of the corresponding investigations, both theoretical and experimental, and, on the other hand, the scattering-matrix components are not needed for solution of many practical problems. For example, it is sufficient to know the scattering or attenuation coefficients in many cases.

The matrix M has its simplest form in the case of molecular scattering:

$$M(\theta) = \frac{3}{4+3d}\begin{pmatrix} 1+\cos^2\theta+d & -\sin\theta & 0 & 0 \\ -\sin^2\theta & 1+\cos^2\theta & 0 & 0 \\ 0 & 0 & 2\cos\theta & 0 \\ 0 & 0 & 0 & 2\cos\theta \end{pmatrix}. \qquad (7.8)$$

Generally speaking, the matrix M may have all 16 components different in the scattering of radiation by atmospheric-aerosol particles. However, the symmetry of various particles and of their spatial orientation reduces the number of independent components of the matrix and causes some of them to vanish. Thus, the matrix M has the following form for spherical particles [504]:

$$M(\theta) = \begin{pmatrix} M_{11} & M_{12} & 0 & 0 \\ M_{21} & M_{22} & 0 & 0 \\ 0 & 0 & M_{33} & M_{34} \\ 0 & 0 & M_{43} & M_{44} \end{pmatrix}, \qquad (7.9)$$

where $M_{11} = M_{22}$, $M_{12} = M_{21}$, $M_{33} = M_{44}$, $M_{34} = M_{43}$. Thus, there are only four independent components for particles of spherical shape, and these can be calculated using the appropriate formulas of the Mie theory. An example of a calculation of this kind is found in V.S. Malkova's paper [505], in which all four components of $M(\theta)$ were calculated for values of ρ from 0.1 to 1.0, $\theta = 0(5)180°$, and 13 values of the complex refractive index of water that are characteristic for the wavelength range from 2 to 12 μ. /283

The most complete experimental data on the scattering-matrix components were obtained by G.V. Rozenberg's group [16, 506, 507, 897, 898], which began the corresponding investigations in the ground layer of the atmosphere in 1959, using specially developed equipment. Reduction of a large number of measurements made in various segments of the spectrum under various sets of meteorological conditions enabled G.V. Rozenberg et al. to obtain quantitative data on all components of the matrix M. Analyzing these data, they were able to draw important conclusions concerning the presence of typical aerosol states in the ground layer of the atmosphere (fog, foggy haze, haze with drizzle, and simple haze). A unique set of angular dependences of the components of matrix M corresponds to each of these states. Here we refer not to specific dependences of the components on the angle θ, but of sets, since G.V. Rozenberg et al. actually obtained data for various specific conditions each of which may compare to a greater or lesser degree with the condition characteristic for one of the above four aerosol states of the atmosphere's ground layer.

4. ENERGY CHARACTERISTICS OF SCATTERING OF VISIBLE AND INFRARED WAVES BY CLOUDS AND FOGS

In solving many problems in the propagation of visible and infrared waves in clouds and fogs, it is necessary first of all to know what fraction of the radiant flux incident on the layer is diverted by this layer from its original direction through aerosol attenuation, i.e., by scattering and absorption by particles of the layer. To answer this question, it is necessary to have the attenuation coefficients $\alpha(\lambda)$. For this reason, the present

section concentrates its attention on this quantity for water clouds and fogs. Data on the coefficients $\alpha(\lambda)$ for supercooled and crystalline clouds and fogs have not yet been obtained.

1. Analytical expressions for the attenuation coefficient and the averaged attenuation factor. Let f(a) be the size-distribution function of the particles of a cloud or fog. Then, assuming that we are dealing with spherical particles, we may write for the coefficient $\alpha(\lambda)$ and the geometrical cross section Q of particles of unit volume /284

$$\alpha(\lambda) = N\int_0^\infty \pi a^2 K(\rho, m) f(a)\, da, \tag{7.10}$$

$$Q = N\int_0^\infty \pi a^2 f(a)\, da. \tag{7.11}$$

The quantity

$$F = \frac{\alpha(\lambda)}{Q} = \frac{\int_0^\infty \pi a^2 K(\rho, m) f(a)\, da}{\int_0^\infty \pi a^2 f(a)\, da} \tag{7.12}$$

will be called the averaged attenuation efficiency factor. This name is justified by relation (7.12), which defines F as the ordinary statistical mean of the attenuation efficiency factor for a single particle $K(\rho, m)$ with a density function $\pi a^2 f(a)$. The function F is numerically equal to the ratio of the optical cross section of the particles in a unit volume to the geometrical cross-section.

As we see from (7.12), the function F does not depend on N and characterizes the volume attenuation coefficient accurate to within a constant multiplier. The values of F are determined by m and λ (F depends on λ through $\rho = 2\pi a/\lambda$). The relation

$$\frac{F(\lambda_1, m)}{F(\lambda_2, m)} = \frac{\alpha(\lambda_1)}{\alpha(\lambda_2)}, \tag{7.13}$$

follows directly from (7.10) and (7.12) and is valid for given f(a) and r.

The volume attenuation coefficients $\alpha(\lambda)$ and the averaged attenuation efficiency factors $F(\lambda, m)$ are fundamental quantitative characteristics of the attenuation of radiation by polydisperse aerosols. Naturally, the form of the expressions for $\alpha(\lambda)$ and $F(\lambda, m)$ depends strongly on the form of the particle size distribution function. /285

To ascertain the influence of the form of f(a) on the numerical values of $F(\lambda, m)$, we used methods that will be set forth below to calculate values of F with the logarithmically normal and gamma distributions taken for f(a). As we have noted, both of these distributions approximate satisfactorily the experimental curves of the particle-size spectra for clouds and fogs. The calculation showed that either distribution can be used in calculating the function F. The choice between (5.3) and (5.4) for f(a) depends on the specific problem.

A formula for the function F that is valid for all values of the parameter ρ and $m = 1.33$ was obtained by L.M. Levin [508] on the basis of an approximating expression that he proposed for the function $K(\rho)$ and the gamma distribution as the function f(a).

Using the van de Hulst [461] approximate expression (6.42) for $K(\rho, m)$ and the gamma distribution for the function f(a), K.S. Shifrin and V.F. Raskin [509] obtained a formula for the polydisperse scattering coefficient of "soft" transparent particles.

The spectral transparencies of water clouds and fogs in the visible region and for those parts of the infrared where the complex nature of the refractive index of water can be disregarded are easily calculated with the tables given in [509].

Using his approximating expressions (6.45) and (6.46) for $K(\rho, m)$, Deirmenjian [489] calculated coefficients $\alpha(\lambda)$ with consideration of the complex nature of the water refractive index in the infrared and obtained values of $\alpha(\lambda)$ for one cloud model in the visible and infrared regions up to a wavelength $\lambda = 13\ \mu$.

Using the logarithmically normal law as the aerosol particle distribution function, S.D. Tvorogov [510] demonstrated that the function F is in this case a solution of a parabolic-type equation with a defined initial condition. Reference [510] gives three parabolic equations, each with its own initial conditions, which are satisfied by the function F.

We stress that no limitations whatever are imposed on the function $K(\rho, m)$ in the proof of this statement. Thus the basic conclusion of [510] remains in force if the function $K(\rho, m)$ is replaced by the scattering or absorption efficiency, the scattering indicatrix, or any other component of the scattering matrix. In this sense, the result obtained in [510] is universal. /286

In [511] and [512], S.D. Tvorogov developed methods for solving the parabolic equations that he had derived in [510]. The results of [510-512] can be used to calculate any averaged scattering-matrix component.

Analytical expressions were obtained in our papers [513-515] for the function F, using the gamma distribution as the function

f(a). We present the formulas for the function F:

$$F=\frac{\int_0^\infty \tau^2 f(\tau) K(x\tau, m)\, d\tau}{\int_0^\infty \tau^2 f(\tau)\, d\tau}=F(x, \mu, m), \tag{7.14}$$

where

$$\tau=\frac{a}{r}, \quad x=\frac{2\pi r}{\lambda}, \tag{7.15}$$

r and μ are the parameters of the gamma distribution.

Expression (7.14) follows directly from (7.12) when (7.15) is applied.

Substituting (5.4) into (7.14), we obtain

$$F(x, \mu, m)=\frac{\mu^{\mu+3}}{\Gamma(\mu+3)}\int_0^\infty \tau^{\mu+2} e^{-\mu\tau} K(x\tau, m)\, d\tau. \tag{7.16}$$

If we now substitute (6.36)-(6.42) for the function K(ρ, m) = = K(xτ, m), into (7.16), we can easily obtain concrete formulas for F(x, μ, m) for various cases. Omitting the derivation, we present here only the expression for F(x, m, μ) that will be used below, which is obtained on substitution into (7.16) of formulas (6.40) and (6.41), which describe the function K(xτ, m) in the case of "soft" large particles: /287

$$F(x, \mu, m)=2-\frac{4}{\mu+2}\frac{\sin[(\mu+2)\varphi-\beta][\cos(\varphi+\beta)]^{\mu+3}}{\sin\varphi[\cos\beta]^{\mu+2}}- \\ -\frac{4}{(\mu+2)(\mu+1)}\frac{\cos[(\mu+1)\varphi-2\beta][\cos(\varphi+\beta)]^{\mu+3}}{\sin^2\varphi[\cos\beta]^{\mu+1}}+ \\ +\frac{4\cos^2\beta\cos^2(\varphi+\beta)}{(\mu+2)(\mu+1)\sin^2\varphi}; \tag{7.17}$$

$$\operatorname{tg}\varphi=\frac{u}{1+u\operatorname{tg}\beta}; \quad \operatorname{tg}\beta=\frac{\varkappa}{n-1}; \quad u=\frac{x'}{\mu}; \quad x'=2x(n-1). \tag{7.18}$$

In the particular case of real m, we obtain from (7.17) and (7.18)

$$F(x, \mu, m) = 2 - \frac{4}{(\mu+2)} \frac{\sin[(\mu+2)\varphi][\cos\varphi]^{\mu+3}}{\sin\varphi} -$$
$$- \frac{4}{(\mu+2)(\mu+1)} \frac{\cos[(\mu+1)\varphi][\cos\varphi]^{\mu+3}}{\sin^2\varphi} + \frac{4\operatorname{ctg}^2\varphi}{(\mu+2)(\mu+1)}, \qquad (7.19)$$

where

$$\operatorname{tg}\varphi = u = \frac{2}{\mu} x(n-1).$$

Formula (7.19) is also given in [509].

We note the following limit relations:

$$\lim_{x\to\infty} F(x, \mu, m) = 2, \quad \lim_{\mu\to 0} F(x, \mu, m) = 2,$$
$$\lim_{\mu\to\infty} F(x, \mu, m) = K(x, m). \qquad (7.20)$$

Let us now consider the approximate method that we proposed in [513, 514] for calculating the averaged efficiency factor for attenuation of radiation by water clouds and fogs in the visible and infrared regions. The method assumes consideration of the complexity of the refractive index of water and the real particle-size spectra of the clouds and fogs, as described by the gamma distribution. The method is based on use of expressions (6.45)-(6.46) for the single-particle attenuation efficiency K(ρ, m) obtained by Deirmenjian [489] by an approximation method.

Substituting (6.45) and (6.46) into (7.16), we obtain

$$F(x, \mu, m) = F_1(x, \mu, m) + F_2(x, \mu, m). \qquad (7.21)$$

Here the function F_1 is determined by expressions (7.17) and (7.18), and /288

$$F_2(x, \mu, m) = \frac{\mu^{\mu+3}}{\Gamma(\mu+3)} \sum_{j=1}^{4} \int_{h_j}^{h_{j+1}} D_j(x'\tau_m) \times$$
$$\times K(x'\tau, m)\, \tau^{\mu+2} e^{-\mu\tau} d\tau, \qquad (7.22)$$

where

$$h_1 = 0; \quad h_2 = 5(n-1); \quad h_3 = \frac{4{,}08}{1+3\operatorname{tg}\beta}; \quad h_4 = \frac{4{,}08}{1+\operatorname{tg}\beta}; \quad h_5 = \infty.$$

We tabulated the function F for various values of ϕ, β, and μ, which were so selected that the range of their variations ensured acquisition of volumetric coefficients for the attenuation of visible and infrared radiation by clouds and fogs with the wide variety of microstructural characteristics encountered under natural conditions.

Since $D(x'\tau)$ is a continuous function, the expression for F_2 can be written in terms of F_1 and D after application of the law of the mean to (7.22):

$$F_2(x, \mu, m) = F_1(x, \mu, m) D(x', \tau, m), \tag{7.23}$$

where $\bar{\tau}$ is a quantity that depends, generally speaking, on n, β, μ, and x'.

The function F_2 was calculated by (7.22) using numerical integration for various x', μ, β, and n, and then τ was found from (7.23). It was found that the results of calculation by (7.22) and (7.23) agree within 5% if we set

$$\bar{\tau} = \frac{\mu+3}{\mu}. \tag{7.24}$$

Thus, substituting (7.23) into (7.21), we finally obtain for F

$$F(x, \mu, m) = F_1(x, \mu, m)[1 + D(x'\tau, m)]. \tag{7.25}$$

We used expressions (7.25) and (7.24) to calculate the function $F(x, \mu, m)$ and the volumetric attenuation efficiencies $\alpha(\lambda)$ for clouds and fogs. Our estimates indicated that the approximate method described above gives errors no greater than 5-7% in the values of $F(x, \mu, m)$ as compared with the results obtained using the values of the function $K(\rho, m)$ tabulated in [470] by the exact formulas of the Mie theory. This accuracy is quite adequate for practical purposes and for quantitative interpretation of experimental data. /289

2. **Calculation of attenuation coefficients.** The most complete calculated data on the attenuation coefficients $\alpha(\lambda)$ for water clouds and fogs in the spectral region from 0.5 to 14 μ with consideration of the real polydisperse nature of the particles and the complexity of the refractive index were obtained in our study [516], which is described in detail in the monograph [1]. The results of Deirmenjian's calculation of $\alpha(\lambda)$ for two specific cloud models [489, 517] in the 0.45-16-μ region and L.M. Levin's calculated data [508] for various cloud models without

consideration of the complexity of the water refractive index are also analyzed in [1].

Our calculations and those of Deirmenjian were based on data on the complex refractive indices of water that were published by Centeno back in 1941 [518], which were regarded until recently as the most complete and reliable figures. However, a detailed comparison that we made of all known values of the components of the complex refractive index of water in the infrared revealed the presence of wide scatter in the data from different investigators. In view of this fact and the fact that the coefficients $\alpha(\lambda)$ depend strongly both on the real part n and the imaginary part κ of the complex refractive index of water, our laboratory undertook a new determination of these quantities. The coefficients $\alpha(\lambda)$ were recalculated on the basis of the data obtained on n and κ for various wavelengths in the range from 0.5 to 25 μ. Below we set forth concisely the results from investigation of the components of the complex refractive index of water and data from the corresponding calculations of the coefficients $\alpha(\lambda)$.

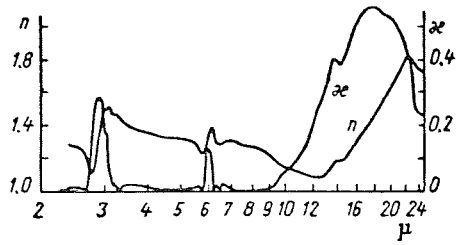

Figure 7.1. Refractive Index n and Absorption Index κ of Water as Functions of Wavelength in the Spectral Region from 2.5 to 25 μ.

1. Components of the complex refractive index of water in the spectral region from 0.5 to 25 μ. The apparatus and method used to measure the refractive and absorption indices of water in the spectral region from 0.5 to 25 μ are described in detail in our papers [519]-[521].

Figure 7.1 shows the curves obtained in [520] for the refractive index n and absorption index κ as functions of wavelength in the region of the spectrum from 2.5 to 25 μ. Figure 7.2 presents a comparison of our values of n and κ /290 in various regions of the spectrum with those of other authors.

The method used in [519]-[520] to determine κ from reflection spectra in regions of small κ did not yield satisfactory accuracy. In [521], therefore, the quantity κ was redetermined in these regions by a method based on the use of transmission spectra. In addition, the spectral range of the n and κ measurements was widened in [521]. The results appear in Figs. 7.3 and 7.4. To find the absorption-index values $\kappa(\nu)$ from known data on $\alpha(\lambda)$, it is necessary to apply the formula

$$\varkappa(\nu)=\frac{\alpha(\nu)}{4\pi\nu}. \qquad (7.26)$$

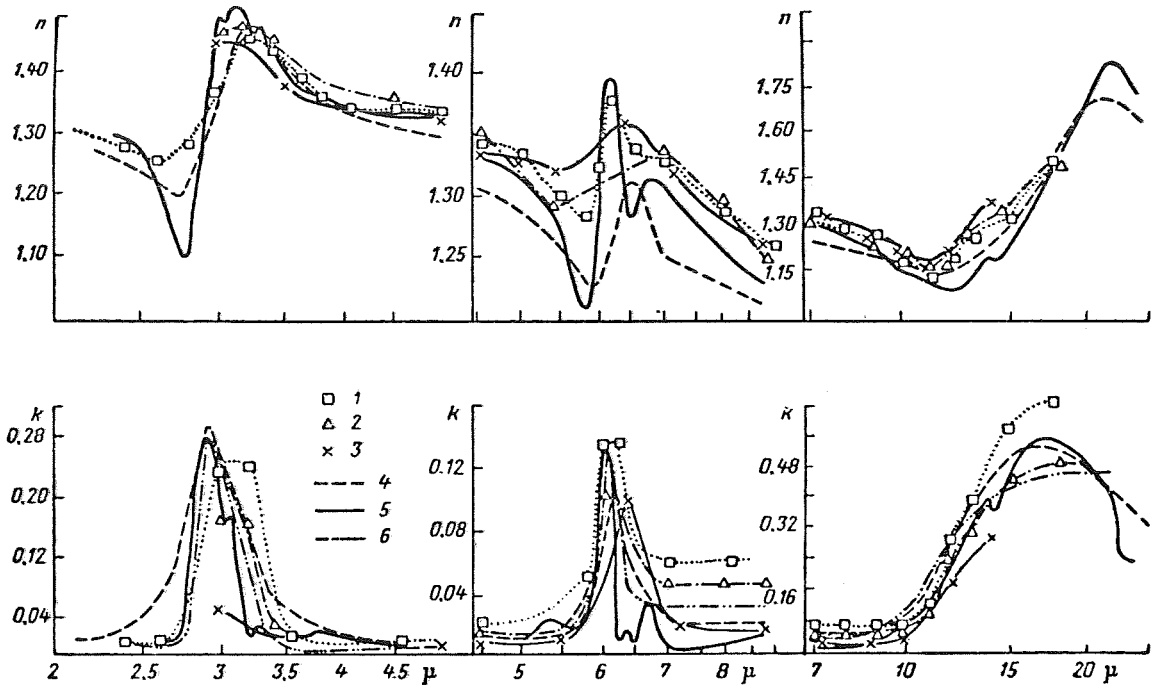

Figure 7.2. Refractive Index n and Absorption Index κ of Water in the Region from 2.5 to 25 μ: 1) [522]; 2) [467]; 3) [518]; 4) [523]; 5) [520]; 6) [524].

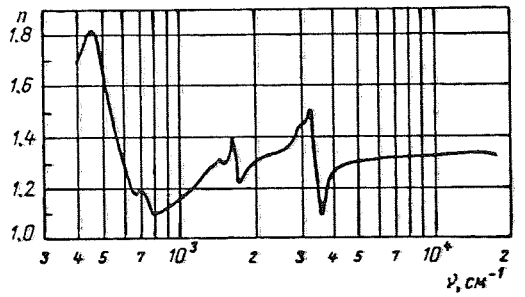

Figure 7.3. Refractive Index of Water as a Function of Wavelength in the Spectral Region from 0.5 to 25 μ.

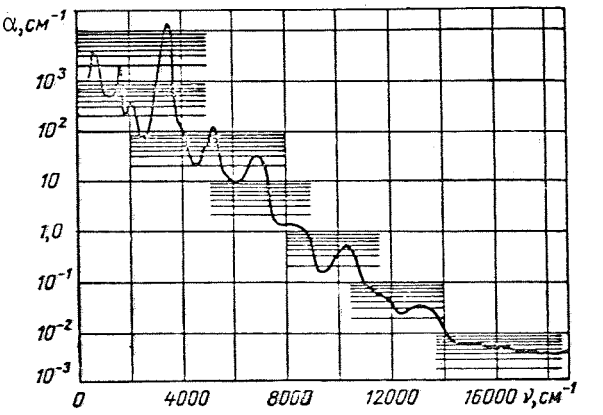

Figure 7.4. Absorption Coefficient of Water as a Function of Wavelength in the Spectral Region from 0.5 to 25 μ.

The data in Figs. 7.3 and 7.4 were determined with a relative error of no more than 1% for n and 4% for α.

In view of the trouble encountered in the use of graphs in practical work, Appendix 2 presents our detailed tabular data on

n and κ in the spectral region from 0.54 to 25 μ.

2. Attenuation coefficients. The approximate method described under 1) was used in a new series of calculations of the attenua-

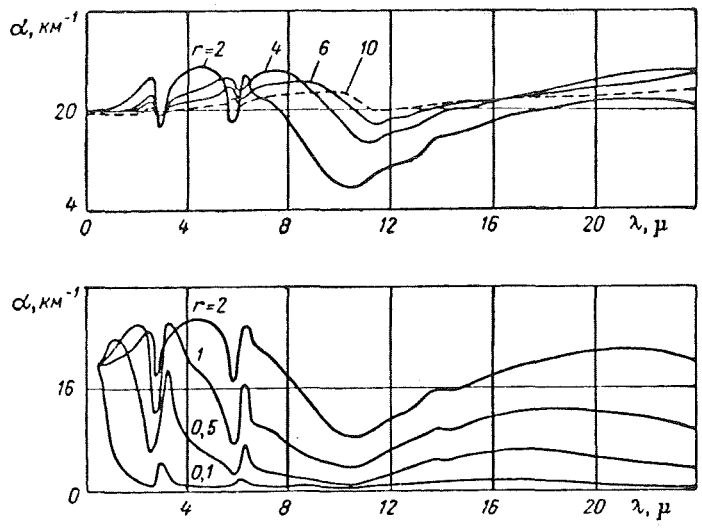

Figure 7.5. Attenuation Coefficients of Water Clouds and Fogs in the Wavelength Range from 0.5 to 25 μ for μ = 2, r = 0.1, 0.5, 1, 2, 4, 6, and 10 μ, and S_m = 0.2 km.

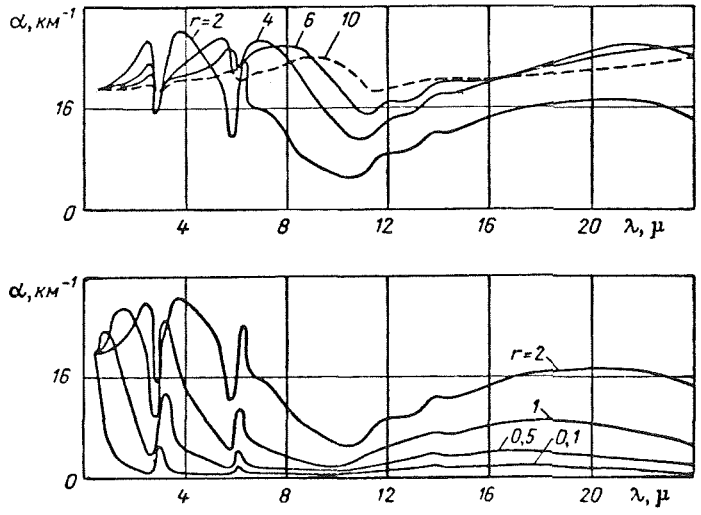

Figure 7.6. Attenuation Coefficients of Water Clouds and Fogs in the Wavelength Range from 0.5 to 25 μ for μ = 4, r = 0.1, 0.5, 1, 2, 4, 6, and 10 μ, and S_m = 0.2 km.

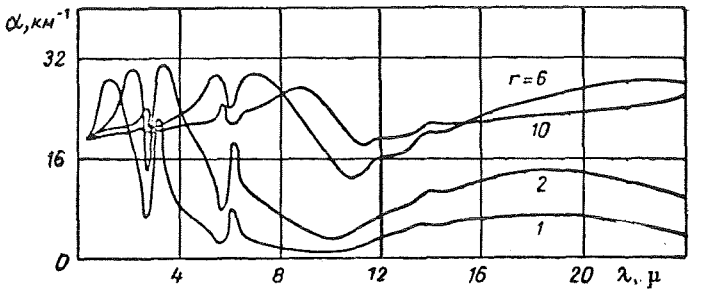

Figure 7.7. Coefficients of Attenuation of Water Clouds and Fogs in the Wavelength Range from 0.5 to 25 μ for μ = 10, r = 1, 2, 6, and 10 μ, and S_m = 0.2 km.

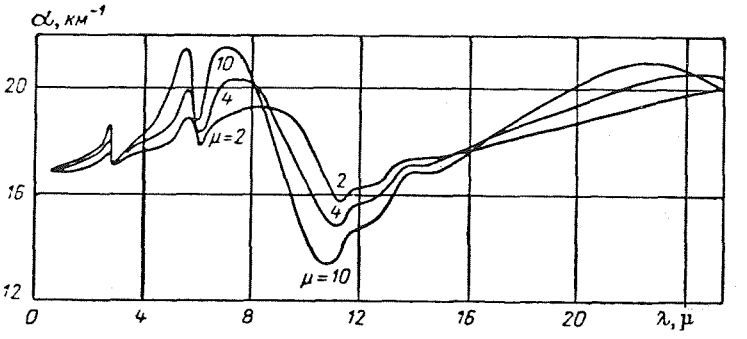

Figure 7.8. Attenuation Coefficients of Water Clouds and Fogs in the Wavelength Range from 0.5 to 25 μ at r = 6 μ, μ = 2, 4, and 10, and S_m = 0.2 km.

tion coefficient $\alpha(\lambda)$ of water clouds and fogs with consideration of the real particle-size spectra and the data that we had obtained on the components of the complex refractive index of water. The calculations were made for the following values of the microstructure parameters r (the most probable particle radius) and μ (a characteristic of the distribution half-width): 0.1, 0.5, 1.0, 2.0, 6.0, and 10.0 μ and 1, 2, 3, 6, and 10, respectively. The set of wavelengths for which $\alpha(\lambda)$ were calculated was governed by the corresponding trend of the components of the complex refractive index of water. We attempted to take account of all features of this dependence. In addition, we selected a series of wavelengths corresponding to the radiating frequencies of the most commonly used lasers. /292

The article [555] contains detailed data from our calculations. Figures 7.5-7.8 and Table 7.3 present certain illustrations of these results, which indicate the strong influence of /294

TABLE 7.3. COEFFICIENTS $\alpha(\lambda)$ FOR THE MOST PROBABLE VALUES OF CLOUD AND FOG MICROSTRUCTURE PARAMETERS AT A METEOROLOGICAL VISIBILITY S_m = 0.2 km OR A PARTICLE CONCENTRATION N = 28 cm^{-3}

λ	α (λ)	λ	α (λ)	λ	α (λ)	λ	α (λ)
0,31	19,5	1,18	19,9	2,94	20,1	6,15	21,6
0,51	19,6	1,24	19,9	3,12	20,3	6,21	21,9
0,53	19,6	1,26	20,0	3,34	20,6	6,27	22,1
0,56	19,6	1,39	20,0	3,39	20,7	6,44	22,9
0,59	19,7	1,43	20,0	3,51	20,8	6,66	23,1
0,625	19,7	1,45	20,0	3,58	20,9	7,69	24,1
0,63	19,7	1,47	20,1	3,85	21,0	8,36	24,6
0,67	19,7	1,56	20,1	4,17	21,4	10,04	22,0
0,69	19,7	1,67	20,1	4,55	21,6	10,6	19,6
0,71	19,7	1,79	20,2	4,77	21,8	11,29	17,3
0,77	19,7	1,82	20,2	5,00	22,0	11,42	17,5
0,81	19,7	1,89	20,2	5,13	22,1	11,56	18,0
0,84	19,7	1,94	20,2	5,27	22,2	12,42	18,6
0,91	19,8	2,00	20,3	5,41	22,6	13,79	20,5
0,97	19,8	2,22	20,4	5,56	23,5	14,18	20,6
1,01	19,8	2,36	20,5	5,82	23,7	14,38	20,6
1,05	19,9	2,50	20,6	5,87	22,7	16,81	21,8
1,06	19,9	2,63	20,8	5,93	22,0	17,39	22,0
1,11	19,9	2,71	21,0	5,98	21,6	22,47	24,5
1,13	19,9	2,78	20,0	6,03	21,4	25,31	25,8
1,15	19,9	2,91	20,0	6,09	21,4		

Note: Commas represent decimal points.

the microstructure-parameter values and the components of the complex refractive index of water on the attenuation coefficient $\alpha(\lambda)$ and its spectral variation.

Table 7.3 presents data on the attenuation coefficients $\alpha(\lambda)$ of clouds and fogs for the following characteristics, which are those most frequently encountered in nature: 1) most probable radius r = 6 μ; 2) distribution half-width parameter μ = 2; 3) meteorological visibility S_m = 0.2 km.

The coefficients $\alpha(\lambda)$ for other values of S_m are easily obtained from the data of Table 7.3, since $\alpha(\lambda)$ is inversely proportional to S_m.

Figure 7.9 presents a comparison of the results of our calculations for the coefficient $\alpha(\lambda)$, which were performed on the basis of Centeno's data on the complex refractive index of water and our own. It will be seen from the figure that our new figures for the coefficients $\alpha(\lambda)$ differ markedly from the old ones in a number of spectral bands.

It should be noted that the calculation in [525] covers practically all possible realistic values of the microstructure

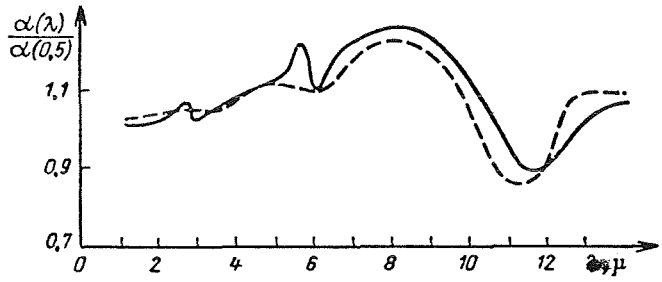

Figure 7.9. Comparison of Results of Calculation of Attenuation Coefficients of Water Clouds and Fogs in the Wavelength Range from 0.5 to 14 μ Performed on the Basis of Centeno's Data [518] (dashed curve) and the Author's Data [520] (solid curve) on the Components of the Complex Refractive Index of Water for the Microstructure Parameters μ = 2 and r = 6 μ.

parameters of water clouds and fogs except for the formations with the largest drop sizes, for which, as will be seen from Figs. 7.5-7.8 and as follows from qualitative considerations, $\alpha(\lambda)$ may be considered independent of wavelength with satisfactory accuracy. /296 We note further that the gamma distribution, which describes single-peak particle-size spectrum curves, was used as the particle-size distribution function in the calculation. The calculated results cannot be applied to other particle-size distributions. However, as was shown in Chapter 5, most data on the particle-size spectra of clouds and fogs are approximated well enough by the gamma distribution.

Finally, we stress once again that the coefficients $\alpha(\lambda)$ describe the attenuation of radiation propagating on a straight line from the source to the receiver. In experimental studies of the aerosol component of cloud and fog transparency for visible and infrared waves, the receiving system registers scattered radiation along with the direct attenuated radiation. The question as to the limits of applicability of the data obtained on the coefficients $\alpha(\lambda)$ for determination of cloud and fog transparencies for various specific sources and receivers will be examined in §9.

3. Experimental investigations of the attenuation coefficients. The most complete experimental data on the coefficients $\alpha(\lambda)$ for various values of the microstructure parameters of artificial fogs were obtained in our papers [513, 526-529, 702], which are described in detail in the monograph [1], which also examines /297 the basic results of other investigators [379, 530-537].

Reference [1] presents an analysis of available experimental data and compares them with calculated values of $\alpha(\lambda)$. It was found as a result of this analysis that the experimental data of various authors are in satisfactory qualitative agreement with one another. In most cases, quantitative comparisons cannot be drawn because the published papers do not give the necessary information on the microstructures of the clouds and fogs in which the measurements were made.

Comparison of the experimental and calculated data obtained in our papers on $\alpha(\lambda)$ showed substantial discrepancies between them. A number of other investigators have also remarked on this disagreement. As a rule, the measured coefficients $\alpha(\lambda)$ were found to be larger than those calculated from simultaneous microstructural investigations. It was therefore very important to establish the causes of these discrepancies.

On analysis of the results from the first series of measurements, the hypothesis was advanced that the absolute particle concentration was not determined correctly with the flow-through traps used for this purpose. Assuming that for some reason, the traps do not collect all droplets from a given volume, we arrive immediately at the conclusion that the coefficients calculated from trap microstructural data would be smaller than the experimental coefficients.

To check this hypothesis, the second series of measurements was supplemented by special photometer measurements of the coefficients $\alpha(0.42)$ and measurements of water content by two methods – one using filters [529] and one based on microstructural-measurement data.

It was found as a result of these experiments that the water contents determined with the filters were in all cases greater than those calculated from simultaneous microstructural measurements with the flow-through trap. The coefficient $\alpha(0.42)$ measured with the photometer was found to be directly proportional to the water content determined by the filtration method. The resulting relationship is approximated by the expression

$$\alpha(0.42)\,[\text{cm}^{-1}] = 2.04 \cdot 10^{-3} q\,[\text{g/m}^3]. \tag{7.27}$$

An analogous relation is easily obtained from the formulas

$$\alpha(0.42) = 2Q = 2N\frac{\pi d_2^2}{4}10^{-8}\,[\text{cm}^{-1}], \tag{7.28}$$

$$q = N\frac{\pi d_3^3}{6}10^{-6}\,[\text{g/m}^3]. \tag{7.29}$$

Here d_2 and d_3 are the root-mean-square and root-mean-cube diameters of the droplet size distributions (in microns).

We obtain from (7.28) and (7.29)

$$\alpha(0.42) = 3\frac{d_2^2}{d_3^3}10^{-2}q[\text{cm}^{-1}]. \qquad (7.30)$$

The d_2^2/d_3^3 were calculated for each water-content value on the basis of the microstructure measurements in order to compare the empirical (7.27) and theoretical (7.30) curves of $\alpha(0.42)$ vs. q. The mean value of this ratio was found to be 0.0714, which, on substitution in (7.30), gives the expression

$$\alpha(0.42) = 2.14\cdot10^{-3}q. \qquad (7.31)$$

As we see from (7.27) and (7.31), these expressions are very closely similar.

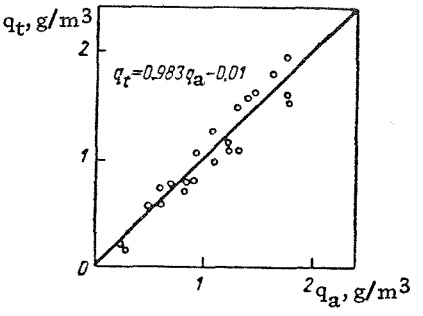

Figure 7.10. Relation Between Calculated q_t and Experimentally Determined q_a Water Contents of Artificial Fog.

A more detailed comparison of the water contents measured by the filter method and calculated from (7.30) for each measurement appears in Fig. 7.10. To calculate q from (7.30), the values of $\alpha(0.42)$ were found from measurements with a photometer, and the ratio d_2^2/d_3^3 was determined from flow-through-trap data. It was found that the relation between the calculated and measured values q_t and q_a of the water content is approximated by the equation of a straight line: /299

$$q_t = 0.983q_a - 0.01, \qquad (7.32)$$

indicating good agreement between the calculated and measured water contents.

Thus, these coordinated measurements confirmed our hypothesis that the large discrepancies between the calculated and measured absolute values of the volumetric attenuation coefficients were due to incorrect data obtained with the flow-through traps on the absolute particle concentration.

4. Recurrence of various meteorological visibilities in clouds and fogs. Solution of many problems requires knowledge of how often a given cloud or fog with a given value of either the meteorological visibility S_m or the particle concentration N or the water

content Q is encountered. These quantities are interrelated as follows:

$$N = \frac{3.912\mu^2}{S_m F(0.5)\,\pi r^2 (\mu+2)(\mu+1)}, \tag{7.33}$$

$$Q = \frac{3.912 \cdot 4r(\mu+3)d}{3 \cdot S_m F(0.5)\,\mu} \tag{7.34}$$

and by formula (7.11), where μ and r are the parameters of the gamma particle-size distribution, F(0.5) is the effective attenuation factor for the wavelength λ = 0.5 μ, and d is the density of water.

We know of only a single paper, that of G.M. Zabrodskiy [535], in which a recurrence table of various values of the meteorological visibility S_m in clouds and fogs was obtained on the basis of direct measurements in the Arctic during the warm season (203 measurements in fogs, 1,457 measurements in St, 433 in Sc, and 148 in Ns-As) (see Table 7.4).

TABLE 7.4. RECURRENCE IN % OF METEOROLOGICAL VISIBILITY S_m IN VARIOUS CLOUDS AND FOGS DURING THE WARM SEASON IN THE ARCTIC ACCORDING TO G.M. ZABRODSKIY [535]

Cloud type	S_m, m					
	Below 26	27–50	51–100	101–200	201–300	301–400
St	0,1	2,0	21,7	36,1	21,4	5,6
Sc	0,5	2,1	18	35,6	21,1	7,1
Ns—As	8,1	5,4	10,1	33,1	20,3	12,2
Fogs	1,0	5,4	10,3	32,9	21,7	11,3

Cloud type	S_m, m						
	401–500	501–600	601–700	701–800	801–900	901–1000	Above 1000
St	4,4	4,2	2,7	1,5	0,7	0,1	—
Sc	5,3	4,9	0,2	1,8	1,1	0,7	0,5
Ns—As	2,7	2,0	1,3	2,7	1,4	0,7	—
Fogs	6,9	6,4	1,0	0,6	1,0	0,5	1,0

Note: Commas represent decimal points.

TABLE 7.5. WATER CONTENT Q AND PARTICLE CONCENTRATION N OF CERTAIN WATER CLOUDS AND FOGS

Nature of cloud	Microstructure parameters		S_M, km	Q, g/m^3	N, cm^{-3}
	r, μ	μ			
Fine-droplet	1 1	2 10	0.2	0.031 0.015	971 2050
Cloud with medium particle sizes	6 6	2 10	0.2	0.194 0.101	28 65
Large-drop	10 10	2 10	0.2	0.324 0.168	10 2.3

If formula (7.33) is used with the data on the recurrence of cloud water contents obtained by V.Ye. Minervin [391] by reducing 5,000 aircraft measurements of water content in various regions of the USSR, values of S_m from 388 to 130 meters are obtained for the /301 range of most probable meteorological visibilities. This interval was obtained by using the most probable values of the water contents, which lie in the range from 0.1 to 0.3 g/m^3 [391] and microstructural parameters r = 6 μ and μ = 2.

In conclusion, we list in Table 7.5 values of the water content Q and particle concentration N in clouds and fogs for certain characteristic sets of values of the microstructure parameters at a meteorological visibility S_m = 0.2 km. The tabulated data were calculated by formulas (7.33) and (7.34). The table shows that the water content and particle concentration may vary in the range from 0.015 to 0.324 g/m^3 and from 2.3 to 2,050 particles per cm^3 in different clouds and fogs at the same value S_m = 0.2 km.

5. Determination of aerosol component of transparency in the infrared from transparency data in the visible region of the spectrum. The possibility of determining the spectral transparencies of clouds and fogs in the infrared from data on their transparencies in the visible region is very tempting, since the theoretical and experimental solutions of the latter problem are much simpler. It is sufficient to say that the visible-region transparency $T_a(0.5)$ can be determined from visual measurements of the meteorological visibility S_m by use of the well-known [5, 539] relationship (taking a value of 0.02 for the contrast-sensitivity threshold of the eye)

$$T_a(0.5) = e^{-3.912 \frac{l}{S_m}}, \qquad (7.35)$$

where l is the distance and

$$\alpha(0.5) = \frac{3.912}{S_m}. \qquad (7.36)$$

We write the expression for the spectral transparency at wavelength λ:

$$T_a(\lambda) = e^{-\alpha(\lambda) l}.$$

We obtain from this last relation and (7.36)

$$T_a(\lambda) = e^{-\omega(\lambda) 3{,}912 \frac{l}{S_m}} = [T_a(0.5)]^{\omega(\lambda)}, \qquad (7.37)$$

where

$$\omega(\lambda) = \frac{\alpha(\lambda)}{\alpha(0.5)} = \frac{F[x(\lambda), \mu]}{F[x(0,5), \mu]}. \qquad (7.38)$$

We obtained the ratios $\alpha(\lambda)/\alpha(0.5)$ for various values of the microstructure parameters of liquid-drop clouds and fogs for the 0.5-25-μ wavelength range on the basis of new data on the complex refractive index of water (see Par. 2 of this section). /302

The stated problem is solved by use of these data together with an assigned value of the meteorological visibility S_m or the coefficient $\alpha(0.5)$.

As will be seen from Figs. 7.5-7.8, different transparencies $T_a(\lambda)$ for a given wavelength in the infrared correspond, depending on the values of the microstructure parameters r and μ, to a given value of the meteorological visibility S_m or, what is the same thing, a given transparency $T_a(0.5)$ of the atmosphere in the visible region. A unique relation exists between $T(\lambda)$ and $T(0.5)$ or S_m for specific values of these parameters.

In practical application of this method in solution of many problems, the ranges of variation of the parameters r and μ can be narrowed sharply to their most probable values, which are given in Table 5.2 for various clouds and fogs. The most frequently encountered values of the meteorological visibility S_m in various types of clouds and in fogs are given in Table 7.4.

An important advantage of the proposed method of determining the spectral transparencies of clouds and fogs in the infrared from data on their transparencies in the visible region is that it eliminates the need for data on the aerosol-particle concentration, which is difficult to determine experimentally.

5. ENERGY CHARACTERISTICS OF THE SCATTERING OF VISIBLE AND INFRARED WAVES BY HAZE

1. Attenuation coefficients. 1. Theoretical investigations. K.S. Shifrin and V.F. Raskin [540-542] investigated theoretically the attenuation coefficients of a polydisperse aerosol consisting of "soft" transparent particles with size-distribution functions described by the Junge formula, the gamma distribution with the parameter μ = 2, and the generalized gamma distribution.

L.S. Ivlev and Ye.L. Yanchenko [821] calculated the attenuation coefficients of a polydisperse aerosol consisting of transparent particles with refractive indices m = 1.5 and 1.33. The /303
particle-size distribution functions used were the Junge formula with values of the parameter β = 2, 2.5, 3, 3.5, and 4 and lower and upper size limits a_1 = 0.08 μ and a_2 = 1, 3, and 10 μ and distributions of the types obtained in [810] and [811]. It was shown in [821] that in the real atmosphere, the attenuation coefficients in the visible region may differ substantially both in spectral variation and in their absolute values.

Deirmenjian [489, 517] calculated the attenuation coefficients $\alpha(\lambda)$ for several haze models with consideration of the complexity of the refractive index of water in the spectral region up to 13 μ.

The coefficients $\alpha(\lambda)$ were calculated in [543] for a haze whose particle-size spectrum is described by the Junge formula with values of 3, 4, and 5 for the parameter β and with consideration of the complexity of the refractive index of water. Values of 0.1 and 1.0 μ were taken as the minimum and maximum particle radii. The calculation was carried out in the wavelength range from 0.5 to 14 μ. It was found expedient to represent the values obtained for the coefficient $\alpha(\lambda)$ in the form of ratios $\alpha(\lambda)/\alpha(0.5) = \omega(\lambda)$.

Knowing $\omega(\lambda)$, it is easy to calculate the attenuation coefficient $\alpha(\lambda)$ of an atmospheric haze for various values of the meteorological visibility S_m:

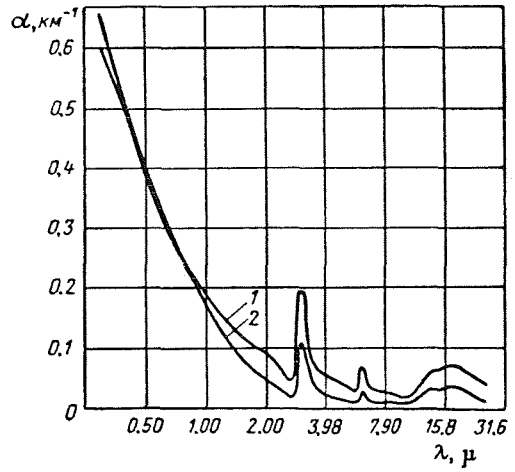

Figure 7.11. Attenuation Coefficients of Haze in the 0.3-25-μ Wavelength Range for S_m = 10 km, β = 4, a_1 = 0.1 μ, a_2 = 1.0 μ (curve 1), β = 4, a_1 = 0.01 μ, a_2 = 10 μ (curve 2).

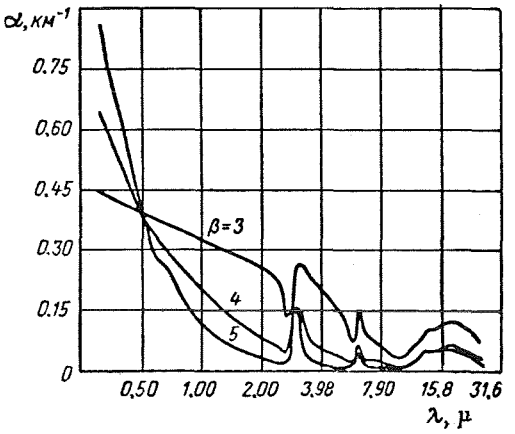

Fig. 7.12. Attenuation Coefficients of Haze in the Wavelength Range of 0.3-25 μ for S_m = 10 km, a_1 = 0.05 μ, a_2 = 5.0 μ.

$$\alpha(\lambda) = \frac{3.912}{S_m}\omega(\lambda) \ [\text{km}^{-1}]. \qquad (7.39)$$

We obtained a new series of data on the coefficients α(λ) on the basis of improved values of the complex refractive index of water (see §4 and Appendix 2).

The calculations were made for many wavelengths in the visible and infrared, from 0.3 to 25 μ. Several values were taken for the minimum and maximum particle sizes, namely a_1 = 0.01, 0.05, and 0.1 μ and a_2 = 1.0, 5.0, and 10 μ. This made it possible to ascertain the contributions to the coefficient α(λ) from particle fractions with different sizes. The results of the new calculations of α(λ) were set forth in detail in the paper [544]. Some of the data obtained are displayed in Figs. 7.11-7.13.

As will be seen from these diagrams, the parameter β, which characterizes the slope of the particle-size distribution curve described by the Junge formula, has the strongest influence on the spectral variation of the coefficients α(λ) in haze. The contribution of the small-drop fraction of the haze particles (dimensions a_1 from 0.1 to 0.01 μ) to the attenuation coefficient is negligibly small despite the fact that the concentration of these particles is very high according to the Junge formula. /305

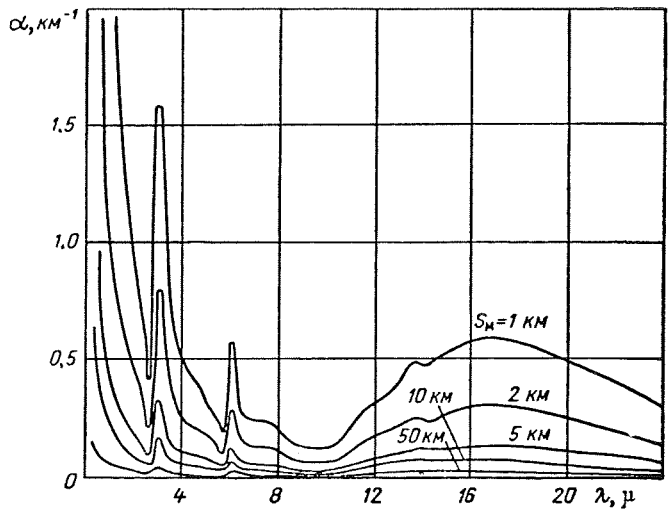

Figure 7.13. Attenuation Coefficients of Haze in the 0.3-25-μ Wavelength Range for Various Values of S_m and $\beta = 4$, $a_1 = 0.05$ μ, $a_2 - 5.0$ μ.

Figure 7.14 presents a comparison of the first and second series of our calculations for the coefficients $\alpha(\lambda)$, which indicates appreciable disagreement between the two sets of data in certain segments of the spectrum.

Figures 7.15-7.17 show curves of the aerosol component of the spectral transparency $T_a(\lambda)$ of haze that were calculated from the new data on the coefficients $\alpha(\lambda)$.

Table 7.6 presents the values that we obtained for the coefficients $\alpha(\lambda)$ with the most probable values of the haze-microstructure parameters: $\beta = 4$, $a_1 = 0.05$ μ, $a_2 = 5.0$ μ and a meteorological visibility $S_m = 10$ km in the ground layer of the atmosphere. /307
Coefficients $\alpha(\lambda)$ for other values of S_m can be obtained directly from Table 7.6, since they are inversely proportional to S_m.

Let us now consider the limits of applicability of the data /308
obtained on the coefficients $\alpha(\lambda)$. We shall analyze two assumptions made in the calculations: 1) the haze particles were assumed to be spherical water particles; 2) their size spectrum was described by the Junge empirical formula.

The results are, strictly speaking, not applicable to a haze that consists not only of liquid-drop particles but also of two-layered particles with solid nuclei. However, as was shown in [484, 486], the error admitted by neglect of the two-layered

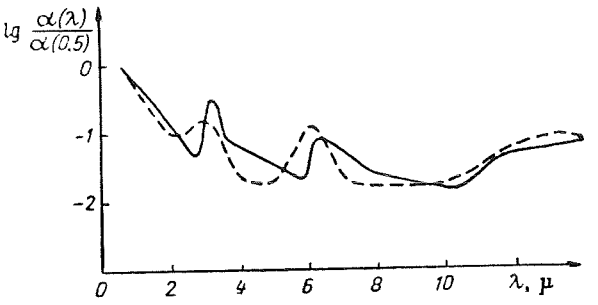

Figure 7.14. Comparison of Attenuation Coefficients of Haze in the 0.5-14.0-μ Wavelength Band as Calculated from Centeno's Data [518] on the Complex Refractive Index and the Author's Data [520] for the Microstructure Parameters $\beta = 4$, $a_1 = 0.1$ μ, $a_2 = 1$ μ.

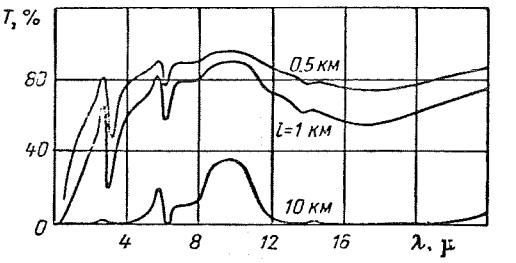

Figure 7.15. Aerosol Component of Spectral Transparency of Haze in the Wavelength Range of 0.3-25 μ for S_m = 10 km, $\beta = 4$, $a_1 = 0.05$ μ, $a_2 = 5.0$ μ.

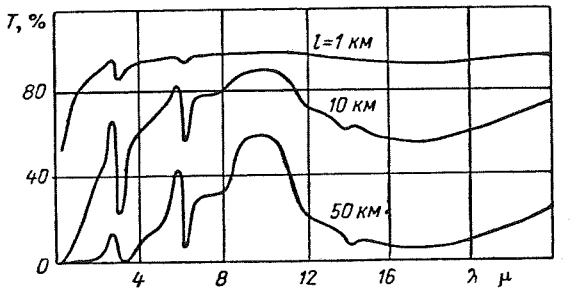

Figure 7.16. Aerosol Component of Spectral Transparency of Haze in the Wavelength Range of 0.3-25 μ for S_m = 10 km, $\beta = 4$, $a_1 = 0.05$ μ, $a_2 = 5.0$ μ.

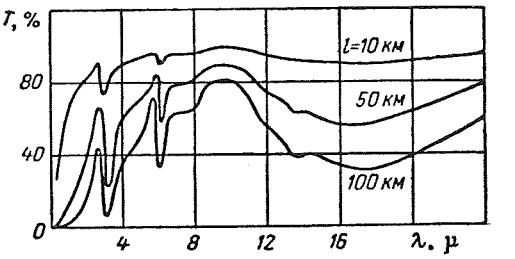

Figure 7.17. Aerosol Component of Spectral Transparency of Haze in the Wavelength Range of 0.3-25 μ for S_m = 50 km, $\beta = 4$, $a_1 = 0.05$ μ, $a_2 = 5.0$ μ.

structure of the particles is small when the dimensions of the solid nuclei are much smaller than those of the water envelopes. If the haze particles are nonspherical, the results obtained must be regarded as a certain approximation of reality in view of the fact that the chaotic orientation of the particles makes it possible, in principle, to find a spherical-particle size spectrum that is equivalent as regards attenuation.

As we noted in Chapter 5, the Junge formula gives an approximate picture of the real particle-size spectra of the atmospheric aerosol, one that is obtained, as a rule, after averaging a large

TABLE 7.6. COEFFICIENTS $\alpha(\lambda)$ FOR HAZE AT THE MOST PROBABLE VALUES OF THE MICROSTRUCTURE PARAMETERS AND A METEOROLOGICAL VISIBILITY S_m = 10 km IN THE GROUND LAYER OF THE ATMOSPHERE

λ, μ	$\alpha(\lambda)$, km^{-1}	λ, μ	$\alpha(\lambda)$, km^{-1}	λ, μ	$\alpha(\lambda)$, km^{-1}	λ, μ	$\alpha(\lambda)$, km^{-1}
0,31	0,65	1,18	0,17	2,94	0,16	6,15	0,05
0,50	0,40	1,24	0,15	3,12	0,13	6,21	0,04
0,53	0,38	1,26	0,15	3,34	0,09	6,27	0,04
0,56	0,36	1,39	0,14	3,39	0,08	6,44	0,03
0,59	0,34	1,43	0,13	3,51	0,07	6,66	0,02
0,625	0,32	1,45	0,13	3,58	0,06	7,69	0,02
0,63	0,32	1,47	0,13	3,85	0,05	8,36	0,01
0,67	0,30	1,56	0,12	4,17	0,05	10,04	0,01
0,69	0,29	1,67	0,11	4,55	0,04	10,6	0,01
0,71	0,26	1,79	0,10	4,77	0,04	11,29	0,02
0,77	0,26	1,82	0,10	5,00	0,03	11,42	0,02
0,81	0,25	1,89	0,10	5,13	0,03	11,56	0,03
0,84	0,24	1,94	0,09	5,27	0,03	12,42	0,03
0,91	0,22	2,00	0,09	5,41	0,03	13,79	0,05
0,97	0,21	2,22	0,08	5,56	0,02	14,18	0,05
1,01	0,20	2,36	0,07	5,82	0,02	14,38	0,05
1,05	0,19	2,50	0,06	5,87	0,02	16,81	0,06
1,06	0,18	2,63	0,05	5,93	0,03	17,39	0,06
1,11	0,18	2,71	0,04	5,98	0,04	22,47	0,04
1,13	0,17	2,78	0,06	6,03	0,05	25,31	0,02
1,15	0,17	2,91	0,15	6,09	0,06		

Note: Commas represent decimal points.

number of real particle-size distributions. As a result, the data obtained on the polydisperse attenuation coefficients in hazes must be regarded as average characteristics of a sort. In each concrete case, the coefficients $\alpha(\lambda)$ will differ from those calculated with the Junge formula. However, the available data on the real particle-size distributions are still totally inadequate for calculation of the corresponding $\alpha(\lambda)$.

2. Experimental investigations. Most of the experimental studies have been concerned with the visible region of the spectrum. This is explained by the relative facility of measurements in this range and the practical absence of absorption by the atmospheric gases; as a result, the quantity in which we are interested is easily obtained from measurement results that have been corrected for molecular scattering, for which quite accurate characteristics are available.

We also take note of the fundamental difficulty of experimental determination of the attenuation coefficients $\alpha(\lambda)$ in the infrared region. It stems not only from the need to take account of selective absorption by the gaseous component of the atmosphere, but also from the presence of continuous absorption by the limbs of distant strong lines lying in the corresponding

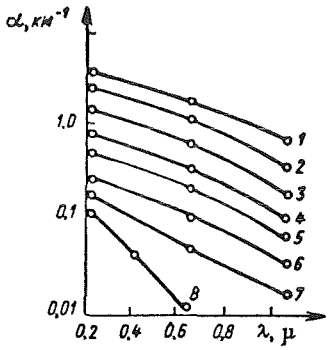

Figure 7.18. Scattering Coefficients in Hazes for Various S_m According to [545]: 1) S_m = 1.6 km; 2) S_m = 2.5 km; 3) S_m = 4.3 km; 4) S_m = 8.4 km; 5) S_m = 13.4 km; 6) S_m = 29.6 km; 7) S_m = 58.5 km; 8) Rayleigh scattering coefficient.

vibrational-rotational and purely rotational absorption bands. Quantitative data on this continuous absorption are still inadequate (see §6 of Chapter 3). /309

Thus, the most reliable experimental data on the coefficients $\alpha(\lambda)$ from direct measurements in the atmosphere can be obtained in the visible region and in the shortest-wavelength transparency "windows" in the infrared, where the continuous-absorption effect is not yet a significant factor.

O.I. Popov [545] measured the transparency of hazes for wavelengths of 0.313, 0.546, and 1.024 μ for various meteorological visibilities S_m (1.6-58 km) in the ground layer of the atmosphere. Extrapolating the results to other wavelengths within the range investigated, he constructed spectral curves of the coefficient $\alpha(\lambda)$ in hazes for various S_m; these appear in Fig. 7.18.

Curcio [546] and Knestrick, Cosden, and Curcio [547] report measurements of the coefficients $\alpha(\lambda)$ in ten narrow regions of the spectrum between 0.4 and 2.27 μ. The effects of absorption by water vapor and methane were eliminated from the values of $\alpha(\lambda)$ for wavelengths of 1.65 and 2.27 μ. The data on the absorption by water vapor and methane were taken from Passman and Larmore's paper [548]. All measurements were made in the ground layer of the atmosphere on paths 5.5 and 16.3 km long at various meteorological visibilities. /310 Figure 7.19 shows the curves of the attenuation coefficients as functions of wavelength for various S_m as obtained from the experimental data.

In [547], the coefficient α for λ = 0.56 μ was found to correlate with relative humidity at values of the latter above 70%. At lower relative humidities, α remains constant. This result is regarded as consistent with the data of early [549, 550] and recent [551, 552] studies and confirms Middleton's statement [553] that the radii of the condensation nuclei change comparatively little as the relative humidity varies up to 70%.

This conclusion stands in contradiction to the results of Yu. S. Georgiyevskiy [554, 899], who found the attenuation coefficient to depend on relative humidity as the latter increases from 30 to 35% This fact, together with a complex analysis of the results of

other optical investigations of the atmospheric aerosol led G.V. Rozenberg [538] to the important conclusion that at relative humidities r ≤ 30% and under the conditions of the measurements, the dry (dust) aerosol fraction, which creates a minor degree of turbidity, is responsible for the attenuation of light in the atmosphere. As humidity increases, the air becomes much more turbid as a result of formation of a moist haze.

/311

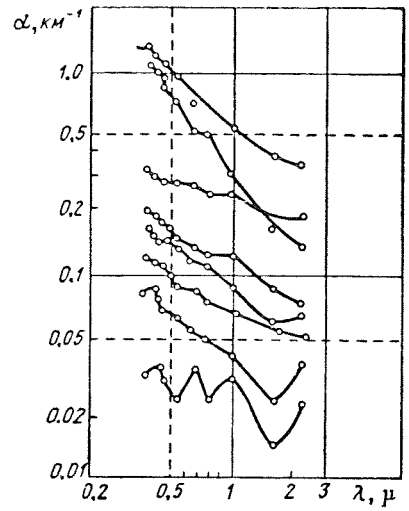

Figure 7.19. Coefficients of Aerosol Attenuation of Haze at Various Meteorological Visibilities (from S_m = 4 km to S_m = 160 km) According to [546].

/312

The authors of [872] measured the attenuation coefficients of hazes in the winter and autumn. The results (Fig. 7.20) for these seasons differ in the spectral trend of the attenuation coefficients in the 0.5-5.0-μ range.

Dennis [555] carried out an original investigation of the aerosol attenuation coefficients in the infrared at wavelengths of 2, 4, 8, and 10 μ. His method completely eliminates the influence of both selective and continuous absorption by the gaseous component of the atmosphere, but the accuracy of the measured results can hardly be considered satisfactory.

To summarize our examination of the experimental studies, we note an important deficiency that is common to all of them. This consists in the fact that the microstructure of the aerosols responsible for the turbidity of the atmosphere was not investigated concurrently with the optical measurements. This makes it practically impossible to compare the experimental data with the corresponding theoretical data without ambiguities.

2. Aerosol component of haze transparency at various heights and on slant paths in the atmosphere. 1. Theoretical investigations. We write the general formulas for the aerosol component of haze spectral transparency for slant paths in the atmosphere:

$$T_a(\lambda) = e^{-\tau}, \tag{7.40}$$

$$\tau = \int_0^l \alpha(\lambda, l)\, dl, \tag{7.41}$$

$$\alpha(\lambda, l) = N(l) \int_{a_1}^{a_2} \sigma(\lambda, a)\, f(a, \beta)\, da, \tag{7.42}$$

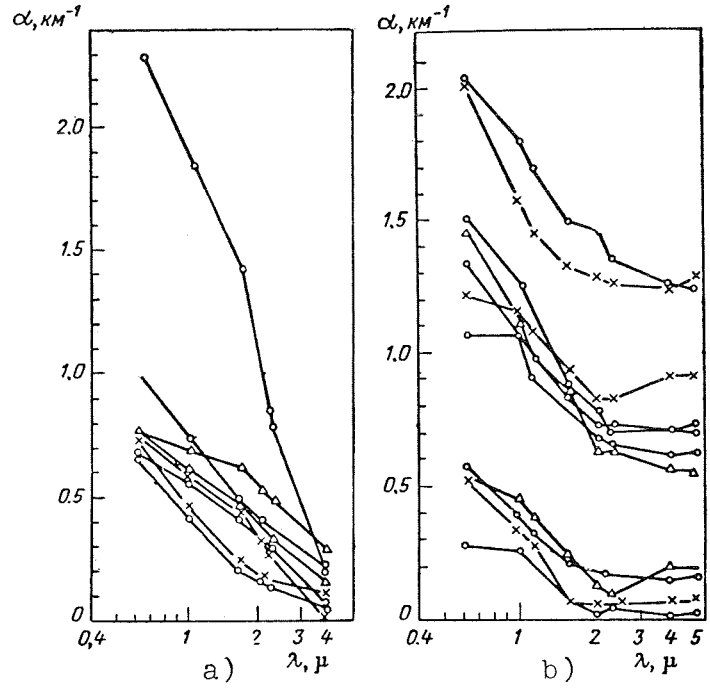

Figure 7.20. Coefficients of Aerosol Attenuation of Hazes in the Range from 0.5 to 5.0 μ According to Winter (a) and Autumn (b) Measurements [872].

$$\sigma(\lambda, \alpha) = \pi a^2 K(\rho, m), \tag{7.43}$$

where $T_a(\lambda)$ is the component of the spectral transparency of the haze that owes its origin solely to the aerosol attenuation, l is the distance traveled by the radiation, N is the particle concentration, which varies along the ray path, $\sigma(\lambda, a)$ is the attenuation coefficient of a particle of radius a, and K is the efficiency of attenuation by the particle.

The altitude distribution of particle concentrations can be described by fromulas (5.8), which we selected on the basis of approximation of Junge's data on the concentrations of optically active aerosol particles at various heights.

Formulas (7.40)-(7.43) and (5.8), together with the formulas and tabular data for the function $K(\rho, m)$ that we considered in Chapter 6 permit calculation of the aerosol component of haze spectral transparency along slant paths in the atmosphere. A calculation of $T_a(\lambda)$ made by this scheme indicated that the aerosol attenuation may be disregarded in atmospheric layers above

/313

5 km when the radiation propagates at all possible angles and over distances up to 1000 km for the atmospheric model described by (5.8). Consequently, only the aerosol attenuation in the lowermost 5-km layer of the atmosphere with its exponential decrease in particle concentration with height [see (5.8)] can be of practical interest. In this case, a relatively simple formula can be obtained for calculation of $T_a(\lambda)$.

Introducing the notation $C' = \int_{a_1}^{a_2} \pi a^2 f(a, \beta)\, da$, we can write

$$\alpha(\lambda) = QF = N(z)\, C'F, \tag{7.44}$$

where Q is the geometrical cross section of the particles in the unit volume [see formula (7.11)];

$$F = \frac{\int_{a_1}^{a_2} \pi a^2 K\left(\frac{2\pi a}{\lambda}, m\right) f(a, \beta)\, da}{\int_{a_1}^{a_2} \pi a^2 f(a, \beta)\, da}. \tag{7.45}$$

Applying (7.44), we write (7.40) in the differential form

$$dT_a(\lambda) = -N(z)\, C'F\, dl. \tag{7.46}$$

The initial condition of Eq. (7.46) is $T_a(\lambda) = 1$ at $l = 0$.

Let the ray cover a certain distance between heights z_1 and z_2 at an angle θ to the vertical. Then $dl = \sec\theta dz$. We shall assume that only particle concentration changes with height, and that the parameter β in formula (5.6) for the particle-size distribution function does not depend on height. Assuming that in this case C' and F are also independent of height, integration of (7.46) with respect to height and transformation of the resulting equation gives the following formulas for the quantity τ, which appears in the expression for $T_a(\lambda)$ [see formula (7.40)]: /314

$$\tau(\lambda, z_1, z_2, \theta) = \sec\theta \frac{3.912}{S_m} \omega(\lambda) \frac{1}{b} (e^{-bz_1} - e^{-bz_2}), \tag{7.47}$$

or

$$\tau(\lambda, z_1, z_2, \theta) = \sec\theta\, [\tau(z_1) - \tau(z_2)], \tag{7.48}$$

where

$$\tau(z) = \frac{3.912}{S_m}\omega(\lambda)\frac{e^{-bz}}{b}, \tag{7.49}$$

$$\omega(\lambda) = \frac{\int_{a_1}^{\infty} \pi a^2 K\left(\frac{2\pi a}{\lambda}, m\right) f(a, \beta)\, da}{\int_{a_1}^{a_2} \pi a^2 K\left(\frac{2\pi a}{0.5}, m\right) f(a, \beta)\, da} = \frac{\alpha(\lambda)}{\alpha(0.5)}. \tag{7.50}$$

Making use of the fact that N(5) = 0.03 [see the second formula in (5.8)], we obtain with (7.36), (7.42), and (7.50)

$$b = 2.78 - 0.460 \lg S_m(0), \tag{7.51}$$

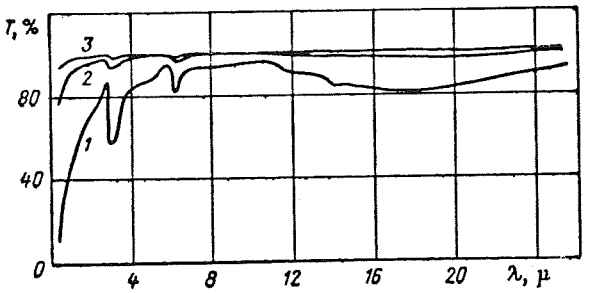

Figure 7.21. Aerosol Component of Haze Spectral Transparency in the Vertical Direction in the Lowermost 5-km Layer of Atmosphere for: 1) $S_m(0)$ = 1 km; 2) $S_m(0)$ = 10 km; 3) $S_m(0)$ = 50 km.

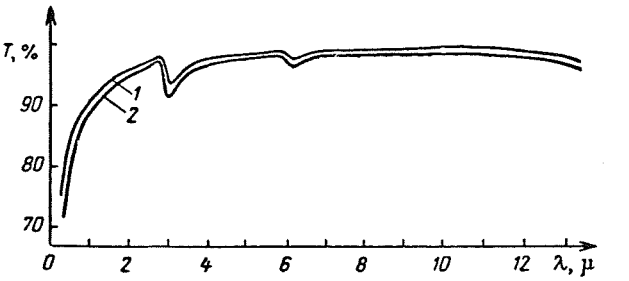

Figure 7.22. Aerosol Component of Haze Spectral Transparency in the Vertical Direction in the Atmospheric Layers: 1) 0-0.5 km; 2) 0-5.0 km at $S_m(0)$ = 5 km.

where $S_m(0)$ is the meteorological visibility at the earth's surface.

Formulas (7.47), and (7.51) and Table 7.6 are sufficient for solution of the problem of the aerosol component of haze spectral transparency for various geometries of the source and receiver locations in the lowermost 5-km layer of the atmosphere. Figure 7.21 presents calculated results for $T_a(\lambda)$ in the vertical direction for $\beta = 4$, $a_1 = 0.05$ μ, and $a_2 = 5$ μ. Figure 7.22 illustrates the role of certain layers in haze attenuation in the vertical direction.

It must be remembered that these $T_a(\lambda)$ were obtained for an atmospheric model with a certain average statistical distribution of the concentration of particles of atmospheric aerosol with respect to altitude. The particle-size spectrum was regarded as height-independent. In each concrete case, the actual distribution of particle concentration and size may differ to a greater or lesser degree from that described by the model adopted. Moreover, it is also necessary to remember the remarks made in the preceding paragraph of this section concerning the limits of applicability of data on the coefficients $\alpha(\lambda)$. /315

The quantitative data obtained in [544] and those discussed above, which characterize scattering on haze particles along slant paths in the atmosphere, pertain principally to the infrared. Analytical expressions for the scattering coefficients and optical thicknesses in the visible region for slant-path propagation in the atmosphere were obtained by K.S. Shifrin and I.N. Minin in [555], a paper devoted to the development of a theory of off-horizontal visibility.

2. Experimental investigations. Substantial progress has been made in recent years in experimental study of aerosol scattering at various heights and in a broad wavelength range. Just a few years ago, the available data were chiefly for the visible region of the spectrum and had been obtained in measurements from the ground and a limited number of aircraft observations. A respectable number of investigations has now been made at various heights in both the visible and infrared regions. The sun is used as the radiation source in all measurements, and the receiving apparatus has been placed on aircraft, balloons, and artificial earth satellites, or on the ground, in which case the work is done by the method of probing the atmosphere with searchlight and laser beams and by the twilight and certain other methods. /316

The most important results from research on the vertical profiles of the aerosol attenuation coefficients, which were concerned with description of the atmosphere as a scattering medium, were examined in Chapter 5. Let us briefly outline the studies that were not included in the survey in Chapter 5. The most detailed aircraft data were obtained by G.P. Faraponova [556], B.I. Rabinovich [436, 558, 559], and G.P. Gushchin [435, 561, 562]. The measurements were made for a number of wavelengths in the visible and nearest infrared regions at various heights up to 6-7 km over various areas of the USSR. The results of the studies reduce to the following. The values of the aerosol attenuation coefficient at various heights and the aerosol optical thickness of the atmosphere above a given height vary through 1-2 orders from one case to another. The dependence of the average aerosol attenuation coefficients on height is approximated by an exponential curve accurate to 15-20%. The lowermost 1-km layer plays the dominant role in the over-all attenuation of radiation by the entire thickness of the atmosphere. The same conclusion was drawn

in [563-565].

The exponential decrease of the aerosol-attenuation coefficients with height reduces them by 1-2 orders at heights of 3-5 km as compared with the value at the ground surface. Nevertheless, the Rayleigh attenuation coefficients are found to be equal to or slightly larger than the aerosol coefficients only in the violet and blue regions of the spectrum at these heights. In the red region, and even more so in the infrared, parts of the aerosol-coefficient spectrum exceed the corresponding Rayleigh segments at all heights investigated in the studies under consideration. Aerosol coefficients in excess of the Rayleigh coefficients were also observed for great heights: up to 50 km in [433] and to 100 km in [434]. /317

The measurements of G.P. Faraponova revealed a practically neutral spectral variation of the aerosol attenuation coefficients — which is equivalent to a zero exponent n in the familiar empirical Angstrom formula, which describes the scattering coefficient α as a function of wavelength λ:

$$\alpha = C\lambda^{-n}, \qquad (7.52)$$

where C is an experimentally determined constant.

Yu.I. Rabinovich obtained a similar result for atmospheric layers above 1 km; in the lowermost one-kilometer layer and for the entire thickness of the atmosphere, the exponent n in (7.52) was found to be approximately unity. In measurements from the ground, G.P. Gushchin determined the average value at $n \approx 1.32$; the minimum and maximum were 1.03 and 1.48, respectively.

A neutral spectral trend of the attenuation coefficient would be understandable if large particles were assumed to be present in the corresponding atmospheric layers. Such an assumption would be consistent with the data of [432, 563, 566, and 567].

We note that the Angstrom formula has come into rather extensive use in describing experimental data on the spectral variation of the aerosol attenuation coefficient. Different investigators have obtained different values of n. Thus, Shmolinskiy [568] gives $n = 0.92 \pm 0.25$, Curcio [546] obtained $n = 1.3 \pm 0.6$, T.P. Toropova [565] found n = 1.1, 2.1, and 2.3, K.S. Shifrin and V.F. Raskin [540], using a gamma particle size distribution with $\mu = 2$ and average particle radii of 0.05, 0.1, 0.2, and 0.5 μ, obtained theoretical values of n equal respectively to 3.3, 3.0, 2.5, and 2.1. Foitzik and Zskhaeck [569] found from measurements at $S_m > 7.5$ km that n = 1.2-1.5; for $S_m \approx 2$ km, $n \approx 0.9$. For the 49-60% transparency range, O.P. Popov [545] obtained $n \approx 2$ for $\Delta\lambda = 0.313\text{-}0.546$ μ and $n \approx 1.2\text{-}1.3$ for $\Delta\lambda = 1.014\text{-}0.546$ μ. In [820],

n varied from 0.30 to 2.15, with an average value of 0.81. The authors of [820] remark correctly that formula (7.52) is valid in far from all cases. /318

In balloon experiments, K.Ya. Kondrat'yev's group [445] obtained vertical profiles for the layerwise attenuation of solar radiation (in 1.0-km layers) by the atmospheric aerosol for heights up to 25-30 km. The resulting profiles differ somewhat from those determined by V.V. Nikolayeva-Tereshkova and G.V. Rozenberg [822] from spacecraft measurements. In the latter study, two maxima were observed in the vertical trend of the attenuation coefficient (Fig. 7.23). In [445], these maxima are not as distinct and are shifted somewhat toward lower heights. Reference [445] also reported additional maxima in the altitude profile of the attenuation coefficients, e.g., near the 6-km level.

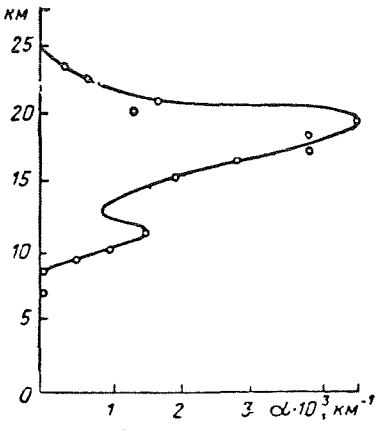

Figure 7.23. Vertical Profile of Aerosol Attenuation Coefficient According to [822].

The existence of an aerosol layer with a higher attenuation coefficient was also detected at heights around 19 km in twilight and daytime measurements made from the Vostok and Voskhod spacecraft [823].

On the basis of measurements made with balloons, Newkirk [440, 446] detected extremely thin layers with elevated scattering-coefficient values. These layers were approximately 50 meters thick. /319 The intervals between them were occupied by layers of relatively clear air with vertical depths of the order of 300 m.

Maxima are observed in the vertical profile of the aerosol attenuation coefficient all the way up to the heights of the ionospheric layers. The upper boundary of the atmospheric aerosol is placed at 100 to 150 km according to various investigators [824].

G.V. Rozenberg [895] constructed a summary diagram of the aerosol attenuation coefficient as a function of height on the basis of the optical measurements made in [432, 559, 822, 901-905]. The data of these sources, which were obtained by various methods, were found to mesh nicely and form a complete picture of the approximately exponential decrease in the attneuation coefficient for a number of wavelengths in the visible region all the way up to a height of 100 km. The attenuation coefficient decreases through approximately 6 orders for all wavelengths as height changes from 0 to 100 km. The aerosol attenuation coefficient was found to be at least several times the molecular scattering coefficient for all heights. An exception is found in two narrow height intervals

(approximately from 5 to 8-9 km and from 25 to 30 km) with very small values of the aerosol attenuation coefficients.

In summarizing data from experimental studies of aerosol scattering at various heights, we must first of all stress the very wide variability of the vertical scattering-coefficient profiles and the presence of a layered structure in these profiles over the entire aerosol layer of the atmosphere. The maxima in the height curve of the scattering coefficients are due to the presence of the corresponding aerosol layers. Some of these layers are time-stable (for example, the layer around 20 km), while the others appear in random fashion. Despite the considerable number of papers devoted to experimental study of the aerosol component of atmospheric transparency for visible and infrared waves, the data obtained are still insufficient for definite conclusions as to the average statistical vertical profiles of the attenuation coefficients and their variability.

As in the case of the experimental studies considered in subsection 1, none of the measurements of the aerosol attenuation coefficients at various heights was accompanied by simultaneous studies of aerosol microstructure. This precludes correct comparison of the experimental results obtained with the theory. /320

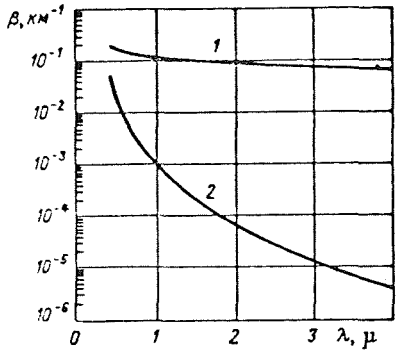

Figure 7.24. Aerosol Attenuation Coefficients (1) and Molecular Scattering Coefficients (2) in the Ground Layer of the Atmosphere as Functions of Wavelength in the Elterman Model [447].

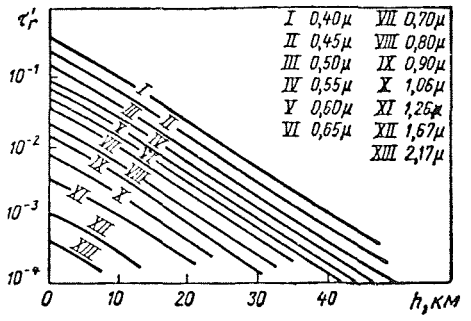

Figure 7.25. Optical Rayleigh-Scattering Thicknesses of Vertical Columns of Atmosphere from Various Heights for Various Wavelengths, in the Elterman Model [447].

3. Elterman model of aerosol attenuation in the atmosphere. Generalizing the experimental data of foreign investigators on the size spectra, particle concentration, and attenuation coefficients in the ground layer, Elterman [447] constructed an optical model

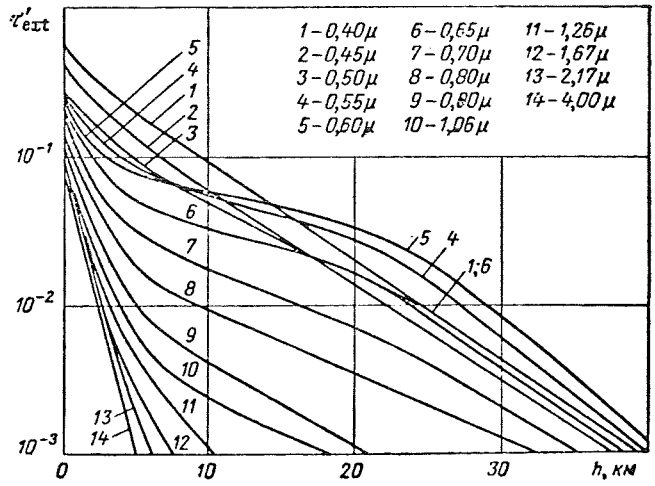

Figure 7.26. Altitude Dependence of Total Optical Thickness for Various Wavelengths in the Elterman Model [447].

of the cloudless atmosphere for $S_m(0) = 25$ km. The model was constructed for the following wavelengths: 0.27, 0.28, 0.30, 0.32, 0.34, 0.36, 0.38, 0.40, 0.45, 0.50, 0.55, 0.60, 0.65, 0.70, 0.80, 0.90, 1.06, 1.26, 1.67, 2.17, 3.50, and 4.00 μ. Tables of the molecular-scattering, aerosol-attenuation, and ozone molecular-absorption coefficients were compiled for all of these wavelengths. The last coefficients were given for wavelengths subject to absorption by ozone: 0.27, 0.28, 0.30, 0.32, 0.34, 0.36, 0.45, 0.50, 0.55, 0.60, 0.65, 0.70, and 0.80 μ. In addition, the model includes the optical molecular-scattering thickness and the resultant optical thickness due to molecular scattering, aerosol attenuation, and ozone absorption for all wavelengths. All data are given for 1-km height intervals from 0 to 50 km. The aerosol coefficients are assumed equal to zero above 30 km.

Using the data of the Elterman model, we have constructed a /321
number of graphs that demonstrate the role of aerosol attenuation and molecular scattering in the atmosphere (Figs. 7.24-7.26). It must be remembered that the aerosol-scattering data were obtained in this model for $S_m(0) = 25$ km. The coefficients $\alpha(\lambda)$ for other S_m are easily obtained directly from the tables, since $\alpha(\lambda)$ is inversely proportional to $S_m(0)$.

We note that the Elterman model gives a very rough description of aerosol scattering at various heights. It does not take account of the inflection in the height curve of aerosol-particle concentration at a height of 5 km or the presence of aerosol layers. It also assumes that the aerosol attenuation vanishes above 30 km. However, no better model has been forthcoming.

6. ENERGY CHARACTERISTICS OF SCATTERING OF VISIBLE AND INFRARED WAVES BY PRECIPITATION

For the visible and infrared regions, the particles of precipitation may be regarded as large particles, for which we may put $K(\rho, m) = 2$. In this case, if the particles are assumed spherical, we obtain for the attenuation coefficient

$$\alpha(\lambda) = N \int_0^\infty \pi a^2 K(\rho, m) f(a)\, da = 2Q,$$

where Q is the geometrical cross section of particles of unit volume as defined by (7.11).

Raindrops may be considered spherical without equivocation. Thus, the attenuation coefficient of rain does not depend on wavelength and is uniquely defined by the geometrical cross section Q, which is uniquely related to water content for a given set of microstructure characteristics.

Ye.A. Polyakova's measurements [453] have shown that the dependence of the coefficient $\alpha(\lambda)$ on the microstructure parameters of rain is negligible by comparison with the correlation between the coefficient $\alpha(\lambda)$ and the intensity I of the rainfall:

$$\alpha = 0{,}21 I^{0{,}74}, \tag{7.53}$$

where I is given in mm/h and α in km^{-1}. The coefficient of correlation between log α and log I was found equal to 0.95 ± 0.01. An even higher correlation has been discerned between log α and log ω, where ω is the water content of the rain in g/m^3 (correlation coefficient 0.97 ± 0.01).

A similar correlation between the coefficient α and the rate of snowfall was obtained by Ye.A. Polyakova and V.D. Tret'yakov in [570]. The correlation coefficient was found to be 0.91 ± 0.02. The correlations obtained in [453] and [570] between the coefficients α and the rates of rain- and snowfall were confirmed by Jefferson in [571]. /323

Thus, the coefficients of attenuation of visible and infrared light by precipitation particles can be considered practically independent of wavelength. This conclusion is valid at least for wavelengths meeting the condition $\lambda < 15\text{-}20\ \mu$. The numerical values of the coefficients are easily determined if the rate of precipitation is known.

7. SCATTERING INDICATRICES OF POLYDISPERSE AEROSOLS

Analytical expressions useful for calculation of the scattering indicatrices of polydisperse aerosols consisting of "soft" transparent particles with various size-distribution functions were obtained by K.S. Shifrin and V.F. Raskin [540-542]. The distribution functions used were the gamma distribution with the parameter $\mu = 2$, the generalized gamma distribution, and the Junge formula with $\beta = 4$, 5, and 6. Data on the scattering indicatrices for the Junge distribution and a Junge-type distribution with values of the parameter $\beta = 3$, 4, 5, 6, and 8, minimum sizes $a_1 =$ 0.0175, 0.052, and 0.082 μ and refractive indices $n = 1.33$, 1.44, 1.50 [2, 105], were obtained by K.S. Shifrin and Ye.A. Chayanova in [572]. Tables for calculation of the scattering indicatrix in the region of small scattering angles were obtained in [573].

Deirmenjian [517] calculated the scattering indicatrix for two haze models and one cloud model with allowance for the complexity of particle refractive index for various wavelengths in the range from 0.45 to 16.6 μ.

Polydisperse scattering indicatrices were calculated by T.P. Toropova [825, 826] for media with Junge particle-size distributions at values of $n = 1.25$ and 1.50 for five wavelengths in the visible region. The parameter β and the upper limit of particle sizes assumed various values.

A considerable number of papers has been devoted to experimental study of the scattering indicatrices of visible light under various conditions in the ground layer of the atmosphere and in measurements of the scattering of solar radiation in the cloudless sky. The results of these studies are generalized in the monographs [583, 820, 827, 828]. /324

All indicatrices were grouped into 10 classes on the basis of the asymmetry coefficient K, which equals the ratio of the luminous fluxes scattered forward and backward. Indicatrices whose K differ by a factor of one and a half were included in each class. The first case of a near Rayleigh scattering indicatrix with $K = 1$ and $\alpha = 0.0136$ km^{-1} or $S_m = 220$ km was reported from one of the series of observations on Mount El'brus. The maximum value of K was 35.

The measurements indicated that there is no unique relation between the shape of the indicatrix and atmospheric transparency. It is noted in [574] that this conclusion is consistent with the measured data of V.F. Belov [575], although in the papers of Foitzik and Zskhaeck [569], Hulbert [576], Bullrich [577, 578], and Reger and Siedentopf [579], a given transparency interval is juxtaposed to a given value of K. It is said in [574] that this conclusion was drawn from analysis of an inadequate number of measurements.

The possibility of using a nephelometric transparency-measurement method was indicated in [580] on the basis of an analysis of the results of [574]. A theoretical defense of this method is given by K.S. Shifrin and E.Ya. Chaynova [829].

T.P. Toropova's measurements [565, 581, 582] of the scattering indicatrix of visible light in the ground layer also lead to the conclusion that there is no unique relation between the coefficient K and atmospheric transparency. In [581], the values of K were determined separately for the complete indicatrix and its aerosol part. The ranges of their variation were 1.57-8.75 and 1.69-15.1, respectively, with average values of 3.29 and 6.23. It is noted in [581] that the average values found in the measurements of Bullrich [577], Foitzik and Zskhaeck [569], and Reger and Siedentopf [579] were 6.41, 8.17, and 11.5, respectively. /325

The intensity ratio of the light scattered at angles of 10 and 140°, which characterizes the elongation of the indicatrix and varies from 8.8 to 63.8, was found in [582]. The ratios of the intensities scattered at various angles to the corresponding intensities for the case of Rayleigh scattering were also determined in the same study. For example, these ratios varied from 8 to 314 and 1.1 to 9.6 for the minimum and maximum scattering angles, 10° and 160°, respectively.

In [565], the indicatrices were measured for two narrow segments of the spectrum with effective wavelengths λ_{ef} = 0.428 and 0.560 μ. It was found that the elongation of the indicatrix increases with wavelength. The same effect was observed for the entire thickness of the atmosphere by Ye.V. Pyaskovskaya-Fesenkova [583]. This effect, which is mystifying at first glance ($\rho = 2\pi a/\lambda$ decreases with increasing λ, which should shorten the indicatrix in the case of monodisperse ash), is explained in detail by V.G. Kastrov [584] in an analysis of the contributions of small and large particles to the indicatrix of a polydisperse aerosol.

Yu.S. Lyubovtseva and G.V. Rozenberg [585, 906] made a detailed study of the coronal part of the scattering indicatrix in the ground layer of the atmosphere for narrow segments of the spectrum approximately 50 Å wide and centered around 0.47, 0.585, and 0.888 μ. Analysis of the results permitted the conclusion that there exist three qualitatively different optical states of the ground layer of the atmosphere: haze, foggy haze, and fog. Each of these states is characterized by its own angular variation of the intensity of light scattered at small angles and its own fluctuations of the coronal part of the indicatrix. An extremely sharp drop in the intensity $I(\theta)$ is observed for fogs. As the scattering angle changes from 10' to 7°, $I(\theta)$ changes by 3-7 orders! Coronas are observed in the case of foggy haze, indicating the presence of particle fractions with certain dimensions.

The fluctuations of the coronal scattering indicatrices are small in haze and stable foggy haze. During the transformation of a foggy haze to a fog, the brightness of light scattered at angles of 10'-3° may change through 2-3 orders within a few seconds! The authors of [585] report that there are practically no recurring cases in the very large number of coronal indicatrices that they obtained. /326

A considerable number of scattering indicatrices for the ground layer of the atmosphere was obtained by G.V. Rozenberg and G.I. Gorchakov [506, 507] in experimental studies of the scattering-matrix components (see §3 of Chapter 6). Curves of the angular dependence of the scattering-matrix component M_{11} (the scattering indicatrix) for haze, dense haze, fog, and drizzle are given in [507].

Free-atmosphere scattering indicatrices were measured at various heights by V.F. Belov [586], B.A. Chayanov [587], and Kompaniyets [588]. The results of these measurements indicate that the prolateness of the indicatrix varies from one measurement to the next. Its asymmetry persists at all heights studied up to 20 km, increasing in the region of the tropopause.

V.Ye. Pavlov [830] measured the atmospheric scattering indicatrix for certain wavelengths in the visible and ultraviolet regions at scattering angles around 0° and 180°. In the range of small scattering angles, he detected an increase in the prolateness of the indicatrix with increasing wavelength and increasing absolute magnitude of the corona around the sun. In the ultraviolet region, the scattering indicatrix approximates that of Rayleigh scattering.

We note in conclusion that in the studies known to us, the scattering indicatrices of polydisperse aerosols have been investigated experimentally under natural and laboratory conditions almost exclusively for certain wavelengths in the visible and nearest infrared regions (not beyond 0.9 μ). In most cases, there were no simultaneous measurements of aerosol microstructure, and this precludes quantitative comparison of the experimental data with one another and with the corresponding calculated results. The latter are available in more or less adequate quantity for the visible and nearest infrared regions. Polydisperse scattering indicatrices for the infrared have been calculated with consideration of the complexity of particle refractive index only for a few concrete models of the size-distribution function of water spheres. /327 It should be noted that we still lack the necessary chemical-composition data for calculations of the polydisperse scattering indicatrices of nonaqueous aerosols, not to mention data on the components of their complex refractive indices [589].

8. SCATTERING OF LASER RADIATION IN THE ATMOSPHERE

The coherence, the high degree of monochromaticity, the strong directivity and the power of laser radiation may, generally speaking, give rise to corresponding peculiarities in the propagation behavior of this radiation in the atmosphere. These features may be manifested both in the absorption of the radiation and in its scattering, both in the region of linear optics, in which Bouguer's law is valid, and in the region of nonlinear optics.

We examined the peculiarities of absorption of laser light in the linear-optics region in §14 of Chapter 3. The nonlinear effects that accompany the absorption and scattering of powerful laser radiation in the atmosphere will be described in Chapter 10. Here we shall examine only the energetics of laser radiation propagating in a scattering medium, in which case the Bouguer law may be considered to apply.

Purely qualitative reasoning indicates that the attenuation coefficients for laser light and noncoherent radiation from thermal sources with the same spectral composition should not differ greatly. Indeed, coherence of a wave incident on a layer of scattering particles may be governed by interference of the waves scattered by the particles. This results in a distribution of the intensities of the light scattered in various directions that differs from the corresponding pattern produced when noncoherent radiation strikes the layer. M.V. Kabanov [590] obtained an experimental proof of this statement in our laboratory. The effect is due to the different values of the effective field for particles in different zones of the cross section of the laser beam. However, if the particles are distributed uniformly in the medium and these effective-field increases are not sufficient to produce nonlinear effects, we should expect the attenuation of the beam, averaged over its cross section, not to differ greatly from the attenuation /328 that would be obtained on irradiation of this same layer of the medium by incoherent radiation with the same spectral composition.

These purely qualitative observations require experimental verification. This verification is the more necessary since the attenuation coefficients for laser light were found in [591] to differ from those of noncoherent radiation of the same spectral composition.

Measurements of water-fog attenuation coefficients for the radiation from lasers and thermal sources with appropriate interference filters were made by a group of colleagues of our laboratory [592]. The types of lasers used and some of their characteristics are given in Table 7.7.

Figure 7.27 presents the results of comparison of the attenuation coefficients for the light of the He-Ne laser at 0.63 μ, the ruby laser (λ = 0.69 μ), and the attenuation coefficients for a

TABLE 7.7. CERTAIN TYPES OF LASERS AND THEIR CHARACTERISTICS

Laser type	Radiating wavelength λ, μ	Operating mode
He-Ne gas	0.63	Continuous, multimode
Ruby solid	0.69	Pulsed, multimode
Nd-doped glass solid	1.06	Pulsed, multimode
He-Ne gas	1.15	Continuous, multimode
He-Ne gas	3.39	Continuous, multimode

thermal source with the appropriate interference filters. We see from Fig. 7.27 that all three attenuation coefficients are closely similar. The equation of the line passing through the experimental points takes the form

$$\alpha(0.63)=\alpha(0.69)=1.06\alpha_f, \qquad (7.54)$$

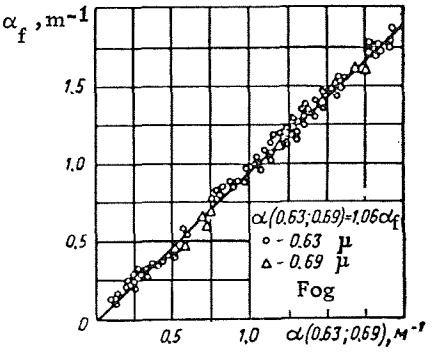

Figure 7.27. Comparison of Attenuation Coefficients for Radiation from Lasers at Wavelenghts of 0.63 and 0.69 μ and Attenuation Coefficient of Thermal Source with the Same Wavelengths in an Artificial Water Fog. /329

where $\alpha(0.63)$, $\alpha(0.69)$, and α_f are the respective attenuation coefficients for the radiation from the lasers at 0.63 and 0.69 μ and from the thermal sources with the interference filters. Similarity of the attenuation-coefficient values for laser and thermal-source radiations may be inferred in the same way for the 1.06-, 1.15-, and 3.39-μ lasers, even though the attenuation coefficients for the radiation from the thermal source were measured in these cases for a wavelength of 0.4 μ. We note that the measurements of the attenuation coefficients of laser radiation and radiation from a thermal source at various wavelengths that were reported in [593] show a difference in the values obtained for the coefficients that was not precisely interpreted.

Harris, Sherman, and Morse [594] recently published the results of careful laboratory studies of the angular dependence of the intensity of radiation scattered by latexes. The radiation sources used were a He-Ne gas laser with a wavelength of 6328 Å and a high-pressure xenon arc lamp that radiated a band about 100 Å wide and centered around 6328 Å. The diameters of the latex

scatterers were varied from 0.088 to 3.49 μ. Analysis of the measurement results led the authors of [494] to the conclusion that the scattering indicatrices of the laser and xenon-lamp radiations coincide within the limits of measurement error. Coincidence of the /330
indicatrices is equivalent to coincidence of the attenuation coefficients.

We note in conclusion that the results obtained in [592] and [594] naturally do not constitute proof that there is no difference in the propagation of coherent and noncoherent radiation of the same spectral composition in scattering media. We may speak only of approximate equality of the attenuation coefficients of these radiations.

9. INFLUENCE OF MEASUREMENT APPARATUS ON THE RESULTS OF EXPERIMENTAL INVESTIGATIONS OF THE SCATTERING OF VISIBLE AND INFRARED WAVES IN THE ATMOSPHERE

The theoretical data on the attenuation coefficients of clouds, fogs, and hazes that have been examined in this chapter characterize the attenuation of direct monochromatic radiation propagating through the medium in question. We have noted that, strictly speaking, conditions under which only the attenuated direct light is registered cannot be realized in an experiment. Any receiving system registers, together with the direct radiation that has been attenuated by the scattering medium, scattered light whose intensity must depend on the visual angle of this system, the properties of the scattering medium, and the directivity of the incident radiation. Thus, the measured attenuation coefficient and the measured layer transparency should differ from the theoretical values. Another cause of differences between the measured values and those predicted by theory consists in the fact that we do not deal with strictly monochromatic radiation in the experiment as we do in theory.

Our problem is to analyze the influence of experimental conditions and the measurement apparatus on the rssults of the corresponding measurements. This problem is examined in detail in the monograph [1]. Below we give a basic summary of the results that have been obtained by various investigators. Here it is assumed that the influence of source nonmonochromaticity on the measured results can be disregarded. This assumption is not critical since the widely used methods of monochromatizing the radiation from thermal sources ensure isolation of relatively narrow segments of the radiated spectrum within which the coefficient of aerosol at- /331
tenuation may be considered independent of wavelength.

1. Measured scattering coefficient as a function of photometered atmospheric thickness. This dependence was first observed by Sinclair [595], who measured the scattering coefficients of lycopodium-powder particles (particle sizes 15 ± 1 μ) situated at various distances from the receiver. As the distance was varied

from 5.5 m to 15 cm, the measured scattering coefficient of a parallel beam of visible light assumed values from $2\pi a^2$ to πa^2. The Mie theory gives $2\pi a^2$ for this case.

K.S. Shifrin [467] gave a theoretical solution of the problem for large particles with arbitrary electrical properties. The case of an opaque sphere was analyzed theoretically by Brillouin [596]. It is reported in [597] that Moulin and Reynolds obtained a similar result for the case of a cylinder. Studies of other nonspherical particles subsequently led to similar conclusions [598]. The cause of the dependence of the measured scattering coefficient on distance lies in the quite unique shape of the scattering indicatrices of large particles. Depending on the distance between the particle and the receiver, the latter may receive a larger or smaller fraction of the energy scattered by the particle. Thus, the measured scattering coefficient is found to depend on the scheme of the experiment. K.S. Shifrin [467] showed that the measured scattering coefficient can be written

$$\alpha_{\text{meas}} = \pi a^2 [2 - \varphi(z)] = 2\pi a^2 \left[1 - \frac{\varphi(z)}{2}\right], \tag{7.55}$$

where $z = \frac{2\pi a}{\lambda} \frac{d}{2l}$; a is the droplet radius, λ is the wavelength of the scattered light, d is the diameter of the receiver entrance aperture, l is the distance from the droplet to the receiver, and $\phi(z)$ is a function that takes account of the shape of the indicatrix and has been tabulated in [467].

Ye.A. Polyakova [599] tested formula (7.63) experimentally for the case of raindrops.

Gumprecht and Sliepcevich [597] described the measured coefficient of a localized layer with the expression

$$\alpha_{\text{meas}} = \pi a^2 R(z), \tag{7.56}$$

where

$$R(z) = 1 + J_0^2(z) + J_1^2(z); \tag{7.57}$$

$j_0(z)$ and $j_1(z)$ are Bessel functions of the first kind and of zeroth and first order.

V.A. Timofeyeva found the measured scattering coefficient to depend on receiver aperture in studies of scattering in a milky

medium [600, 601].

M.V. Kabanov [602] derived an expression for the function B(z) that appears in the formula for α_{meas} in the case of large particles:

$$\alpha_{meas}=\frac{1}{2}\alpha B(z), \tag{7.58}$$

where z has the same significance as in (7.55).

Calculated results for B(z) are given in [602] and [1] for various z from 0 to 15. As z varies from 0 to ∞, the function B(z) runs through values from 2 to 1. Consequently, the measured large-particle scattering coefficient may differ from the true coefficient by at most a factor of 2. It is also shown in [602] that in the case of small particles, α_{meas} is practically independent of distance and differs little from α under atmospheric conditions. The results of experimental studies of the measured scattering coefficient as a function of receiver parameters and the photometered thickness of atmosphere are described in [1]. The measurements were made with artificial fogs. The results were found to agree satisfactorily with theory.

2. Influence of scattered light on measured atmospheric transparency. If the radiation from the source is concentrated in a definite solid angle, the receiver registers not only the radiation propagating along a straight line from the source, but also radiation scattered by particles off the source-to-receiver line. We shall refer to these parts of the radiation sensed by the receiver as the direct and dispersed radiations, respectively. In this case, the illumination E created by these radiations may be written

$$E=E_d+E_D=\frac{I_0}{l^2}e^{-\frac{1}{2}\alpha B(z)l}+E_D, \tag{7.59}$$

where E_d and E_D are, respectively, the illuminations created on the sensitive area of the receiver by the direct and dispersed radiations and I_0 is the intensity of the radiation incident on a scattering layer of thickness l.

Thus, the signal at the receiver, which is usually assumed proportional to the transparency of the atmosphere, will be governed by the illuminations created by both the direct and dispersed radiation. In most studies concerned with atmospheric-transparency measurements, the latter factor is not taken into account, and this may result in gross errors, as will be shown below. /333

The first estimates of the role of singly dispersed radiation in the atmosphere were made by Middleton [603], who calculated the illuminations created by the direct E_d and once-dispersed E_D radiations for the following conditions: a = 2.5 μ, N = $= 10^8$ m^{-3}, l = 0.2, 0.5, and 1.0 μ; a = 10 μ, N = $6.25 \cdot 10^6$ m^{-3} and l = 0 and 5 μ, θ = 0.02, 0.10, 0.20, and 1.0 rad, $0 \leq \Psi \leq 0.05$ rad. Here a, N, l, θ, and Ψ are, respectively, the radius and concentration of the particles, the distance between the source and the receiver, half the angle of the emitting cone of the source, and half the visual angle of the receiver (see Fig. 7.28). Under the conditions studied, the ratio E_D/E_d reached a maximum value of 1.6. Middleton confirmed the calculated data in an experiment in fog, obtaining $E_D/E_d \approx 2$ for a distance of 114 m with θ = 0.30, Ψ = 0.008, and a meteorological visibility of 125 m.

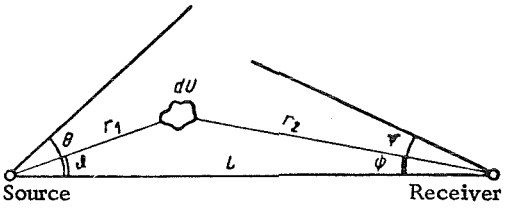

Figure 7.28. Diagram Showing Propagation of Radiation from Source to Receiver.

To obtain data on the role of singly-dispersed radiation in the case of a slightly turbid atmosphere, Stewart and Curcio [604] conducted experiments for long distances (3.7 and 16.7 km) and a broad range of Ψ (from 1.5 to 13°) for individual segments of the spectrum in the 0.36-0.61-μ band, which were isolated by filters. Reduction of the measured results yielded the following empirical formula for the relation of the true transparency T to the measured transparency T_Ψ:

$$T_\Psi = T + 0.5(1-T)(1-e^{-2\Psi}). \qquad (7.60)$$

Formula (7.60) was obtained for T > 0.70; the coefficient 0.5 is related to the albedo of the underlying surface. /334

Gibbons et al. [605-607] made extensive studies of the role of singly-dispersed radiation. For the illumination E_D they obtained the formula

$$E_D = gI_0 \int_v \frac{F(\varphi) e^{-\alpha(r_1+r_2)} \cos\Psi}{r_1^2 r_2^2} dv, \qquad (7.61)$$

where g varies from 0.5 to 1 depending on the nature of the underlying surface, v is the scattering volume, $F(\phi)$ is the scattering indicatrix, $\phi = \psi + \vartheta$ and the remaining nomenclature is that of

Fig. 7.27. We note that formula (7.61) had been obtained earlier by V.M. Meshkov [608], and for double as well as single dispersion.

Gibbons calculated E_D by numerical integration of formula (7.61) with the following parameter values: $\theta = \pi/2$, $\Psi = 8°20'$, 25, 50, 75, and 90°, $\tau = \alpha l = 0.1$, 0.3, 0.9, 1.2, and 3.6.

Gibbons' experimental studies were performed for large distances, large Ψ, and low atmospheric turbidities over San Francisco Bay and in the Nevada desert. In the former case, the distances varied from 1.18 to 14.37 miles, and in the latter from 0.51 to 13.17 miles. The studies were made for wavelengths of 0.40, 0.50, 0.70, 0.83, and 0.90 μ.

Eldridge and Johnson [609] made similar measurements for slant paths in the atmosphere with $\Psi = 1.5$, 15, and 75° in the visible region and in the bands from 0.35 to 2 μ and 0.75 to 2 μ for atmospheric thicknesses from 0.5 to 9 km under a variety of weather conditions. They obtained more detailed data for fogs and hazes for an isotropic source and a receiver with $\Psi = \pi$ [610]. The empirical formula obtained for the transmission function deviates from Bouguer's law; the authors explain this as being due to the substantial influence of the dispersed radiation.

Theoretical and experimental studies of the effect of scattered radiation on the measured atmospheric transparency were reported in our papers [611-615]. First of all, we attempted to simplify formula (7.61) in such a way as to permit calculation of E_D for a broad range of conditions in the atmosphere. Essentially, /335 this simplification reduces to the following.

Substituting the variables ϑ and ϕ for r and ψ in (7.61) in accordance with the usual rules [616], putting g = 1, $F(\phi) = \alpha/4\pi f(\phi)$, where $f(\phi)$ is the normalized scattering indicatrix, and remembering that $\phi = \psi + \vartheta$, we obtain

$$E_D = \frac{\alpha I_0}{2l} \int_0^{\Psi} d\psi \int_0^{\theta} e^{-kl \frac{\sin\psi + \sin\vartheta}{\sin(\vartheta+\psi)}} f(\psi+\vartheta)\cos\psi\, d\vartheta. \qquad (7.62)$$

For small ψ or ϑ, the exponential function in (7.62) can be taken outside the integral:

$$E_D = \frac{\alpha I_0 e^{-\alpha l}}{2l} \int_0^{\Psi} d\psi \int_0^{\theta} f(\psi+\vartheta)\cos\psi\, d\vartheta. \qquad (7.63)$$

It is easily seen from (7.63) that for the given experimental conditions, the double integral does not depend on the distance between the receiver and the source. We introduce the nomenclature

$$D=D(\rho, \Psi, \theta)=\frac{1}{2}\int_0^{\Psi}\int_0^{\theta} f(\psi+\vartheta)\cos\psi\, d\psi\, d\vartheta, \tag{7.64}$$

whereupon

$$E_D=\frac{\alpha I_0 e^{-\alpha l}}{l} D. \tag{7.65}$$

The dependence of D on ρ enters (7.64) through the scattering indicatrix $f(\psi, \vartheta)$.

As the estimates showed, formula (7.63) describes E_D with an error that is definitely smaller than 5% at values of $\Psi \leq 0.1$ and atmospheric transmissions $T \geq 0.1$, which are encountered in most cases of atmospheric-transparency measurement.

A formula for the total illumination on the receiver's sensing surface is easily obtained from (7.61), (7.63), and (7.64):

$$E=E_r+E_D=\frac{I_0}{l^2} e^{-\alpha l}[1+\alpha l D(\rho, \Psi, \theta)], \tag{7.66}$$

whence follows the simple relation

$$\frac{E_D}{E_r}=\tau D, \tag{7.67}$$

where $\tau = \alpha l$ is the optical thickness of the medium.

We note that with $\Psi \leq 0.1$, formulas (7.63)-(7.66) can be used /336 for any wavelength band and any homogeneous scattering medium with a known scattering indicatrix.

The method and results of calculation of D for various ρ, Ψ, and θ are described in detail in [1]. Here we present only one figure to illustrate the dependence of D on Ψ for various ρ and two values of θ: $\pi/2$ and $\pi/6$ (Fig. 7.29).

The numerical values obtained for D for various ρ, θ, and Ψ permit quantitative estimation of the role of singly dispersed light under various experimental conditions in the atmosphere. From these data, for example, it follows that for relatively small $\Psi = 0.1$, the quantity D may reach values of 0.5-0.7 for large

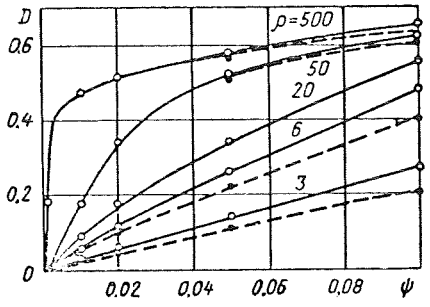

Figure 7.29. Curves of the Function D vs. Receiver Aperture for Various ρ and Two Values of the Half-Angle of the Source Radiation Cone: ———) $\theta = \pi/2$; ---) $\theta = \pi/6$.

particles; at the τ of a few units that are often encountered in practice, this is equivalent to a contribution to the signal from the dispersed light that is several times larger than the contribution from the direct attenuated light. Consequently, failure to take this fact into account in experimental studies of atmospheric transparency may give measured transparency values several times larger than the true transparency.

The monograph [1] gives a detailed description of experimental studies of D that were carried out in an artificial-fog chamber and in natural fogs and snows. Comparison of the results of measurements in the artificial fogs with their known microstructure and the calculated values of D indicated satisfactory agreement between experiment and theory. /337

A.P. Ivanov and N.Ya. Khayrullina [617] made a detailed experimental study of the influence of source radiating cone angle and receiver angular aperture on the results of attenuation-coefficient measurements made at various optical thicknesses of model scattering media. The latter were so selected as to have microphysical and optical properties (for example, photon-survival probabilities) conforming to those of the natural media. Tables of $(\alpha_{meas} - \alpha)\alpha^{-1}$ were compiled in [617] for various Ψ, θ, and τ (the notation is ours).

Hodkinson and Greenfield [618] calculated the scattering of white light by a polydisperse aerosol with allowance for the parameters of the instrument used for the measurement. The calculation was based on the Mie theory for values of the refractive index n = = 1,2 (0.2) 2.4 and Mie parameters in the range $0.1 < \rho < 100$.

The above results from study of E_D pertain to rather broad beams of radiation. In recent years, however, with the use of lasers in communications, data-transmission, radar, distance-measurement, and other similar systems, study of the role of scattered radiation in the results of measurements of various quantities that characterize the scattering properties of the medium in propagation of narrow collimated light beams through it has become an urgent practical necessity. The results of the corresponding studies will be examined in Chapter 9.

Part Three /338

PROPAGATION OF SPATIALLY LIMITED BEAMS OF LIGHT IN THE ATMOSPHERE

Chapter 8

CHARACTERISTICS OF RADIATION FROM VARIOUS TYPES OF LASERS

INTRODUCTION

The object of this chapter is to examine briefly those characteristics of the radiation from lasers that are of importance in the problem of laser-light propagation in the atmosphere. Foremost among these characteristics are: 1) spectrum, 2) energy and power, 3) coherence, 4) directivity, 5) operating mode, and 6) the polarization of the radiation. We do not propose to give a complete survey of all of the work done to date with acquisition of various concrete data on the radiating properties of specific lasers. We shall be interested primarily in data on the values recently attained in those parameters of various types of lasers that are of importance for the problem of propagation of their radiation in the atmosphere.

The overwhelming majority of presently known lasers can be assigned to one of four classes: 1) ionic-crystal lasers; 2) glass lasers; 3) gas lasers; 4) semiconductor lasers. Below we shall describe the basic characteristics of the radiation from these types of lasers, chiefly on the basis of surveys published over the past 2-3 years [619-643, 701, 831].

1. IONIC-CRYSTAL LASERS

As we know, the first laser was developed around a ruby crystal — a sapphire (Al_2O_3) single crystal doped with the trivalent chromium ion Cr^{3+}. This type of laser is now the most widely used, although emission has been obtained on many other ionic /340 crystals.

Ionic-crystal lasers are characterized by a high concentration of the working particles (10^{17} - 10^{20} cm^{-3}), which are distributed more or less uniformly through the volume of the crystal, and by a large lifetime of the working levels of the ions ($\sim 10^{-3}$ sec). These properties of the working bodies of the lasers under consideration are responsible for the high radiant-energy yields in free generation and the giant powers developed in Q-switched operation with a relatively simple solution of the problem of

TABLE 8.1. LIST OF CRYSTALS AND DOPING IONS GOVERNING LASER RADIATION AT VARIOUS WAVELENGTHS [624, 628]

Crystal	Doping-ion	Doping-ion concentration, %	Wavelenght of laser radiation, Å
CaF_2	H_0^{3+}		5 512
LaF_3	Pr^{3+}	1	5 985
Y_2O_3	Eu^{3+}	5	6 113
Al_2O_3	Cr^{3+}	0.05	6943, 6 934, 6 929
SrF_2	Sm^{2+}	0.01	6 969
Al_2O_3	Cr^{3+}	0.5	7 009, 7 041, 7 670
CaF_2	Sm^{2+}	0.01	7 083
$CaWO_4$	Nd^{3+}	1	9 145, 10 580, 13 392
$Y_3Al_5O_{12}$	Yb^{3+}		10 296
CaF_2	Nd^{3+}	1	10 460
$CaWO_4$	Pr^{3+}	0.5	10 468
$CaMoO_4$	Nd^{3+}	1.8	10 610
$Y_3Al_5O_{12}$	Nd^{3+}		10 648
CaF_2	Tm^{2+}	0.01	11 160
Er_2O_3	Tm^{3+}		13 340
$Ca(NbO_3)_2$	Er^{3+}		16 100
$CaWO_4$	Er^{3+}	1	16 120
MgF_2	Ni^{2+}	1	16 220
$Y_3Al_5O_{12}$	Er^{3+}		16 602
MgF_2	Co^{2+}	1	17 500, 18 030
$CaWO_4$	Tm^{3+}		19 110
$Y_3Al_5O_{12}$	Tm^{3+}		20 132
$CaWO_4$	Ho^{3+}	0.5	20 460
$Y_3Al_5O_{12}$	Ho^{3+}		20 975
SrF_2	U^{3+}		24 070
CaF_2	Dy^{2+}	0.01	25 588
ZnF_2	Co^{2+}	1	26 113
CaF_2	U^{3+}	0.05	26 130

cooling the working bodies.

The following materials are used as the base of the working body in ionic-crystal lasers: Al_2O_3, CaF_2, $CaWO_4$, SrF_2, BaF_2, $SrCl_2$, LaF_3, CeF_3, $SrWO_4$, $CaMoO_4$, $PbMoO_4$, YO_3, Er_2O_3, $Y_3Ga_5O_{12}$, $Gd_3Ga_5O_{12}$, MgF_2, ZnF_2, and $Ca(NbO_3)_2$ (Table 8.1). Crystals of Al_2O_3, CaF_2, and $CaWO_4$ and synthetic garnets are most widely used.

Depending on operating mode, all ionic-crystal lasers can be classed into three groups: 1) continuous-duty; 2) free-generating pulsed; 3) Q-switched pulsed.

TABLE 8.2. CHARACTERISTICS OF THE RADIATION OF THE MOST EFFICIENT IONIC-CRYSTAL LASERS OPERATING IN THE CONTINUOUS-GENERATION MODE [628]

Working body	Radiation wave lenght, μ	Efficiency, %	Power, W	Working temperature, °K
$Al_2O_3+Cr^{3+}$	0.69	0.1	1	300
$Y_3Al_5O_{12}+Nd^{3+}$	1.06	0.2	200	300
$Y_3Al_5O_{12}+Ho^{3+}$	2.12	5	15	77
CaF_2+Dy^{2+}	2.36	1—1.5	100	77

To obtain continuous radiation from a laser, it is necessary to have a certain excess of excited ions per unit volume of the working body as a result of continuous pumping. Known optical-pumping sources yield this ion excess in far from all laser working bodies. Continuous generation of radiation becomes possible when this condition is met. The parameters of this radiation (see, for example, Table 8.2) depend on many factors that will not be discussed here.

It is much easier to obtain pulsed radiation from ionic-crystal lasers. Pulsed pumping stimulates emission in a substantially larger number of ionic crystals than continuous pumping. The power attained is substantially larger in pulsed operation, and the energies released range into the thousands of joules. /341

Fantastic powers are attained in Q-switched operation. For example, one industrial ruby-laser model has put out a power of 10^9 W in Q-switched operation with a pulse duration of 20 nsec and a divergence of one part in one billion. Special mode-synchronizing measures (known as mode locking) can be used to obtain radiated powers of the order of 10^{10} - 10^{12} W with pulse durations from 10^{-11} to 10^{-13} sec, which can be estimated only by indirect methods, since the best low-inertia radiation detectors cannot register pulses with such durations.

Let us dwell briefly on the spectral characteristics of the radiation of ionic-crystal lasers. Table 8.1 listed radiated wavelengths that characterize the center of the narrow spectral interval radiated by the laser. Unless special measures are taken, the radiation from the laser is multimode and occupies a segment several tenths of an angstrom wide with a characteristic spiked structure of the frequency and time distributions of intensity. Special measures narrow the emission band of the laser significantly, down to the order of 10^{-3} Å. Without collimating systems, the divergence angles of ionic-crystal lasers depend on the geometrical dimensions of the working bodies, the wavelength of the radiation, the material of the working body, and the number of

modes generated. Divergence angles of a few milliradians are common. Use of special reflectors with selective distribution of the reflection coefficient as a function of incidence angle makes it possible to obtain near-diffraction divergences. As a rule, the energy is nonuniformly distributed in the cross section of the radiation beam.

The coherence of the radiation from ionic-crystal lasers depends on the number of modes. Each of the modes emits light with a definite degree of coherence. The same should be said concerning the degree of polarization of the radiation.

2. GLASS LASERS

/342

A distinctive feature of lasers working with glass doped by trivalent ions of neodymium, ytterbium, holmium, and erbium is related to the properties of glass, which can be varied over a rather broad range by varying its chemical composition (Table 8.3).

TABLE 8.3. CERTAIN CHARACTERISTICS OF RADIATION FROM GLASS LASERS DOPED WITH TRIVALENT NEODYMIUM, YTTERBIUM, HOLMIUM, AND ERBIUM IONS [629]

Composition of glass	Doping-ion	Wavelenght of radiation, μ
Na—La—Si	Nd^{3+}	0,92
Li—Mg—Al—Si	Yb^{3+}	1,015
K—Ba—Si	Nd^{3+}	1,06
K—Ba—Si	Yb^{3+}	1,06
Li—Mg—Al—Si	Ho^{3+}	1,35
La—Ba—Th—B	Nd^{3+}	1,37
Yb—Na—K—Ba—Si	Er^{3+}	1,54
Li—Mg—Al—Si	Er^{3+}	1,55

In addition, working bodies of various shapes and sizes, ranging from fiberoptic elements a few microns in diameter and up to 10 m long to very large rods up to 60 mm in diameter and 2 m long, can be made from glass. Neodymium-glass lasers are most widely used.

The most powerful laser has been built with neodymium glass; its pulse energy reaches 5000 J at a working-rod length of 90 cm and a diameter of 30 mm. Operating in the Q-switched mode, the neodymium glass laser radiates a pulse with a power ranging up to several tens of gigawatts and lasting 10-50 nsec.

The radiation of glass lasers is characterized by more or less uniform distribution over the beam cross section. The divergence of the beam is approximately the same as in the ionic-crystal lasers.

Glass lasers have a much broader radiated-frequency band than ionic-crystal lasers. Unless special measures are taken, glass /343
lasers usually radiate a band several tens of angstroms wide. Separation of specific emission lines narrows the radiation spectrum of the laser significantly. Neodymium-glass lasers now radiate in a spectral segment of the order of 10^{-3} Å wide.

The coherence of glass-laser radiation depends strongly on the number of modes, as in the case of ionic-crystal lasers.

Glass lasers can be made to operate in a mode in which the spontaneous radiation that arises at one end of the rod is fully saturated on reaching the other end (the superluminescence mode). In this case, uniform intensity distribution over the contour of the spontaneous-emission line is observed in the radiated spectrum, and the radiation itself is found to be unpolarized. Its power reaches 10^9 W at a pulse duration of 70 nsec.

3. GAS LASERS

The gas lasers are the most common of all of the laser types. The basic qualitative difference between these lasers and others consists in the high monochromaticity of their radiation and their high frequency stability, which are little affected by external conditions. These properties of gas lasers result in much higher coherence of the radiation than is observed for other lasers. The radiations of gas lasers occupy a much broader and continuously expanding range of wavelengths. At the present time, this range extends from 2315.5 Å (the emission line of Xe II) to 1 mm. Gas lasers yield the highest powers in continuous operation.

All gas lasers can be divided into the following four classes: 1) neutral-atom lasers; 2) ion lasers; 3) molecular lasers and 4) chemical lasers. The emission line lies in one or another region of the spectrum depending on the particles in which the corresponding energy transition is effected. High-energy electron transitions of ions fall into the ultraviolet and visible regions; electron transitions in atoms yield emission lines in the visible and nearest infrared. Vibrational-rotational and purely rotational transitions of molecules give rise to generation of lines /344
filling a broad band of wavelengths from the near infrared into the microwave region. The radiation wavelengths of chemical lasers depend on the energy levels between which the corresponding transition takes place in particles formed as a result of a chemical reaction.

Lasers operating on helium-neon mixtures are most common among the neutral-atom gas lasers. In turn, lasers radiating

wavelengths of 6328 Å, 1.15 μ and 3.39 μ are most common among these lasers. The most powerful of the atomic lasers, which radiates at 6328 Å, delivers a continuous-duty power of 1 W from a discharge tube 5 meters long. Commercial models of this laser have powers no greater than 100 mW.

Pulsed atomic lasers working on self-limited transitions have recently been developed with powers on the order of a few kilowatts and durations on the order of a few nanoseconds. A copper-vapor laser was recently developed. It is expected that the efficiency of this laser will reach 30%.

Ion lasers deliver higher radiated powers (up to 50-100 W) in continuous operation in the visible region of the spectrum than any other type of laser. Among the ion lasers, the most common type is the ionized-argon laser, which emits a whole series of lines in the range from 0.48 to 0.52 μ.

The molecular-nitrogen and carbon-dioxide lasers are commonest among the molecular lasers. In the former case, a self-limited electron-vibrational transition is used to obtain radiation at λ = 3371 Å with a duration of 20 nsec and a maximum power of 0.3-2.5 mW in pulses with a repetition frequency of 300 Hz. The commercial model has a power of 100 kW, a pulse duration of 10 nsec, repetition frequencies from 1 to 100 Hz, and an average maximum power of 100 W.

The CO_2 laser is the most powerful among all known continuous-duty lasers in any wavelength band. A laser with a continuous-duty power of several kilowatts at a wavelength of 10.6 μ was recently built. Another advantage of CO_2 as a laser working medium consists in the fact that generation can take place on a whole series of transitions in a spectral interval of the order of 100 cm^{-1} in the region of the atmosphere's long-wave transparency window. In addition, the large lifetime of the upper level of CO_2 (more than 1 msec) permits Q-switched operation of this laser. /345

The first of the chemical gas lasers was one in which radiation appears as a result of a transition between the metastable and ground states of iodine. The iodine atoms are produced on photodissociation of the CH_3I molecule under the action of ultraviolet light. The wavelength at which this laser radiates is 1.315 μ. Use of the photodissociation of the CF_3I molecule delivered higher efficiency and an energy of 60 J in a pulse lasting 100 μsec. A chemical laser in which the chemical reaction between chlorine and hydrogen is utilized is considered highly promising. The spectrum of its radiation lies in the 3-μ region.

Let us now consider the spectral characteristics of gas-laser radiation. As we know, the width of the spectral segment in which multimode gas lasers radiate is determined by the Doppler contour. The latter's width is known quite exactly for the emission of the

helium-neon laser at 6328 Å (1700 MHz). The Doppler width decreases in inverse proportion to wavelength. It is 920 and 310 MHz for helium-neon lasers with wavelengths of 1.15 and 3.39 μ, respectively, and about 60 MHz for carbon dioxide lasers.

The Doppler width of an ion laser is considerably greater than those of atomic and molecular lasers. This is because generation occurs at high temperatures in ion lasers. For argon lasers, the Doppler-contour width is 3500 MHz, and 2500 MHz for krypton and xenon lasers.

When gas lasers are used, it is easier to obtain single-mode, single-frequency continuous generation with exceptionally high stability of the radiated frequency than it is with other types of lasers. The short-term frequency stability may range to 10^{-9} and better. The long-term stability is several times 10^{-8} and practically independent of external conditions.

The single-frequency continuous gas laser is the best among all types of lasers in respect to the coherence of the radiation /346 in space and time.

The directivity of the radiation is highest for gas lasers. The divergence angles of gas lasers depend on the geometrical dimensions of the laser and on radiated wavelength. Without collimating systems, the angles subtended by commercial models of the lasers are fractions of a milliradian.

4. SEMICONDUCTOR LASERS

The exceptionally high concentration of the working particles in semiconductor lasers (on the order of 10^{22} cm^{-3}) makes it

TABLE 8.4. CERTAIN CHARACTERISTICS OF THE RADIATION FROM SEMICONDUCTOR LASERS [631]

Material	Radiation wavelenght, μ	Pumping method
ZnS	0.32	Electron beam
ZnO	0.38	Electron beam
CdS	0.50	Electron beam; optical
CdS_xSe_{1-x}	0.50—0.69	Electron beam
GaScSe	0.59	Electron beam
$Ga(As_xP_{1-x})$	0.64—0.88	p-n junction
CdSe	0.68	Electron beam
CdTe	0.79	Electron beam
CdS_xSe_{1-x}	0.83	p-n junction

TABLE 8.4. (Cont'd.)

Material	Radiation wavelenght, μ	Pumping method
CaAs	0.84	p-n junction , optical, avalanche breakdown, electron beam
InP_xAs_{1-x}	0.89	p-n junction
InP	0.90	p-n junction
GaSb	1.51	p-n junction, electron beam
InAs	3.13	p-n junction, electron beam, optical
Te	3.65	Electron beam
$Hg_xCd_{1-x}Te$	3.76—4.13	Optical
PbS	4.27	p-n junction, electron beam
InSb	5.38	p-n junction, electron beam, optical
PbTe	6.54	p-n junction, electron beam, optical
$Pb_xSn_{1-x}Te$	6.54—16.67	Optical
PbSe	8.55	p-n junction, electron beam

possible to obtain generation using working bodies of very small volume, and, in turn, this causes wide divergence of the radiation (on the order of 10°).

The gallium arsenide laser, which radiates a band a few tens of angstroms wide around 0.84 μ, is the most common semiconductor laser. A maximum radiated power of 3 W has been obtained from this laser in continuous duty with an efficiency of 15%.

Semiconductor lasers (Table 8.4) can operate in both continuous and pulsed modes. In the latter case, the pulse-repetition frequency can be varied through a very broad range.

5. VARIATION OF LASER EMISSION PARAMETERS DUE TO VARIOUS CAUSES /347

Strictly speaking, the emission parameters of all laser types may vary under the influence of various factors. In some cases, these causes are related to generation conditions, while in others they are introduced deliberately into the particular experiment.

The influence of the temperature of the laser's working medium on its emission spectrum is an example of factors of the first type. This influence is especially conspicuous in the case of the ruby laser. Direct experiments performed by various investigators have shown that the emitted wavelength changes by an average of 1 Å when the temperature of the ruby is changed by 13°C. This shift varies slightly from specimen to specimen. We recall that a shift of the emission of a laser by even a tenth of an angstrom

in the 0.69-μ region may change its absorption in the atmosphere appreciably (see Fig. 3.10). The influence of temperature on the emission parameters of other lasers has not yet been adequately studied. /348

The temperature at which generation occurs may influence not only the emission of solid-state lasers, but also that of gas and gas-mixture lasers. Thus, for example, the CO_2 laser may generate in different lines depending on generation temperature.

In addition to temperature variation, the characteristics of laser emission may also be influenced by the concentration of doping impurities, their volume distribution, the quality of the resonators, ambient temperature, the total and partial pressures of the gases in the case of gas lasers, etc.

In addition to the above factors of influence on the emission characteristics of lasers, which are related to frequently uncontrollable generation conditions, there are cases in which the investigators deliberately change certain parameters to obtain control of the laser's emission characteristics and, first of all, the spectral characteristics of the emission.

A number of methods have now been developed for varying the spectral characteristics of laser emission:

1) isolation of specific modes in the laser emissions;

2) parametric emission;

3) Harmonic emission;

4) stimulated Raman scattering, etc.

The simplest method of isolating specific laser emission modes consists in the introduction of additional mirrors into the laser's resonator. Introduction of one mirror forms an auxiliary Fabry-Perot interferometer, whose reflection coefficients depend on emission frequency. This increases the Q of certain modes and suppresses undesirable modes. Here the energy of the suppressed modes can be pumped into generating modes. The selection of generated modes increases if two mirrors are introduced into the laser resonator or the mirror system is matched in a certain way. Rotation of the mirror introduced into the resonator changes the Q of the corresponding modes, thus making it possible to obtain selection of first one and then another mode or to scan the generated modes over the luminescence contour [643].

Smooth scanning of laser emission along the luminescence contour has recently been accomplished experimentally [644]. /349

Selection of individual modes has made it possible to obtain ruby-laser emission with the following data. The laser was made to generate single-mode with a spectral emission-line width smaller than 0.001 Å, a pulse power of 5 mW, and wavelength stability of ±0.005 Å without special control of working-body temperature [645]. Powers of 14 and 25 mW were obtained with emission-line widths of 0.005 Å and 0.008 Å. Single-mode generation has also been obtained in neodymium-glass lasers.

The monochromatism and radiated power obtained from ruby and neodymium-glass lasers have made it possible to use the methods of parametric generation, second-harmonic generation (SHG), and stimulated Raman scattering (SRS). Here the width of the emitted band may be held constant or even narrowed under certain conditions as compared with its value in the driving laser. Combination of the SHG and SRS techniques makes it possible to obtain coherent emission of various wavelengths. Generation has been obtained by this method at more than 40 wavelengths in the 0.4-1.2-μ region of the spectrum.

Use of the parametric-generation method permits scanning of laser emission in relatively narrow segments of the spectrum. Models of frequency-tunable lasers that use nonlinear KDP and $LiNbO_3$ crystals have recently been built. The following concrete data have been obtained. When the second-harmonic emission of a neodymium-glass laser (wavelength 0.53 μ, pulse power 30-35 MW/cm^2, pulse duration $2.5 \cdot 10^{-8}$ sec, pump divergence 7'-8') was passed through a KDP crystal, the wavelength of the radiation was retuned into the 9571-11,775-Å region. The output-signal power was 0.5-1 kW, and the spectral half-width 0.03-0.07 cm^{-1} [644]. Frequency retuning has been obtained in the 0.684-2.335-μ region using the same second harmonic of a neodymium-glass laser as the stimulating radiation and an $LiNbO_3$ crystal. At a stimulating radiation power of $5 \cdot 10^4$ W, the output-signal power was 50 W [645]. It is suggested that this crystal might be used for frequency retuning in the 0.59-5-μ region if the temperature of the crystal were also varied in the measurements. /350

Finally, we take note of the possibility of laser-emission frequency scanning by means of a magnetic field in which the laser is placed. Relatively small magnetic fields can be used to frequency-scan the emission of gas lasers over several tenths of a reciprocal centimeter. This frequency shift might cause a substantial change in the absorption coefficient for laser light propagating in the earth's atmosphere.

Chapter 9 /351

PROPAGATION OF SPATIALLY LIMITED BEAMS OF OPTICAL RADIATION IN ATMOSPHERIC AEROSOLS

During the propagation of spatially limited light beams in an aerosol atmosphere, the radiation is attenuated and a particle-scattered light field appears. On superposition of the direct and scattered radiation, the brightness distribution of the radiation over the beam cross section depends in a complex manner on the optical thickness of the layer, the geometrical dimensions of the beam, the properties of the scattering medium, and the polarization state of the incident radiation. This pattern may be distorted by the instruments used in experimental studies.

The task of the present chapter is to examine these patterns in the propagation of spatially limited beams of radiation (with emphasis on laser emission) in various atmospheric aerosols. Attention will be concentrated on srructural analysis of the light field at small scattering angles (forward scattering) and scattering angles around 180° (backward scattering), since it is of prime importance to have data on the forward and back scattering for use of lasers in communications, data-transmission, optical-radar, distance-measuring, and other systems.

1. BRIGHTNESS OF FORWARD-SCATTERED RADIATION

1. Theoretical investigations. The light field due to scattering of radiation on aerosol particles is described by a transfer equation whose solution involves major mathematical difficulties in the general case [646]. At small scattering angles, the brightness of the forward-scattered radiation can be calculated by the small-angle approximation of the transfer equation [647-649]. However, this method has substantial limitations, since it /352 does not take account of polarization effects and is suitable only for beams of unlimited width and large particles (strongly elongated scattering indicatrices). Forward-scattered brightnesses were calculated by the small-angle approximation in various scattering media in [650], which also established the limits of applicability of A.A. Gershun's formula [651], which describes the brightness of forward-scattered light with only single scattering taken into account.

In the case of narrow collimated pencils of light, theoretical determination of the brightness of forward-scattered radiation is a very complex task. It has thus far been solved only for certain particular cases. Ye.M. Feygel'son [652] derived an approximate formula for the brightness B of light scattered at small angles in a searchlight beam:

$$B = B_0 \frac{f(0)}{4\Gamma_2} e^{-\tau} \varphi(\tau) \theta^2, \tag{9.1}$$

where

$$\varphi(t) = \begin{cases} \left[\tau + \ln\left(\frac{\Gamma_2}{2} + \frac{\Gamma_1}{2} e^{-\tau}\right)\right], & \tau \leqslant \tau_0 (z \leqslant z_0), \\ \left[\tau + \ln\left(\frac{\Gamma_2}{2} + \frac{\Gamma_1}{2} e^{-\tau_0}\right)\right] + \tau_0 \left(1 - \frac{z_0}{z}\right), & \\ \tau \geqslant \tau_0 (z \geqslant z_0); & \end{cases} \tag{9.2}$$

Γ_1 and Γ_2 are the radiations scattered into the forward and back hemispheres, respectively; the quantity z_0 corresponds to the focal length of the searchlight and is reckoned along a z axis that coincides with the propagation direction of the beam; θ is the divergence angle of the beam, which is linked to the beam radius a by the relation $\theta = a/z_0$; $f(0)$ is the scattering indicatrix in the forward direction, and τ is the optical thickness. As we should expect, parameters characterizing the dimensions of the light beam appear in the formula.

More general formulas for limited beams were derived in [653] and [654], but their use for the corresponding quantitative calculations is difficult.

M.V. Kabanov [656] derived expressions that can be used to calculate the brightness of singly scattered light for various geometrical parameters of a narrow beam whose divergence equals the visual angle of the receiving system:

$$V = V_0 e^{-\tau} \left[1 + \tau \frac{1}{2} \int_0^{\theta} \int_0^{\Psi} f(m, \rho, \psi + \vartheta)\, d\psi\, d\vartheta\right] = V_0 e^{-\tau} [1 + \tau D], \tag{9.3}$$

/353

where V_0 is the magnitude of the signal in the absence of attenuation in the medium, τ is the optical thickness of the layer, θ and Ψ are the field angles of the radiation source and the receiving system, and $f(m, \rho, \psi + \vartheta)$ is the normalized scattering indicatrix, which depends on the scattering angle $\phi = \psi + \vartheta$, the parameter ρ, and the complex refractive index of the scatterers. The quantity D defines the singly scattered radiation at various parameters Ψ and θ in various scattering media.

If the distance between the source and receiver of the radiation satisfies the condition $l >> d/\theta$, where d is the diameter of the receiving lens, formula (9.3) can be used to describe the attenuation of a narrow collimated beam.

In [656], an expression was derived for the function D for the case in which θ and Ψ are small and equal to one another and the scattering indicatrix is represented in terms of Legendre polynomials:

$$D=\frac{1}{2}\left[\Psi\theta+\sum_{n=1}^{\infty}a_n\int_0^{\Psi}\int_0^{\theta}P_n\left[\cos\left(\psi+\vartheta\right)\right]d\psi\,d\vartheta\right]\cong$$

$$\cong\frac{1}{2}\varphi^2\sum_{n=0}^{\infty}a_n=\frac{1}{2}\varphi^2A_n, \qquad (9.4)$$

where $\phi = \Psi = \theta$ and the a_n are the coefficients of the Legendre polynomials, which depend on the optical properties of the scattering medium.

As was shown in [656], (9.4) may be replaced by a simpler expression when $\rho \geq 5$; this is obtained from (9.4) by applying the Penndorf approximation formula [657]:

$$D=\frac{\rho^2\varphi^2}{2}\frac{K(\rho,m)}{2}, \qquad (9.5)$$

where K(ρ, m) is the scattering efficiency of a particle.

Expressions (9.4) and (9.5) cannot be used for very large ρ, since they were derived without consideration of the angular dependence of the Legendre polynomials at small ϕ. Accordingly, a formula for D was obtained in [656] using a representation of the scattering indicatrix in terms of Bessel functions:

$$D=\frac{1}{2}\int_0^{\varphi}\int_0^{\varphi}f(\psi+\vartheta)\,d\psi\,d\vartheta=\rho\varphi\int_{\rho\varphi}^{2\rho\varphi}\left[2\frac{J_1(z)}{z}\right]^2dz$$
$$+2\left[1-J_0^2(\rho\varphi)-J_1^2(\rho\varphi)\right]-\left[1-J_0^2(2\rho\varphi)-J_1^2(2\rho\varphi)\right], \qquad (9.6)$$

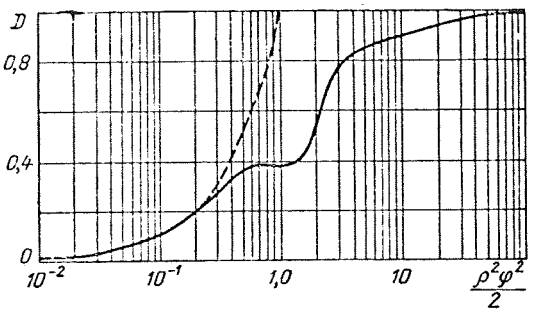

/354

Figure 9.1. Curves Obtained for D as a Function of the Parameter ρ on the Basis of Calculations by Formulas (9.5) (dashed curve) and (9.6) (solid curve).

where J_0 and J_1 are the Bessel functions.

We note that representation of the scattering indicatrix in terms of Bessel functions describes the angular distribution of scattered-light intensity in a range of scattering angles ϕ amounting to a few degrees accurate to within 3% for particles with $\rho \geq \geq 60$.

Figure 9.1 presents calculated results for D according to formulas (9.5) and (9.6). The calculated results indicate that when the field angles of the receiving system and the source are the same for narrow collimated beams of radiation with divergences of a few thousandths of a radian, the singly forward-scattered radiation can be disregarded as small by comparison with the direct radiation of the beam up to optical-thickness values in the tens in fogs and even higher in hazes. In the case of rain, D approaches unity under the same conditions, so that even at $\tau = 1$, the singly-scattered light in the beam zone may be as bright as the direct beam.

The statistical-test (Monte Carlo) method is, in our view, highly promising for solution of problems in the radiative transfer of spatially limited light beams in scattering and absorbing media. The Monte Carlo method is highly efficient in solution of multidimensional radiative-transfer problems in media with various optical characteristics for finite source and receiver geometry. The relatively slow convergence of the method depends only on the number of statistical tests and the quality of modelling. The development of various modifications of the method, along with the use of modern electronic computers, has made it possible to solve many problems in atmospheric optics. /355

A rather large number of papers has been devoted to the theory of the Monte Carlo method as applied to the problem of radiative transfer (see, for example, [832]). Application of the method to solution of atmospheric-optics problems was examined by G.I. Marchuk and G.A. Mikhaylov [655]. G.A. Mikhaylov and G.M. Krekov perfected certain modifications of the method, derived algorithms, and solved a number of problems in the propagation of spatially limited light beams in various scattering media [658, 659, 783, 833-837, 843]. Some of the results obtained will be analyzed below. Here we shall briefly examine the results of investigations of multiple forward scattering of radiation as it occurs in the propagation of various spatially limited light beams and is registered by receivers with various sensitive-area dimensions. The program of the calculation assumes the possibility of varying the optical properties of the medium and the geometry of the source and receiver through very broad ranges. We shall confine ourselves to description of certain characteristic cases.

The angular intensity distribution of multiply scattered light in the receiver plane was calculated in [837] for the

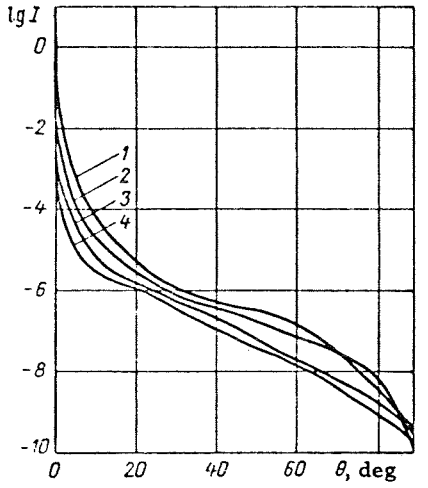

Figure 9.2. Calculated Results for Angular Intensity Distribution of Multiply Forward-Scattered Radiation (λ = 0.45 μ) in a Water Cloud with Optical Thickness τ = 5.0 for Various Source Divergence Angles: θ = 6' (curve 1); 1° (curve 2); 5° (curve 3); 10° (curve 4) (source and receiver diameters 4 and 150 mm, respectively).

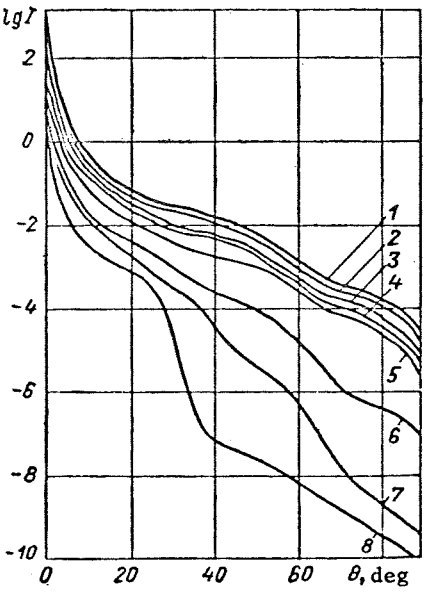

Figure 9.3. Calculated Results for Angular Intensity Distribution of Multiply Forward-Scattered Radiation (λ = 0.45 μ) in a Water Cloud with Optical Thickness τ = 4.0 for Various Receiver Diameters D(r) = 4.0 m (curve 1); 3.0 m (2); 1.5 m (3); 1.0 m (4); 0.5 m (5); 0.2 m (6); 0.15 m (7) (the diameter and divergence angle of the source are 4 mm and 30', respectively).

following numerical-experiment conditions. The radiating and receiving surfaces are circular in shape. The optical axes of the source and receiver collimators coincide. The intensity of the source radiation is uniformly distributed in cones with angles θ equal to 6', 1°, 5°, and 10°. The wavelengths of the radiation are 0.45 and 0.7 μ. The radiation propagates in the water cloud whose indicatrix and attenuation coefficient were obtained in Deirmenjian's paper [517]. The source and receiver diameters D_1 and D_2 are 4 and 150 mm, respectively. The optical thicknesses τ traversed by the direct radiation of the beam are 3.0, 5.0, and 10.0. /357

Figure 9.2 presents calculated results for the angular intensity distribution of multiply forward-scattered radiation in the receiver plane.

For each of the source divergence angle values studied, the intensity of the radiation arriving at the indicator sensing area

at various angles Ψ is varied through 9-12 orders as Ψ varies from 0° to 90°. We note that figures of the type of Fig. 9.2 were plotted using data for the angles Ψ = 0.30', 1°, 2°, 5°, 10°, 15°, 20°, 30°, 40°, 50°, 60°, 70°, 80°, and 90°. As would be expected, the strongest angle dependence of the forward-scattered radiation incident on the receiver is observed at small Ψ and θ.

Figure 9.3 shows the calculated results for the angular intensity distribution for various indicator sensing-area sizes.

The calculated results permit quantitative analysis of the intensity variation of the multiply forward-scattered radiation registered by the receiver with various source and receiver geometries. Comparison of the calculated data with the corresponding experimental results indicates that the results of calculation are quite satisfactory.

2. Experimental investigations. Our laboratory has made detailed experimental studies of the brightness of forward-scattered light for the propagation of laser radiation in various media [660-665, 781].

The apparatus designed for the studies incorporated the following basic components: 1) lasers with working wavelengths of 6328 Å (gas laser in continuous emission, beam diameter about 1.4 cm, divergence angle 6') and 6943 Å (pulsed ruby laser, beam diameter 20-100 mm, divergence angle 30"-40"); 2) collimated thermal sources fitted with narrow-band interference filters with transmission maxima around wavelengths of 0.63 and 0.69 μ; 3) a receiving system that provided for photometry of specific sections of the focal source-image pattern and the background in the direction /358 of small scattering angles.

The brightness distribution of the radiation was registered in the receiving-system focal plane either photographically or photoelectrically, depending on the method used to stop down the focal pattern.

The measurements were made in a chamber with a capacity of 30 m^3, in which wood smokes (particle diameters 0.8-1.0 μ) and artificial water fogs (root-mean-square droplet diameter 8-15 μ) were created. The scattering media were selected with a view to obtaining data suitable for analysis of the propagation behavior of narrow collimated beams in the earth's atmosphere. The brightnesses of the direct and scattered radiations were measured with two measurement systems. In one variant, the radiation source and the receiving system were on a straight line (direct-beam setup). The length of the ray path was 4 meters in this case. In the other variant, the light beam from the source was turned back by a plane mirror into a receiving device situated beside the /359 source (reflected-beam setup). Here the length of the ray path

was increased to 8.3 meters; the angle ϕ through which the beam was rotated by the mirror could be varied from 1°30' to 8°30'.

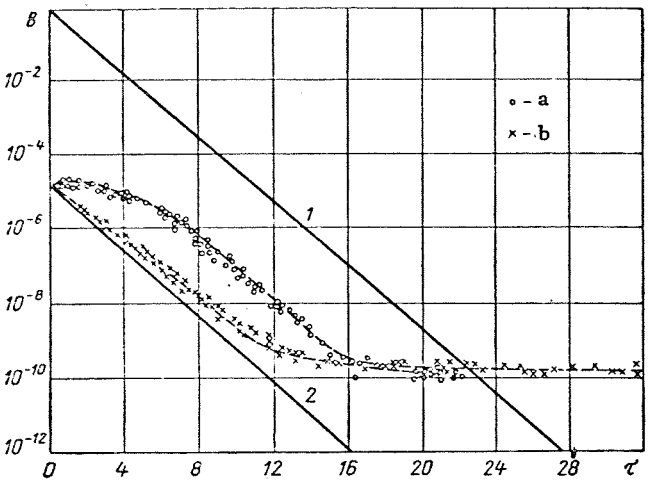

Figure 9.4. Total Brightness of Forward- and Backward-Scattered Radiation as a Function of Optical Thickness τ in Fogs (circles) and Smokes (crosses). Lines 1 and 2 characterize the decrease in the brightness of the direct beam radiation and the initial source background with increasing τ according to Bouguer's law.

By measuring simultaneously the brightnesses of the direct radiation from the laser and a thermal source in the scattering medium, it was possible to investigate the specifics of coherent-radiation attenuation as compared with that of noncoherent radiation.

Figure 9.4 presents the results of brightness measurements of the forward-scattered radiation in artificial water fogs and smokes as obtained with the reflected-beam setup and a gas laser. All measurements were reduced to an initial source brightness B = 1.

As we see from Fig. 9.4, the background brightness is nonzero at an optical thickness $\tau = 0$. To find the background brightness due solely to scattering of the light, it is necessary to subtract the brightness of the initial source background from the measured total background brightness. It can be assumed that the attenuation of the initial source background is described by Bouguer's law (line 2). The contribution of the latter to the total background is found to be substantial for fogs with $\tau < 4$ and for smokes with $\tau < 14$. With consideration of the above remarks, we may state that the background brightness becomes equal to the

brightness of the direct radiation at optical thicknesses $\tau \cong 22$-24 for both fogs and smokes — media that differ strongly in their scattering-particle sizes. In the approximate optical-thickness range from 2 to 13, the background brightness in fogs is approximately 1-1.5 orders higher than that in smokes. Beginning at a certain optical thickness in smokes and fogs, an inflection begins to appear on the background-brightness curves. It intervenes at a smaller τ in smokes than in fogs. At optical thicknesses greater than 20, the background-brightness curves practically coincide for the smokes and fogs and become independent of τ.

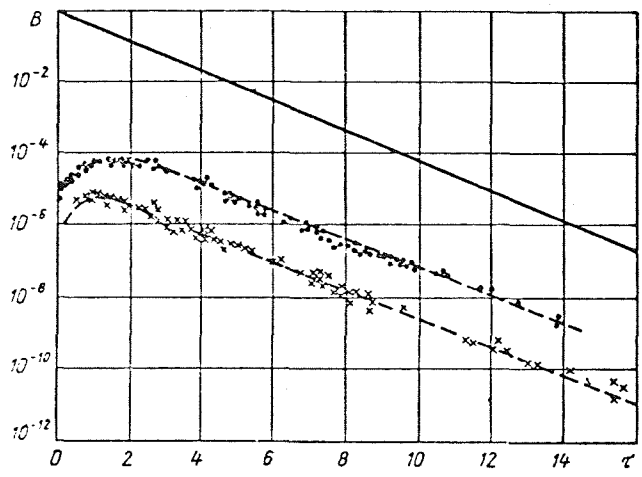

Figure 9.5. Brightness of Forward-Scattered Radiation as a Function of Optical Thickness in Fogs (dots) and Smokes (crosses). The dashed curves were plotted on the basis of calculations by single-scattering theory; the straight line describes the attenuation of the direct radiation according to Bouguer's law.

The reflected-beam setup was used to obtain the measured results shown in Fig. 9.4 for background brightness in the fogs and smokes. This means that the measurements registered not only the background due to scattering forward at small angles, but also the background due to scattering backward at small angles during propagation of the beam from the source to the rotating mirror. It was felt that interest would attach to values of the brightnesses of both background components. For this purpose, the rotating mirror was masked off and the background brightness due solely to backscattering was measured. These measurements indicated that the /360
background brightness is determined chiefly by backward scattering of the radiation at large τ.

Figure 9.5 presents the results of brightness measurements made on the forward-scattered radiation in fogs and smokes with the direct-beam setup. It shows that the background brightness is much lower than the brightness of the direct radiation over the entire range of τ studied. The variation of background brightness is described satisfactorily by values calculated using the single-scattering formula.

In addition to these measurements in the artificial-fog chamber, we also investigated the brightness of forward-scattered radiation in model media (a slightly turbid solution of milk in water with a root-mean-square particle diameter of 3.5 ± 1.5 μ and a suspension of lycopodium in an alcohol-water mixture with particle radii 15 ± 0.5 μ). The width of the beam was characterized by the optical diameter

$$\Delta = \alpha d, \qquad (9.7)$$

where α is the attenuation coefficient and d is the geometrical diameter of the beam. The value of Δ in the measurements was 0.34. The angular aperture of the receiver was equal to the divergence angle of the source radiation.

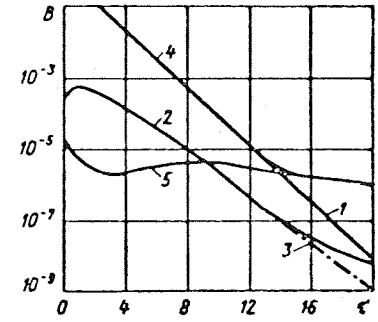

Figure 9.6. Total Brightness of Direct Radiation and Radiation Scattered in the Beam Zone as a Function of Optical Thickness of a Slightly Turbid Solution of Milk. /361

Figure 9.6 presents the measured results for the slightly turbid milk solution. In these figures, the abscissa is the optical thickness of the medium and the ordinate is the measured brightness of the direct and scattered light. The brightness of the direct laser radiation in the absence of a scattering medium was assumed equal to unity. The curves in the figures were drawn through experimental points whose brightness-value scatter did not exceed 5%. Curve 1 characterizes the brightness variation of the direct radiation and that scattered in the beam zone for a receiving-lens optical diameter Δ = 0.5; curve 2 was obtained under the same conditions and describes the brightness variation of only the scattered radiation; curve 3, which coincides with curve 2 at values of τ < 15, was plotted from the results of calculations of the brightness of singly scattered radiation under the measurement conditions of curve 2; curve 4 is analogous to curve 1, except that it was obtained with a receiving-lens optical diameter Δ = 9; curve 5 describes the brightness variation of multiple scattering only for a receiving-lens optical diameter Δ = 9.

We see from Fig. 9.6 that in the zone of the light beam, which is characterized by a divergence of 6' and an optical diameter $\Delta = 0.34$ with a receiving-lens optical diameter of 0.50, the brightness of the scattered light is described by the single-scattering formulas [651] all the way up to an optical thickness of $\tau = 15$, while its absolute value is at least an order smaller than the brightness of the direct radiation attenuated in accordance with Bouguer's law in the range of τ from 0 to 18. An increase in the optical diameter of the receiving lens, which was equivalent in our experiments to a corresponding increase in its geometrical diameter, since the beam width and scatterer density did not change, caused a substantial increase in the importance of multiple scattering in the shaping of the forward-scattered radiation at various optical thicknesses. Thus, at values of $\tau > 15$ (receiving-lens optical diameter 9.0), the multiple-scattering brightness is found to exceed that of the direct radiation. The absolute magnitude of the multiple-scattering brightness exceeds the single-scattering brightness at $\tau > 9$, with a weak dependence on τ. /362

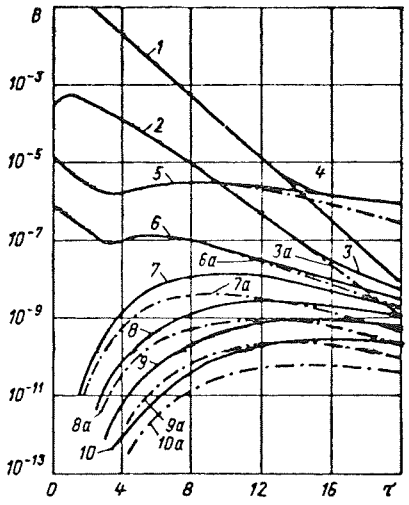

Figure 9.7. Variation of Brightness of Multiply Forward-Scattered Radiation in Various Zones of Receiving-Lens Cross Section for Two Values of the Photon-Survival Probability $\lambda = 0.99$ (curves 6-10) and $\lambda = 0.92$ (curves 6a-10a). Curves 1-5 have been transferred from Fig. 9.4.

To determine the dependence of the brightness distribution of multiply forward-scattered light over the beam cross section on receiving-lens diameter, brightness measurements were made in isolated annular zones, which were cut out by diaphragms set up in front of the receiving lens. The beam zone (zone 1) was, as before, screened with a diaphragm that set $\Delta = 0.5$; zones 2-6 were isolated in such a way that each one of them characterized a 1.70 increase in receiving-lens optical diameter. Figure 9.7 presents the measurement results. Curves 6-10 characterize the brightness change in the multiply scattered radiation as a function of τ in zones 2-6 for a photon-survival probability $\lambda = 0.99$, while curves 6a-10a were obtained for the same zones with a medium having $\lambda = 0.92$. Curves 1-5 have been transferred from Fig. 9.4 and bear the same numeration. It was not possible to eliminate the source-background effect in zone 2 in obtaining curves 6 and 6a.

Results qualitatively similar to those examined above were obtained in the studies with a lycopodium

suspension in a water-alcohol solution. Multiple scattering of the light in the beam zone was found to be more important than in the case of the slightly turbid milk solution, and this produced a corresponding difference in the elongations of the scattering indicatrices of these media.

To test the accuracy of the Monte Carlo method in brightness calculations for multiply forward-scattered radiation in various scattering media and with various source and receiver geometries, the conditions of the described experiments were reconstituted in [837] and the corresponding calculation carried out. Figure 9.8 compares the calculated results with experimental data of Fig. 9.7. The calculated data are entered in the form of points through which vertical segments of length characterizing the rms deviation have been drawn. We see from Fig. 9.8 that the calculated results agree quite satisfactorily with the experimental data. Some disagreement between the results in the range of small τ on curve 2 is due to the initial source background, which was not taken into account in the experimental studies.

/363

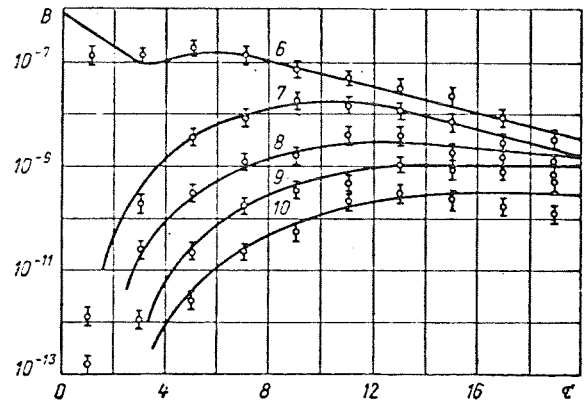

Figure 9.8. Results of Comparison of Experimental Data of Fig. 9.7 (curves 6-10) with Calculated Data Obtained by the Monte Carlo Method [837].

It was considered worthwhile to determine the limiting optical-thickness values at which single scattering, calculation of which is relatively simple, retains the dominant role in forward scattering in various scattering media. /364

The intensity of the singly forward scattered radiation is written [651] in the form

$$I_s = I_0 \tau e^{-\tau} \frac{\omega}{4\pi} f(0), \qquad (9.8)$$

where I_0 is the intensity of the radiation incident on the scattering layer, τ is the optical thickness of the layer, ω is the solid angle of beam divergence, and f(0) is the value of the scattering indicatrix for the direction of the scattering angle θ = 0 (forward scattering). For small collimation angles, we may set ω = $= \pi\alpha^2$, where α is the divergence angle of the beam. If we use

Penndorf's approximation formula [656]

$$\frac{\omega}{4\pi} f(\theta) = \frac{\alpha^2\rho^2}{4} K(\rho, m), \tag{9.9}$$

we obtain from (9.8)

$$I_s \quad I_0\tau e^{-\tau}\frac{\alpha^2\rho^2 K(\rho, m)}{16}, \tag{9.10}$$

where $K(\rho, m)$ is the efficiency of attenuation by a particle of radius a, $\rho = 2\pi a/\lambda$, and λ is the wavelength.

Formula (9.10) can be rewritten /365

$$I_s = I_0\tau e^{-\tau\eta}, \tag{9.11}$$

where

$$\eta = \frac{\alpha^2\rho^2 K(\rho, m)}{16} \tag{9.12}$$

is a parameter characterizing the fraction of light scattered forward by the particle. The value of this parameter can be found by using the experimentally measured I_s.

The boundary values of η determined by experiment made it possible to find the limiting optical thicknesses at which the effects of multiple scattering can be disregarded in determining the forward-scattered radiation. It was found that for beam divergences in the range α = 30'-10", the formulas that describe the intensity of the forward-scattered light due solely to single scattering are valid up to optical-thickness values $\tau < 18$ for particles with the parameter ρ in the range from 1 to 3000. For the visible and infrared regions of the spectrum, this range of values of the parameter ρ covers practically the entire range of atmospheric-aerosol particle sizes (haze, clouds, fog, drizzle, smoke, dust).

A.P. Ivanov and A.Ya. Khayrullina [617, 838, 839] conducted experiments to investigate the brightness of forward-scattered light propagating in various model media for optical thicknesses $\tau \leq 20$. The parameters characterizing the source of the radiation, the receiver, and the scattering media were varied over broad ranges (source divergence angles from 7' to 1°44'; receiver

angular apertures from 16" to 7°; optical diameter of radiation beam from 0 to 0.30, and optical diameter of radiation receiver from 0 to 0.40). The results enabled the authors to obtain a quantitative estimate of the systematic error of measurement of the scattering-medium attenuation coefficient due to registration of forward-scattered radiation by the receiver. This error is uniquely defined if the optical characteristics of the scattering medium and the source and receiver geometries are known.

In conclusion, we examined briefly the results of experimental studies of the brightness of forward-scattered light at very large optical thicknesses, at which the so-called depth condition intervenes. V.A. Timofeyeva [666-668] made a series of measurements of light scattering in strongly turbid media. According to the results of these measurements, the brightness of forward-scattered radiation varies exponentially with increasing optical thickness τ of the medium, but the attenuation coefficient is smaller than in the case of small optical thicknesses. At very large τ, the brightness of radiation scattered at various angles diminishes by the same exponential law as the brightness of forward-scattered light. The range of τ in which this relation prevails is commonly known as the range of the depth or stationary condition. In this case, the brightness of the radiation in the direction of the angle θ takes the form

/366

$$B(\theta) = B_0'\varphi(\theta)\,e^{-k'(z-z_0)};\ B_0' = B_0C, \tag{9.13}$$

where B_0 is the initial brightness of the beam in the forward direction, C is a constant that depends on the boundary conditions and the geometrical parameters of the light beam, $\phi(\theta)$ is the angular distribution of brightness in the depth condition, z is the geometrical thickness of the scattering layer, z_0 is the geometrical thickness of the scattering layer beginning at which the depth condition prevails, k' is an attenuation coefficient related to the attenuation coefficient α in the range of small τ by

$$k' = \sqrt{A\alpha}; \tag{9.14}$$

A is a parameter that depends on the optical properties of the scattering medium and is linked to the absorption coefficient α_a of the medium by the linear relation

$$A = b\alpha_a. \tag{9.15}$$

The constant b in (9.15) depends on the scattering indicatrix of the medium.

For a constant distance between the source and the receiver, the following formula can be obtained from (9.13)-(9.15) for the brightness of the forward-scattered radiation at a depth with optical thickness τ:

$$B(0) = B_0 C e^{-1\sqrt{b\alpha_a z}\left(1\tau - \sqrt{\frac{z_0\tau_0}{z}}\right)} = B_0 C' e^{-k\sqrt{\tau}}, \tag{9.16}$$

$$C' = C e^{-k\sqrt{\frac{z_0\tau_0}{z}}}; \quad k = \sqrt{b\alpha_a z}. \tag{9.17}$$

In the case of a purely scattering medium ($\alpha_a = 0$), as we see from (9.16) and (9.17), the brightness of the forward-scattered light is independent of the optical thickness τ. The presence of absorption in the medium ($\alpha_a \neq 0$) causes B(0) to attenuate with τ. /367

In the depth condition, the angular-distribution diagram of the scattered-light brightness is a circle. In the case of a purely scattering medium, the pole of the diagram is at the center. In the presence of absorption in the medium, this pole shifts backward in the propagation direction of the light beam and the brightness diagram itself becomes somewhat elongated. With increasing τ, the form of the diagram remains unchanged and is characterized by

$$R = \frac{B(0)}{B(\theta)} = 1 + \mu\frac{\alpha_a}{\alpha_s}, \tag{9.18}$$

where μ is a parameter that depends on the scattering indicatrix of the medium.

G.V. Rozenberg obtained a formula similar to (9.18) from theoretical considerations [669].

A.P. Ivanov et al. [670-677] made an extensive series of scattered-radiation brightness measurements in the depth condition in various model scattering media. The geometrical parameters of the light beam were varied for the measurements. At small light-beam diameters, the depth condition intervened at optical thicknesses $\tau > 500$. Analysis of the experimental data led to the following empirical formula, which describes the illumination of the medium at great depths below a parallel light beam:

(9.19)

where τ_0 is the optical thickness beginning at which the depth condition prevails, q is a parameter that depends on the scattering indicatrix, $S = k^2Q$ is the optical cross sectional area of the beam, k is the attenuation coefficient, Q is the geometrical cross section of the beam, and p is a parameter that depends on the absorption and scattering coefficients and the scattering indicatrix.

Formula (9.19) can be rewritten

$$B = B_0'(1 - e^{-p' \frac{d}{\tau}}), \qquad (9.20)$$

where d is the beam diameter, τ is the optical thickness, and p' is a parameter that depends on the optical characteristics of the medium.

In [670-677], proportionality was observed between the brightness of the scattered light and the divergence angle of a narrow collimated beam in the depth condition. /368

2. ATTENUATION OF DIRECT RADIATION IN SCATTERING MEDIA. LIMITS OF APPLICABILITY OF BOUGUER'S LAW

The direct monochromatic radiation of a collimated beam propagating in a scattering medium that does not self-radiate is attenuated in accordance with Bouguer's law if the particles of the medium scatter the radiation independently of one another. The direct radiation usually carries some sort of useful information. From the standpoint of practical application, therefore, it is very important to know the limiting conditions under which the direct radiation can be separated from the background of forward-scattered radiation. Obviously, this can be done when the brightness of the direct radiation exceeds that of the background. If, on the other hand, the background brightness exceeds the direct-radiation brightness, insurmountable obstacles may arise in the extraction of the useful information carried by the beam owing to the fact that the forward-scattered radiation is created, in the final analysis, by the beam itself. In this case, selection of the direct-radiation signal against the scattered-radiation background requires that the signal brightness exceed the brightness of the forward-scattered light. It is readily understood that the most favorable conditions for measurement of the useful signal are those under which the angular aperture of the receiver and the source divergence angle are the same. In this case, the receiving system will grasp the entire beam and a minimum of scattered-background radiation, since the background-noise signal will be stronger for a given useful-signal level the larger the entrance pupil (see §1).

When the useful signal is considerably stronger than the signal from the forward-scattered light, we may speak of applicability of Bouguer's law for description of the measured attenuation of a narrow collimated beam propagating in the scattering medium and subject to full coverage by the receiving system. Thus, investigation of the limits of applicability of Bouguer's law for description of the measured attenuation in a medium enables us to answer the question as to the effective range of a system in which narrow collimated light beams are used to transmit useful information through various scattering media. /369

A detailed investigation of the limits of applicability of Bouguer's law for various specific measurement systems in various scattering media was carried out during the work of our laboratory that was cited in the preceding section, in which the brightness of the direct beam was determined simultaneously with measurement of the brightness of the forward-scattered radiation. Here we report certain results of these studies with a bearing on the limits of applicability of Bouguer's law. We stress once again that we are speaking of the limits of applicability of Bouguer's law for description of the experimentally measurable attenuation of a light beam propagating through a scattering medium. It is clear that these limits must depend not only on the optical properties of the scattering medium, but also on the geometry of the beam and the receiving system. Let us consider the case in which the beam divergence angle and the receiver angular aperture are equal.

Figure 9.9 presents the results of measurements of the brightness B of a laser beam as a function of the optical thickness of milk diluted with water. A gas laser with a divergence of 6' and a beam diameter $d = 0.4$ cm was used in the measurements. Each of the curves in the figure pertains to a definite value $\Delta = \alpha d$ of the beam optical diameter. The diameter Δ was varied from 0.09 to 12.0 by increasing the scatterer density. All measured results were reduced to a unit brightness of the beam incident on the scattering layer.

The criterion for applicability of Bouguer's law to describe the attenuation of the measured brightness of a beam with τ is the presence of a linear relation between log B and τ. We see from Fig. 9.9, in which B is plotted logarithmically, that the straight-line segments of the curves depend strongly on the optical diameter of the beam. A particularly sharp change in the limiting values of τ occurs at small Δ ($\Delta < 0.74$). As Δ increases, the limiting values of τ decrease more and more slowly, and at $\Delta > 1.48$ they are practically independent of Δ and approximately equal to $\tau = 12$.

The relation obtained for the limits of applicability of Bouguer's law for description of the change in measured beam brightness with τ as a function of beam optical diameter can be explained by the varying importance of multiple scattering in the /370

beam zone for different Δ. With the increase in Δ due to particle-concentration change at constant beam geometrical diameter or to an increase in the latter with scatterer concentration constant, multiple scattering becomes more important in shaping the light scattered in the beam zone as compared to the singly scattered radiation. At large Δ, the contribution of multiple scattering is "saturated." At small Δ, single scattering makes a larger contribution to the forward-scattered field. This shifts the limits of applicability of Bouguer's law for description of the measured attenuation of the beam in the direction of larger τ.

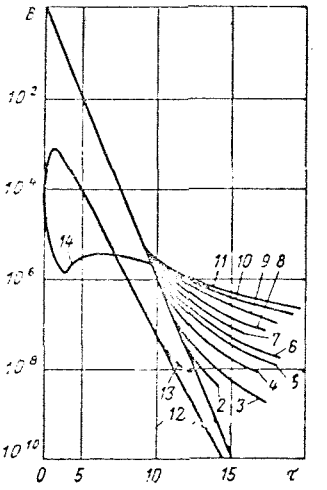

Figure 9.9. Limits of Applicability of Bouguer's Law for Description of Measured Attenuation of a Narrow Collimated Light Beam in a Scattering Medium as Functions of Beam Optical Diameter Δ: 1) Δ = 0,09; 2) 0,34; 3) 0,74; 4) 1,11; 5) 1,48; 6) 2,22; 7) 2,96; 8) 3,56; 9) 7,12; 10) 9,0; 11) 12,0. /371

It follows from §1 that similar changes take place in the limits of applicability of Bouguer's law as the optical diameter of the receiving-collimator lens increases while the optical diameter of the light beam is held constant.

The model-medium measured results shown in Fig. 9.9 permit a number of inferences as to the applicability of Bouguer's law to describe the attenuation of narrow collimated light beams in various atmospheric aerosols. The optical diameters of these beams in the optically densest aerosols — clouds and fogs — at a meteorological visibility S_m = 50 m and a geometrical beam diameter d = 0.4 cm do not exceed the smallest of the Δ values studied in Fig. 9.9 in the visible region of the spectrum. Actually, the attenuation coefficient in the case under consideration (see Chapter 7) is approximately $8 \cdot 10^{-4}$ cm^{-1}, so that Δ = 0.0003 for d = 0.4 cm. Clouds and fogs on the one hand and a dilute solution of milk in distilled water on the other do not differ sharply in their microphysical and optical properties. Thus the results shown in Fig. 9.9 can be used for approximate analysis of the limits of applicability of Bouguer's law to describe the attenuation of a collimated beam in clouds and fogs. Bearing in mind that in a dense cloud or fog (S_m = 50 m), the value of Δ at d = 0.4 cm is much smaller than its smallest value in Fig. 9.6, we may state with confidence that the limits of applicability of Bouguer's law are beyond τ = 25 in this case. This statement is fully consistent with the experimental data that we obtained in [660] in measurements made in artificial water fogs. We may

expect this limit to obtain even when the beam geometrical diameter is 100 cm, since in this case $\Delta = 0.08$.

The optical diameters of beams propagating through haze, precipitation, and dry aerosols are generally smaller than those in clouds and fogs. Bouguer's law can therefore describe the measured attenuation of collimated light beams when the divergence and diameter of the beam do not exceed 6' and 100 cm and the receiver angular aperture equals the divergence of the beam in all atmospheric aerosols with optical thicknesses τ no smaller than 25 in the visible region of the spectrum. We note that the radiation receivers most sensitive in the visible region register radiation that has passed through a layer of medium with $\tau \cong 30$-35 if the energy density incident on the layer equals 10^3 W. This conclusion may also be extended to the infrared, which differs from the visible region in having relatively smaller values of the parameter ρ and larger values of the absorption coefficient for the medium. Both factors only increase the limiting values of τ at which Bouguer's law can still be used to describe the measured attenuation of a beam in a scattering medium. /372

3. BRIGHTNESS OF BACKWARD-SCATTERED RADIATION

Knowledge of the brightness of back-scattered radiation is important for solution of many applied problems, e.g., in the use of narrow collimated beams of light for radar, ranging in scattering media, determination of the aerosol component of the transparency of these media, determining the albedos of various surfaces, and in solving a number of other problems. In the present section we examine briefly the results recently obtained in theoretical and experimental research on back scattering in the atmosphere.

1. Theoretical investigations. Ye.M Feygel'son [652] calculated the albedos of clouds for various zenith distances of the sun by numerical solution of the transfer equation. From the fact of the weak dependence of cloud albedos on the sun's zenith distance, the author of [652] concludes that the back-scattered radiation depends only weakly on scattering angle. The dependence of the albedos of clouds on their optical thicknesses τ is stronger; the increase in albedo with τ becomes slower at large optical thicknesses, tending to "saturate." Thus, the brightness of back-scattered radiation is determined by a certain finite scattering layer. The optical thickness of this effective layer decreases, as shown by L.M. Romanova [678], when absorption occurs in the medium. Cloud albedos are calculated in Bartky's paper [679] for various solar zenith distances in the 1.9-4.3-μ region of the infrared.

References [680-682] contain calculated data on the intensity of back-scattered radiation, which are necessary for determination of the aerosol component of atmospheric transparency. The amount

of light scattered backward by an aerosol layer is found to be proportional to the degree of atmospheric turbidity. The calculations were made for various haze and fog models. K.S. Shifrin and I.L. Zel'manovich [683] made detailed calculations of the quantities that appear in the expression for the back-scattering coefficient. /373

V.P. Kozlov and Ye.O. Fedorova [684] calculated the intensities of singly back-scattered light for illumination of fogs with a narrow collimated light beam.

Munick [685] derived a formula for the intensity of light scattered backward by turbulent inhomogeneities in the atmosphere. A calculation performed by this formula indicated that the intensity of light from a ruby laser (wavelength $\lambda = 0.69$ μ), scattered backward on turbulent inhomogeneities, represents $5.9 \cdot 10^{-7}$ of the radiant intensity scattered backward by molecular scattering.

Using the Monte Carlo method, G.M. Krekov [837] made detailed calculations of the deformation of an instantaneous light pulse reflected from scattering media. We shall examine some of the resulting data in § 5, which sets forth the results of study of the propagation of light pulses in scattering and absorbing media.

2. Experimental investigations. Our laboratory made experimental studies of the brightness of back-scattered light for various scattering media illuminated by narrow collimated beams of radiation [660, 686]. These studies were dictated by the lack of appropriate data, either theoretical or experimental, on back-scattering by atmospheric aerosols.

Lasers emitting at wavelengths of 0.63 μ (continuous helium-neon laser), 0.69 μ (pulsed ruby laser) and 1.06 μ (pulsed neodymium-glass laser) were used for the measurements. The measurements at 0.63 and 0.69 μ were performed in artificial fogs and smokes, and those at 1.06 μ under natural conditions in the presence of haze and falling snow.

Measured results for the brightness of gas-laser radiation ($\lambda = 0.63$ μ, beam diameter 1 cm, divergence 6') scattered at an angle of 171°30' in artificial fogs with various optical thicknesses are entered in Fig. 9.10 (crosses). The same figure shows measured data for the total brightness of the forward- and backward-scattered radiations (circles) as obtained in a source-rotating mirror-receiver scheme (beam rotation angle 8°30'). The rotating mirror was masked for measurement of the brightness of the radiation scattered at 171°30'. /374

If the initial source background is excluded from the measured results, it can be seen that as the optical thickness increases from 0 to 1, the brightness of the back-scattered light increases, reaches a maximum, and then decreases again, comparatively rapidly at first and then slowly, with increasing τ. For

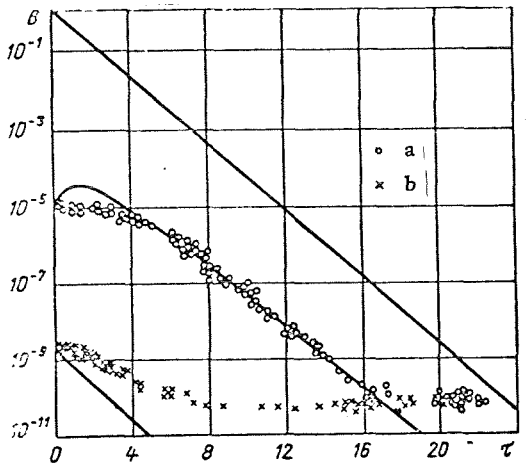

Figure 9.10. Total Brightness of Forward- and Backward-Scattered Radiation as a Function of the Optical Thickness of Fogs (circles) and the Brightness of the Backward-Scattered Radiation (crosses). The straight lines characterize the decrease in direct-radiation brightness of the beam and the initial source-radiation background according to Bouguer's law.

$\tau > 8$, it remains practically constant, reaching a value equal to the brightness of the direct beam at $\tau \cong 23$.

Measurements of the brightness of gas-laser radiation scattered at an angle of 171°30' by wood smokes indicated that its values coincide with those obtained in fogs at $\tau > 20$. At smaller τ, the brightness of light scattered backward by fogs is lower than that from smokes.

Figure 9.11 shows the results of brightness measurements on laser light with wavelength 0.63 μ after scattering at an angle of 172° by fogs and smokes. The measurements were made without the rotating mirror, using a beam 0.4 cm in diameter with a divergence of 6'. The optical axes of the receiver and source crossed at an 8° angle. The values of the optical thickness τ entered on the figure pertain to the scattering layer from the source to the receiver. The brightness values have been referred to the initial brightness of the direct beam. Each of the points on the figure was obtained by averaging the results of 5-10 measurements. /375

Figure 9.11 shows that the absolute brightness values of light scattered at an angle of 172° in fogs and smokes in the range of optical thicknesses studied represent, in order of magnitude, $\sim 10^{-8} - 10^{-9}$ of the initial direct-beam brightness.

Measurements of back scattering in haze and falling snow made with a pulsed neodymium-glass laser ($\lambda = 1.06$ μ) made it possible to obtain certain preliminary estimates of the back scattering. In the presence of hazes characterized by meteorological visibilities $S_m = 3\text{-}7$ km, the back-scattered brightness is of the order of 10^{-10} of the initial brightness of the direct beam. Falling snow causes practically no change in the brightness of the backward-scattered laser radiation at 1.06 μ.

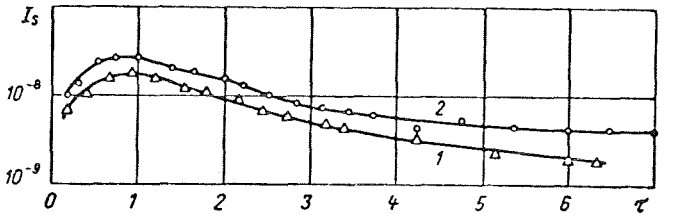

Figure 9.11. Brightness Variation of Radiation of Laser at $\lambda = 0.63$ μ Scattered at an Angle of 172° by Fogs (1) and Wood Smokes (2).

4. POLARIZATION CHARACTERISTICS OF SCATTERED RADIATION

The polarization state of radiation scattered at various angles is important in the solution of many applied problems related to transmission of data with a narrow beam of radiation. In fact, if the scattering layer of medium is illuminated by linearly-polarized radiation, the particles of the layer may depolarize /376 this radiation on scattering. Polarizing devices may be used in the reception of direct and scattered radiation to reduce the contribution of the scattered field to the signal as compared with the contribution of the direct beam radiation to this quantity. This may make it possible to increase the effective range of the technical system in question. Thus, it is shown in [687] that the use of polaroids in receiving systems at least doubles underwater visibility. A similar effect may also be expected in the atmosphere.

Theoretical analysis of the question as to the polarization state of scattered radiation by solving the general transfer equation is an extremely complex problem. As we have noted, no solution of the transfer equation without consideration of the polarization characteristics of the incident and scattered fields has as yet been obtained for narrow collimated beams. Information on the polarization state of the scattered radiation, which is needed for solution of many problems, is therefore obtained experimentally. However, most of the experimental studies also pertain to the polarization characteristics of the scattered radiation for an elementary volume [506, 507, 688] or for broad beams and scattering media with large optical thicknesses [672, 689-691].

The use of lasers emitting linearly polarized radiation as radiation sources opens new possibilities for experimental study of the scattered-field polarization characteristics in the propagation of narrow collimated light beams in scattering media. Of prime importance here is study of the polarization state of radiation scattered at small angles forward and backward in various scattering media. An attempt at an investigation of this kind has been made in our laboratory [692].

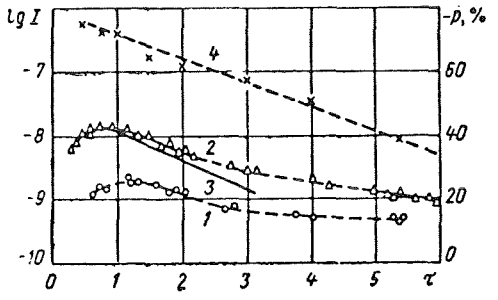

Figure 9.12. Curves of Optical Thickness of Fog Against: 1) intensity of backward-scattered light with vector $\vec{E}$ lying in the scattering plane; 2) intensity of backward-scattered light with vector $\vec{E}$ lying in plane perpendicular to the scattering plane; 3) intensity of backward-scattered radiation calculated by the single-scattering theory; 4) degree of polarization of backward-scattered radiation.

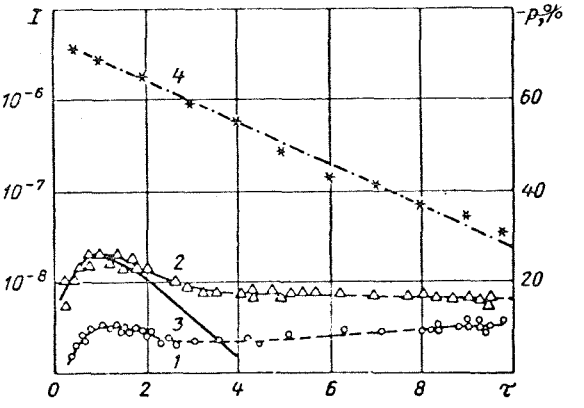

Figure 9.13. Optical Thickness of Wood Smoke Plotted Against 1) intensity of backward-scattered light with vector $\vec{E}$ lying in the scattering plane; 2) intensity of backward-scattered light with vector $\vec{E}$ lying in plane perpendicular to scattering plane; 3) intensity of backward-scattered radiation calculated by the single-scattering theory; 4) degree of polarization of backward-scattered radiation.

The polarization characteristics of the scattered radiation were measured for angles of 1°30' (forward direction) and 172° (backward direction). The quantities measured were the intensity I_1 of light with vector $\vec{E}$ lying in the scattering plane and the intensity I_2 of light with vector $\vec{E}$ perpendicular to the scattering plane. The ratio $\Delta = I_1/I_2$ characterizes the depolarization of the radiation. Knowledge of Δ enables us to determine the degree of polarization of the scattered light: /377

$$p = \frac{1-\Delta}{1+\Delta}. \qquad (9.21)$$

Figures 9.12 and 9.13 show the measured results for I_1 and I_2 and the degree of polarization p of the backward-scattered radiation in fogs and wood smokes as calculated from these intensities. The values of I_1 and I_2 have been referred to the initial intensity of the direct radiation beam incident on the scattering layer. The figures show that the dependence of the degree of polarization of the backward-scattered radiation on the optical thickness τ of the layer can be approximated in the range of τ studied by the straight line

$$p(\tau) = p_0 - k\tau. \qquad (9.22)$$

where p_0 and k are empirical parameters whose values depend on the properties of the scattering medium and vary weakly as the source divergence angle varies from 40" to 6'.

The degree of polarization of the back-scattered radiation differs from the p of the source even at the smallest value of τ studied: $\tau \cong 0.5$. Extrapolation of the linear relation (9.22) to zero τ gives a p smaller than that of the source. (The degree of polarization of the source radiation was above 0.99 according to measurements that were made.) This means that the dependence of p on τ cannot be linear in the range of small τ.

/378

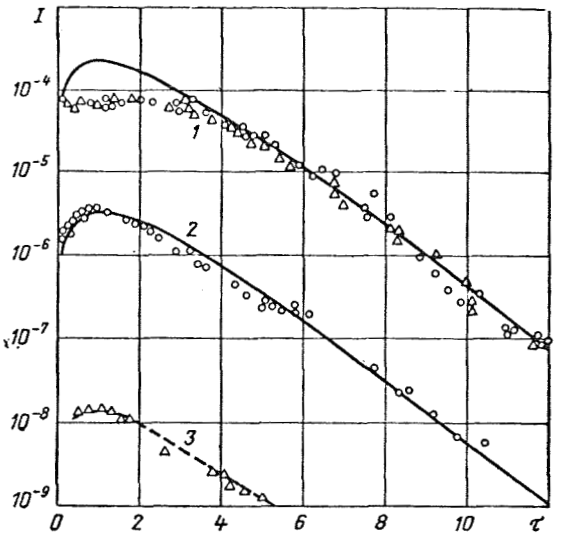

Figure 9.14. Total Intensity $I_1 + I_2$ (triangles) and Intensity I_1 (circles) of Forward-Scattered Radiation in Fogs as Functions of Optical Thickness (curve 1); Intensities I_1 (curve 2) and I_2 (curve 3) as Functions of τ in Wood Smokes. The solid and dashed curves were calculated by the formula of single-scattering theory.

Figure 9.14 presents measured results for the intensities I_1 and I_2 of the radiation scattered forward at 1°30' in fogs and smokes with various optical thicknesses. As we should expect, the sum $I_1 + I_2$ from measurements in fog did not differ from I_1 within the limits of measurement error, indicating that the forward-scattered radiation is not depolarized. As the figure shows, I_1 is 2.5 orders larger than I_2. Thus, practically no depolarization of the radiation takes place in small-angle forward scattering even in the case of wood smokes. The solid and dashed curves in the figure were obtained by calculation using the formula that describes single scattering. They give a satisfactory description of the measured results in the range of optical-thickness values studied, $\tau \leq 12$.

/379

5. PROPAGATION OF A PULSE OF DIRECTIONAL RADIATION IN A SCATTERING AND ABSORBING MEDIUM

The creation and practical use of pulsed lasers with short pulse durations in radar, distance-measuring, and other systems

designed to work through the atmosphere requires study of the laws governing nonstationary scattering of light in media with various photon-survival probabilities. This last quantity can vary widely in the atmosphere depending on the wavelength at which the pulse is generated. /380

One of the most important problems of nonstationary scattering of radiation is that of investigating the space-time variations in the shape of a pulse in propagation to various optical depths in absorbing and scattering media. First of all, it is necessary to know the shape change of an infinitesimally short pulse, since any pulse can be represented in the form of a set of pulses of vanishingly small duration.

Detailed calculations of the deformation of an instantaneous pulse propagating in various scattering media were made by the Monte Carlo method in [836]. Let us examine some of the results.

The photon path distribution registered by a receiver of diameter D_2 = 15 cm on irradiation of a water cloud with a delta pulse from a source of diameter D_1 = 8 mm with a divergence angle θ = 31' was calculated for wavelengths of 0.45 and 0.7 μ. The choice of wavelengths was governed by the available data on the scattering coefficients and indicatrices of the water cloud [517]. The dimensionless photon path $t = t'c\sigma$ was taken as a measure of the spreading of the pulse; here t' is the true path time, $t' = l/c$; l is the path, c is the speed of light, and $\sigma = 0.016525\ m^{-1}$ is the attenuation coefficient. The parameter t has the sense of the optical thickness pierced by the photon on its path from the source to the receiver. The calculation was made for optical thicknesses τ = 1.0, 2.0, 5.0, and 10.0. In constructing the intensity curve of the multiply forward-scattered radiation as a function of the angle at which this radiation strikes the receiver, the parameter t was varied with a 0.05 step for τ = 1.0, 2.0, and 5.0 and with a 0.1 step for τ = 10. For τ = 5.0, for example, the parameter t assumed the values t = 5.0, 5.05, 5.1, and so forth. We note that the parameter increment Δt = 0.05 corresponds approximately to a time of 10 nsec at $\sigma = 0.016525\ m^{-1}$. The angles of arrival of the photons at the detector's sensitive surface were set equal to 0°, 0.5°, 1°, 2°, 5°, 10°, 15°, 20° (10°) 90°.

The calculated results were plotted in the form of a family of curves, which gives a complete picture of the angle and time distributions of the photon flux for the given values of the source and receiver parameters, the optical thickness, and the wavelength of the radiation. Figure 9.15 presents an illustration of the resulting calculated data for τ = 5.0 and λ = 0.7 μ. The abscissa is the angle at which the photon impinges on the receiver's sensitive surface (reckoned from the normal to this surface), and the ordinate is the logarithm of radiant intensity. Curve 1 characterizes the angular distribution of the flux of photons that have travelled distances equivalent to values of τ in the range from /381

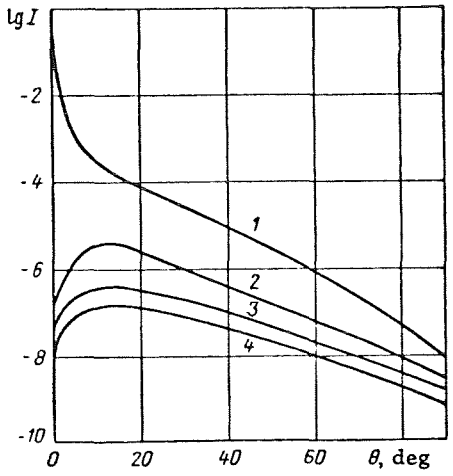

Figure 9.15. Calculated Results for Angular Distribution of Photon Flux in Plane of Receiver 150 mm in Diameter in Propagation of a Light Beam 8 mm in Diameter with a Divergence Angle of 30' and a Wavelength of 0.7 μ in a Water Cloud of Optical Thickness τ = = 5.0. Curves 1-4 were plotted for values of the parameter t taken at intervals t = 0.05 ≈ ≈ 10 nsec.

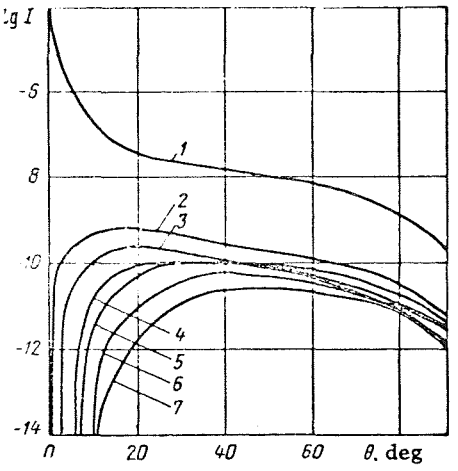

Figure 9.16. Calculated Results for Angular Distribution of Photon Flux in Plane of Receiver 150 mm in Diameter in Propagation of a Light Beam 8 mm in Diameter with a Divergence Angle of 30' in a Haze with τ = 2.0 at a Particle Index of Refraction n = 1.5. Curves 1-7 differ from one another by successive 0.05 or approximately 1.56-μsec changes in the parameter t.

5.0 to 5.05. In other words, this curve defines the fraction of photons that have arrived at the indicator's receiving surface with a time delay not exceeding 10 nsec. Curves 2, 3, and 4 are those of photons with time delays from 10 to 20, from 20 to 30, and from 30 to 40 nsec.

Figure 9.16 presents some of the calculated results for the angular photon-flux distribution when a haze with the Junge particle-size distribution (parameter β = 4) and τ = 2.0 is considered /382 as the scattering medium. The data on the scattering indicatrix for an index of refraction n = 1.50 were taken from [572]. The attenuation coefficient was assumed equal to $\sigma = 0.00010555\ m^{-1}$.

The angle and time characteristics of the distribution of photons with various scattering multiplicities were also investigated in [843] for cases in which the optical thickness of a water cloud between the source and receiver assumes values of τ = 1.0, 3.0, 5.0, and 10.0. The scattering indicatrix and coefficient were taken from [517]. The calculation was performed for source and receiver diameters of 4 and 150 mm, respectively, and

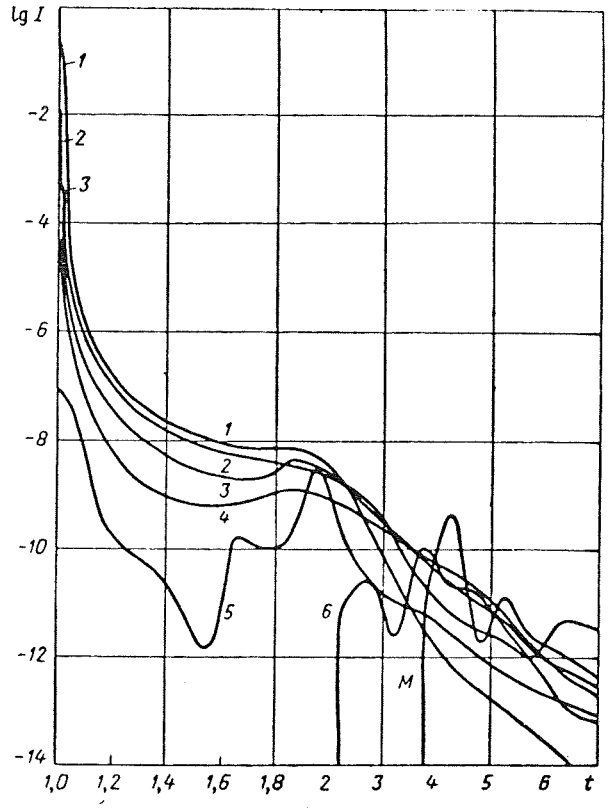

Figure 9.17. Calculated Intensity-Time Curves of Radiation Due to Photons of Various Scattering Multiplicities for a Wavelength of 0.7 μ and τ = 1.0 in a Water Cloud. The source and receiver diameters are 4 and 150 mm. Curves 1, 2, ..., 6 correspond to scattering multiplicities of 1, 2, ..., 6, and curve M represents all scattering multiplicities greater than 6.

a source divergence angle of 30'.

Figures 9.17 and 9.18 present time curves of the intensity of radiation due to photons of varying scattering multiplicity for τ = 1.0 and 10.0 and a wavelength λ = 0.7 μ. The figures clearly show the redistribution of the contributions made by various scattering multiplicities to the deformation of an instantaneous light pulse as the optical thickness varies from 1.0 to 10.0. /383

Figure 9.19 shows some of the calculated results for backscattering of a delta pulse of radiation in a narrow light beam

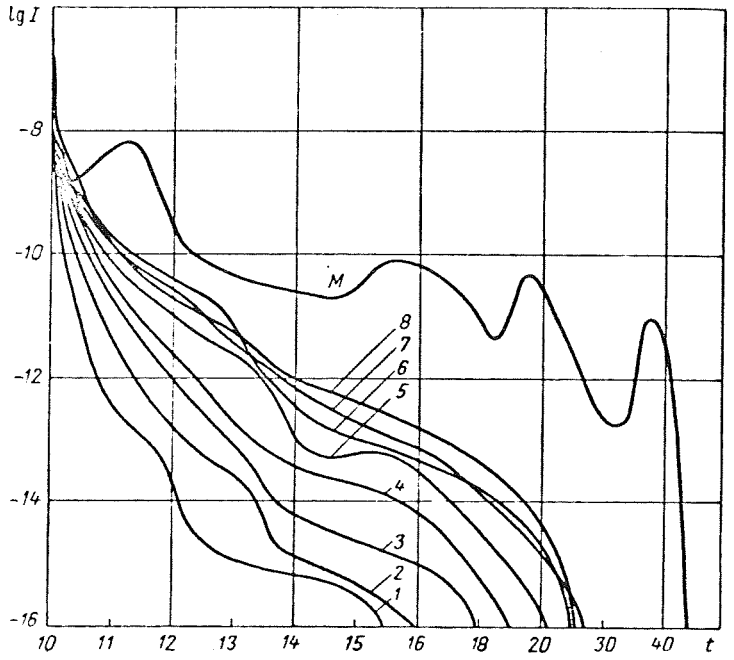

Figure 9.18. Calculated Intensity-Time Curves of Radiation Due to Photons of Various Scattering Multiplicities for a Wavelength of 0.7 μ and τ = 10.0 in a Water Cloud. The source and receiver diameters are 4 and 150 mm. Curves 1, 2, ..., 8 correspond to scattering multiplicities of 1, 2, ..., 8 and curve M represents all scattering multiplicities greater than 8.

propagating in a cloud medium.

On the basis of an approximate solution of the nonstationary transfer equation for an unbounded beam, L.M. Romanova [693-695] investigated the path-length distribution of photons in the reflected and arriving light for isotropic scattering of an infinitesimally short radiation pulse. The calculations showed that the unbounded layer of medium next to the radiation source is the basic factor in shaping the signal reflected from a scattering medium on illumination of the latter by a delta pulse. /384

The nonstationary transfer equation for a narrow collimated beam was formulated and solved in [842] in the single- and double-scattering approximations. A spherical scattering indicatrix was used in the calculations. The solutions of the equation are valid for media with photon-survival probabilities smaller than 0.8 (the absorption coefficient of the medium is one-quarter of the /385

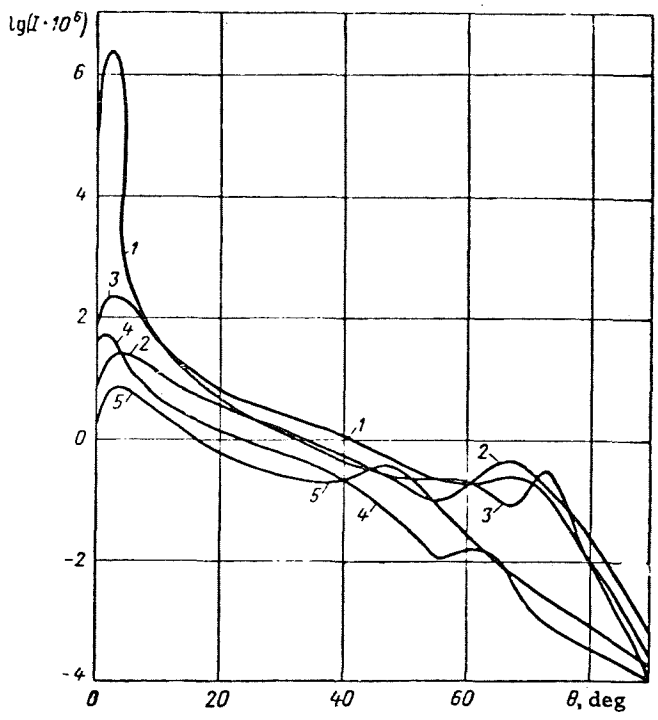

Figure 9.19. Calculated Results for Backward Scattering of Delta Pulse by a Cloud. Curve 1: source and receiver together. Curves 2, 3, 4, 5: receiver at various distances from source.

scattering coefficient). The calculations showed that the distortion of a square pulse during passage through a layer of medium is due chiefly to double scattering and depends strongly on the relation between the duration of the pulse incident on the layer and the receiver aperture. The shape of the reflected-pulse front is determined by both singly- and doubly-scattered radiation.

A.B. Ivanov and I.A. Katsev [840, 841] considered the reflection of a short pulse from an infinite layer of a medium with a strongly forward-elongated scattering indicatrix (which is more characteristic for conditions in the atmosphere than the preceding case). The scattering indicatrix was assigned as the ratio of the radiant flux scattered forward by a volume element to the sum of the fluxes scattered forward and backward. The results of the calculations indicated that the higher the photon-survival probability and the stronger the forward elongation of the scattering pulse. At the same time, the reflected-pulse duration is inversely proportional to the attenuation index of the medium. /386

Experimental research on the propagation of short-duration pulses in various scattering media is still in the stage in which the first results are being acquired.

In [852], an attempt is made to find a relation between atmospheric transparency and the parameters of a pulse signal reflected from it. In measurements in natural fogs, the duration of the reflected pulse and its delay in the medium were observed to depend on the attenuation coefficient α. As α varied from 0.001 to 0.01 m^{-1}, the duration of the reflected pulse varied from 2-3 to 0.5 μsec.

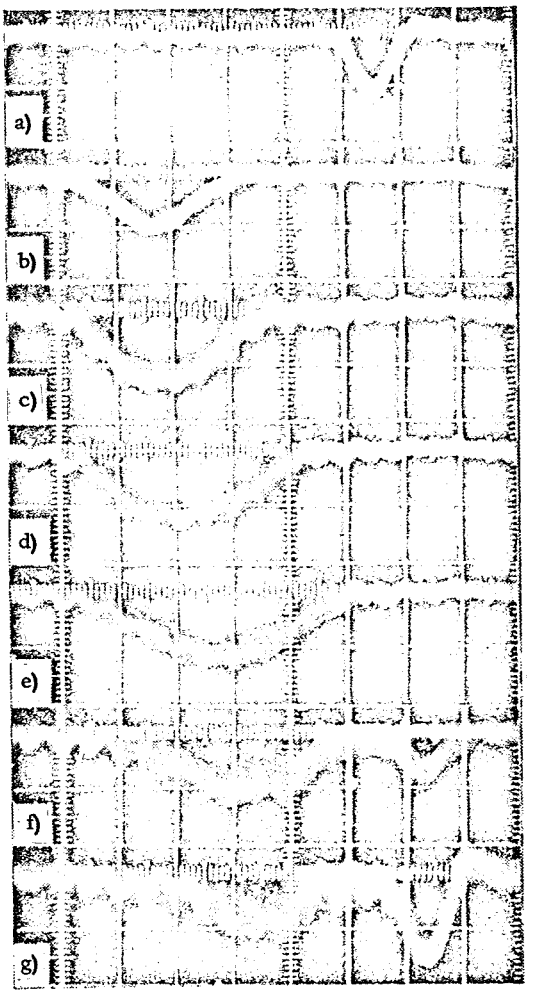

Figure 9.20. Oscillograms of Radiation Pulses Reflected from Layers of Fog with Various Attenuation Coefficients: a) source radiation pulse; b) α = 1.5 m^{-1}; c) α = 0.84 m^{-1}; d) α = = 0.43 m^{-1}; e) α = 0.25 m^{-1}; f) α = 0.13 m^{-1}; g) α = 0.08 m^{-1}.

The author's laboratory made an experimental study of the deformation of a radiation pulse from a gallium arsenide semiconductor laser (wavelength 0.84 μ) on reflection from artificial water fogs and smokes [853]. The duration of the original pulse at 0.5 amplitude level was 8 nsec. The attenuation coefficient of the medium was varied from 0.02 to 1.0 m^{-1}. The receiver and source of the radiation were set up in such a way that their optical axes crossed inside the medium under investigation at a 1° angle at a distance of 7 meters from its forward boundary.

Figure 9.20 presents some of the results from study of the deformation of pulses reflected from fogs with various densities. The vertical lines in the figure are 10 nsec apart. The source pulse is shifted 50 nsec to the right from its true position and reduced in amplitude by a factor of 10^5.

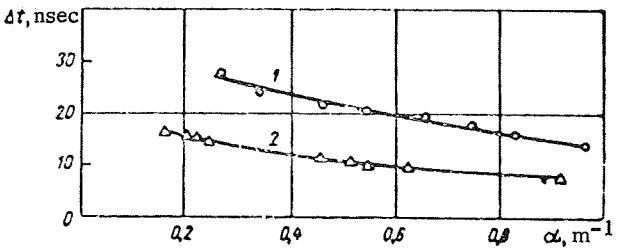

Figure 9.21. Duration of Pulses Reflected from Fogs and Smokes as a Function of the Attenuation Coefficients.

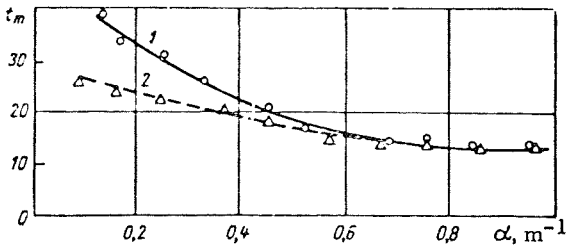

Figure 9.22. Delay of Pulses Reflected from Fogs and Smokes as a Function of the Attenuation Coefficients.

The figure shows that as the attenuation coefficient decreases or, which is the same thing, as the optical thickness of the medium decreases, the duration of the reflected-pulse front /388
increases and its slope diminishes. At the same time, the trailing-edge duration of the reflected pulse also increases at first, but then begins to decrease. The latter is due to the influence of the rear boundary of the scattering medium. The sharp pulse at the right side of the lower oscillogram owes its origin to reflection of radiation from the rear wall of the chamber in which the measurements were made.

Figure 9.21 shows the duration Δt of pulses reflected from fogs (upper curve) and smokes (lower curve) as a function of attenuation coefficient. The figure shows that in both cases, the duration of the reflected pulses decreases with increasing attenuation coefficient and tends to the duration of the source pulse. This is because the reflected signal is shaped primarily in the /389
layers directly adjacent to the source. The extent of these layers diminishes with increasing density of the medium. The differing durations of pulses reflected from fogs and smokes at

the same α are apparently due to the corresponding difference between the scattering indicatrices of these media.

Figure 9.22 shows the delays t_m of pulses reflected from fogs (1) and smokes (2) as functions of the attenuation-coefficient values. We note that the pulse delay spoken of here is the time interval between transmission of the pulse and the maximum of the received signal. The figure shows that t_m diminishes more rapidly with increasing α for fogs than for smokes. The difference between the t_m values for fogs and smokes practically disappears at $\alpha > 0.5$ m. The following qualitative explanation can be given for the differing behavior of t_m at samll α in fogs and smokes. At small optical densities of the medium, the basic factor in shaping the reflected signal is the small scattering multiplicities, for which the difference between the scattering indicatrices of the media has a strong influence on the resultant shape of this signal. The reflected pulse is shaped by more distant layers in fogs than in smokes.

We note in conclusion that the described results from experimental study of the deformation of pulses reflected from fogs were also obtained by calculation using the Monte Carlo method [835]. The calculated and experimental data were found to be in satisfactory agreement, which once again confirms the effectiveness of the Monte Carlo method as applied to investigate the qualitative laws of propagation of spatially limited light beams in scattering and absorbing media.

Chapter 10 /390

NONLINEAR EFFECTS ATTENDING THE PROPAGATION OF STRONG OPTICAL RADIATION IN THE ATMOSPHERE

The atmospheric propagation of optical radiation of the giant powers attainable from certain pulsed lasers in Q-switched operation and the high energies of a number of lasers operated in pulsed free and continuous emission give rise to a whole series of nonlinear effects, which accompany the propagation of such radiation in the atmosphere.

First of all, these effects render Bouguer's law invalid for description of the attenuation due either to molecular absorption by the gaseous components of the atmosphere or to scattering on aerosol particles.

Some of the other relationships in the propagation of optical waves that were described in the preceding chapters of this monograph also become inapplicable at high powers and energies of the optical radiation.

The present chapter examines certain multiphoton effects that do not require consideration of interference phenomena (multiphoton ionization and dissociation, which cause breakdown of a layer of pure air), the spectroscopic saturation effect, which causes partial brightening of the absorbing gas layer, the beam self-focusing effect, which is due to the nonlinear dependence of the index of refraction of the medium when it is illuminated by a powerful radiant flux, and effects in which aerosol particles are vaporized under exposure to pulsed and continuous radiation sources of high power and energy.

1. PROBABILITY OF MULTIPHOTON PROCESSES /391

Rather numerous papers, analyses and detailed bibliographies of which will be found in the surveys [857-860], have been devoted to theoretical investigations of multiphoton processes. Reference [857] examines sources in which the usual variant of perturbation theory is used to describe multiphoton processes caused by the corresponding interaction of the radiation field with matter. Two-photon processes, and, in particular, resonant scattering of light by an atom, are considered in greatest detail in [857].

In [858], the formalism of scattering theory is used to describe multiphoton processes. The probabilities of these processes are calculated by the diagram method of perturbation theory.

Multiphoton transitions in the optical range of wavelengths are considered in the review [859]. Studies of multiphoton ionization in inert gases are analyzed in detail.

The breakdown of gases, the multiquantum photoeffect, and a number of other related problems are considered in [860].

In this chapter, the problem of multiphoton processes in the propagation of strong optical radiation in gaseous media is expounded systematically on the basis of the scheme developed by S.D. Tvorogov and L.I. Nesmelova [696]. Throughout the discussion, references are made only to those sources with a direct bearing on the subject matter.

Let us first consider the problem of calculating the probability of transition of a certain quantum system from one fixed state to another.

We shall denote the system Hamiltonian by H. The evolution of the system wave function ψ is then described by the Schrödinger equation

$$i\hbar \frac{\partial \psi}{\partial t} = H\psi. \tag{10.1}$$

The formal solution of (10.1) can be written

$$\psi(t) = S(t)\psi(0), \tag{10.2}$$

where $\psi(0)$ is the initial value of the wave function and S(t) is a unitary operator that describes the evolution of the system in time. It follows from (10.1) and (10.2) that

$$i\hbar \frac{\partial S}{\partial t} = HS, \quad S(0) = 1. \tag{10.3}$$

Relations (10.3) fully define the mathematical problem of calculating the operator S. /392

Let us examine a certain operator M with eigenfunctions ϕ_n. If our system is in a state described by a certain ϕ_n, the quantity corresponding to the operator M assumes a certain fixed value M_n.

Let us now select a certain function ϕ_n as the initial condition for ψ. In virtue of the orthonormality of ϕ_n, the function

$\psi(t)$ can be written

$$\psi(t) = \sum C_m(t)\,\varphi_m. \tag{10.4}$$

According to the general rule of quantum mechanics, the quantity $|C_m(t)|^2$ determines the probability that the investigated system will be in the state described by the function ϕ_m at time t.

Substituting (10.4) into (10.2) and setting $\psi(0) = \phi_n$ in virtue of the initial-condition selection, we have

$$\sum_{m'} C_{m'}(t)\,\varphi_{m'} = S(t)\,\varphi_n. \tag{10.5}$$

Multiplying both parts of (10.5) on the left by ϕ_m^*, integrating the function ϕ with respect to the variables ξ, and applying the relation $\int \phi_m^* \phi_{m'} d\xi = \delta_{mm'}$, we find that $C_m = \langle \phi_m | S(t) | \phi_n \rangle$. Here the symbol < > signifies the scalar product defined in the usual manner:

$$\langle f | S | g \rangle = \int f^*(\xi)\, Sg(\xi)\, d\xi.$$

We shall denote by W_{mn} the probability of transition of our system from state ϕ_n to state ϕ_m during time t. It follows from the sense of C_m that

$$W_{mn} = |\langle \varphi_m | S(t)\,\varphi_n \rangle|^2. \tag{10.6}$$

We now apply the result (10.6) to analysis of a system consisting of a certain molecule (atom) and an electromagnetic field. In this case, the total Hamiltonian of the system

$$H = H_0 + H_R + H_{0R}, \tag{10.7}$$

where H_0 is the Hamiltonian of the molecule, H_R is the Hamiltonian of the radiation field, and H_{0R} is the field-molecule-interaction Hamiltonian.

We shall denote by $\kappa_n(x)$ and $\psi_{n_k}(\xi)$ the eigenfunctions of H_0 and H_R. The function $\kappa_n(x)$ depends on the molecular variables x and describes a certain state of the molecule. The function $\psi_{n_k}(\xi)$ determines the state of a field with n_k photons and depends on the field variables. We shall henceforth consider a monochromatic field. /393

We set $M = H_0 + H_R$. Then $\phi_n = \kappa_n(x)\psi_{n_k}(\xi)$ in virtue of the commutation of H_0 and H_R, since these operators operate on different variables. The functions written out above define the situation in which the molecule is in state κ_n and the field contains n_k photons. Let us assume that the molecule has gone over to a certain state κ_m and that this transition has resulted in absorption of n photons. Then the final state of the molecule-plus-field system will be determined by the function $\phi_m = \kappa_m\psi_{n_k-N}$. According to (10.6), the probability of the described transition can be calculated by the formula

$$W = |\langle \varkappa_m \psi_{n_k-N} | S | \varkappa_n \psi_n \rangle|^2. \qquad (10.8)$$

The operator S can be found from (10.2) after substitution of (10.7) into (10.3). The operator H_0 is the ordinary operator of the molecule or atom, taking account of all interactions of the particles of the atom or molecule. In the long-wave approximation, the other two operators in (10.7) take the form

$$H_R = \hbar\omega a^* a,$$
$$H_{0R} = \beta P(a + a^*) + \alpha(a + a^*)^2,$$

where

$$\beta = -(e/m)(2\pi\hbar/\omega)^{1/2}, \quad \alpha = e^2\pi\hbar/m\omega c;$$

ħ is Planck's constant, c is the velocity of light, ω is the field frequency, a and a* are the photon production and annihilation operators, P is the projection of the vector $m\vec{v}$ onto the direction of polarization of the photon, and m, e, and $\vec{v}$ are the mass, charge, and velocity operator of the particle. We note further that the eigenfunctions of H_R are the eigenfunctions of a harmonic oscillator.

Formula (10.8) can be used to calculate the probability of N-photon absorption during time t. Usually, the matrix elements are integrals of rapidly oscillating functions. We may therefore write the following relation for the transition probability F per unit time: /394

$$F = \lim_{t\to\infty} \frac{d}{dt} |\langle \varkappa_m \psi_{n_k - N} | S | \varkappa_n \psi_{n_k} \rangle|^2. \qquad (10.9)$$

The energy spectrum of the operator H_0 consists of discrete levels and a continuum. The wave functions that correspond to the energy values of the continuous spectrum describe dissociated or ionized states of the atom or molecule. If these functions are substituted for κ_m, Eq. (10.9) will give the probability of N-photon dissociation or ionization.

2. CALCULATION OF TRANSITION PROBABILITY BY SUCCESSIVE APPROXIMATIONS

On substituting (10.7) into (10.3), we obtain an equation for calculation of the operator S:

$$i\hbar \frac{\partial S}{\partial t} = (H_0 + H_R + H_{0R}) S. \qquad (10.10)$$

We convert to the interaction representation by setting S = g(t) $\exp[(t/i\hbar)(H_0 + H_R)]$. It then follows from (10.10) that

$$i\hbar \frac{\partial g}{\partial t} = H'_{0R}(t) g(t), \quad g(0) = 1, \qquad (10.11)$$

and $H'_{0R}(t) = \exp[-(t/i\hbar)(H_0 + H_R)] H_{0R} \exp[(t/i\hbar)(H_0 + H_R)]$. We set $g(t) = \sum_{n=0}^{\infty} g_n(t)$ and obtain the recursion equations $i\hbar(\partial g_n/\partial t) = H'_{0R} g_{n-1}(t)$ and $g_0 = 1$ by the usual iteration scheme. On successive solution of these equations, we can calculate F.

The final result for F takes the form [696]:

$$F = \sum_{n=n'}^{\infty} F_n \sum_{k=k'}^{2n-1} n_k^k \beta^{2(2n-k)} \alpha^{2(k-n)} \times \\ \times (C_k^{\frac{k+N}{2}})^2 \cdot |\{P_{2n-k}, I_{k-n}\}|^2. \qquad (10.12)$$

Here C_j^j, is the binomial coefficient, n' = (N + 1)/2 if N is odd and n' = N/2 for even N; k' = N for n ≤ N and k' = n for n > N; the prime on the second sum signifies that the terms for which (k + N)/2 is a whole number must be retained in the summation over k; /395

$$F_n = \frac{2\pi}{\hbar^2} \times$$
$$\times \left\{ \frac{\delta(E_A/\hbar - E_B/\hbar - n\omega)}{(E_B - E_{A_1} + \hbar\omega)^2 (E_B - E_{A_2} + 2\hbar\omega)^2 \ldots (E_B - E_{A_{n-1}} + (n-1)\hbar\omega)^2} + \right.$$
$$+ \frac{\delta[E_A/\hbar - E_{A_1}/\hbar - (n-1)\omega]}{(E_{A_1} - E_B - \hbar\omega)^2 (E_{A_1} - E_{A_2} + \hbar\omega)^2 \ldots (E_{A_1} - E_{A_{n-1}} + (n-2)\hbar\omega)^2} + \ldots$$
$$\left. \ldots + \frac{\delta(E_A/\hbar - E_{A_{n-1}}/\hbar - \omega)}{(E_{A_{n-1}} - E_B - (n-1)\hbar\omega)^2 (E_{A_{n-1}} - E_{A_1} - (n-2)\hbar\omega)^2 \ldots \ldots (E_{A_{n-1}} - E_{A_{n-2}} - \omega)^2} \right\},$$

where E_B and E_A are the energies of the initial and final states of the system, respectively, and the E_C are the eigenvalues of the operator H_0.

The expression defined by the symbol $\{P_{2n-k}, I_{k-n}\}$ is constructed as follows. The matrix element $\langle \varphi_{A_n} | N(PI) | \varphi_B \rangle$, where ϕ_{A_1} are the eigenfunctions of the operator H_0 and N(PI) denotes the sum of all possible permutations of (2n - k) operators P and k - n unit operators I, is written out. The intermediate indices are written in the sequence A_n, A_{n-1}, A_{n-2}, ..., B, and then the summation over these indices is taken.

In the expression for F_n, the summation is carried out over all indices A_1, A_2, ..., A_1, ...

The index n that figures in (10.12) actually numbers the various orders of perturbation theory (with respect to the operator H_{0R}). If only the first term is considered in the operator H_{0R}, the summation over n will be performed with n' = N.

Then, as follows from the corresponding estimates, it is necessary to consider both terms of the interaction operator H_{0R} in the analysis of F. We note that multiphoton processes were calculated in [697, 861] on the basis of only the first term of the interaction operator. Processes in which several photons of different frequencies participate, and which are also referred to as multiphoton processes, are analyzed in [698]. However, the authors of [698] consider only cases that can be called single-photon processes in the sense of (10.8) (N = 1). Needless to say,

it is sufficient to consider only the first term of the operator H_{0R} in discussing such situations, a fact that is stated by the authors of the cited reference in the form of a special theorem. /396

In the case of transitions to the continuous spectrum (multiphoton dissociation and ionization processes), relation (10.12) must be integrated over the energy of the final state after first multiplying it by the density of these states. The presence of the δ-functions in this relationship reduces the integration to substitution of $\hbar\rho$ for the δ functions, where ρ is the aforementioned density of states:

$$\rho = (m\hbar^2)(2\pi)^{-3} k\, d\Omega;$$

$d\Omega$ is the elementary solid angle, $k = \hbar^{-1}\sqrt{E/m}$, $E = E_{A_l} + (n - l)\hbar\omega - E'$, E' is the energy of the dissociation or ionization, and the indices n and l are defined in accordance with the construction scheme of F_n.

3. ESTIMATES OF THE PROBABILITY OF MULTIPHOTON PHOTOIONIZATION AND PHOTODISSOCIATION

Concrete calculations of the probability of a multiphoton process can be performed if the matrix elements of the dipole mo-

TABLE 10.1. VALUES OF F FOR VARIOUS λ

$N = 2$		$N = 3$		$N = 4$	
λ, μ	F, sec^{-1}	λ, μ	F, sec^{-1}	λ, μ	F, sec^{-1}
0.135	$7\cdot10^{-30}n_k^2$	0.258	$10^{-50}n_k^3$	0.344	$2\cdot10^{-72}n_k^4$
0.128	$2\cdot10^{-29}n_k^2$	0.253	$10^{-50}n_k^3$	0.335	$10^{-72}n_k^4$
0.124	$9\cdot10^{-29}n_k^2$	0.248	$10^{-50}n_k^3$	0.326	$6\cdot10^{-73}n_k^4$
0.122	$2\cdot10^{-25}n_k^2$	0.243	$2\cdot10^{-48}n_k^3$	0.317	$6\cdot10^{-73}n_k^4$
0.118	$3\cdot10^{-29}n_k^2$	0.238	$10^{-51}n_k^3$	0.310	$5\cdot10^{-73}n_k^4$
0.113	$2\cdot10^{-30}n_k^2$	0.234	$10^{-51}n_k^3$	0.302	$5\cdot10^{-73}n_k^4$

Note: n_k is the number of photons per unit volume (cm^{-3}) and N is the number of absorbed photons.

ment and the energy levels of the molecule or atom are known. On the basis of available literature data on the energy spectra and

matrix elements of dipole transitions, the ionization probability of the hydrogen atom has been calculated for two-, three-, and four-photon absorption. The values obtained for F for specific wavelengths are given in Table 10.1.

In analyzing these processes for the molecules of atmospheric gases, it is necessary to deal with the electron states of the molecule. Calculation of the matrix elements and energy levels is an exceptionally complex task in this case. At the present time, the appropriate data are available only for the simplest atoms and molecules. The situation is similar as regards analysis of the wave function of a dissociated polyatomic molecule, knowledge of which is necessary for calculation of the dipole-moment matrix elements that appear in (10.12).

TABLE 10.2. VALUES OF INDIVIDUAL TERMS IN THE SUM OF (10.12)

N	F, sec^{-1}					
	1	2	3	4	5	6
1	$10^{-9,82}n_k$					
2	$10^{-32,10}n_k^2$					
3	$10^{-52,6}n_k^3$	$10^{-94,0}n_k^5$				
4	$10^{-74,0}n_k^4$	$10^{-116,2}n_k^6$				
5	$10^{-95,4}n_k^5$	$10^{-136,7}n_k^7$	$10^{-178,2}n_k^9$			
6	$10^{-117,7}n_k^6$	$10^{-158,7}n_k^8$	$10^{-199,9}n_k^{10}$			
7	$10^{-133,3}n_k^7$	$10^{-179,5}n_k^9$	$10^{-220,6}n_k^{11}$			
8	$10^{-160,5}n_k^8$	$10^{-201,2}n_k^{10}$	$10^{-242,6}n_k^{12}$	$10^{-284,1}n_k^{14}$		
9	$10^{-181,2}n_k^9$	$10^{-222,0}n_k^{11}$	$10^{-263,5}n_k^{13}$	$10^{-304,8}n_k^{15}$	$10^{-346,3}n_k^{17}$	
10	$10^{-203,2}n_k^{10}$	$10^{-244,0}n_k^{12}$	$10^{-285,3}n_k^{14}$	$10^{-326,5}n_k^{16}$	$10^{-367,9}n_k^{18}$	
11	$10^{-224,1}n_k^{11}$	$10^{-265}n_k^{13}$	$10^{-306,1}n_k^{15}$	$10^{-347,4}n_k^{17}$	$10^{-388,8}n_k^{19}$	$10^{-430,2}n_k^{21}$
12	$10^{-246,2}n_k^{12}$	$10^{-287}n_k^{14}$	$10^{-327,8}n_k^{16}$	$10^{-369,1}n_k^{18}$	$10^{-412,3}n_k^{20}$	$10^{-451,3}n_k^{22}$

In view of the above facts, we shall present below estimates for only some of the quantities that characterize multiphoton processes. It is assumed in these estimates that the dipole-moment /397
matrix elements are quantities of the order of 10^{-18} CGS electrostatic units. The characteristics of the N-photon process are estimated without regard to the particular process taking place (photoionization, photodissociation, change in electronic or vibrational-rotational state).

TABLE 10.3. VALUES OF THE QUANTITIES a AND b THAT APPEAR IN THE EXPRESSIONS $n_k = 10^a$ AND $F = 10^b$

N	a						
	18	19	20	21	22	20,5	21,5
1	8,2	9,2	10,2	11,2	12,2	10,7	11,7
2	3,6	5,6	7,6	9,6	11,6	8,6	10,6
3	1,4	4,4	7,4	11,1	16,0	9,5	13,6
4	−2,9	1,1	5,1	9,8	15,8	7,3	12,8
5	−5,4	−0,1	4,6	11,1	19,8	7,5	15,3
6	−9,7	−3,7	2,3	10,3	20,1	5,8	15,0
7	−12,1	−5,1	1,9	10,9	23,7	6,0	17,2
8	−16,5	−8,5	−0,5	10,1	23,9	4,0	17,0
9	−19,3	−10,3	−1,3	10,9	27,7	3,9	19,2
10	−23,2	−13,2	−3,2	10,8	28,1	2,5	19,2
11	−26,1	−15,2	−4,1	11,5	31,8	2,0	21,3
12	−30,2	−18,2	−6,2	10,7	32,7	0,3	21,7

Note: Commas represent decimal points.

Table 10.2 presents various terms of the sum in (10.12) for N from 1 to 12 as calculated for the indicated conditions.

Table 10.3 presents data on the probabilities of multiphoton processes (N = 1(1) 12) for various n_k. The table gives the value of the b that appears in the expression $F = 10^b$ for various a in the expression $n_k = 10^a$.

Having data on the probabilities of the corresponding processes, we can estimate the absorption coefficient τ of the multiphoton process. The relation [71]

$$\tau\,[\mathrm{cm}^{-1}] = \frac{F(I)\,n_0}{Ic} \qquad (10.13)$$

obtains between τ and F; n_0 is the number of absorbing molecules per unit volume, and I is the radiant intensity, which is given in the plane-wave case by

$$I \quad c\hbar\omega_k n_k. \qquad (10.14)$$

Now the differential relation giving the absorbed radiation takes the form /399

$$dI = -\tau(I)\, I\, dx, \qquad (10.15)$$

where x is the distance traveled by the light beam in the medium.

For a homogeneous medium, we obtain from (10.15) and (10.13)

$$x = -\frac{c}{n_0}\int \frac{dI}{F(I)}. \qquad (10.16)$$

The integral in (10.16) can always be evaluated, because in our case F is a certain polynomial in I according to (10.12) and (10.14). However, to write concrete expressions, it is necessary to have exact knowledge of the corresponding coefficients. After evaluation of the integral, I(x) can be found by solving the resulting equation. The entire task described above can be carried out in general form for arbitrary N.

The familiar exponential intensity decrease follows from /400 (10.16) for the single-photon process. We have for the two-photon process

$$T = \frac{I_0 x \gamma_2 n_0}{c+1},$$

where $T = I/I_0$, I_0 is the intensity of the radiation incident on the layer of medium, and γ_2 is the coefficient of I^2 in the expression for F in the case of a two-photon process. For a three-photon process, we have the equation

$$x = \Gamma_1 I^{-2} + \Gamma_2 \ln I + \Gamma_3 \operatorname{arctg} \Gamma_4 I + \text{const},$$

where Γ_j is a certain constant.

This last expression is no longer sufficient to permit writing an explicit expression for T. Equation (10.16) becomes even more complex for N > 3.

Analysis of the data in Tables 10.2 and 10.3 shows that for certain N and n_k, the sum (10.12) can be cut off at a certain term. Then $F(I) = \gamma_j I^{b_j}$, and we have for the ratio I/I_0

TABLE 10.4. DISTANCES TRAVELLED BY LIGHT AT VARIOUS N, n_k, $n_0 = 2.4 \cdot 10^{19}$ AND T = 0.1

N	n_k, cm^{-3}				
	10^{17}	10^{18}	$10^{18,5}$	10^{19}	10^{20}
2	$3 \cdot 10^{4}$	$3 \cdot 10^{3}$	$3 \cdot 10^{2,5}$	$3 \cdot 10^{2}$	$3 \cdot 10^{1}$
3	$2 \cdot 10^{6}$	$2 \cdot 10^{4}$	$2 \cdot 10^{2}$	2	$2 \cdot 10^{-4}$
4	∞	$3 \cdot 10^{7}$	$2 \cdot 10^{3,5}$	$2 \cdot 10^{1}$	$2 \cdot 10^{-4}$
5	∞	$5 \cdot 10^{5}$	$5 \cdot 10^{4}$	$8 \cdot 10$	0
6	∞	$7 \cdot 10^{7}$	$4 \cdot 10^{4,5}$	4	0
7	∞	∞	$2 \cdot 10^{5}$	$2 \cdot 10^{-1}$	0
8	∞	∞	$3 \cdot 10^{6,5}$	3	0
9	∞	∞	10^{7}	2	0
10	∞	∞	$8 \cdot 10^{7,5}$	$8 \cdot 10^{-1}$	0
11	∞	∞	∞	$8 \cdot 10^{-2}$	0
12	∞	∞	∞	$9 \cdot 10^{-2}$	0

$$\frac{I}{I_0} = \frac{1}{\sqrt[b_j]{\frac{I_0^{b_j-1} x}{\sigma} + 1}}, \tag{10.17}$$

$$\sigma = \frac{c}{n_0 k (b_j - 1) (\hbar \omega_k c)^{b_j - 1}}. \tag{10.18}$$

For large I_0, the unity in (10.17) can be dropped to give the equation

$$x = \sigma \left(\frac{I/I_0}{I_0} \right)^{b_j - 1}, \tag{10.19}$$

which enables us to calculate the distance x corresponding to a given transparency $T = I/I_0$ (Table 10.4).

We note that the estimates indicate that the results of such a calculation depend insignificantly on the value chosen for T. A zero in the table indicates that the required absorption occurs at the very beginning of propagation in the medium (the phenomenon should be explosive in nature), and a ∞ indicates that the corresponding distance is greater than 10^7 cm.

The quantity F can be used to determine the time needed for decay of a given fraction of the molecules or atoms. The corresponding expression follows from the familiar decay relation /401

TABLE 10.5. VALUES OF τ^0 IN SECONDS FOR VARIOUS N AND n_k AT $n/n_0 = 0.1$

N	n_k		
	10^{18}	10^{19}	10^{20}
2	$10^{-3.2}$	$10^{-5.2}$	$10^{-7.2}$
3	10^{-1}	10^{-4}	10^{-7}
4	$10^{3.3}$	$10^{0.7}$	$10^{-4.7}$
5	∞	$10^{0.8}$	$10^{-4.2}$
6	∞	$10^{1.1}$	$10^{-1.9}$
7	∞	∞	$10^{-1.5}$
8	∞	∞	$10^{0.9}$
9	∞	∞	$10^{1.7}$
10	∞	∞	$10^{3.6}$
11	∞	∞	$10^{4.5}$
12	∞	∞	$10^{6.6}$

TABLE 10.6. DISSOCIATION ENERGY E_D OF THE MOLECULES O_2, N_2, CO_2, AND H_2O: IONIZATION ENERGY E_I OF THE ATOMS N, O, C, AND H AND THE ORDERS OF MULTIPHOTON PROCESSES FOR NEODYMIUM-GLASS LASER RADIATION AT $\lambda = 1.06$ μ (N_1) AND RUBY-LASER RADIATION AT $\lambda = 0.69$ μ (N_2)

Molecule	O_2	N_2	CO_2	H_2O	Atom	N	O	C	H
E_D, ev	5.08	9.76	2.8	5.1	E_I, ev	14.5	13.6	11.27	13.6
N_1	5	9	3	5	N_1	13	12	10	12
N_2	3	6	2	3	N_2	9	8	7	8

$$n = n_0 e^{-Ft}, \tag{10.20}$$

where n and n_0 are the numbers of "preserved" molecules (atoms) at the times t and t = 0. If the partial decay time t^0 is defined as the interval in which the ratio n/n_0 reaches a certain value, we have

$$\tau^0 = \frac{\ln n_0/n}{F}. \qquad (10.21)$$

Table 10.5 gives values of τ^0 for $n/n_0 = 0.1$ and various N and n_k. In this table, the sign ∞ means that τ^0 exceeds 10^4 sec.

The process under consideration can be realized in the decay of molecules or atoms of the medium at the focus of a certain lens. The relation between the photon density n_{k_t} at the focus of the lens and the density n_k in the incident beam can be established from the correspondence principle. If R is the radius of the lens and f is its focal length, we have /402

$$n_{k_t} = n_k \frac{R^5 \omega_k^2}{8 f^3 c^2}. \qquad (10.22)$$

The order of the N-photon process is easily evaluated from the relation

$$N = \left[\frac{E_1 - E_2}{\omega_k}\right],$$

where the symbol [ ] denotes the integral part of the number, /403 E_1 is the ionization or dissociation energy, and E_2 is the energy of the lower (usually the ground) state.

Table 10.6 lists the dissociation energies of molecules of the principal atmospheric gases and the ionization energy of their atoms.

4. THE SPECTROSCOPIC SATURATION EFFECT

For the case of elastic collisions between molecules, the spectroscopic saturation effect has been investigated quite thoroughly, e.g., in [699, 700]. We shall give a full analysis of the quantum variant of this effect, in which it is possible to examine inelastic collisions of molecules in a single-photon process of light absorption. The problem of saturation in multiphoton processes is described in [862].

The Hamiltonian of the present problem can be written

$$H = H_1 + H_2 + H_c(t) + H_R + H_{1R}, \qquad (10.23)$$

where H_1, H_2, and H_R are the Hamiltonians of the first and second molecules and the radiation field. The operator $H_c(t)$ takes account of the time-dependent interaction between the two molecules (the collision), and H_{1R} of the interaction between the field and the first (light-absorbing) molecule. The second molecule does not absorb radiation (at least in the single-photon interaction), but only deforms the state of the first molecule.

Since we deal in our problem with bound states, the initial condition must be formulated for a certain point in time t = 0, which may be regarded as coinciding with the beginning of a certain collision. The solution of problem (10.23) must then be sought for a time $t \geq \tau$, where τ is a certain critical (correlation) time that depends on the nature of the interaction $H_c(t)$. With a certain approximation, τ may be understood as the average time spent by one molecule in the neighborhood of the other, or the molecular collision time.

Reasoning almost identical to that set forth in §1 yields the result

$$P_{BA} = |\langle \psi_{n_{k-1}}(\tau)\varphi_m(\tau)|S|\psi_{n_k}(0)\varphi_n(0)\rangle|^2. \qquad (10.24)$$

Here P_{BA} is the probability of transition of the system from state A to state B during time τ; state A is defined as a certain state of the field with n_k photons and the n-state of the interacting molecules; state B is the m-state of the molecules and the state of the field with n_{k-1} photons. The following nomenclature has been introduced in (10.24): ψ_{n_k} for the eigenfunctions of the operator H_R, $\phi_n(0)$ for the eigenfunctions of the operator $H_1 + H_2$, and $\phi_n(t) - S_c(t)\phi_n(0)$. The operators S and S_c satisfy the equations

/404

$$i\hbar \frac{\partial S}{\partial t} = HS, \qquad (10.25)$$

$$i\hbar \frac{\partial S_c}{\partial t} = (H_1 + H_2 + H_c(t))\, S_c. \qquad (10.26)$$

The function $\psi_{n_{k-1}}(\tau) = S_R \psi_{n_{k-1}}$ and $S_R = \exp\left(\frac{t}{i\hbar} H_R\right)$. In (10.24), therefore, $\psi_{n_{k-1}}(\tau)$ may be replaced by $\psi_{n_{k-1}}(0)$.

Expression (10.24) must then be summed over m to take account of all possible transitions from the fixed state to any other state that are accompanied by absorption of a single photon. After this operation,

$$\sum_{(B)} P_{BA} = \langle P_n(0) \mid F \mid \varphi_n(0) \rangle, \tag{10.27}$$

$$F = \int \bar{\psi}_{n_k}(p)\, U^{-1}(p, q)\, \psi_{n_k-1}(p)\, \psi_{n_k-1}(p') \times \times U(p', q)\, \psi_{n_k}(p')\, dp\, dp', \tag{10.28}$$

where the P are the variables of the field functions and the q are the variables of the molecular functions. The operator $U = SS'^{-1}$, $S' = S_c S_R$. Unitarity of the operator U implies that the operator F is Hermitian.

Equation (10.27) must then be averaged over the initial states of the molecules. According to the general rule, averaging a quantity of this type leads to the relation

$$P = S_p \rho_0 F. \tag{10.29}$$

Here P denotes the sum $\sum_{(A)} P_{BA}$ averaged over the initial states of the molecules and ρ_0 is the Boltzmann density matrix for the Hamiltonian $H_1 + H_2$.

We note that the result (10.29) can be obtained starting from the expression for the density matrix ρ, which satisfies the equation /405

$$i\hbar \frac{\partial \rho}{\partial t} = H\rho - \rho H \tag{10.30}$$

with the system Hamiltonian (10.23) and the initial conditions

$$\rho^{(0)}_{nn_k,\, nn_k} = 1, \quad \rho^{(0)}_{mm_k,\, nn_k} = 0. \tag{10.31}$$

Then expression (10.24) for the probability of the A → B transition is written as the diagonal element of the density matrix $\rho_{mn_k-1,\, mn_k-1}$; after the operations of summing over the final states and averaging over the initial states of the system $H_1 + H_2$, we arrive at expression (10.29).

The expression for P must be averaged over the collisions. Technically, this is done by the scheme used in [71].

Equation (10.25) is then solved in the third order of perturbation theory with respect to the interaction operator H_{1R}. The integrals in (10.28) are evaluated by the familiar rules applying to the photon production and annihilation operators. A method based on the theory of rotation-group representations is given in [71, 56] for calculating the sums in (10.29). Since they are cumbersome, we shall omit all intermediate calculations and present the final expression written directly for the function

$$\omega = \frac{P}{n_k c \tau}, \tag{10.32}$$

which has the sense of an absorption coefficient calculated for a single absorbing molecule:

$$\omega = 2\gamma \sum_{\substack{a, b \\ \alpha, \beta}} \frac{\rho_{aa}^{(\omega)}}{2a+1} \times \times \frac{|\langle a\alpha | \mu | b\beta \rangle|^2 (\sigma_{ba}^{(r)})^2}{(\omega_k - \omega_{ba} + \sigma_{ba}^{(i)})^2 + (\sigma_{ba}^{(r)})^2 + 2\eta\tau n_k (\sigma_{ba}^{(2)}) |\langle a\alpha | \mu | b\beta \rangle|^2}. \tag{10.33}$$

The following nomenclature has been introduced in (10.33): $\gamma = 2\pi\omega_k/\hbar c$, $\eta = 2\pi\omega_k \hbar^{-1}$, $\sigma_{ba}^{(r)}$ is the half-width, $\sigma_{ba}^{(i)}$ the shift, and ω_{ba} the center of the spectral line; $\rho_{aa}^{(0)}$ are the diagonal matrix elements of the Boltzmann density matrix for the operator H_1, $\langle a\alpha|\mu|b\beta\rangle$ are the matrix elements of the dipole moment in the representation of the degenerate eigenfunctions of operator H_1, and c is the velocity of light. We note also that only terms containing the frequency difference were taken into account in the calculation (10.33). /406

The n_k-dependent term in the denominator formally constitutes the content of the saturation effect. Actually, the calculation described above stresses a familiar notion: the saturation effect is a result of the fact that the molecule's density matrix differs from the Boltzmann matrix in the presence of a strong field.

5. ABSORPTION OF LIGHT WITH CONSIDERATION OF THE SATURATION EFFECT

Applying (10.33), we can write the following expression for the absorption coefficient for light of frequency ν:

$$k(\nu, I) = \sum_j \frac{a_j}{b_j(\nu) + c_j(\nu) I} \cdot \qquad (10.34)$$

Here the summation is carried out over all lines contributing to absorption of light of the given frequency, $a_j = S_j\gamma_j/\pi$, $b_j = (\nu - \nu_j)^2 + \gamma_j^2$, $c_j = \tau\gamma_j |\mu_j|^{-2}c^{-2}$, S_j, γ_j, ν_j and μ_j are the intensity, half-width, center, and the square of the matrix element of the dipole moment j of the line, and I is the intensity of the radiation. We note that ν_j and γ_j are measured in reciprocal centimeters.

The relation describing the change of radiant intensity in the medium takes the form

$$dI = -k(I) I \, d\omega, \qquad (10.35)$$

where ω is the precipitated layer of the absorbing gas. The initial condition for (10.35) is the usual one: $I = I_0$ at $\omega = 0$.

Equation (10.35) follows, in essence, from the definition (10.32) of ω as the ratio of the amount of absorbed energy to the intensity of the incident radiation.

Equation (10.35) can be integrated exactly for a homogeneous medium. Here, however, it is necessary to deal with cumbersome numerical calculations. It is therefore simpler to solve (10.35) by successive approximations, taking advantage of the smallness of $c_j I$. For this purpose, Eq. (10.35) should be written in the form $dI/I = -k(i)d\omega$ and the zeroth approximation should be $I^{(0)} = I_0 \cdot \exp(-k_0\omega)$, where $k_0 = \Sigma a_j/b_j$. We obtain after simple calculations /407 [703]

$$T = T_0 \prod_j \left(\frac{1 + I_0\varkappa_j}{1 + I_0\varkappa_j T_0}\right)^{\frac{a_j}{b_j k_0}}. \qquad (10.36)$$

Here $T = I/I_0$, $T_0 = \exp(-k_0\omega)$, $\varkappa_j = c_j/b_j$.

It follows from the expressions for a_j and b_j that k_0 has the sense of the attenuation coefficient calculated without consideration of the dependence of the molecular density matrix on the field. Then T_0 is the transparency ordinarily determined for a given radiation frequency. It follows from (10.36) that $T = T_0$ for $I_0\varkappa_j \ll 1$.

Relation (10.36) can be used to estimate the influence of the saturation effect on the transparency of the absorbing-medium

layer. If

$$I_0 \varkappa_j T_0 \gg 1, \text{ then } T = 1. \tag{10.37}$$

The quantity τ can be estimated from the following considerations. The collision time may be regarded as the time for transition of the colliding molecules from one straight-line trajectory segment of their motion to another. Using the corresponding results from solution of this problem [704], we can write that

$$\tau = \tau_0 P^{-1/2} T^{-1/6}. \tag{10.38}$$

In (10.38), T is the absolute temperature, P is the pressure, and τ_0 is a certain nearly constant quantity. If P is expressed in atmospheres, τ_0 is of the order of 10^{-11}.

Making use of this last observation, we can use (10.37) to estimate the intensity at which the saturation effect appears. In the spirit of the estimates in §3, we set further $\alpha_j = 0.1$ cm^{-1} and $T_0 = 0.1$ and obtain a value of the order of 10^{14} erg/cm^2·sec for I_0.

6. SELF-FOCUSING OF THE LASER BEAM

The propagation of powerful laser radiation in a medium may lead to a change in the index of refraction in the beam channel. The difference between the values of the medium's index of refraction in the beam channel and outside it may be such that the divergence of the beam is eliminated. This phenomenon has come to be known as self-focusing of the laser beam. A substantial number of papers have already been devoted to its investigation [705-719, 844 and others].

It is found that when the beam has a divergence ϕ, its elimination requires changing the index of refraction in the beam channel by an amount Δn approximately equal to ϕ^2 from its value outside the channel. /408

If the first nonlinear term in the expansion of the polarization vector in terms of the field in the medium is proportional to the third power of the electric field strength E, the index of refraction of this medium can be written

$$n = n_0 + n_2 E^2, \tag{10.39}$$

where n_0 is the ordinary index of refraction and n_2 is a

coefficient that characterizes the nonlinear properties of the medium. Formula (10.39) has been written on the assumption that the subsequent nonlinear terms in the expansion are small by comparison with the first two.

The nonlinear dependence of the medium's index of refraction on electric field strength is governed chiefly by the Kerr and electrostriction effects. In addition, when absorption occurs in the medium, the corresponding nonlinear effects may be due to thermal expansion of the gas owing to its heating by energy absorbed from the wave.

As we know, the Kerr effect is related to the orientation of the dipole moments of the molecules in the direction of a strong electric field, which explains the practically inertialess manifestation of anisotropy in the properties of the refracting medium. In the electrostriction effect, an additional volumetric pressure

$$P=\frac{1}{8\pi}\rho\frac{\partial\varepsilon}{\partial\rho}E^2 \qquad (10.40)$$

and a force

$$F=\operatorname{grad}P \qquad (10.41)$$

appear in the region of influence of the radiation; here ρ is the density of the medium and ε its dielectric constant.

By solving the electrodynamic equations and the linearized equations of perturbation of the dielectric constant, it is possible to obtain expressions for the threshold power P_{thr} of the self-focusing due to the Kerr and electrostriction effects.

The threshold self-focusing power can be estimated approxi- /409
mately from the simple formula

$$P_{\text{thur}}\approx\frac{\lambda c}{n_2}, \qquad (10.42)$$

where λ is the wavelength of the radiation and c is the velocity of light.

Thus, the threshold self-focusing power may be smaller the shorter the wavelength and the stronger the nonlinear properties of the medium. Certain liquids have the lowest self-focusing thresholds, of the order of tens of kilowatts. The threshold

powers for gases run into the tens and hundreds of thousands of kilowatts. This means that the appearance of self-focusing conditions should be expected when laser radiation propagates in the atmosphere. It will be recalled that the pulse powers of many lasers greatly exceed the threshold self-focusing powers indicated above for gases.

Isolated measurements made in the atmosphere have confirmed the presence of laser-beam self-focusing and shown that, together with focusing of the beam as a whole, thin filaments form inside the beam. It should be noted that self-focusing theory predicts the decomposition of light beams into individual components when the power of the radiation substantially exceeds P_{thr}. However, thin filaments have been observed experimentally at powers not exceeding P_{thr}. At this time, it is difficult to give a definite qualitative interpretation of this filament phenomenon. One possible mechanism may involve fluctuations of the index of refraction of air due to turbulent motions in the atmosphere. It appears that these fluctuations may contribute to the self-focusing effect at powers below threshold for a homogeneous medium.

Detailed investigations of the laser-beam self-focusing effect in the atmosphere have not yet been carried out.

7. EFFECT OF STRONG RADIATION FIELD ON ATMOSPHERIC-AEROSOL PARTICLES

Illumination of atmospheric-aerosol particles with strong directional radiation is accompanied by a number of effects that lead to changes in propagation conditions for radiation in the medium. Among these effects, vaporization of particles by the energy that they absorb from the field is of greatest practical interest. A change in particle size causes a corresponding change in the bulk polydisperse attenuation coefficients. Thus, the transparency of the scattering-medium layer comes to depend on the intensity of the incident radiation. /410

Slow vaporization of particles in a thermal field has been studied in considerable detail. The most complete review of the completed theoretical and experimental research will be found in the monograph by N.A. Fuks [720]. The results obtained in these studies cannot be used to estimate the vaporization of particles in a powerful radiation field. Investigations of this phenomenon were begun only recently. Below we set forth some of the results.

Williams [721] examined the vaporization of solid and liquid spherical particles in a radiation field in a gaseous medium of infinite extent. The author of [721] found the rate of particle evaporation by using the Knudsen kinetic equation. However, the vaporization coefficient that appears in the Knudsen equation remains undetermined. Only tentative estimates have been made for it.

K.S. Shifrin and Zh.K. Zolotova [722] analyzed the kinetics of vaporization of a drop under exposure to solar radiation. Use of a stationary-vaporization hypothesis yielded simple analytical expressions that describe the change in drop radius with time:

$$\left.\begin{aligned} r &= r_0 e^{-\eta t}, \quad \frac{8\pi\varkappa}{\lambda} r \ll 1, \\ r &= r_0 - \eta' t, \quad \frac{8\pi\varkappa}{\lambda} r \gg 1, \end{aligned}\right\} \tag{10.43}$$

where r_0 and r are the radii of the drop before and after radiation exposure, t is time, η and η' are parameters, κ is the absorption index of the particle material, and λ is wavelength.

We see from (10.43) that for a given wavelength, the radii of large drops vary linearly with time under exposure to solar radiation, while those of small particles vary exponentially.

Theoretical studies of the vaporization of atmospheric-aerosol particles under exposure to powerful radiation have recently been carried out in the author's laboratory [723-725]. Below we set forth briefly the principal results of these studies. /411

1. General equations. In deriving the general equations, the process of heat and mass transport is described on the basis of the Enskog-Chapman mathematical theory of inhomogeneous gases [726]. In a spherical coordinate system, the final equations obtained for the distribution of the water vapor partial pressure and temperature outside the particle take the form

$$\frac{\partial p}{\partial t} - \frac{p}{T^l}\frac{\partial T^l}{\partial T} = D\left(\frac{2}{\rho}\frac{\partial p}{\partial \rho} + \frac{\partial^2 p}{\partial \rho^2}\right)\frac{P}{P-p} + D\frac{P}{(P-p)^2}\left(\frac{\partial p}{\partial \rho}\right)^2, \tag{10.44}$$

$$\frac{\partial T^l}{\partial t} = \frac{\lambda^l R_n}{C_p}\frac{T^l}{\mu^a P - (\mu^a - \mu^v)P}\left(\frac{\partial^2 T^l}{\partial \rho^2} + \frac{2}{\rho}\frac{\partial T^l}{\partial \rho}\right) + D\frac{T^l}{P-p}\left(\frac{\partial^2 p}{\partial \rho^2} + \frac{2\partial p}{\rho\,\partial \rho}\right) + D\mu^v P\frac{T^l}{(P-p)^2\left[\mu^a P - (\mu^a - \mu^v)p\right]}\left(\frac{\partial p}{\partial \rho}\right)^2, \tag{10.45}$$

where p is the water vapor partial pressure, P is the total pressure in the medium, T^l is the temperature of the medium, D is the diffusion coefficient of water vapor in air, ρ is the polar radius of the particle, λ^l is the thermal conductivity of the medium, C_p is the heat capacity of the medium at constant pressure, R_n is the

universal gas constant, μ^a is the molecular weight of air, and μ^v is the molecular weight of water vapor.

The temperature field inside a particle is described by the inhomogeneous thermal diffusivity equation

$$\frac{\partial T^i}{\partial t} = \varkappa^i \left(\frac{\partial^2 T^i}{\partial \rho^2} + \frac{2}{\rho} \frac{\partial T^i}{\partial \rho} \right) + I, \tag{10.46}$$

where T^i is the temperature inside the particle, κ^i is the thermal diffusivity of the particle material, and I is the source function

$$I = \frac{3\mathcal{J}\omega(t) K_a(r, \lambda, m)}{4 C_L \gamma_L r^3}. \tag{10.47}$$

In this last formula, $\mathcal{J}$ is the heat equivalent of work, ω is the power of the radiant flux, C_L and γ_L are the heat capacity and density of the particle material, and K_a is the optical absorption cross section of the particle.

Equations (10.44)-(10.46) determine the kinetics of vaporization of a single particle in the radiation field. The boundary conditions for these equations take the form: /412

initial conditions:

$$t = 0;\ p(\rho, 0) = p_\infty;\ T^l(\rho, 0) = T^i(\rho, 0) = T_\infty, \tag{10.48}$$

boundary conditions:

$$\begin{gathered} \rho = r,\ T^l(r, t) = T^i(r, t) \equiv T_0(r, t),\ \rho(r, t) = p_0(T_0), \\ L j_m^0 + j_Q^0 = \lambda^i \left(\frac{\partial T^i}{\partial \rho} \right)_{\rho = r}, \\ \rho \to \infty,\ T^l \to T_\infty,\ p \to p_\infty, \end{gathered} \tag{10.49}$$

where T_0 is the surface temperature of the particle and j_m and j_Q are the vapor mass and heat fluxes.

The initial conditions are formulated on the hypothesis of thermodynamic equilibrium between the particle and the surrounding medium before the radiation acts. The function $p_0(T_0)$ in (10.49) characterizes the saturation vapor pressure as a function of particle surface temperature. For particles with radius r > 1 μ,

this function takes the form

$$p_0(T_0) = p_r e^{L\mu^v/R_n T_r} e^{-L\mu^v/R_n T_0}, \qquad (10.50)$$

where L is the specific heat of vaporization. For particles with $r \leq 1$ μ, appropriate corrections must be applied to (10.50).

Analysis of the hypotheses used in deriving (10.44)-(10.46) enables us to establish the limits of their applicability. The equations obtained are valid for description of the mass and heat transport process in the system formed by a water drop in air at $p = p_{cr} < P$, $T^1 = T_b$; $v = v_{so}$, where T_b is the boiling point of water, v is the mass flowrate, and v_{so} is the speed of sound.

In cases when p, T^1, and v reach values exceeding p_{cr}, T_b, and v_{so}, the vapor mass and heat fluxes can be described by approximate states if it is assumed that

$$j_m = \frac{\mu^v p}{R_n T^l} v_{so}, \qquad (10.51)$$

$$j_Q = C_p \gamma_g T^l v_{so}, \qquad (10.52)$$

where γ_g is the density of the vapor-gas mixture.

In this case, the boundary conditions assume the form /413

$$L\frac{\mu^v p_0}{R_n T_0} v_{so} + C_p^v \frac{\mu^v p_0}{R_n} v_{so} = \lambda^i \left(\frac{\partial T^i}{\partial \rho}\right)_{\rho=r}, \qquad (10.53)$$

and the vaporization kinetics of the drop is described by the equation

$$\frac{dr}{dt} = -\frac{1}{\gamma_L}\frac{\mu^v p_0}{R_n T_0} v_{so}. \qquad (10.54)$$

Equations (10.44) and (10.45) can be solved only by numerical methods. The appropriate algorithms and computer programs have therefore been written in the ALGOL-60 language.

2. Quasistationary fields. In the case of quasistationary temperature and water vapor partial pressure fields, in which they

are determined only by the surface temperature of the particle, Eqs. (10.44) and (10.45) yield expressions for the partial pressure p and temperature T^1 in the form

$$p = P - \frac{(P-p_0)\frac{T^l}{T_0}\frac{r}{\rho}}{(P-p_\infty)\frac{T^l}{T_\infty}\left(\frac{r}{\rho}-1\right)}, \tag{10.55}$$

$$T^l = \frac{r}{\rho}(T_0 - T_\infty) + \frac{C_p D}{\lambda^l R_n} \times$$
$$\times \left[\mu^{v} P \ln\frac{P-p}{P-p_\infty} - (\mu^a - \mu^v)(p-p_\infty)\right] +$$
$$+ \frac{r}{\rho}\frac{C_p D}{\lambda^l R_n}\left[\mu^{v} P \ln\frac{P-p_\infty}{P-p_0} - (\mu^a - \mu^v)(p_\infty - p_0)\right] + T_\infty. \tag{10.56}$$

Asymptotic expressions for p in which T^1 does not appear and an expression for T^1 that does not contain p for $(\rho - r) \ll 1$ (points near the surface of the particle) can be obtained from these equations. However, they are too cumbersome to be given here.

In calculating the vaporization rate of a drop, it is necessary to know the temperature of its surface, which depends on both the fields outside the particle and the temperature distribution in its volume. To determine the temperature inside the drop, it is necessary to solve the boundary-value problem known in mathematical physics as the third boundary-value problem for equations of the parabolic type. Solving this problem has made it possible /414 to obtain the following transcendental equation for determination of the drop surface temperature T_0:

$$T_0 + \frac{2r}{\varkappa^{i2}}\sum_{n=1}^{\infty}\frac{(-1)^n \pi n}{\pi^3 n^3 (1+n^2\pi^2)}\left\{I_r + \frac{2\varkappa^{i2}}{r^2}\times\right.$$
$$\left.\times\theta\left[1-(-1)^n\right]\right\}\left(1 - e^{-\left(\frac{\varkappa^i n\pi}{r}\right)^2 t}\right) + \frac{2}{r}\sum_{n=1}^{\infty}\frac{(-1)^n}{1+n^2\pi^2}\times$$
$$\times\left\{T_\infty r - \theta\frac{(-1)^n\left[n^2\pi^2+2\right]-2}{n^2\pi^2}\right\} e^{\left(\frac{\varkappa^i n\pi}{r}\right)^2} + \frac{\theta}{r} = 0, \tag{10.57}$$

where

$$\theta = \frac{\lambda^l}{\lambda^i}T_0 r - \frac{D\mu^{v} P r}{\lambda^i R_n}\ln(P-p_0)\left(C_g + \frac{L}{T_0}\right) +$$
$$+ \frac{C_p D r}{\lambda^i R_n}(\mu^a - \mu^v)p_0 - \frac{\lambda^l T_\infty}{\lambda^i}r + \frac{D\mu^{v} P r}{\lambda^i R_n}\times$$
$$\times\ln(P-p_\infty)\left(C_p + \frac{L}{T_\infty}\right) - \frac{C_p D}{\lambda^i R_n}(\mu^a - \mu^v). \tag{10.58}$$

If the solution of (10.57) for T_0 is known, no great difficulty is encountered in calculating the vaporization rate of the drop; this can be done by the formulas

$$\frac{dr}{dt} = -\frac{1}{\gamma_L} j_m^0, \tag{10.59}$$

$$j_m^0 = \frac{\mu_V D p}{r R_n}\left[\frac{1}{T_\infty}\ln(P-p_\infty) - \frac{1}{T_0}\ln(P-p_0)\right]. \tag{10.60}$$

3. Stationary vaporization of a drop under continuous illumination. When a time-constant radiant flux acts continuously on the drop, it can be assumed that the heat fluxes absorbed by the drop and removed from it with the vapor are the same. This circumstance enables us to write the balance equation

$$4\pi\lambda'(T_0-T_\infty) + 4\pi r L(T) D[c_V(T_0) - c_{V\infty}] = \pi J\omega K_a(r) r^2, \tag{10.61}$$

where c_V is the water-vapor concentration in the medium.

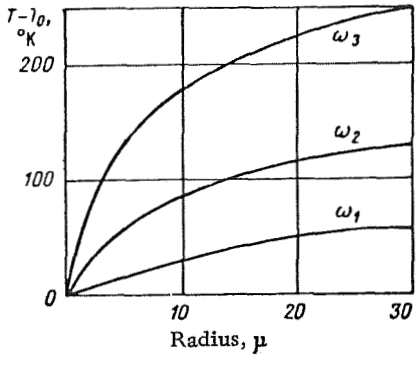

Figure 10.1. Calculated Temperature Variations for Droplets of Various Sizes Under Continuous Illumination with Radiant Fluxes of $\omega_1 = 10^2$ W/cm^2, $\omega_2 = 10^3$ W/cm^2, $\omega_3 = 10^4$ W/cm^2, $T_0 = 273°K$, $\lambda = 10.6$ μ.

Equation (10.61) can be used to determine the surface temperature of the drop. /415

Figure 10.1 presents results of graphical solution of (10.61).

The vaporization rate of the drop can be estimated by integrating the kinetic equation of stationary vaporization:

$$r\frac{dr}{dt} = -\frac{\dot{D}}{\gamma_L}[c_V(T) - c_{V\infty}]. \tag{10.62}$$

Approximate graphical integration of this last equation using tabular data for $c_V(T)$ for parameter values the same as those in Fig. 10.1 made it possible to obtain curves of drop radius as a function of time (Fig. 10.2). These curves are approximated satisfactorily by the equation

$$r(t)=\begin{cases} r_0-0{,}494\omega^{1{,}102}t, & pr\gg 1,\\ r_0e^{-0{,}494\omega^{1{,}102}t}, & pr\ll 1, \end{cases} \qquad (10.63)$$

where $p=8\pi\varkappa/\lambda$; $q=\exp[-0.2(|m|-1)]$; m is the complex index of refraction of water.

4. Vaporization of drop under the action of single radiation pulses. If a single pulse acts on the drop for a time such that the process of energy absorption by the drop can be considered adiabatic, the temperature of the drop after exposure to the pulse can be determined from the formula

$$T_h=T_\infty+\frac{1.8\cdot 10^3K_a(r_0)E}{r_0}, \qquad (10.64)$$

where E is the energy of the pulse in joules per square centimeter and r_0 is the initial radius of the drop in microns.

Estimates show that for $T_h \leq 400°K$ produced by a single pulse, the vaporization from the drop has little effect on its radius.

There is no point in examining values of $T_h \geq T_{cr} = 647°K$. Thus, interest attaches to the effects of exposure of the drop to a single pulse when the temperature T_h lies in the range

$$400°K \leqslant T_h \leqslant T_{cr}. \qquad (10.65)$$

Assuming that the temperature of the drop is uniformly distributed through its volume, it can be found for any given time from the simple relation

$$C_L m\,dT = L\,dm, \qquad (10.66)$$

from which it is easy to obtain an expression for the temperature

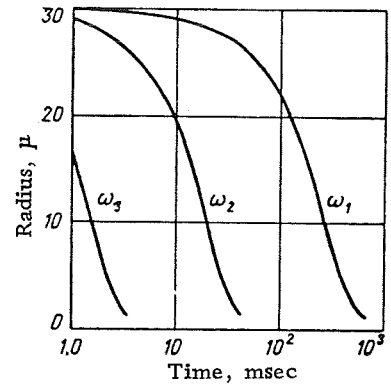

/416

Figure 10.2. Calculated Time Curves of Drop Radius for Continuous Illumination of Drop by a Flux with Wavelength 10.6 μ and Powers $\omega_1 = 10^2$ W/cm², $\omega_2 = 10^3$ W/cm², $\omega_3 = 10^4$ W/cm². Initial drop radius $r_0 = 30$ μ.

of the drop as a function of its radius: /417

$$T = T_h + \beta \ln \frac{r}{r_0}, \qquad (10.67)$$

where

$$\beta = \frac{6L(T_h)L(T_\infty)}{C_L[L(T_h)+L(T_\infty)]}. \qquad (10.68)$$

Eq. (10.67) yields an expression for the final radius of the drop after it has been subjected to a single pulse:

$$r_f = r_0 e^{-(T_h - T_\infty)/\beta}. \qquad (10.69)$$

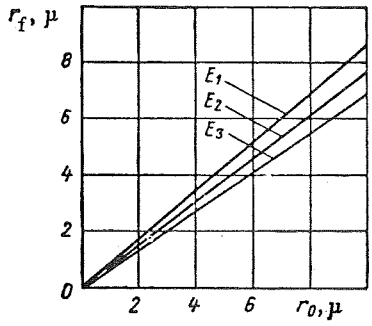

Figure 10.3. Calculated Final Drop Radius as a Function of Initial Radius for Pulse Energies $E_1 = 2.00 \cdot 10^3$ J/cm^2; $E_2 = 2.66 \cdot 10^3$ J/cm^2; $E_3 = 2.93 \cdot 10^3$ J/cm^2.

Figure 10.3 presents the results of a calculation of the final radius of a drop that has been subjected to illumination with a single pulse at a wavelength of 10.6 μ. We note that in the general case, the final radius of the particle is not a linear function of its initial radius, since the difference $T_h - T_\infty$ and β depend on r_0.

Formula (10.69) implies that the final radius of the drop can equal zero only when $T_h = T_{cr} = 647°K$, when $\beta = 0$, since $L(T_{cr}) = 0$.

The above formulas are valid when the pulse duration is shorter than the time within which the size and temperature of the drop can change appreciably. Estimates indicate that this time should be of the order of 10^{-4} sec.

When $T_h > T_{cr}$, we should expect the drop to explode, with /418 the water vapor impinging on the air under high pressure and forming a compression wave. Estimates show that this wave equalizes the vapor pressure in the medium surrounding the drop; at a distance of approximately $10r_0$ from the drop, the products of the explosion have yielded their energy to the air. It is found that the time within which this phenomenon unfolds is expressed by the simple formula

$$t = \frac{r_0}{U_x} \frac{10^3}{3} \text{ [sec]}, \qquad (10.70)$$

where U_x is the propagation velocity of the compression wave. For water drops with radii of 10 μ, the explosion time is found to be of the order of 10^{-6} sec.

5. Radiation effects on polydisperse aerosol. To determine the radiation effect on a polydisperse aerosol, it is necessary to know the change which this effect makes in the particle size distribution function. It can be assumed in first approximation that the disturbance affects each particle of the polydisperse aerosol independently. This assumption is justified by the fact that in most cases, the moisture content of the aerosol particles in a unit volume is much lower than that of the air containing the aerosol.

With the above assumption, it is easy to obtain an expression for the particle size distribution function f(r, t) involving time. In the case of continuous illumination of a polydisperse aerosol with an initial particle size distribution function described by the gamma distribution [see (5.4)], we can obtain the following expression for f(r, t):

$$f(r, t)=\begin{cases} \frac{1}{\Gamma(\mu+1)}\mu^{\mu+1}\frac{1}{\bar{r}_0}\left(\frac{r+S}{\bar{r}_0}\right)^{\mu}e^{-\mu\left(\frac{r+S}{\bar{r}_0}\right)}, & (10.71) \\ \frac{e^{\mu pS}}{\Gamma(\mu+1)}\mu^{\mu+1}\frac{1}{\bar{r}_0}\left(\frac{re^{pS}}{\bar{r}_0}\right)e^{-\mu\left(\frac{re^{pS}}{\bar{r}_0}\right)}, & (10.72) \\ pr \ll 1, \end{cases}$$

where μ is a parameter that characterizes the half-width of the distribution, $S=0.494q\omega^{1.102}t$; $\bar{r}$ is the most probable particle radius.

Substituting (10.71) and (10.72) into (7.3), we can calculate the bulk attenuation coefficient. /419

In the case of large particles, when the function K(ρ, m) = = 2, a rather simple expression with μ = 2 is obtained for the bulk attenuation coefficient:

$$\alpha(\omega, t)=2\pi N_0(S^2+3\bar{r}_0S+3\bar{r}_0^2)e^{-2S/\bar{r}_0}, \quad (10.73)$$

where N_0 is the number of particles per unit volume.

For small and "soft" particles,

$$\alpha(\omega, t) = \frac{\pi N_0}{\Gamma(\mu+1)}\mu^{\mu+1}\times$$
$$\times\left[\frac{32\pi(n-1)(\operatorname{tg}\beta)r^{-3}\Gamma(\mu+4)}{3\lambda\mu^{\mu+1}}e^{-3pS}+\right.$$
$$\left.+\frac{8\pi^2(1-\operatorname{tg}^2\beta)\bar{r}_0^4\Gamma(\mu+5)}{\lambda^2\mu^{\mu+5}}e^{-4pS}\right], \qquad (10.74)$$

where $\tan\beta = \kappa/(n-1)$; n is the index of refraction of water.

When pulsed radiation strikes a polydisperse aerosol, the particle size distribution function is defomed as a whole when the relation between the final and initial particle radii can be considered linear, with a change in the most probable particle radius. In this case, the bulk coefficient can be calculated by the usual formulas, except that $\bar{r}_0 k$, where k is a parameter that depends on the pulse energy and the particle optical cross section, must be taken for the most probable radius.

The foregoing approximate theory of spherical-particle vaporization under the action of strong continuous, quasicontinuous, and pulsed optical radiation represents a first attempt at quantitative description of a highly complex phenomenon. As usual, its reliability can be determined in appropriate experimental studies, the first results from which have been published in [727, 728]. However, the sources used for the measurements in these studies were too small to permit definite conclusions as to the agreement between theory and experiment.

We note also that vaporization of drops is by no means the only effect attending propagation of strong optical radiation in a polydisperse water aerosol. When a water aerosol is acted upon by high-powered, short-duration light pulses, the aerosol particles acquire a directional motion as a result of their nonuniform heating. The particles may coagulate as a result of thie directional motion. /420

At high powers of the radiation incident on the aerosol, it may be found necessary to consider the effect of light pressure, calculation of which presents no major difficulties. It appears that nonstationary vaporization of water-aerosol particles should lead to the appearance of conditions for defocusing and anomalous refraction of the directional radiation in the beam channel.

Study of these effects and their influence on particle vaporization is a matter for the future. All that can be said now is that from the standpoint of the energy losses of strong optical radiation in a water aerosol, the particle-vaporization effect is dominant apart from the losses of the directional radiant flux due to scattering on particles.

Chapter 11 /421

PROPAGATION OF LIMITED BEAMS OF LIGHT IN A TURBULENT ATMOSPHERE

In addition to the energy losses caused by absorption and scattering phenomena, a light wave propagating in the real atmosphere experiences amplitude and phase fluctuations that owe their origin to the random space-time distribution of the index of refraction of the air. The latter is a result of turbulent motions in the atmosphere, which cause random variation of the temperature and of the index of refraction, which is related to it. Estimates indicate that a 1°K change in air temperature changes the index of refraction by an amount of the order of 10^{-6} [729]. The amplitude of the observed air-temperature fluctuations at a given point ranges into the tenths of a degree; the period of the fluctuations varies from milliseconds to seconds. The amplitude of the temperature pulsations along horizontal paths in the atmosphere may reach several degrees for points separated by distances of the order of 10^2 - 10^3 meters [730].

The influence of the space-time fluctuations of the atmosphere's index of refraction on the characteristics of unlimited plane and spherical waves has been investigated in considerable detail, both theoretically and experimentally. The well-known monographs of V.I. Tatarskiy [463, 731] set forth the theory systematically and examine the results of experimental studies. However, the theoretical and experimental results obtained for unlimited beams cannot, generally speaking, be applied directly for quantitative estimation of the corresponding parameters of limited beams. This fact calls for new theoretical and experimental investigations, the results of which have great applied importance /422
in connection with the possibility of using limited laser beams in communications, data-transmission, radar, and ranging systems and in other devices designed to work through the atmosphere.

The present chapter discusses the basic results of research on the influence of the turbulent atmosphere on the parameters of spatially limited light beams under various propagation conditions.

1. GENERAL REMARKS

Turbulent motions in the atmosphere give rise to inhomogeneities whose extent varies from many hundreds of meters (macroinhomogeneities) to dimensions l_0 of the order

$$l_0 \sim \sqrt[4]{\nu^3/\varepsilon}, \qquad (11.1)$$

where the quantity l_0 is the so-called internal scale of the turbulence, ν is the kinematic viscosity, and ε is the rate of thermal dissipation of the energy of the inhomogeneity. The dimension l_0 is of the order of 1 mm near the ground.

The field of the index of refraction n of a medium with random inhomogeneities is usually characterized by the structure function [463]

$$D_n(r) = \overline{[n(r_1+r) - n(r_1)]^2}, \tag{11.2}$$

where r is the distance between the points.

The structure function for the temperature field is introduced in analogous fashion:

$$D_T(r) = \overline{[T(r_1+r) - T(r_1)]^2}. \tag{11.3}$$

The form of the functions $D_n(r)$ and $D_T(r)$ in the inertial range [731] was obtained by A.M. Obukhov [732] on the assumption of locally isotropic and homogeneous turbulence. The corresponding relationships have come to be known as the Kolmogorov-Obukhov two-thirds law:

$$D_n(r) = C_n^2 r^{2/3}, \tag{11.4}$$

$$D_T(r) = C_T^2 r^{2/3}, \tag{11.5}$$

where $l_0 < r < L_0$, L_0 is the external turbulence scale.

The quantities C_n and C_T are known as the structure constants /423 of the index of refraction and the air-temperature pulsations and are related as follows for a wavelength of 0.5 μ:

$$C_n\,[\mathrm{cm}^{-1/3}] = \frac{79{,}2\cdot 10^{-6} P\,[\mathrm{mb}]}{T^2\,[^\circ\mathrm{K}]}\, C_T\,[\mathrm{deg}\cdot\mathrm{cm}^{-1/3}]. \tag{11.6}$$

In the ground layer of the atmosphere, C_n ranges from 10^{-7} to 10^{-9} $\mathrm{cm}^{-1/3}$ [741]. Methods of determining the structure constant of the index of refraction are based on use of data on the average values of the meteorological-field characteristics [733, 846] and data on temperature pulsations [847]. Optical methods of determining C_n have been developed in recent years [848-850].

The mean square of the log-intensity fluctuations of an unbounded plane monochromatic wave propagating in a turbulent atmosphere is given by the relation

$$\sigma^2 = 2.24k^{7/6}\int_0^L C_n^2 (L-x)^{5/6}\,dx, \qquad (11.7)$$

where k is the wave number and L is the distance traveled by the wave in the atmosphere.

In the case of an atmosphere that is homogeneous from the standpoint of turbulence conditions, C_n^2 does not change over the entire path L, and (11.7) yields

$$\sigma_0^2 = 1.23C_n^2k^{7/6}L^{11/6}. \qquad (11.8)$$

The quantity C_n depends on the height of the layer of atmosphere:

$$C_n^2(z) = C_n^2(z_0)\left(\frac{z}{z_0}\right)^{-\alpha}, \qquad (11.9)$$

where z_0 is a fixed height ($z > z_0$), and the exponent $\alpha = 2/3$ in the presence of dynamic turbulence in the atmosphere and $\alpha = 4/3$ in the case of free convection [463].

The formulas for the variance of the log-intensity fluctuations correctly describe the case of so-called weak fluctuations, defined by the condition $\sigma << 1$. In solving the wave equation in the approximation of geometrical optics, V.I. Tatarskiy [851] obtained a formula for the mean-square σ_x^2 of the log-amplitude fluctuations in the strong-fluctuation case: /424

$$\sigma_x^2 = 1 - [1 + 6\sigma_0^2]^{-1/6},$$

which agrees well with the experimental data of [751], although the conditions for applicability of geometrical optics were not satisfied in the experiment.

The mean square of the fluctuations of the angle of arrival of an infinite plane wave in the focal plane of a lens is expressed by the relation [463]

$$\sigma_\varphi^2 = 2.8b^{-1/3} \sec\theta \int_{z_0}^{\infty} C_n^2(z)\,dz, \qquad (11.10)$$

where θ is the source zenith angle, z_0 is the height at which the receiving lens is situated, and b is the diameter of the lens.

Aircraft measurements made by L.R. Tsvang [734] showed that formula (11.9) with $\alpha = 4/3$ is valid up to the heights of formation of cumulus clouds. Taking this height as infinity, a simple expression for σ_ϕ^2 can be obtained at once from (11.10) and (11.9) [735]:

$$\sigma_\varphi^2 = 2.8b^{-1/3} \sec\theta\, z_0 3C_n^2(z_0). \qquad (11.11)$$

The quantity σ_ϕ^2 is related to the frequency spectrum of the arrival-angle fluctuations by the relation

$$\sigma_\varphi^2 = \int \omega_\varphi(f)\,df. \qquad (11.12)$$

A formula was derived in [736] for the frequency spectrum of the angle-of-arrival fluctuations in the case of a homogeneous turbulent atmosphere:

$$\omega_\varphi(f) = 0.045\sigma_\varphi^2 \sin^2\left(\frac{\pi b f}{v_1}\right)\left(\frac{b}{v_1}\right)^{-5/3} f^{-8/3}, \qquad (11.13)$$

where f is the frequency and v_1 is the wind-speed component perpendicular to the propagation direction of the wave for the frozen-in turbulence model.

2. THEORETICAL INVESTIGATIONS OF PARAMETER FLUCTUATIONS OF LIMITED BEAMS PROPAGATING IN THE ATMOSPHERE

/425

A. I. Kon and V.I. Tatarskiy [737] derived expressions for use in calculating the fluctuations of the phase and the effective divergence of a limited beam propagating in a turbulent atmosphere.

The problem was solved in the approximation of the Rytov-Obukhov smooth-perturbation method. Into the expression for the logarithm of the small perturbation of the field ψ, which is a solution of the wave equation and is expressed in terms of the characteristics of the incident and perturbed fields as follows:

$$\psi_1 = \psi - \psi_0 = \ln \frac{A}{A_0} + i(s - s_0) \qquad (11.14)$$

(A, A_0 and s, s_0 are the amplitudes and phases of the perturbed and incident fields, respectively), they substituted the value of the unperturbed field, whose amplitude is distributed over the beam cross section in accordance with the law

$$A_0 = A_0' \exp\left(-\frac{y^2+z^2}{a^2}\right), \qquad (11.15)$$

A_0' is the amplitude of the incident wave on the axis of the beam, a is the dimension of the beam, and y and z are the coordinates in the plane of the cross section of the beam, which propagates in the direction of the x axis. An expression containing $s_1 = \mathrm{Im}\,\psi_1$ was then written for the structure function D_S of the phase fluctuations. This was followed by an approximate calculation of the integrals in the expression for D_S, using the conditions

$$g = 2L/ka^2 \ll 1 \ (\text{or } a^2 \gg \lambda L), \qquad (11.16)$$

$$a^4 \gg \lambda^3 L^3 l_0^2. \qquad (11.17)$$

Only the fluctuations of the propagation direction are determined; use is therefore made of the value of D_S for $|\vec{\rho}| \ll \underline{l}_0$, where $\vec{\rho} = \vec{\rho}_1 - \vec{\rho}_2$, $\vec{\rho}_1$ and $\vec{\rho}_2$ are the radius vectors of points in the plane $x = L$. A formula that differs by small corrections from the corresponding expression in the case of an infinite plane wave is obtained for D_S in the geometrical-optics approximation ($\sqrt{\gamma L} \ll \underline{l}_0$). When the expression for D_S is found for $\sqrt{\gamma L} \gg \underline{l}_0$ (the practically important case), a parameter θ is introduced: /426

$$\theta^2 = 2L^2\varkappa_m^2/k^2a^2, \qquad (11.18)$$

where κ_m is the wave number characterizing the internal turbulence scale. The parameter θ characterizes the ratio of the diffracted-beam width to the geometrical beam width.

In the asymptotic case $\theta \gg 1$, the following expression is obtained for the structure function D_S:

$$D_s(\rho, R) = 0.46k^3aC_n^2k_m^{-2/3}\rho^2 \ln 2\theta^2 \times$$
$$\times\left[2{}_1F_1\left(\frac{1}{6}, 1, \frac{2R^2}{a^2}\right) - {}_1F_1\left(\frac{1}{6}, 2, \frac{2R^2}{a^2}\right)\right], \qquad (11.19)$$

where ${}_1F_1$ is the degenerate hypergeometric function, R is the numerical value of the vector $\vec{R} = \frac{1}{2}(\vec{\rho}_1 + \vec{\rho}_2)$ (the vectors $\vec{\rho}$ and $\vec{R}$ are assumed parallel; the line joining the observation points $\vec{\rho}_1$ and $\vec{\rho}_2$ passes through the center of the beam). Formula (11.19) differs substantially from the corresponding expression for D_S in the infinite-wave case.

Applying (11.19), the authors of [737] found an approximate expression for the effective mean square of the arrival-angle fluctuations:

$$\sigma_{\varphi\ \mathrm{eff}}^2 \cong 0.1C_n^2kal_0^{2/3}\ln 2\theta^2, \qquad (11.20)$$

whence it follows that at large θ (large L), the increase of $\sigma^2_{\phi\ \mathrm{eff}}$ slows down sharply with distance (it becomes proportional to ln L rather than L, as in the case of the infinite wave). This is explained by the fact that in the limited-beam case, the scattered waves are knocked out of the beam at large L and cease to contribute to the fluctuations. For θ = 10 (beam width 50 cm, l_0 = 1 m, L = 5 km, λ = 0.5 μ), σ^2_ϕ differs by a factor of 4 from that calculated by (11.10) for the infinite wave. We note that $\sigma^2_{\phi\ \mathrm{eff}}$ is the value of σ^2_ϕ averaged over the beam cross section with consideration of the amplitude distribution (11.15).

A formula that determines the linear expansion of the beam as a function of the distance traveled in the turbulent medium was also obtained in [737]. The random broadening of the beam over a distance L equals /427

$$R = \int_0^L \Delta\varphi(x)\,dx. \qquad (11.21)$$

Assuming that the longitudinal correlation coefficient for $\Delta\phi(x)$ is close to unity [738] and applying (11.20), the authors of [737] obtained the formula

$$R_{\mathrm{eff}} = \sqrt{\langle R^2\rangle} = \mathrm{const}\, C_n l_0^{1/3}(ka\ln\theta)^{1/2}L, \qquad (11.22)$$

which indicates that at large L ($\theta \gg 1$) R_{eff} is proportional to L and not to $L^{3/2}$, as in the case $\theta \ll 1$.

A calculation of the amplitude fluctuations of a spatially limited beam showed that the corresponding expression for σ^2 differs from (11.7) by small corrections of the order of g^2 in the case of the unlimited wave.

Formula (11.15), which describes the law of wave-amplitude distribution over the beam cross section, does not always conform to experimental conditions; however, the authors of [737] stress that the basic qualitative conclusions of the study also remain valid for other expressions for the function $A_0(y, z)$.

Z.I. Feyzulin and Yu.A. Kravtsov [739] considered the problem of broadening of a spatially limited beam propagating in a turbulent atmosphere. They took account of both the blurring of the beam and its diffractive divergence and its rocking as a whole about the propagation direction. The total broadening of the beam is written in the form

$$\overline{\langle \rho^2 \rangle} = \overline{\Delta\rho^2} + \overline{\rho_c^2}, \tag{11.23}$$

where

$$\overline{\langle \rho^2 \rangle} = \frac{\int_S \rho^2 \overline{I_s(\vec{\rho})}\, d\vec{\rho}}{\int_S \overline{I_s(\vec{\rho})}\, d\vec{\rho}}; \tag{11.24}$$

$$\overline{\rho_c^2} = \frac{\int_S \int \overline{(\vec{\rho}_1, \vec{\rho}_2)\, I_s(\vec{\rho}_1)\, I_s(\vec{\rho}_2)}\, d\vec{\rho}_1\, d\vec{\rho}_2}{\left(\int_S \overline{I_s(\vec{\rho})}\, d\vec{\rho}\right)^2}. \tag{11.25}$$

The term $\overline{\rho_c^2}$ characterizes the rocking of the beam as a whole about its propagation direction, and $\overline{\Delta\rho^2}$ determines the broadening of the beam about the perturbed position of its center. Expressions for the average intensity $I_S(\rho)$ of the field at a point with radius vector $\vec{\rho}$ and for the intensity correlation function $\overline{I_s(\vec{\rho}_1)\, I_s(\vec{\rho}_2)}$ in a plane S perpendicular to the propagation direction of the beam are found in [739]. A plane propagating wave is assumed. The method of smooth perturbations [463] is used in calculating the statistical characteristics that appear in the sought expressions. /428

We cite one of the terms of the expression obtained in [739] for $\overline{\langle \rho^2 \rangle}$, one that characterizes the broadening of the beam due to scattering on fluctuations of the index of refraction of air in the case in which isotropic turbulence prevails:

$$\frac{L^2}{2k^2}\Delta D_\psi(\theta) = 2.19C_n^2 l_0^{-1/3}L^3, \qquad (11.26)$$

where D_ψ is the structure function of the complex phase.

The expression for $\overline{\langle\rho^2\rangle}$ is greatly simplified in the case of a Gaussian field distribution over the beam cross section:

$$\overline{\langle\rho^2\rangle} = a^2 + \frac{L^2}{k^2a^2} + 2.19C_n^2 l_0^{-1/3}L^3. \qquad (11.27)$$

This formula does not imply that the increase in beam width becomes slower with increasing distance at large L, as was inferred in [737]. The authors of [739] explain the difference in the results as due to the different measures of beam width used in their work and in [737].

Subsequently, [739] analyzes two defined cases of rocking of the beam's "center of gravity:" the case of large-scale inhomogeneities, when the beam dimensions are much smaller than those of the inhomogeneities, and the case of small-scale inhomogeneities (inhomogeneity dimensions much smaller than beam width). It is shown that the beam is not broadened in the former case, but merely shifted as a whole around the propagation direction. In the latter case, quantitative analysis is difficult. It follows from qualitative considerations that the shift of the beam "center of gravity" should be insignificant in this case.

The values of the total beam broadening were determined in [739] for the following parameter values: a = 35.7 cm, l_0 = 0.1 cm, /429 λ = 0.5 μ, $C_n = 0.02 \cdot 10^{-6}$ $cm^{-1/3}$, and distances L_1 = 15 km and L_2 = 145 km; the results were about 91 cm and 25.5 m, respectively.

Let us briefly describe the results obtained in other theoretical investigations. Quantitative theoretical data on the fluctuations of laser-beam parameters during propagation in a turbulent atmosphere were analyzed in Davis' review paper [741] as affecting the performance of laser systems. Fried and Schmeltzer [744] made a detailed calculation of the effects of atmospheric fluctuations on optical communications links. The variance of the log amplitude of a laser beam propagating on a horizontal path in the atmosphere was estimated in the paper by Fried and Seidman [745].

Hufnagell and Stanley [750] constructed a statistical theory of the transfer of an optical image through a turbulent atmosphere. A formula was obtained in [750] for the optical transmission function, which characterizes the coefficient of transmission of spatial frequencies through the atmosphere:

$$M(\lambda Rf) = e^{-\frac{1}{2}k^2\langle[S(p)]^2\rangle},$$

where f = p/λR is the spatial frequency, p are the linear dimensions of the object observed, R is the focal length of the receiving lens, and

$$\langle S^2\rangle = 2.91p^{5/3}\int_0^z C_n^2(z')\,dz'.$$

The angle brackets indicate rather extensive averaging over time.

Fried [742, 743] made a theoretical study of the influence of the atmosphere's turbulence state on the optical resolution, as defined by the optical transmission function, for long and short photographic exposure times and at the limit of resolution of images obtained by photography from top to bottom through the atmosphere.

A number of quantitative estimates of the effects of atmospheric turbulence on the parameters of spatially limited light beams were also obtained in [740, 746-749, 752] and others. The limiting dimensions of the radiation source and receiver at which there is still no disturbance to the spatial coherence of the light beam due to atmospheric turbulence are estimated in [747]. The authors of [749] estimated the limiting light-beam diameter beyond which turbulent motions in the atmosphere greatly reduce the spatial coherence of the beam. An expression was obtained in [740] for the normalized variance of the intensity fluctuations with averaging over the aperture, which is referred to as the aperture-averaging factor. The strength of source flicker is investigated in [752] as a function of source angular dimensions. /430

3. EXPERIMENTAL STUDIES OF PARAMETER FLUCTUATIONS OF SPATIALLY LIMITED BEAMS PROPAGATING IN A TURBULENT ATMOSPHERE

1. Intensity fluctuations. The measured intensity fluctuations of a spatially limited laser beam propagating in a turbulent atmosphere depend on weather conditions, the optical length of the ray path, the aperture diameters of the source and receiver, the receiver time constant, the time of measurement (exposure), the radiation of the wavelength, and the focusing of the beam.

The theory uses the following quantities as quantitative measures of the fluctuations of the beam intensity I:

$$\sigma^2 = \overline{(\ln I - \overline{\ln I})^2}, \qquad (11.28)$$

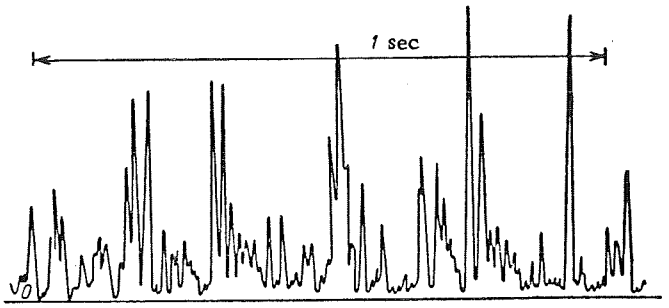

Figure 11.1. Sample Trace Showing Fluctuation of Signal Propagating in the Atmosphere According to [751].

or [759]

$$M^2 = \overline{I^2(t)}/\overline{I(t)}^2, \qquad (11.29)$$

$$\overline{I(t)} = \lim_{T\to\infty} \frac{1}{2T} \int_{-T}^{T} I(t)\,dt;$$

$$\overline{I^2(t)} = \lim_{T\to\infty} \frac{1}{2T} \int_{-T}^{T} [I(t) - \overline{I(t)}]^2\,dt, \qquad (11.30)$$

and the standard deviation of the measured signal from its mean value,

$$\sigma_n = \sqrt{M^2}. \qquad (11.31)$$

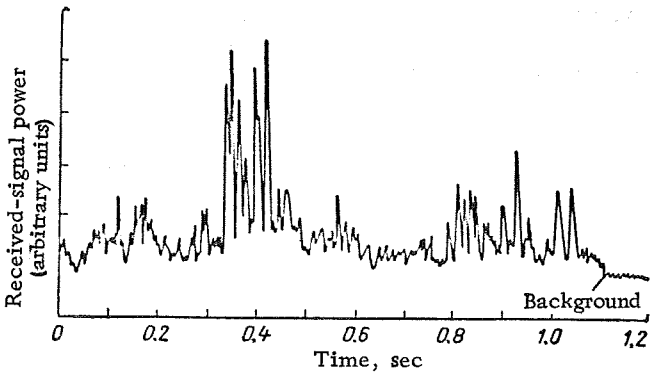

Figure 11.2. Example Showing Time Dependence of Signal Propagating in the Atmosphere, According to [766].

The experimentally measurable quantities are /431

$$\bar{I} = \frac{1}{N}\sum_{i=1}^{N} I_i, \tag{11.32}$$

$$\overline{I^2} = \frac{1}{N}\sum_{i=1}^{N} I_i^2, \tag{11.33}$$

$$\sigma_k^2 = \frac{\overline{I^2} - \bar{I}^2}{\bar{I}^2}. \tag{11.34}$$

Assuming validity of the logarithmically normal distribution law for the fluctuations of the intensity I, the relation between σ_k^2 and σ^2 is

$$\sigma^2 = \ln(1 + \sigma_k^2). \tag{11.35}$$

A general impression of the nature and amplitude of signal-intensity fluctuations is given by Figs. 11.1 and 11.2, which show signal traces obtained in [751] and [766].

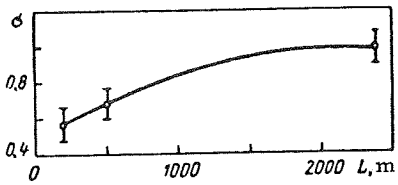

Figure 11.3. σ as a Function of Distance L Between Source and Receiver According to [755].

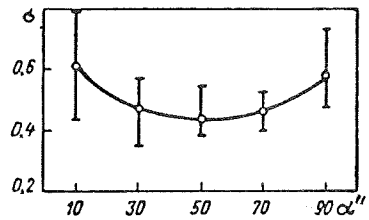

Figure 11.4. σ as a Function of Laser-Light Divergence Angle According to [755].

Figures 11.3-11.5 present results obtained in the author's laboratory for the quantity σ as a function of distance between the source and the receiver, the divergence angle of the laser beam, and the receiver aperture diameter [755]. In all figures, the curves are drawn through points corresponding to the arithmetic mean values of σ and the vertical line segments indicate the /432 ranges of σ in the individual measurements due both to measurement errors and changes in the meteorological conditions under which the measurements were made. All curves were obtained using a helium-neon laser radiating the wavelength λ = 6328 Å in continuous operation. The measurements were made at night.

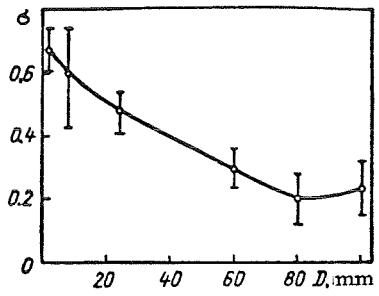

Figure 11.5. σ as a Function of Receiver Aperture Diameter According to [755].

The curve in Fig. 11.3 was plotted from measurements made on paths 0.1, 0.25, and 1.2 km long. A rotating plane mirror was placed at the end of each path. Thus, the light beam travelled distances of 0.2, 0.5, and 2.4 km in the measurements. The beam diameter at the exit from the collimating system was 14.4 cm, and its divergence angle was 10" for the distances L = 0.2 and 0.5 km and 17" for the 2.4-km distance. The receiving-aperture diameter was 4 mm for L = 0.2 and 0.5 km and 14 mm for L = = 2.4 km. As we see from the figure, σ changes by a factor of about 1.5 in the range of distances studied. The lack of distances between 0.5 and 2.4 km precludes a definite answer to the question as to saturation in the dependence of σ on L. We note that a dependence of σ on L sharper than that shown in Fig. 11.3 was observed in [751]. Saturation of σ was observed at a distance of 0.55 km in Buck's study [766].

In the measurements to determine σ as a function of beam angular divergence, the latter was varied from 10" to 90" with a beam diameter of 12.5 cm at the exit from the collimating system, a 500-meter measuring distance, and a receiver entrance aperture diameter of 1.6 mm. The curve in Fig. 11.4 shows that as the angular divergence α of the beam increases from 10" to 50", the value of σ decreases; it increases with further increase in α. /433 /434

In the measurements of σ as a function of receiving-system aperture diameter D (see Fig. 11.5), the diameters chosen were 0.2, 0.8, 2.4, 6.0, 8.0, and 10.0 cm, the distance L = 0.5 km, the diameter of the beam at the collimating-system exit was 12.5 cm, and the angular divergence was 70". As D increased from 0.2 to 8.0 cm, σ decreased to approximately one-third; at D = 10 cm, the measured value was found to be slightly larger than at D = 8 cm.

Fried [768] made detailed studies of the intensity fluctuations of the radiation from a 0.63-μ gas laser (beam diameter 3.5 mm at 0.7 level) as functions of the receiving-aperture diameter using a measurement path 8 km long. The results of the measurements indicate a smooth decrease of the variance σ^2 as the receiving-aperture diameter increases from 1.0 to 10 cm. A further increase in the diameter to 1 meter has practically no effect on σ^2. A logarithmically normal intensity distribution was observed for all receiving-aperture diameters. Fried's calculations [854], which were based on the formulas of the existing theory [731], gave results for the variance of the intensity fluctuations at various receiving apertures that contradicted the data from his own experiment with large receiving aperture. The hypothesis was

therefore advanced in [768] that there are two independent effects that determine the variance of the beam-intensity fluctuations in propagation in a turbulent atmosphere. One of the effects is responsible for the normal intensity distiibution at large apertures, and the other gives rise to a logarithmically normal distribution. However, the latter effect is dominant.

We note that disagreement between the theory of weak fluctuations and experiment was also observed in experimental studies made in the author's laboratory [754] with large receiving apertures. The measurements were made with a 70-cm receiving aperture. The diameter of the light beam at the exit and its divergence were 25 cm and 30', respectively. The variance of the fluctuations in these measurements was found to be larger than predicted by theory, and the intensity distribution conformed to the logarithmically normal law. Further, no dependence of the fluctuation variance on /435 the wavelength of the radiation was discerned within the limits of measurement error.

In [766], measurements with a large receiving-aperture diameter, in which the entire beam was intercepted by the receiving system, yielded values of σ smaller than 0.02, and the signal could have been regarded as practically stable and time-independent. This circumstance indicated smallness of the signal fluctuations due to the corresponding variations of molecular absorption and aerosol scattering in the course of the measurements.

The authors of [767] and [755] investigated the intensity distribution of laser beams of wavelength 6328 Å propagating over various distances in the atmosphere. In the first study cited, the measurements were made over distances of 4.5 and 14.5 km with a beam 0.35 cm in diameter where it entered the atmosphere. The beam used in [755] had an initial diameter of 1.4 cm and travelled distances of 0.2, 0.5, 2.4, and 7.0 km. Sixty-eight intensity distributions were processed in [767], and 28 in [755]; of these, 51 and 23, respectively, were found to be logarithmically normal.

Chu [855] investigated the intensity fluctuations of the light from three lasers of different wavelengths: 0.63, 3.51, and 10.6 μ. The measurements were made over a 2.6-km course with receiving-aperture values of 5, 12.5, and 15 cm, respectively, for the three wavelengths indicated. The frequency spectrum of the intensity fluctuations was investigated with a spectrum analyzer. The signal is observed to decrease exponentially with frequency up to 100 Hz. The decrease becomes slower at higher frequencies, possibly as a result of earth noise. The dependence of the intensity fluctuations on radiation wavelength was found to be slower than $\lambda^{-1/2}$, which follows from the theory for the frozen-in turbulence model. This result cannot be explained by the different receiving apertures in measurements with different wavelengths.

Höhn [769] investigated the intensity-fluctuation frequency spectra of a laser beam (λ = 6328 Å) with an initial diameter of 0.35 cm for distances of 4.5 and 14.5 km. It was found that the normalized intensity-fluctuation spectrum U(f), where f is the frequency, depends weakly on the receiving-aperture diameter, which was varied from 0.5 to 8.0 cm in the experiments. Data on the characteristic frequency of the fluctuations or the frequency corresponding to the maximum of the U(f) curve were also obtained in [769]. The dependence of this frequency on distance and the average-wind-speed component perpendicular to the propagation direction of the beam differs both from that predicted by theory and from the relation that follows from the empirical formula derived by V.I. Tatarskiy [463]. The experimental data of Ruznar [761] were found to agree satisfactorily with this relation. /436

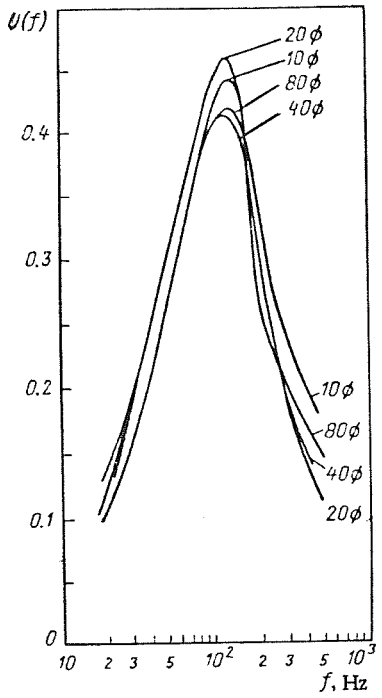

Figure 11.6. Spectra of the Function U(f) for Various Receiving Apertures According to One Series of Measurements in [769].

Figure 11.6 presents U(f) spectra for various receiving-aperture diameters, as obtained in one of the measurement series in [769]. The values of the frequency f_m corresponding to the maximum on the U(f) curve varied from measurement to measurement in the approximate range from 40 to 140 Hz. The half-width of the distribution varied from 4 to 18. This half-width is

$$\gamma_{1/2}=f_2/f_1, \tag{11.36}$$

where f_2 and f_1 are the frequencies that satisfy the condition

$$U(f_2)=U(f_1)=\frac{1}{2}U(f_m). \tag{11.37}$$

A study of the spatial structure of pulsed laser radiation propagating in a turbulent atmosphere was made in the author's laboratory [770]. The measurements were made with a ruby laser (wavelength 0.69 μ) operating in the free-generation mode (single pulses on the order of 0.5 msec in duration, power several hundred watts, beam divergence 6'). The structure of the laser radiation was investigated at distances of 0.25, 1.2, 3.5, and 10 km from the source. The corresponding patterns of this structure were photographed from screens set up at these distances. Use of neutral filters made it possible to obtain photographs of normal density. Sections /437

across the resulting images were photometered to obtain no fewer than 10 intensity readings in the region of the theoretical correlation radius, which was approximately equal to $\sqrt{\lambda L}$ [731]. Two to six sections were photometered along each frame and one section across it. The photometric sections were processed on an electronic computer, by means of which the correlation functions of the intensity fluctuations, the variance, and the mean intensity value were calculated.

TABLE 11.1. VALUES OF CORRELATION RADIUS ρ DETERMINED EXPERIMENTALLY AND FROM CALCULATION

Distance L, km	Experimental Values of ρ, cm			Calculated value of ρ, cm	Number of photometric sections
	Minimum	Maximum	Average		
0.25	4.7	17	9.1	1.3	37
1.2	4	12.8	10	2.9	23
3.5	3	14	9.5	4.9	15
10.0	—	—	8.1	8.3	52

Table 11.1 presents values of the correlation radius determined from reduction of the experimental data and from a calculation by the formula $\rho = \sqrt{\lambda L}$.

Analysis of the resulting experimental data from the standpoint of the intensity-distribution law indicated that there were no deviations from the normal distribution of the natural logarithm of intensity for distances of 0.25, 1.2, and 3.5 km. In this case, formula (11.35) can be used to determine σ^2 from the experimental data. Intensity distributions that did not follow the logarithmically normal law were observed in the measurements over a distance of 10 km. /438

When the logarithmically normal intensity distribution prevailed, the dependences of σ^2 on distance and the beam-divergence angle of the laser light were determined. It was found that σ^2 increases up to a distance L = 3.5 km and then falls off slowly. The curve of σ^2 as a function of beam divergence angle ϕ shows a minimum corresponding to a ϕ of approximately 50". We note that the value of the beam-divergence angle determined from the dimensions of the radiation spot and the distance in measurements made on short paths is taken as ϕ in this case.

Experimental data on the intensity fluctuations of narrow light beams were also obtained in [753, 758, 760, 762-765, 892].

The intensity of the fluctuations and their frequency spectrum in the radiation of a gas laser ($\lambda = 0.63\ \mu$) were investigated in [758] as functions of receiving-aperture diameter, which was varied from 3.5 to 50 cm. The polarization fluctuations of radiation from the same laser due to intensity fluctuations were studied in [765] over a distance of 5 miles in the ground layer of atmosphere. To explain the nature of the observed polarization fluctuations, it will be necessary to conduct careful additional studies capable of resolving the measured fluctuations with sufficient accuracy into the components due to atmospheric aerosols and turbulent inhomogeneities in the atmosphere.

The intensity fluctuations of a searchlight beam were investigated in [892] in the ground layer of the atmosphere at distances from 1 to 30 km. The distribution of the intensity-fluctuation logarithm was found to be approximately normal. Also investigated in [892] were the frequency spectrum of the intensity fluctuations and the percentage modulation of the radiation by the atmosphere at various receiving-aperture diameters from 13 to 4 cm. Percentage modulation was defined as the ratio of the average range of the signal fluctuations to the average signal value. It was found that the percentage modulation is inversely proportional to the receiving-aperture diameter. Saturation was observed in the relationship at small values of the latter. /439

2. Variation of beam diameter with distance. Turbulent motions in the atmosphere cause broadening of the beam over and above that due to geometry and diffraction. Exploration of this problem has thus far been totally inadequate.

Certain data that permit inferences as to the possible broadening of laser beams under various conditions in the atmosphere were obtained in [757, 766, 770]. In [757], 8" and 13" increases in beam divergence were observed in measurements over distances of 15 and 145 km, respectively. In [766], the results of measurements of the beam diameter D at various distances up to 145 km with an initial diameter of 10 cm in a weakly turbid nighttime atmosphere were processed to obtain the following empirical formula for D:

$$D = \alpha L^{\beta}, \tag{11.38}$$

where $\alpha = 4.5 \cdot 10^{-6}$ and $\beta = 1.2$, D was measured in centimeters and L in meters. It is noted in [766] that under hazy conditions and during the daytime, the beam diameter may increase to several times the value obtained from (11.38).

The diameter of a focused beam was also investigated in [766] as a function of initial diameter. In propagation in a vacuum, these quantities are inversely proportional. Measurements in a

turbulent atmosphere showed that a decrease in the diameter of the focused beam from the source aperture diameter occurs only until the latter reaches a value of 11 cm. Focusing does not improve on a further increase of the initial beam diameter. Figure 11.7 shows an experimental curve of this type (upper curve, on which the vertical-segment lengths characterize the scatter of the experimental data). The lower curve in this figure represents the case of propagation of a focused beam in a vacuum. The slight upturn of the upper curve at source aperture diameters greater than 11 cm is explained in [766] as due to aberrations of the optical system.

The radiation spot from a pulsed ruby laser was found in [770] to have varying linear dimensions in measurements made over the same distance. Thus, the linear dimensions of the beam cross section varied approximately from 0.7 to 2 m at a distance of 10 km in pulses that followed one another at 45-second intervals.

/440

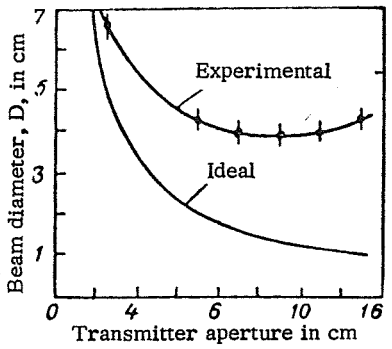

Figure 11.7. Diameter of Focused Beam as a Function of its Initial Diameter According to [766].

3. Fluctuations of the angle of arrival of a spatially limited radiation beam. Fluctuations of the arrival angle of the radiation with which the image is formed in the focal plane of a lens causes the image to shift and blur. Image shifting takes place when the dimensions of the inhomogeneities due to turbulent motion in the atmosphere are greater than the diameter of the lens. Small-scale inhomogeneities shift specific elements of the radiation beam and cause "blurring" of the image.

The author's laboratory has made experimental studies of the angle-of-arrival fluctuations of the radiation from a gas laser in propagation in the ground layer of the atmosphere [756]. The measuements were made over a distance of 1.2 km with a helium-neon laser (wavelength 6328 Å) operated in axial-mode continuous generation and a thermal source whose incandescent body was appropriately stopped down. The initial diameter d_0 of the beam and its divergence ϕ were 2.5 mm and 110". /441

When telescopes with lens diameters d = 19, 27, and 38 mm were used, the beam divergence angle was near the diffraction limit at 20"-70". The receiving-lens diameters were 2.4, 4.8, 8.0, and 10.0 cm. The source images were registered on moving high-speed photographic film. The time to obtain random fluctuations of image position on the film was 20-30 seconds. A total of 96 arrival-angle records was obtained.

The measure used for source shake was

$$\sigma_\varphi = \sqrt{\frac{\sum_i \Delta_i^2}{n}}, \tag{11.39}$$

where Δ_i is the arrival-angle deviation measured at 0.2-sec intervals, n is the number of measurements of Δ_i, and the summation is extended over all deviations for the particular realization.

The variance of the arrival-angle fluctuations was calculated by the formula

$$\sigma_\varphi^2 = \frac{\sum_i x_i^2 n_i}{n}, \tag{11.40}$$

where x_i is the deviation of the image trace from its average value. The average value of σ_ϕ^2 was determined as the arithmetic mean over all realizations for each beam-diameter value and each entrance aperture. The error in the determination of σ_ϕ^2 varied in the approximate range from 10 to 20%.

The distribution functions of the arrival-angle fluctuations were determined. It was found that of 64 distributions, 62 were normal with σ_ϕ^2 ranging from 0.8 to 10.8 square seconds of arc.

For an uncollimated beam, σ_ϕ^2 is given by the following relation as a function of receiving-lens diameter D_{rec} in centimeters:

$$\sigma_\varphi^2 \sim (D_{rec})^{-1/3}. \tag{11.41}$$

The numerical values of σ_ϕ^2 vary widely for each D_{rec}, depending on the meteorological conditions under which the measurements were made.

When the initial beam diameter increases from 2.5 to 27 mm, /442
the variance of the arrival angles increases sharply, apparently because of a spherical-to-plane wave transition. A further increase in beam diameter results in a slight decrease in the variance of the arrival-angle fluctuations.

In addition to the high-frequency arrival-angle fluctuations, a slow displacement of the angles is also observed when laser

radiation beams propagate in the atmosphere.

Buck [766] observed deviations of the beam from a $\lambda = 6328$ Å laser as a whole, ranging up to 4 meters over a 10-km distance in 30 minutes.

4. Investigations of the coherence of laser radiation propagating in a turbulent atmosphere. The distortion of the phase front of the wave and the redistribution of intensity in the cross section of the light beam due to turbulent motions in the atmosphere are detrimental to the spatial and temporal coherence of laser radiation. This has substantial influence on the efficiency of communications systems based on optical heterodyning.

The quantitative measure of the coherence of radiation is the coherence function, whose normalized value is the same as the optical transmission function characterizing the resolution of optical receivers used to register the images of objects through the atmosphere [750, 856]. Measurement of the coherence function may help solve an inverse problem — determination of the atmosphere's turbulence parameters on the basis of data from such measurements. Thus, study of the coherence function of radiation propagating in the atmosphere is of great applied importance.

Experimental study of the coherence of radiation propagating in the atmosphere consists of analyzing the interference pattern formed on superposition of the fields of the beam that has passed through the layer of atmosphere and a reference beam. Long-base interferometric studies [771-773] used photography to register interference fringes of finite width. The possibility of observing the interference fringes with high clarity was pointed out in these studies. V.I. Vaytsel' and S.S. Khmelevtsov [774] developed an interference method that can be used to determine the characteristics of atmospheric turbulence from measurements of the coherence of optical radiation. Data on the coefficient C_n were obtained with this method. The same authors studied the influence of atmospheric turbulence on the resolution of interference receivers [775] and the spectrum of the signal from the photomultiplier in an optical-heterodyne setup [776]. V.V. Pokasov and S.S. Khmelevtsov [777,778] studied the spatial coherence of laser radiation and the effects of atmospheric turbulence upon it. The measurements were made in the ground layer of atmosphere on paths 100 and 200 meters long. Two methods, the fundamentals of which were developed in [863, 856, 864, and 750], were used. The results of studies of the coherence function of the radiation as it depends on the temperature gradient were found to agree satisfactorily with theory. The dependence of the coherence function on distance between points in the beam cross section is inconsistent with the theoretical predictions; the authors explain this as due to the limitations of the geometrical-optical approximation used in the theory.

/443

Values of the structure constant C_n of the index of refraction were obtained in [777] on the basis of experimental coherence-function data. The values of C_n were determined simultaneously from measurements of the meteorological elements at heights of 20 cm and 2.0 m. Comparison of the C_n values obtained by the two methods indicated that they agree satisfactorily at temperature gradients $\Delta T \leq 0.6°C$ (the case with $\Delta T = 0$, in which $C_n = 0$ according to the meteorological data and $C_n = 0.008 \cdot 10^{-6}$ $cm^{-1/3}$ according to the second method, is an exception). For $\Delta T > 0.6°C$ the values of C_n determined from measured results for the coherence function and from meteorological data differ increasingly as ΔT increases. Thus, at $\Delta T = 1.0°C$, the difference is 100%, and at $\Delta T = 2.2°C$, 200%. In all cases, the C_n determined from the measured meteorological elements was found to be smaller than that obtained from the coherence-function measurements. This means that for $\Delta T > 0.6°C$, the spatial coherence of the radiation decreases much more rapidly than would follow from the theory. It should be noted that the wind speed did not exceed 0.2-0.3 m/sec in any of the measurements.

APPENDIX I

1. ARDC Atmospheric Model for Heights from 0 to 30 km [3]

Height, km	Temperature, °K	Pressure, mbar	Density, g-cm^{-3}	Number of molecules per unit volume, cm^{-3}	Height of homogeneous atmosphere, km
0	288,16	$1,01325 \cdot 10^{3}$	$1,2250 \cdot 10^{-3}$	$2,5476 \cdot 10^{19}$	8,4344
1	281,66	$8,9876 \cdot 10^{2}$	1,1117	2,3118	8,2468
2	275,16	7,9501	1,0066	2,0933	8,0591
3	268,67	7,0121	$9,0926 \cdot 10^{-4}$	1,8909	7,8713
4	262,18	6,1660	8,1935	1,7039	7,6835
5	255,69	5,4048	7,3643	1,5315	7,4957
6	249,20	4,7217	6,6011	1,3728	7,3077
7	242,71	4,1105	5,9002	1,2270	7,1198
8	236,23	3,5651	5,2578	1,0934	6,9317
9	229,74	3,0800	4,6706	$9,7130 \cdot 10^{18}$	6,7436
10	223,26	2,6500	4,1351	8,5993	6,5554
11	216,78	2,2700	3,6480	7,5864	6,3672
12	216,66	1,9399	3,1194	6,4870	6,3656
13	216,66	1,6579	2,6659	5,5441	6,3676
14	216,66	1,4170	2,2785	4,7385	6,3696
15	216,66	1,2112	1,9475	4,0501	6,3716
16	216,66	1,0353	1,6647	3,4619	6,3736
17	216,66	8,8496·10	1,4230	2,9593	6,3756
18	216,66	7,5652	1,2165	2,5298	6,3776
19	216,66	6,4674	1,0399	2,1627	6,3796
20	216,66	5,5293	$8,8909 \cdot 10^{-5}$	1,8490	6,3816
21	216,66	4,7274	7,6015	1,5808	6,3836
22	216,66	4,0420	6,4995	1,3516	6,3856
23	216,66	3,4562	5,5575	1,1557	6,3876
24	216,66	2,9554	4,7522	$9,8828 \cdot 10^{17}$	6,3896
25	216,66	2,5273	4,0639	8,4513	6,3916
26	219,34	2,1632	3,4359	7,1453	6,4728
28	225,29	1,5949	2,4663	5,1290	6,6525
30	231,24	1,1855	1,7861	3,7144	6,8323

Note: Commas represent decimal points.

2. Heights of Isobaric Surfaces in the Layer from 25 to 100 km, in Geopotential Kilometers [3]

Level in atmosphere, mbar	Latitude								
	0°	10°	20°	30°	4 °	50°	60°	70°	80°
20	26,5	26,5	26,6	26,9	27,1	27,3	27,4	27,5	27,6
16	27,9	28,0	28,1	28,4	28,6	28,8	28,9	29,0	29,1
12	29,8	29,9	30,0	30,3	30,6	30,8	30,9	31,0	31,1
10	31,1	31,1	31,2	31,6	31,8	32,1	32,2	32,3	32,4
8	32,6	32,6	32,8	33,1	33,4	33,7	33,8	33,9	34,0
6	34,6	34,6	34,8	35,2	35,5	35,7	35,9	36,0	36,1
4	37,5	37,5	37,8	38,2	38,5	38,8	38,9	39,0	39,1
3	39,7	39,7	40,0	40,4	40,7	41,0	41,1	41,2	41,2
2,5	41,1	41,1	41,4	41,8	42,2	42,5	42,5	42,6	42,6
2,0	42,8	42,9	43,2	43,6	44,0	44,2	44,3	44,4	44,3
1,6	44,6	44,6	44,9	45,4	45,8	46,1	46,1	46,1	46,0
1,2	47,0	47,0	47,3	47,7	48,2	48,5	48,5	48,5	48,4

(Cont'd.)

Level in atmosphere, mbar	Latitude								
	0°	10°	20°	30°	40°	50°	60°	70°	80°
1,0	48,4	48,5	48,8	49,2	49,7	50,1	50,1	50,0	49,9
0,8	50,3	50,3	50,6	51,1	51,6	52,0	52,0	51,9	51,8
0,6	52,7	52,7	53,0	53,4	54,0	54,4	54,5	54,4	54,2
0,4	—	56,0	56,2	56,6	57,2	57,7	57,8	57,8	57,6
0,3	—	—	58,4	58,8	59,4	60,0	60,1	60,1	59,9
0,2	—	—	—	61,8	62,3	63,0	63,2	—	—
0,15	—	—	—	63,9	64,4	65,1	65,4	—	—
0,10	—	—	—	66,7	67,1	67,8	68,2	—	—
0,08	—	—	—	68,3	68,6	69,3	70,0	—	—
0,04	—	—	—	72,7	73,0	73,6	74,0	—	—
0,02	—	—	—	77,0	77,1	77,6	78,0	—	—
0,01	—	—	—	81,1	81,1	81,4	81,8	—	—
0,004	—	—	—	86,6	86,4	86,5	86,7	—	—
0,002	—	—	—	90,9	90,6	90,6	90,5	—	—
0,001	—	—	—	95,4	95,1	94,9	94,7	—	—
0,0005	—	—	—	100,2	99,8	99,5	99,2	—	—

Level in atmosphere, mbar	Latitude								
	0°	10°	20°	30°	40°	50°	60°	70°	80°
20	26,1	26,1	26,2	26,2	26,2	26,1	25,7	25,2	25,0
16	27,5	27,5	27,6	27,6	27,6	27,5	27,1	26,6	26,3
12	29,4	29,4	29,5	29,5	29,4	29,3	28,8	28,3	28,0
10	30,6	30,6	30,7	30,6	30,6	30,4	30,0	29,4	29,0
8	32,1	32,1	32,2	32,1	32,0	31,8	31,3	30,7	30,3
6	34,1	34,0	34,1	34,0	33,9	33,7	33,1	32,4	32,0
4	37,0	37,0	37,0	36,8	36,6	36,3	35,7	34,9	34,5
3	39,1	39,0	39,0	38,9	38,7	38,2	37,6	36,7	36,2
2,5	40,4	40,4	40,4	40,2	40,0	39,5	38,8	37,9	37,6
2,0	42,1	42,1	42,1	41,9	41,6	41,1	40,3	39,3	38,8
1,6	43,9	43,8	43,8	43,6	43,2	42,6	41,8	40,8	40,3
1,2	46,2	46,1	46,1	45,8	45,4	44,7	43,8	42,8	42,2
1,0	47,6	47,6	47,5	47,2	46,8	46,1	45,1	44,0	43,5
0,8	49,5	49,4	49,3	49,0	48,5	47,7	46,7	45,6	45,0
0,6	51,8	51,8	51,6	51,3	50,7	49,8	48,7	47,6	47,0
0,4	55,2	55,1	55,0	54,5	53,9	52,9	51,7	50,4	49,7
0,3	—	57,4	57,2	56,8	56,1	55,1	53,8	52,5	51,8
0.2	—	60,5	60,4	60,0	59,3	58,3	56,9	55,5	54,8
0,15	—	—	—	62,1	61,4	60,4	59,1	—	—
0,10	—	—	—	65,0	64,4	63,6	62,2	—	—
0,08	—	—	—	66,5	66,0	65,2	63,9	—	—
0,04	—	—	—	71,1	70,6	70,0	68,9	—	—
0,02	—	—	—	75,4	75,0	74,4	73,5	—	—
0,01	—	—	—	79,6	79,2	78,6	77,8	—	—
0,004	—	—	—	85,0	84,7	84,3	83,7	—	—
0.002	—	—	—	89,3	89,1	88,9	88,4	—	—
0,001	—	—	—	93,7	93,7	93,6	93,3	—	—
0,0005	—	—	—	98,4	98,6	98,6	98,3	—	—

Note: Commas represent decimal points.

3. Temperature in the Layer of Atmosphere from 25 to 100 km, °K [3]

Summer

Level in atmosphere, mbar	Latitude								
	0°	10°	20°	30°	40°	50°	60°	70°	80°
20	220	220	222	224	226	230	233	235	236
16	223	223	225	227	229	232	234	236	237
12	227	227	229	231	233	236	237	239	239
10	230	230	232	234	237	239	240	242	242
8	234	234	237	239	242	244	244	245	244
6	240	240	243	246	249	251	250	250	248
4	251	251	254	257	261	261	259	257	254
3	260	260	263	266	269	267	264	261	257
2.5	265	265	267	270	273	271	267	264	260
2.0	271	271	272	274	277	276	273	268	265
1.6	274	274	276	277	281	282	279	274	271
1.2	278	278	279	279	285	290	289	284	279
1.0	279	279	280	279	285	293	293	289	283
0.8	280	280	280	278	283	291	294	292	288
0.6	280	279	277	274	277	285	290	291	290
0.4	—	274	270	265	265	272	276	278	280
0.3	—	—	262	259	254	261	267	269	270
0.2	—	—	—	248	244	247	254	—	—
0.15	—	—	—	242	237	238	245	—	—
0.10	—	—	—	233	227	226	232	—	—
0.08	—	—	—	228	222	220	226	—	—
0.04	—	—	—	214	208	205	203	—	—
0.02	—	—	—	202	197	189	186	—	—
0.01	—	—	—	200	194	186	180	—	—
0.004	—	—	—	208	202	194	185	—	—
0.002	—	—	—	218	212	204	195	—	—
0.001	—	—	—	229	226	217	210	—	—
0.0005	—	—	—	241	243	238	234	—	—

Winter

Level in atmosphere, mbar	Latitude								
	0°	10°	20°	30°	40°	50°	60°	70°	80°
20	214	213	213	214	214	214	209	204	201
16	218	217	216	216	214	214	208	203	200
12	222	221	220	218	216	213	208	203	199
10	226	225	223	220	217	213	208	203	199
8	230	229	228	224	220	214	209	203	199
6	237	236	234	230	225	218	212	206	202
4	246	245	243	239	234	226	219	212	208
3	253	253	251	247	240	232	224	217	213
2.5	257	257	256	252	245	236	228	220	217
2.0	263	262	260	256	249	241	233	225	221
1.6	268	267	264	260	253	244	236	229	225
1.2	274	273	269	265	257	248	238	232	229
1.0	277	276	272	267	260	250	239	233	231
0.8	279	279	274	270	262	252	241	235	232
0.6	281	280	277	273	265	255	245	237	234
0.4	276	276	275	274	268	259	250	243	239
0.3	—	270	269	269	267	262	255	247	244
0.2	—	257	256	257	259	263	259	254	251
0.15	—	—	—	249	253	261	262	—	—
0.10	—	—	—	236	243	254	262	—	—
0.08	—	—	—	232	237	247	258	—	—
0.04	—	—	—	218	220	224	229	—	—
0.02	—	—	—	207	209	211	216	—	—
0.01	—	—	—	200	204	207	214	—	—

(Cont'd.)

Level in atmosphere, mbar	Latitude								
	0°	10°	20°	30°	40°	50°	60°	70°	80°
0.004	—	—	—	205	210	218	224	—	—
0.002	—	—	—	214	220	228	236	—	—
0.001	—	—	—	224	233	239	244	—	—
0.0005	—	—	—	236	245	250	250	—	—

APPENDIX 2

Values of the Absorption Coefficient α, Absorption Index κ, and Refractive Index n of Pure Water According to Data of the Author and Co-Workers for Various Wavelengths in the Range from 0.55 to 25.3 μ

No.	ν, $см^{-1}$	λ, μ	α, $см^{-1}$	κ	n
1	395	25,31	1130	0,229	1,700
2	405	24,65	1190	0,234	1,702
3	415	24,09	1230	0,236	1,709
4	425	23,52	1210	0,227	1,738
5	435	22,98	1300	0,238	1,784
6	445	22,47	1790	0,320	1,833
7	455	21,97	2300	0,402	1,802
8	465	21,50	2590	0,444	1,763
9	475	21,05	2800	0,470	1,722
10	485	20,61	3010	0,495	1,695
11	495	20,21	3180	0,511	1,665
12	505	19,80	3370	0,531	1,637
13	515	19,41	3480	0,537	1,601
14	525	19,04	3540	0,537	1,575
15	535	18,69	3710	0,552	1,544
16	545	18,34	3780	0,552	1,516
17	555	18,01	3870	0,553	1,496
18	565	17,69	3980	0,560	1,459
19	575	17,39	4070	0,563	1,421
20	585	17,09	4100	0,557	1,394
21	595	16,80	4110	0,550	1,367
22	605	16,52	4150	0,546	1,329
23	615	16,26	4150	0,536	1,324
24	625	16,00	4130	0,526	1,292
25	635	15,74	4020	0,504	1,280
26	645	15,50	3990	0,492	1,248
27	655	15,26	3970	0,483	1,242
28	665	15,03	3960	0,474	1,222
29	675	14,81	3850	0,454	1,192
30	685	14,59	3680	0,427	1,177
31	695	14,38	3520	0,403	1,175
32	705	14,18	3380	0,382	1,194
33	715	13,98	3520	0,392	1,192
34	725	13,79	3600	0,396	1,166

Note: Commas represent decimal points.

(Cont'd.)

No.	ν, см⁻¹	λ, μ	α, см⁻¹	κ	n
35	735	13,61	3510	0,380	1,147
36	745	13,42	3350	0,358	1,126
37	755	13,24	3220	0,339	1,115
38	765	13,07	3100	0,323	1,107
39	775	12,91	2940	0,302	1,102
40	785	12,73	2750	0,279	1,097
41	795	12,57	2620	0,262	1,096
42	805	12,42	2470	0,245	1,095
43	815	12,26	2360	0,230	1,096
44	825	12,12	2270	0,219	1,100
45	835	11,97	2170	0,207	1,102
46	845	11,83	2020	0,190	1,103
47	855	11,69	1960	0,182	1,107
48	865	11,56	1930	0,177	1,113
49	875	11,42	1690	0,154	1,110
50	885	11,29	1520	0,137	1,112
51	896	11,16	880	0,122	1,118
52	946	10,57	800	0,067	1,144
53	996	10,04	580	0,047	1,105
54	1047	9,55	550	0,042	1,180
55	1098	9,11	530	0,038	1,203
56	1148	8,71	530	0,037	1,228
57	1198	8,35	540	0,036	1,250
58	1249	8,01	540	0,034	1,262
59	1300	7,69	560	0,034	1,277
60	1350	7,41	560	0,033	1,292
61	1401	7,14	560	0,032	1,303
62	1451	6,89	600	0,033	1,316
63	1502	6,66	610	0,032	1,301
64	1553	6,44	720	0,037	1,297
65	1595	6,27	1130	0,056	1,379
66	1611	6,21	1140	0,056	1,401
67	1626	6,15	2180	0,107	1,371
68	1641	6,09	2940	0,143	1,342
69	1656	6,03	2760	0,133	1,275
70	1671	5,98	2390	0,114	1,239
71	1686	5,93	1730	$0,815 \cdot 10^{-1}$	1,224
72	1701	5,87	1090	$0,511 \cdot 10^{-1}$	1,202
73	1716	5,83	550	$0,211 \cdot 10^{-1}$	1,208
74	1731	5,77	445	$0,205 \cdot 10^{-1}$	1,222
75	1746	5,72	467	$0,213 \cdot 10^{-1}$	1,231
76	1761	5,67	650	$0,294 \cdot 10^{-1}$	1,261
77	1797	5,57	271	$0,125 \cdot 10^{-1}$	1,275
78	1848	5,41	232	$0,105 \cdot 10^{-1}$	1,287
79	1898	5,27	232	$0,103 \cdot 10^{-1}$	1,309
80	1949	5,13	249	$0,107 \cdot 10^{-1}$	1,312
81	1999	5,00	309	$0,123 \cdot 10^{-1}$	1,317
82	2046	4,89	362	$0,136 \cdot 10^{-1}$	1,321
83	2096	4,77	386	$0,142 \cdot 10^{-1}$	1,323
84	2146	4,66	386	$0,138 \cdot 10^{-1}$	1,327
85	2196	4,55	348	$0,122 \cdot 10^{-1}$	1,329
86	2246	4,45	296	$0,100 \cdot 10^{-1}$	1,329
87	2296	4,36	252	$0,083 \cdot 10^{-1}$	1,329
88	2396	4,17	181	$0,559 \cdot 10^{-2}$	1,335
89	2446	4,09	160	$0,521 \cdot 10^{-2}$	1,338
90	2496	4,01	134	$0,428 \cdot 10^{-2}$	1,343
91	2546	3,93	127	$0,397 \cdot 10^{-2}$	1,347
92	2596	3,85	116	$0,359 \cdot 10^{-2}$	1,357
93	2646	3,78	122	$0,369 \cdot 10^{-2}$	1,364
94	2696	3,71	134	$0,398 \cdot 10^{-2}$	1,370
95	2746	3,64	166	$0,484 \cdot 10^{-2}$	1,376
96	2796	3,58	218	$0,621 \cdot 10^{-2}$	1,394

(Cont'd.)

No.	ν, $см^{-1}$	λ, μ	α, $см^{-1}$	x	n
97	2846	3,51	290	$0,813 \cdot 10^{-2}$	1,398
98	2896	3,45	418	$0,115 \cdot 10^{-1}$	1,416
99	2946	3,39	630	$0,170 \cdot 10^{-1}$	1,478
100	2996	3,34	900	$0,240 \cdot 10^{-1}$	1,458
101	3006	3,33	313	$0,828 \cdot 10^{-2}$	1,460
102	3021	3,31	417	$0,111 \cdot 10^{-1}$	1,468
103	3036	3,29	680	$0,179 \cdot 10^{-1}$	1,467
104	3051	3,28	1300	$0,338 \cdot 10^{-1}$	1,458
105	3066	3,26	990	$0,257 \cdot 10^{-1}$	1,452
106	3081	3,25	1010	$0,261 \cdot 10^{-1}$	1,463
107	3096	3,23	1180	$0,303 \cdot 10^{-1}$	1,465
108	3111	3,71	1410	$0\ 361 \cdot 10^{-1}$	1,478
109	3126	3,20	1740	$0,443 \cdot 10^{-1}$	1,489
110	3141	3,18	2100	$0,532 \cdot 10^{-1}$	1,492
111	3156	3,17	3060	$0.637 \cdot 10^{-1}$	1,495
112	3171	3,15	3070	$0,772 \cdot 10^{-1}$	1,504
113	3186	3,16	3690	$0,923 \cdot 10^{-1}$	1,509
114	3201	3,12	4420	0,110	1,513
115	3216	3,11	5320	0,132	1,514
116	3231	3,10	6660	0,164	1,515
117	3246	3,08	7610	0,187	1,489
118	3261	3,07	6910	0,171	1,467
119	3276	3,05	7930	0,193	1,494
120	3291	3,03	9250	0,224	1,469
121	3306	3,02	9950	0,240	1,451
122	3321	3,01	10390	0,249	1,430
123	3336	2,99	10830	0,259	1,414
124	3351	2,98	11120	0,264	1,396
125	3366	2,97	11280	0,266	1,374
126	3381	2,96	11350	0,267	1,353
127	3396	2,94	11660	0,273	1,337
128	3411	2,93	11750	0,274	1,314
129	3426	2,92	11880	0,276	1,288
130	3441	2,91	12230	0,283	1,260
131	3456	2,89	11670	0,269	1,232
132	3471	2,88	11080	0,254	1,210
133	3486	2,87	10770	0,237	1,190
134	3501	2,86	9940	0,226	1,175
135	3516	2.84	9310	0,210	1,147
136	3531	2.83	8610	0,194	1,131
137	3546	2,82	7530	0,169	1,110
138	3561	2,81	5940	0,133	1,094
139	3576	2,79	4890	0,109	1,088
140	3591	2,78	4480	$0,994 \cdot 10^{-1}$	1,100
141	3606	2,77	3600	$0,794 \cdot 10^{-1}$	1,108
142	3621	2,76	2950	$0,648 \cdot 10^{-1}$	1,112
143	3636	2,75	2360	$0,517 \cdot 10^{-1}$	1,133
144	3651	2,74	1780	$0,384 \cdot 10^{-1}$	1,138
145	3666	2,73	1050	$0,227 \cdot 10^{-1}$	1,141
146	3696	2,71	730	$0,157 \cdot 10^{-1}$	1,181
147	3746	2,67	247	$0,526 \cdot 10^{-2}$	1,221
148	3796	2,63	183	$0,386 \cdot 10^{-2}$	1,234
149	3846	2,60	146	$0,304 \cdot 10^{-2}$	1,245
150	3896	2,57	128	$0,263 \cdot 10^{-2}$	1,255
151	3946	2,53	119	$0,240 \cdot 10^{-2}$	1,261
152	3996	2,50	103	$0,206 \cdot 10^{-2}$	1,264
153	4046	2,47	88,9	$0,175 \cdot 10^{-2}$	1
154	4096	2,44	63,8	$0,124 \cdot 10^{-2}$	1,269
155	4146	2,41	56,3	$0,108 \cdot 10^{-2}$	
156	4196	2,38	48,6	$0,921 \cdot 10^{-3}$	
157	4246	2,36	40,4	$0,757 \cdot 10^{-3}$	1,274
158	4296	2,33	34,0	$0,631 \cdot 10^{-3}$	
159	4346	2,30	29,9	$0,548 \cdot 10^{-3}$	

(Cont'd.)

No.	ν, см⁻¹	λ, μ	α, см⁻¹	κ	n
160	4396	2,27	27,2	$0,492 \cdot 10^{-3}$	1,286
161	4446	2,25	25,3	$0,453 \cdot 10^{-3}$	
162	4496	2,22	24,5	$0,424 \cdot 10^{-3}$	1,289
163	4546	2,19	24,9	$0,436 \cdot 10^{-3}$	
164	4596	2,18	25,9	$0,449 \cdot 10^{-3}$	1,294
165	4646	2,15	27,5	$0,471 \cdot 10^{-3}$	
166	4696	2,13	29,6	$0,502 \cdot 10^{-3}$	1,297
167	4746	2,11	32,7	$0,548 \cdot 10^{-3}$	
168	4780	2,09	37,0	$0,616 \cdot 10^{-3}$	1,300
169	4830	2,07	40,6	$0,669 \cdot 10^{-3}$	
170	4878	2,05	45,5	$0,743 \cdot 10^{-3}$	1,304
171	4938	2,03	48,3	$0,778 \cdot 10^{-3}$	
172	4987	2,01	55,8	$0,891 \cdot 10^{-3}$	1,304
173	5040	1,98	70,3	$0,111 \cdot 10^{-2}$	
174	5105	1,96	85,2	$0,133 \cdot 10^{-2}$	1,306
175	5165	1,94	106	$0,163 \cdot 10^{-2}$	
176	5208	1,92	123	$0,187 \cdot 10^{-2}$	1,305
177	5277	1,89	119	$0,179 \cdot 10^{-2}$	
178	5333	1,88	68,4	$0,102 \cdot 10^{-2}$	1,303
179	5376	1,86	25,0	$0,371 \cdot 10^{-3}$	
180	5449	1,84	15,5	$0,227 \cdot 10^{-3}$	1,309
181	5602	1,78	13,6	$0,193 \cdot 10^{-3}$	
182	5635	1,77	12,6	$0,177 \cdot 10^{-3}$	
183	5710	1,75	12,4	$0,173 \cdot 10^{-3}$	1,310
184	5880	1,70	9,71	$0,131 \cdot 10^{-3}$	
185	6030	1,66	9,71	$0,128 \cdot 10^{-3}$	1,311
186	6200	1,61	9,71	$0,125 \cdot 10^{-3}$	
187	6370	1,57	10,7	$0,133 \cdot 10^{-3}$	1,312
188	6470	1,55	14,6	$0,179 \cdot 10^{-3}$	
189	6570	1,52	17,6	$0,213 \cdot 10^{-3}$	1,313
190	6660	1,50	21,8	$0,253 \cdot 10^{-3}$	
191	6770	1,48	28,5	$0,335 \cdot 10^{-3}$	1,313
192	6690	1,43	30,9	$0,352 \cdot 10^{-3}$	1,314
193	7100	1,41	24,0	$0,269 \cdot 10^{-3}$	
194	7210	1,39	14,5	$0,160 \cdot 10^{-3}$	1,314
195	7275	1,37	6,91	$0,756 \cdot 10^{-4}$	
196	7420	1,35	3,33	$0,347 \cdot 10^{-4}$	1,315
197	7540	1,33	2,21	$0,233 \cdot 10^{-4}$	
198	7670	1,30	1,62	$0,169 \cdot 10^{-4}$	1,315
199	7800	1,28	1,33	$0,136 \cdot 10^{-4}$	
200	7920	1,26	1,33	$0,133 \cdot 10^{-4}$	1,316
201	8060	1,24	1,38	$0,136 \cdot 10^{-4}$	
202	8180	1,22	1,44	$0,141 \cdot 10^{-4}$	1,316
203	8320	1,20	1,49	$0,143 \cdot 10^{-4}$	
204	8460	1,18	1,48	$0,139 \cdot 10^{-4}$	1,317
205	8600	1,16	1,41	$0,131 \cdot 10^{-4}$	
206	8760	1,14	1,13	$0,102 \cdot 10^{-4}$	1,317
207	8900	1,12	0,423	$0,378 \cdot 10^{-5}$	
208	9040	1,11	0,242	$0,212 \cdot 10^{-5}$	1,318
209	9190	1,09	0,190	$0,176 \cdot 10^{-5}$	
210	9350	1,07	0,161	$0,137 \cdot 10^{-5}$	1,319
211	9500	1,05	0,187	$0,156 \cdot 10^{-5}$	
212	9660	1,04	0,243	$0,199 \cdot 10^{-5}$	1,320
213	9800	1,02	0,321	$0,260 \cdot 10^{-5}$	
214	9950	1,01	0,402	$0,322 \cdot 10^{-5}$	1,321
215	10100	0,99	0,508	$0,401 \cdot 10^{-5}$	
216	10200	0,98	0,522	$0,408 \cdot 10^{-5}$	0,323
217	10350	0,97	0,456	$0,352 \cdot 10^{-5}$	
218	10450	0,96	0,363	$0,277 \cdot 10^{-5}$	1,325

(Cont'd.)

No.	ν, $см^{-1}$	λ, μ	α, $см^{-1}$	$\varkappa$	n
219	10650	0,94	0,221	$0,165 \cdot 10^{-5}$	
220	10800	0,93	0,171	$0,126 \cdot 10^{-5}$	1,326
221	10900	0,92	0,121	$0,88 \cdot 10^{-6}$	
222	11000	0,91	$0,853 \cdot 10^{-1}$	$0,62 \cdot 10^{-6}$	1,327
223	11200	0,89	$0,749 \cdot 10^{-1}$	$0,53 \cdot 10^{-6}$	
224	11300	0,88	$0,673 \cdot 10^{-1}$	$0,47 \cdot 10^{-6}$	1,329
225	11450	0,87	$0,606 \cdot 10^{-1}$	$0,42 \cdot 10^{-6}$	
226	11600	0,86	$0,563 \cdot 10^{-1}$	$0,39 \cdot 10^{-6}$	1,330
227	11700	0,85	$0,533 \cdot 10^{-1}$	$0,36 \cdot 10^{-6}$	
228	11820	0,85	$0,510 \cdot 10^{-1}$	$0,34 \cdot 10^{-6}$	1,331
229	11950	0,84	$0,466 \cdot 10^{-1}$	$0,31 \cdot 10^{-6}$	
230	12100	0,83	$0,386 \cdot 10^{-1}$	$0,25 \cdot 10^{-6}$	1,331
231	12150	0,82	$0,306 \cdot 10^{-1}$	$0,20 \cdot 10^{-6}$	
232	12300	0,82	$0,250 \cdot 10^{-1}$	$0,16 \cdot 10^{-6}$	
233	12400	0,81	$0,248 \cdot 10^{-1}$	$0,16 \cdot 10^{-6}$	
234	12550	0,80	$0,241 \cdot 10^{-1}$	$0,15 \cdot 10^{-6}$	1,333
235	12650	0,79	$0,263 \cdot 10^{-1}$	$0,17 \cdot 10^{-6}$	
236	12800	0,78	$0,287 \cdot 10^{-1}$	$0,18 \cdot 10^{-6}$	
237	12900	0,78	$0,300 \cdot 10^{-1}$	$0,19 \cdot 10^{-6}$	
238	13000	0,77	$0,312 \cdot 10^{-1}$	$0,19 \cdot 10^{-6}$	1,333
239	13150	0,76	$0,318 \cdot 10^{-1}$	$0,19 \cdot 10^{-6}$	
240	13300	0,75	$0,319 \cdot 10^{-1}$	$0,19 \cdot 10^{-6}$	
241	13450	0,74	$0,312 \cdot 10^{-1}$	$0,18 \cdot 10^{-6}$	1,333
242	13550	0,74	$0,295 \cdot 10^{-1}$	$0,17 \cdot 10^{-6}$	
243	13650	0,73	$0,226 \cdot 10^{-1}$	$0,13 \cdot 10^{-6}$	
244	13800	0,72	$0,159 \cdot 10^{-1}$	$0,92 \cdot 10^{-7}$	
245	13850	0,72	$0,131 \cdot 10^{-1}$	$0,75 \cdot 10^{-7}$	
246	14000	0,71	$0,100 \cdot 10^{-1}$	$0,57 \cdot 10^{-7}$	1,333
247	14100	0,71	$0,86 \cdot 10^{-2}$	$0,49 \cdot 10^{-7}$	
248	14300	0,70	$0,73 \cdot 10^{-2}$	$0,47 \cdot 10^{-7}$	
249	14300	0,70	$0,68 \cdot 10^{-2}$	$0,38 \cdot 10^{-7}$	
250	14500	0,70	$0,62 \cdot 10^{-2}$	$0,34 \cdot 10^{-7}$	1,333
251	14600	0,68	$0,60 \cdot 10^{-2}$	$0,33 \cdot 10^{-7}$	
252	14750	0,68	$0,68 \cdot 10^{-2}$	$0,37 \cdot 10^{-7}$	1,332
253	14900	0,67	$0,59 \cdot 10^{-2}$	$0,32 \cdot 10^{-7}$	
254	14950	0,67	$0,56 \cdot 10^{-2}$	$0,30 \cdot 10^{-7}$	1,332
255	15100	0,662	$0,57 \cdot 10^{-2}$	$0,30 \cdot 10^{-7}$	
256	15200	0,644	$0,55 \cdot 10^{-2}$	$0,29 \cdot 10^{-7}$	
257	15300	0,653	$0,55 \cdot 10^{-2}$	$0,29 \cdot 10^{-7}$	
258	15400	0,649	$0,52 \cdot 10^{-2}$	$0,27 \cdot 10^{-7}$	
259	15500	0,645	$0,51 \cdot 10^{-2}$	$0,28 \cdot 10^{-7}$	
260	15600	0,641	$0,52 \cdot 10^{-2}$	$0,27 \cdot 10^{-7}$	1,3318
261	15700	0,636	$0,52 \cdot 10^{-2}$	$0,26 \cdot 10^{-7}$	
262	15800	0,632	$0,49 \cdot 10^{-2}$	$0,25 \cdot 10^{-7}$	
263	15850	0,630	$0,50 \cdot 10^{-2}$	$0,25 \cdot 10^{-7}$	1,3314
264	16000	0,625	$0,48 \cdot 10^{-2}$	$0,24 \cdot 10^{-7}$	
265	16050	0,623	$0,51 \cdot 10^{-2}$	$0,25 \cdot 10^{-7}$	
266	16200	0,617	$0,51 \cdot 10^{-2}$	$0,25 \cdot 10^{-7}$	
267	16250	0,615	$0,50 \cdot 10^{-2}$	$0,25 \cdot 10^{-7}$	1,3314
268	16350	0,611	$0,50 \cdot 10^{-2}$	$0,24 \cdot 10^{-7}$	
269	16450	0,607	$0,49 \cdot 10^{-2}$	$0,24 \cdot 10^{-7}$	
270	16500	0,606	$0,45 \cdot 10^{-2}$	$0,22 \cdot 10^{-7}$	1,3314
271	16700	0,598	$0,43 \cdot 10^{-2}$	$0,21 \cdot 10^{-7}$	
272	16900	0,591	$0,39 \cdot 10^{-2}$	$0,18 \cdot 10^{-7}$	
273	17050	0,586	$0,37 \cdot 10^{-2}$	$0,17 \cdot 10^{-7}$	
274	17200	0,581	$0,36 \cdot 10^{-2}$	$0,17 \cdot 10^{-7}$	
275	17400	0,574	$0,39 \cdot 10^{-2}$	$0,18 \cdot 10^{-7}$	1,3314
276	17550	0,569	$0,39 \cdot 10^{-2}$	$0,18 \cdot 10^{-7}$	
277	17650	0,566	$0,39 \cdot 10^{-2}$	$0,18 \cdot 10^{-7}$	
278	17900	0,558	$0,36 \cdot 10^{-2}$	$0,16 \cdot 10^{-7}$	
279	18100	0,552	$0,39 \cdot 10^{-2}$	$0,17 \cdot 10^{-7}$	
280	18300	0,546	$0,41 \cdot 10^{-2}$	$0,18 \cdot 10^{-7}$	1,3314

REFERENCES

/455

1. Zuyev, V.Ye. Prozrachnost' atmosfery dlya vidimykh i infrakrasnykh luchey (Transparency of the Atmosphere for Visible and Infrared Rays), Izd-vo "Sovetskoye radio," 1966.
2. Kondrat'yev, K.Ya. Aktinometriya (Actinometry), Gidrometeoizdat, 1965.
3. Gudi (Goody), R.M. Atmosfernaya radiatsiya, Ch. 1. Osnovy teorii (Atmospheric Radiation, Part 1. Fundamentals of Theory), Izd-vo "Mir," 1966.
4. Fligl', R. and Buzinger, Dzh. Vvedeniye v fiziku atmosfery (Introduction to Atmospheric Physics), Izd-vo "Mir," 1965.
5. Tverskoy P.N. Kurs meteorologii (Textbook of Meteorology), Gidrometeoizdat, 1962.
6. Gutnik, M. Appl. Optics, 1962, Vol. 1, No. 5, p. 670.
7. Malkevich, M.S., Samsonov, Yu.B., and Koprova, L.I. Usp. Fiz. Nauk, 1963, Vol. 80, No. 1, p. 93.
8. Houghton, J.T. In collection entitled: "Les problems meteorologiques de la stratosphere et de la mesosphere." (Meteorological Problems of the Stratosphere and the Mesosphere). Presses Universitaires de France 108, Boulevard Saint-Germain, Paris, 1966.
9. Komarov, V.S. Izv. Akad. Nauk SSSR, seriya Fizika atmosfery i okeana, 1968, Vol. IV, No. 11, p. 1160. Trudy Nauchno-issledovatel'skogo instituta aeroklimatologii (Transactions of the Scientific Research Institute of Aeroclimatology), 1968, No. 47.
10. Howard, J.N. and Garing, J.S. Infrared Phys., 1962, Vol. 2, No. 3, p. 155.
11. Komarov, V.S. and Marchenko, A.S. Trudy nauchno-issledovatel'skogo instituta aeroklimatologii, 1969, No. 58.
12. Komarov, V.S. Meteorologiya i gidrologiya, 1969, No. 1.
13. Komarov, V.S. Trudy Nauchno-issledovatel'skogo instituta aeroklimatologii, 1968, No. 47; 1969, No. 58.
14. Carion, H.R. Appl. Optics, 1965, Vol. 4, No. 9, p. 1089.
15. Bazhenov, V.A., Ivanova, R.N., and Miroshnikov, M.M. Izv. Akad. Nauk SSSR, seriya fizika atmosfery i okeana, 1966, Vol. 2, No. 3, p. 248.
16. Rozenberg, G.V. Sumerki (Twilight), Fizmatgiz, 1963.
17. Fedynskiy, A.V., Perov, S.P., and Chizhov, A.F. Izv. Akad. Nauk SSSR, ser. fizika atmosfery i okeana, 1967, Vol. 3, No. 5, p. 557.
18. "Atmosfernyy ozon" (Atmospheric Ozone), Edited by A.Kh. Khrgian, Izd-vo MGU, 1961.
19. Khrgian, A.Kh., Kuznetsov, G.I., and Kondrat'yeva, A.M. Issledovaniye atmosfernogo ozona (Investigation of Atmospheric Ozone). Izd. Akad. Nauk SSSR, 1965.
20. Khvostikov, I.A. Fizika ozonosfery i ionosfery (Physics of the Ozonosphere and Ionosphere), Akad. Nauk SSSR, 1963.

21. Gushin, G.P. Ozon i aerosinopticheskiye usloviya v atmosfere (Ozone and Aerosynoptic Conditions in the Atmosphere), Gidrometeoizdat, 1964.
22. Dütsch, H.U. Archiv Meteorol. Geophys., Biocl., Ser. A, 1959, Vol. 11. /456
23. Yakovleva, A.V., Kudryavtseva, L.A., Britayev, A.S. et al. In collection entitled: "Iskusstvennye sputniki Zemli" (Artificial Earth Satellites), No. 14, Izd-vo Akad. Nauk SSSR, 1962, p. 57.
24. Haldane, J.B.C. Nature, 1936, Vol. 137, No. 3466.
25. Callendar, G.S. Quart. Journ. Roy. Met. Soc., 1938, Vol. 64, No. 275; 1940, Vol. 66, No. 287.
26. Glücauf, E. Nature, 1944, Vol. 153, No. 3890, p. 620.
27. Buch, K. Geophys., 1948, Vol. 3, p. 63.
28. Revelle, R. and Suess, H.E. Tellus, 1957, Vol. 9, No. 1.
29. Slocum, G. Monthly Weather Rev., 1955, Vol. 83, No. 10.
30. Fonselius, S., Koroleff, F., and Wärme, K.E. Tellus, 1956, Vol. 8, No. 2.
31. Bray, J.R. Tellus, 1959, Vol. 11, No. 2.
32. Bishof, W. Tellus, 1960, Vol. 12, No. 2.
33. Lyutsarev, S.V. Trudy instituta okeanologii AN SSSR (Transactions of the Oceanology Institute, USSR Academy of Sciences), 1961, Vol. 47, p. 199.
34. Bruyevich, S.V. and Lyutsarev, S.V. Dokl. Akad. Nauk SSSR, 1961, Vol. 136, No. 2, p. 405.
35. Suess, H.E. Science, 1958, Vol. 122, p. 415.
36. Arnold, J.R. and Andersen, E.C. Tellus, 1957, Vol. 9, No. 1.
37. Keeling, C.D. Tellus, 1960, Vol. 12, No. 2.
38. Takanashi, T. Journ. Geoph. Res., 1961, Vol. 60, No. 2.
39. Tomislav, P. Meteorol. Zpravy, Vol. VIII, 1955, No. 5.
40. Misra, R.K. Ind. Journ. Meteor. and Geoph., 1950, No. 1.
41. Voytikova, T.D. Trudy Glavnoy geofizicheskoy observatorii (Transactions of the Main Geophysical Observatory), 1961, No. 118, p. 82.
42. Seeley, J.S. and Houghton, J.T. Infrared Physics, 1961, Vol. 1, No. 2, p. 116.
43. Migeotte, M., Neven, L., and Swenson, J. Met. Soc. Sci., Liege (spec. issue), 1956.
44. Bouman, R.L. and Shaw, J. Appl. Optics, 1963, Vol. 2, No. 2, p. 176.
45. Shaw, J.H. Astrophys. Journ., 1958, Vol. 128, p. 428.
46. Funk, U., Rank, D.H., and Wiggins, T.A. Journ. Optic. Soc. Amer., 1964, Vol. 54, No. 4, p. 472.
47. Goody, R.M. Fizika stratosfery (Physics of the Stratosphere), Gidrometeoizdat, 1958.
48. Birkeland, J.W. and Shaw, J.H. Journ. Optic. Soc. Amer., 1959, Vol. 49, No. 6, p. 637.
49. McMath, R.R., Pierce, A.K., Mohler, O.C., Goldberg, L., and Donovan, R.A. Phys. Rev., 1950, Vol. 78, p. 65.
50. Gertsberg, G. Spektry i stroyeniye dvukhatomnykh molekul (Spectra and Structure of Diatomic Molecules), Izd-vo inostrannoy literatury, 1949.

51. Yel'yashevich, M.A. Atomnaya i molekulyarnaya spektroskopiya (Atomic and Molecular Spectroscopy), Fizmatgiz, 1962.
52. Erlandsson, J. Arkiv für Fysik, 1956, Vol. 10, p. 65.
53. Gordi, V., Smit, V., and Tramborulo, R. Radiospektroskopiya (Radiospectroscopy), Gostekhizdat, 1955.
54. Kondrat'yev, V.N. Struktura atomov i molekul (Structure of Atoms and Molecules), Fizmatgiz, 1959.
55. Lorents, H.A. Proc. Amst. Acad. Soc., 1906, Vol. 8, p. 591.
56. Anderson, P.W. Phys. Rev., 1949, Vol. 76, p. 647; 1950, Vol. 80, p. 511. /457
57. Benedict, W.S. and Kaplan, L.D. Journ. Chem. Phys. 1959, Vol. 30, p. 388.
58. Benedict, W.S. and Kaplan, L.D. Journ. Quant. Spectrosc. Rad. Transfer, 1964, Vol. 4, No. 3, p. 453.
59. Galibina, L.I. and Zuyev, V.Ye. Izv. vuzov SSSR, seriya fizika, 1962, No. 4, p. 69.
60. Plyler, E.K., Gailar, N.M., and Wiggins, T.A. Journ. Res. Nat. Bur. Stand., 1952, Vol. 48, p. 221.
61. Madden, R.F. Journ. Chem. Phys., 1961, Vol. 35, p. 2083.
62. Drayson, S.R. Appl. Optics, 1966, Vol. 5, No. 3, p. 385.
63. Goldberg, L. In collection entitled: The Earth as a Planet, ed. Kuiper, G.P., Chicago Univ. Press, 1954, p. 434.
64. Dufay, J. Ann. d'astrophys., 1942, Vol. 5.
65. Dianov-Klokov, V.I. Optika i spektroskopiya, 1964, Vol. 16, p. 409.
66. Rank, D.N., Pierre, A.G.St., and Wiggins, T.A. Journ. Molecul. Spectr., 1965, Vol. 18, No. 4, p. 418.
67. Breen, R.G. The Shift and Shape of Spectral Lines, Pergamon Press, Oxford-London-New York-Paris, 1961.
68. Traving, G. Über die Theorie der Druckverbreiterung von Spektrallinien (The Theory of the Pressure Broadening of Spectral Lines), Karlsruhe, Braun, 1960.
69. Sobel'man, I.I. Usp. Fiz. Nauk, 1954, Vol. 54, No. 4, p. 551.
70. Chen, S.Y., Takeo, M. Rev. Mod. Phys., 1957, Vol. 29, p. 20.
71. Tsao, C.J. and Curnutte, B. Journ. Quant. Spectr. Rad. Transf., 1962, Vol. 2, No. 1, p. 41.
72. Rautian, S.G. and Sobel'man, I.I. Usp. Fiz. Nauk, 1966, Vol. 90, No. 2, p. 209.
73. Plass, G.N. and Fivel, D.I. Astrophys. Journ., 1953, Vol. 117, p. 225.
74. Surtees, W.J. Journ. Optic. Soc. Amer., 1965, Vol. 55, No. 7, p. 893.
75. Fried, B.D. and Conte, S.D. The Plasma Dispersion Function, Academic Press, New York, 1961.
76. Young, C. Journ. Quant. Spectr. Rad. Tr., 1965, Vol. 5, No. 3, p. 549.
77. Shved, G.M. and Tsaritsyna, I.V. In collection entitled: "Problemy fiziki atmosfery" (Problems of Atmospheric Physics), No. 1, Izd-vo Leningradskogo Universiteta, 1963, p. 71.
78. Winters, B.H., Silverman, S. and Benedict, W.S. Journ. Quant. Spectr. Rad. Transfer, 1964, Vol. 4, p. 527.

79. Kyle, T.G., Murcray, D.G., Murcray, F.H., and Williams, W.J. Journ. Opt. Soc. Amer., 1966, Vol. 56, No. 11, p. 1421.
80. Burch, D.E., Patty, R.R., and Gryvnak, D.A. Journ. Optic. Soc. Amer., 1965, Vol. 55, No. 5, p. 606.
81. Burch, D.E. and Gryvnak, D.A. Journ. Quant. Spectr. Rad. Transf., 1966, Vol. 6, No. 3, p. 229.
82. Landenburg, R. and Reiche, F. Ann. d. Phys., 1913, Vol. 42, p. 181.
83. Elsasser, W.M. Harvard Met. Studies, 1942, No. 6.
84. Kondrat'yev, K.Ya. Perenos dlinnovolnovogo izlucheniya v atmosfere (Transfer of Long-wave Radiation in the Atmosphere), Gostekhizdat, 1950. /458
85. Zuyev, V.Ye. and Tvorogov, S.D. Izv. vuzov SSSR, seriya fizika, 1965, No. 1, p. 185.
86. Zuyev, V.Ye. and Tvorogov, S.D. Izv. vuzov SSSR, seriya fizika, 1965, No. 2, p. 170.
87. Matossi, F., Mayer, R., and Rauscher, E. Phys. Rev. 1949, Vol. 76, No. 6, p. 1049.
88. Zuyev, V.Ye. and Tvorogov, S.D. Izv. vuzov SSSR, seriya fizika, 1966, No. 4, p. 26.
89. Elsasser, W.M. Heat Transfer by Infrared Radiation in the Atmosphere, Harvard, 1942.
90. Kondrat'yev, K.Ya. Luchistyy teploobmen v atmosfere (Radiant Heat Transfer in the Atmosphere), Gidrometeoizdat, 1956.
91. Goody, R.M. Quart. Journ. Roy. Met. Soc., 1952, Vol. 78, p. 336.
92. Plass, G.N. Journ. Opt. Soc. Amer., 1958, Vol. 48, No. 10, p. 690.
93. Godson, W.L. Journ. Opt. Soc. Amer., 1955, Vol. 12, No. 3; Proc. Toronto Meteorol. Conf., Toronto, 1953, 1954.
94. Kaplan, L. Proc. Toronto Meteor. Conf., Toronto, 1953, Vol. 43.
95. Soshnikov, V.N. "Optika i spektroskopiya," 1961, Vol. 10, No. 4, p. 448.
96. Wyatt, P.J., Stull, V.R., and Plass, G.N. Journ. Optic. Soc. Amer., 1962, Vol. 52, No. 11, p. 1209.
97. Soshnikov, V.N. "Optika i spektroskopiya," 1962, Vol. 12, No. 1, p. 123.
98. Plass, G.N. Advances Molecul. Spectrosc. Vol. 3, Oxford-London-New York-Paris, Pergamon Press, 1962, p. 1326.
99. Godson, W.L. Archiv für Meteorol., Geophys. und Bioklim., 1962, Vol. 12, No. 1, p. 1.
100. Godson, W.L. Archiv für Meteorol. Geophys. und Bioklim., 1963, Vol. 13, No. 2, p. 196.
101. Gershun, A.A. Ocherk po istorii fotometrii. Izbrannyye trudy po fotometrii i svetotekhnike (Outlines of the History of Photometry. Selected Works on Photometry and Illumination Engineering), Fizmatgiz, 1958.
102. Strong. F.S. Annal. Chem., 1952, Vol. 24, p. 338.
103. Vavilov, S.I. Mikrostruktura sveta (The Microstructure of Light), Izd-vo Akad. Nauk SSSR, 1950.
104. Houghton, J.T. Quart. Journ. Roy. Met. Soc., 1963, Vol. 89, No. 381, p. 332.

105. Angstrom, K. Oversing of K. Vetensk. Akad. Förh., 1889, Vol. 46, p. 546; 1890, Vol. 47, p. 331; Phys. Rev., 1892, Vol. 1, p. 597; Ann. d. Phys., 1901, Vol. 6, p. 163; Arkiv f. Mathem., Astronom. och Fysik, 1907, Vol. 4, No. 30.
106. Schaefer, C. Ann. d. Physik, 1905, Vol. 16, p. 93.
107. Eva von Bahr. Ann. d. Phys., 1909, Vol. 29, p. 780; 1910, Vol. 33, p. 585; Phys. Zeit., 1911, Vol. 12, p. 1167; Verh. deutsche Phys. Ges. 1913, Vol. 15, p. 673, 710.
108. Rank, D.H., Guenther, A.H., Shearer, J.H., and Wiggins, T.A. Journ. Opt. Soc. Amer., 1957, Vol. 47, p. 144.
109. Plyler, E.K. and Blaine, L.K. Journ. Res. Nat. Bur. Stand., 1959, Vol. 62, No. 1.
110. Rank, D.H., Eastman, D.P., Bertley, W.B., Skorinko, G., and Wiggins, T.A. Journ. Opt. Soc. Amer., 1960, Vol. 50, No. 8. p. 821.
111. Nielsen, J.R., Thornton, V., and Dalle, E.B. Rev. Modern Phys., 1944, Vol. 16, p. 307. /459
112. Howard, J.N., Burch, D.E., and Williams, D. Journ. Optic. Soc. Amer., 1956, Vol. 46, p. 186, 237, 242, 334, 452.
113. Zuyev, V.Ye., Elyashberg, M.Ye., and Safronova, G.I. Izv. vuzov SSSR, seriya fizika, 1960, No. 5, p. 77.
114. Zuyev, V.Ye. and Koshelev, B.P. Izv. vuzov SSSR, seriya fizika, 1961, No. 6, p. 172.
115. Kozlov, V.P. and Fedorova, Ye.O. "Optika i spektroskopiya," 1961, Vol. 10, No. 5.
116. Dmitriyevskiy, O.D., Neporent, B.S., and Nikitin, V.A. Usp. Fiz. Nauk, 1958, Vol. 64, p. 447.
117. Rautian, S.G. Usp. Fiz. Nauk, 1958, Vol. 66, p. 475.
118. Petrash, G.G. "Optika i spektroskopiya," 1959, Vol. 6, No. 6, p. 792; 1960, Vol. 8, No. 1, p. 122; 1960, Vol. 9, No. 3, p. 423.
119. Petrash, G.G. and Rautian, S.G. "Inzhenerno-fizicheskiy zhurnal," 1958, Vol. 1, p. 61, p. 80.
120. Dmitriyevskiy, O.D. and Nikitin, V.A. "Zhurnal optiko-mekhanicheskaya promyshlennost'," 1947, No. 4, p. 9; "Optika i spektroskopiya," 1960, Vol. 8, No. 1, p. 120.
121. Nikitin, V.A. "Optika i spektroskopiya," 1958, Vol. 4, p. 523.
122. Kyle, T.G. and Green, J.O. Journ. Opt. Soc. Amer., 1965, Vol. 55, No. 7, p. 895.
123. Rank, D.H. and Wiggins, T.A. Journ. Quant. Spectr. Rad. Tr., 1963, Vol. 3, No. 4, p. 377.
124. Dennison, D. Rev. Mod. Phys., 1931, Vol. 3, p. 280.
125. Bonner, L.J. Phys. Rev., 1934, Vol. 47, p. 458.
126. Escart, C. Phys. Rev., 1959, Vol. 47, p. 552.
127. Khachkuruzov, G.A. Trudy Gosudarstvennogo instituta prikladnoy khimii (Transactions of the State Institute of Applied Chemistry), 1959, Vol. 42, p. 51.
128. Wang, S.E. Phys. Rev., 1929, Vol. 34, p. 243.
129. Ray, B.S. Zeit. für Phys., 1932, Vol. 78, p. 74.
130. Hainer, R.M., Cross, P.S., and King, G.W. Journ. Chem. Phys., 1943, Vol. 11, p. 27.

131. Hainer, R.M., Cross, P.C., and King, G.W. Journ. Chem. Phys., 1949, Vol. 17, p. 826.
132. Wilson, E.B. and Howard, B. Journ. Chem. Phys., 1936, Vol. 4, p. 260.
133. Wilson, E.B. Journ. Chem. Phys., 1937, Vol. 5, p. 617.
134. Yel'yashevich, M.A. Trudy Gosudarstvennogo opticheskogo instituta (Transactions of the State Optical Institute), 1939, Vol. 4, No. 106.
135. Shaffer, W.H. and Nielsen, H.H. Phys. Rev. 1939, Vol. 56, p. 188.
136. Majumdar, D. Proc. Phys. Soc., 1954, Vol. 67, p. 351; 1958, Vol. 72, p. 635.
137. Majumdar, D. and Gosh, A.K. Spectrochem. Acta, 1962, Vol. 18, p. 615.
138. Benedict, W., Gailar, N., and Plyler, E.K. Journ. Chem. Phys., 1956, Vol. 24, p. 1139.
139. Zuyev, V.Ye., Ippolitov, I.I., Makushkin, Yu.S., Orlov, A.A., and Fomin, V.V. Dokl. Akad. Nauk SSSR, 1968, Vol. 179, No. 1, p. 51.
140. Zuyev, V.Ye., Ippolitov, I.I., Makushkin, Yu.S., Orlov, A.A., /460 and Fomin, V.V. "Optika i spektroskopiya," 1968, Vol. 25, No. 1.
141. Zuyev, V.Ye., Ippolitov, I.I. Makushkin, Yu.S., and Fomin, V.V. Doklad na XIV General'noy assambleye MGGS (Paper at Fourteenth General Assembly of the IUGG (Switzerland, September 1967).
142. Makushkin, Yu.S. Izv. vuzov SSSR, seriya fizika, 1966, No. 6, p. 70.
143. Makushkin, Yu.S. Izv. vuzov SSSR, seriya fizika, 1967, No. 2, p. 79.
144. Makushkin, Yu.S. Izv. vuzov SSSR, seriya fizika, 1967, No. 3, p. 153.
145. Makushkin, Yu.S. In collection entitled: "Trudy mezhvuzovskogo soveshchaniya po spektral'noy prozrachnosti atmosfery" (iyun' 1965 g.) Transactions of Interinstitute Conference on the Spectral Transparency of the Atmosphere (June 1965)), Izd-vo Tomskogo Gosudarstvennogo universiteta, 1968.
146. Makushkin, Yu.S. "Optika i spektroskopiya," Vol. 25, No. 1.
147. Ippolitov, I.I. and Makushkin, Yu.S. "Optika i spektroskopiya," 1968, Vol. 24, No. 4, p. 530.
148. Nielsen, H.H. Rev. Mod. Phys., 1951, Vol. 23, p. 90.
149. Goldsmith, M., Amat, G., and Nielsen, H.H. Journ. Chem. Phys., 1956, Vol. 24, p. 1178.
150. Podolsky, B. Phys. Rev., 1928, Vol. 32, p. 812.
151. Goldsmith, M., Amat, G., and Nielsen, H.H. Journ. Chem. Phys., 1957, Vol. 27, p. 838.
152. Amat, G. and Nielsen, H.H. Journ. Chem. Phys., 1957, Vol. 27, p. 845.
153. Amat, G. and Nielsen, H.H. Journ. Chem. Phys., 1962, Vol. 36, p. 1859.
154. Blokhintsev, D.I. Osnovy kvantovoy mekhaniki (Fundamentals of Quantum Mechanics), Izd-vo "Vysshaya shkola," 1963.

155. Sleator, W.W. Astrophys. Journ., 1918, Vol. 48, p. 125.
156. Sleator, W.W. and Phelps, E.R. Astroph. Journ. 125, Vol. 62, p. 28.
157. Plyler, E.K. and Sleator, W.W. Phys. Rev., 1931, Vol. 37, p. 1493.
158. Plyler, E.K. Phys. Rev., 1932, Vol. 39, p. 77.
159. Mecke, R. Zeit. für Phys., 1933, Vol. 81, p. 313.
160. Boumann, W. and Mecke, R. Zeit. für Phys., 1933, Vol. 81, p. 445.
161. Freudenberg, K. and Mecke, R. Zeit. für Phys., 1933, Vol. 81, p. 465.
162. Nielsen, H.H. Phys. Rev., 1941, Vol. 59, p. 565; 1942, Vol. 62, p. 422.
163. Nelson, R.C. and Benedict, W.S. Phys. Rev. 1948, Vol. 74, p. 703.
164. Benedict, W.S. and Plyler, E.K. Journ. Res. Nat. Bur. Stand., 1951, Vol. 46, p. 246.
165. Benedict, W.S. Bull. Amer. Phys. Soc., 1948, Vol. 23, p. 54; Phys. Rev., 1948, Vol. 74, p. 1246.
166. Benedict, W.S., Claassen, H.H., and Shaw, J.H. Journ. Res. Nat. Bur. Stand., 1952, Vol. 49, p. 91.
167. Dalby, F.W. and Nielsen, H.H. Journ. Chem. Phys., 1956, Vol. 25, p. 934.
168. Benedict, W.S., Bass, A.M., and Plyler, E.K. Journ. Res. Nat. /461 Bur. Stand., 1954, Vol. 52, p. 64.
169. Barnes, R.B. and Benedict, W.S. Phys. Rev., 1935, Vol. 47, p. 918.
170. Randall, H.M., Dennison, D.M., Ginsberg, N., and Weber, L.R. Phys. Rev., 1937, Vol. 52, p. 160.
171. Dennison, D.M. Rev. Modern Phys., 1940, Vol. 12, p. 175.
172. Yaroslavskiy, N.G. and Stanevich, A.Ye. "Optika i spektroskopiya," 1958, Vol. 5, p. 384; 1959, Vol. 7, p. 626.
173. Furashov, N.I. Optika i spektroskopiya, 1966, Vol. 20, No. 3, p. 427.
174. Minnaert, M., Mulders, G.F., and Houtgast, J. Photometric Atlas of the Solar Spectrum λ 3612 to λ 8771, Amsterdam, 1940.
175. Babcock, H.D. and Moore, C.E. The Solar Spectrum, λ 6600 to λ 13,495, Washington: Carnegie Institute of Washington Publ. 579, 1947.
176. Mohler, O.C., Pierce, A.K., McMath, R.R., and Goldberg, L. Atlas of the Solar Spectrum from 0.84 to 2.55 Microns, Univ. of Mich. Press, Ann Arbor, Mich., 1950.
177. Mohler, O.C. and Benedict, W.S. Phys. Rev., 1948, Vol. 74, p. 702.
178. Mohler, O.C. Tables of Solar Spectrum Wave Lengths 1.20-2.55 Microns, Univ. of Mich. Press, Ann Arbor, Mich., 1955.
179. Shaw, J.H., Chapman, R.M., Howard, J.N., and Oxholm, M.L. Astrophys. Journ., 1951, Vol. 113, p. 268.
180. Shaw, J.H., Oxholm, M.L., and Claassen, H.H. Astrophys. Journ., 1952, Vol. 116, p. 354.
181. Migeotte, M., Neven, L., and Swenson, J. The Solar Spectrum from 2.8 to 23.7 Microns, University of Liege, Final Report, Part I, 1956; Part II, 1957.

182. Migeotte, M., Neven, L., Swenson, J., and Benedict, W.S. The Solar Spectrum from 2.8 to 23.7 Microns, Part II, Institute of Astrophysics, Liege University, 1957.
183. Delbouille, L. and Roland, G. Atlas Photometrique du spectre solair de λ 7498 a λ 12,016 (Photometric Atlas of the Solar Spectrum from λ 7498 to λ 12,016), Liege, 1963.
184. Farmer, C.B. and Key, P.J. Appl. Opt., 1965, Vol. 4, No. 9, p. 1051.
185. Curcio, I.A., Drummeter, L.F., and Knestrick, G.L. Appl. Optics, 1964, Vol. 3, No. 12, p. 1401.
186. Moore, C.E., Minnaert, M.G.J., and Houtgast, J. Tables of Spectral Lines of the Atmosphere from λ 2935 to λ 8770 Å, Washington, Gov. Print. Off., 1966.
187. Oppenheim, U.P. and Goldman, A. Atlas and Wave-Number Tables of Water Vapor Absorption at 1200°K in the 1.9 and 2.7 μ Regions, Scientific Report No. 1, AFEOAR 63-111, Haifa, Israel, 1964.
188. Schwendenman, R.H. and Laurie, V.W. Tables of Line Strengths for Rotational Transmissions of Asymmetric Rotor Molecules, Pergamon Press, New York, 1958.
189. Calfee, R.F. Journ. Quant. Spectr. Rad. Transfer, 1966, Vol. 6, No. 3, p. 221.
190. Ippolitov, I.I. Izv. vuzov SSSR, seriya fizika, 1967, No. 7, /462 p. 145.
191. Cross, P.C., Hainer, R.M., and King. G.W. Journ. Chem. Phys., 1944, Vol. 12, p. 210.
192. Ippolitov, I.I. "Optika i spektroskopiya," 1969, Vol. 27, No. 3, p. 458.
193. Khachkuruzov, G.A. Trudy Gosudarstvennogo instituta prikladnoy khimii (Transactions of the State Institute of Applied Chemistry), 1960, Vol. 46, p. 66.
194. Papousek, D. and Pliva, J. Collect. Czech. Chem. Comm., 1964, Vol. 29, p. 1973.
195. Vasilevskiy, K.P. and Neporent, B.S. "Optika i spektroskopiya," 1959, Vol. 7, p. 572.
196. Vasilevskiy, K.P. and Neporent, B.S. "Optika i spektroskopiya," 1958, Vol. 4, p. 474.
197. Vasilevskiy, K.P. "Optika i spektroskopiya," 1961, Vol. 11, p. 207.
198. Sanderson, R.B. and Ginsburg, N. Journ. Quant. Spectr. Rad. Tr., 1963, Vol. 3, No. 4, p. 435.
199. Saidy, F. Quart. Journ. Roy. Met. Soc., 1961, Vol. 87, No. 384, p. 578.
200. Bolle, H.J. Journ. Optic. Soc. Amer., 1966, Vol. 56, No. 4, p. 560.
201. Goldman, A. and Oppenheim, U.P. Appl. Optics, 1966, Vol. 5, No. 6, p. 1073.
202. Jaffe, J.H. and Benedict, W.S. Journ. Quant. Spectr. Rad. Transf., 1963, Vol. 3, No. 1, p. 87.
203. Hirshfeld, M.A., Jaffe, J.H., and Ross, G. Journ. Quant. Spectr. Rad. Transf., 1966, Vol. 6, No. 3, p. 311.
204. Landay, L.D. and Lifshits, Ye.M. Teoriya polya (Field Theory), Fizmatgiz, 1962.

205. Davydov, A.S. Kvantovaya mekhanika (Quantum Mechanics), Fizmatgiz, 1963.
206. Zuyev, V.Ye. In collection entitled: "Trudy mezhvuzovskogo soveshchaniya po spektral'noy prozrachnosti atmosfery" (iyun' 1965 g., Tomsk) (Transactions of Interinstitute Conference on the Spectral Transparency of the Atmosphere (June 1965, Tomsk)), Izd-vo Tomskogo Gosudarstvennogo Universiteta, 1968.
207. Gradshteyn, I.S. and Ryzhik, I.M. Tablitsy integralov, summ, ryadov i proizvedeniy (Tables of Integrals, Sums, Series, and Products), Fizmatgiz, 1962.
208. Becker, G.E. and Autler, S.H. Phys. Rev., 1946, Vol. 70, p. 300.
209. Cowling, T.G. Phil. Mag., 1950, Vol. 41, p. 109.
210. Benedict, W.S. Journ. Opt. Soc. Amer., 1957, Vol. 47, p. 1056.
211. Kondrat'yev, K.Ya. and Timofeyev, Yu.M. Izv. Akad. Nauk SSSR, seriya fizika atmosfery i okeana, 1966, Vol. 2, No. 3, p. 272.
212. Plass, G.N. and Stull, V.R. Theoretical Study of High Temperature Emissivities and Atmospheric Transmission, Contract, Bedford, 1960.
213. Howard, J.N., Burch, D.E., and Williams, D. Near Infrared Transmission Through Synthetic Atmosphere, Contract, Ohio University, 1955.
214. Stull, V.R., Wyatt, P.J., and Plass, G.N. The Infrared Absorption of Water Vapor, Report SSD-TDR-62-127, Vol. II, Space Systems Division, Air Force Systems Command, Los Angeles, Calif., 1962.
215. Stull, V.R., Wyatt, R.J., and Plass, G.N. The Infrared Absorp- /463
tion of Carbon Dioxide, Report SSD-TDR-62-127, Vol. III, Space Systems Division, Air Force Systems Command, Los Angeles, Calif., 1962.
216. Burch, D.E., Gryvnak, D., Singlton, E.B., France, W.L., and Williams, D.W. Infrared Absorption by CO_2 Water Vapor and Minor Atmospheric Constituents, AFCRL-62-698, AFCRL, Bedford, Mass., July, 1962.
217. Wyatt, P.J., Stull, V.R., and Plass, G.N. Appl. Optics, 1964, Vol. 3, No. 2, p. 229.
218. Oppenheim, U.P. and Ben-Aryeh, Y. Journ. Quant. Spectrosc. Rad. Transf., 1964, Vol. 4, No. 4, p. 559.
219. Zuyev, V.Ye., Nesmelova, L.I., Sapozhnikova, V.A., and Tvorogov, S.D. In collection entitled: "Aktinometriya i optika atmosfery" (Trudy V mezhvedomstvennogo soveshchaniya po aktinometrii i optike atmosfery) (Actinometry and Atmospheric Optics (Transactions of Fifth Interdepartmental Conference on Actinometry and Atmospheric Optics)), Edited by G.V. Rozenberg, Izd-vo "Nauka," 1964.
220. Zuyev, V.Ye. In collection entitled: "Yubileynyy sbornik trudov Tomskogo universiteta po fizike" (Anniversary Collection of Tomsk University Physics Transactions), Izd-vo Tomskogo Gosudarstvennogo Universiteta, 1970.

221. Burch, D.E. and Williams, D.W. Appl. Optics, 1963, Vol. 2, No. 6.
222. Larmor, L. and Passman, S. Proc. IRIS, 1956, Vol. 1, No. 1, p. 1; 1956, Vol. 1, No. 2, p. 15.
223. Langer, R.M. Proc. IRIS, Part 2, July, 1958.
224. Roach, W.T. Quart. Journ. Roy. Met. Soc., 1961, Vol. 87, No. 373, p. 346.
225. Zuyev, V.Ye. Izv. vuzov SSSR, seriya fizika, 1961, No. 3, 6; 1962, No. 1, 3, 6; Collection entitled: "Rasseyaniye i polyarizatsiya sveta v zemnoy atmosfere" (Scattering and Polarization of Light in the Earth's Atmosphere), Izd-vo Akad. Nauk Kaz. SSR, 1962.
226. Burch, D.E., Singleton, E.B., and Williams, D. Appl. Optics, 1962, Vol. 1, No. 3, p. 359.
227. Palmer, C.H. Journ. Optic. Soc. Amer., 1960, Vol. 50, p. 1232.
228. Izatt, J. Ph. D. Dissertation, Johns Hopkins Univ., 1960.
229. Goody, R.M. and Wormell, T.W. Proc. Roy. Soc. A, 1951, Vol. 209, p. 178.
230. Cross, P.S. and Daniels, F. Journ. Chem. Phys., 1934, Vol. 2, p. 6.
231. Edwards, D.K. Journ. Opt. Soc. Amer., 1960, Vol. 50, p. 617.
232. Stauffer, F.R. and Walsh, T.E. Journ. Opt. Soc. Amer., 1966, Vol. 56, No. 3, p. 401-406.
233. Palmer, C.H. Journ. Opt. Soc. Amer., 1957, Vol. 47, p. 1024.
234. Burch, D.E. and Reisman, E. Journ. Opt. Soc. Amer., 1966, Vol. 56, No. 4, p. 556.
235. Goldstein, R. Journ. Quant. Spectr. Rad. Transfer, 1964, Vol. 4, No. 2, p. 343.
236. Ludwig, C.B., Ferriso, C.C., and Abeyta, C.N. Journ. Quant. Spectr. Rad. Transf., 1965, Vol. 5, No. 2, p. 281.
237. Gray, L.D. and Penner, S.S. Journ. Quant. Spectr. Rad. Transf., 1965, Vol. 5, No. 4, p. 611.
238. Ferriso, C.C., Ludwig, C.B., and Thomson, A. Journ. Opt. Soc. Amer., 1965, Vol. 55, No. 5, p. 617.
239. Ferriso, C.C. and Ludwig, C.B. Journ. Opt. Soc. Amer., 1966, /463 Vol. 56, No. 4, p. 560.
240. Goldman, A. and Oppenheim, U.P. Journ. Opt. Soc. Amer., 1965, Vol. 55, No. 7, p. 794.
241. Edwards, D.K., Flornes, B.J., Glassen, L.K., and Sun, W. Appl. Optics, 1965, Vol. 4, No. 6, p. 715.
242. Ferriso, C.C. and Ludwig, C.B. Journ. Quant. Spectrosc. Rad. Transf., 1964, Vol. 4, p. 215.
243. Ferriso, C.C. and Ludwig, C.B. Journ. Chem. Phys., 1964, Vol. 41, p. 1668.
244. Möller, F. Beit. Geophys., 1942, Vol. 58, p. 27.
245. Gebbie, H.A., Harding, W.R., Hilsum, C., Pryce, A.W., and Roberts, Proc. Roy. Soc., 1951, Vol. 206, No. 1084, p. 87.
246. Taylor, J. and Yattes, H.W. Journ. Opt. Soc. Amer., 1957, Vol. 47, No. 3, p. 223.
247. Adel, A. Astrophys. Journ., 1939, Vol. 89, p. 1.
248. Anthony, R. Phys. Rev., 1952, Vol. 85, p. 674.
249. Feygel'son, Ye.M. Izv. Akad. Nauk SSSR, seriya geofizicheskaya, 1951, No. 4, p. 92.

250. Roach, W.T. and Goody, R.M. Quart. Journ. Roy. Met. Soc., 1958, Vol. 84, p. 319.
251. Volz, F. Ann. d. Meteorol., 1957, Vol. 8, p. 34.
252. Bignell, K., Saiedy, F., and Sheppard, P.A. Journ. Optic. Soc. Amer., 1963, Vol. 53, No. 4, p. 466.
253. Kondrat'yev, K.Ya., Badinov, I.Ya., Ashcheulov, S.V., and Andreyev, S.D. Izv. Akad. Nauk SSSR, seriya fizika atmosfery i okeana, 1965, Vol. 1, No. 4, p. 363.
254. Kaplan, L.D. In collection entitled: Les problems meteorologiques de la Stratosphere et de la mesosphere (Meteorological Problems of the Stratosphere and the Mesosphere), Presses Universitaires de France 108, Boulevard Saint-Germain, Paris, 1966, p. 307.
255. Kaplan, L.D. Journ. Chem. Phys., 1950, V. 18, No. 2, p. 186.
256. Yamomoto, G. and Sasamory, T. Sci. Reports, Tohoku Univers., Series 5, Geophys., 1958, Vol. 10, No. 2, p. 37; 1961, Vol. 13, p. 1.
257. Gordon, H.R. and McCubbin, T.K. Jr. Journ. Molecul. Spectrosc., 1965, Vol. 18, No. 1, p. 73.
258. Kaplan, L.D. and Eggers, D.F. Journ. Chem. Phys., 1950, Vol. 25, p. 876.
259. Nielsen, A.H. and Yao, Y.T. Phys. Rev., 1945, Vol. 68, p. 173.
260. Benedict, W.S., Herman, R.C., and Silverman, S. Journ. Chem. Phys., 1951, Vol. 19, No. 10, p. 1325.
261. Courtoy, C.P. Canad. Journ. Phys., 1957, Vol. 35, p. 608.
262. Gray, L.D. and Selvidge, J.E. Journ. Quant. Spectrosc. Rad. Transf., 1965, Vol. 5, No. 2, p. 291.
263. Calfee, R.F. and Benedict, W.S. Appl. Optic., 1966, Vol. 5, No. 10, p. 1695. Carbon Dioxide Spectral Line Positions and Intensities Calculated for 2.05 and 2.7 Micron Regions, Nation. Bur. of Standards, Washington, D.C., 1966.
264. Williams, D. Appl. Optics, 1966, Vol. 5, No. 10, p. 1696.
265. Gordon, H.R. and McCubbin, T.K. Jr. Journ. of Molec. Spectr., 1966, Vol. 19, No. 2, p. 137.
266. Vasilevskiy, K.P., Kazbanov, V.A., and Derviz, T.Ye. "Optika i spektroskopiya," 1967, Vol. 23, No. 6, p. 888.
267. Boese, R.W., Miller, J.H., and Inn, E.C.J. Journ. Quant. Spectr. Rad. Transf., 1966, Vol. 6, No. 6, p. 717. /465
268. Gorchakova, I.A. and Malkevich, M.S. Izv. Akad. Nauk SSSR, seriya fizika atmosfery i okeana, 1966, Vol. 2, No. 6, p. 585.
269. Stull, V.R., Wyatt, P.J., and Plass, G.N. Appl. Opt., 1964, Vol. 3, No. 2, p. 243.
270. Megill, L.R. and Jamnick, P.M. Journ. Optic. Soc. Amer., 1961, Vol. 51, No. 11, p. 1294.
271. Gray, L.D. Journ. Opt. Soc. Amer., 1966, Vol. 56, No. 4, p. 555.
272. Gray, L.D. and McClatchey, R.A. Journ. Opt. Soc. Amer., 1965, Vol. 55, No. 11, p. 1567.
273. Burch, D.E., Gryvnak, D.A., and Williams, D. Appl. Opt., 1962, Vol. 1, No. 6, p. 759.

274. Edwards, D.K. and Menard, W.A. Appl. Opt., 1964, Vol. 3, No. 7, p. 847.
275. Edwards, D.K. and Sun, W. Appl. Opt., 1964, Vol. 3, No. 12, p. 1501.
276. Varanasi, P. and Lauer, J.L. Journ. Quant. Spectr. Rad. Transf., 1966, Vol. 6, No. 1, p. 127.
277. Clough, S.A. and Kneizys, F.X. Journ. Chem. Phys., 1966, Vol. 44, No. 5, p. 1855.
278. Clough, S.A. and Kneizys, F.X. Ozone Absorption in the 9.0 Micron Region, AFCRL-65-862, Report, Air Force Cambridge Research Laboratories, 1965.
279. White, J.U., Alpert, N.L., Debell, A.G., and Chapman, R.M. Journ. Opt. Soc. Amer., 1957, Vol. 47, No. 5, p. 358.
280. Walshaw, C.D. An Experimental Investigation of the 9.6 Micron Band of Ozone, Thesis, Cambridge University, 1954.
281. Nexsen, W.E. Jr. Sci. Report No. 1, Contract AF19(604)-1003 with the Ohio State University AFCRL-TN-56-265, 1965.
282. McCaa, D.J. and Shaw, J.H. Appl. Optics, 1963, Vol. 2, p. 581.
283. Trajmar, S. Paper Presented at Symposium on Molecular Structure and Spectroscopy, Columbus, Ohio, 1963.
284. Trajmar, S. and McCaa, D.J. Journ. Molec. Spectrosc., 1964, Vol. 14, No. 3, p. 244.
285. Gora, E.K. Journ. Molec. Spectrosc., 1959, Vol. 3, p. 78.
286. Gebbie, H.A., Stone, N.W.B., Topping, G., Gora, E.K., Clough, S.A., and Kneizys, F.X., Journ. of Molecul. Spectrosc., 1966, Vol. 19, No. 1, p. 7.
287. Walshaw, C.D. Quart. Journ. Roy. Met. Soc., 1957, Vol. 83, No. 357, p. 315.
288. Altshuller, T.L. Infrared Transmission of Clear Atmosphere, Document 61SD199, General Electric Company, Philadelphia, Penna., Dec. 1961.
289. Elsasser, W.M. and Culbertson, M.F. Metrol. Monogr., Vol. 4, No. 23, Am. Met. Soc., 1960.
290. Allen, H.C. and Plyler, E.K. Journ. Chem. Phys., 1957, Vol. 26, No. 4, p. 972.
291. Herranz, J. and Thyagarajan, G. Journ. Molec. Spectrosc., 1966, Vol. 19, No. 3, p. 247.
292. Herranz, J., Morcillo, J., and Gomes, A. Journ. of Molecul. Spectrosc., 1966, Vol. 19, No. 3, p. 266. /466
293. Burch, D.E. and Williams, D. Appl. Optics, 1962, Vol. 1, No. 4, p. 473.
294. Burch, D.E. and Williams, D. Appl. Optics, 1962, Vol. 1, No. 5, p. 587.
295. Long., R.L. Atmospheric Absorption and Laser Radiation, Ohio State University Engineering Publications, Bulletin 199, Columbus, Ohio, 1967.
296. Howard, J.N. and Garing, J.S. In book entitled: U.S. National Report, 14th General Assembly, Transactions, American Geophysical Union, 1967, Vol. 48, No. 2, p. 471
297. Gray, L.D. Appl. Optics, 1965, Vol. 4, No. 11, p. 1494.
298. Abels, L.L. and Ford, D.L. Journ. Opt. Soc. Amer., 1965, Vol. 55, No. 5, p. 617.

299. Oppenheim, U.P. and Goldman, A. Journ. Opt. Soc. Amer., 1966, Vol. 56, No. 5, p. 675.
300. Rank, D.H., Slomba, A.F., Gardner, F.F., and Wiggins, T.A. Journ. Opt. Soc. Amer., 1962, Vol. 52, No. 8, p. 858.
301. Dorman, F. and Lin, C.C. Journ. of Molecul. Spectrosc., 1964, Vol. 12, No. 2, p. 119.
302. Gordon, H.R. and McCubbin, T.K. Journ. Molec. Spectrosc., 1965, Vol. 18, No. 1, p. 73.
303. Abels, L.L. and Shaw, J.H. Journ. Optic. Soc. Amer., 1963, Vol. 53, No. 7, p. 856.
304. Yamada, H. and Person, W.S. Journ. Chem. Phys., 1966, Vol. 45, No. 6, p. 1861.
305. Hathaway, C.E., Hoover, G.M., and Williams, D. Journ. Opt. Soc. Amer., 1966, Vol. 56, No. 4, p. 555.
306. Edwards, D.K. Appl. Optics, 1965, Vol. 4, No. 10, p. 1352.
307. Benedict, W.S., Herman, R., Moore, G.E., and Silverman, S. Astrophys. Journ., 1962, Vol. 135, No. 1, p. 277.
308. Shaw, J.H. and France, W.L. Intensities and Widths of Single Lines of the 4.7 Microns CO Fundamental, Scientific Rep. 4 on Project 587, Ohio State Univ., 1956.
309. Dowling, J.M. and Hall, R.T. Journ. Molecul. Spectr., 1966, Vol. 19, No. 1, p. 108.
310. Weinberg, J.M., Fishburne, E.S., and Rao, K.N. Journ. of Molec. Spectrosc., 1965, Vol. 18, No. 4, p. 428.
311. Gryvnak, D.A. and Shaw, J.H. Journ. Opt. Soc. Amer., 1962, Vol. 52, No. 5, p. 539.
312. Hathaway, C.E., Hoover, G.M., Tubbs, L.D., and Williams, D. Journ. Opt. Soc. Amer., 1966, Vol. 56, No. 10, p. 1422.
313. Abu-Romia, M.M. and Tien, C.L. Journ. Quant. Spectrosc. Rad. Transf., 1966, Vol. 6, No. 2, p. 143.
314. Shaw, J.H. and Houghton, J.T. Appl. Optics, 1964, Vol. 3, No. 6, p. 773.
315. Hoover, G.M., Hathaway, C.E., and Williams, D. Appl. Optics, 1967, Vol. 6, No. 3, p. 481.
316. Gray, L.D. and McClatchey, R.A. Appl. Optics, 1965, Vol. 4, p. 1624.
317. Penner, S.S. and Varanasi, P. Journ. Quant. Spectr. Rad. Transf., 1966, Vol. 6, No. 2, p. 181. /467
318. Sakai, H. and Stauffer, F.R. Journ. Opt. Soc. Amer., 1964, Vol. 54, p. 759.
319. Sakai, H. Journ. Opt. Soc. Amer., 1966, Vol. 56, No. 1, p. 127.
320. Plass, G.N. Journ. Opt. Soc. Amer., 1965, Vol. 55, No. 1, p. 104.
321. Sakai, H. Journ. Opt. Soc. Amer., 1966, Vol. 56, No. 4, p. 556.
322. Plass, G.N. Journ. Opt. Soc. Amer., 1965, Vol. 55, No. 5, p. 593.
323. Plass, G.N. Appl. Optics, 1965, Vol. 4, p. 69.
324. Balandin, N.I., Kuznetsova, E.S., and Podkladenko, M.V. "Prikladnaya spektroskopiya," 1964, Vol. 1, No. 1, p. 66.

325. Podkladenko, M.V. Trudy Mezhvuzovskogo nauchnogo soveshchaniya po spektral'noy prozrachnosti atmosfery v vidimoy i infrakrasnoy oblastyakh spektra (Transactions of Interinstitute Scientific Conference on the Spectral Transparency of the Atmosphere in the Visible and Infrared Regions of the Spectrum), Izd-vo Tomskogo Gosudarstvennogo Universiteta, 1968, p. 106.
326. Curcio, J.A. and Buttrey, D.V.E. Appl. Optics, 1966, Vol. 5, No. 2, p. 231.
327. Zuyev, V.Ye. Izv. vuzov SSSR, seriya fizika, 1967, No. 3, p. 138.
328. Zuyev, V.Ye. Izv. vuzov SSSR, seriya fizika, 1967, No. 10, p. 53.
329. Zuyev, V.Ye., Pokasov, V.V., Pkhalagov, Yu.A., Sosnin, A.V., and Khmelevtsov, S.S. Izv. Akad. Nauk SSSR, seriya fizika atmosfery i okeana, 1968, Vol. 4, No. 1, p. 63.
330. Antipov, B.A., Zuyev, V.Ye., and Sapozhnikova, V.A. Izv. vuzov SSSR, seriya fizika, 1967, No. 7, p. 142.
331. Antipov, B.A., Zuyev, V.Ye., and Sapozhnikova, V.A. Izv. vuzov SSSR, seriya fizika, 1967, No. 6, p. 158.
332. Edwards, B.N. and Burch, D.E. Journ. Opt. Soc. Amer., 1965, Vol. 55, No. 2, p. 174.
333. Chu, T.S. and Hogg, D.C. The Bell System Technical Journ., 1966, Vol. 45, No. 2, p. 301.
334. Long, R. and Lewis, T.H. In collection entitled: Lasers and Applications, Columbus, Ohio, USA, 1963, p. 209.
335. McCubbin, T.K. Jr. and Darone, R. Journ. Opt. Soc. Amer., 1966, Vol. 56, No. 4, p. 555.
336. Long, R.K. and McCoy, J.H. Journ. Opt. Soc. Amer., 1967, Vol. 57, No. 4, p. 570.
337. Howe, J.A. and McFarlane, R.A. Journ. Molecul. Spectrosc., 1966, Vol. 19, No. 2, p. 224.
338. Calfee, R.F. and Gates, D.M. Appl. Optics, 1966, Vol. 5, No. 2, p. 287.
339. Zuyev, V.Ye. and Tvorogov, S.D. Izv. vuzov SSSR, seriya fizika, 1965, No. 6, p. 84.
340. Plass, G.N. Appl. Optics, 1963, Vol. 2, No. 5, p. 515.
341. Plass, G.N. Transmittance Tables for Slant Paths in the Stratosphere, SSD-TDR-62-127, Vol. V, Space Systems Division, Air Force Systems Command, Los Angeles, Calif., (22 May 1963).
342. Plass, G.N. Appl. Optics, 1964, Vol. 3, No. 4, p. 479.
343. Makushkin, Yu.S. "Prikladnaya spektroskopiya," 1968, Vol. 8, No. 6, p. 1068.
344. Kondratyev, K.Y., Badinov, I.J., Gaevskaya, G.N., Nicolsky, G.A., and Shved, G.M. In collection entitled: "Les problems meteorologiques de la Stratosphere et de la mesosphere," (Meteorological Problems of the Stratosphere and the Mesosphere), Presses universitaires de France, 108, Boulevard Saint-Germain, Paris, 1966, p. 271. /468
345. Murcray, D.G., Murcray, F.H., and Williams, W.J. Journ. Opt. Soc. Amer., 1965, Vol. 55, No. 10, p. 1239.
346. Murcray, D.G., Murcray, F.H., Williams, W.J., and Leslie, F.E. Journ. Geophys. Res., 1960, Vol. 65, p. 11; Journ. Optic.

Soc. Amer., 1961, Vol. 51, No. 2, p. 186.
347. Murcray, D.G., Murcray, F.H., and Williams, W.J. Journ. Geophys. Res., 1962, Vol. 67, No. 2, p. 759.
348. Neporent, B.S. and Kiseleva, M.S. "Optika i spektroskopiya," 1964, Vol. 16, No. 5, p. 803.
349. Yates, D.M. Journ. Optic. Soc. Amer., 1960, Vol. 50, No. 12, p. 1299.
350. Yates, D.M. and Harrop, W.J. Appl. Optics, 1963, Vol. 2, No. 9, p. 887.
351. Houghton, J.T. and Seeley, J.S. Quart. Journ. Roy. Met. Soc., 1960, Vol. 86, No. 369, p. 358.
352. Houghton, J.T., Hughes, N.D.P., Moss, T.S., and Seeley, J.S. Phil. Trans. Roy. Soc., 1962, Vol. 254, No. 1043, p. 47.
353. Houghton, J.T. Quart. Journ. Roy. Meteor. Soc., 1963, Vol. 89, No. 381, p. 319.
354. Cumming, C. Stratospheric Composition from Infrared Solar Spectra. Thesis, International Symposium on Radiation Processes, Leningrad, 1964.
355. Stauffer, F. and Strong, J. Applied Optics, 1962, Vol. 1, No. 2, p. 129.
356. Brown, A.H. and Roberts, V. Journ. Sci. Instr., 1953, Vol. 30, No. 1, p. 5.
357. Jones, F.H. and Roberts, V. Proc. Roy. Soc., A, 1956, Vol. 236, No. 1205, p. 171.
358. Levin, L.M. Issledovaniya po fizike grubodispersnykh aerozoley (Studies in the Physics of Coarse-Disperse Aerosols), Izd-vo Akad. Nauk SSSR, 1961.
359. Borovikov, A.M. et al. In collection entitled: "Fizika oblakov," (The Physics of Clouds), Edited by Khrgian, A.Kh., Gidrometeoizdat, 1961.
360. Huang Mei-Yuan, Izv. Akad. Nauk SSSR, seriya geofizicheskaya, 1963, No. 2, p. 362.
361. Mason, B.J. "Fizika oblakov" (The Physics of Clouds), Gidrometeoizdat, 1961.
362. Rittberger, W. Archiv. für Meteorol., Geophys. und Bioklim., Ser. A, 1959, Vol. 11, No. 3, p. 333.
363. Best, A.C. Quart. Journ. Roy. Met. Soc., 1951, Vol. 77, p. 418.
364. Khrgian, A.Kh. and Mazin, I.P. Trudy Tsentral'noy aerologicheskoy observatorii (Transactions of the Central Aerological Observatory), 1952, No. 7, p. 56.
365. Borovikov, A.M. Trudy Tsentral'noy aerologicheskoy observatorii, 1948, No. 3, p. 3.
366. Levin, G.M. Dokl. Akad. Nauk SSSR, 1954, Vol. 94, No. 6, p. 1045.
367. Kolmogorov, A.N. Dokl. Akad. Nauk SSSR, 1941, Vol. 31, No. 2, p. 99.
368. Levin, L.M. Izv. Akad. Nauk SSSR, seriya geofizicheskaya, 1958, No. 10, p. 1211.
369. Shifrin, K.S. Trudy Glavnoy geofizicheskoy observatorii (Transactions of the Main Geophysical Observatory), 1955, No. 46, p. 5. /469
370. Fuks, N.A. Mekhanika aerozoley (Mechanics of Aerosols), Izd-vo Akad. Nauk SSSR, 1955.

371. D'yachenko, P.V. Trudy Glavnoy geofizicheskoy observatorii, 1959, No. 101, p. 3.
372. Khrgian, A.Kh. and Mazin, I.P. Trudy Tsentral'noy aerologicheskoy observatorii, 1956, No. 17, p. 36.
373. Dergach, A.L. Trudy Arkticheskogo i antarkticheskogo nauchno-issledovatel'skogo instituta (Transactions of the Arctic and Antarctic Scientific Research Institute), 1959, Vol. 228, p. 55.
374. Nikandrov, V.Ya. Trudy Arkticheskogo i antarkticheskogo nauchno-issledovatel'skogo instituta, 1959, Vol. 228, p. 146.
375. Dolgin, I.M. Trudy Arkticheskogo i antarkticheskogo nauchno-issledovatel'skogo instituta, 1962, Vol. 239, p. 5.
376. Voskresenskiy, A.I. Trudy Arkticheskogo i antarkticheskogo nauchno-issledovatel'skogo instituta, 1962, Vol. 239, p. 64.
377. Voskresenskiy, A.I. and Dergach, A.L. In collection entitled: Issledovaniye oblakov, osadkov i grozovogo elektrichestva (Research on Clouds, Precipitation, and Lightning), Izd-vo Akad. Nauk SSSR, 1961, p. 101.
378. Kazas, V.I. Izv. Akad. Nauk SSSR, seriya geofizicheskaya, 1963, No. 5, p. 805.
379. Arnulf, A., Bricard, T., Cure, E. and Veret, C. Journ. Opt. Soc. Amer., 1957, Vol. 47, No. 6, p. 491.
380. Wiener, F.M., Ball, J.H., and Gogos, C.M. Journ. Geoph. Res., 1961, Vol. 66, No. 11, p. 3974.
381. Eldridge, R.G. Journ. Meteorol., 1961, Vol. 18, No. 5, p. 671.
382. May, K.R. Quart. Journ. Roy. Met. Soc., 1961, Vol. 87, No. 374, p. 535.
383. Okita, T. Journ. Meteor. Soc. Japan, 1962, Vol. 40, No. 1, p. 39.
384. Eldridge, R.G. Journ. Atm. Sci., 1966, Vol. 23, No. 5, p. 605.
385. Mazin, I.P. and Skosyreva, V.D. Trudy Tsentral'noy aerologicheskoy observatorii, 1961, No. 36, p. 43.
386. Nikandrova, G.T. Trudy Glavnoy geofizicheskoy observatorii, 1962, No. 126, p. 70.
387. Selezneva, Ye.S. Meteorologiya i gidrologiya, 1948, No. 2.
388. Pedersen, K. and Todsen, M. Geophys. Publ., 1960, Vol. 21, No. 7.
389. Minervin, V.Ye. Trudy Tsentral'noy aerologicheskoy observatorii, 1961, No. 36, p. 62.
390. Schumacher, P. Journ. Aircraft, 1964, Vol. 1, No. 1.
391. Minervin, V.Ye. In collection entitled: Issledovaniye oblakov, osadkov i grozovogo elektrichestva (Research on Clouds, Precipitation and Lightning), Izd-vo Akad. Nauk SSSR, 1961, p. 91.
392. Borovikov, A.M., Mazin, I.P., and Nevzorov, A.N. Trudy Tsentralinoy aerologicheskoy observatorii, 1961, No. 36.
393. Borovikov, A.M., Mazin, I.P., and Nevzorov, A.N. Izv. Akad. Nauk SSSR, ser. fizika atmosfery i okeana, 1965, Vol. 1, No. 3, p. 291.
394. Okita, T. Tellus, 1961, Vol. 13, No. 4, p. 509.
395. Petrenchuk, O.P. and Drozdova, V.M. Trudy Glavnoy geofizicheskoy observatorii, 1966, No. 185, p. 117.

396. Junge, C.E. Advances in Geophys., 1958, Vol. 4, p. 1.
397. Makhon'ko, K.P. Izv. Akad. Nauk SSSR, seriya geofizicheskaya, /470
1963, No. 1, p. 183.
398. Twomey, S. and Severynse, G.T. Journ. Atm. S., 1964, Vol. 21, No. 5, p. 558.
399. Fedorov, M.M. Dokl. Akad. Nauk SSSR, 1958, Vol. 118, No. 4, p. 691.
400. Makhon'ko, K.P. Izv. Akad. Nauk SSSR, seriya geofizicheskaya, 1959, No. 8, p. 1235.
401. Spurny, K. and Pich, J. Studia Geophys. et Geolog., 1961, Vol. 5, No. 11, p. 85.
402. Hatch, T. and Choate, S.J. Frankl. Institute, 1929, Vol. 207.
403. Voegtlin, C. and Hodge, H. Pharmacology and Toxicology of Uranium Compounds, New York, 1949.
404. Podzimek, J. Studia Geoph. et Geolog., 1959, Vol. 3, No. 4.
405. Podzimek, J. and Cernoch, I. Geoph. Pure et Appl., 1961, Vol. 50, No. 3, p. 96.
406. Junge, C.E. Journ. Meteorol., 1955, Vol. 12, p. 13.
407. Laktionov, A.G. Izv. Akad. Nauk SSSR, seriya geofizicheskaya, 1958, No. 3, p. 419.
408. Laktionov, A.G. Izv. Akad. Nauk SSSR, seriya geofizicheskaya, 1960, No. 4, p. 566.
409. Plass, G.N. Appl. Optics, 1966, Vol. 5, No. 1, p. 149.
410. Okita, T. Journ. Meteorol. Soc. Japan, 1957, Vol. 35, No. 2.
411. Junge, C.E., Chagnon, C.W., and Manson, J.E. Science, 1961, Vol. 133, No. 3463, p. 1478.
412. Junge, C.E. and Manson, J.E. Journ. Geoph. Res., 1961, Vol. 66, No. 7, p. 2163.
413. Friedlander, C.K. Journ. Meteorol., 1960, Vol. 17, No. 3, p. 373; 1961, Vol. 18, No. 6, p. 753.
414. Idlis, G.M. Izv. Astrofizicheskogo instituta Akad. Nauk KazSSR, 1957, Vol. 4, Nos. 5-6, p. 3.
415. Goetz, A., Priening, O. and Kallai, T. Geophys. Pure et Appl., 1961, Vol. 50, No. 3, pp. 67, 79.
416. Khrgian, A.Kh. Fizika atmosfery (Atmospheric Physics), Gostekhizdat, 1953.
417. Laktionov, A.G. Izv. Akad. Nauk SSSR, seriya geofizicheskaya, 1960, No. 9, p. 1397.
418. Gayvoronskiy, I.I. Trudy Tsentral'noy aerologicheskoy observatorii, 1949, No. 4, p. 46.
419. Penndorf, R. Journ. Meteorol., 1954, Vol. 11, No. 3, p. 245.
420. Selezneva, Ye.S. and Yudin, M.I. Trudy Glavnoy geofizicheskoy observatorii, 1960, No. 105, p. 37.
421. Selezneva, Ye.S. In collection entitled: "Issledovaniye oblakov, osadkov i grozovogo elektrichestva" (Studies of Clouds, Precipitation, and Lightning), Izd-vo Akad. Nauk SSSR, 1961, p. 96; Trudy Glavnoy geofizicheskoy observatorii, 1962, No. 134, p. 3.
422. Dergach, A.L. Trudy Glavnoy geofizicheskoy observatorii, 1960, No. 105, p. 30.
423. Junge, C.E., Chagnon, C.W., and Manson, J.E. Journ. Meteorol., 1961, Vol. 18, No. 1, p. 81.

424. Chagnon, C.W. and Junge, C.E. Journal Meteorology, 1961, Vol. 18, No. 6, p. 746.
425. Manson, J.E., Junge, C.E., and Chagnon, C.W. Chem. Reactions Lower and Upper Atmosphere, New York-London, Interscience, 1962, p. 139.
426. Junge, C.E. Journ. Meteorol., 1961, Vol. 18, No. 4.
427. Durbin, W.S. Geoph. Pure et Appl., 1959, Vol. 42, No. 1, p. 11. /471
428. Durbin, W.S. and White, G.D. Tellus, 1961, Vol. 13, No. 2, p. 260.
429. Singleton, F., and Durbin, W.G. Quart. Journ. Roy. Meteor. Soc., 1961, Vol. 88, No. 377, p. 315.
430. Wright, F.W. and Hodge, P.W. Nature, 1962, Vol. 195, No. 4838, p. 269.
431. Laktionov, A.G. Trudy Vsesoyuznogo naùchnogo meteorologicheskogo soveshchaniya (Transactions of All-Union Scientific Meteorological Conference), Gidrometeoizdat, 1963, Vol. VI, p. 60.
432. Georgiyevskiy, Yu.S., Driving, A.Ya., et al. Prozhektornyy luch v atmosfere (The Searchlight Beam in the Atmosphere), Edited by Prof. G.V. Rozenberg, Izd-vo Akad. Nauk SSSR, 1960.
433. Rossler, F. and Vassy, E.C.R. Acad. Sci., 1962, Vol. 254, No. 11, p. 2041.
434. Mikirov, A.Ye. Dokl. Akad. Nauk SSSR, 1962, Vol. 142, No. 3, p. 587.
435. Gushchin, G.P. Trudy Glavnoy geofizicheskoy observatorii, 1960, No. 105, p. 43.
436. Rabinovich, Yu.I. Trudy Glavnoy geofizicheskoy observatorii, 1962, No. 125, p. 54.
437. Collis, R.T.H. and Ligda, M.G.H. Journ. Atmosph. Sci., 1966, Vol. 23, No. 2, p. 255.
438. Fiocco, G. and Grams, G. Journ. Atmosph. Sci., 1964, Vol. 21, No. 3, p. 323.
439. Deirmendjian, D. Journ. Geoph. Res., 1965, Vol. 70, No. 3.
440. Newkirk, G. and Kroening, J.L. Journ. Atmosph. Sci., 1965, Vol. 22, No. 5, p. 567.
441. Elterman, L. and Campbell, A.B. Journ. Atm. Sci., 1964, Vol. 21, No. 4, p. 457.
442. Elterman, L. Journ. Opt. Soc. Amer., 1965, Vol. 55, No. 11, p. 1583.
443. Elterman, L. Appl. Optics, 1966, Vol. 5, No. 11, p. 1769.
444. Elterman, L. An Atlas of Aerosol Attenuation and Extinction Profiles for the Troposphere and Stratosphere, Environmental Research Papers, No. 241, AFCRL, Mass., 1966.
445. Kondrat'yev, K.Ya., Nikol'skiy, G.A., and Yesipova, Ye.N. Izv. Akad. Nauk SSSR, seriya fizika atmosfery i okeana, 1966, Vol. 5, No. 4.
446. Newkirk, G.Jr., and Eddy, J.A. Journ. Atmosph. Sci., 1964, Vol. 21, No. 1, p. 35.
447. Elterman, L. Atmospheric Attenuation Model, 1964, in the Ultraviolet, Visible, and Infrared Regions for Altitudes to 50 km. Environmental Research Papers, No. 46, AFCRL, Mass. 1964.

448. Elterman L. Appl. Optics, 1964, Vol. 3, No. 6, p. 745.
449. Kelkar, V.N. Indian Journ. Meteor. and Geophys., 1962, Vol. 13, No. 2, p. 173.
450. Mason, B.J. and Andrews. Quart. Journ. Roy. Met. Soc., 1960, Vol. 86, p. 346.
451. Polyakova, Ye.A. and Shifrin, K.S. Trudy Glavnoy geofizicheskoy observatorii, 1953, No. 42, p. 84.
452. Polyakova, Ye.A. Trudy Glavnoy geofizicheskoy observatorii, 1957, No. 68, p. 92.
453. Polyakova, Ye.A. Trudy Glavnoy geofizicheskoy observatorii, 1960, No. 100, p. 45. /472
454. Marshall, T.S. and Palmer, W. Journ. Meteor., 1948, Vol. 5, No. 4, p. 165.
455. Zel'manovich, I.L. Trudy Glavnoy geofizicheskoy observatorii, 1960, No. 100, p. 58.
456. Tvorogov, S.D. Izv. vuzov SSSR, Seriya fizika, 1965, No. 3, p. 147.
457. Green, H.S. and Wolf, E. Proc. Phys. Soc., 1953, Vol. 66A, p. 1129.
458. Wolf, E. Proc. Phys. Soc., 1959, Vol. 74, p. 269.
459. Roman, P. Acta Phys. Hung., 1957, Vol. 4, p. 209.
460. Tvorogov, S.D. Izv. vuzov SSSR, seriya fizika, 1965, No. 3, p. 175.
461. Van de Hulst, H.C. Light Scattering by Small Particles, New York-London, 1957, Russian translation: Van-de-Khyulst, G. Rasseyaniye sveta malymi chastitsami, Edited by V.V. Sobolev, Izd-vo inostrannoy literatury, 1961.
462. Schiff, L.J. Phys. Rev., 1956, Vol. 103, p. 443.
463. Tatarskiy, V.I. Teoriya fluktuatsionnykh yavleniy pri rasprostranenii voln v turbulentnoy atmosfere (Theory of Fluctuation Phenomena in the Propagation of Waves in the Turbulent Atmosphere), Izd-vo Akad. Nauk SSSR, 1959.
464. Born, M. and Wolf, E. Principles of Optics, New York, 1959.
465. Sokolov, V.V. and Tvorogov, S.D. "Zhurnal prikladnoy spektroskopii," 1968, Vol. 8, No. 3, p. 493.
466. Landau, L.D. and Lifshits, Ye.M. Elektrodinamika sploshnykh sred (Electrodynamics of Continuous Media), Gostekhizdat, 1957.
467. Shifrin, K.S. Rasseyaniye sveta v mutnoy srede (Scattering of Light in a Turbid Medium), Gostekhizdat, 1951.
468. Tvorogov, S.D. Izv. vuzov SSSR, seriya fizika, 1961, No. 1, p. 87.
469. Shifrin, K.S. Trudy Glavnoy geofizicheskoy observatorii, 1951, No. 26, p. 83.
470. Johnson, J.C. and Terrell, J.R. Journ. Opt. Soc. Amer., 1955, Vol. 45, No. 6, p. 451.
471. Penndorf, R.B. Journ. Opt. Soc. Amer., 1956, Vol. 46, p. 1001; 1957, Vol. 47, p. 603, Journ. Meteor., 1956, Vol. 13, p. 219; Journ. Phys. Chem., 1958, Vol. 62, p. 1537.
472. Deirmendjian, D., Clasen, R., and Viezee, W. Journ. Opt. Soc. Amer., 1961, Vol. 51, No. 6, p. 620.
473. Stephens, J.J. and Gerhardt, J.R. Journ. Meteor., 1961, Vol. 18, No. 6, p. 818.

474. Herman, B.M. Quart. Journ. Roy. Met. Soc., 1962, Vol. 88, No. 376, p. 143.
475. Penndorf, R. Research in Aerosol Scattering in the Infrared, Sci. Rep. 5, Tech. Rep. RAD-TR-61-32, U.S. Dept. of Commerce, Office of Technical Services, 1961.
476. Irvine, W.M. Bull. Astronom. Inst. Netherlands, 1964, Vol. 17, No. 4, p. 266.
477. Irwine, W.M. Journ. Opt. Soc. Amer., 1965, Vol. 55, No. 1, p. 16.
478. Orchard. S.E. Journ. Opt. Soc. Amer., 1965, Vol. 55, No. 9, p. 1190.
479. Plass, G.N. Appl. Optics, 1966, Vol. 5, No. 2, p. 279.
480. Kattawar, G.W. and Plass, G.N. Appl. Optics, 1967, Vol. 6, No. 8, p. 1377. /473
481. Shifrin, K.S. and Zel'manovich, I.L. Tablitsy po svetorasseyaniyu. t. I., Uglovyye funktsii (Light Scattering Tables. Vol. I. Angle Functions), Gidrometeoizdat, 1966.
482. Shifrin, K.S. and Zel'manovich, I.L. Tablitsy po svetorasseyaniyu, t. II. Tablitsy matrits rasseyaniya i sostavlyayushchikh rasseyannogo polya (Light Scattering Tables. Vol. II. Tables of Scattering Matrices and Scattered-Field Components), Gidrometeoizdat, 1968.
483. Shifrin, K.S. and Zel'manovich, I.L. Tablitsy po svetorasseyanuyu. t. III. Koeffitsiyenty oslableniya, rasseyaniya i luchevogo davleniya (Light Scattering Tables. Vol. III, Attenuation, Scattering, and Light-Pressure Coefficients), Gidrometeoizdat, 1968.
484. Shifrin K.S. Izv. Akad. Nauk SSSR, seriya geofizicheskaya, 1952, No. 2, p. 15.
485. Kerker, M., Kratohvil, J.P., and Matijevic, E. Journ. Opt. Soc. Amer., 1962, Vol. 52, No. 5, p. 551.
486. Fenn, R.W. and Oser, H. Appl. Optics, 1965, Vol. 4, No. 11, p. 1504.
487. Kerker, M., Kauffman, L.H., and Farone, W.A. Journ. Opt. Soc. Amer., 1966, Vol. 56, No. 8, p. 1053.
488. Plass, G.N. Appl. Optics, 1965, Vol. 4, No. 12, p. 1616.
489. Deirmenjian, D. Quart. Journ. Roy. Met. Soc., 1960, Vol. 86, p. 371.
490. Penndorf, R. Journ. Opt. Soc. Amer., 1962, Vol. 52, No. 4, p. 402.
491. Clark. G.C. Journ. Opt. Soc. Amer., 1957, Vol. 47, No. 1.
492. Volz, F. Ber. Deut. Wetterd., 1954, Vol. 2, No. 13.
493. Penndorf, R. Journ. Opt. Soc. Amer., 1957, Vol. 47, No. 2, p. 176.
494. Foldy, L. Phys. Rev., 1945, Vol. 67, p. 107.
495. Lax, M. Rev. Mod. Phys., 1951, Vol. 23, p. 287; Phys. Rev., 1952, Vol. 85, p. 621.
496. Waterman, P.C. and Truell, R. Journ. Math. Phys., 1961, Vol. 2, p. 512.
497. Twersky, V. Journ. Math. Phys., 1962, Vol. 3, p. 700.
498. Gnedin, Yu.N. and Dolginov, A.Z. Zh. Eksp. Teor. Fiz., 1963, Vol. 45, p. 1136.

499. Gnedin, Yu.N. and Dolginov, A.Z. "Astronomicheskiy zhurnal," 1966, Vol. 43, p. 800.
500. Borovoy, A.G. Izv. vuzov SSSR, seriya fizika, 1966, No. 2, p. 175.
501. Borovoy, A.G. Izv. vuzov SSSR, seriya fizika, 1966, No. 6, p. 50.
502. Borovoy, A.G. Izv. vuzov SSSR, seriya fizika, 1967, No. 4, p. 97.
503. Borovoy, A.G. Izv. vuzov SSSR, seriya fizika, 1967, No. 5, p. 7.
504. Rozenberg, G.V. Usp. Fiz. Nauk, 1955, Vol. 56, No. 1, p. 77.
505. Malkova, V.S. Izv. Akad. Nauk SSSR, seriya fizika atmosfery i okeana, 1965, Vol. 1, No. 1, p. 109-113.
506. Gorchakov, G.I. Rozenberg, G.V. Izv. Akad. Nauk SSSR, seriya fizika atmosfery i okeana, 1965, Vol. 1, No. 12, p. 1279.
507. Gorchakov, G.I. Izv. Akad. Nauk SSSR, seriya fizika atmosfery i okeana, 1966, Vol. 2, No. 6, p. 595.
508. Levin, L.M. In collection entitled: "Issledovaniye po eksperi-/474 mental'noy i teoreticheskoy fizike" (Research in Experimental and Theoretical Physics), Memoirs of Academician G.S. Lansberg, Izd-vo Akad. Nauk SSSR, 1959, p. 121.
509. Shifrin, K.S. and Raskin, V.F. "Optika i spektroskopiya," 1961, Vol. 11, No. 2, p. 268.
510. Tvorogov, S.D. Izv. vuzov SSSR, seriya fizika, 1961, No. 1, p. 87.
511. Tvorogov, S.D. Izv. vuzov SSSR, seriya fizika, 1962, No. 4, p. 175.
512. Tvorogov, S.D. Izv. vuzov SSSR, seriya fizika, 1962, No. 3, p. 174.
513. Zuyev, V.Ye., Kabanov, M.V., Koshelev, B.P., Tvorogov, S.D., and Khmelevtsov, S.S. In collection entitled: "Aktinometriya i optika atmosfery" (Trudy V Mezhvedomstvennogo soveshchaniya po aktinometrii i optike atmosfery) (Actinometry and Atmospheric Optics (Transactions of Fifth Interdepartmental Conference on Actinometry and Atmospheric Optics)), Edited by G.V. Rozenberg, Izd-vo "Nauka," 1964.
514. Zuyev, V.Ye., Kabanov, M.V., Koshelev, B.P., Tvorogov, S.D., and Khmelevtsov, S.S. Izv. vuzov SSSR, seriya fizika, 1964, No. 3, p. 92.
515. Tvorogov, S.D. Izv. vuzov SSSR, seriya fizika, 1965, No. 3, p. 147.
516. Zuyev, V.Ye. and Tvorogov, S.D. Izv. vuzov SSSR, seriya fizika, 1966, No. 2, p. 143.
517. Deirmenjian, D. Appl. Opt., 1964, Vol. 3, No. 2, p. 187.
518. Centeno, M. Journ. Opt. Soc. Amer., 1941, Vol. 31, p. 244.
519. Sonchik, V.K., Lopasov, V.P., and Chernyavskaya, N.A. In collection entitled: "Trudy mezhvuzovskogo soveshchaniya po spektral'noy prozrachnosti atmosfery v vidimoy i infrakrasnoy oblasti (iyun' 1965 g) (Transactions of Interinstitute Conference on the Spectral Transparency of the Atmosphere in the Visible and Infrared Regions (June 1965)), Izd-vo Tomskogo Gosudarstvennogo Universiteta, 1958.

520. Zuyev, V.Ye., Lopasov, V.P., and Sonchik, V.K. Izv. Akad. Nauk SSSR, seriya fizika atmosfery i okeana, 1967, Vol. 3, No. 1, p. 16.
521. Zuyev, V.Ye. and Sonchik, V.K. Izv. Akad. Nauk SSSR, seriya fizika atmosfery i okeana, 1969, Vol. 5, No. 7, p. 745.
522. Rubens, H. and Ladenburg, E. Verh. D. Ges., 1909, Vol. 11, No. 16.
523. Kislovskiy, L.F. "Optika i spektroskopiya," 1959, Vol. 7, No. 3, p. 311.
524. Kondrat'yev, K.Ya., Burgova, M.P., Gaynulin, I.F., and Togunova, G.F. In collection entitled: "Problemy fiziki atmosfery," (Problems of Atmospheric Physics), No. 2, Izv. LGU, 1963.
525. Zuyev, V.Ye., Sokolov, V.V., and Tvorogov, S.D. Doklad na Vsesoyuznom mezhvedomstvennom soveshchanii po rasseyaniyu sveta v atmosfere (Paper Presented at All-Union Interdepartmental Conference on the Scattering of Light in the Atmosphere), Chernovtsy, 1967.
526. Zuyev, V.Ye., Kabanov, M.V., Koshelev, B.P., Tvorogov, S.D., and Khmelevtsov, S.S. Izv. vuzov SSSR, seriya fizika, 1964, No. 2, p. 90.
527. Zuyev, V.Ye., Koshelev, B.P. Tvorogov, S.D., and Khmelevtsov, S.S. Izv. vuzov SSSR, seriya fizika, 1966, No. 3, p. 121.
528. Zuyev, V.Ye., Koshelev, B.P., Tvorogov, S.D., and Khmelevtsov, S.S., Izv. Akad. Nauk SSSR, seriya fizika atmosfery i okeana, 1965, No. 5, p. 509.
529. Koshelev, B.P. Izv. vuzov SSSR, seriya fizika, 1966, No. 3, p. 126. /475
530. Arnulf, A. and Bricard, J. Beit. Phys. Atmosph., 1960, Vol. 33, No. 1/2, p. 9.
531. Kurnick, S.W., Zitter, R.N., and Williams, D.W. Journ. Opt. Soc. Amer., 1960, Vol. 50, p. 578.
532. Gates, D.M. and Shaw, C.D. Journ. Opt. Soc. Amer., 1960, Vol. 50, p. 876.
533. Bocharov, Ye.I. Izv. Akad. Nauk SSSR, seriya geofizicheskaya, 1958, No. 5, p. 678.
534. Zabrodskiy, G.M. and Morachevskiy, V. G. Trudy Arkticheskogo i antarkticheskogo instituta, voprosy fiziki oblakov i tumanov (Transactions of the Arctic and Antarctic Institute, Problems of the Physics of Clouds and Fogs), 1959, Vol. 228, No. 1, p. 68.
535. Zabrodskiy, G.M. Trudy Arkticheskogo i antarkticheskogo instituta, voprosy fiziki oblakov i tumanov, 1962, Vol. 239, No. 2, p. 48; Trudy Vsesoyuznogo nauchnogo meteorologicheskogo soveshchaniya (Transactions of All-Union Scientific Meteorological Conference), 1963, Vol. VI, p. 102.
536. Trappenberg, R. Arch. Meteor., Geoph., Biokl., A.12, 1960, No. 1, p. 125.
537. McCubbin, T.K. Journ. Opt. Soc. Amer., 1952, Vol. 42, p. 876.
538. Rozenberg, G.V. Izv. Akad. Nauk SSSR, seriya fizika atmosfery i okeana, 1967, Vol. 3, No. 9, p. 936.
539. Sharonov, V.V. Izmereniye i raschet vidimosti dalekikh predmetov (Measurement and Calculation of the Visibility of

Distant Objects), Gostekhizdat, 1947.
540. Shifrin, K.S., and Raskin, V.F. Trudy Glavnoy geofizicheskoy observatorii, 1960, No. 100, p. 3.
541. Shifrin, K.S. and Raskin, V.F. In collection entitled: "Aktinometriya i atmosfernaya optika" (Actinometry and Atmospheric Optics), Gidrometeoizdat, 1961, p. 178.
542. Shifrin, K.S. and Raskin, V.F. Trudy Glavnoy geofizicheskoy observatorii, 1961, No. 109, pp. 155, 161.
543. Zuyev, V.Ye., Sokolov, V.V., and Tvorogov, S.D. Izv. vuzov SSSR, seriya fizika, 1966, No. 3, p. 7.
544. Zuyev, V.Ye., Sokolov, V.V., and Tvorogov, S.D. Izv. vuzov SSSR, seriya fizika, 1969, No. 1, p. 107.
545. Popov, O.I. "Optika i spektroskopiya," 1957, Vol. 3, No. 4, p. 504.
546. Curcio, J. Journ. Opt. Soc. Amer., 1961, Vol. 51, No. 5, p. 548.
547. Knestrick, G.L. Cosden, T.H., and Curcio, J.A. Journ. Opt. Soc. Amer., 1962, Vol. 52, No. 9, p. 1010.
548. Passman, S. and Larmore, L. Proc. IRIS, 1956, Vol. 1, No. 2, p. 15.
549. Junge, C. Gerlands Beit. Geoph., 1935, Vol. 46, p. 108.
550. Wright, H.L. Quart. Journ. Roy. Met. Soc., 1940, Vol. 66, p. 66.
551. Boilean, A.R. Scripps Institute of Oceanography, University of California, Feb. 1959, p. 1.
552. Buma, T.J. Bull. Amer. Meteor. Soc., 1960, Vol. 41, p. 357.
553. Middleton, W.E.K. Vision Through the Atmosphere, The University of Toronto Press, Toronto, 1952, Chap. 3, p. 24.
554. Georgiyevskiy, Yu.S. Izv. Akad. Nauk SSSR, seriya fizika atmosfery i okeana, 1966, Vol. 2, No. 5, p. 494.
555. Shifrin, K.S. and Minin, I.N. Trudy Glavnoy geofizicheskoy observatorii, 1957, No. 68, p. 5.
556. Faraponova, G.P. Trudy Tsentral'noy aerologicheskoy observatorii, 1957, No. 23, p. 52; 1959, No. 32, p. 3. /476
557. Handbook of Geophysics and Space Environments AFCRL, Office of Aerospace Research US Air Force, 1965.
558. Rabinovich, Yu.I. In collection entitled: "Aktinometriya i atmosfernaya optika" (Actinometry and Atmospheric Optics), 1961, Gidrometeoizdat, p. 146; Trudy Glavnoy geofizicheskoy observatorii, 1961, No. 118, p. 18.
559. Rabinovich, Yu.I. and Guseva, L.N. Trudy Glavnoy geofizicheskoy observatorii, 1961, No. 118, p. 69.
560. "Atmosfernyy ozon" (Atmospheric Ozone), Edited by G.P. Gushchin, Materialy III. Mezhduvedomstvennogo soveshchaniya po atmosfernomu ozonu 21-23 maya 1963 g (Materials of 3rd Interdepartmental Conference on Atmospheric Ozone, May 21-23, 1963), Gidrometeoizdat, 1965.
561. Gushchin, G.P. In collection entitled: "Aktinometriya i atmosfernaya optika," Gidrometeoizdat, 1961, p. 218.
562. Gushchin, G.P. Issledovaniye atmosfernogo ozona (Investigation of Atmospheric Ozone), Gidrometeoizdat, 1963.
563. Penndorf, R. Journ. Meteor., 1954, Vol. 11, No. 3.

564. Packer, D. and Lock, C. Journ. Opt. Soc. Amer., 1951, Vol. 41, No. 7.
565. Toropova, T.P. Izv. Astrofizicheskogo instituta Akad. Nauk KazSSR, 1960, Vol. 10, p. 71.
566. Zuyev, V.Ye., Kabanov, M.V., and Pkhalagov, Yu.A. Izv. Akad. Nauk SSSR, seriya fizika atmosfery i okeana, 1968, Vol. 4, No. 7, p. 778.
567. Driving, A.Ya., and Smirnova, A.I. Izv. Akad. Nauk SSSR, seriya geofizicheskaya, 1958, No. 3, p. 337.
568. Schmolinsky, F. Meteor. Zeit., 1944, Vol. 61, No. 6.
569. Foitzik, L. and Zskhaeck, H. Zeit. für Meteorol., 1953, Vol. 7. No. 1, p. 1.
570. Polyakova, Ye.A. Tret'yakov, V.V. Trudy Glavnoy geofizicheskoy observatorii, 1960, No. 100, p. 53.
571. Jefferson, G.J. Meteor. Mag., 1961, Vol. 90, No. 1067, p. 163.
572. Shifrin, K.S. and Chayanova, E.A. Trudy Glavnoy geofizicheskoy observatorii, 1965, No. 170, p. 93.
573. Shifrin, K.S., Perel'man, A.Ya., and Punina, V.A. Trudy Glavnoy geofizicheskoy observatorii, 1966, No. 183, p. 18.
574. Barteneva, O.D. Izv. Akad. Nauk SSSR, seriya geofizicheskaya, 1960, No. 12, p. 1852.
575. Belov, V.F. Izmereniye osnovnykh opticheskikh kharakteristik prizemnogo sloya vozdukha (Measurement of the Basic Optical Characteristics of the Ground Layer of Air), Gidrometeoizdat, 1956.
576. Hulbert, E.O. Journ. Opt. Soc. Amer., 1941, Vol. 31.
577. Bullrich, K. Meteor. Zeit., 1944, Vol. 61, p. 270.
578. Bullrich, K. and Möller, F. Optik, 1947, Vol. 2.
579. Reger, E. and Siedentopf, Optik, 1946, Vol. 1, p. 15.
580. Barteneva, O.D. and Bashilov, G.Ya. Izv. Akad. Nauk SSSR, seriya geofizicheskaya, 1961, No. 4, p. 613.
581. Toropova, T.P. Izv. Astrofizicheskogo instituta Akad. Nauk KazSSR, 1959, Vol. 9, p. 108.
582. Boyko, P.N., Lifshits, G.Sh., and Toropova, T.P. Izv. astrofizicheskogo instituta Akad. Nauk KazSSR, 1959, Vol. 8, p. 98.
583. Pyaskovskaya-Fesenkova, Ye.V. Issledovaniya rasseyaniya sveta /477 v zemnoy atmosfere (Studies of Light Scattering in the Earth's Atmosphere), Izd-vo Akad. Nauk SSSR, 1957.
584. Kastrov, V.G. Trudy Tsentral'noy aerologicheskoy observatorii, 1959, No. 32, p. 84.
585. Lyubovtseva, Yu.S. and Rozenberg, G.V. Izv. Akad. Nauk SSSR, seriya fizika atmosfery i okeana, 1966, Vol. 2, No. 3, p. 248.
586. Belov, V.F. Trudy Tsentral'noy aerologicheskoy observatorii (Transactions of the Central Aerological Observatory), 1957, No. 23, p. 63; Trudy Vsesoyuznogo nauchnogo meteorologicheskogo soveshchaniya (Transactions of All-Union Scientific Meteorological Conference), 1963, Vol. VI, p. 52.
587. Chayanov, B.A. Trudy Tsentral'noy aerologichesnoy observatorii, 1959, No. 32, p. 17.
588. Kompaniyets, A.I. Izv. Akad. Nauk SSSR, seriya fizika atmospery i okeana, 1965, Vol. 1, No. 3, p. 335.

589. Bullrich, K. Adv. in Geophys., 1964, Vol. 10, p. 101.
590. Kabanov, M.V. In collection entitled: Trudy Mezhvuzovskogo soveshchaniya po spektral'noy prozrachnosti atmosfery v vidimoy i infrakrasnoy oblasti (iyun' 1965 g) (Transactions of Interinstitute Conference on the Spectral Transparency of the Atmosphere in the Visible and Infrared Regions (June 1965)), Izd-vo Tomskogo gosudarstvennogo universiteta, 1968.
591. Carrier, L.W. and Nugent, L.J. Appl. Optics, 1965, Vol. 4, No. 11, p. 1457.
592. Bukatyy, V.I., Kabanov, M.V., Koshelev, B.P., Smirnov, B.A., Savel'yev, B.A., and Khmelevtsov, S.S. Izv. vuzov SSSR, seriya fizika, 1967, No. 8, p. 139.
593. Woodward, D.H. Appl. Optics, 1963, Vol. 2, No. 11, p. 1205.
594. Harris, F.S. Jr., Sherman, G.C. and Morse, E.L. IEEE Transactions on Antennas and Propagation, 1967, Vol. AP-15, No. 1, p. 141.
595. Sinclair, D. Journ. Opt. Soc. Amer., 1947, Vol. 37, p. 475.
596. Brillouin, L. Journ. Appl. Phys., 1949, Vol. 20, No. 11, p. 1110.
597. Gumprecht, R.O. and Sliepcevich, C.M. Journ. Phys. Chem., 1953, Vol. 57, p. 90.
598. King, R. and Wu-T'ai Tsun. Rasseyaniye i difraktsiya elektromagnitnykh voln (Scattering and Diffraction of Electromagnetic Waves), Izd-vo inostrannoy literatury, 1962.
599. Polyakova, Ye.A. Trudy Glavnoy geofizicheskoy observatorii, 1957, No. 68, p. 88.
600. Timofeyeva, V.A. Trudy morskogo gidrofizicheskogo instituta (Transactions of Marine Hydrophysical Institute), 1953, Vol. 3, p. 35.
601. Timofeyeva, V.A. and Koveshnikova, L.A. Izv. Akad. Nauk SSSR, seriya fizika atmosfery i okeana, 1966, Vol. 2, No. 3, p. 320.
602. Kabanov, V.A. In collection entitled: "Aktinometriya i optika atmosfery" (Trudy V Mezhvedomstvennogo soveshchaniya po aktinometrii i optike atmosfery) (Actinometry and Atmospheric Optics (Transactions of Fifth Interdepartmental Conference on Actinometry and Atmospheric Optics)) Edited by G.V. Rozenberg, Izd-vo "Nauka," 1964.
603. Middleton, W.E.K. Journ. Opt. Soc. Amer., 1949, Vol. 39, No. 7.
604. Stewart, H.S. and Curcio, J.A. Journ. Opt. Soc. Amer., 1952, Vol. 42, p. 801.
605. Gibbons, M.G. Journ. Opt. Soc. Amer., 1958, Vol. 48, p. 550; 1959, Vol. 49, p. 702.
606. Gibbons, M.G., Nichols, J.R., Laughridge, F.I., and Rudkin. /478
Journ. Opt. Soc. Amer., 1961, Vol. 51, p. 633.
607. Gibbons, M.G., Laughridge, F.I., Nichols, J.R., and Krause, N.A. Journ. Opt. Soc. Amer., 1962, Vol. 52, p. 38.
608. Meshkov, V.V. Osnovy svetotekhniki (Fundamentals of Illumination Engineering), Part 1, Gosenergoizdat, 1957.
609. Eldridge, R.G. and Johnson, J.C. Journ. Opt. Soc. Amer., 1958, Vol. 48, p. 463.

610. Eldridge, R.G. and Johnson. J.C. Journ. Opt. Soc. Amer., 1962, Vol. 52, p. 787.
611. Zuyev, V.Ye., Kabanov, M.V., and Borovoy, A.G. Izv. vuzov SSSR, seriya fizika, 1963, No. 6, p. 162.
612. Zuyev, V.Ye. and Kabanov, M.V. Izv. vuzov SSSR, seriya fizika, 1964, No. 1, p. 168.
613. Zuyev, V.Ye., Kabanov, M.V., and Savel'yev, B.A. Izv. vuzov SSSR, seriya fizika, 1964, No. 5, p. 80.
614. Zuyev, V.Ye. and Kabanov, M.V. In collection entitled: "Aktinometriya i optika atmosfery" (Trudy V Mezhvedomstvennogo soveshchaniya po aktinometrii i optike atmosfery). Editor: G.V. Rozenberg, Izd-vo "Nauka," 1964.
615. Zuyev, V.Ye. and Kabanov, M.V. Izv. vuzov SSSR, seriya fizika, 1965, No. 6, p. 175.
616. Smirnov, V.I. Kurs vysshey matematiki (Textbook of Higher Mathematics), Vol. 2, Gostekhizdat, 1948.
617. Ivanov, A.P. and Khayrullina, A.Ya. Izv. Akad. Nauk SSSR, seriya fizika atmosfery i okeana, 1966, Vol. 2, No. 7, p. 721.
618. Hodkinson, J.R. and Greenfield, J.R. Appl. Optics, 1965, Vol. 4, No. 11, p. 1463.
619. Prokhorov, A.M. Usp. Fiz. Nauk, 1965, Vol. 85, p. 599.
620. Basov, N.G. Usp. Fiz. Nauk, 1965, Vol. 85, p. 585.
621. Akhmanov, S.A. and Khokhlov, R.V. Usp. Fiz. Nauk, 1966, Vol. 88, No. 3, p. 439.
622. Meyman, "Elektronika," 1965, Vol. 38, No. 8, p. 55.
623. Tauns, Ch. Usp. Fiz. Nauk, 1966, Vol. 88, No. 3, p. 461.
624. Kalinskiy, A.A. and Osiko, V.V. Izv. Akad. Nauk SSSR, seriya neorganicheskiye materialy, 1965, Vol. 1, No. 12, p. 2049.
625. Kiss, Z.J. and Pressley, R.J. TIIER (Trans. IEEE in Russian translation), 1966, Vol. 54, No. 10, p. 7.
626. Bridges, W.B. and Chester, A.N. Appl. Optics, 1965, Vol. 4, No. 5, p. 573.
627. Johnson. "Elektronika," 1966, Vol. 39, No. 8, p. 3.
628. Kiss, Z.J. and Pressley, R.J. Appl. Optics, 1966, Vol. 5, No.10, p. 1474.
629. Snitzer, E. Appl. Optics, 1966, Vol. 5, No. 10, p. 1487.
630. Bloom, A.L. Appl. Optics, 1966, Vol. 5, No. 10, p. 1500.
631. Nathan, M.I. Appl. Optics, 1966, Vol. 5, No. 10, p. 1514.
632. Khokhlov, R.V. Usp. Fiz. Nauk, 1965, Vol. 87, p. 17.
633. Pimental, G.S. Scientific Americ., 1966, Vol. 214, No. 4, p. 32.
634. "Opticheskiye kvantovyye generatory. Noveyshiye issledovaniya i primeneniya opticheskoy kvantovoy elektroniki" (Lasers. Current Research on and Applications of Optical Quantum Electronics), Collected papers edited by F.V. Bunkin, Izd-vo "Mir," 1966.
635. Labuda, E.F., Gordon, E., Miller, R.C. IEEE Journ. Quant. Electron., 1965, Vol. 1, No. 6, p. 273. /479
636. Polanyi, I.C. Appl. Optics, 1965, Suppl., No.2, p. 109.
637. Paananen, R.A. IEEE Spectrum, 1966, Vol. 3, No. 6, p. 88.
638. Bogoroditskiy, N.P., Pikhtin, A.N., and Yas'kov D.A. "Izvestiya Leningradskogo elektrotekhnicheskogo instituta,"

1966, Vol. 57, No. 21, p. 3.
639. Patel, C.K.N. Chim. Phys. et Phys. Chim. Biocl., 1967, Vol. 64, No. 1, p. 82.
640. Walter, W.T., Solimene, N., Piltch, M., and Gould, G. IEEE Journ. Quant. Electron., 1966, Vol. 2, No. 9, p. 474.
641. Johnson, A.R.I. Laser Focus, 1966, Vol. 2, No. 17, p. 19.
642. Survey of Laser Products Microwaves, 1966, Vol. 5, No. 10, pp. 56, 58, 62.
643. Manger, H. Zeitschrift für angewandte Phys., 1965, Vol. 18, No. 4, p. 265.
644. Akhmanov, S.A., Kovrigin, A.I., Kolesov, V.A., Piskarskas, A. S., and Fadeyev, V.V. Pis'ma v Zh. Eksp. Teor. Fiz., 1966, Vol. 3, No. 9, p. 372.
644a. Danileyko, M.V., Kravchenko, V.I., Odulov, S.G., Pogorelyy, O.N., and Soskin, M.S. "Ukrainskiy fizicheskiy zhurnal," 1967, Vol. 12, No. 4, p. 669.
645. Müller, R.C. and Nordland, W.A. Appl. Phys. Letters, 1967, Vol. 10, No. 2, p. 53.
646. Sobolev, V.V. Perenos luchistoy energii v atmosferakh zvezd i planet (Transfer of Radiant Energy in the Atmospheres of Stars and Planets), Gostekhizdat, 1956.
647. Wang, M.C. and Guth, E. Phys. Rev. 1951, Vol. 84, No. 6, p. 1092.
648. Romanova, L.M. "Optika i spektroskopiya," 1962, Vol. 13, No. 3, p. 429.
649. Romanova, L.M. "Optika i spektroskopiya," 1962, Vol. 13, No. 6, p. 819.
650. Kabanov, M.V. and Savel'yev, B.A. Izv. Akad. Nauk SSSR, seriya fizika atmosfery i okeana, 1967, Vol. 3, No. 6, p. 658.
651. Gershun, A.A. Izbrannyye trudy po fotometrii i svetotekhnike (Selected Works in Photometry and Illumination Engineering), Fizmatgiz, 1958.
652. Feygel'son, Ye.M. Radiatsionnyye protsessy v sloistoobraznykh oblakakh (Radiation Processes in Stratiform Clouds), Izd-vo "Nauka," 1964.
653. Dolin, L.S. Izv. vuzov SSSR, seriya Radiofizika, 1966, Vol. 9, No. 1, p. 61.
654. Kolesov, A.K. Vestnik LGU, seriya matematika, mekhanika, astronomiya, 1966, No. I, p. 160.
655. Marchuk, G.I. and Mikhaylov, G.A. Izv. Akad. Nauk SSSR, seriya fizika atmosfery i okeana, 1967, Vol. 3, No. 3, p. 258.
656. Kabanov, M.V. Izv. vuzov SSSR, seriya fizika, 1967, No. 8, p. 26.
657. Penndorf, R.B. Journ. Opt. Soc. Amer., 1962, Vol. 52, No. 7, p. 797.
658. Krekov, G.M., Mikhaylov, G.A., and Kargin, B.A. Izv. vuzov SSSR, seriya fizika, 1968, No. 4, p. 110.
659. Krekov, G.M., Mikhaylov, G.A., and Kargin, B.A. Izv. vuzov SSSR, seriya fizika, 1968, No. 5, p. 54.
660. Zuyev, V.Ye., Kabanov, M.V., and Savel'yev, B.A. Dokl. Akad. Nauk SSSR, 1967, Vol. 175, No. 2, p. 327. /480

661. Zuyev, V.Ye., Kabanov, M.V., and Savel'yev, B.A. Izv. Akad. Nauk SSSR, seriya fizika atmosfery i okeana, 1967, Vol. 3, No. 7, p. 724.
662. Kabanov, M.V, and Savel'yev, B.A. Izv. Akad. Nauk SSSR, seriya fizika atmosfery i okeana, 1968, Vol. IV, No. 9, p. 960.
663. Kabanov, M.V., Savel'yev, B.A., and Fadeyev, V.Ya. Izv. vuzov SSSR, seriya fizika, 1967, No. 7, p. 140.
664. Savel'yev, B.A. Izv. vuzov SSSR, seriya fizika, 1967, No. 12, p. 135.
665. Savel'yev, B.A. Izv. vuzov SSSR, seriya fizika, 1967, No. 12, p. 136.
666. Timofeyeva, V.A. Trudy morskogo gidrofizicheskogo instituta, 1953, Vol. 3, p. 35.
667. Timofeyeva, V.A. Dokl. Akad. Nauk SSSR, 1957, Vol. 113, p. 556.
668. Timofeyeva, V.A. Izv. Akad. Nauk, SSSR, seriya geofizicheskaya, 1957, No. 2, p. 265.
669. Rozenberg, G.V. Dokl. Akad. Nauk SSSR, 1962, Vol. 145, No. 4, p. 775.
670. Ivanov, A.P. and Makarevich, S.A. Izv. Akad. Nauk SSSR, seriya geofizicheskaya, 1963, No. 11, p. 1754.
671. Ivanov, A.P. and Sherbaf, I.D. Dokl. Akad. Nauk Belorusskoy SSR, 1963, Vol. 7, No.10, p. 673.
672. Ivanov, A.P. and Sherbaf, I.D. In collection entitled "Aktinometriya i optika atmosfery" (Actinometry and Atmospheric Optics), Izd-vo "Nauka," 1964.
673. Ivanov, A.P. and Il'ich, G.K. Dokl. Akad. Nauk Belorusskoy SSR, 1965, Vol. 9, No. 5, p. 301.
674. Ivanov, A.P. and Sherbaf, I.D. Optika i spektroskopiya, 1965, Vol. 18, No. 14, p. 698.
675. Ivanov, A.P. and Il'ich, G.K. Dokl. Akad. Nauk Belorusskoy SSR, 1965, Vol. 9, No. 7, p. 438.
676. Ivanov, A.P. and Sherbaf, I.D. Izv. Akad. Nauk SSSR, seriya fizika atmosfery i okeana, 1966, Vol. 2, No. 3, p. 312.
677. Ivanov, A.P. and Sherbaf, I.D. "Zhurnal prikladnoy spektroskopii," 1966, Vol. 5, No. 2, p. 195.
678. Romanova, L.M. "Optika i spektroskopiya," 1963, Vol. 14, No. 2, p. 262.
679. Bartky, C.E. Appl. Optics, 1965, Vol. 4, No. 7, p. 847.
680. Twomey, S. and Howell, H.B. Appl. Optics, 1965, Vol. 4, No. 4. p. 501.
681. Fenn, R.W. Appl. Optics, 1966, Vol. 5, No. 2, p. 293.
682. Gavrilov, V.A. Vidimost' v atmosfere (Visibility in the Atmosphere), Gidrometeoizdat, 1965.
683. Shifrin, K.S. and Zel'manovich, I.L. Trudy Glavnoy geofizicheskoy observatorii, 1965, No. 170, p. 61.
684. Kozlov, V.P. and Fedorova, Ye.O. Optiko-mekhanicheskaya promyshlennost', 1967, Vol.1, No. 3, p. 1.
685. Munick, R.J. Journ. Opt. Soc. Amer., 1965, Vol. 55, No. 7, p. 893.
686. Donchenko, V.A., Kabanov, M.V., Savel'yev, B.A., and Samokhvalov, I.V. Izv. vuzov SSSR, seriya fizika, 1968, No. 1, p. 158.

687. Gilbert, G.D. and Pernika, J.C. Appl. Optics, 1967, Vol. 6, No. 4, p. 741. /481
688. Eiden, R. Appl. Optics, 1966, Vol. 5, No. 4, p. 569.
689. Timofeyeva, V.A. Izv. Akad. Nauk SSSR, seriya geofizicheskaya, 1961, No. 5, p. 766.
690. Timofeyeva, V.A. Dokl. Akad. Nauk SSSR, 1962, Vol. 147, No. 3, p. 604.
691. Timofeyeva, V.A., Vostroknutov, A.A. and Koveshnikova, L.A. Izv. Akad. Nauk SSSR, seriya fizika atmosfery i okeana, 1966, Vol. 2, No. 12, p. 1259.
692. Kabanov, M.V., Savel'yev, B.A., and Samokhvalov, I.V. Izv. Akad. Nauk SSSR, seriya fizika atmosfery i okeana, 1968, Vol. 4, No. 10.
693. Romanova, L.M. Izv. Akad. Nauk SSSR, seriya fizika atmosfery i okeana, 1965, Vol. 1, No. 6, p. 599.
694. Romanova, L.M. Izv. Akad. Nauk SSSR, seriya fizika atmosfery i okeana, 1965, Vol. 1, No. 10, p. 1022.
695. Romanova, L.M. Izv. Akad. Nauk SSSR, seriya fizika atmosfery i okeana, 1966, Vol. 2, No. 8, p. 844.
696. Nesmelova, L.I. and Tvorogov, S.D. Izv. vuzov SSSR, seriya fizika, 1967, No. 5, p. 141.
697. Bebb, H.B. and Gold, A. Phys. Rev., 1966, Vol. 143, No. 1, p. 1.
698. Cohan, N.V. and Hameka, H.F. Phys. Rev., 1966, Vol. 151, No. 4, p. 1076.
699. Tauns, Ch. and Shavlov, A. Radiospektroskopiya (Radiospectroscopy), Izd-vo inostrannoy literatury, 1959.
700. Karplus, R. and Schwinger, J. Phys. Rev., 1949, Vol. 73, No. 9, p. 1020.
701. Akhmanov, S.A. and Khokhlov, R.V. Usp. Fiz. Nauk, 1968, Vol. 95, No. 1, p. 231.
702. Zuyev, V.Ye. In collection entitled: "Yubileynyy sbornik trudov Tomskogo gosudarstvennogo universiteta po fizike," Izd-vo Tomskogo gosudarstvennogo universiteta, 1970.
703. Nesmelova, L.I. and Tvorogov, S.D. In collection entitled: "Trudy Mezhvuzovskogo soveshchaniya po spektral'noy prozrachnosti atmosfery v vidimoy i infrakrasnoy oblasti," Izd-vo Tomskogo gosudarstvennogo universiteta, 1968.
704. Landau, L.D. and Lifshits, Ye.M. Mekhanika (Mechanics), Fizmatgiz, 1966.
705. Askar'yan, G.A. Zh. Eksp. Teor. Fiz., pis'ma, 1966, Vol. 4, No. 10, p. 400.
706. Rayzer, Yu.P. Zh. Eksp. Teor. Fiz., pis'ma, 1966, Vol. 4, No. 1, p. 3.
707. Rayzer, Yu.P. Zh. Eksp. Teor. Fiz., pis'ma, 1966, Vol. 4, No. 4, p. 124.
708. Rayzer, Yu.P. Zh. Eksp. Teor. Fiz., pis'ma, 1966, Vol. 4, No. 8, p. 286.
709. Yankauskas, Z.K. Izv. vuzov SSSR, seriya Radiofizika, 1966, Vol. 9, No. 2, p. 412.
710. Litvak, A.G. Izv. vuzov SSSR, seriya Radiofizika, 1966, Vol. 9, No. 3, p. 629.

711. Shen. I.R. Journ. Opt. Soc. Amer., 1966, Vol. 56, No. 10, p. 1425.
712. Chiao, R.Y., Garmire, E., and Townes, C.H. Phys. Rev. Letters, 1964, Vol. 13, p. 479; erratum, Phys. Rev. Lett., 1965, Vol. 14, p. 1056.
713. Akhmanov, S.A., Sukhorukov, A.P., and Khokhlov, R.V. Zh. Eksp. Teor. Fiz., 1966, Vol. 50, No. 6, p. 1537.
714. Barkhudarova, G.M., Voronov, G.S., Gorbunkov, V.M., and Delone, N.B. Zh. Eksp. Teor. Fiz., 1965, Vol. 49, No. 2, p. 386.
715. Wang, C.C. Phys.Rev. Letters, 1966, Vol. 16, p. 344. /482
716. Akhmanov, S.A. and Khokhlov, R.V. Problemy nelineynoy optiki (Problems in Nonlinear Optics), Izd. Akad. Nauk SSSR, 1964.
717. Akhmanov, S.A., Sukhorukov, A.P., and Khokhlov, R.V. Usp. Fiz. Nauk, 1967, Vol. 93, No. 1, p. 19.
718. Zel'dovich, Ya.B. and Rayzer, Yu.P. Zh. Eksp. Teor. Fiz., pis'ma, 1966, Vol. 3, No. 3, p. 137.
719. Akhmanov, S.A., Krindach, D.P., Sukhorukov, A.P., and Khokhlov, R.V. Zh. Eksp. Teor. Fiz., pis'ma, 1967, Vol. 6, No. 2, p. 509.
720. Fuks, N.A. Ispareniye i rost kapel' v gazoobraznoy srede (Evaporation and Growth of Drops in a Gaseous Medium), Izd. Akad. Nauk SSSR, 1958.
721. Williams, T.A. Journ. Heat and Mass Transfer, 1965, Vol. 8, p. 575.
722. Shifrin, K.S. and Zolotova, Zh.K. Izv. Akad. Nauk SSSR, seriya fizika atmosfery i okeana, 1966, Vol. 2, No. 12, p. 1311.
723. Kuzikovskiy, A.V. and Khmelevtsov, S.S. Izv. Akad. Nauk SSSR, seriya fizika atmosfery i okeana, 1968, Vol. 4, No. 3, p. 363.
724. Kuzikovskiy, A.V. Izv. vuzov SSSR, seriya fizika, 1970, No. 5, p. 95.
725. Kuzikovskiy, A.V. and Khmelevtsov, S.S. Trudy IX Vsesoyuznoy konferentsii po rasprostraneniyu radiovoln (Transactions of Ninth All-Union Conference on Radio Wave Propagation), Khar'kov, 1969.
726. Chepmen, S. and Kauling, T. Matematicheskaya teoriya neodnorodnykh gazov (Mathematical Theory of Inhomogeneous Gases), Izd-vo inostrannoy literatury, 1960.
727. Bukatyy, V.I. and Pogodayev, V.A. Izv. vuzov SSSR, seriya fizika, 1970, No. 1, p. 141.
728. Bukatyy, V.I. and Khmelevtsov, S.S. Izv. vuzov SSSR, seriya Fizika, 1968, No. 1, p. 91.
729. Khodara, Trudy IIER (Trans. IEEE in Russian translation), Vol. 54, No. 3, p. 36.
730. Zaytsev, V.A. and Ledokhovich, A.A. Trudy Glavnoy geofizicheskoy observatorii, 1964, No. 156, p. 118.
731. Tatarskiy, V.I. Rasprostraneniye voln v turbulentnoy atmosfere (Wave Propagation in the Turbulent Atmosphere), Izd-vo "Nauka," 1967.
732. Obukhov, A.M. Izv. Akad. Nauk SSSR, seriya geofizicheskaya, 1949, Vol. 13, p. 58.

733. Bovsheverov, V.M., Gurvich, A.S., and Kalistratova, M.A. Izv. vuzov SSSR, seriya Radiofizika, 1961, Vol. 4, No. 5, p. 886.
734. Tsvang, L.R. Izv. Akad. Nauk SSSR, seriya geofizicheskaya, 1963, No. 10, p. 1594.
735. Kalistratova, M.A. Izv. vuzov SSSR, seriya Radiofizika, 1966, Vol. 9, No. 1, p. 50.
736. Golitsyn, G.S., Gurvich, A.S., and Tatarskiy, V.I. "Akusticheskiy zhurnal," 1960, Vol. 6, No. 2, p. 187.
737. Kon, A.I. and Tatarskiy, V.I. Izv. vuzov SSSR, seriya Radiofizika, 1965, Vol. 8, No. 5, p. 870.
738. Chernov, L.A. Rasprostraneniye voln v srede so sluchaynymi neodnorodnostyami (Wave Propagation in a Medium with Random Inhomogeneities), Izd. Akad. Nauk SSSR, 1958.
739. Feyzulin, Z.I. and Kravtsov, Yu.A. Izv. vuzov SSSR, seriya Radiofizika, 1967, Vol. 10, No. 1, p. 68.
740. Fried, D.L. Journ. Opt. Soc. Amer., 1967, Vol. 57, No. 2, p. 169.
741. Davis, J.I. Appl. Optics, 1966, Vol. 5, No. 1, p. 139. /483
742. Fried, D.L. Journ. Opt. Soc. Amer., 1966, Vol. 56, No. 10, p. 1372.
743. Fried, D.L. Journ. Opt. Soc. Amer., 1966, Vol. 56, No. 10, p. 1380.
744. Fried, D.L. and Schmeltzer, R.A. Applied Optics, 1967, Vol. 6, No. 10, p. 1729.
745. Fried, D.L. and Seidman, Journ. Opt. Soc. Amer., 1967, Vol. 57, No. 2, p. 181.
746. Munick, R.J. Journ. Opt. Soc. Amer., 1965, Vol. 55, No. 5, p. 594.
747. Straub, H.W. Appl. Optics, 1965, Vol. 4, No. 7, p. 875.
748. Shah, B.R. Journ. Opt. Soc. Amer., 1966, Vol. 56, No. 4, p. 559.
749. Consortini, A., Ronchi, L., Scheggi, A.M., and Toraldo di Francia, G. Radio Sci. Journ. Res., 1966, Vol. 1. p. 523.
750. Hufnagell, R.E. and Stanley, N.R. Journ. Opt. Soc. Amer., 1964, Vol. 54, p. 52.
751. Gracheva, M.Ye. and Gurvich, A.S. Izv. vuzov SSSR, seriya Radiofizika, 1965, Vol. 8, No. 4, p. 717.
752. Kon, A.I. and Tatarskiy, V.I. Izv. vuzov SSSR, seriya Radiofizika, 1964, Vol. 7, No. 2, p. 306.
753. Gurvich, A.S. and Kon, A.I. Izv. vuzov SSSR, seriya Radiofizika, 1964, Vol. 7, No. 4, p. 790.
754. Kabanov, M.V., Pershin, A.A., and Pkhalagov, Yu.A. Izv. vuzov SSSR, seriya fizika, 1968, No. 9, p. 121.
755. Khmelevtsov, S.S. and Tsvyk, R.Sh. Izv. vuzov SSSR, seriya Radiofizika, 1970, No. 1.
756. Borisov, B.D., Sazanovich, V.M., and Khmelevtsov, S.S. Izv. vuzov SSSR, seriya fizika, 1969, No. 1.
757. Hinchman, W.R. and Buck, A.L. Proc. IEEE, 1964, Vol. 52, p. 305.
758. Mevers, G.E., Fried, D.L., and Keister, M.P. Journ. Opt. Soc. Amer., 1965, Vol. 55, No. 11, p. 1575.
759. Edwards, B.N. and Steen, R.R. Appl. Optics, 1965, Vol. 4, No. 3, p. 311.

760. Collings, S.A. and Mouroe, M. Journ. Opt. Soc. Amer., 1966, Vol. 56, No. 4, p. 560.
761. Ryznar, E. Appl. Optics, 1965, Vol. 4, p. 1416.
762. Subramanian, M. and Collinson, J.A. Bell System Tech. Journ., 1967, Vol. 46, No. 3.
763. Subramanian, M. and Collinson, J.A. Bell System Tech. Journ., 1965, Vol. 44, p. 543.
764. Goldstein, B.S., Miles, P.A., and Chabot, A. Proc. IEEE, 1965, Vol. 53, p. 1172.
765. Fried, D.L. and Mevers, G.E. Journ. Opt. Soc. Amer., 1965, Vol. 55, p. 740.
766. Buck, A.L. Appl. Optics, 1967, Vol. 6, No. 4, p. 703.
767. Höhn, D.H. Appl. Optics, 1966, Vol. 5, No. 9, p. 1427.
768. Fried, D.L., Mevers, G.E., and Keister, M.P. Journ. Opt. Soc. Amer., 1967, Vol. 57, No. 6, p. 787.
769. Höhn, D.H. Appl. Optics, 1966, Vol. 5, No. 9, p. 1433.
770. S"yedin, V.Ya. and Khmelevtsov, S.S. Izv. vuzov SSSR, seriya Radiofizika, 1970, No. 1.
771. Herrick, R.B. and Mayer-Arrendt, J.R. Appl. Optics, 1966, /484
Vol. 5, No. 6, p. 981.
772. Marocuma, T., Nefflen, K.F., Lawrence, T.R., and Klucher, T.M. Journ. Opt. Soc. Amer., 1963, Vol. 53, No. 3.
773. McNish, A.G. Science, 1964, Vol. 146, p. 117.
774. Vaytsel' V.I. and Khmelevtsov, S.S. Tezisy doklada na I Konferentsii po perenosu informatsii lazernym izlucheniyem (Abstract of Paper at First Conference on Data Transmission by Laser Radiation), Izd-vo Kiyevskogo gosudarstvennogo universiteta, 1968.
775. Vaytsel' V.I. and Khmelevtsov, S.S. Tezisy doklada na I konferentsii po perenosu informatsii lazernym izlucheniyem, Izd-vo Kiyevskogo gosudarstvennogo universiteta, 1968.
776. Vaytsel' V.I. and Khmelevtsov, S.S. Izv. vuzov SSSR, seriya fizika, 1968, No. 6, p. 87.
777. Pokasov, V.V. and Khmelevtsov, S.S. Izv. vuzov SSSR, seriya fizika, 1968, No. 5, p. 82.
778. Pokasov, V.V. and Khmelevtsov, S.S. "Optika i spektroskopiya," 1968, Vol. XXV, No. 6, p. 945.
779. Zuyev, V.Ye., Ippolitov, I.I., and Makushkin, Yu.S. Trudy mezhdunarodnogo simpoziuma po radiatsionnym protsessam v atmosfere (Transactions of International Symposium on Radiation Processes in the Atmosphere) (Bergen, Norway, August 1968).
780. Zuyev, V.Ye., Marchuk, G.I., Galin, V.Ya., Ippolitov, I.I., Makushkin, Yu.S., Tvorogov, S.D., and Fomin, V.V. Trudy mezhdunarodnogo simpoziuma pc radiatsionnym protessam v atmosfere (Bergen, Norway, August, 1968).
781. Zuyev, V.Ye., Kabanov, M.V., Savel'yev, B.A., Samokhvalov, I.V., Sokolov, V.V., and Tvorogov, S.D. Trudy mezhdunarodnogo simpoziuma po radiatsionnym protessam v atmosfere (Bergen, Norway, August, 1968).
782. Antipov, B.A., Zuyev, V.Ye., Sapozhnikova, V.A., Sosnin, A. V., and Khmelevtsov, S.S. Trudy mezhdunarodnogo simpoziuma

po radiatsionnym protessam v atmosfere (Bergen, Norway, August, 1968).
783. Krekov, G.M. and Mikhaylov, G.A. Trudy Mezhdunarodnogo simpoziuma po radiatsionnym protessam v atmosfere (Bergen, Norway, August, 1968).
784. Kostkowski, H.J. and Bass, A.M. Journ. Opt. Soc. Amer., 1956, Vol. 46, p. 1060.
785. Seshadri, K.S. and Jones, R.N. Spectrochemica Acta, 1963, Vol. 19, p. 1013.
786. Bastin, J.Q., Grear, A.E., Jons, G.O., Smith, H.J.T., and Wright, P.J. Proceedings of the Royal Society, 1964, Vol. 278, No. 1375, p. 543.
787. Ryadov, V.Ya. and Furashov, N.I. Izv. vuzov SSSR, seriya Radiofizika, 1966, Vol. 9, No. 5, p. 1075.
788. Dryagin, Yu.A., Kislyakov, A.G., Kukin, L.M., Naumov, A.I., Fedoseyev, L.I. Izv. vuzov SSSR, seriya Radiofizika, 1966, Vol. 9, No. 5, p. 1078.
789. Ryadov, V.Ya. and Furashov, N.I. Optika i spektroskopiya, 1968, Vol. 24, No. 2, p. 178.
790. Zuyev, V.Ye., Nesmelova, L.I., and Tvorogov, S.D. In collection entitled: "Trudy mezhvuzovskogo soveshchaniya po spektral'noy prozrachnosti atmosfery v vidimoy i infrakrasnoy /485
oblasti" (Tomsk, iyun', 1965 g.) (Transactions of Inter-institute Conference on the Spectral Transparency of the Atmosphere in the Visible and Infrared Regions (Tomsk, June 1965)), Izd-vo Tomskogo gosudarstvennogo universiteta, 1968.
791. Golubitskiy, B.M. and Moskalenko, N.I. Izv. Akad. Nauk SSSR, seriya fizika atmosfery i okeana, 1968, Vol. 4, No. 1, p. 85.
792. Golubitskiy, B.M., Mirumyants, S.O., and Moskalenko, N.I. Doklad na VII Vsesoyuznom soveshchanii po aktinometrii i atmosfernoy optike (Paper Presented at Seventh All-Union Conference on Actinometry and Atmospheric Optics) May 27-31, 1968, Leningrad.
793. Moskalenko, N.I. Izv. Akad. Nauk SSSR, seriya fizika atmosfery i okeana, 1968, Vol. IV, No. 7, p. 777. Doklad na VII Vsesoyuznom soveshchanii po aktinometrii i atmosfernoy optike. May 27-31, 1968, Leningrad.
794. Kiseleva, M.S. "Optika i spektroskopiya," 1968, Vol. 24, No. 3, p. 401.
795. Rossetti, C. and Barchewitz, P. Comptes Rendus Acad. Sc. Paris, 1966, Ser. B, Vol. 262, p. 1966.
796. Rossetti, C., Bourbonneux, F., Farreng, R., and Barchewitz, P. Comptes Rendus Acad. Sc. Paris, 1966, ser. B, Vol. 262, p. 1684.
797. Farreng, R., Rossetti, C., Bourbonneux, F., and Barchewitz, P. Comptes Rendus Acad. Sc. Paris, 1966, Ser. B, Vol. 263, p. 241.
798. Gertsberg, G. Kolebatel'nyye i vrashchatel'nyye spektry mnogoatomnykh molekul (Vibrational and Rotational Spectra of Polyatomic Molecules), Izd-vo inostrannoy literatury, 1949.

799. Babcock, H.D. and Herzberg, L. Astrophys. Journ., 1948, Vol. 108, p. 167.
800. Adiks, T.G. and Dianov-Klokov, V.I. Izv. Akad. Nauk SSSR, seriya fizika atmosfery i okeana, 1968, Vol. IV, No. 10, p. 1052.
801. Schlapp, R. Phys. Rev., 1937, Vol. 51, No. 5.
802. Wark, D.Q. and Mercer, D.H. Appl. Optics, 1965, Vol. 4, No. 7.
803. Malkevich, M.S. Trudy Glavnoy geofizicheskoy observatorii, 1964, No. 166, p. 282.
804. Saiedy, F., Hilleary, D.T. and Morgan, W.A. Appl. Optics, 1965, Vol. 4, No. 4.
805. Moeller, G. and Rigden, J.D. Appl. Phys. Letters, 1966, Vol. 8, p. 69.
806. Zuyev, V.Ye., Sosnin, A.V., and Khmelevtsov, S.S. Izv. Akad. Nauk SSSR, seriya fizika atmosfery i okeana, 1969, Vol. V, No. 2, p. 201.
807. Kondratyev, K.J., Andreev, S.D., Badinov, I.J., Grishechkin, V.S., and Popova, L.V. Appl. Optics, 1965, Vol. 4, No. 9, p. 1069.
808. Neporent, B.S., Kiseleva, M.S., Makogonenko, A.G., and Shlyakhov, V.I. Appl. Optics, 1967, Vol. 6, No. 11, p. 1845.
809. Kiseleva, M.S., Reshetnikova, I.N., and Fedorova, Ye.O. Doklad na VII Vsesoyuznom soveshchanii po aktinometrii i atmosfernoy optike (Paper Presented at Seventh All-Union Conference on Actinometry and Atmospheric Optics), May 27-31, 1968, Leningrad).
810. Ivlev, L.S., Bursakova, N.S., and Surikov, O.M. In collection /486 entitled: "Problemy fiziki atmosfery" (Problems of Atmospheric Physics), 1968, No. 6, izd-vo Leningradskogo Gosudarstvennogo universiteta.
811. Fenn, R. Beitr. Physik d. Atmosph., 1964, Vol. 37, p. 69.
812. Bullrich, K., Eiden, R., Jaenicke, R., and Novak, W. Mainz. Final Technical Report, Contract DA-91-591-EUC-3458, 1966.
813. Ivlev, L.S. and Surikov, O.M. In collection entitled: "Problemy fiziki atmosfery," 1968, No. 8, Izd-vo Leningradskogo gosudarstvennogo universiteta.
814. Tanaka, M. Special Contributions, Geophysical Institute, Kyoto University, 1966, No. 6, p. 47.
815. Toba, Y. Special Contributions, Geophysical Institute, Kyoto University, 1966, No. 6, p. 59.
816. Toba, Y. and Tanaka, M. Special Contributions, Geophysical Institute, Kyoto University, 1965, No. 5, p. 81.
817. Toba, Y. and Tanaka, M. Journ. Meteor. Soc. Japan, 1963, ser. II, Vol. 41, No. 3, p. 135.
818. Toba, Y. Tellus, 1965, Vol. 27, No. 1, p. 131; No. 3, p. 366.
819. Toba, Y. Tellus, 1966, Vol. 28, No. 1, p. 132.
820. Ivanov, A.I., Livshits, G.Sh., Pavlov, V.Ye., Tashenov, B.T., and Teyfel', Ya.A. Rasseyaniye sveta v atmosfere (Scattering of Light in the Atmosphere), Izd-vo "Nauka" Kazakhskoy SSR, 1968.
821. Ivlev, L.S. and Yanchenko, Ye.L. Doklad na Vsesoyuznom soveshchanii po rasseyaniyu sveta v atmosfere (Paper at All-Union Conference on the Scattering of Light in the Atmos-

phere), Alma-Ata, November 1969.
822. Nikolayeva-Tereshkova, V.V. and Rozenberg, G.V. Izv. Akad. Nauk SSSR, seriya fizika atmosfery i okeana, 1965, Vol. 1, No. 4, p. 386.
823. Feoktistov, K.P., Rozenberg, G.V., Sandomirskiy, A.B., Sergeyevich, V.N., and Sonechkin, D.M. In collection entitled: Trudy Vsesoyuznoy konferentsii po fizike kosmicheskogo prostranstva (Transactions of All-Union Conference on the Physics of Outer Space), Izd-vo "Nauka," 1965.
824. Bunakova, A.M. and Ivlev, L.S. In collection entitled: "Problemy fiziki atmosfery" (Problems of Atmospheric Physics), No. 5, Izd-vo Leningradskogo Gosudarstvennogo universiteta, 1967.
825. Toropova, T.P. In collection entitled: "Trudy Astrofizicheskogo instituta AN Kaz. SSR." Voprosy astrofiziki i atmosfernoy optiki (Transactions of the Astrophysical Institute, Academy of Sciences of the Kazakh SSR. Problems of Astrophysics and Atmospheric Optics), Vol. VIII, Izd-vo "Nauka," Kaz.SSR, 1967.
826. Toropova, T.P. and Obasheva, S.O. In collection entitled: "Trudy Astrofizicheskogo instituta AN Kaz.SSR. Voprosy astrofiziki i atmosfernoy optiki," Vol. VIII, Izd-vo "Nauka," KazSSR, 1967.
827. Livshits, G.Sh. Rasseyaniye sveta v atmosfere, ch.1, "Trudy Astrofizicheskogo instituta AN KazSSR," (Scattering of Light in the Atmosphere. Part 1. Transactions of the Astrophysical Institute, Academy of Sciences of the Kazakh SSR), Vol. VI, 1965.
828. Barteneva, O.D., Davgyallo, Ye.N., and Polyakova, Ye.A. Experimental Research on the Optical Properties of the Ground Layer of the Atmosphere. Trudy Glavnoy geofizicheskoy observatorii, No. 220, Gidrometeoizdat, 1967.
829. Shifrin, K.S. and Chayanova, E.A. Izv. Akad. Nauk SSSR, seriya fizika atmosfery i okeana, 1967, Vol. 3, p. 274.
830. Pavlov, V.Ye. "Astronomicheskiy zhurnal," 1964, Vol. 41, No. 1, p. 122; No.3, p. 546.
831. Tychinskiy, V.P. Usp. Fiz. Nauk, 1967, Vol. 91, No. 3, p. 389.
832. "Metod Monte-Karlo v probleme perenosa izlucheniy" (The Monte Carlo Method in the Problem of Radiant Transfer), Collection of Papers Edited by Corresponding Member of the USSR /487
Academy of Sciences G.I. Marchuk, Atomizdat, 1967.
833. Krekov, G.M., Mikhaylov, G.A., and Kargin, B.A. Izv. vuzov SSSR, seriya fizika, 1968, No. 9. p. 99.
834. Krekov, G.M. and Mikhaylov, G.A. Izv. vuzov SSSR, seriya fizika, 1968, No. 10, p. 145.
835. Krekov, G.M., Krekova, M.M., and Samokhvalov, I.V. Izv. vuzov SSSR, seriya fizika, 1969, No. 5.
836. Krekov, G.M. Izv. vuzov SSSR, seriya fizika, 1969, No. 6, p. 74.
837. Krekov, G.M. Trudy IX Vsesoyuznoy konferentsii po rasprostraneniyu radiovoln (Transactions of the Ninth All-Union Conference on the Propagation of Radio Waves), Khar'kov, 1969.

838. Ivanov, A.P. and Khayrullina, A.Ya. Izv. Akad. Nauk SSSR, seriya fizika atmosfery i okeana, 1967, Vol. 3, No. 5, p. 537.
839. Khayrullina, A.Ya., and Ivanov, A.P. "Zhurnal prikladnoy spektroskopii," 1967, Vol. 7, No. 2, p. 255.
840. Ivanov, A.P. and Katsev, I.L. Izv. Akad. Nauk SSSR, seriya fizika atmosfery i okeana, 1967, Vol. 3, No. 7, p. 714.
841. Katsev, I.L. and Ivanov, A.P. "Zhurnal prikladnoy spektroskopii," 1967, Vol. 7, No. 5, p. 714.
842. Belyantsev, A.N., Dolin, L.S., and Savel'yev, V.A. Izv. vuzov SSSR, seriya radiofizika, 1967, Vol. 10, No. 4, p. 489.
843. Krekov, G.M. Izv. vuzov SSSR, seriya fizika, 1969, No. 7, p. 7.
844. Armand, S.A. "Radiotekhnika i elektronika," 1969, Vol. 14, No. 4, p. 587.
845. Saiedy, F., Jacobonritz, H., and Wark, D.Q. Journ. Atm. Sci., 1967, Vol. 21, No. 1.
846. Monin, A.S. and Obukhov, A.M. Trudy geofizicheskogo instituta, 1954, No. 24, p. 151.
847. Tsvang, L.R. Izv. Akad. Nauk SSSR, seriya geofizicheskaya, 1960, No. 8, p. 1252.
848. Gurvich, A.S. and Meleshkin, B.N. Izv. Akad. Nauk SSSR, seriya fizika atmosfery i okeana, 1966, Vol. 2, No. 7, p. 688.
849. Rogers, C.B. Journ. Opt. Soc. Amer., 1965, Vol. 55, No. 9, p. 1151.
850. Ward, R.C. and Berry, G.V. Appl. Optics, 1967, Vol. 6, No. 6, p. 1136.
851. Tatarskiy, V.I. Izv. vuzov SSSR, seriya Radiofizika, 1967, Vol. 10, No. 1, p. 48.
852. Richard, T., Brown, Jr. 12th Conference Radar Meteorology, Norman, Okla., 1966.
853. Kabanov, M.V., and Samokhvalov, I.V. Izv. vuzov SSSR, seriya fizika, 1969, No. 3, p. 80.
854. Fried, D.L. Journ. Opt. Soc. Amer., 1967, Vol. 57, No. 2, p. 169.
855. Chu, T.S. Appl. Optics, 1967, Vol. 6, No. 1, p. 163.
856. Beran, M.J. Journ. Optic. Soc. Amer., 1966, Vol. 56, No. 11, p. 1475.
857. Bonch-Bruyevich, A.M. and Khodovoy, V.A. Usp. Fiz. Nauk, 1965, Vol. 85, No. 1, p. 3.
858. Wallace, R. Molec. Phys., 1966, Vol. 11, p. 457.
859. Lukaszewski, M. Postepy fiz, 1967, Vol. 18, p. 287.
860. Rayzer, Yu.P. Usp. Fiz. Nauk, 1965, Vol. 87, No. 1.
861. Morton, V.M. Proc. Phys. Soc., 1967, Vol. 92, p. 301.
862. Pierre, N. and Pierre, V.C.R. Acad. Sci., 1966, Vol. AB 262, B.1337.
863. Beran, M. and Parrent, J. Theory of Partial Coherence, Englewood Cliffs,(N.J.), 1964.
864. Taylor, L. Journ. Opt. Soc. Amer., 1967, Vol. 57, No. 3, p. 304.
865. "Atmosfernyy ozon" (Atmospheric Ozone), Edited by G.P. Gushchin, Gidrometeoizdat, 1966.
866. Vasilevskiy, K.P. Kazbanov, V.A., and Boldyrev, V.A. Doklad na VII Vsesoyuznom soveshcnanii po aktinometrii i atmos-

fernoy optike (Paper Presented at Seventh All-Union Conference on Actinometry and Atmospheric Optics), May 27-31, 1968, Leningrad.
867. Golubitskiy, B.M. and Moskalenko, N.I. Izv. Akad. Nauk SSSR, seriya fizika atmosfery i okeana, 1968, Vol. 4, No. 1, p. 90.
868. Golubitskiy, B.M. and Moskalenko, N.I. Izv. Akad. Nauk SSSR, seriya fizika atmosfery i okeana, 1968, Vol. 4, No. 3, p. 346.
869. Moskalenko, N.I., Golubitskiy, B.M., and Mirumyants, S.O. Doklad na VII Vsesoyuznom soveshchanii po aktinometrii i atmosfernoy optike (Paper Presented at Seventh All-Union Conference on Actinometry and Atmospheric Optics), May 27-31, 1968, Leningrad.
870. Golubitskiy, B.M. and Moskalenko, N.I. Izv. Akad. Nauk SSSR, seriya fizika atmosfery i okeana, 1968, Vol. 4, No. 3, p. 360.
871. Farmer, C.V. and Houghton, J.T. Nature, 1966, Vol. 209, No. 5030.
872. Golubitskiy, B.M., Mirumyants, S.O., Tantashev, M.V., Filippov, V.L., and Artem'yeva, L.M. Doklad na VII Vsesoyuznom soveshchanii po aktinometrii i atmosfernoy optike (Paper Presented at Seventh All-Union Conference on Actinometry and Atmospheric Optics), May 27-31, 1968, Leningrad.
873. Filippov, V.L. and Mirumyants, S.O. Izv. Akad. Nauk SSSR, seriya fizika atmosfery i okeana, 1969, Vol. 5, No. 6, p. 638.
874. Ashcheulov, S.V., Kondrat'yev, K.Ya., and Styro, D.B. In collection entitled: "Problemy fiziki atmosfery," (Problems of Atmospheric Physics), No. 5, Izd-vo Leningradskogo gosudarstvennogo universiteta, 1967.
875. Bolle, H.J. Memoires de la Societe Royale des Sciences de Liege, Vol. 26, 1964.
876. Davis, P.A. and Viezee, W. Journ. Geophys. Res., 1964, Vol. 69, No. 18.
877. Kiseleva, M.S., Milinina, I.N., and Fedorova, Ye.O. Doklad na VII Vsesoyuznom soveshchanii po aktinometrii i atmosfernoy optike (Paper Presented at Seventh All-Union Conference on Actinometry and Atmospheric Optics), May 27-31, 1968, Leningrad.
878. Wacker, P.F. and Pratto, M.R. Microwave Spectral Tables, Vol. II, Line Strengths of Asymmetric Rotors, NBS Monograph 70, National Bureau of Standards, Washington, D.C., 1964.
879. Gates, D.M., Calfee, R.F., and Hansen, W. Appl. Optics, 1963, Vol. 2, No. 11, p. 1117.
880. Gates, D.M., Calfee, R.F., Hansen, D.W. and Benedict, W.S. Line Parameters and Computed Spectra for Water Vapor Bands at 2.7 μ, NBS Monograph 71, National Bureau of Standards, 1964.
881. Benedict, W.S., Calfee, R.F., Line Parameters for the 1.9 and 6.3 Micron Water Vapor Bands, ESSA Professional Paper 2, U.S. Department of Commerce, Washington, D.C., 1967.

/489

882. Pokrovskiy, A.G. In collection entitled: "Problemy fiziki atmosfery," (Problems of Atmospheric Physics), No. 5, Izd-vo Leningradskogo gosudarstvennogo universiteta, 1967.
883. Timofeyev, Yu.M. In collection entitled: "Problemy fiziki atmosfery," No. 5, Izd-vo Leningradskogo gosudarstvennogo universiteta, 1967.
884. Kondrat'yev, K.Ya. and Timofeyev, Yu.M. Doklad na VII Vsesoyuznom soveshchanii po aktinometrii i atmosfernoy optike (Paper Presented at Seventh All-Union Conference on Actinometry and Atmospheric Optics), May 27-31, 1968, Leningrad.
885. Ben Aryeh, Y. Journ. Quant. Spectr. Rad. Transfer, 1967, Vol. 7, No. 1, p. 211.
886. Sakai, H. Line Strengths and Widths in the ν_2 Water Band.
887. Pongtongcharoen, P. Intensities in Heated Water Vapor in the Region 4-5 μ. M.S.Thesis, Catholic Univ., Washington, D.C., 1965.
888. Kiriyenko, G.A., Toropova, T.P., Kharitonova, G.A., and Ibragimov, N.M. Doklad na VII Vsesoyuznom soveshchanii po aktinometrii i atmosfernoy optike (Paper Presented at Seventh All-Union Conference on Actinometry and Atmospheric Optics), May 27-31, 1968, Leningrad.
889. Gal'tsev, A.P., and Osipov, V.M., Doklad na VII Vsesyouznom soveshchanii po aktinometrii i atmosfernoy optike (Paper Presented at Seventh All-Union Conference on Actinometry and Atmospheric Optics), May 27-31, 1968, Leningrad.
890. Gal'tsev, A.P. In collection entitled: "Problemy fiziki atmosfery," (Problems of Atmospheric Physics), No. 5, Izd-vo Leningradskogo gosudarstvennogo universiteta, 1967.
891. Kozhevnikov, N.I., Sarychev, A.P., Sitnik, G.F., and Khlystov, A.I., Doklad na VII Vsesoyuznom soveshchanii po aktinometrii i atmosfernoy optike, 27-31 May 1968, Leningrad.
892. Siedentopf, H. and Mayer, U. Optik, 1965, Vol. 22, No. 9, p. 626.
893. Zuyev, V.Ye., Sosnin, A.V., and Khmelevtsov, S.S. Doklad na VII Vsesoyuznom soveshchanii po aktinometrii i atmosfernoy optike, May 27-31, 1968, Leningrad.
894. Yunge, Kh. Khimicheskiy sostav i radioaktivnost' atmosfery (Chemical Composition and Radioactivity of the Atmosphere), Izd-vo "Mir," 1965.
895. Rozenberg, G.V. Usp. Fiz. Nauk, 1968, Vol. 95, No. 1, p. 157.
896. Shedlovsky, J.P. and Blifford, I.H. Jr. Doklad na XIV General'noy assambleye MGGS (Paper at the Fourteenth General Assembly of the IUGG) Geneva, September, 1967.
897. Gorchakov, G.I. and Rozenberg, G.V. Izv. Akad. Nauk SSSR, seriya fizika atmosfery i okeana, 1967, Vol. 3, No. 6, p. 611.
898. Rozenberg, G.V. and Gorchakov, G.I. Izv. Akad. Nauk SSSR, seriya fizika atmosfery i okeana, 1967, Vol. 3, No. 7, p. 699.
899. Georgiyevskiy, Yu.G. Doklad na Vsesoyuznom mezhvedomstvennom soveshchanii po rasseyaniyu sveta v atmosfere (Paper Presented at All-Union Interdepartmental Conference on the Scattering of Light in the Atmosphere), Chernovtsy, June, 1967.

900. Selezneva, Ye.S. Atmosfernyye aerozoli (Atmospheric Aerosols), Gidrometeoizdat, 1966.
901. Sandomirskiy, A.B., Al'tovskaya, N.P., and Trifonova, G.I. Izv. Akad. Nauk SSSR, seriya Geofizicheskaya, 1964, No. 7, p. 121. /490
902. Pyldmaa, V.K. and Rozenberg, G.V. Izv. Akad. Nauk SSSR, seriyz fizika atmosfery i okeana, 1966, Vol. 2, No. 8, p. 820.
903. Koprova, L.I. Doklad na Vsesoyuznom mezhvedomstvennom soveshchanii po rasseyaniyu sveta v atmosfere (Paper at All-Union Interdepartmental Conference on the Scattering of Light in the Atmosphere), Chernovtsy, June, 1967.
904. Rozenberg, G.V., Sandomirskiy, A.B., and Pyldmaa, V.K. In collection entitled:"Serebristyye oblaka." Trudy mezhdunarodnogo simpoziuma (Noctilucent Clouds. Transactions of International Symposium), (Tallin, 1966), Izd-vo VINITI, 1967, p. 94.
905. Rozenberg, G.V. and Sandomirskiy, A.B. Izv. Akad. Nauk SSSR, seriya fizika atmosfery i okeana, 1967, Vol. 3, No. 2, p. 151.
906. Rozenberg, G.V. and Lyubovtseva, Yu.S. Izv. Akad. Nauk SSSR, seriya fizika atmosfery i okeana, 1967, Vol. 3, No. 2, p. 172.
907. Zuyev, V.Ye., Ippolitov, I.I., and Makushkin, Yu.S. Doklad na VII Vsesoyuznom soveshchanii po aktinometrii i atmosfernoy optike (Paper Presented at Seventh All-Union Conference on Actinometry and Atmospheric Optics), May 27-31, 1968, Leningrad.
908. Zuev, V.E., Kabanov, M.V., and Savelev, B.A. Appl. Optics, 1969, Vol. 8, No. 1.
909. Zuyev, V.Ye. Doklad na VII Vsesoyuznom soveshchanii po aktinometrii i atmosfernoy optike, May 27-31, 1968, Leningrad.
910. Zuyev, V.Ye. Doklad na VII Vsesoyuznom soveshchanii po atkinometrii i atmosfernoy optike, May 27-31, 1968, Leningrad.

INDEX

Absorption coefficients 68, 73, 76, 77, 123, 144-147, 148-154, 199, 200, 231, 335, 336
in gas medium 68, 73, 77, 123, 144-154, 335, 336
in scattering medium 199, 200, 231
Absorption functions 69, 70
calculation and use of spectrum models 77-85, 111-112, 124, 125
carbon dioxide 123-126
carbon monoxide 131, 132
direct calculation of 76, 77, 109-111, 124
experimental determination of 85, 112-116, 125, 126, 167, 168
groups of overlapping lines 76-85, 132-134
in inhomogeneous atmosphere 153-157
approximate method 157, 158, 161-163
calculation of curvature of the earth 164-167
methane 129, 130
nitrous oxide 130, 131
oxygen 128
ozone 127, 128
of a single line 74-76
water vapor 109-116, 168
Absorption of overlapping lines and bands 76-85, 132-134
Absorption of selective radiation 134-136
Anharmonic oscillator 36-38
Atmosphere
aerosol characteristics 175-193
clouds and fogs 175-183
hazes 183-193
precipitation 193, 194
characteristics of turbulence 349-352, 367
correlation function 349, 350, 355
correlation radius 363
structure constants 350, 351, 353, 355, 356, 368
structure function 350, 351, 353
concentration of carbon dioxide in 21-23
concentration of minor impurities in 22, 23
concentration of oxygen in 1, 2
concentration of ozone in 20, 21
concentration of water vapor in 5-19
gas composition of 1, 2
pressure 1, 2
temperature 2, 3
Attenuation coefficients 200, 202, 205, 231, 235, 239, 242-247, 251-257, 266
Backward scattering 306-308, 316-319
Bouguer's law 68, 85-89, 153, 232, 233, 249, 250, 257, 258, 274-278, 335, 336
limits of applicability for absorbing media 85-89
limits of applicability for scattering media 273-278, 303-306
Broadening of spectral lines (see Spectral lines)
Carbon dioxide 21-23, 57-62, 120-126, 151, 152

Carbon dioxide (cont'd)
absorption coefficients 151, 152
absorption functions 124-126
components of fine structure 120-123
concentration in atmosphere 21-23
general characteristics of absorption spectra 57-62
Carbon monoxide 21-23, 67, 131, 132
absorption function in 131, 132
concentration in atmosphere 21-23
fine structure in spectrum of 131, 132
general characteristics of spectrum 67
Clouds and fogs 175-184, 239, 242-249, 267-269, 308-311
attenuation coefficients 239, 240, 242-247
chemical composition of particles 183
microstructure parameters 178-180, 182
particle concentration 180, 249
polarization of scattered radiation 309-311
recurrence of meteorological visibility 247-249
scattering indicatrices 267-269
spectra of particle dimensions 175-178
water content of 180-182, 249
Complex refractive index 211, 239-243
Correlation radius 363
Depth condition 301-303
Doppler effect 45, 49, 50
Effective field 270
Fluctuations of light-beam parameters in turbulent atmosphere 349-368
beam shifting 356
coherence 367, 368
fluctuation cross sections 364, 365
fluctuations of angle of arrival 365-367
intensity fluctuations 357-364
Forward scattering 289-304, 311-316
experimental investigations 294-303
Monte Carlo method 292-294, 312-316
solution of transfer equation 289
Fresnel zone 352, 353, 362, 363
Hamiltonian 91-94, 105, 320-324, 332-334
Harmonic oscillator 36-38
Hazes 183-193, 250-264, 266-269
attenuation coefficients 251-257
chemical composition of particles 191-193
particle concentration 186-193
scattering indicatrices 267-269
size spectra of particles 184-186
transparency in horizontal direction 253
transparency on slant paths 257-263
Integral absorption 70
Integral strength of bands 70, 116, 117, 126
Lasers 279-288
absorption of radiation in atmosphere 120-152
coherence 282, 283, 285

Lasers (cont'd)
divergence 281, 285
gas 283-285
generation mode 279-288
glass 282, 283
ionic-crystal 279-282
parameter fluctuations in atmosphere 357-368
power and energy 279-288
radiation spectra 279-285, 287, 288
scattering radiation in atmosphere 269-272, 293-297, 303-319
semiconductor 285, 286
Linear molecules 26-29, 41
Matrix element 51, 52, 101-103
Meteorological visibilities 191, 247-249, 260
Methane 21-23, 65-67, 129, 130, 149, 150-152
absorption functions 128-130
absorption of radiation from lasers $\lambda = 3.39$ μm 148-150
concentration in atmosphere 21-23
fine structure of spectra 128, 129
general characteristics of spectra 65-67
Models of absorption bands 76-85, 111-113, 124, 125
combined model 81, 82
Elsasser model 78, 79, 130
quasistatistical model 82, 83
statistical model 79-81
Molecular scattering 228-230
Molecular spectra 24-26
carbon dioxide 57-62
carbon monoxide 67
electron 43
methane 65-67
nitrogen 52
nitrous oxide 64, 65
oxygen 62-64
ozone 61, 62
pure rotational 26-34
vibrational-rotational 35-43
water vapor 52-66
Molecules of asymmetrical-top type 32-35, 42, 43
Molecules of spherical-top type 29, 30, 41, 42
Molecules of symmetrical-top type 30-32, 42
Moments of inertia of a molecule 26, 27, 30, 31, 53
Nitrous oxide 21-23, 64, 65, 130, 131
absorption of individual bands 131
concentration in atmosphere 21-23
fine structure of spectra 130, 131
general characteristics of absorption spectra 64, 65
Nonlinear effects 320-348
multiphoton processes 320-332
saturation effect 332-337
self-focusing of laser beam 337-339
vaporization of particles 339-348

Nonstationary scattering 312–319
Optical thickness 68
Oxygen 1, 62–64, 128
  coefficients and absorption functions 128
  concentration in atmosphere 1, 2
  diffuse absorption complexes 64
  fine structure of spectra 128
  general characteristics of spectra 62–64
Ozone 20, 21, 61, 62, 126–128
  absorption function in 126, 127
  concentration in atmosphere 20, 21
  fine structure in spectrum of 126, 127
  general characteristics of spectrum 62
Parametric laser-emission frequency scanning 287, 288
Perturbation theory 93–96
Polarization of scattered radiation 309–311
Precipitation 183, 193, 266
  attenuation coefficient of 266
  chemical composition of 183
  intensity 193, 194
  ranges of particle sizes 193, 194
  scattering indicatrices 267
Production and annihilation operators 323
Pulsed light 281, 282, 288, 311–319
  deformation of propagation in medium of 311–319
Quantum numbers 27–29, 35–54
Scattering coefficients 199, 200, 228–231
Scattering matrix 198, 313, 314
Schrödinger equations 91, 92, 321
Single-particle scattering of light 195–227
  efficiency factors of attenuation, scattering and absorption 211–224
    approximating expressions 223
    large particles 213
    results of tabulation 214–223
    small particles 212
    "soft" particles 213
  of inhomogeneous field 206–211
  by nonspherical particles 226, 227
  by plane monochromatic wave 197, 198
  scalar approximation 202–206
  scattering, absorption, and attenuation coefficients 199–202
  scattering indicatrices 224–226
  scattering matrix 197
  Stokes parameters 196, 197
Spectral absorption 68, 69, 153–155, 168–174
  in inhomogeneous medium 153–155, 168–174
Spectral line 43–52, 70–77, 90–98, 109, 116–120
  absorption function 74–77
  center positions 90–98, 109
  contour shape 43–50, 71–74
    Doppler broadening 45, 46
    half-width 44, 45, 47–50

Spectral line (cont'd)
molecular-collision broadening 46-49
natural broadening 44, 45
shape of far limbs 50, 116-120
integral absorption 70, 74-77
strength of 50-52
Spectral-line strength 49, 50, 98-104, 109
Spectral propagation 68, 69, 153-155, 168-174
in inhomogeneous medium 153-155, 168-174
Structure constants 350, 368
Structure functions 350
Water vapor 5-19, 52-57, 90-115, 144-147, 149-151
absorption by far limbs of lines 117-120
absorption functions 109-116, 167, 168
concentration in atmosphere 5-19
general characteristics of absorption spectra 52-57
half-widths of lines 104-109
line center positions 90-98, 109
line strengths 98-104, 109
Wave function 91, 94, 95, 101, 105, 320-324, 332-334

****

Translated for the National Aeronautics and Space Administration by Scripta Technica, Inc. NASW-2036.

NATIONAL AERONAUTICS AND SPACE ADMISTRATION
WASHINGTON, D.C. 20546

OFFICIAL BUSINESS
PENALTY FOR PRIVATE USE $300

FIRST CLASS MAIL

POSTAGE AND FEES PAID
NATIONAL AERONAUTICS AND
SPACE ADMINISTRATION

U.S.MAIL

NASA 451

POSTMASTER: If Undeliverable (Section 158 Postal Manual) Do Not Return

"The aeronautical and space activities of the United States shall be conducted so as to contribute . . . to the expansion of human knowledge of phenomena in the atmosphere and space. The Administration shall provide for the widest practicable and appropriate dissemination of information concerning its activities and the results thereof."

—NATIONAL AERONAUTICS AND SPACE ACT OF 1958

NASA SCIENTIFIC AND TECHNICAL PUBLICATIONS

TECHNICAL REPORTS: Scientific and technical information considered important, complete, and a lasting contribution to existing knowledge.

TECHNICAL NOTES: Information less broad in scope but nevertheless of importance as a contribution to existing knowledge.

TECHNICAL MEMORANDUMS: Information receiving limited distribution because of preliminary data, security classification, or other reasons.

CONTRACTOR REPORTS: Scientific and technical information generated under a NASA contract or grant and considered an important contribution to existing knowledge.

TECHNICAL TRANSLATIONS: Information published in a foreign language considered to merit NASA distribution in English.

SPECIAL PUBLICATIONS: Information derived from or of value to NASA activities. Publications include conference proceedings, monographs, data compilations, handbooks, sourcebooks, and special bibliographies.

TECHNOLOGY UTILIZATION PUBLICATIONS: Information on technology used by NASA that may be of particular interest in commercial and other non-aerospace applications. Publications include Tech Briefs, Technology Utilization Reports and Technology Surveys.

Details on the availability of these publications may be obtained from:

SCIENTIFIC AND TECHNICAL INFORMATION OFFICE

NATIONAL AERONAUTICS AND SPACE ADMINISTRATION

Washington, D.C. 20546